AD-A060 343 PRATT AND WHITNEY AIRCRAFT GROUP WEST PALM BEACH FL G--ETC F/G 21/5
TURBINE EXIT GUIDE VANE PROGRAM.(U)
NOV 77 W S MITCHELL, J F SOILEAU F33615-74-C-2060
UNCLASSIFIED PWA-FR-8932 AFAPL-TR-77-75 NL

1 OF 4
AD A060343



AD A060343

DDC FILE COPY

AFAPL-TR-77-75

LEVEL II

TURBINE EXIT GUIDE VANE PROGRAM

United Technologies Corporation
Pratt & Whitney Aircraft Group
Government Products Division
P.O. Box 2691
West Palm Beach, Florida 33402

DDC
DISTRIBUTED
OCT 25 1978
F

November 1977

Final Report March 1974 - October 1977

Approved for public release;
distribution unlimited

Prepared for
Air Force Aero Propulsion Laboratory
Air Force Systems Command
United States Air Force
Wright-Patterson AFB, Ohio

78 10 19 066

NOTICE

When Government drawings, specifications, or other data are used for any purpose other than in connection with a definitely related Government procurement operation, the United States Government thereby incurs no responsibility nor any obligation whatsoever; and the fact that the government may have formulated, furnished, or in any way supplied the said drawings, specifications, or other data, is not to be regarded by implication or otherwise as in any manner licensing the holder or any other person or corporation, or conveying any rights or permission to manufacture, use, or sell any patented invention that may in any way be related thereto.

This report has been reviewed by the Information Office (OI) and is releasable to the National Technical Information Service (NTIS). At NTIS, it will be available to the general public, including foreign nations.

This technical report has been reviewed and is approved for publication.

Wayne A. Tall

WAYNE A. TALL
Tech Area Manager - Turbines
Components Branch

FOR THE COMMANDER

Ernest C. Simpson

ERNEST C. SIMPSON
Director
Turbine Engine Division

A

"If your address has changed, if you wish to be removed from our mailng list, or if the addressee is no longer employed by your organization please notify AFAPL/TBC, W-PAFB, OH 45433 to help us maintain a current mailing list."

Copies of this report should not be returned unless return is required by security considerations, contractual obligations, or notice on a specific document.

AIR FORCE/56780/8 September 1978 — 100

UNCLASSIFIED

SECURITY CLASSIFICATION OF THIS PAGE (When Data Entered)

REPORT DOCUMENTATION PAGE	READ INSTRUCTIONS BEFORE COMPLETING FORM
1. REPORT NUMBER: AFAPL-TR-77-75	2. GOVT ACCESSION NO. / 3. RECIPIENT'S CATALOG NUMBER
4. TITLE (and Subtitle): TURBINE EXIT GUIDE VANE PROGRAM.	5. TYPE OF REPORT & PERIOD COVERED: Final Report, March 1974 - Oct 1977.
	6. PERFORMING ORG. REPORT NUMBER: PWA FR-8932
7. AUTHOR(s): W. S. Mitchell, J. F. Soileau	8. CONTRACT OR GRANT NUMBER(s): F33615-74-C-2060
9. PERFORMING ORGANIZATION NAME AND ADDRESS: ~~United Technologies Corporation~~ Pratt & Whitney Aircraft Group, Government Products Division, West Palm Beach, Florida 33402	10. PROGRAM ELEMENT, PROJECT, TASK AREA & WORK UNIT NUMBERS: 30660624 / 96
11. CONTROLLING OFFICE NAME AND ADDRESS: Air Force Aero Propulsion Laboratory (TBC), Air Force Systems Command, United States AF, Wright-Patterson AFB, Ohio	12. REPORT DATE: Nov 1977 / 13. NUMBER OF PAGES: 316 (317 p.)
14. MONITORING AGENCY NAME & ADDRESS (if different from Controlling Office)	15. SECURITY CLASS. (of this report): Unclassified / 15a. DECLASSIFICATION/DOWNGRADING SCHEDULE

16. DISTRIBUTION STATEMENT (of this Report)

Approved for public release; distribution unlimited.

17. DISTRIBUTION STATEMENT (of the abstract entered in Block 20, if different from Report)

62203F

18. SUPPLEMENTARY NOTES

19. KEY WORDS (Continue on reverse side if necessary and identify by block number)

Gas turbine engines, turbine exit guide vanes, diffusing airfoil cascades, non-series airfoils, NASA series airfoils, secondary flow, secondary losses, endwall modifications, cutback leading edge, uncambered trailing edge, plane cascade, annular cascade, flow visualization.

20. ABSTRACT (Continue on reverse side if necessary and identify by block number)

This report summarizes the results of an Air Force-sponsored Turbine Exit Guide Vane (EGV) Technology Development Program. In the EGV program, non-series EGV airfoils, designed for spanwise maximum inlet Mach numbers of 0.75 and average gas turnings of 38.0 deg (loading levels above those typical of state-of-the-art EGV's) demonstrated high diffusion efficiencies (72.0%) and low total pressure losses (1.5%). The non-series EGV airfoils were designed (using computer graphics design techniques with predicted pressure distributions and predicted boundary layer characteristics) by tailoring the airfoil camber and thickness distributions to

DD FORM 1 JAN 73 1473 EDITION OF 1 NOV 65 IS OBSOLETE
S/N 0102-LF-014-6601

UNCLASSIFIED

SECURITY CLASSIFICATION OF THIS PAGE (When Data Entered)

78 10 19 066

392 887

minimize the airfoil suction surface rate of diffusion, therefore reducing the potential for flow separation. The non-series EGV airfoils also demonstrated performance improvements relative to equivalent NASA series airfoils.

The EGV program cascade data was correlated using a Pratt & Whitney Aircraft correlation for diffusing compressor cascades in order to develop, in conjunction with the non-series airfoil design technology, an EGV design system.

Experimental investigations were conducted to identify airfoil-endwall modifications which influence cross-channel secondary flow and reduce the associated total pressure losses. Endwall modifications, located within the airfoil pressure side-endwall fillet and identified as endwall protrusions, resulted in significant performance improvements, reducing total pressure loss, and increasing diffusion and gas turning.

SUMMARY

Advanced engine designs call for increasing turbine stage loadings which raise turbine exit Mach numbers and tangential swirls above state-of-the-art levels. Improved turbine exit guide vanes (EGV's) are required to provide flow conditions which are compatible with engine exhaust systems and/or augmentors. To meet these requirements, an EGV technology development program was sponsored by the Air Force Aero Propulsion Laboratory.

The EGV program was conducted in four phases. Phase I was concerned primarily with two-dimensional airfoil design techniques and the reduction of secondary losses with airfoil and/or endwall modifications. Phases II and III extended the Phase I design technology to three-dimensional design applications. Phase IV was a critique of Phases I, II, and III.

PHASE I — FLOW VISUALIZATION AND PLANE CASCADE STUDIES

In Phase I, the evaluation of NASA series airfoils for highly loaded design applications indicated that the suction surface rate of diffusion was too high, increasing the potential for flow separation. Therefore, non-series airfoils, specifically designed to minimize the suction surface rate of diffusion, were selected for the Phase I test airfoils. The non-series airfoils were designed using computer graphics design methods; optimum airfoils were identified with predicted surface pressure distributions and boundary layer characteristics. By tailoring the airfoil camber and thickness distributions, the non-series airfoil suction surface rate of diffusion was minimized and the potential for flow separation reduced.

Three non-series EGV airfoils, designed for gas turnings of 30-, 40- and 50-deg and inlet Mach numbers of 0.5, 0.675 and 0.85, respectively, were evaluated in a high Mach number plane cascade test rig. Relative to equivalent state-of-the-art series airfoils, the non-series airfoils demonstrated improved performance, reducing total pressure loss and increasing diffusion. However, the non-series airfoils were found to be more sensitive to incidence variations.

A flow visualization study was conducted during Phase I to determine methods to reduce secondary losses by improving the flow near the endwalls. Using a low Mach number (0.33) two-dimensional flow visualization wind tunnel for rapid screening of airfoil and endwall models, a total of 63 different airfoil-endwall configurations were tested. Optimum configurations which were subsequently tested in the 40-deg plane cascade included: cutback leading edge, uncambered trailing edge, reduced suction surface camber, and pressure side endwall protrusions.

Results of the 40-deg plane cascade testing indicated that the spanwise average static pressure rise increased with each modified airfoil-endwall configuration. The largest increase in static pressure rise was obtained with the combined airfoil-endwall modifications. Except for the pressure side endwall protrusion, each modification reduced the amount of secondary loss but also decreased the gas turning. The endwall protrusion resulted in an increase in gas turning; however, the total pressure loss also increased.

The Phase I 30-, 40- and 50-deg performance data was correlated using a Pratt & Whitney Aircraft (P&WA) equivalent cone angle (θeq) correlation. This correlation (presented in figure 62) equates the diffusing airfoil cascade to equivalent conical diffusers, permitting the airfoil aspect ratio and gap/chord ratio to be selected for maximum diffusion efficiency. The θeq correlation, in conjunction with the nonseries airfoil design technology, was used to design optimum performance highly loaded EGV's in Phase II.

PHASE II — ANNULAR CASCADE DESIGN AND TESTING

In Phase II, the design technology identified in Phase I was used to design an EGV for an advanced engine, single-stage, fan drive turbine with a mean exit swirl of 38 deg and an exit Mach number of 0.539. The EGV design was required to diffuse the flow to a Mach number at or below 0.4 and turn the flow to the axial direction. A maximum allowable total pressure loss of 2.0% was selected for the design. The experimental investigations conducted during this phase were made in an annular cascade test rig which was designed to simulate the engine turbine exit Mach number and swirl distributions.

The equivalent cone angle correlation was used to select the Phase II EGV aspect ratio and gap/chord ratio. The optimum diffusion efficiency was obtained with an equivalent conical angle of 6.1 deg for an aspect ratio of 2.478 and a gap/chord ratio of 0.55. The test rig EGV axial chord was set at 1.54 in., resulting in a full annulus design with 48 airfoils. Using the non-series design technology, airfoil sections were designed for each of five spanwise or radial positions which were curve-line faired during fabrication.

Two EGV annular cascades were tested during Phase II. The first cascade tested was the basic non-series airfoil. The second cascade was identical to the first except for airfoil-endwall modifications which were made to reduce secondary losses. These modifications were similar to those tested in Phase I and included the cutback leading edge, uncambered trailing edge and pressure side endwall protrusions.

The performance of the unmodified non-series airfoil exceeded the design performance goals of 2% loss and 0.4 exit Mach number. Across the airfoil cascade the loss was 1.5% and the exit Mach number was 0.395. For the combined cascade and downstream diffuser, the loss was 2.3% and the exit Mach number was 0.34.

Performance results of the modified airfoil showed, relative to the unmodified airfoil, increased diffusion (static pressure rise coefficient = 0.376 vs 0.357) and increased gas turning (exit air angle = 91.5 deg vs 94.0 deg). However, the total pressure loss increased also, 2.3% vs 1.5%.

The measured diffusion efficiency for the unmodified airfoil was 73.3%. The predicted diffusion efficiency, based on the equivalent cone angle correlation, was 71.5%. The close agreement between measured and predicted diffusion efficiencies substantiates the cone angle correlation. The correlation, although based on plane cascade (2-D) data, can be applied directly to annular cascade (3-D) designs.

PHASE III — SUPPLEMENTARY ANNULAR CASCADE TESTING

Three supplementary annular cascade tests were conducted during Phase III to further evaluate the Phase I and Phase II airfoil-endwall modifications. Results of these tests showed that, contrary to the Phase I test results, the cutback leading edge and uncambered trailing edge airfoil modifications decreased performance, increasing the total pressure loss and decreasing the gas turning. The endwall modifications (pressure side protrusions) showed, relative to a cutback-uncambered airfoil, an improvement in performance. The protrusions decrease the total pressure loss and increase the static pressure rise and gas turning. A reduced size protrusion, approximately one-half the size of the full protrusion, resulted in the largest reduction in total pressure loss, indicating that an optimum protrusion size exists.

In addition to the airfoil-endwall modification tests conducted in Phase III, a state-of-the-art series airfoil was tested in the annular cascade test rig in order to identify performance improvements made with the advanced technology non-series airfoils. The 65-series circular arc mean camberline NASA series was selected for the representative state-of-the-art airfoil. The series airfoil geometric design, except for surface curvatures, was identical to the non-series airfoil design (i.e., aspect ratio, gap/chord ratio, etc.)

Performance comparisons made between the series and non-series EGV's showed that the non-series EGV improved performance. The total pressure loss was lower (1.5% vs 2.5%) and the static pressure rise was higher (0.357 vs 0.343). Flow visualization tests made on the series airfoil indicated that the higher total pressure loss was caused by flow separation. Analytical studies made prior to the series airfoil test predicted the flow separation. The non-series airfoil, specifically designed with a reduced suction surface rate of diffusion, as predicted, did not separate.

PHASE IV — CRITIQUE

The Phase I plane cascade data was reviewed in order to establish a data bank for use in predicting the spanwise losses for highly loaded non-series EGV's. A secondary flow expansion angle was defined to predict the location of the secondary flow spanwise endpoints. Between these spanwise locations, the losses are assumed to be profile losses and are estimated using the Phase I profile loss data. Secondary losses are estimated by using equivalent secondary losses which are based on the Phase I secondary loss data. In addition to the loss data review, the plane cascade air angle data was reviewed to identify possible design deviation improvements. In general, the measured non-series EGV gas turning was less than the predicted gas turning. The difference between measured and predicted gas turning increased with inlet Mach number, permitting identification of a Mach number correction to the design deviation prediction system.

Because turbine EGV's are generally required to accommodate rear bearing compartment support rods and oil lines, thick long chord low aspect ratio airfoils are used. This requirement was not considered in the design and selection of the EGV program test airfoils. Therefore, to properly assess the program test results, a low aspect ratio EGV was designed and analytically evaluated for comparison with the Phase II high aspect ratio EGV. Predicted losses for both designs show that the low aspect ratio loss is 0.8% higher. In addition, the amount of suction surface diffusion conducted prior to flow separation was very low, indicating possible additional increases in total pressure loss with decreased diffusion efficiencies. Weight and cost comparisons made between the high and low aspect ratio EGV's showed that the high aspect ratio EGV weighed 17 lb more, and (for a single piece casting) had the same procurement cost.

The EGV program non-series airfoils were designed with small circular leading edges in order to obtain the minimum suction surface rate of diffusion. These airfoils are very sensitive to incidence variations. Therefore an incidence sensitivity study was conducted to compare and evaluate the incidence ranges of series and non-series EGV's.

Using predicted airfoil pressure distributions and an arbitrarily selected minimum leading edge overspeed value of $P_s/P_T = 0.5$, the circular leading edge non-series EGV had an incidence range of 2.0 deg. The 65 series EGV incidence range was 9.0 deg. Redesigning the non-series EGV's with elliptical leading edges increased their incidence range to 6.0 deg.

State-of-the-art advancements made as a result of the EGV technology development program are:

1 Application of non-series airfoil design technology to highly loaded tubine EGV's; the non-series airfoils demonstrating relative to equivalent series airfoils, a reduction in total pressure loss, higher diffusion efficiencies and reduced tendencies for flow separation;

2 Extension of the P&WA equivalent conical angle correlation (θeq) for diffusing cascades into a range of cone angles applicable to advanced engine turbine EGV's; the correlation, based on plane cascade (2-D) data and demonstrated in an annular cascade (3-D) design, was used to obtain optimum diffusion efficiencies;

3 EGV airfoil pressure side protrusions demonstrated reduced secondary losses with improved spanwise gas turning distributions and increased diffusion.

FOREWORD

This final Report was produced in accordance with Contract for Exit Guide Vane Program, No. F33615-74-C-2060, Project No. 3066, Task No. 0624, under the direction of Mr. Wayne A. Tall, TBC of the Air Force Aero Propulsion Laboratory. It presents the work conducted by Pratt & Whitney Aircraft Group of United Technologies Corporation in accordance with Sequence No. 6 of Exhibit A (DD Form 1423) of the contract. The work under the contract was performed under John F. Soileau and William S. Mitchell of Pratt & Whitney Aircraft Group.

TABLE OF CONTENTS

Section		Page
	LIST OF ILLUSTRATIONS	12
	LIST OF TABLES	22
	INTRODUCTION	25
I	PHASE I — FLOW VISUALIZATION AND PLANE CASCADE STUDIES	27
	A. Airfoil and Endwall Analysis and Design	27
	1. Design Point Selection	27
	2. Selection of Model Scale	28
	3. 30-Degree Cascade Airfoil Design	29
	4. 40-Degree Cascade Airfoil Design	39
	5. 50-Degree Cascade Airfoil Design	39
	6. Endwall Designs	39
	B. Flow Visualization Study and Test Setup	48
	1. Test Setup and Test Procedure	48
	2. Test Results	50
	C. Plane Cascade Test Setup and Data Reduction	58
	1. Test Rig and Facility Description	58
	2. Assembly of Airfoil Packs	60
	3. Instrumentation	60
	D. Airfoil Performance Test Results	66
	1. Checkout Tests	66
	2. 30-Degree Airfoil Performance Test Results	73
	3. 50-Degree Airfoil Performance Test Results	73
	4. 40-Degree Airfoil Performance Test Results	85
	5. Data Analysis Using Spanwise Average Total Inlet Pressures	96
	E. Data Correlation Using Equivalent Cone Angle	100
	F. Summary — Phase I	104
II	PHASE II — ANNULAR CASCADE DESIGN AND TESTING	105
	A. Airfoil and Endwall Analysis and Design	105
	1. Design Point Selection	105
	2. Selection of Model Scale and Swirl Vane Design	105
	3. Aerodynamic Design of Configuration 1 (EGV No. 1)	111
	4. Aerodynamic Design of Configuration 2 (EGV No. 2)	117

TABLE OF CONTENTS (Continued)

Section		*Page*
	B. Annular Cascade Test Setup and Data Reduction	128
	1. Facility	128
	2. Test Rig Description	128
	3. Airfoil Inspection	128
	4. Test Rig Instrumentation	134
	5. Data Recording	134
	6. Test Procedure	136
	7. Data Reduction	137
	C. Airfoil Performance Test Results	139
	1. General	139
	2. Checkout Tests	140
	3. EGV No. 1 Performance Test Results	143
	4. EGV No. 2 Performance Test Results	143
	5. Performance Comparison	149
	D. Summary — Phase II	152
III	PHASE III — SUPPLEMENTARY ANNULAR CASCADE TESTING	156
	A. Effect of Leading Edge Cutback	156
	B. Effect of Endwall Protrusions	156
	C. Effect of Root and Tip Section Uncambering	160
	D. State-of-the-Art Series Airfoil Evaluation	169
	E. Series Airfoil Test Results	180
	F. Summary — Phase III	191
IV	PHASE IV — PROGRAM CRITIQUE	196
	A. Non-series EGV Design System Review	196
	1. Loss Prediction System Improvement	196
	2. Deviation System Improvement	201
	B. Low Aspect Ratio Design Study	202
	1. Aerodynamic Performance Comparison	202
	2. Weight Comparison	208
	3. Cost Comparison	208
	C. Series and Non-series EGV Incidence Sensitivity Study	214
	D. State-of-the-Art Advancements	233
	CONCLUSIONS	234

TABLE OF CONTENTS (Continued)

Section		*Page*
	RECOMENDATIONS	235
	REFERENCES	236
	APPENDIX A — Phase I Airfoil Coordinates	237
	APPENDIX B — Phase I Flow Visualization Test Configurations and Results	242
	APPENDIX C — Derivation of Equivalent Conical Angle	276
	APPENDIX D — Phase II Annular Cascade Non-series EGV Airfoil Sections and Airfoil Coordinates	278
	APPENDIX E — Annular Cascade Rig Instrumentation Headers and Instrumentation Locations	289
	APPENDIX F — Phase III 65-Series EGV Airfoil Sections and Airfoil Coordinates	293
	APPENDIX G — Phase IV Low Aspect Ratio Non-series EGV Airfoil Sections and Airfoil Coordinates	304
	APPENDIX H — Design Deviation Prediction Method	313
	ABBREVIATIONS AND SYMBOLS	314

LIST OF ILLUSTRATIONS

Figure		*Page*
1	Exit Guide Vane Cascade Schematic	28
2	Minimum Cascade Reynolds Number	29
3	Diffusion Factor for 30-deg Cascade	30
4	State-of-the-Art Airfoils Considered for 30-deg Cascade	32
5	Comparison of 30-deg Cascade Series Airfoil Suction Surface Pressure Distributions	33
6	Comparison of 30-deg Cascade, 400 Series, and Circular Arc Series Airfoil Suction Surface Skin Friction Coefficient	34
7	30-deg EGV Cascade Non-Series Airfoils	35
8	Comparison of 30-deg Cascade Series and Non-Series Airfoil Suction Surface Pressure Distributions	36
9	Comparison of 30-deg Cascade Series and Non-Series Airfoil Suction Surface Skin Friction Coefficients	37
10	30-deg EGV Cascade Non-Series Airfoil Geometry	38
11	40-deg Cascade Parametric Data (M_2 = 0.675, 0-deg Exit Swirl)	40
12	Comparison of 40-deg Cascade Circular Arc and Non-Series Airfoil Pressure Distributions	41
13	Comparison of 40-deg Cascade Circular Arc and Non-Series Airfoil Suction Surface Skin Friction Coefficients	42
14	40-deg EGV Cascade Non-Series Airfoil Geometry	43
15	50-deg Cascade Parametric Data (M_2 = 0.85, 0-deg Exit Swirl)	44
16	Comparison of 50-deg Cascade Circular Arc and Non-Series Airfoil Pressure Distributions	45
17	Comparison of 50-deg Cascade Circular Arc and Non-Series Airfoil Suction Surface Skin Friction Coefficients	46
18	50-deg EGV Cascade Non-Series Airfoil Geometry	47
19	Flow Visualization Test Facility	48
20	Flow Visualization Cascade Rig Model	49

LIST OF ILLUSTRATIONS (Continued)

Figure		Page
21	Flow Visualization of 30-deg EGV Checkout Test	51
22	Flow Visualization of 40-deg EGV Airfoil Variations (A_3/A_2 = 1.075, Divergence = 5 deg)	55
23	Cutback Leading Edge Configuration with Modified Endwall Section Leading Edge and Uncambered Trailing Edge	57
24	High Mach Number Plane Cascade Test Rig	58
25	Plane Cascade Test Rig Schematic	59
26	Plane Cascade/Annular Cascade Test Facility	59
27	Plane Cascade Rig Test Section Schematic	61
28	Plane Cascade Test Pack Assembly — 7 Airfoil Cascade	62
29	Plane Cascade Test Pack Assembly — 13 Airfoil Cascade	63
30	Endwall Static Pressure Tap Locations	65
31	Inlet Flow Distribution at Midspan (30-deg Cascade)	67
32	Spanwise Inlet Flow Distribution (30-deg Cascade, M_2 = 0.517)	68
33	Effect of Boundary Layer Bleed on Inlet Static Pressure Distribution (30-deg Cascade, M_2 = 0.517)	70
34	Inlet Boundary Layer Velocity Distributions for 30-deg Cascade	71
35	Inlet Boundary Layer Velocity Distributions for 40-deg Cascade	72
36	30-deg EGV Average Performance Data Referenced to Midspan Inlet Total Pressure	74
37	30-deg EGVAirfoil Pressure Distribution (β_2 = 62.5 deg)	75
38	Effect of Incidence on Circular Arc Compressor Cascade Performance	76
39	30-deg EGV Spanwise Exit Air Angle and Loss Distribution	77
40	30-deg EGV Endwall Flow and Pressure Patterns (H_3/H_2 = 1.2, M_2 = 0.513)	78
41	30-deg EGV Endwall Flow and Pressure Patterns (H_3/H_2 = 1.0, M_2 = 0.509)	79
42	50-deg EGV Average Performance Data Referenced to Midspan Inlet Total Pressure	80

LIST OF ILLUSTRATIONS (Continued)

Figure		*Page*
43	50-deg EGV Spanwise Exit Air Angle and Loss Distribution for (H_3/H_2 = 1.0)	81
44	50-deg Airfoil Pressure Distribution (H_3/H_2 = 1.0, β_2 = 48.6 deg, M_2 = 0.841)	82
45	50-deg EGV Endwall Flow and Pressure Patterns (H_3/H_2 = 1.0, M_2 = 0.841)	83
46	Effect of Incidence on Circular Arc Compressor Cascade Performance	84
47	40-deg EGV Airfoil Pressure Distribution (H_3/H_2 = 1.1, β_2 = 55.7 deg, M_2 = 0.671)	85
48	40-deg EGV Airfoil Pressure Distribution (H_3/H_2 = 1.0, β_2 = 45.0 deg, M_2 = 0.634)	86
49	40-deg EGV Average Performance Data Referenced to Midspan Inlet Total Pressure (7-Airfoil Cascade)	87
50	Description of Mod 1 Configuration	88
51	Description of Mod 2 Configuration	89
52	Mod 2 Flow Area Distribution	90
53	40-deg EGV Airfoil Pressure Distribution (H_3/H_2 = 1.0, β_2 = 50 deg, M_2 = 0.702, Baseline Retest)	91
54	40-deg EGV Average Performance Data Referenced to Midspan Inlet Total Pressure (13-Airfoil Cascade)	92
55	40-deg EGV Spanwise Exit Air Angle and Loss Distribution (M_2 = 0.250)	93
56	40-deg EGV Spanwise Exit Angle and Loss Distribution (M_2 = 0.500)	94
57	40-deg EGV Spanwise Exit Air Angle and Loss Distribution (M_2 = 0.675)	95
58	Effect of Incidence on Circular Arc Compressor Cascade Performance (Reference 2)	97
59	40-deg EGV Average Performance Data Referenced to Average Inlet Total Pressure (13-Airfoil Cascade)	98
60	40-deg EGV Total Pressure Loss Distribution Corrected for Inlet Total Pressure Distribution (13-Airfoil Cascade)	99
61	Correlation of Exit Endwall Boundary Layer Displacement Thickness	101
62	Equivalent Conical Angle Correlation of Diffusing Cascade Data	103

LIST OF ILLUSTRATIONS (Continued)

Figure		*Page*
63	F100 Single Stage Low Pressure Turbine Flowpath	106
64	Annular Cascade Design Inlet Air Angle and Mach Number Distribution	107
65	Annular Cascade Rig Schematic	108
66	Annular Cascade Rig Inlet Screen Design Total Pressure Loss and Blockage Characteristics	109
67	Annular Cascade Exit Guide Vane Inlet Absolute Mach Number Distribution	110
68	Annular Cascade Diffusion System Flowpath Restraints (Rig Scale)	111
69	Equivalent Conical Angle Correlation of Diffusing Cascade Data	113
70	EGV Design Characteristics Based on Phase I Cascade Correlation at Optimum Diffuser Efficiency	114
71	EGV Design Characteristics Based on Phase I Cascade Correlation at Optimum Diffuser Efficiency	115
72	Downstream Diffuser Characteristics as a Function of Diffuser Length	116
73	Annular Cascade EGV Root Section Boundary Layer Analysis (M_2 = 0.686)	118
74	Annular Cascade EGV, ¼ Root Section Boundary Layer Analysis (M_2 = 0.631)	119
75	Annular Cascade EGV Mean Section Boundary Layer Analysis (M_2 = 0.527)	120
76	Annular Cascade EGV, ¼ Tip Section Boundary Layer Analysis (M_2 = 0.442)	121
77	Annular Cascade EGV, Tip Section Boundary Layer Analysis (M_2 = 0.342)	122
78	EGV No. 2 Cutback Root Section (Scaled)	123
79	EGV No. 2 Cutback Tip Section (Scaled)	124
80	EGV No. 1 Predicted Spanwise Total Pressure Loss Distribution	125
81	Flow Area Distributions for Selected Root and Tip Streamtubes	126
82	EGV No. 2 Configurations	127

LIST OF ILLUSTRATIONS (Continued)

Figure		*Page*
83	Rear View of 180-deg Segment Annular Cascade Rig	129
84	180-deg Segment Annular Cascade Rig Schematic	130
85	Annular Cascade Test Airfoil, EGV No. 1	131
86	Annular Cascade Test Airfoil, EGV No. 2	132
87	EGV No. 1 Airfoil Inspection	133
88	Annular Cascade Radial-Circumferential Probe Traverse System	135
89	Linear-Rotary Probe Traverse Control System — Radial Traverse and Automotive Air Angle Seeking	136
90	Annular Cascade Rig Wake Rake Element Traverse Positions (Station 2)	138
91	Annular Cascade Checkout Test, Swirl Vane Exit Flow Field Isobars at Design Conditions	140
92	Annular Cascade Checkout Test, Evaluation of Flow Field Periodicity from Swirl Vanes at Design Conditions	142
93	Comparison of EGV Inlet Spanwise Total Pressure Distributions, Measured by the Wake Rake and Radial-Circumferential Traverse Probe at Design Conditions	144
94	Annular Cascade Checkout Test, Spanwise Mach Number, and Air Angle Distribution at Design Conditions	145
95	Annular Cascade Checkout Test, Spanwise Air Angle, and Mach Number Distributions	146
96	Annular Cascade Test EGV Incidence Distribution	147
97	Annular Cascade Average Performance Data Referenced to Maximum Inlet Mach Number (EGV No. 1)	148
98	Annular Cascade Average Performance Data Reference to Maximum Inlet Mach Number (EGV No. 2)	150
99	Comparison of Spanwise Distribution of Total Pressure Loss and Exit Air Angle (M_{2max} = 0.695)	151
100	Boundary Layer Streamline Patterns from Annular Cascade Tests (M_2 = 0.695)	153
101	Flow Field Surveys for EGV No. 1 for M_{2max} = 0.7	154

LIST OF ILLUSTRATIONS (Continued)

Figure		*Page*
102	Equivalent Conical Angle Correlation of Diffusing Cascade Data	155
103	Effect of Leading Edge Cutback, Total Pressure Loss and Exit Air Angle vs Percent Span	157
104	Effect of Leading Edge Cutback, Exit Air Angle and Static Pressure vs Average Inlet Mach Number	158
105	Effect of Leading Edge Cutback, Total Pressure Loss vs Average Inlet Mach Number	159
106	Effect of Endwall Protrusions, Total Pressure Loss and Exit Air Angle vs Percent Span	161
107	Effect of Endwall Protrusions, Exit Air Angle and Static Pressure vs Average Inlet Mach Number	162
108	Effect of Endwall Protrusions, Total Pressure Loss vs Average Inlet Mach Number	163
109	Effect of Uncambered Trailing Edge, Total Pressure Loss and Exit Air Angle vs Percent Span	164
110	Effect of Uncambered Trailing Edge, Exit Air Angle and Static Pressure vs Average Inlet Mach Number	165
111	Effect of Uncambered Trailing Edge, Total Pressure Loss vs Average Inlet Mach Number	166
112	65 Series — Circular Arc Meanline Airfoil Characteristics	171
113	Mean Section Comparison, Series vs Non-series Airfoil	172
114	Mid Range Loss and Minimum Loss vs Inlet Angle, Root Section	172
115	Series and Non-series Airfoil Root Section Surface Pressure Distributions and Skin Friction Coefficients	175
116	Series and Non-series Airfoil ¼ Root Section Surface Pressure Distributions and Skin Friction Coefficients	176
117	Series and Non-series Airfoil Mean Section Surface Pressure Distributions and Skin Friction Coefficients	177
118	Series and Non-series Airfoil ¼ Tip Section Surface Pressure Distributions and Skin Friction Coefficients	178
119	Series and Non-series Airfoil Tip Section Surface Pressure Distributions and Skin Friction Coefficients	179

LIST OF ILLUSTRATIONS (Continued)

Figure		*Page*
120	Series and Non-series EGV Total Pressure Loss vs Inlet Mach Number	181
121	Series and Non-series EGV Static Pressure Rise, Exit Air Angle vs Inlet Mach Number	182
122	Series and Non-series EGV Exit Air Angle, Total Pressure Loss vs Percent Span	183
123	Series and Non-series EGV Diffusion Efficiency vs Inlet Mach Number	184
124	Series and Non-series EGV ¼ Root Section Measured Pressure Distributions	185
125	Series and Non-series EGV Mean Section Measurement Pressure Distributions	186
126	Series and Non-series EGV Average Static Pressure Rise vs Suction Surface Diffusion	187
127	Series and Non-series EGV Average Static Pressure Rise vs Total Pressure Loss	189
128	Flow Visualization — 65 Series Airfoil	190
129	Predicted Effect of Gas Turning on Performance	192
130	Non-series Predicted and Measured Static Pressure Distributions	193
131	65-Series EGV Predicted and Measured Static Pressure Distributions	194
132	65-Series EGV Series Airfoil Predicted/Measured Suction Surface Separation Line	195
133	Phase I Plane Cascade Spanwise Loss Distributions	197
134	Secondary Flow Expansion Angle	198
135	Secondary Flow Expansion Angle vs Inlet Mach Number	198
136	High and Low Aspect Ratio EGV Equivalent Percent Span Locations	199
137	EGV No. 1 Predicted and Measured Spanwise Loss Distributions	200
138	Non-series EGV Measured vs Design Deviation	201
139	Non-series EGV Deviation Correction vs Inlet Mach Number	202

LIST OF ILLUSTRATIONS (Continued)

Figure		*Page*
140	High and Low Aspect Ratio EGV Schematics	203
141	Number of High and Low Aspect Ratio Airfoils vs Mean Gap/Chord Ratio	204
142	High and Low Aspect Ratio EGV Diffusion Factor and Total Pressure Loss vs Mean Gap/Chord Ratio	205
143	Comparison of High and Low Aspect Ratio EGV Mean Sections	206
144	Low Aspect Ratio EGV Root Section Predicted Pressure Distribution and Skin Friction Coefficient	209
145	Low Aspect Ratio EGV ¼ Root Section Predicted Distribution and Skin Friction Coefficient	210
146	Low Aspect Ratio EGV Mean Section Predicted Distribution and Skin Friction Coefficient	211
147	Low Aspect Ratio EGV ¼ Tip Section Predicted Pressure Distribution and Skin Friction Coefficient	212
148	Low Aspect Ratio EGV Tip Section Predicted Pressure Distribution and Skin Friction Coefficient	213
149	65-Series and Non-series EGV Leading Edge Configurations	214
150	65-Series EGV ¼ Root Section Predicted Pressure Distribution at −4.0 deg Incidence	216
151	65-Series EGV ¼ Root Section Predicted Pressure Distribution at −2.0 deg Incidence	217
152	65-Series EGV ¼ Root Section Predicted Pressure Distribution at 0.0 deg Incidence	218
153	65-Series EGV ¼ Root Section Predicted Pressure Distribution at +2.0 deg Incidence	219
154	65-Series EGV ¼ Root Section Predicted Pressure Distribution at +4.0 deg Incidence	220
155	Non-series EGV ¼ Root Section Predicted Pressure Distribution at −4.0 deg Incidence	221
156	Non-series EGV ¼ Root Section Predicted Pressure Distribution at −2.0 deg Incidence	222
157	Non-series EGV ¼ Root Section Predicted Pressure Distribution at 0.0 deg Incidence	223

LIST OF ILLUSTRATIONS (Continued)

Figure		*Page*
158	Non-series EGV ¼ Root Section Predicted Pressure Distribution at +2.0 deg Incidence	224
159	Non-series EGV ¼ Root Section Predicted Leading Edge Region Pressure Distribution for Circular 2/1, 4/1, and 6/1 Elliptical Leading Edges	225
160	4/1 Elliptical Leading Edge Non-series EGV Predicted Pressure Distribution at −6.0 deg Incidence	226
161	4/1 Elliptical Leading Edge Non-series EGV Predicted Pressure Distribution at −5.0 deg Incidence	227
162	4/1 Elliptical Leading Edge Non-series EGV Predicted Pressure Distribution at −4.0 deg Incidence	228
163	4/1 Elliptical Leading Edge Non-series EGV Predicted Pressure Distribution at −2.0 deg Incidence	229
164	4/1 Elliptical Leading Edge Non-series EGV Predicted Pressure Distribution at 0.0 deg Incidence	230
165	4/1 Elliptical Leading Edge Non-series EGV Predicted Pressure Distribution at +2.0 deg Incidence	231
166	4/1 Elliptical Leading Edge Non-series EGV Predicted Pressure Distribution at +4.0 deg Incidence	232
C-1	Equivalent Radius and Cone Angle Derivation	276
D-1	Phase II Annular Cascade Non-series EGV Design, Root Section (Scaled)	279
D-2	Phase II Annular Cascade Non-series EGV Design, ¼ Root Section (Scaled)	281
D-3	Phase II Annular Cascade Non-series EGV Design, Mean Section (Scaled)	283
D-4	Phase II Annular Cascade Non-series EGV Design, ¼ Tip Section (Scaled)	285
D-5	Phase II Annular Cascade Non-series EGV Design, Tip Section (Scaled)	287
E-1	Phase II Annular Cascade Instrumentation Location, Station 1	290
E-2	Phase II Annular Cascade Instrumentation Location, Station 2	290
E-3	Phase II Annular Cascade Instrumentation Location, Station 3	291
E-4	Phase II Annular Cascade Instrumentation Location, Station 4	291

LIST OF ILLUSTRATIONS (Continued)

Figure		*Page*
F-1	65 Circular-Arc Series Airfoil, Root Section	294
F-2	65 Circular-Arc Series Airfoil, ¼ Root Section	296
F-3	65 Circular-Arc Series Airfoil, Mean Section	298
F-4	65 Circular-Arc Series Airfoil, ¼ Tip Section	300
F-5	65 Circular-Arc Series Airfoil, Tip Section	302
G-1	Low Aspect Ratio, Root Section	306
G-2	Low Aspect Ratio, ¼ Root Section	306
G-3	Low Aspect Ratio, Mean Section	308
G-4	Low Aspect Ratio, ¼ Tip Section	308
G-5	Low Aspect Ratio, Tip Section	311
H-1	Maximum Camber Location	313

LIST OF TABLES

Table		*Page*
1	Airfoil Design Parameters	28
2	30-Deg Gas Turning Exit Guide Vane Sections	30
3	Survey of EGV Annulus Area Ratios	40
4	Scoring of Boundary Layer Flow Visualization Patterns	52
5	Comparative Boundary Layer Pattern Scores for Flow Visualization Models.	53
6	Comparison of Flow Visualization Airfoil Variations	56
7	Comparison of Flow Visualization Airfoil Variations — ¼-Chord Cutback Leading Edge	56
8	Test Program Summary	66
9	Phase I Plane Cascade — Inlet Boundary Layer Data Summary	69
10	Phase I Data Summary (Based on Average Inlet Conditions)	100
11	Meanline Conditions for the Selected Single-Stage, Low-Pressure Turbine Design	105
12	Inlet Swirl Vane Design Parameters	111
13	Comparison of Design and Inspected Phase II EGV Airfoil Metal Angles	128
14	Test Program Summary	139
15	Phase II Data Summary	141
16	Comparison of Predicted and Measured Performance at Design Conditions (M_2 = 0.695)	149
17	Comparison of EGV No. 1 and No. 1-1 Performance	156
18	Comparison of EGV Nos. 2, 2-1 and 2-2 Performance	159
19	Comparison of EGV Nos. 1-1 and 2-2 Performance	160
20	Exit Guide Vane Configurations	167
21	Exit Guide Vane Performance Summary	167
22	Summary of Measured Performance of EGV Configurations	168
23	Series Airfoil Evaluation	169

LIST OF TABLES (Continued)

Table		*Page*
24	65 Series/Circular Arc Meanline Performance Comparison at Minimum Loss and Mid-Range	173
25	Comparison of Selected Series Airfoil and Non-series Airfoil	174
26	Predicted and Measured Suction Surface Diffusion ¼ Root Section	188
27	Design Point Performance Summary	189
28	High and Low Aspect Ratio Airfoil Geometry	207
29	High and Low Aspect Ratio Aerodynamic Design	207
30	Suction Surface Static Pressure Rise	208
31	Incidence Sensitivity Study Minimum Leading Edge P_s/P_t	215
A-1	30 Degrees Turning Cascade Section Design	238
A-2	40 Degrees Turning Cascade Section Design	239
A-3	50 Degrees Turning Cascade Section Design	240
A-4	40 Degrees EGV Plane Cascade Design, Root Section	241
B-1	Flow Visualization Tests	243
D-1	Non-series EGV Root Section Design	280
D-2	Non-series EGV ¼ Root Section Design	282
D-3	Non-series EGV Mean Section Design	284
D-4	Non-series EGV ¼ Tip Section Design	286
D-5	Non-series EGV Tip Section Design	288
E-1	Phase II Annular Segment Rig Instrumentation List	292
F-1	EGV Cascade Airfoil 65 Circular-Arc Series Root Section Design	295
F-2	EGV Cascade Airfoil 65 Circular-Arc Series ¼ Root Section Design	297
F-3	EGV Cascade Airfoil 65 Circular-Arc Series Mean Section Design	299
F-4	EGV Cascade Airfoil 65 Circular-Arc Series ¼ Tip Section Design	301
F-5	EGV Cascade Airfoil 65 Circular-Arc Series Tip Section Design	303

LIST OF TABLES (Continued)

Table		*Page*
G-1	Low Aspect Ratio EGV Design, Root Section	305
G-2	Low Aspect Ratio EGV Design, ¼ Root Section	307
G-3	Low Aspect Ratio EGV Design, Mean Section	309
G-4	Low Aspect Ratio EGV Design, ¼ Tip Section	310
G-5	Low Aspect Ratio EGV Design, Tip Section	312

INTRODUCTION

Industry design trends call for increasing turbine stage loading. Studies of advanced highly loaded turbines indicate that aerodynamic performance generally increases with increasing blade reaction levels. The relatively high reaction levels, together with the elevated stage pressure ratios of these advanced turbines, raise exit Mach numbers and tangential swirls above state-of-the-art levels. In downstream turbines, e.g., fan drive turbine stages, these high exit Mach numbers and swirls require improved exit guide vanes (EGV's) to provide compatible flow conditions with engine exhaust systems and/or augmentors. Anticipated inlet conditions for advanced EGV's are Mach numbers in the 0.5 to 0.85 range and swirl angles in the 30- to 50-deg range. The EGV's must turn the flow to the axial direction and diffuse it to a Mach number of approximately 0.4. Recognizing these requirements, the Air Force Aero Propulsion Laboratory has sponsored a technology development program for turbine EGV's.

The program, reported herein, was designed with the objective of developing and demonstrating design techniques for optimizing airfoil and endwall geometries of highly loaded turbine EGV's. The program consisted of four phases and covered a 40-month period.

Phase I of the EGV program was an analytical and experimental investigation conducted to: (1) extend the design and development work previously published for diffusing airfoil cascades (compressor type airfoils) into the Mach number and gas turning ranges applicable to the design of highly loaded turbine EGV's and (2) develop the experimental data for an EGV design system.

The Phase I analytical investigations included the application of computer graphics design techniques to design highly loaded EGV's, and airfoil performance evaluation using predicted pressure distributions and suction surface boundary layer analysis. The experimental investigations were conducted with two-dimensional cascades in the Pratt & Whitney Aircraft Government Products Division high Mach number plane cascade test facility and its low Mach number flow visualization wind tunnel. The flow visualization wind tunnel was used for rapid screening tests of airfoil and endwall models intended to reduce secondary losses by improving the endwall flow field. Promising airfoil and endwall models were subsequently tested in the plane cascade test facility.

Phase II of the EGV program was an experimental and analytical investigation conducted to: (1) evaluate and improve the accuracy of the Phase I design system, and (2) evaluate, in a three-dimensional flow environment, the effects of spanwise variations in Mach number, gas turning and gap/chord ratio. The Phase II experimental investigations were conducted in an annular cascade test facility designed to provide EGV inlet Mach number and swirl distributions which are typical of an advanced engine application.

In this phase, two EGV annular cascades were tested. The first airfoil was a non-series high aspect ratio design which did not have any airfoil or endwall modifications included in the design to reduce secondary losses. The second airfoil was exactly the same as the first except for endwall and airfoil modifications intended to reduce secondary losses. These modifications included (at or near the endwall): cutback leading edge, uncambered trailing edge and pressure side protrusions.

Phase III of the program originally was scheduled to be a full-size rotating rig test to demonstrate the EGV program Phase I and Phase II design technology advancements. However, the Phase II test results raised some question as to which airfoil and endwall modifications (designed to reduce secondary losses) were beneficial. Therefore, three supplementary annular cascade tests were conducted in Phase III to evaluate the individual performance benefits of the cutback leading edge, uncambered trailing edge, and endwall protrusions. In addition, a fourth

annular cascade test was conducted during this phase to define the baseline performance level of a state-of-the-art series airfoil. Performance improvements obtainable with the EGV Program advanced technology non-series airfoils were identified by comparing the series and non-series airfoil test results.

Phase IV of the EGV program was a critique which included: (1) a review of the Phase I non-series EGV design system, (2) a design study of the advantages and disadvantages of low and high aspect ratio EGV's, (3) a design study comparing the incidence sensitivity of series and non-series EGV's, and (4) the definition of state-of-the-art technology advancements made as a result of the EGV program.

SECTION I
PHASE I — FLOW VISUALIZATION AND PLANE CASCADE STUDIES

Phase I of the Exit Guide Vane (EGV) program was an analytical and experimental investigation conducted to: (1) extend the design and development work previously published for diffusing airfoil cascades (compressor type airfoils) into the Mach number and gas turning ranges applicable to the design of highly loaded turbine EGV's, and (2) develop the experimental data for an EGV design system.

The Phase I analytical investigations included the application of computer graphics design techniques to design highly loaded EGV's, and airfoil performance evaluation using predicted pressure distributions and suction surface boundary layer analysis. The experimental investigations were conducted with two-dimensional cascades in the P&WA (Government Products Division), high Mach number, plane cascade test facility and, low Mach number, flow visualization wind tunnel. The flow visualization wind tunnel was used for rapid screening tests of airfoil and endwall models intended to reduce secondary losses by improving the endwall flow field. Promising airfoil and endwall models were subsequently tested in the plane cascade test facility.

A. AIRFOIL AND ENDWALL ANALYSIS AND DESIGN

1. Design Point Selection

The normal procedure for designing turbine exit guide vanes (EGV's) is to use NASA series airfoils. Selection of series airfoils simplifies the design process because it makes use of extensive compressor cascade data. Also thick airfoils are usually selected to accommodate oil tubes and aft bearing supports. Unfortunately, thick airfoils cause high losses due to relatively low critical Mach numbers and airfoil choking, and series airfoils do not permit the geometric tailoring desired to reduce the severe endwall losses encountered with EGV designs. Therefore, it was decided that the test airfoils for this program would be selected to yield promising pressure distributions that avoid boundary layer separation, and that no mechanical restrictions would be placed on airfoil thickness.

During Phase I, three non-series EGV airfoils with turnings of 30, 40, and 50 deg were designed, fabricated, and tested. Table 1 presents a comparison of design parameters for these airfoils. The 30-deg airfoil was representative of current turbine EGV designs in that it was designed for an inlet Mach number of 0.500. For the maximum turning airfoil (50 deg), contractual requirements set the inlet Mach number of 0.85, with diffusion to an exit Mach number of 0.40. For the 40-deg cascade design, an inlet Mach number of 0.675 (midway between the 30- and 50-deg design values) was selected. Note in Table 1 that the aerodynamic loading levels, $\Delta P_s/(P_{T_2} - P_{s_2})$, for the 40- and 50-deg airfoil designs represent a considerable increase over current loading levels typified by the 30-deg airfoil loading level.

TABLE 1
AIRFOIL DESIGN PARAMETERS

EGV Airfoil, deg	30	40	50
Inlet Air Angle, β_2, deg	60	50	40
Exit Air Angle, β_3, deg	90	90	90
Inlet Mach Number, M_2	0.5	0.675	0.85
Exit Mach Number, M_3	0.39	0.38	0.38
Pressure Rise Coefficient, $\Delta P_s/(P_{T_2}-P_{s_2})$	0.365	0.650	0.750
Exit-to-Inlet Channel Height Ratio, H_3/H_2	1.05	1.15	1.05
Suction Side Loading, $\Delta P_s/Q_{max}$	0.569	0.810	0.909
Gap-to-Chord Ratio, τ/b	0.77	0.39	0.38
Thickness Ratio, t/b	0.072	0.073	0.071

2. Selection of Model Scale

The airfoil scale was based on selected test facility capabilities and aspect ratios of interest for engine EGV's. The selected plane cascade test facility had a 3.0 in. wide approach passage. To maintain a Mach number of 0.4 or less in this passage, and thus avoid excessive duct pressure losses and distortion, a vane leading edge span of 1.9 in. was selected for the EGV airfoils. (See Figure 1.) With this span height, the inlet Mach number to the test airfoils was about 0.9 when the approach duct Mach number was 0.4. The vane chord was set at 1.9 in. This selection was based on a review of EGV geometries for operational engines which indicated that an EGV aspect ratio of 1.0 was typical. Figure 2 presents Reynolds number as a function of facility total temperature at a minimum inlet Mach number of 0.5 for the selected chord dimension. The facility was run with an inlet total temperature of 160°F, so the minimum vane Reynolds number was approximately 500,000; hence, the flow was turbulent over the airfoils in all tests.

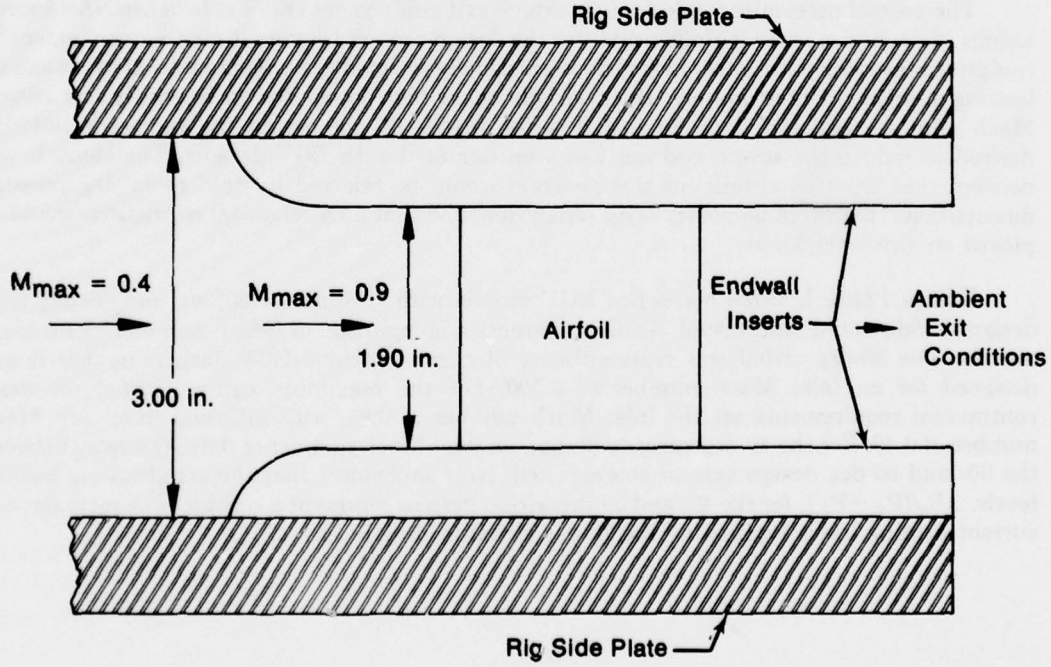


Figure 1. Exit Guide Vane Cascade Schematic

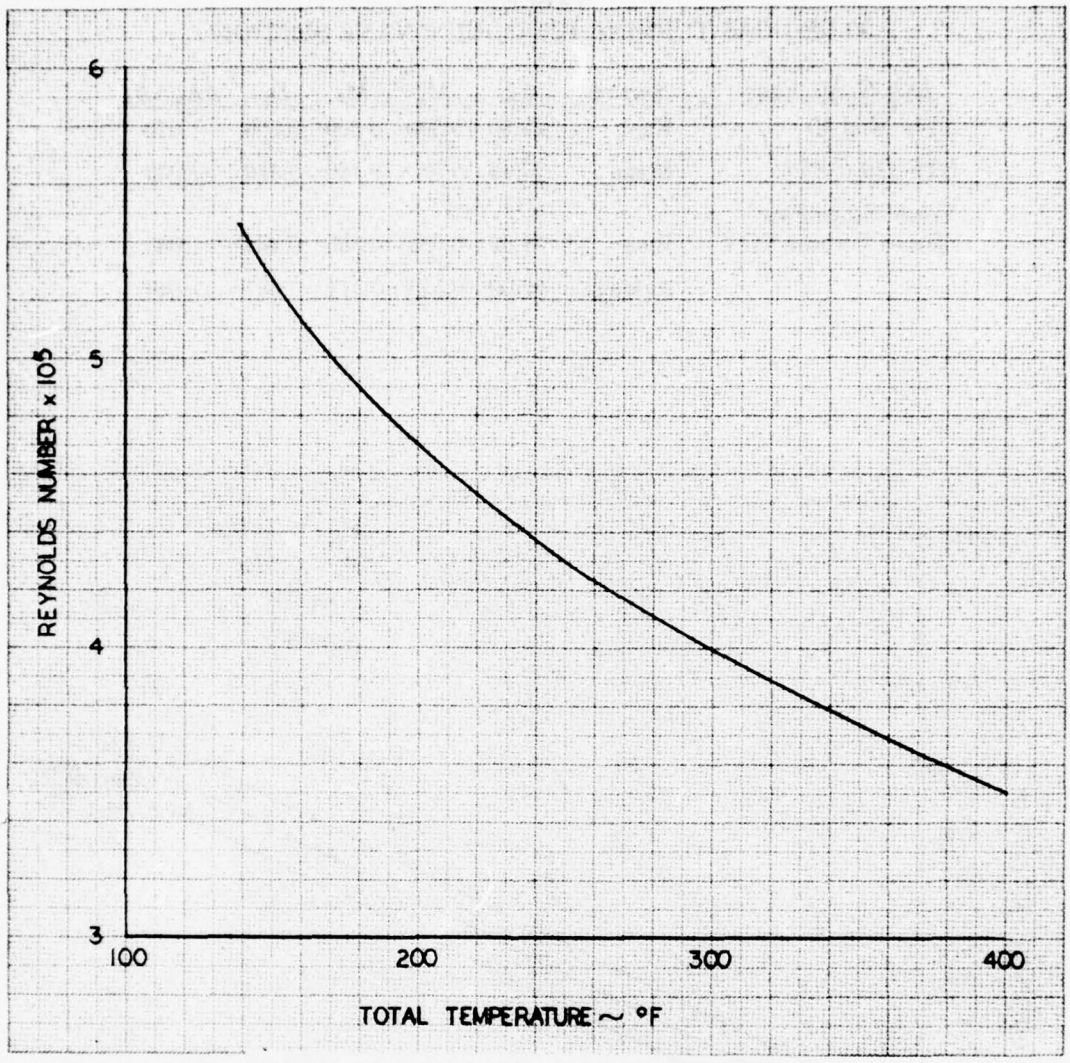


Figure 2. Minimum Cascade Reynolds Number

3. 30-Degree Cascade Airfoil Design

A survey of exiting EGV's was made, and significant design parameters were tabulated for airfoil sections having close to 30-deg gas turning. (Table 2 presents a summary of this survey.) Based on these results, the following design requirements were selected for the 30-deg cascade: $M_2 = 0.5$, $M_3 = 0.4$, $H_3/H_2 = 1.05$, and $0.3 < D_F < 0.4$. Gap/chord ratio selection was based on not exceeding the state-of-the-art D_F range for 30-deg gas turning. A diffusion factor map, based on the selected design parameters, is presented in Figure 3. A gap/chord of 0.8 was selected to satisfy state-of-the-art loading level requirements.

TABLE 2
30-DEG GAS TURNING EXIT GUIDE VANE SECTIONS

Exit Guide Vane	*Section*	θ_{Gas}	M_2	M_3	D_F	AA_3/AA_2
JT11 Mod 10	Root	27.90	0.500	0.390	0.390	1.070
STF 219 (SST)	Mean	27.40	0.520	0.480	0.310	1.030
Single-Stage Fan Drive Turbine EGV	Root	31.99	0.564	0.365	0.462	1.038
	Average	29.09	0.528	0.411	0.387	1.046

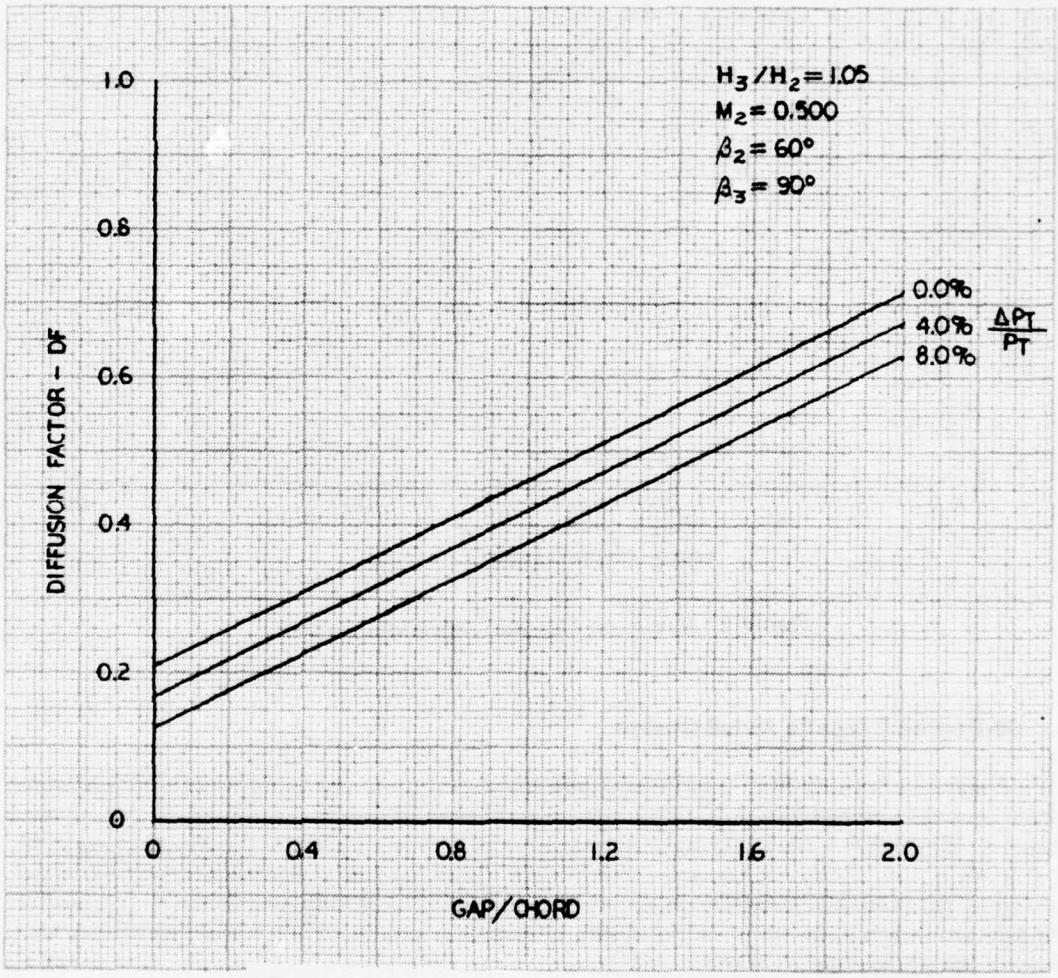


Figure 3. Diffusion Factor for 30-deg Cascade

It has been customary to design thick EGV (t/b = 15%) to accommodate structural and/or service lines. This requirement reduces airfoil choke margin and increases suction surface diffusion. It was decided that aerodynamic performance should not be compromised to maintain traditional thickness. Therefore, the selected thickness/chord ratio of 7.5% was approximately one-half of the current EGV design practice and in the airfoil thickness range used in high-performance compressor airfoils.

The relative merit of using non-series EGV designs for Phase I was evaluated by comparing these designs to state-of-the-art series airfoils on the basis of calculated separation tendencies. Suction surface pressure distributions and friction coefficient (C*f* distributions from boundary layer analyses) were calculated for each potential design. Separation was assumed to occur at the point where C*f* equalled zero. The criterion for improvement was a marked reduction of separation potential over series airfoils with the same design parameters. The series airfoils selected for comparison in the 30-deg EGV design included a 400 series, circular arc, 65 series with a circular arc mean line, and modified 65 series. Figure 4 presents cross sections for each of the selected series airfoils. Calculated suction surface pressure distributions for these airfoils are shown in Figure 5. It can be seen that the rate of diffusion on the suction surface is highest for the 400 series airfoil and lowest for the circular arc design. These two designs were then selected as representative state-of-the-art configurations for boundary layer analysis. It was expected that the 400 series design would be more likely to separate than the circular arc configuration. Figure 6 confirms this conclusion in that the skin friction coefficient on the 400-series airfoil indicates separation at a surface distance of about 0.67 inches. Boundary layer separation is not predicted for the circular arc airfoil, but C*f* does drop to 0.0006 before transition to turbulent flow occurs.

With these series airfoils as baselines, non-series configurations were developed that had the same design parameters, but with reduced suction surface diffusion and no indication of potential separation. This design task was accomplished with a version of the turbine graphics design system that had been modified to accommodate diffusing cascades.

At least 30 different non-series EGV configurations were generated in an effort to select an airfoil with a higher performance potential than the state-of-the-art airfoils. Figure 7 shows three of the most promising non-series designs. Figure 8 presents pressure distributions for these non-series designs, superimposed on those for state-of-the-art airfoils. Design 1 offers improved aerodynamic performance relative to the 400 series; however, when compared to the other series designs, it is not so promising. Designs 2 and 3 represent efforts to further refine the non-series airfoil configurations. For both designs, the minimum pressure levels were raised by shifting the maximum thickness point further downstream.

Boundary layer analyses of the three non-series designs were conducted to evaluate any tendency to separate. (See Figure 9.) The three non-series designs had better boundary layer characteristics (higher average C*f*) than either the 400 series or circular arc airfoils and, hence, were less likely to separate. Design No. 2 was selected as the final airfoil configuration for the 30-deg EGV because it generally had the highest level of C*f* over the entire suction surface. Figure 10 presents the selected 30-deg airfoil cross section and design parameters. Table 1 compares important design parameters of the 30-deg airfoil to those for the 40- and 50-deg airfoils. The 30-deg airfoil coordinates are presented in Appendix A.

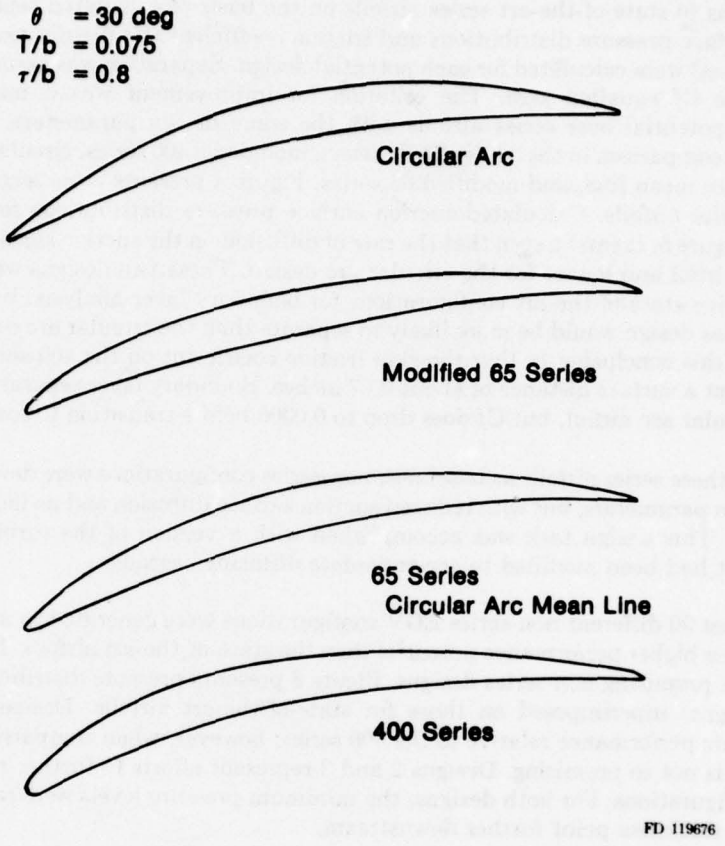


Figure 4. State-of-the-Art Airfoils considered for 30-deg Cascade

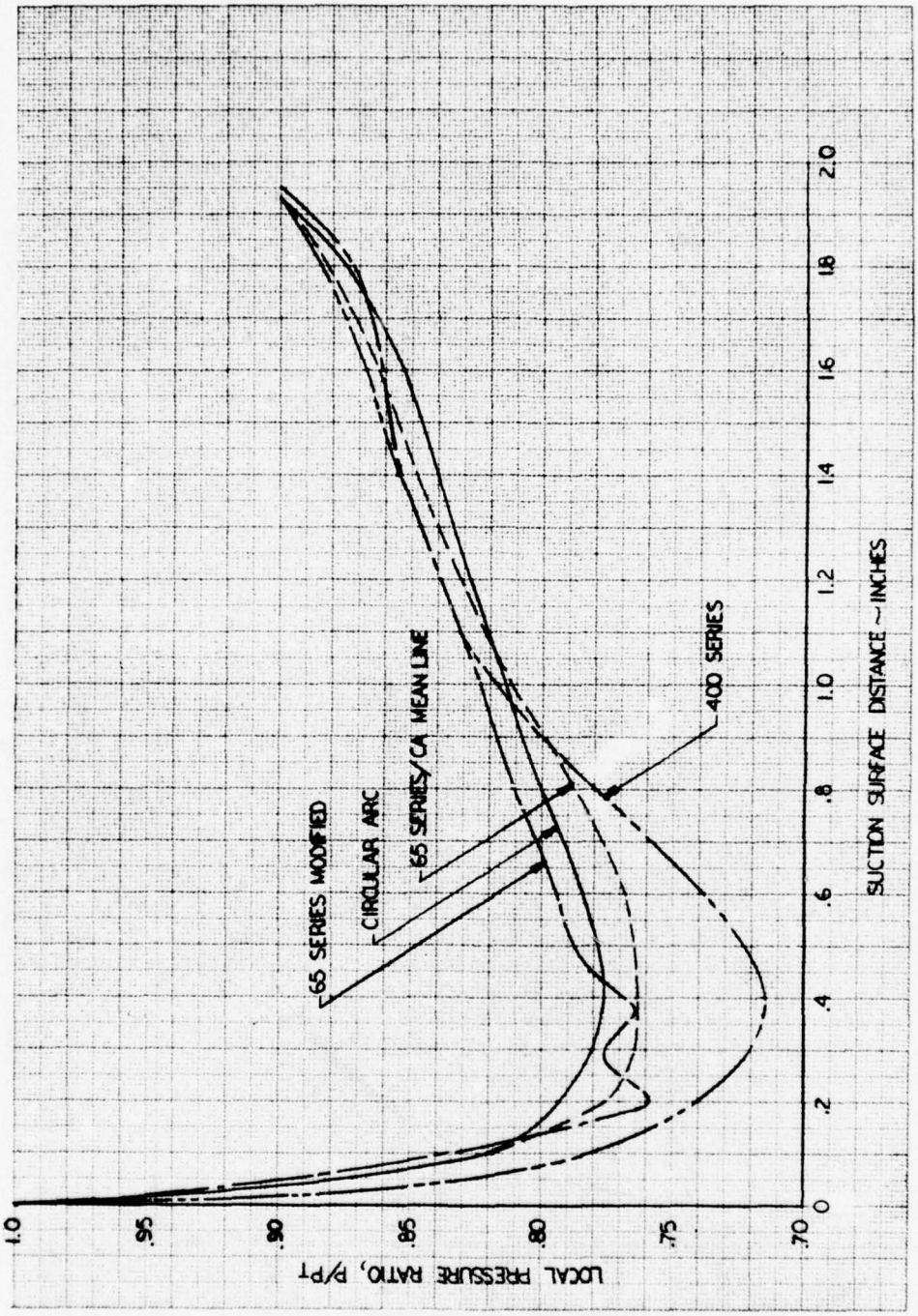


Figure 5. Comparison of 30-deg Cascade Series Airfoil Suction Surface Pressure Distributions

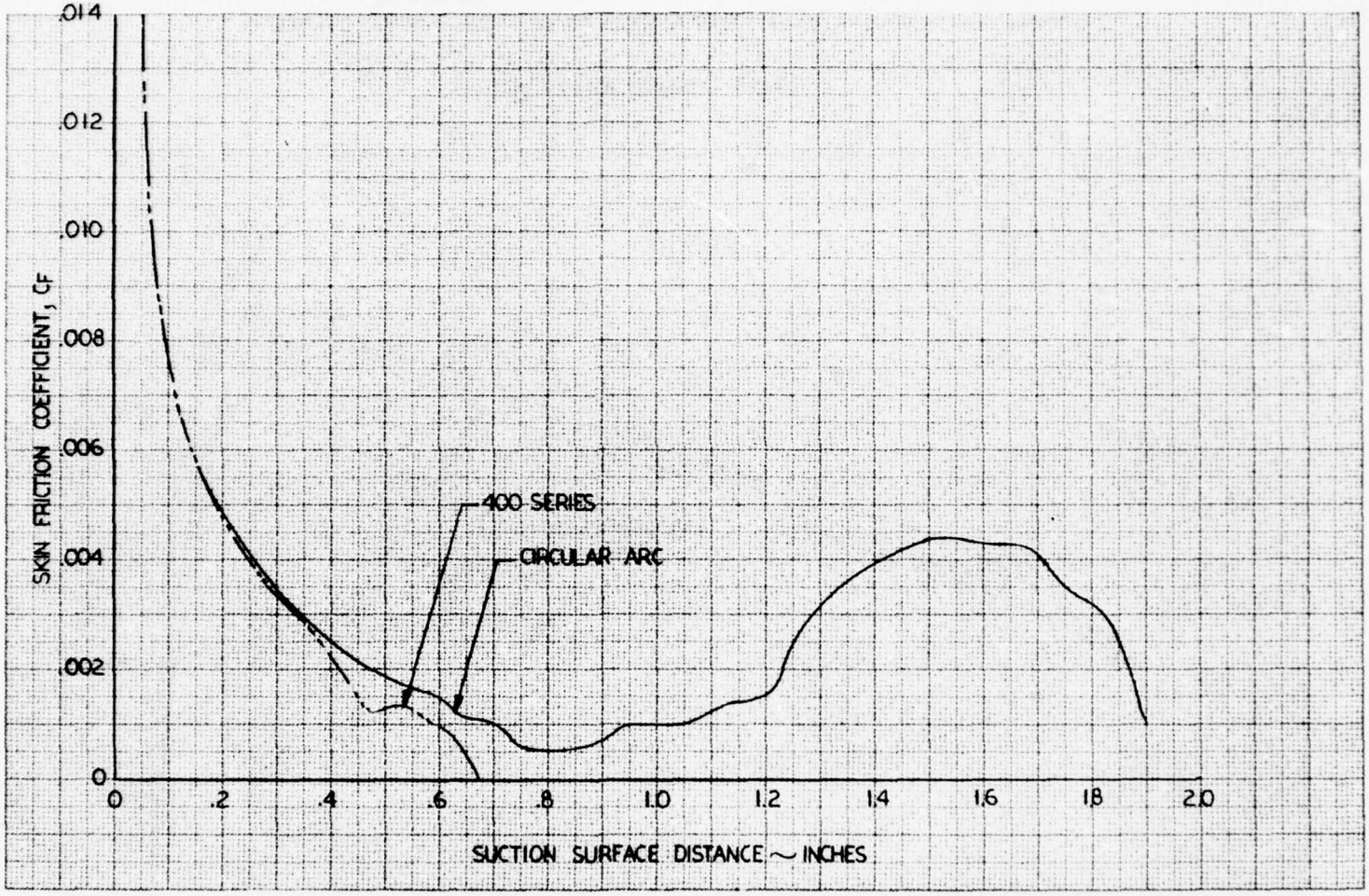


Figure 6. Comparison of 30-deg Cascade, 400 Series, and Circular Arc Series Airfoil Suction Surface Skin Friction Coefficient

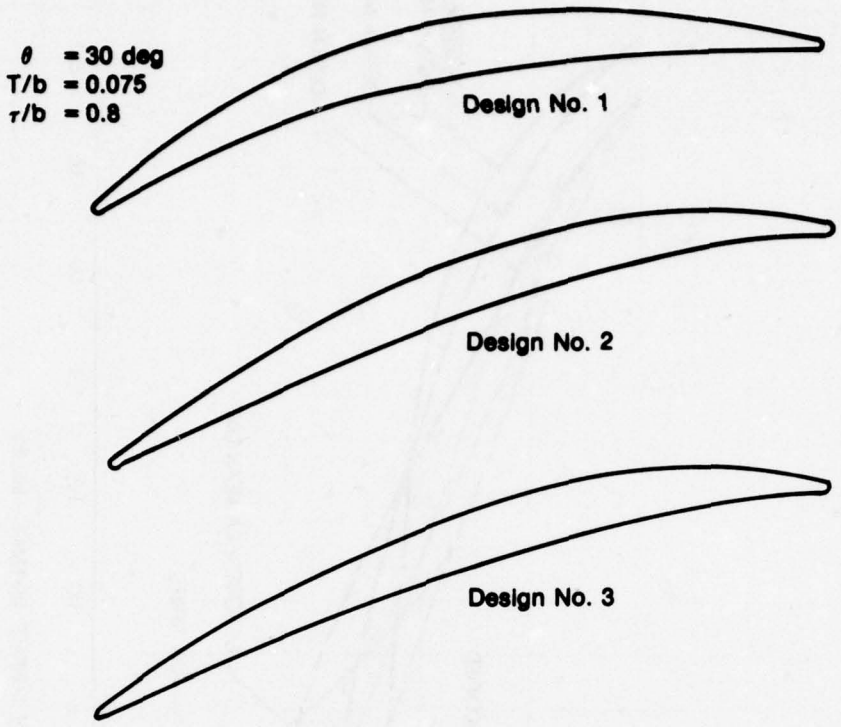


Figure 7. 30-deg EGV Cascade Non-Series Airfoil

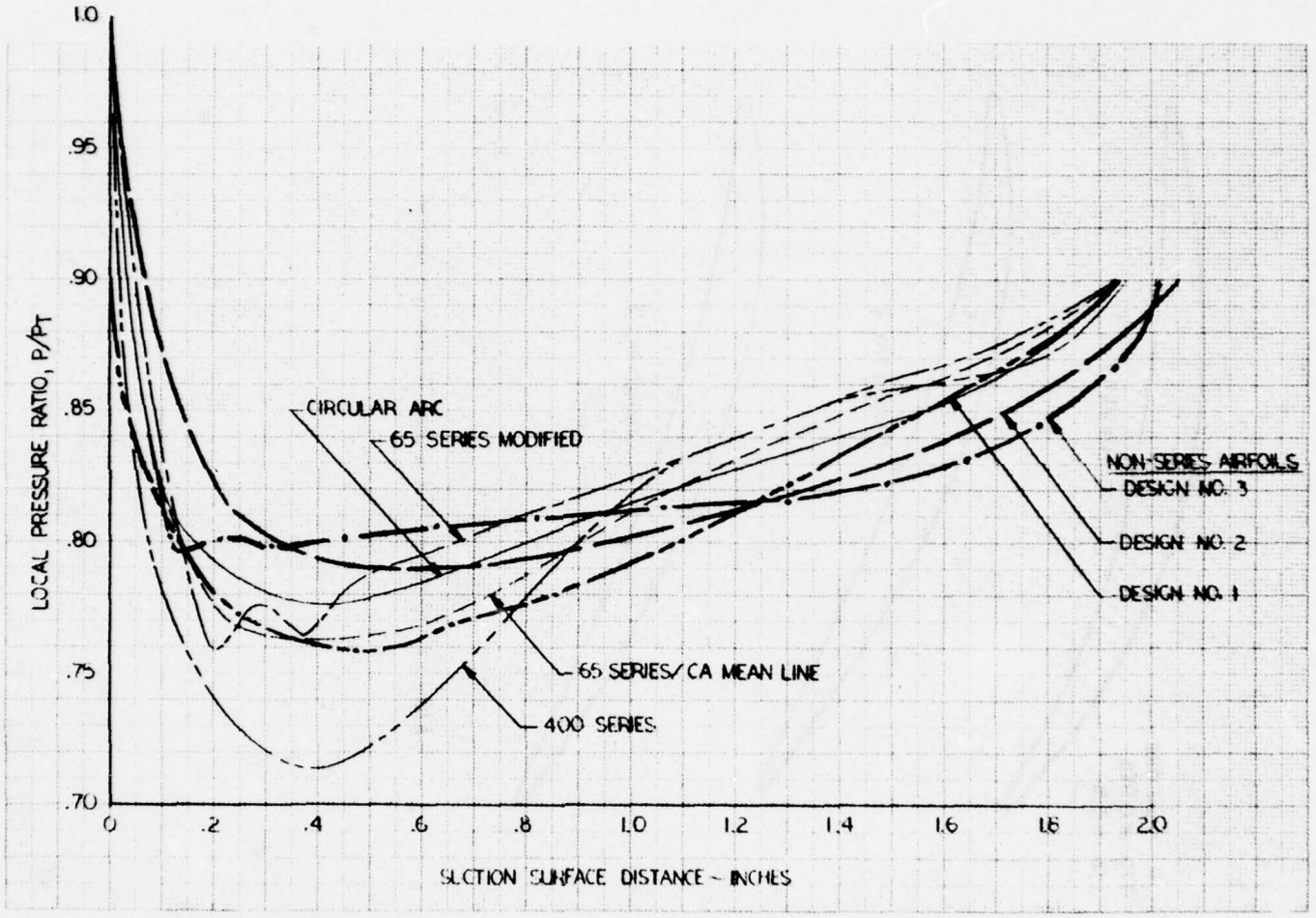


Figure 8. Comparison of 30-deg Cascade Series and Non-Series Airfoil Suction Surface Pressure Distributions

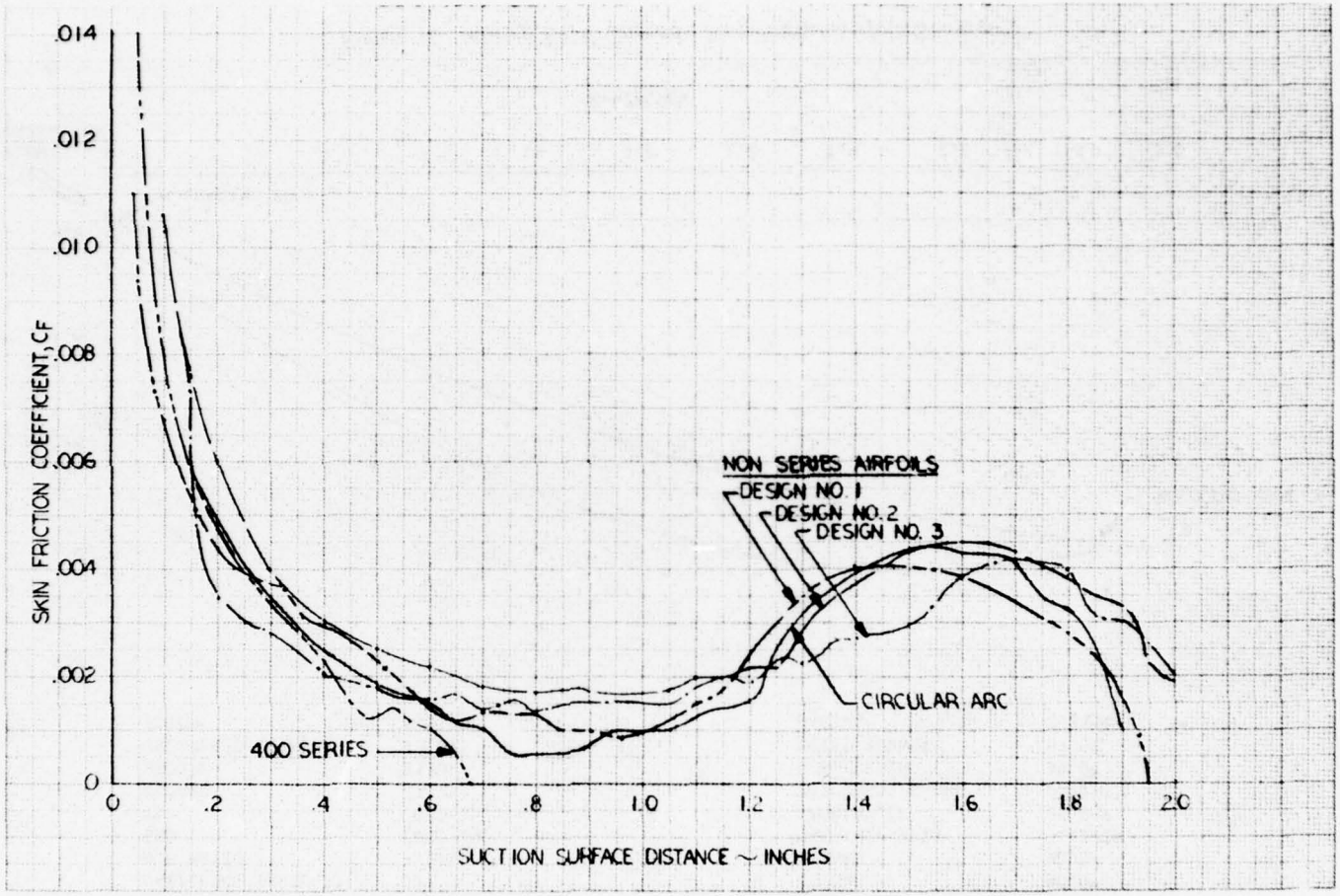


Figure 9. Comparison of 30-deg Cascade and Non-Series Airfoil Suction Surface Skin Friction Coefficients

AXIAL CHORD	1.87 IN.	DBETA2	10.0°
ACTUAL CHORD	1.97 IN.	DBETA3	16.0°
GAP/CHORD (ACTUAL)	.77	BETA2G	60.0°
H/L RATIO	-.325	BETA3G	90.0°
LED	.025 IN.	MAX THICKNESS	.142 IN.
TED	.020 IN.	GAGE ANGLE	55.69°
BETA2F	57.5°	THICKNESS/CHORD	.072
BETA3F	85.0°	GAS TURNING	30.0°
UNCOVERED TURNING	10.07°	METAL TURNING	37.5°
PITCH	1.5199	GAGING	1.2554

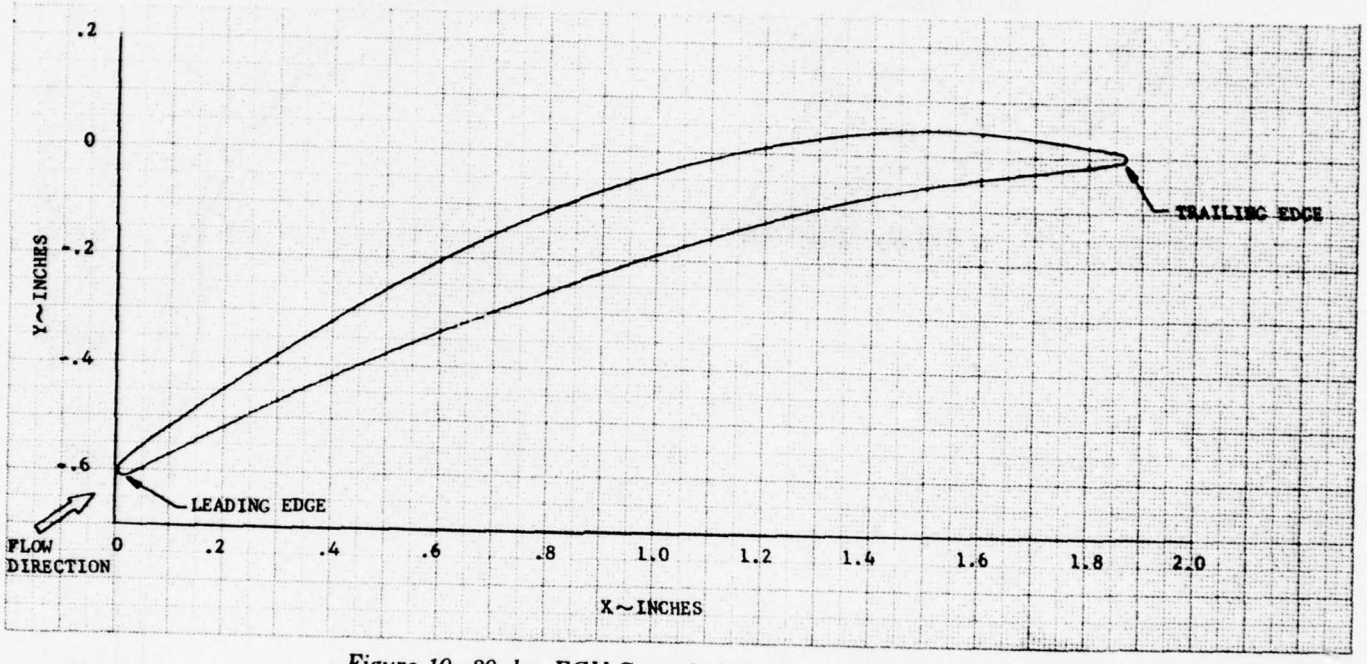


Figure 10. 30-deg EGV Cascade Non-Series Airfoil Geometry

4. 40-Degree Cascade Airfoil Design

Selection of the design axial area ratio for the 40-deg cascade was based on a parametric study to evaluate the effect of axial area ratio and total pressure loss on exit Mach No. The parametric curves are shown in Figure 11. From this study, a design axial area ratio of 1.15 was selected. As the curve shows, this value will permit a total pressure loss up to 5% and still satisfy the design diffusion requirement of an exit Mach number of 0.4. If pressure loss is less than 5%, more diffusion (lower exit Mach number) will be obtained.

The 40-deg airfoil spacing was reduced to a gap-to-chord ratio (τ/b) of 0.39, about one-half the value of the 30-deg EGV; however, even with this close spacing, the cascade was highly loaded (the suction side $\Delta P_s/Q_{max}$ ratio is 0.81). Pressure distributions for the selected non-series design and a state-of-the-art, circular arc airfoil are shown in Figure 12. Results of a boundary layer analysis of the suction surface for both airfoils are presented in Figure 13. It can be seen that the analysis calculated separation (i.e., $Cf = 0.0$) for the circular arc airfoil at a suction surface distance of 0.88 in. Flow on the suction surface of the non-series design transitioned from laminar to turbulent flow and did not separate until very near the trailing edge. Figure 14 shows the selected 40-deg airfoil and pertinent design parameters. Airfoil coordinates are presented in Appendix A.

5. 50-Degree Cascade Airfoil Design

The third and final EGV for the Phase I plane cascade study was designed to have a 50-deg turning capability and diffuse a 0.85 inlet Mach number to an exit Mach number of 0.4. To obtain the required diffusion, a 1.05 design axial area ratio was selected. Figure 15 shows that a 5% pressure loss can be sustained and still satisfy diffusion requirements. The close spacing of the 40-deg EGV was maintained for the 50-deg design (τ/b = 0.38). Pressure distributions for the selected non-series design and a comparable circular arc configuration (representing a state-of-the-art design) are presented in Figure 16. The non-series pressure distribution clearly shows (when compared with the circular arc distribution) how airfoil loading has been shifted back into the covered portion of the channel. This effect has been typical of 30- and 40-deg designs, but is more obvious with the extremely high loading required for the 50-deg EGV. Figure 17 presents the calculated suction surface skin friction coefficient distribution. It can be seen that incipient separation is calculated for the circular arc design at a suction surface distance of only 0.4 in., while separation for the non-series design does not occur until near the trailing edge. Figure 18 presents the selected 50-deg EGV non-series design and pertinent design parameters. Airfoil coordinates are presented in Appendix A.

6. Endwall Designs

Table 3 presents a survey of EGV axial area ratios (AA_3/AA_2) for several modern engines. It can be seen that the area ratios range from 1.03 for the STF 219 to 1.17 for the F401 Redesign II. Based on these results, 1.0, 1.1, and 1.2 axial area ratios were selected for evaluation. The selected ratios covered the range of interest for EGV's, as well as providing a common basis of comparison with data from compressor cascades having no endwall divergence.

Three sets of endwalls, with straight diverging sections from the airfoil leading to trailing edges, were designed for each of the sets of airfoils (i.e., for the 30-, 40-, and 50-deg airfoils). These endwalls and airfoils provide nine diverging endwall cascades to be evaluated.

TABLE 3
SURVEY OF EGV ANNULUS AREA RATIOS

Exit Guide Vane	AA_3/AA_2
F100 EGV Redesign II	1.139
F100 EGV Redesign I	1.116
F100-PW-100	1.122
F401 Redesign II	1.168
F401 Redesign I	1.148
F401-PW-400	1.145
JTF22A-25	1.074
STF 219 (SST Engine)	1.031
JT11D-20 Mod 10	1.068
JT11D-20-J	1.086
WPAFB High Work LPT, EGV	1.147

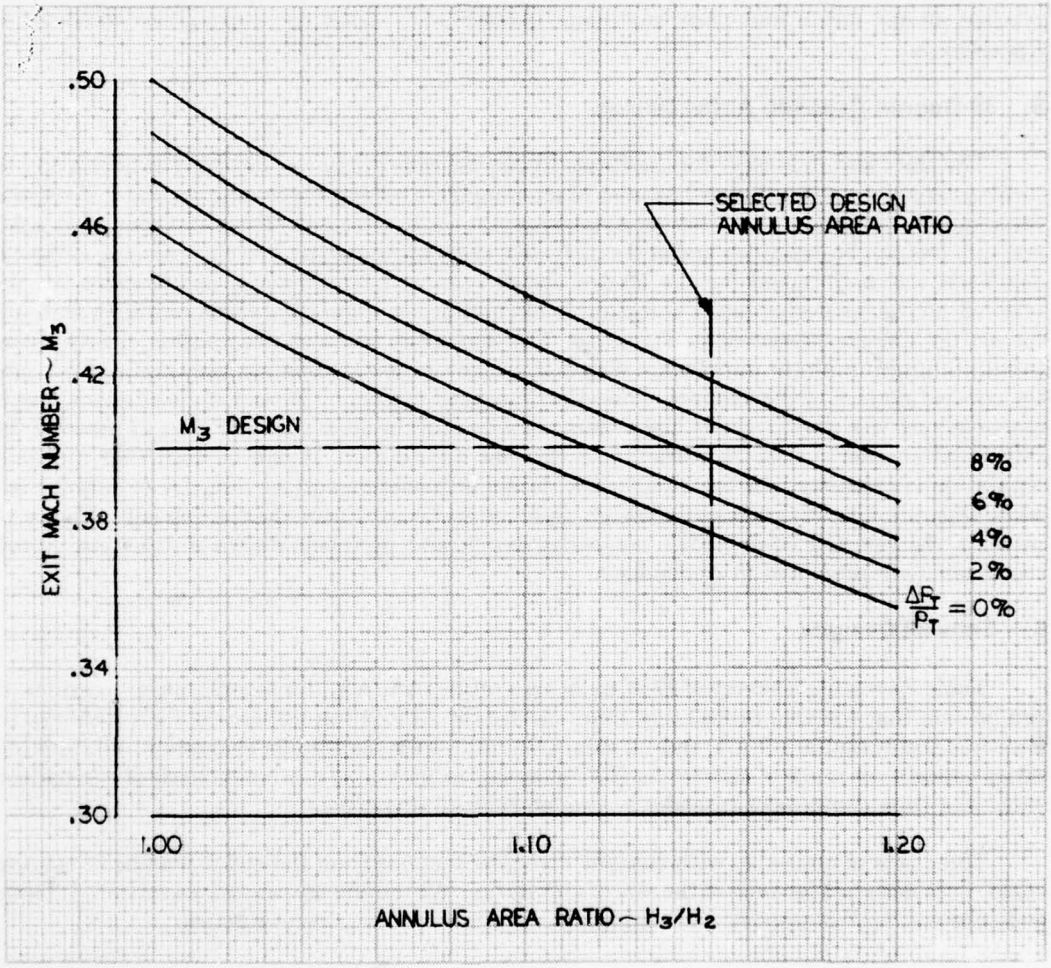


Figure 11. 40-deg Cascade Parametric Data (M_2 = 0.675, 0-deg Exit Swirl)

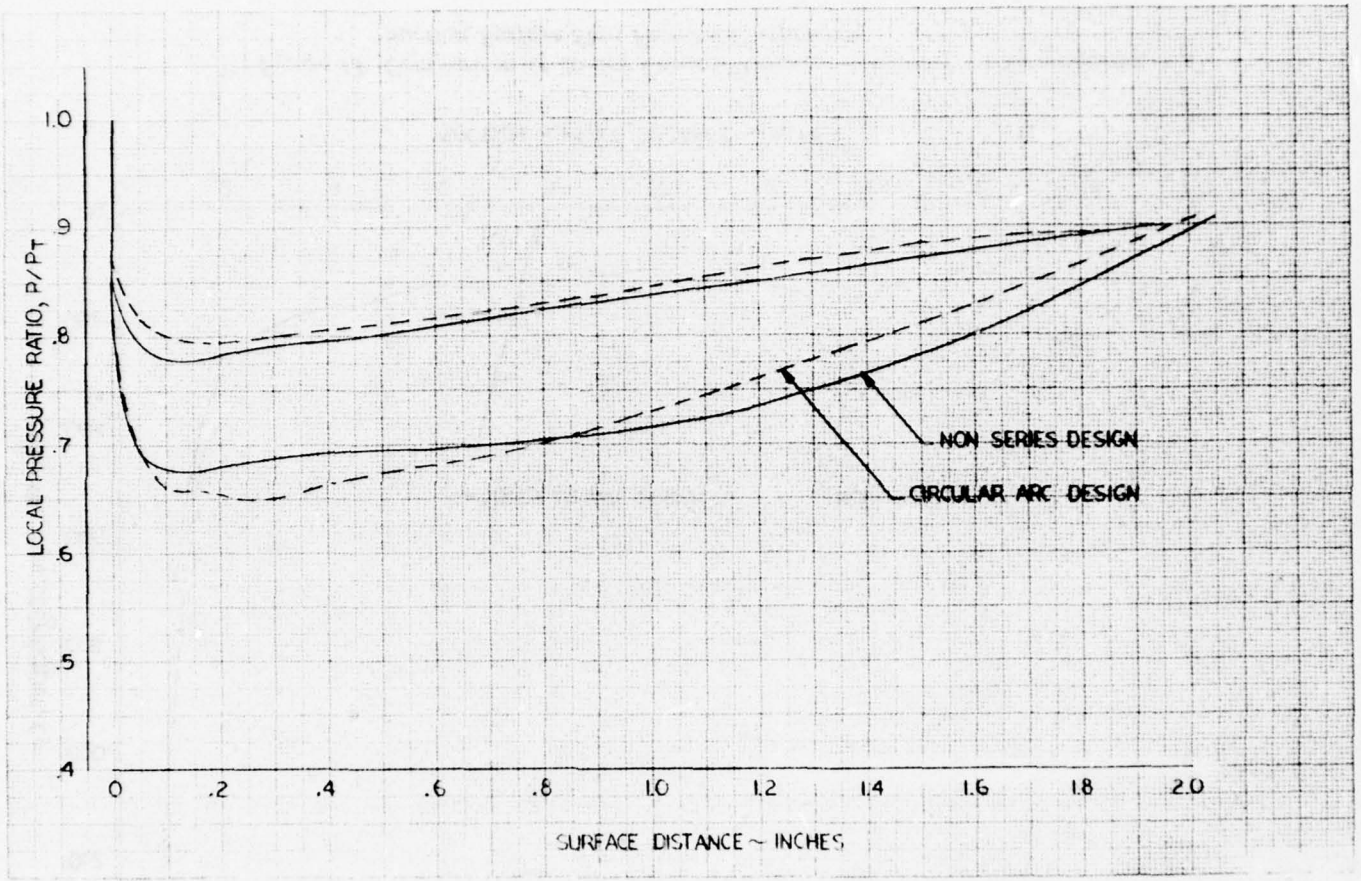


Figure 12. Comparison of 40-deg Cascade Circular Arc and Non-Series Airfoil Pressure Distributions

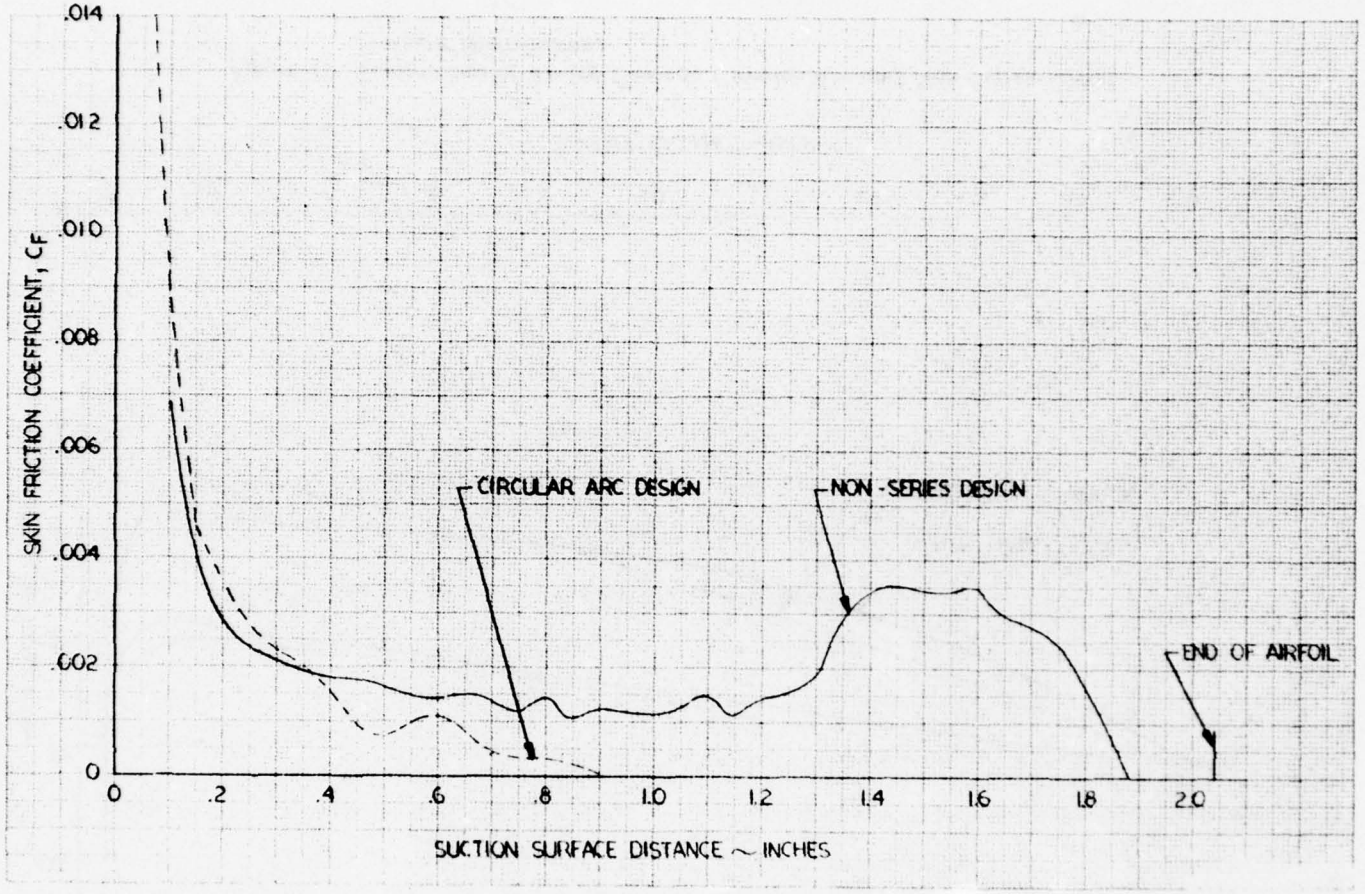


Figure 13. Comparison of 40-deg Cascade Circular Arc and Non-Series Airfoil Suction Surface Skin Friction Coefficients

AXIAL CHORD	1.8447 IN.	DBETA2	7.0°
ACTUAL CHORD	1.940 IN.	DBETA3	18.0°
H/L RATIO	-.325	BETA2G	50.0°
LED	.020 IN.	BETA3G	90.0°
TED	.020 IN.	MAX. THICKNESS	.142 IN.
BETA2F	52.079°	GAGE ANGLE	49.41°
BETA3F	84.0°	THICKNESS/CHORD	.073
UNCOVERED TURNING	6.751°	GAS TURNING	40.0°
PITCH	.760 IN.	METAL TURNING	43.92°
GAP/CHORD (ACTUAL)	.3918	GAGING	.5771 IN.

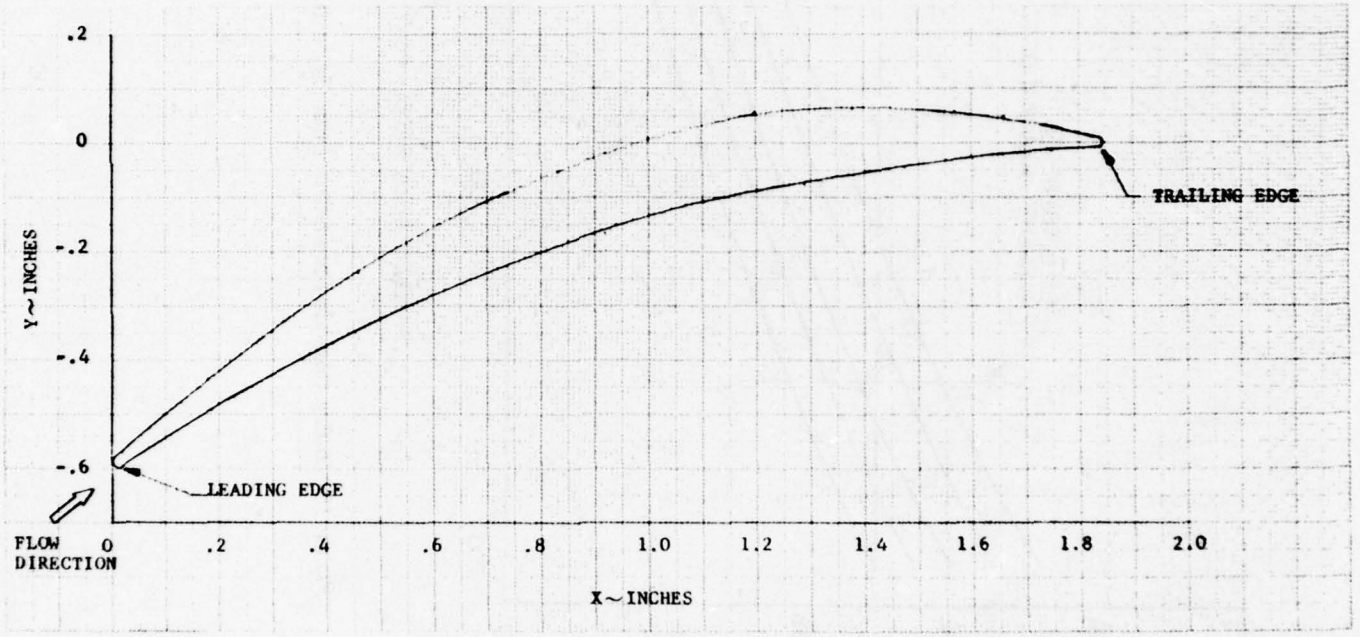


Figure 14. 40-deg EGV Cascade Non-Series Airfoil Geometry

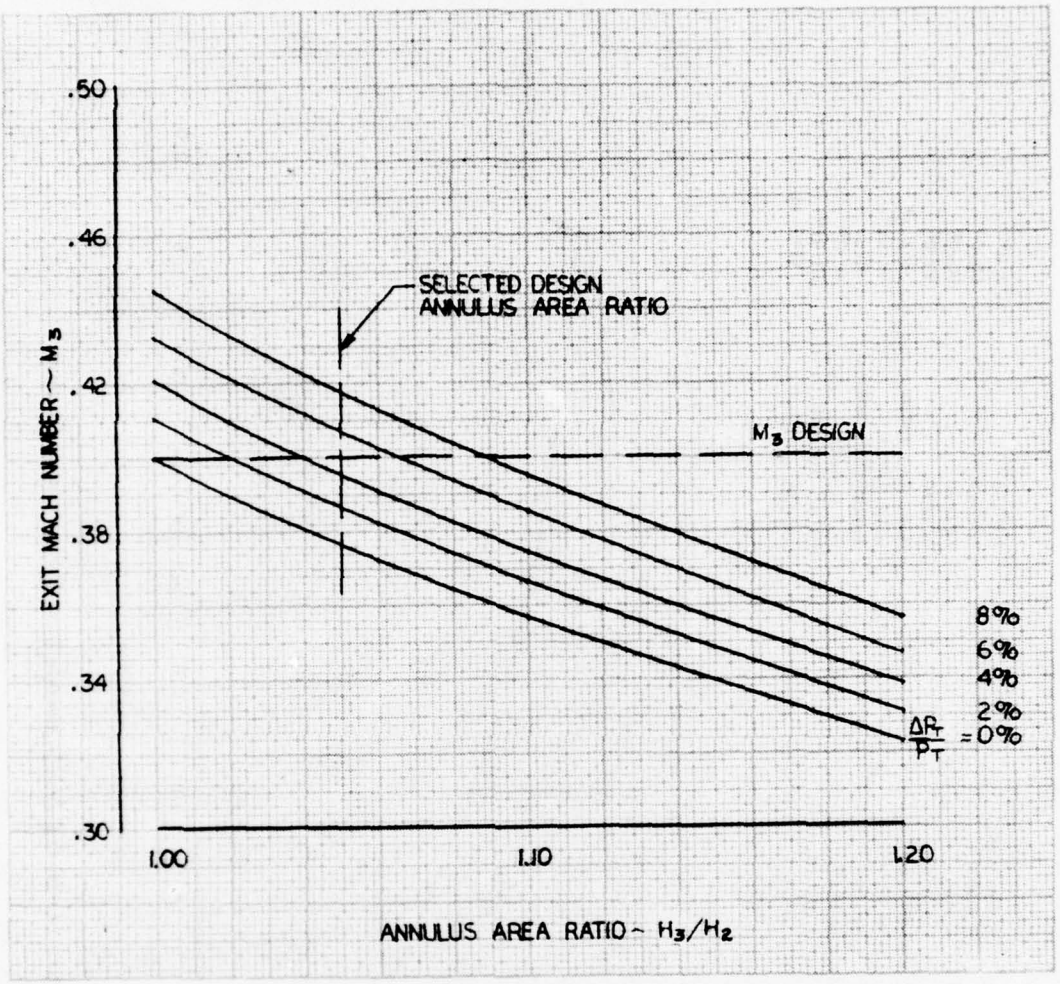


Figure 15. 50-deg Cascade Parametric Data (M_2 = 0.85, 0-deg Exit Swirl)

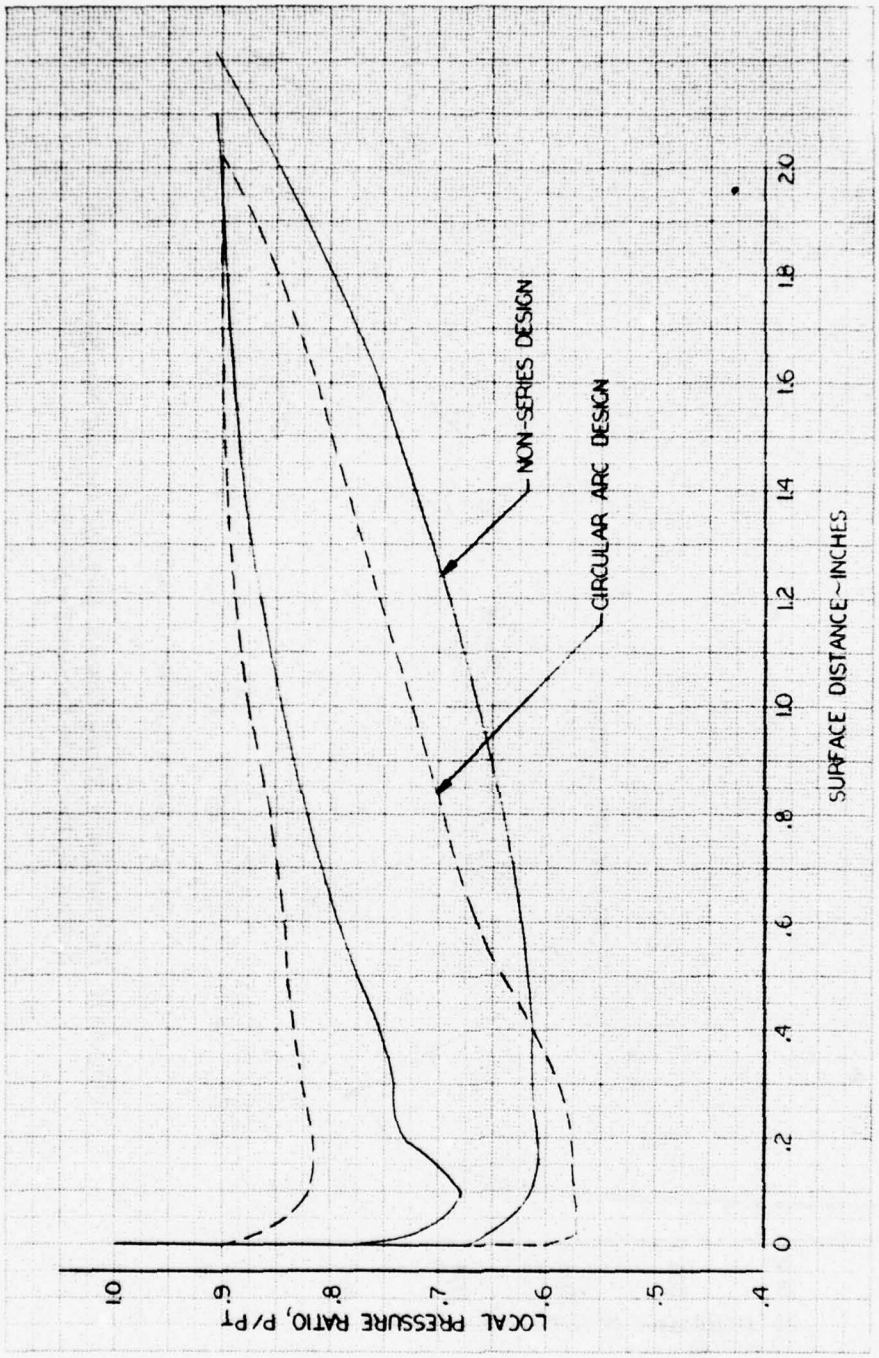


Figure 16. Comparison of 50-deg Cascade Circular Arc and Non-Series Airfoil Pressure Distributions

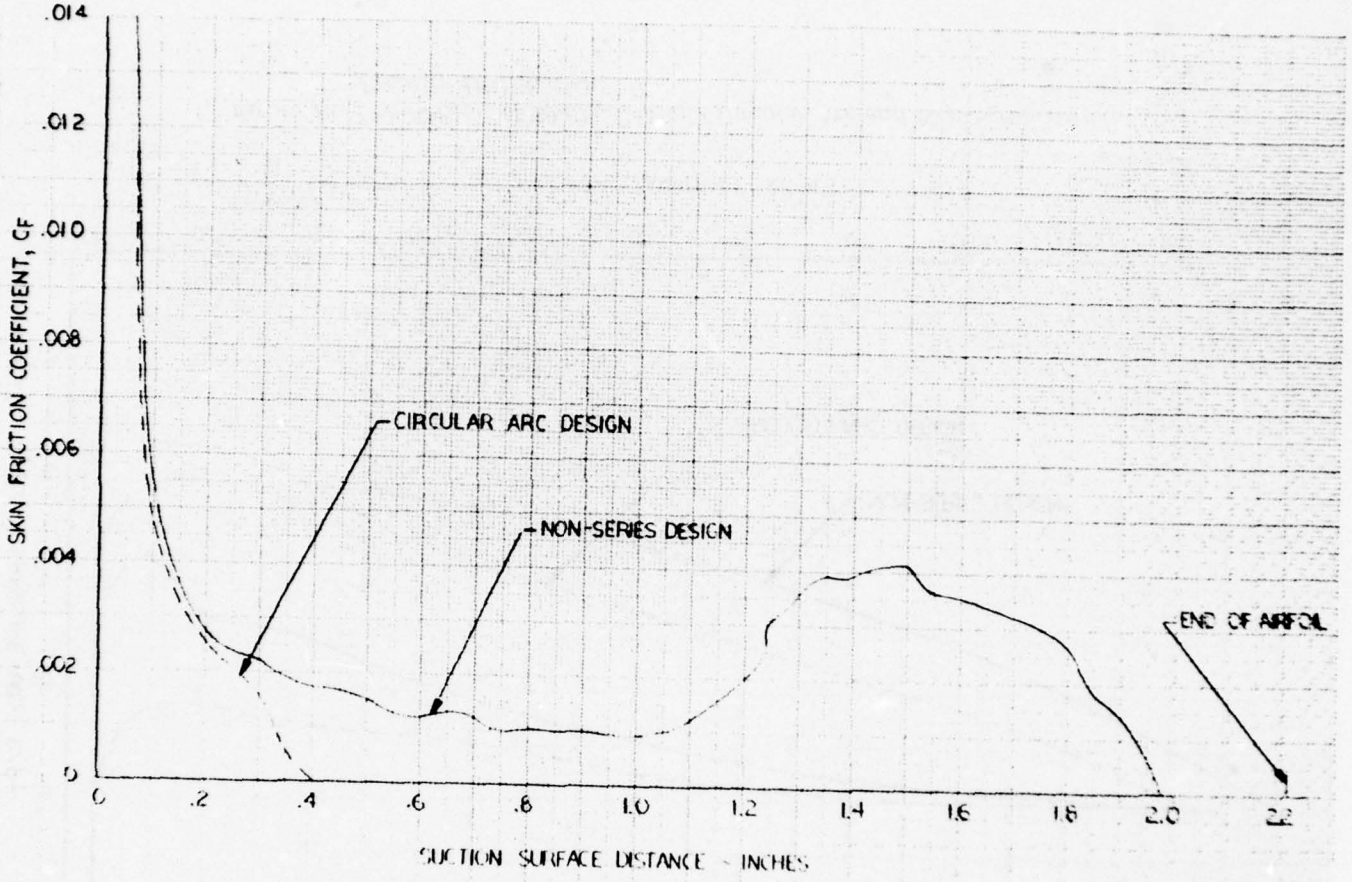


Figure 17. Comparison of 50-deg Cascade Circular Arc and Non-Series Airfoil Suction Surface Skin Friction Coefficients

AXIAL CHORD	1.8694 IN.	DBETA2	6.0°
ACTUAL CHORD	2.05 IN.	DBETA3	19.0°
H/L RATIO	-.450	BETA2G	40.0°
LED	.020 IN.	BETA3G	90.0°
TED	.020 IN.	MAX. THICKNESS	.146 IN.
BETA2F	42.319°	GAGE ANGLE	40.2°
BETA3F	81.80°	THICKNESS/CHORD	.0712
UNCOVERED TURNING	6.912°	GAS TURNING	50.0°
PITCH	.779 IN.	METAL TURNING	55.88°
GAP/CHORD (ACTUAL)	.380	GAGING	.5028 IN.

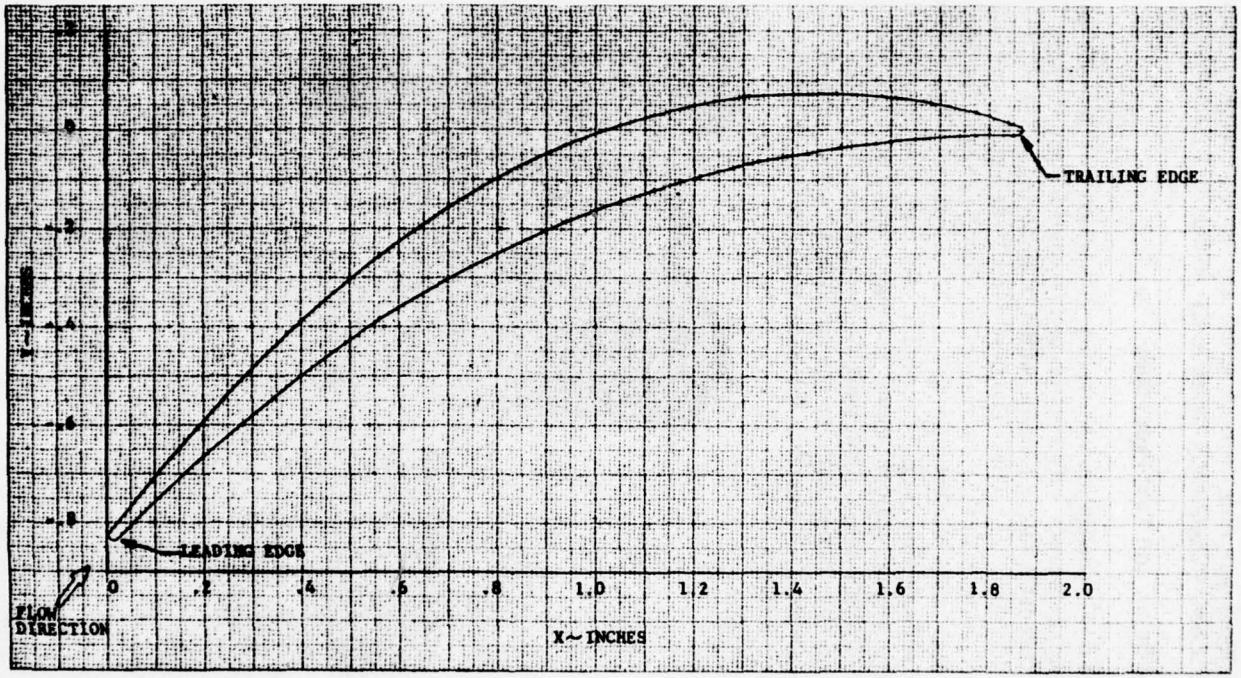


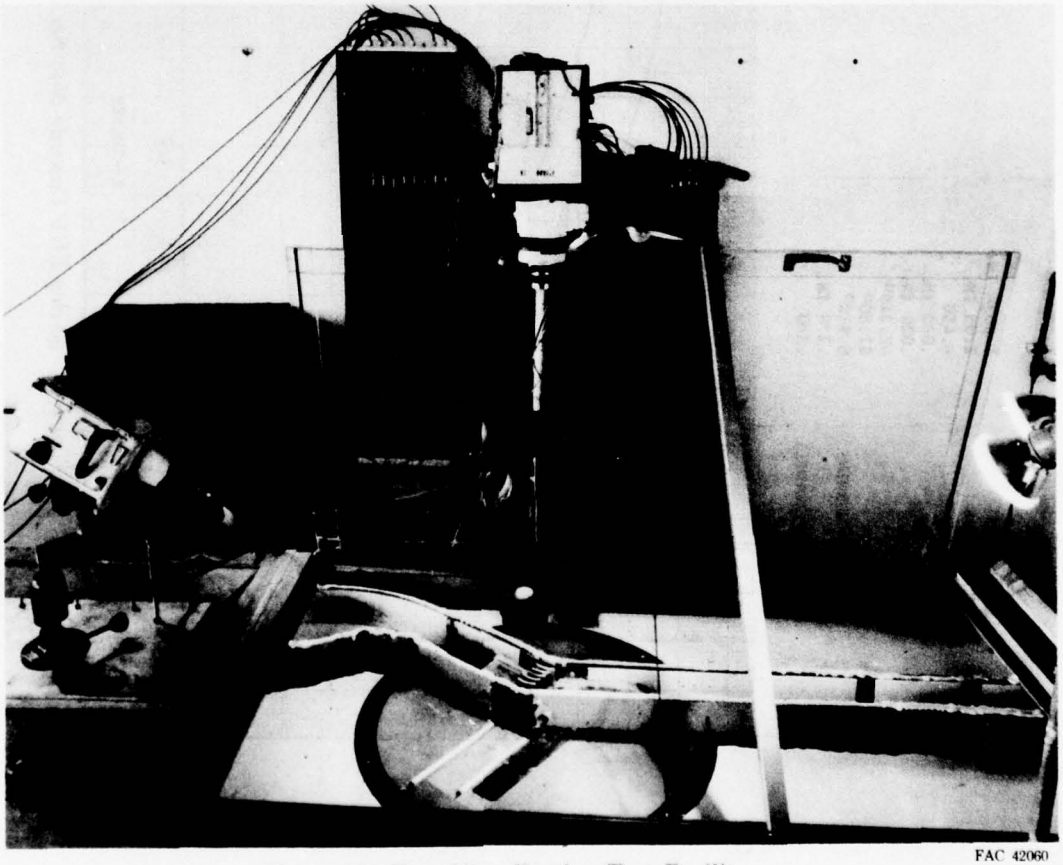
Figure 18. 50-deg EGV Cascade Non-Series Airfoil Geometry

B. FLOW VISUALIZATION STUDY AND TEST SETUP

The objective of the flow visualization study was to determine methods to improve the endwall flow of turbine exit guide vanes. Available analytical tools are inadequate to evaluate geometric variations, which are intended to modify the three-dimensional, viscous flow field in the endwall region. Therefore, a low-speed, two-dimensional, flow visualization wind tunnel was used for rapid screening tests of airfoil and endwall models. Promising airfoil and endwall geometries were subsequently tested in the 40-deg EGV cascade.

1. Test Setup and Test Procedure

The flow visualization test facility, illustrated in Figure 19, draws ambient air through a rectangular bellmouth before entering the cascade test section. The cascade flow exhausts through tailboards into a plenum, which is connected to two 25-hp, constant-speed, axial-flow blowers that operate in series. The flow velocity through the cascade is adjusted by varying the amount of amibent air that is permitted to enter the plenum downstream of the cascade. The top endwall was made of clear plexiglas so the cascade could be observed during operation. The opposite endwall was made of modeling clay from one-chord-length upstream, to one-chord-length downstream of the cascade. The clay endwall could be readily formed into any desired contour. Boundary layer flow patterns were observed by placing dots, which consisted of a mixture of oil and lampblack, on the airfoil and endwall surfaces of interest. The flow patterns were documented by sketches for each configuration. Photographs were made of the more significant patterns.



FAC 42060

Figure 19. Flow Visualization Test Facility

A typical test cascade consisted of five airfoils. These airfoils and the rig sidewalls formed six channels, as shown in Figure 20. A basic model consisted of the desired airfoil design with straight (uncontoured) endwalls. In most cases, there was a preselected axial area change through the cascade (H_3/H_2). The cascade was built on a wooden platform. The clay endwall was formed in a 1.0-in. deep cutout section to permit ample room for endwall contouring. Airfoil dimensions were the same as those used in the plane cascade tests. Therefore, unmodified airfoil configurations made use of the aluminum plane cascade vanes. Modified airfoils were constructed of wood and generally installed in the three center vane positions. The test section span was 1.9 in. at the leading edge. A silicon rubber seal was formed on the airfoil to bear against the plexiglas top endwall.

Preparations for testing in the flow visualization wind tunnel consisted of: attaching the assembled cascade pack to the bottom plate, shaping the clay endwall to the desired contour, and spotting oil and lampblack dots on the endwall and airfoil surfaces. The two electric blower motors were turned on, and the tunnel was permitted to run about five minutes, while boundary layer flow pattern formations were observed through the plexiglas top. Notes and hand sketches of the flow patterns were made for each configuration. Photographs were made for more than half the tests.

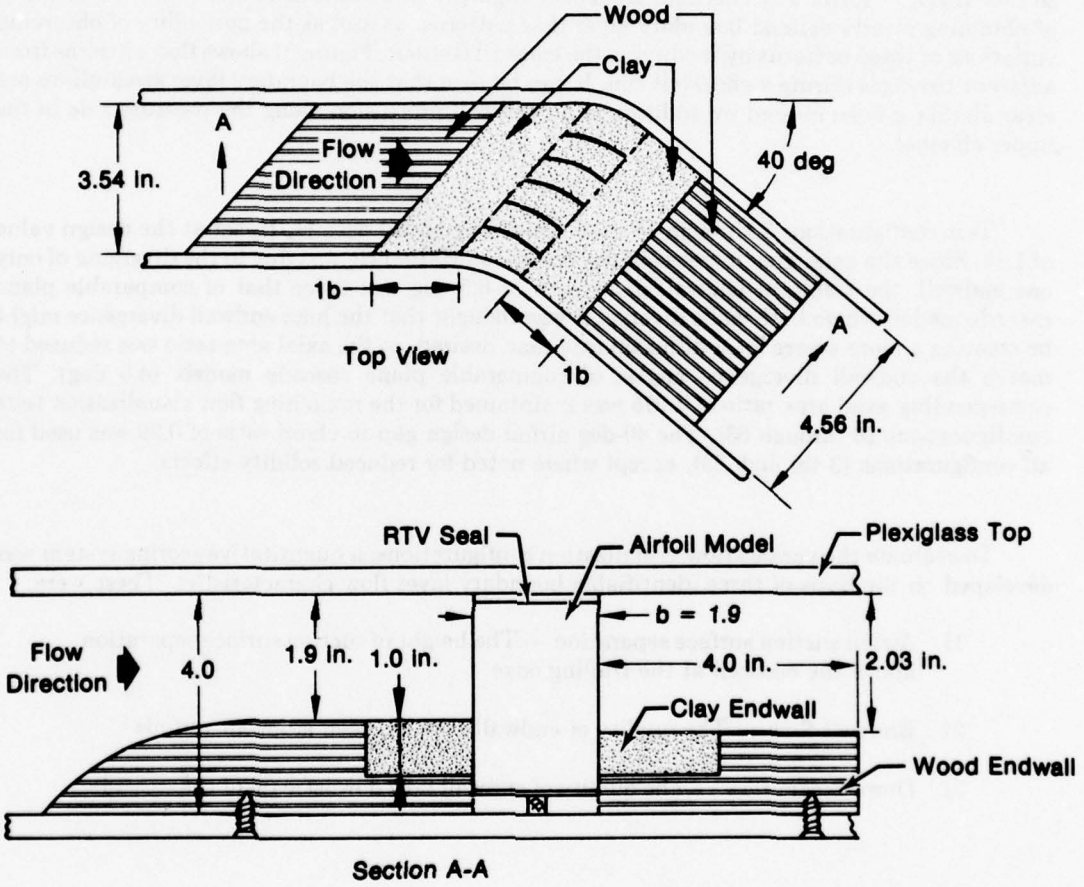


Figure 20. Flow Visualization Cascade Rig Model

The cascade inlet Mach No., determined from static pressure measurements at the cascade inlet, was 0.33. The velocity boundary layer thickness (δ), based on a turbulent flat plate correction of Reference 1 was calculated to be about 0.9 in. The inlet flow direction was set by the orientation of the tunnel sidewall with the plane of the cascade leading edges. Measurement of the inlet boundary layer streamline patterns showed that the inlet flow direction varied about two degrees. This small variation from the desired angle did not affect the qualitative interpretation of data from these tests.

2. Test Results

A total of 63 different airfoil-endwall configurations were tested in the flow visualization study. A description of each configuration and a brief summary of results are presented in Appendix B. With the exception of the first two configurations in which 30-deg airfoils were used, all tests were made with 40-deg airfoils. Spacing of the 30-deg airfoils was at the design gap-to-chord ratio (τ/b) of 0.77; a nominal divergence of the endwall through the cascade was selected so that $H_3/H_2 = 1.075$. The checkout tests of configurations 1 and 2 demonstrated the feasibility of obtaining clearly defined boundary layer flow patterns, as well as the possibility of observing variations of these patterns by modifying the endwall contour. Figure 21 shows flow patterns from adjacent passages during a checkout run. It can be seen that the boundary layer streamlines are clear and have been altered by addition of an endwall protrusion along the pressure side in the upper channel.

Test configurations 3 through 15 used the 40-deg airfoil with H_3/H_2 set at the design value of 1.15. Since the axial area increase in the flow visualization rig was due to the diverging of only one endwall, the resultant endwall divergence of 8.5 deg was twice that of comparable plane cascade models where both walls diverge. It was thought that the high endwall divergence might be creating a more severe local diffusion rate than desired, so the axial area ratio was reduced to match the endwall divergence angles of comparable plane cascade models (4.3 deg). The corresponding axial area ratio of 1.075 was maintained for the remaining flow visualization tests (configurations 16 through 63). The 40-deg airfoil design gap-to-chord ratio of 0.39 was used for all configurations (3 through 63), except where noted for reduced solidity effects.

To evaluate the various flow visualization configurations, a quantitative scoring system was developed on the basis of three identifiable boundary layer flow characteristics. These were:

1) Airfoil suction surface separation — The height of suction surface separation above the endwall at the trailing edge

2) Endwall flow — The quality of endwall flow between adjacent airfoils

3) Downstream flow — The quality of endwall flow downstream of the cascade.

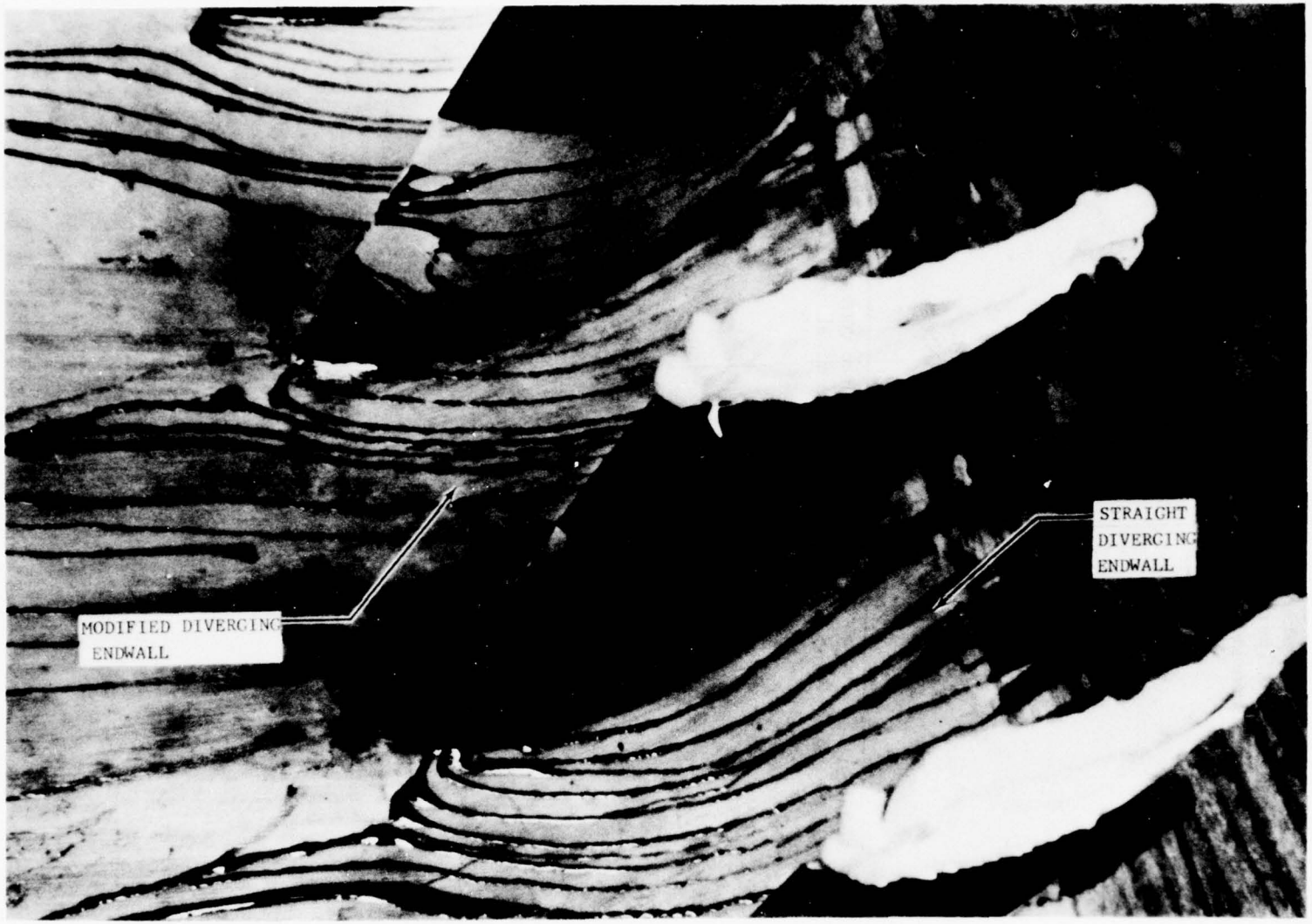


Figure 21. Flow Visualization of 30-deg EGV Checkout Test

The scoring criteria are presented Table 4. Configurations were assigned a score from 0 to 3 in. category. The total configuration score was obtained by adding increments from each category, with a maximum possible of 9.0. The overall scores are given in Table 5 for all configurations for which photographic records were made.

TABLE 4
SCORING OF BOUNDARY LAYER
FLOW VISUALIZATION PATTERNS

Category	*Criteria*	*Score*
Airfoil Suction Surface Separation	Height of suction surface corner separation above the endwall in inches	
	>3/4	0
	9/16 — 3/4	1
	3/8 — 9/16	2
	0 — 3/8	3
Endwall Flow	More than ½-channel blocked and flow reversed	0
	½-channel blocked and flow reversed	1
	Little crossflow, moderate separation, moderate reverse flow	2
	Little crossflow, no separation, no reverse flow	3
Downstream Flow	Gross separation	0
	Reverse flow, no separation	1
	No separation, no reverse flow, over (or under) turned	2
	No separation, no reverse flow	3

TABLE 5
COMPARATIVE BOUNDARY LAYER PATTERN SCORES FOR FLOW VISUALIZATION MODELS

	Category			
Configuration	Airfoil Flow	Endwall Flow	Downstream Flow	Total
3	1	1.5	2	4.5
4	1	0	1	2
9	0	1	1	2
14	1.5	2	1	4.5
15	1	2	1	4
16	1	2.5	2	5.5
17	2	2	0	4
18	0	1.5	1	3.5
26	2	2	2	6
27	1	2	2	5
32	0	2	2	4
33	0	2	1	3
34	2	2	2	6
35	1	1	2	4
37	1	2	2	5
42	0	0	1	1
43	0	2	2.5	4.5
44	0	2	2	4
45	0	1.5	2	3.5
46	2	3	0.5	5.5
47	1	2	2	5
48	1	2	1	4
49	2	3	2.5	7.5
50	3	3	0	6
51	1	1.5	1.5	4
52	1	1.5	1	3.5
53	2	1.5	1.5	5
54	0	2	1.5	3.5
55	0	1	0	1
56	2	2.5	0	4.5
57	0	2.5	2	4.5
58	0	2.5	2.5	5.0
59	2	2	2.5	6.5
60	2	2	2.5	6.5
61	2	1.5	2	5.5
62	1.5	2.5	3	7.0
68	2	3	3	8.0

The flow visualization cascade study was conducted in two parts. The initial effort consisted of configurations 1 through 42 and made use of available airfoils (except for a set of locally uncambered wooden airfoils for configurations 33 and 34). Geometric variations consisted of: endwall modifications; solidity changes; and minor airfoil variations, which could be obtained by

adding modeling clay or leaning the vanes. Evaluation of boundary layer flow patterns from this preliminary study led to the following conclusions:

1) Half the design solidity is more than adequate to turn the endwall boundary layer (configuration 23).

2) An endwall protrusion along the pressure surface, in combination with reduced solidity, resulted in less endwall overturning (configuration 24).

3) Axial endwall convergence to the trailing edge, in combination with reduced solidity and downstream divergence, is beneficial for airfoil-endwall corner separation on the suction surface (configuration 26).

4) Leaning airfoils to form an acute angle between the pressure surface and the endwall increases channel crossflow, but downstream endwall flow is generally uniform and axial with no separation (configuration 27).

5) Uncovered turning (forward loaded airfoils) increased endwall crossflow, inducing severe endwall and airfoil separation (configurations 35 through 42).

The second sequence of flow visualization tests was conducted to more fully characterize promising schemes prior to performance testing in our plane cascade facility at design Mach number. Particular attention was given to airfoil geometry variations, which included:

1) Bowed airfoils to provide spanwise leaning near the endwall
2) Solidity reduction near the endwall (locally shorter chord)
3) Local uncambering near the endwall
4) Combinations, such as local uncambering, with reduced endwall chord.

Five airfoil modifications were selected, consisting of: spanwise bowing near the endwall; two variations of leading edge, cutback near the endwall; and two variations of trailing edge, cutback near the endwall. Figure 22 shows each of these. The airfoils were tested in combination with several endwall modifications, which included: straight diverging, variations of protrusions near the pressure surface, and converging-diverging configurations. Except for the bowed airfoil, configuration changes were made by replacing the three center vanes while retaining unmodified outer vanes. All five airfoils were changed for the bowed airfoil tests.

Sixteen test configurations (43 through 58) were conducted with endwall variations of the modified airfoils. Significant results from these tests are presented in Table 6 for a comparison of airfoil effects and in Table 7 for endwall effects. The first grouping in Table 6 compares major airfoil variations of leaning, ¼-chord cutback leading edge, and ¼-chord cutback trailing edge. In this comparison, the cutback leading edge configuration received the highest total score. Comparision of the ¼- and ½-chord cutback leading edges in the second grouping showed that the larger cutback was not beneficial. Part of the problem observed with the ½-chord cutback resulted from the fact that little boundary layer flow turning occurred ahead of the endwall-airfoil and, as a result, created a high positive incidence. The high incidence caused flow separation near the leading edge of the cutback airfoil section as it entered the endwall channel. It was concluded that another configuration should be tested with a refined cutback leading edge design. Figure 23 presents the refined model configuration. It can be seen that the leading edge has been cut back to about 40% chord and aligned with the approach boundary layer flow. Also the trailing edge was

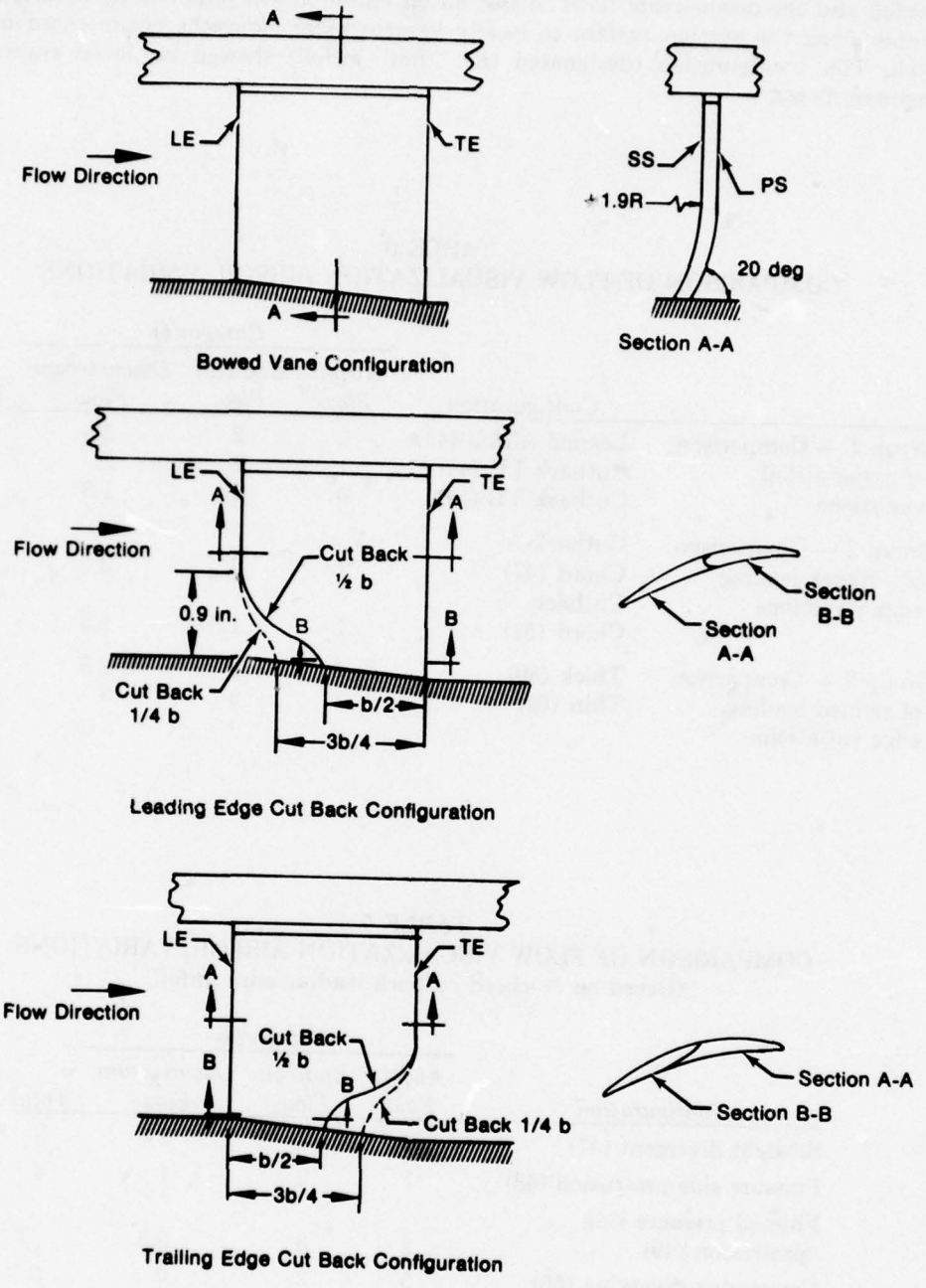


Figure 22. Flow Visualization of 40-deg EGV Airfoil Variations (A_3/A_2 = 1.075, Divergence = 5 deg)

uncambered near the root. The third grouping in Table 6 presents results for this configuration (designated "thick" airfoil). It will be noted that a significant improvement was observed in both the airfoil and the downstream flows. A last airfoil variation was obtained by reducing airfoil thickness along the suction surface to locally lower camber along the entire chord near the endwall. This configuration (designated the "thin" airfoil) showed improved endwall and downstream flows.

TABLE 6
COMPARISON OF FLOW VISUALIZATION AIRFOIL VARIATIONS

		Categories			
	Configuration	*Airfoil Flow*	*Endwall Flow*	*Downstream Flow*	*Total*
Group 1 — Comparison of major airfoil variations	Leaned Airfoil (43)	0	2	2.5	4.5
	Cutback LE (47)	1	2	2	5
	Cutback TE (54)	0	2	1.5	3.5
Group 2 — Comparison of cutback leading edge variations	Cutback ¼ Chord (47)	1	2	2	5
	Cutback ½ Chord (51)	1	1.5	1.5	4
Group 3 — Comparison of refined leading edge variations	Thick (59)	2	2	2.5	6.5
	Thin (62)	2	3	3	8

TABLE 7
COMPARISON OF FLOW VISUALIZATION AIRFOIL VARIATIONS
(Based on ¼-chord cutback leading edge airfoil)

	Categories			
Configuration	*Airfoil Flow*	*Endwall Flow*	*Downstream Flow*	*Total*
Straight divergent (47)	1	2	2	5
Pressure side protrusion (48)	1	2	1	4
Filleted pressure side protrusion (49)	2	3	2.5	7.5
Converging-diverging (50)	3	3	0	6

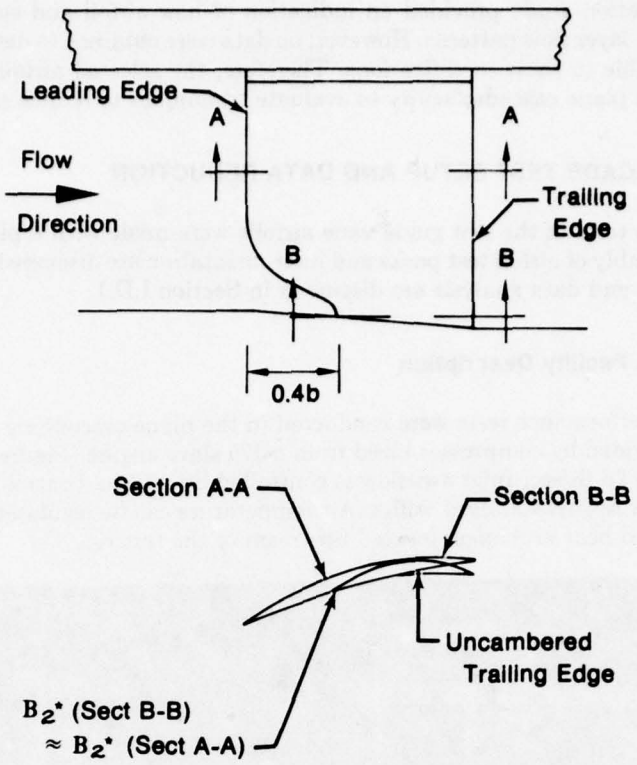


Figure 23. Cutback Leading Edge Configuration with Modified Endwall Section Leading Edge and Uncambered Trailing Edge

As a result of the comparisons in Table 6, several airfoil design features to reduce endwall loss have been identified. These include:

- Cutback leading edge between 25% and 40% chord
- Modify cutback leading edge to offset incidence effect
- Uncamber trailing edge at the endwall
- Minimize suction surface camber at the endwall.

During flow visualization tests with each airfoil configuration, several modifications were made to the clay endwalls. Table 7 presents a comparison of the endwall variations made with the ¼-chord cutback leading edge model. These variations included: a straight diverging endwall, a diverging endwall with a pressure-side protrusion; a filleted pressure-side protrusion extending one-half chord downstream of the trailing edge; and converging-diverging endwall. The filleted pressure side protrusion provided the best overall results. The coverging-diverging configuration resulted in excellent airfoil and endwall flows by unloading the cascade. However, the section downstream of the trailing edges was completely separated due to the rapidly diverging endwall. As a result of comparisons such as those shown in Table 7, several endwall design features have been identified. These include:

- Minimize divergence within the cascade channel
- Provide filleted pressure side protrusion
- Extend any necessary endwall divergence downstream of the cascade as gradually as possible.

The flow visualization study provided an indication of how airfoil and endwall modifications affected boundary layer flow patterns. However, no data were obtained to determine performance benefits attributable to these modifications. Therefore, the selected airfoil endwall geometries were tested in the plane cascade facility to evaluate techniques to reduce endwall loss.

C. PLANE CASCADE TEST SETUP AND DATA REDUCTION

Performance tests of the exit guide vane airfoils were made with a plane cascade test rig. The test rig, assembly of airfoil test packs and instrumentation are discussed in this section. (The airfoil test results and data analysis are discussed in Section I.D.)

1. Test Rig and Facility Description

The airfoil performance tests were conducted in the plane cascade rig shown in Figures 24 and 25. Air is provided by compressor bleed from a J75 slave engine (Figure 26). The maximum airflow capacity is 28 lb/sec. Inlet awirflow is controlled by a 10-in. control valve and measured with a sharp edged ASME standard orifice. Air temperature can be regulated from 160° to 700°F with a water-cooled heat exchanger located upstream of the test rig.

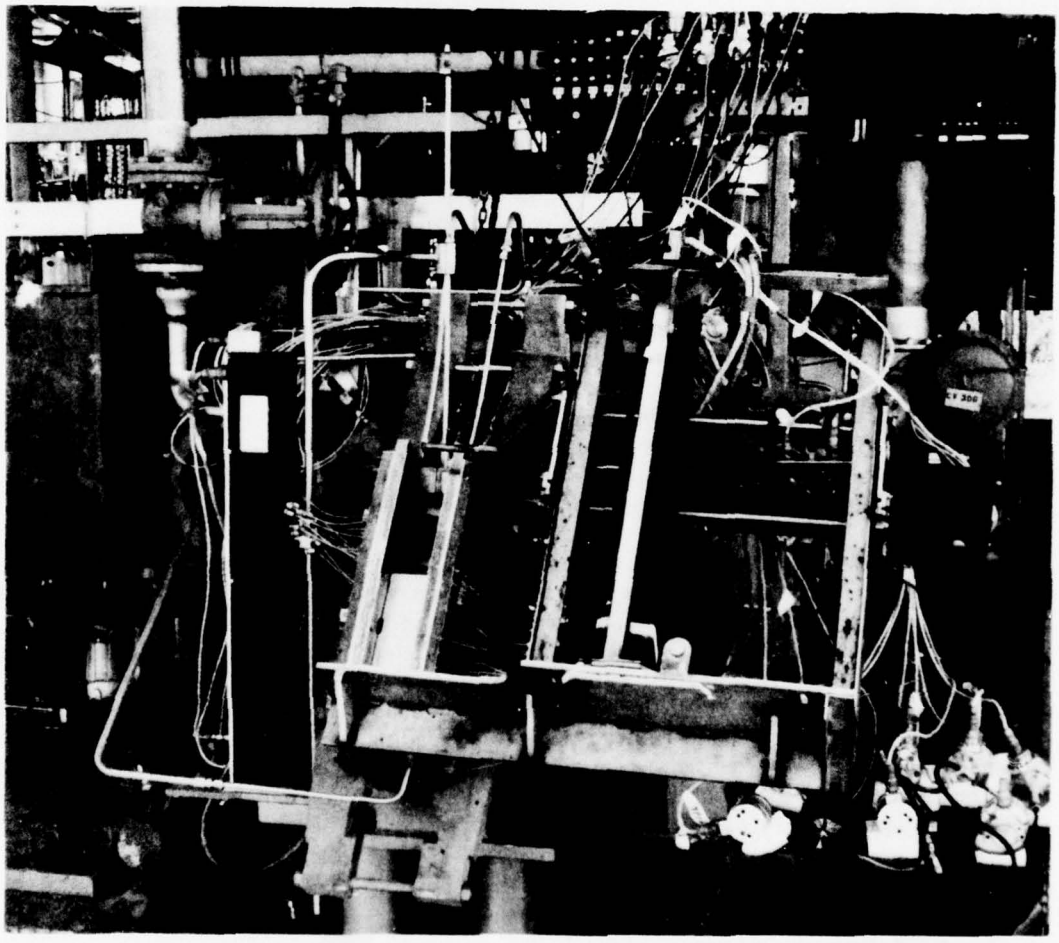


Figure 24. High Mach Number Plane Cascade Test Rig FAE 26698

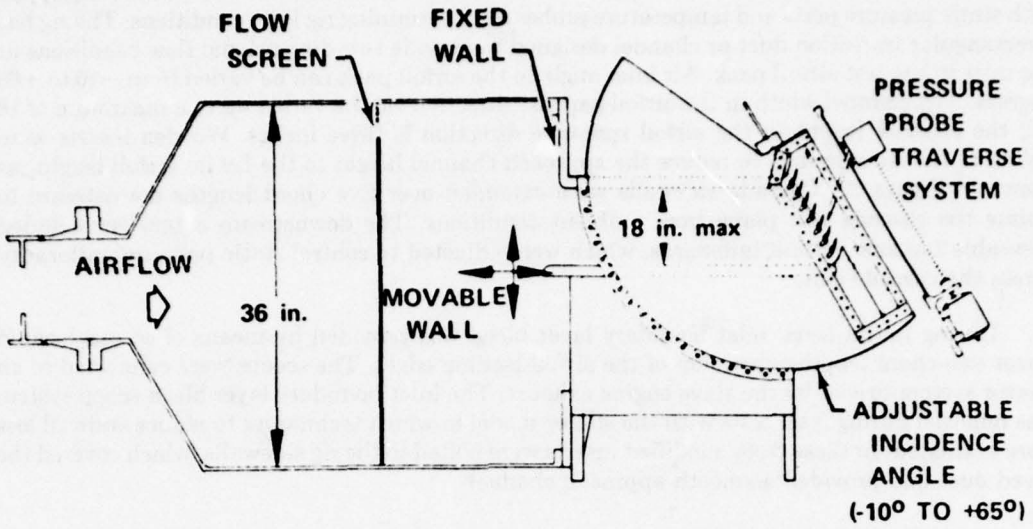


Figure 25. Plane Cascade Test Rig Schematic

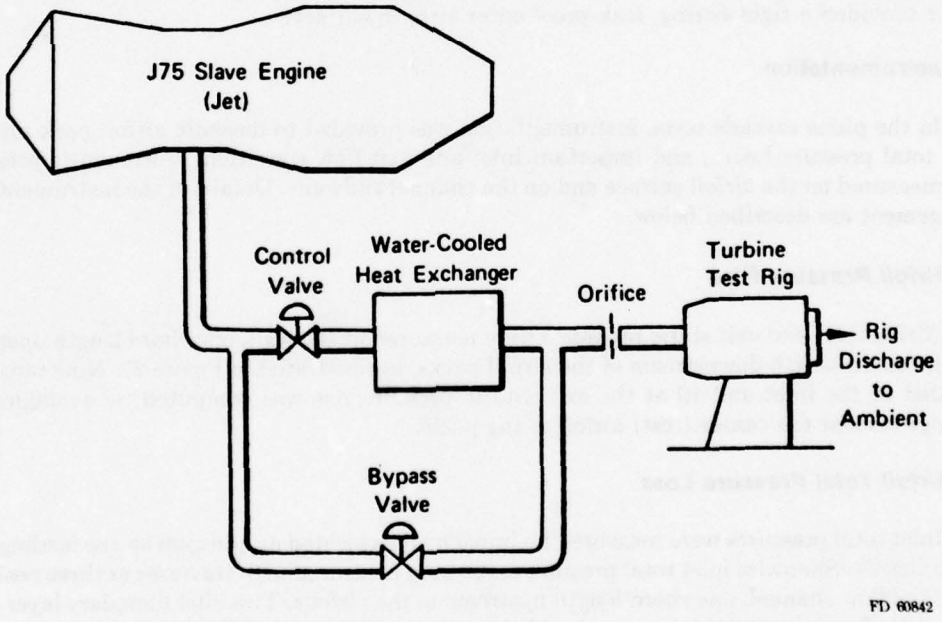


Figure 26. Plane Cascade/Annular Cascade Test Facility

Air flows to the test section through a 36-in. diameter plenum chamber, which is equipped with static pressure ports and temperature probes for determining rig inlet conditions. The rig has a rectangular transition duct or channel designed to provide two-dimensional flow conditions at the inlet to the test airfoil pack. Air inlet angle to the airfoil pack can be varied from −10 to +65 degrees. The channel width in the airfoil gapwise direction can be varied up to a maximum of 18 in.; the channel height in the airfoil spanwise direction is three inches. Wooden inserts were bolted to the rig sidewalls to reduce the approach channel height to the 1.9 in. airfoil height, as shown in Figure 27. Cascade sidewalls were extended over five chord lengths downstream to isolate the cascade exit plane from ambient conditions. The downstream extension included moveable top and bottom tailboards, which were adjusted to control static pressure uniformity across the cascade exit.

During initial tests, inlet boundary layer bleed was provided by means of scoops located about two chord lengths upstream of the airfoil leading edges. The scoops were connected to an ejector system driven by the slave engine exhaust. The inlet boundary layer bleed scoop system was removed during later tests with the 40-deg model in which techniques to reduce endwall loss were evaluated. In these tests, modified inserts were bolted to the rig sidewalls, which covered the bleed duct and provided a smooth approach channel.

2. Assembly of Airfoil Packs

The cascade airfoil packs consisted of multiple constant section aluminum airfoils. In initial tests, packs of seven airfoils, having six flow channels were used. Thirteen airfoils were used in later tests with the 40-deg airfoil. The methods of assembling the cascade test packs are shown in Figures 28 and 29. The airfoils were inserted through metal endwall plates, which had the matching airfoil contours precisely machined at the desired spacings and stagger angles. Silicon rubber was cast onto the plates to provide an easily machinable surface for variation of endwall divergence. The metal endwalls firmly held the airfoils in the proper position while the cast rubber provided a tight-fitting, leak-proof outer airpath surface.

3. Instrumentation

In the plane cascade tests, instrumentation was provided to measure airfoil pack pressure rises, total pressure losses, and important inlet and exit flow conditions. Also, static pressures were measured on the airfoil surface and on the channel endwalls. Details of the instrumentation arrangement are described below.

a. Airfoil Pressure Rise

Airfoil inlet and exit static pressures were measured at the wall, one chord length upstream and one chord length downstream of the airfoil packs, as illustrated in Figure 27. Nine taps were provided at the inlet and 10 at the exit. Static pressure rise was computed by averaging the readings nearest the center (test) airfoil of the packs.

b. Airfoil Total Pressure Loss

Inlet total pressures were measured by impact tubes located at midspan on the leading edge of two airfoils. Spanwise inlet total pressure maps were measured with traverses at three positions across the flow channel, one chord length upstream of the airfoils. Two inlet boundary layer rakes (each with five impact tubes) were provided on the cascade packs. These rakes were near the plane of the airfoil leading edge and located in the airfoil flow channel, as shown in Figure 27.

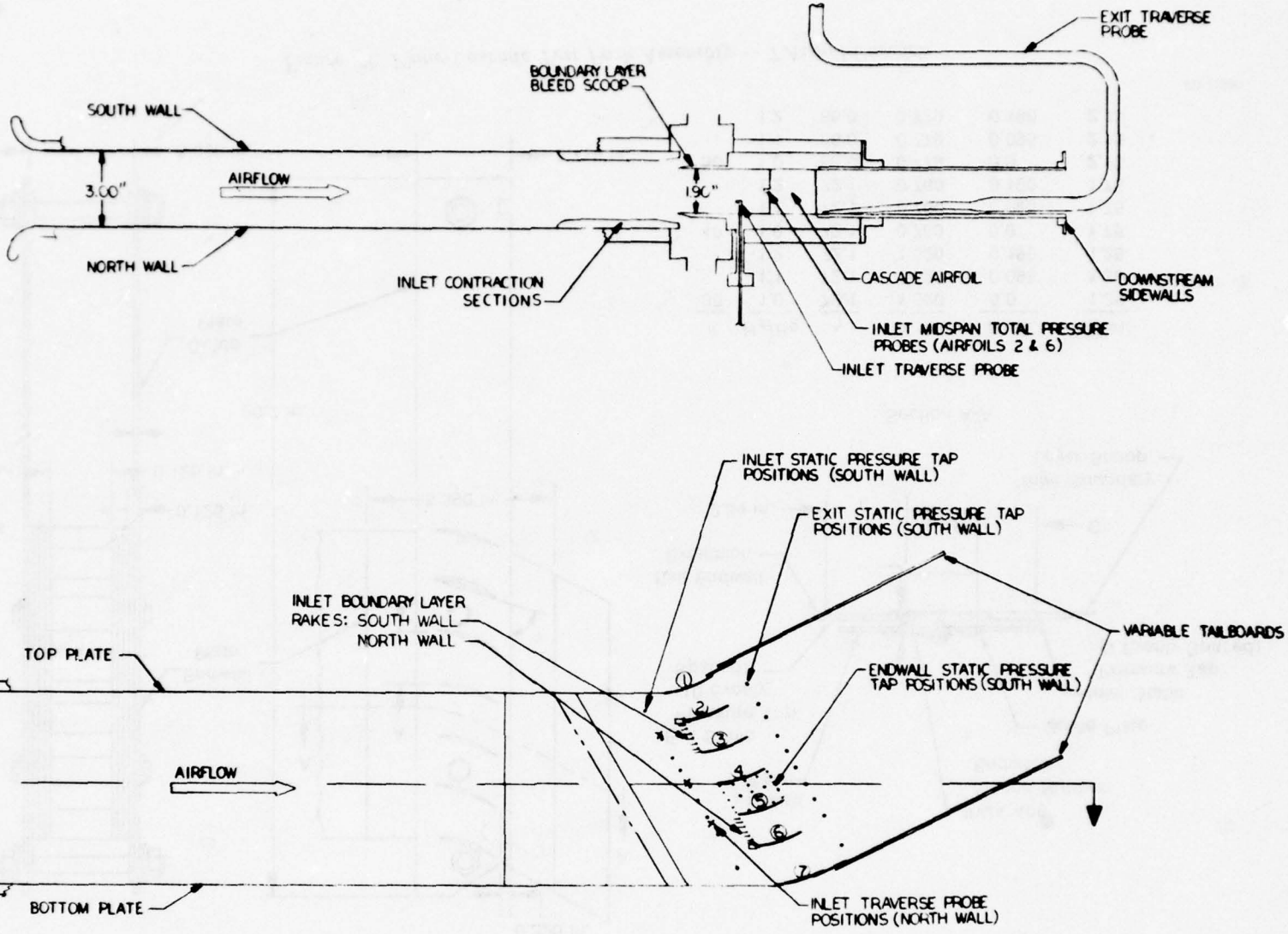
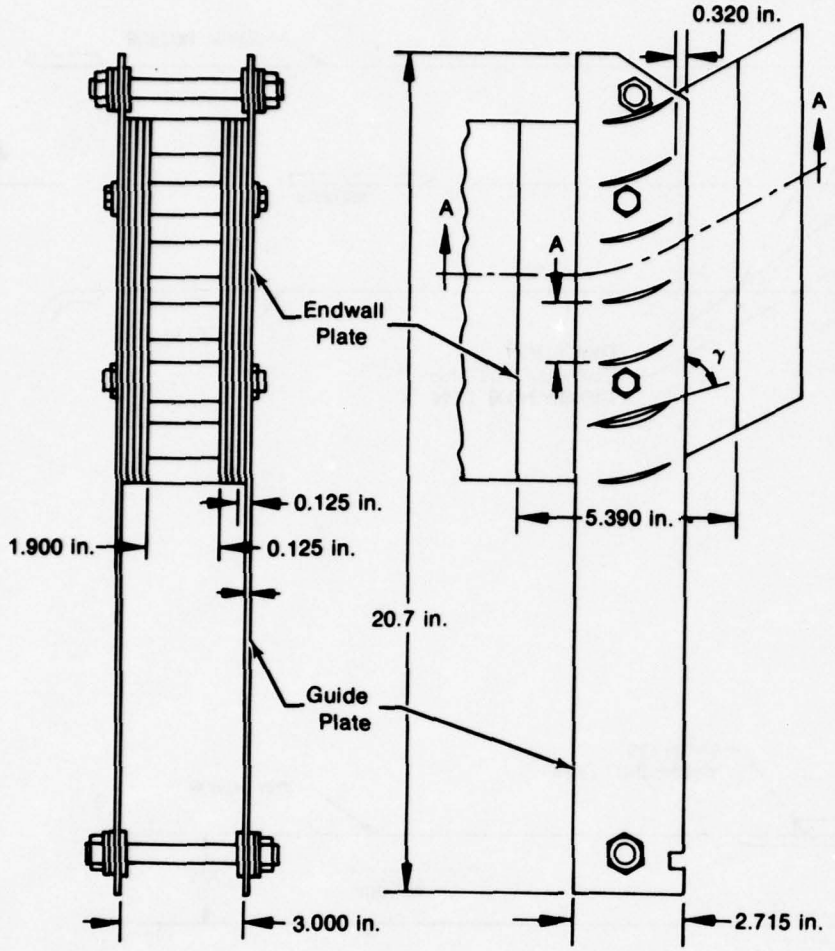
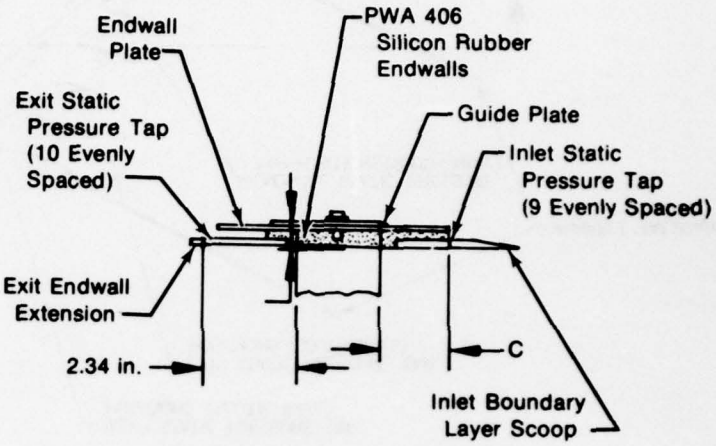


Figure 27. Plane Cascade Rig Test Section Schematic



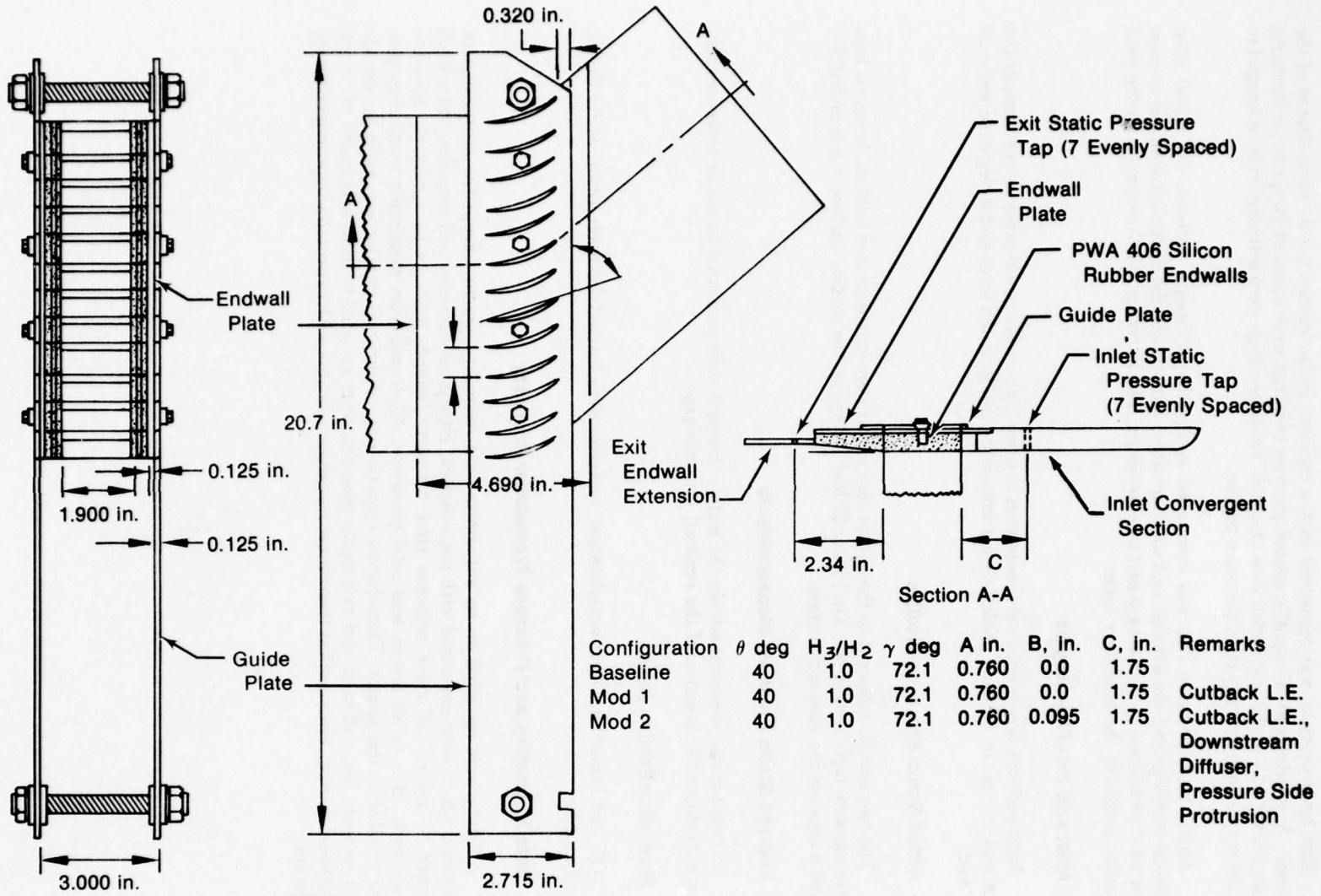


Section A-A

θ	H_3/H_2	γ	A, in.	B, in.	C, in.
30	1.0	72.1	1.520	0.0	1.35
	1.1	72.1	1.520	0.095	1.35
	1.2	72.1	1.520	0.190	1.35
40	1.0	72.1	0.760	0.0	1.75
	1.1	72.1	0.760	0.095	1.75
	1.2	72.1	0.760	0.190	1.75
50	1.0	66.0	0.779	0.0	2.15
	1.1	66.0	0.779	0.095	2.15
	1.2	66.0	0.779	0.190	2.15

FD 119681

Figure 28. Plane Cascade Test Pack Assembly — 7 Airfoil Cascade



Configuration	θ deg	H_3/H_2	γ deg	A in.	B, in.	C, in.	Remarks
Baseline	40	1.0	72.1	0.760	0.0	1.75	
Mod 1	40	1.0	72.1	0.760	0.0	1.75	Cutback L.E.
Mod 2	40	1.0	72.1	0.760	0.095	1.75	Cutback L.E., Downstream Diffuser, Pressure Side Protrusion

FD 119682

Figure 29. Plane Cascade Test Pack Assembly — 13 Airfoil Cascade

Exit total pressure was measured with a traverse probe located 0.2 in. downstream of the cascade. Approximately 45 equally spaced gapwise readings were made at 10 spanwise locations (from 1% to 50%) in the test airfoil flow channel. These readings were arithmetically averaged to obtain a spanwise average total pressure profile.

Airfoil total pressure loss was computed as (1) the difference between the airfoil inlet midspan readings and the average exit total pressure, and (2) the difference between the average inlet total pressure and the average exit total pressure. The latter approach accounts for the total pressure profile of the boundary layer.

c. *Inlet and Exit Flow Angles*

Inlet and exit flow angles were measured in combination with total pressure traverses at the inlet and exit of the cascade pack, using a minicobra probe at the inlet and 9-deg cone probe at the exit.

d. *Airfoil Static Pressure Profiles*

The two airfoils adjacent to the center test airfoil were instrumented with midspan surface static pressure taps. Airfoil No. 3 in Figure 27 had 10 taps on the suction surface, while airfoil No. 5 had 8 taps on the pressure surface.

e. *Endwall Static Pressure Measurements*

Endwall static pressures within the airfoil channels were measured by static pressure taps. Figure 30 shows the position of the endwall pressure taps.

f. *Flow Visualization Data*

Oil and lampblack flow visualization patterns were formed for each airfoil at its design Mach number.

g. *Data Recording and Pressure Transducer Accuracy*

All data were recorded on an automatic data recording system, except the airfoil surface pressures, which were measured with manometers. Exit probe traverse and recording rates were selected to assure sufficient response time for servo-balance systems to accurately measure parameters, such as air angles and total pressures. All transducers measuring transients were close coupled to the sensor. Transducers used to measure critical parameters, such as cascade total pressure loss and inlet and exit static pressure, were selected to have accuracies of $\pm 0.2\%$ of full-scale range. The smallest transducer ranges compatible with expected pressure levels were selected.

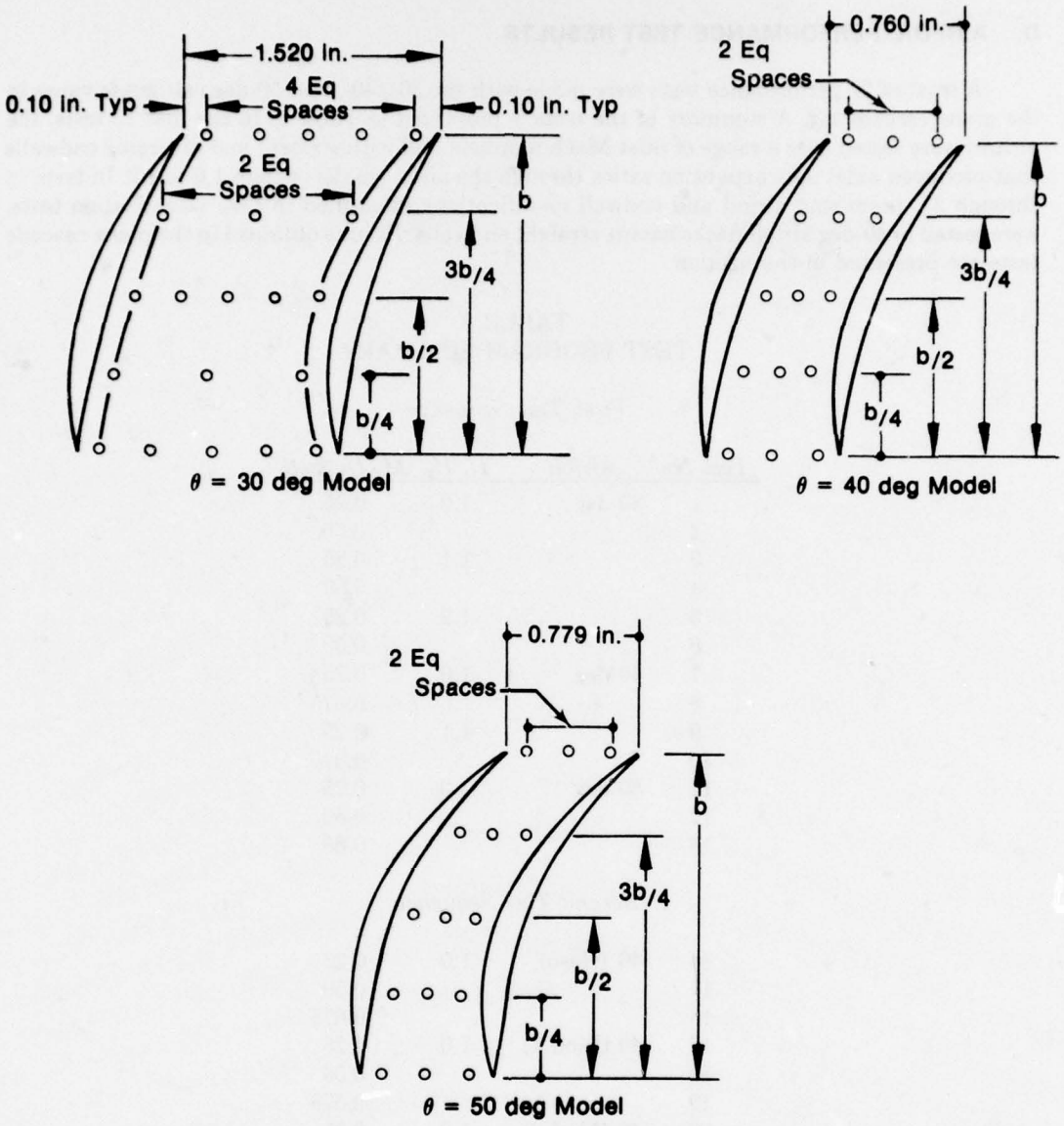


Figure 30. Endwall Static Pressure Tap Locations

D. AIRFOIL PERFORMANCE TEST RESULTS

A total of 22 performance tests were made with the 30-, 40-, and 50-deg exit guide vanes in the plane cascade rig. A summary of the tests is presented in Table 8. In the first 13 tests, the airfoils were tested over a range of inlet Mach numbers and with straight and diverging endwalls that produced axial area expansion ratios through the airfoil packs of from 1.0 to 1.2. In tests 14 through 22, promising airfoil and endwall modifications, identified in flow visualization tests, were tested in 40-deg airfoil packs having straight endwalls. Results obtained in the plane cascade tests are presented in this section.

TABLE 8
TEST PROGRAM SUMMARY

First Test Sequence

Test No.	*Airfoil*	H_3/H_2	M_2 *Desired*
1	30-deg	1.0	0.25
2			0.50
3		1.1	0.25
4			0.50
5		1.2	0.25
6			0.50
7	40-deg	1.0	0.25
8			0.675
9		1.1	0.25
10			0.675
11	50-deg	1.0	0.25
12			0.50
13			0.85

Second Test Sequence

14	40 (Base)	1.0	0.25
15			0.50
16			0.675
17	40 (Mod 1)	1.0	0.25
18			0.50
19			0.675
20	40 (Mod 2)	1.0	0.25
21			0.50
22			0.675

1. Checkout Tests

Checkout tests were conducted with each of the three airfoils. The purpose of these tests was to (1) evaluate the effect of boundary layer bleed on cascade inlet conditions and (2) measure inlet air angle and total pressure distributions. Results are shown in Figures 31 through 35.

Figures 31 and 32 illustrate the uniformity of midspan inlet flow conditions for the 30-deg airfoil pack. Figure 31 shows that (1) static pressure did not vary more than 1%, (2) total pressure was within 1% of the plenum pressure, and (3) negative incidence (<3.0 deg) was induced by the rig. Figure 32 presents inlet total pressure and flow angle measurements for the 30-deg airfoil at different spanwise locations. The data also show total pressure uniformity and negative incidence.

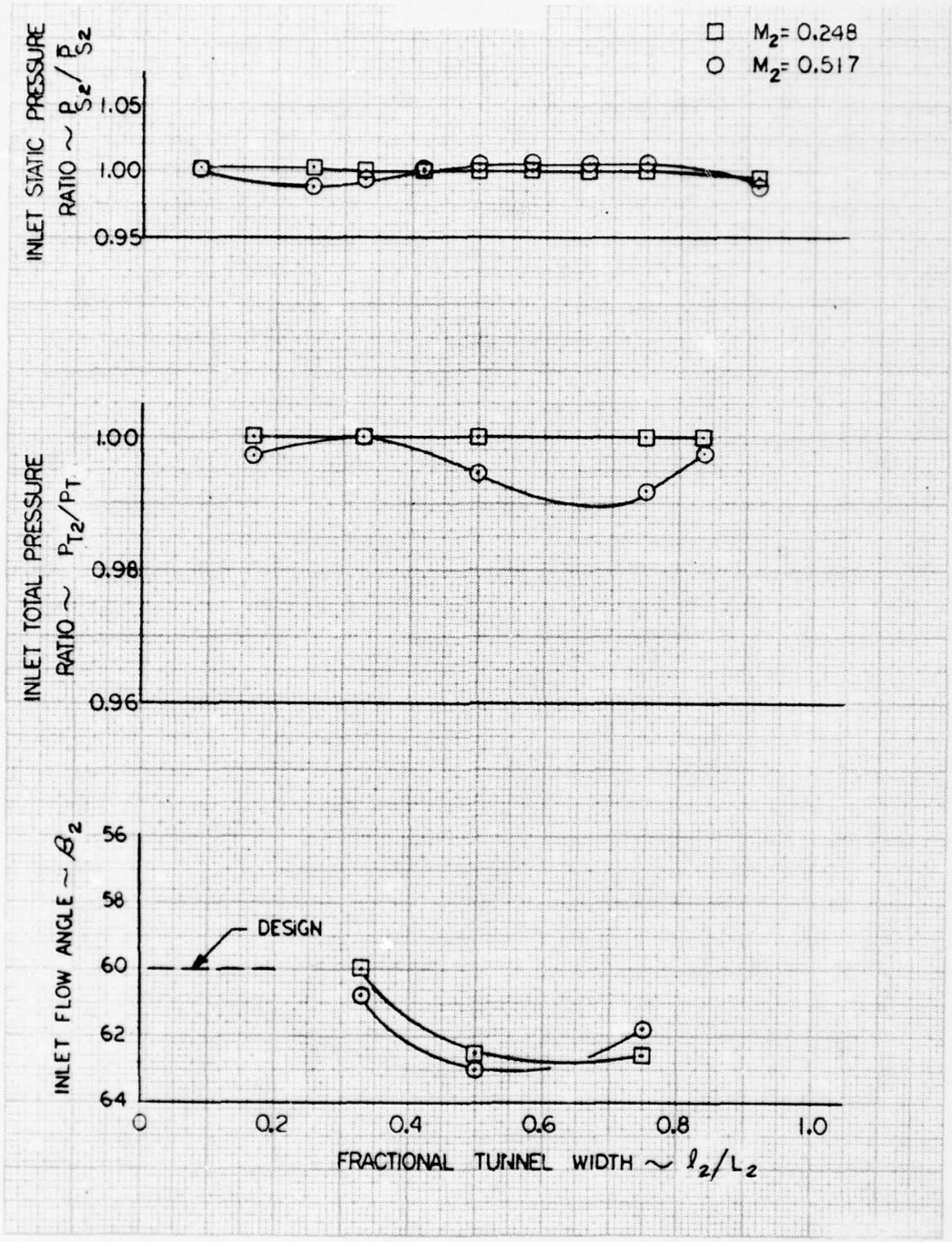


Figure 31. Inlet Flow Distribution at Midspan (30-deg Cascade)

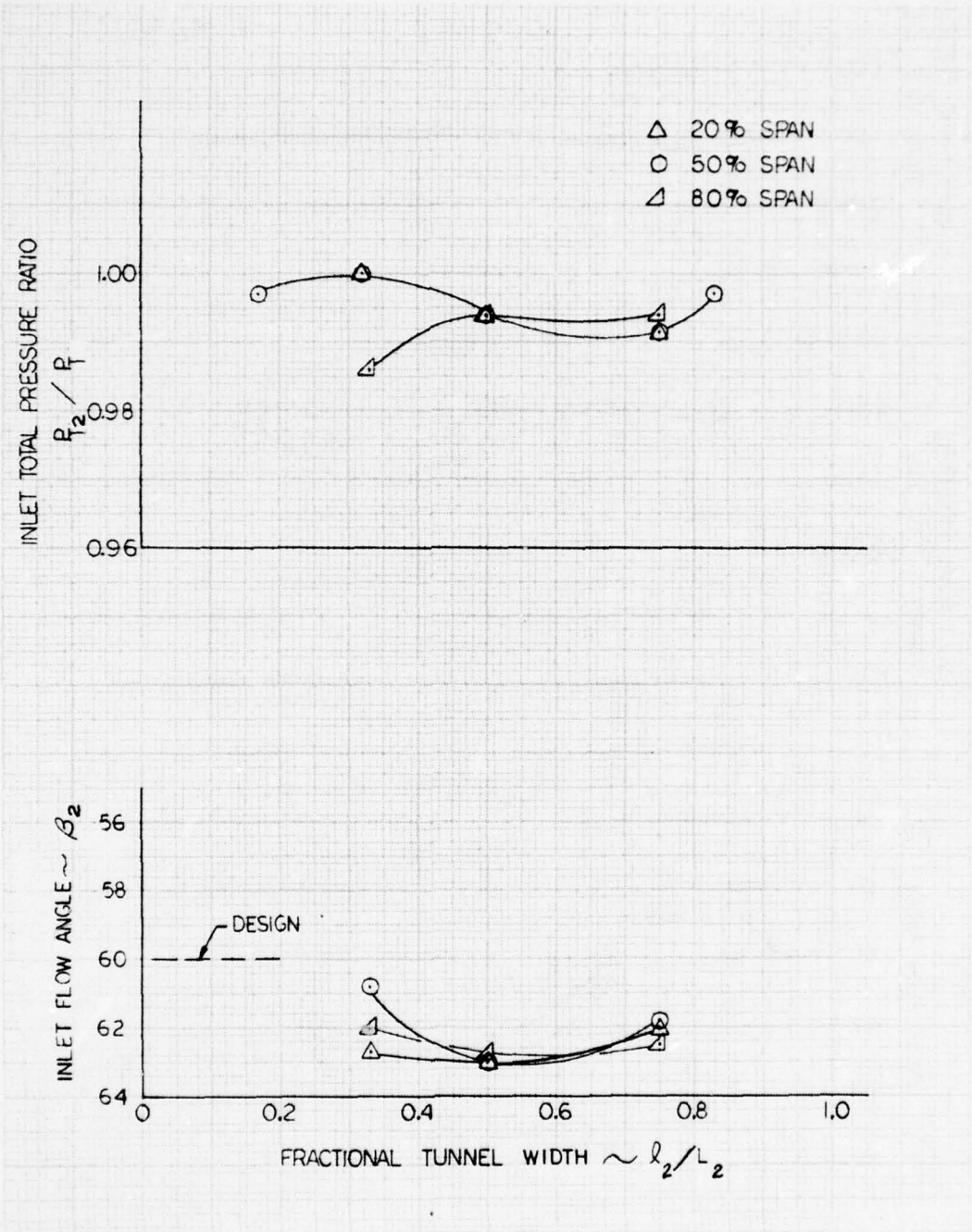


Figure 32. Spanwise Inlet Flow Distribution (30-deg Cascade, $M_2 = 0.517$)

Inlet pressures for the 40- and 50-deg airfoil packs were also uniform. However, the smaller gaps of these packs (the 40- and 50-deg airfoils had gap-to-chord ratios about one-half of the 30-deg airfoils) reduced the rig channel width for the seven airfoil packs to about 3.5 in. The close proximity of endwall plates for these higher turning airfoils caused inlet air angle deviations by as much as 8.9 deg from the design values. In a second series of tests with the 40-deg airfoil, the distance between the endwall plates was doubled by increasing the number of airfoils in the pack. This increased approach channel width effectively eliminated inlet flow deviations so that the approach air angle was generally within ±0.5 deg of the desired value.

Figure 33 shows the effect of boundary layer bleed on inlet static pressure distribution across the width of the channel for the 30-deg airfoil. For both Mach numbers (0.248 and 0.517), bleed had no effect on mid-channel pressure. However, at the higher Mach number, boundary layer bleed improved the static pressure distribution. Figure 34 shows the inlet boundary layer profiles with maximum boundary layer bleed flowrates for the 30-deg cascade at the two test Mach numbers.

During tests with the 50-deg airfoil and initial tests with the 40-deg airfoils, the close spacing of the airfoils reduced rig flowrate by about 50% (relative to that for the 30-deg airfoil) for all test Mach numbers. Since the maximum boundary layer bleed flowrate was essentially constant for each Mach number, it was possible to bleed a higher percentage of total flow for these airfoils. Figure 35 presents the inlet boundary layer profiles for the 40-deg cascade with and without bleed and for several inlet Mach numbers. Table 9 summarizes inlet boundary layer conditions obtained during the plane cascade performance tests.

TABLE 9
PHASE I PLANE CASCADE — INLET BOUNDARY LAYER DATA SUMMARY

Airfoil (deg)	M_2	*Percent Bleed* ($W_{bl}/W_{tot} \times 100$)	δ_2 *(in.)*	δ_2^* *(in.)*
30	0.25	12.0	0.318	0.025
	0.52	8.0	0.400	0.043
40	0.24	25.8	0.110	0.023
	0.63	25.9	0.100	0.017
50	0.30	25.7	0.135	0.025
	0.52	25.5	0.115	0.025
	0.84	25.5	0.103	0.016
40	0.25	0.0	0.275	0.031
(Second Test)	0.50	0.0	0.366	0.056
	0.68	0.0	0.361	0.060

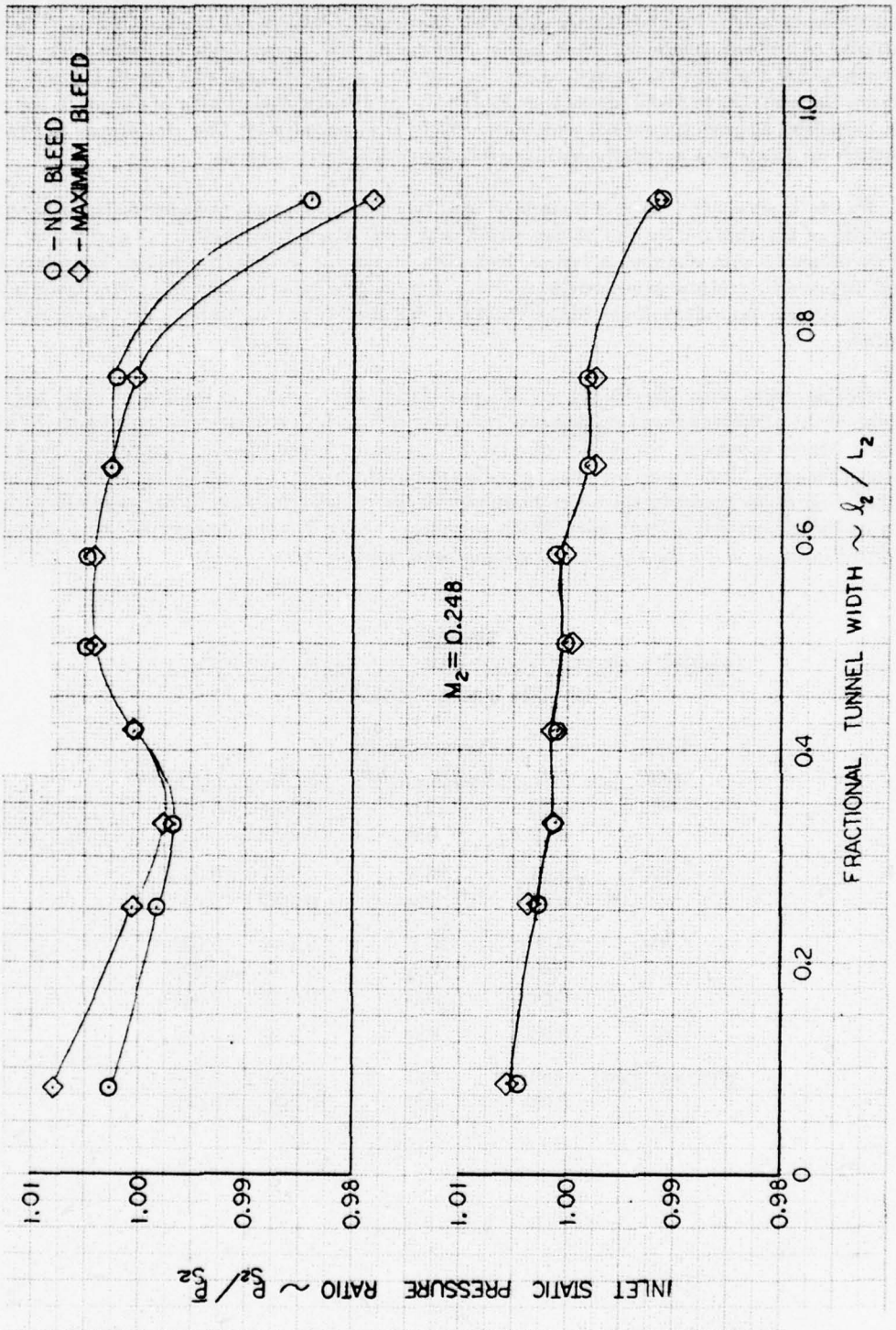


Figure 33. Effect of Boundary Layer Bleed on Inlet Static Pressure Distribution (30-deg Cascade, $M_2 = 0.517$)

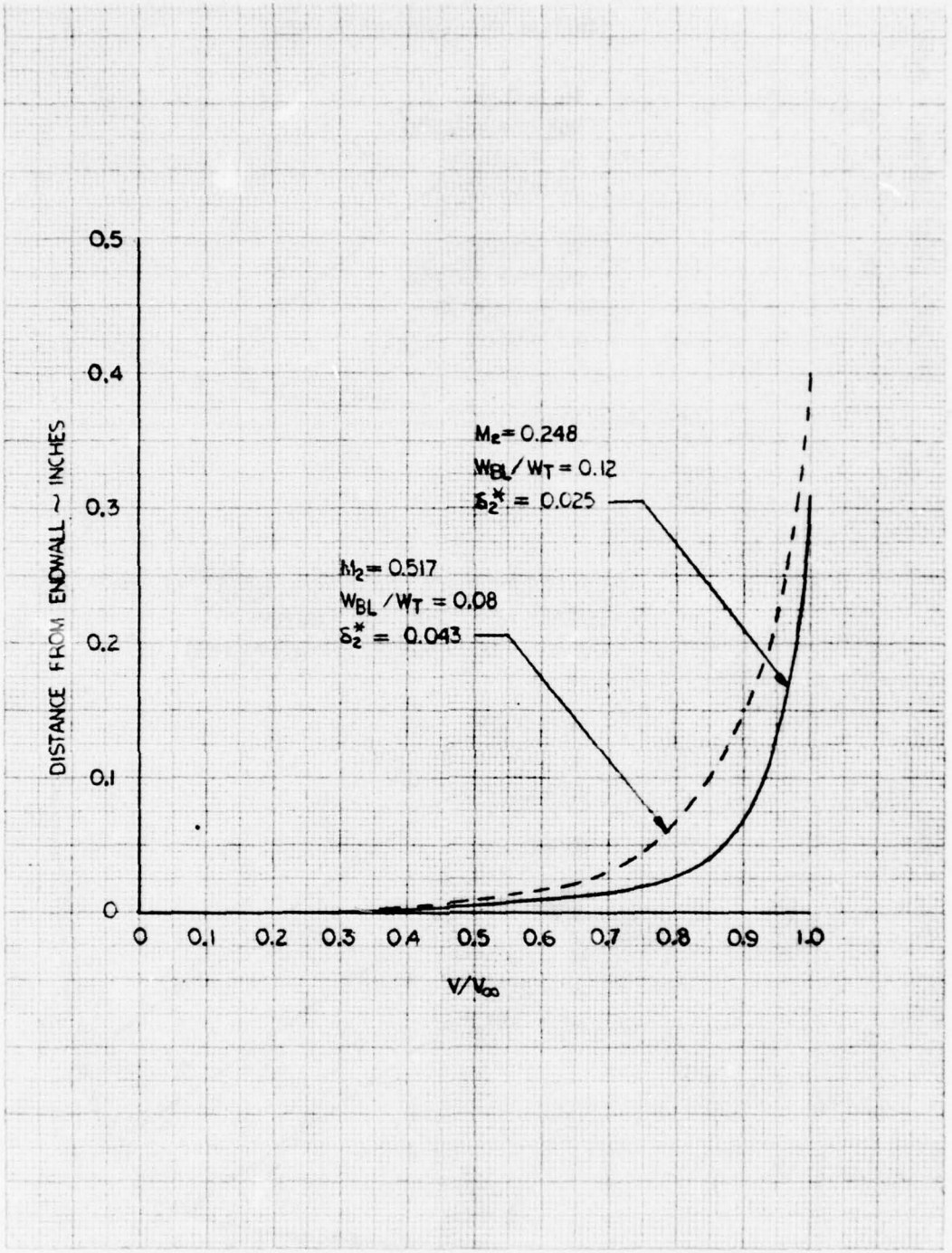


Figure 34. Inlet Boundary Layer Velocity Distributions for 30-deg Cascade

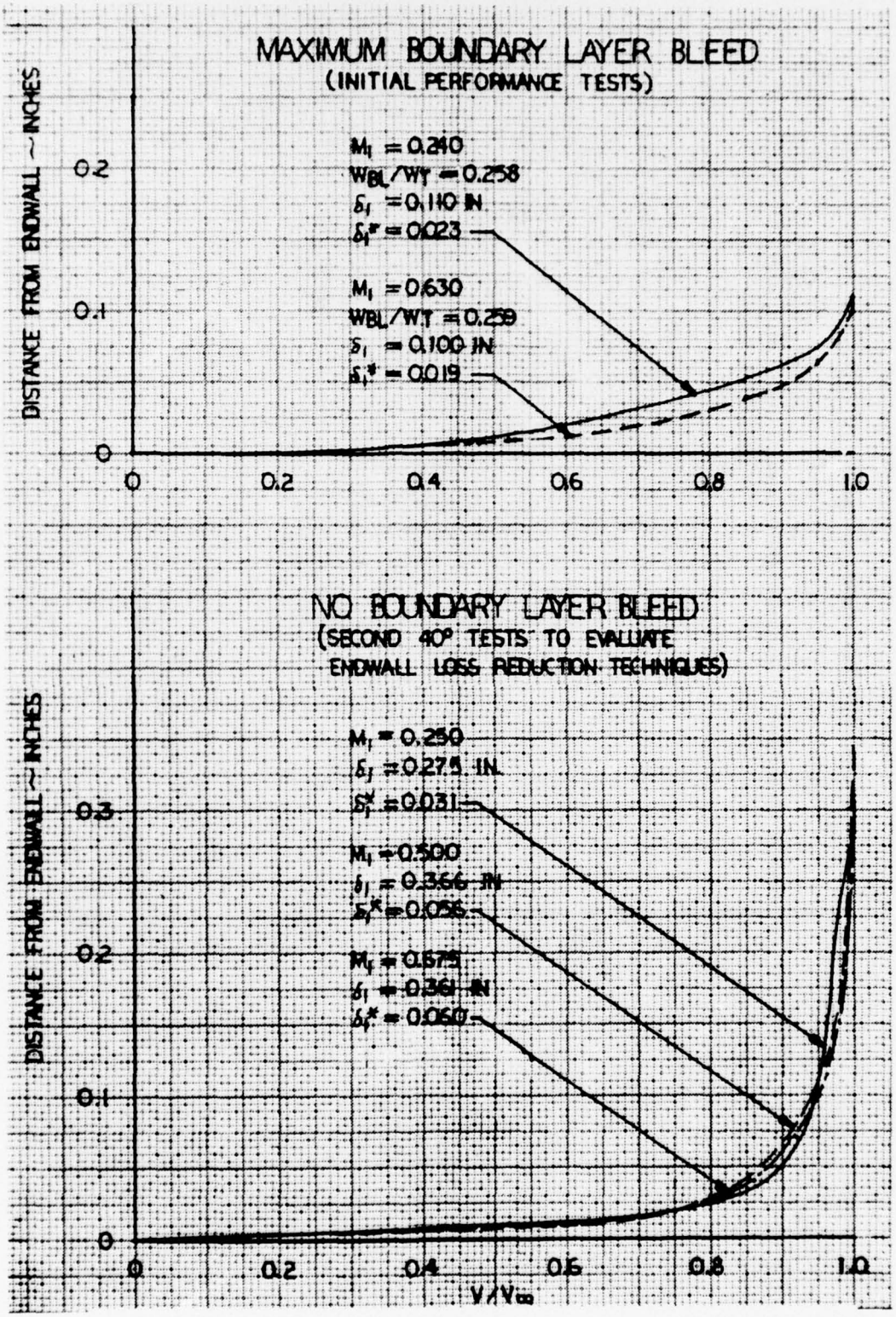


Figure 35. Inlet Boundary Layer Velocity Distributions for 40-deg Cascade

2. 30-Degree Airfoil Performance Test Results

The 30-deg cascade was tested at inlet Mach numbers of approximately 0.25 and 0.50 (design) and with endwalls having axial area ratios (H_3/H_2) of 1.0, 1.1, and 1.2. Data obtained with the 30-deg airfoil packs are summarized in Figure 36, where static pressure rise coefficient, spanwise averaged total pressure loss, and exit air angle are presented as a function of inlet Mach number. Total pressure loss and exit air angle deviation became greater with increasing Mach numbers and axial area ratios. Static pressure rise also increased with larger axial area ratios, but was not a strong function of Mach number.

In all tests with the 30-deg airfoil, incidence was −4.6 deg, which was 2.6 deg greater than the design value of −2.0 deg. The airfoil surface static pressure profiles, Figure 37, shows that pressures on the suction surface are higher than those on the pressure surface.

Figure 38 was prepared to compare the 30-deg EGV airfoil data with that for existing compressor airfoils. It presents the effect of incidence on pressure rise coefficient, exit air angle and loss for a circular arc compressor cascade similar to the 30-deg EGV design. These data are for a cascade with an airfoil AR = 2.0, τ/b = 0.833, and t/b = 0.09 compared to AR = 1.0, τ/b = 0.770, and t/b = 0.075 for the 30-deg EGV. All other geometric parameters are the same. It is significant to note that the non-series 30-deg EGV airfoil achieved higher pressure rise, comparable turning, and a lower loss than the circular arc airfoil.

The total pressure loss presented in Figure 38 is the midspan value measured for the 30-deg EGV airfoil. It is used to be consistent with the circular arc data. As shown in Figure 39, the midspan loss represents an equivalent profile loss for the 30-deg airfoil.

As the axial area ratio (i.e., the endwall divergence) increases, the tendency towards flow separation is increased. With the 30-deg airfoil, the endwalls having axial area ratios of 1.0 and 1.1 did not cause separation. However, with an area ratio of 1.2, separation did occur, as illustrated in Figure 40, where boundary layer streamlines from oil and lampblack traces have been superimposed on the endwall static pressure distributions. Comparable streamlines for the *unseparated test made with straight endwalls are shown in Figure 41.*

3. 50-Degree Airfoil Performance Test Results

The 50-deg airfoils were tested in a pack having straight endwalls (i.e., H_3/H_2 = 1.0) and at inlet Mach numbers of approximately 0.25, 0.50, and 0.85 (design). As with the 30-deg airfoil, the 50-deg airfoil experienced negative incidence in the test. The negative incidence increased with Mach numbers to −6.6 deg at at a Mach number of 0.84 (design incidence was +2.3 deg).

Figure 42 summarizes average spanwise performance data obtained with the 50-deg airfoil pack. This figure illustrates that static pressure rise decreased and total pressure loss increased sharply with increasing Mach number. These trends are indicative of operation at choke (negative) incidence with a high loaded airfoil.

Spanwise distributions of total pressure loss and exit air angle are presented in Figure 43 for three test Mach numbers. It can be seen that there is a large deg of overturning near the endwall due to the strong cross-channel pressure gradient of this highly cambered airfoil. Whereas Mach number appeared to have little effect on air angle distributions, total pressure loss was a very strong function of Mach number. In fact, at a Mach number of 0.84,. midspan losses were as high as those at the endwall. These high losses were due to the complete choking of the cascade, as illustrated by the airfoil pressure distribution in Figure 44. The entire suction surface and part of the pressure surface are supersonic ($P_S/P_T < 0.528$). Figure 44 also shows the effect of negative incidence with the suction surface minimum pressure point shifted back and lower pressures on the pressure surface than on the suction surface near the leading edge.

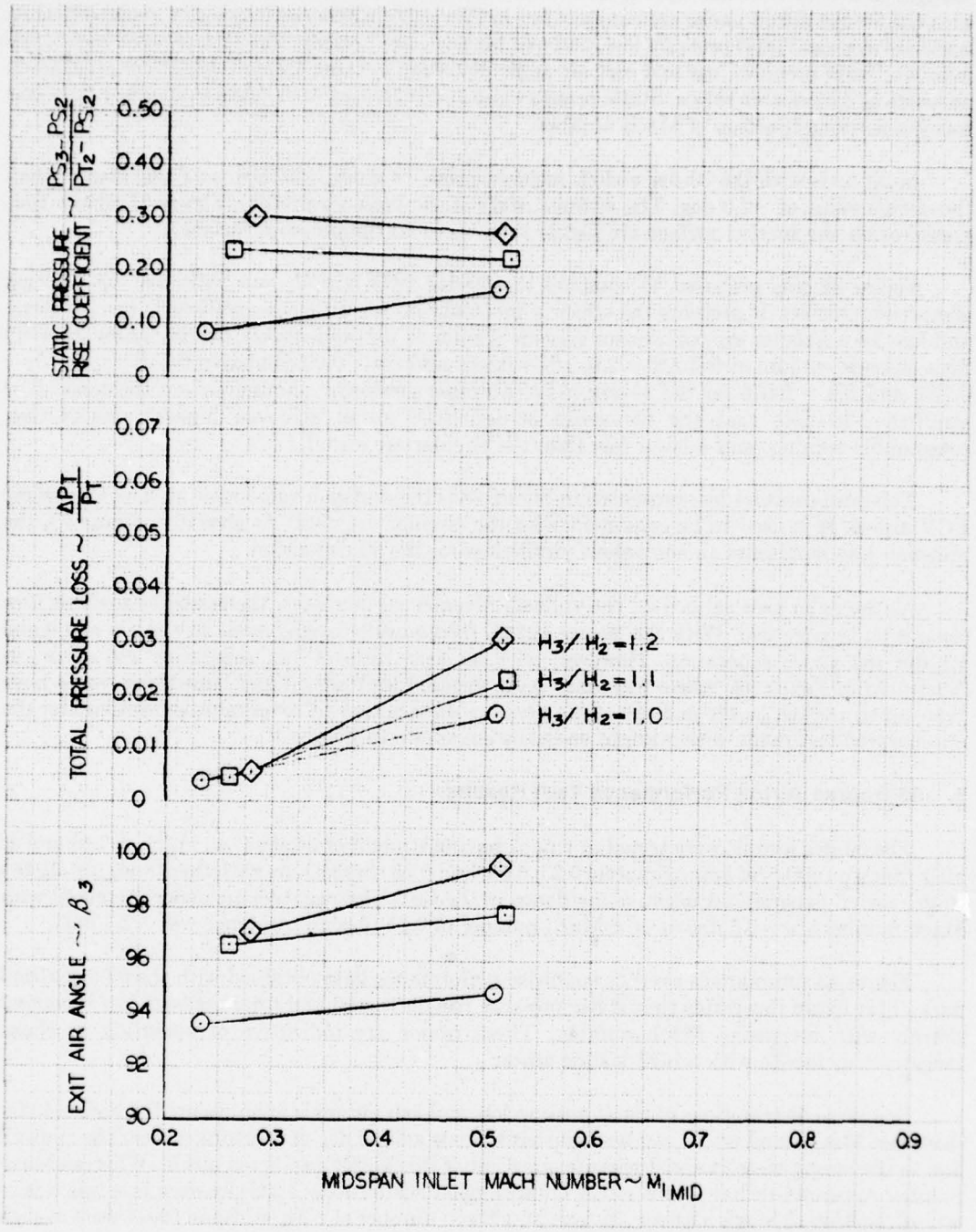


Figure 36. 30-deg EGV Average Performance Data Referenced to Midspan Inlet Total Pressure

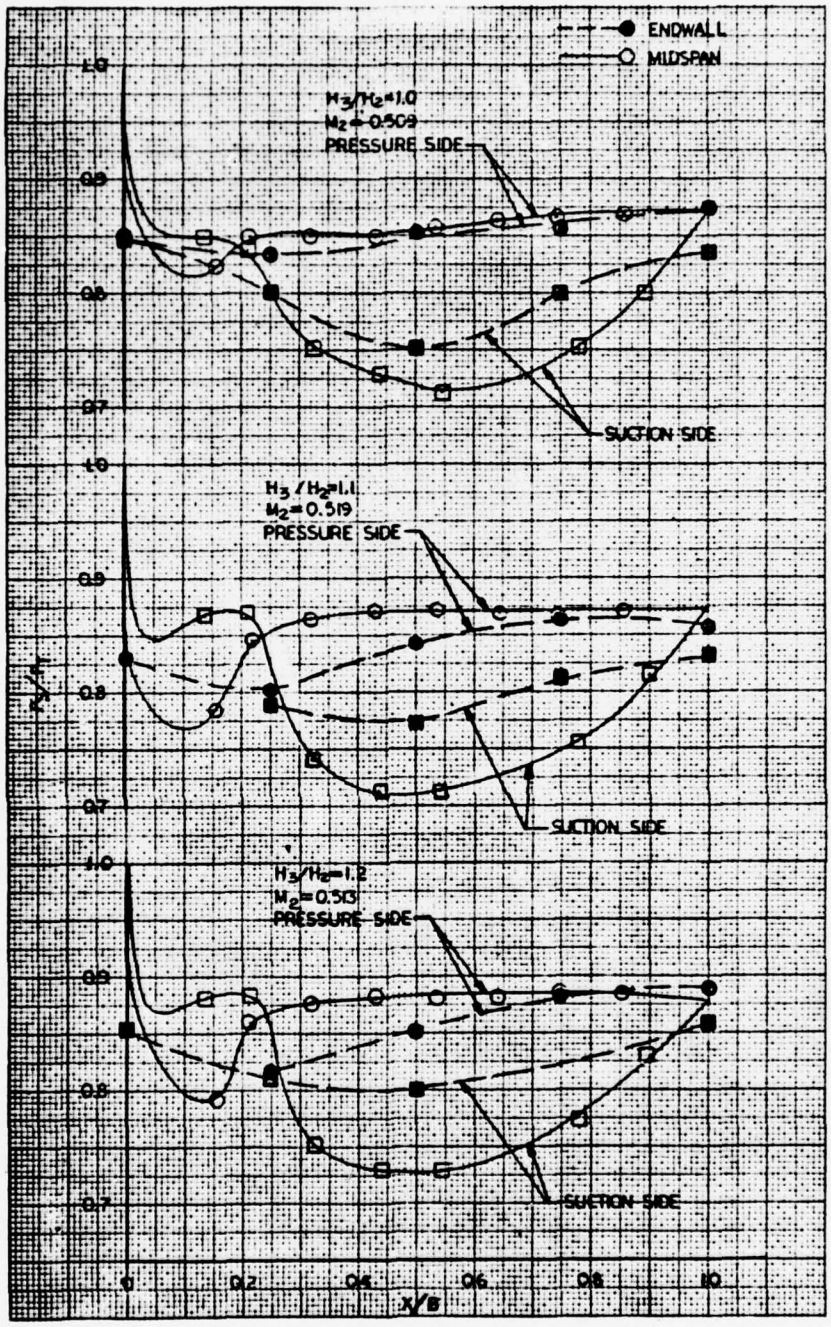


Figure 37. 30-deg EGV Airfoil Pressure Distribution (β_2 = 62.5 deg)

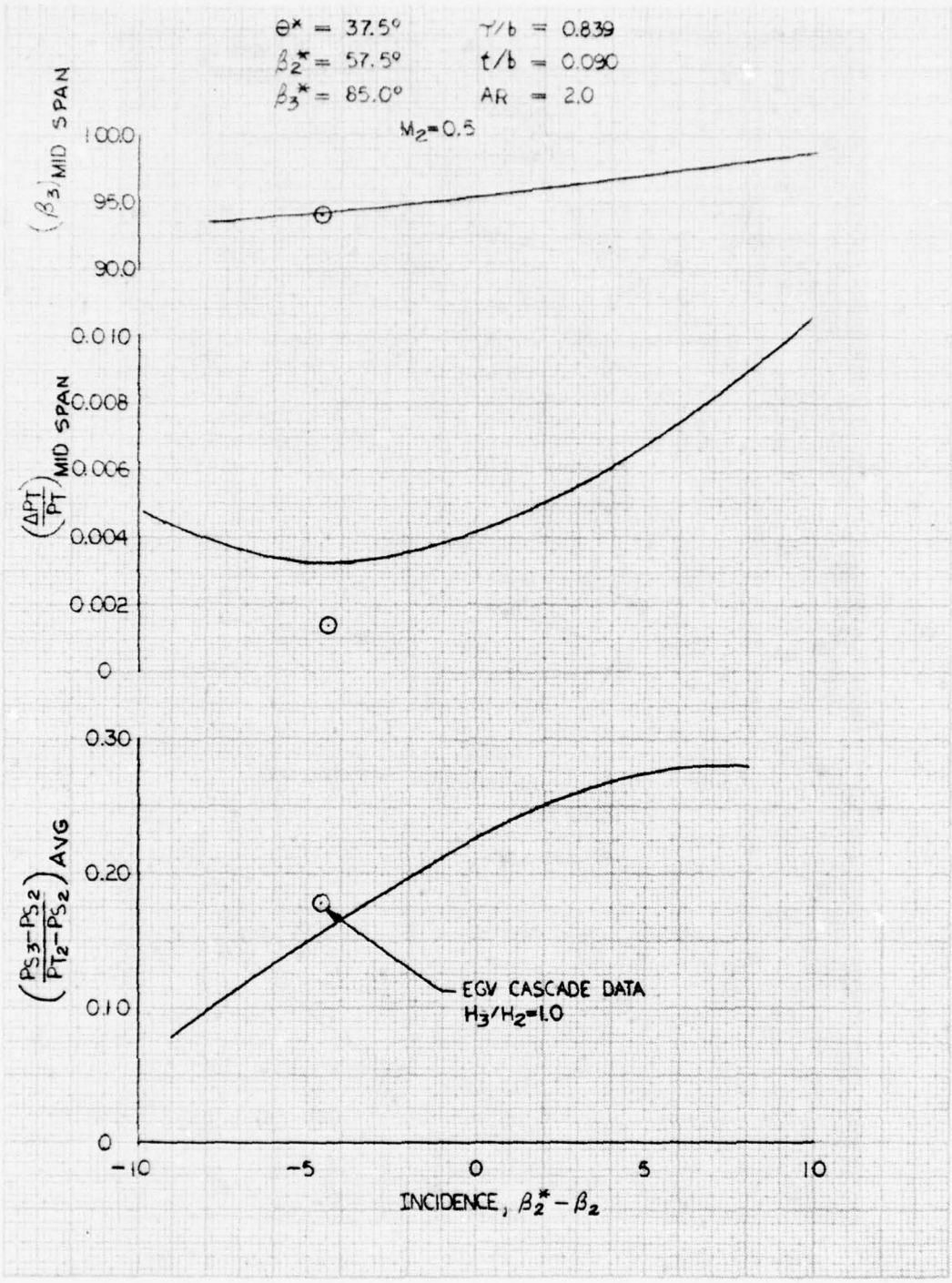


Figure 38. Effect of Incidence on Circular Arc Compressor Cascade Performance

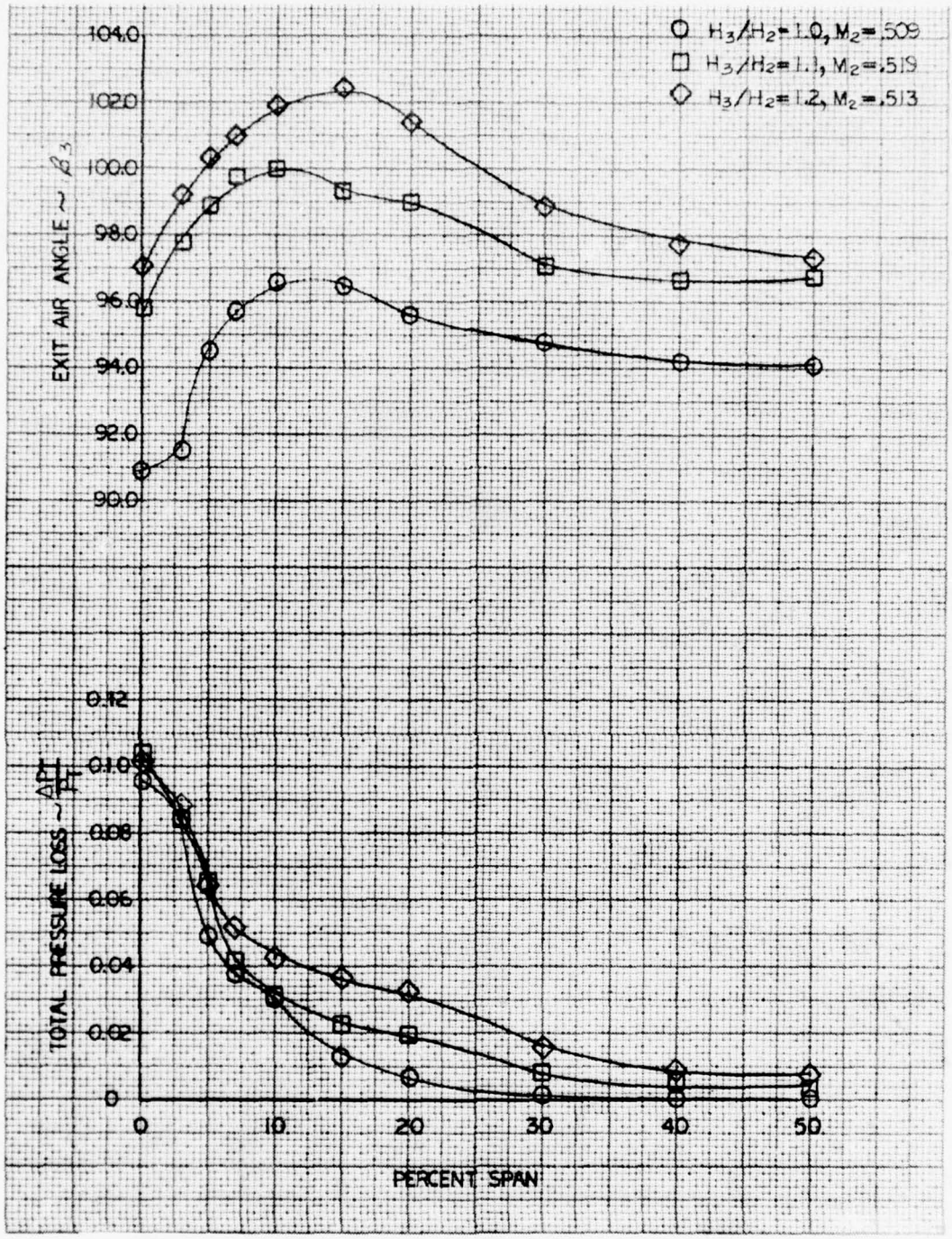


Figure 39. 30-deg EGV Spanwise Exit Air Angle and Loss Distribution

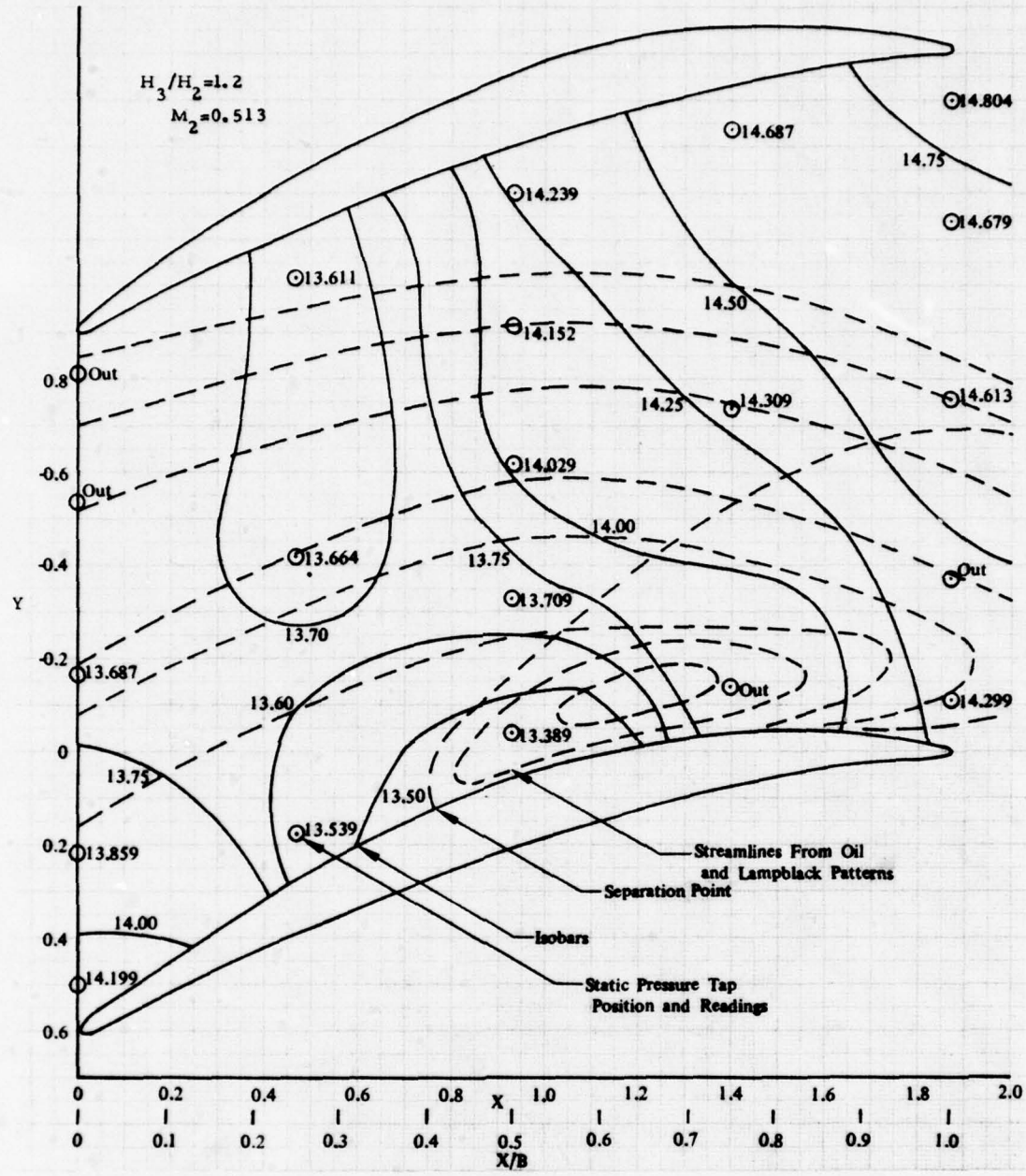


Figure 40. 30-deg EGV Endwall Flow and Pressure Patterns (H_3/H_2 = 1.2, M_2 = 0.513)

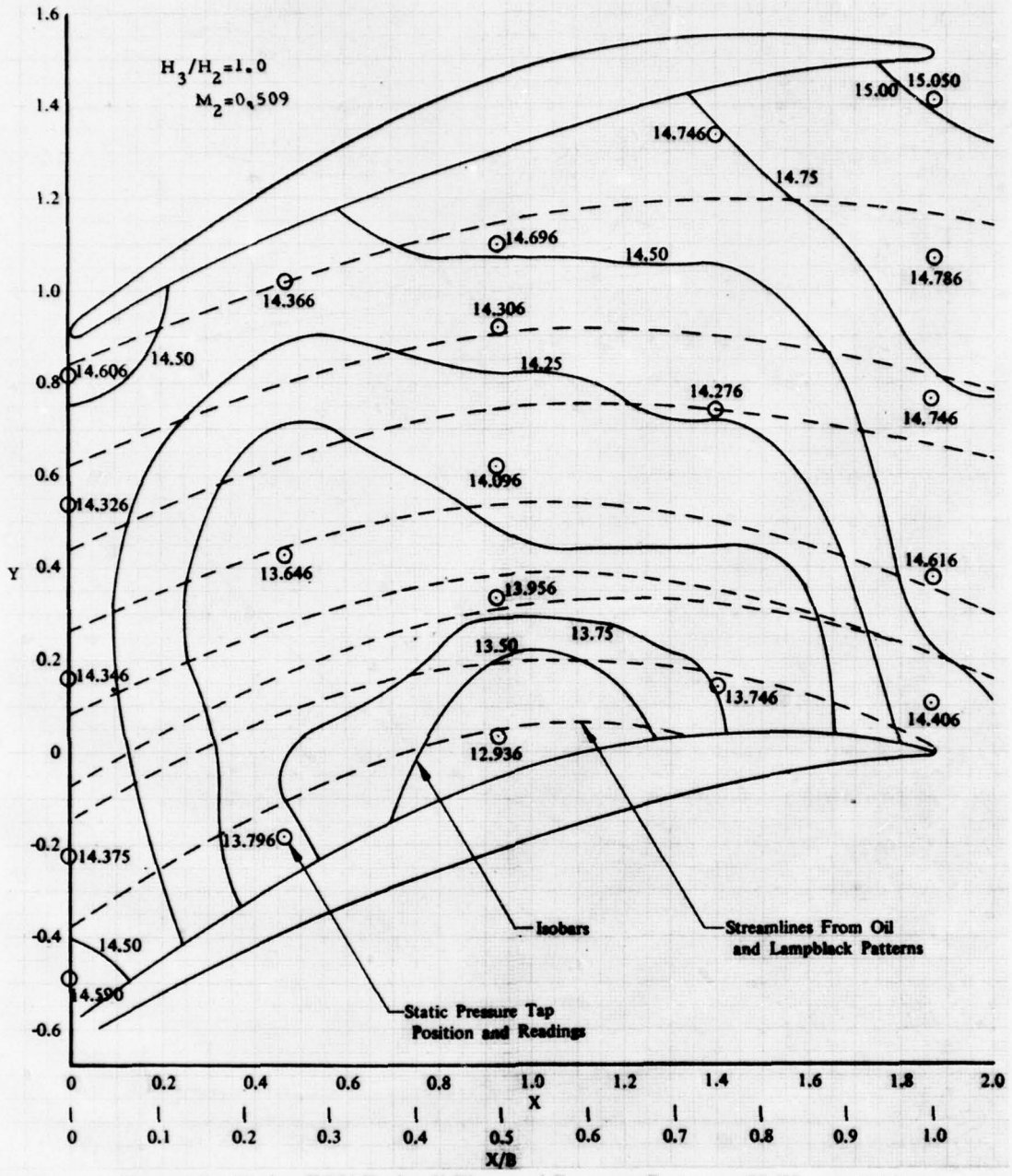


Figure 41. 30-deg EGV Endwall Flow and Pressure Patterns (H_3/H_2 = 1.0, M_2 = 0.509)

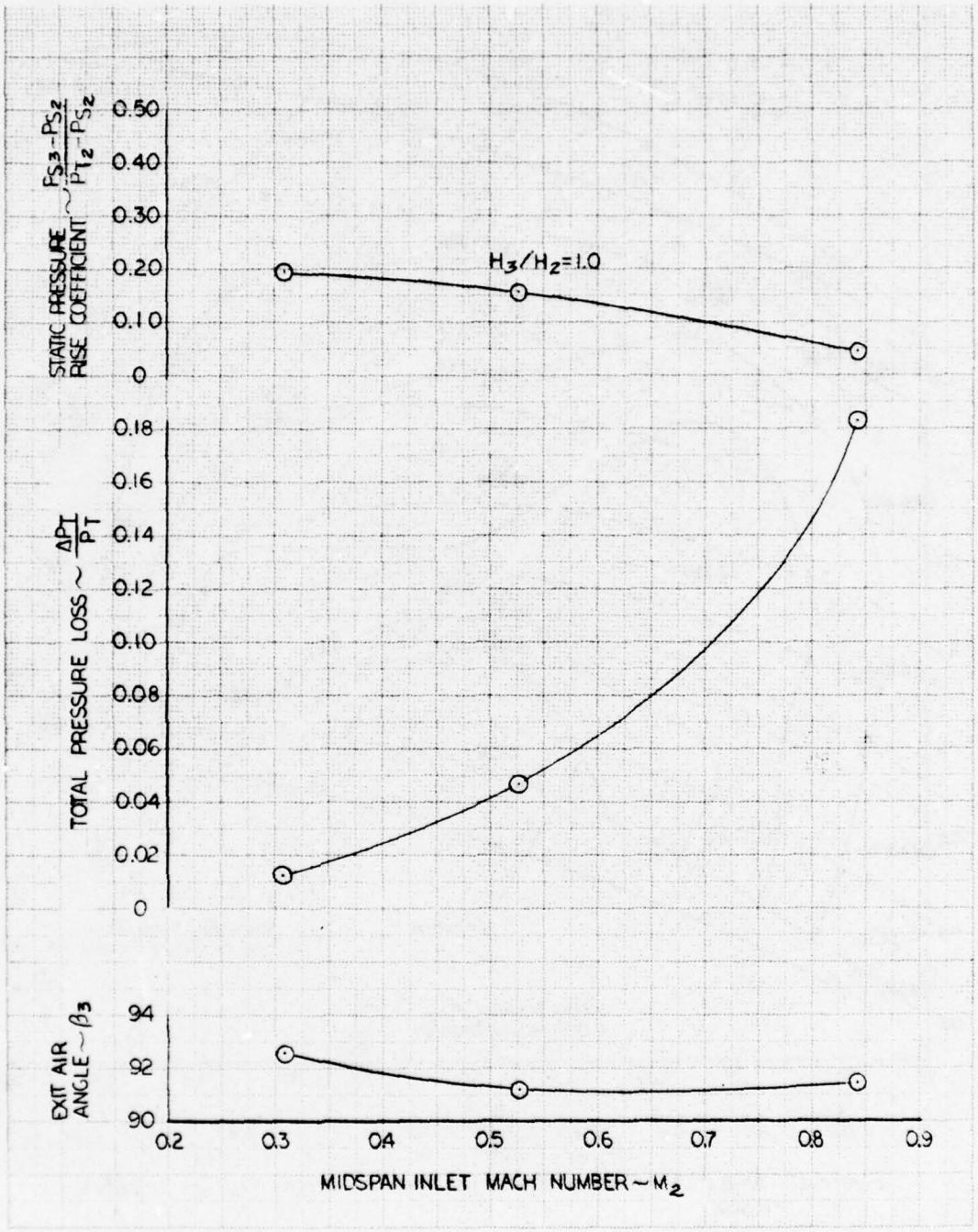


Figure 42. 50-deg EGV Average Performance Data Referenced to Midspan Inlet Total Pressure

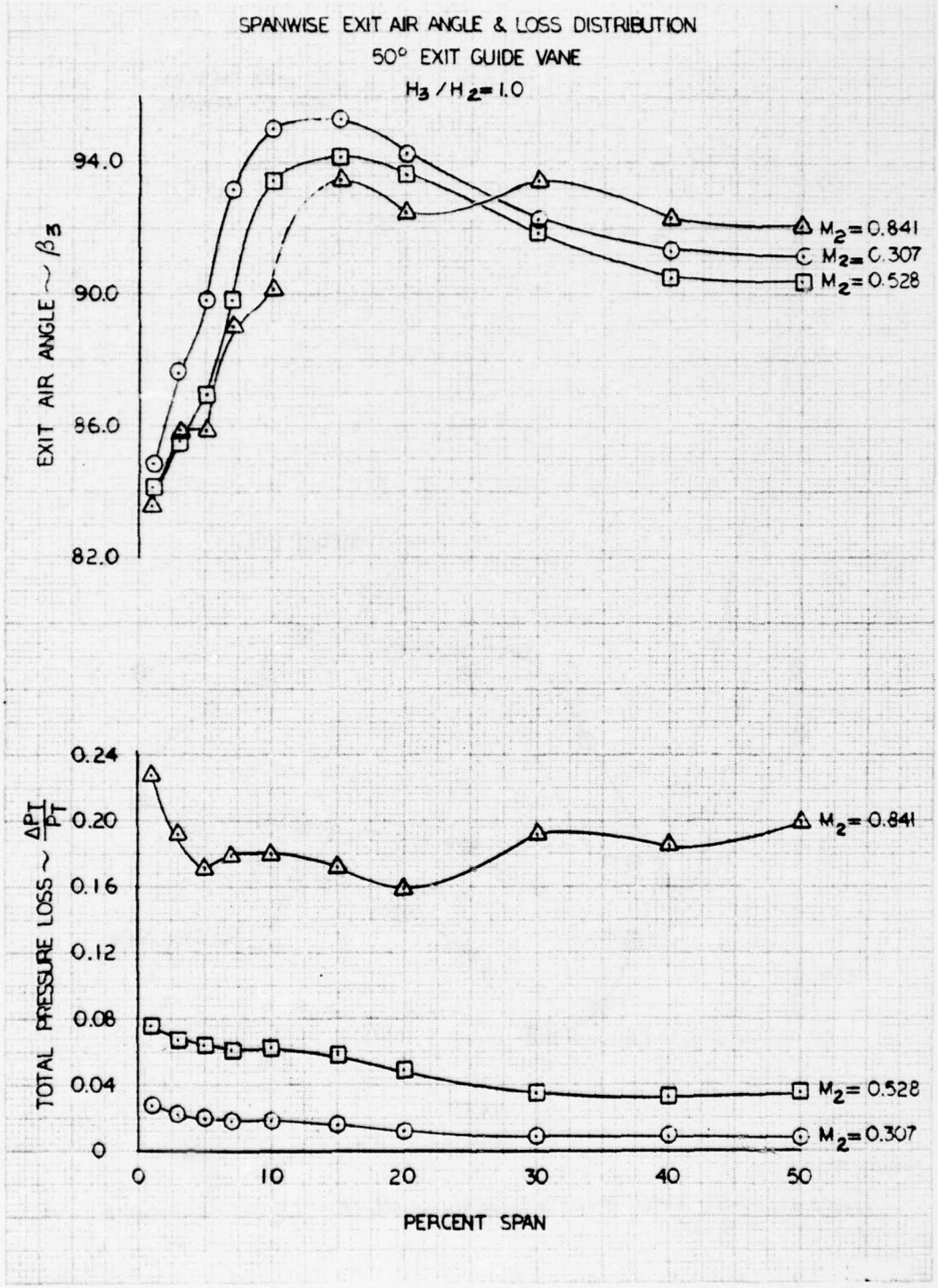


Figure 43. 50-deg EGV Spanwise Exit Air Angle and Loss Distribution for (H_3/H_2 = 1.0)

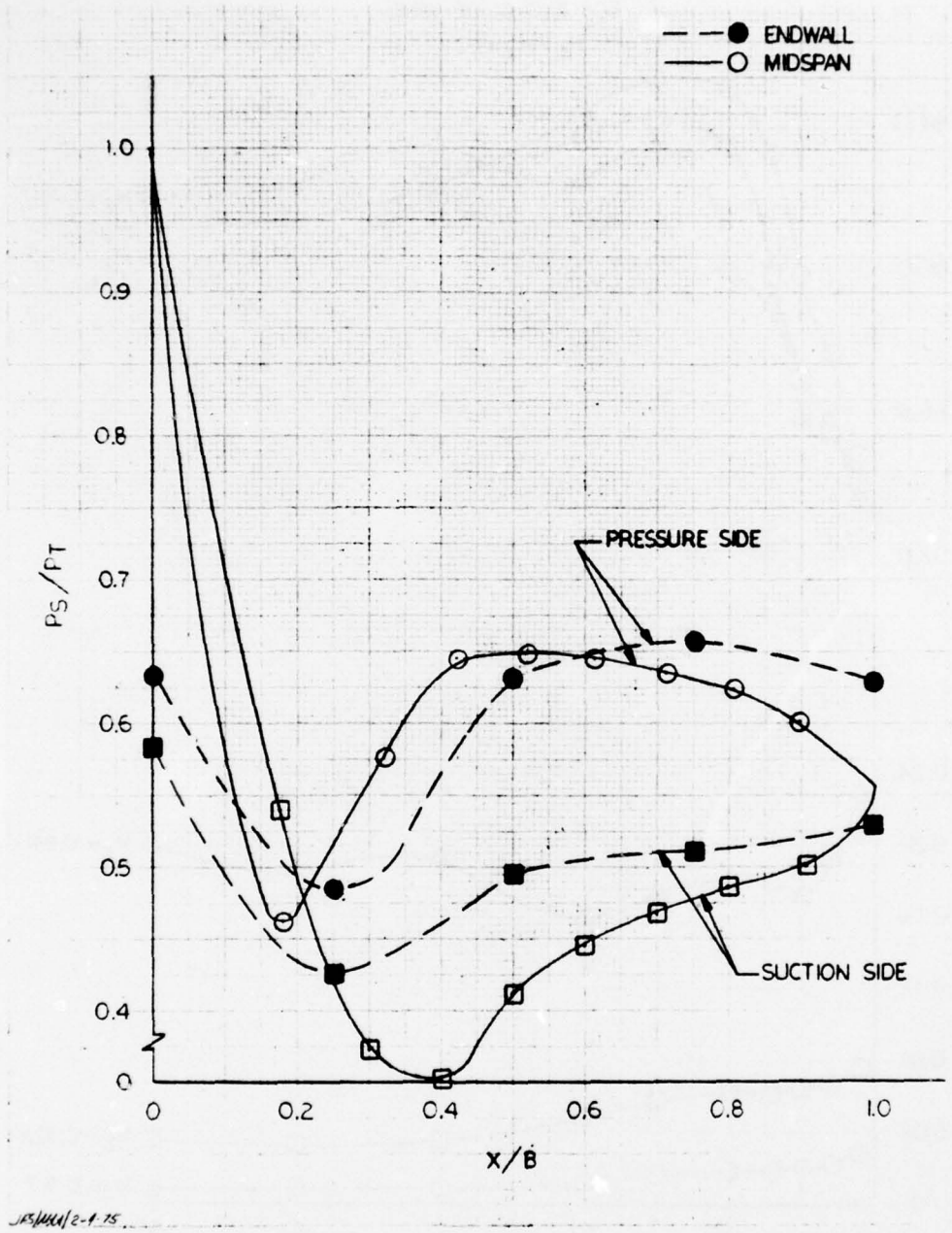


Figure 44. 50-deg Airfoil Pressure Distribution (H_3/H_2 = 1.0, β_2 = 48.6 deg, M_2 = 0.841)

Endwall static pressure distributions and boundary layer streamline patterns are presented in Figure 45 for M_2 = 0.84. The strong cross-channel pressure gradient and sharply overturned streamlines, previously indicated by the spanwise air angle distribution, are obvious.

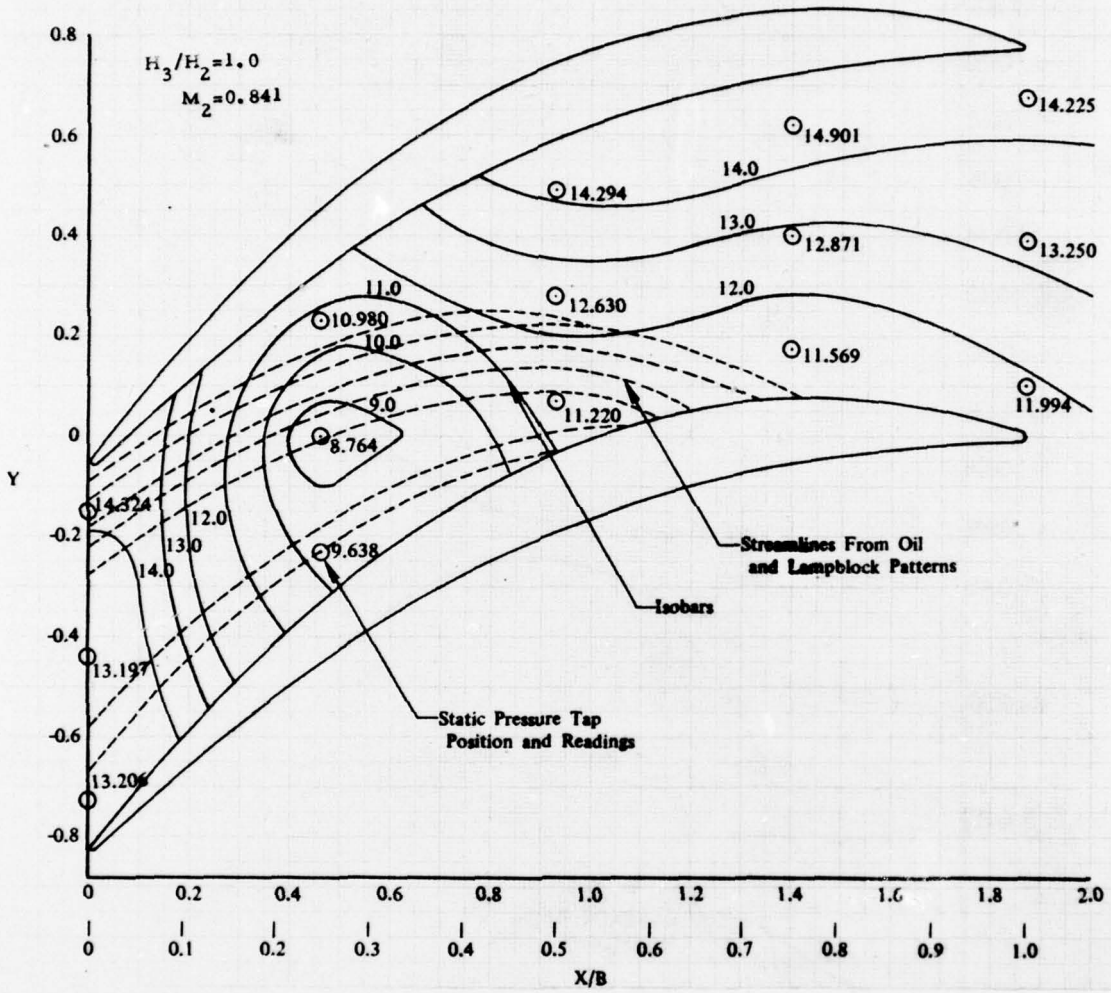


Figure 45. 50-deg EGV Endwall Flow and Pressure Patterns (H_3/H_2 = 1.0, M_2 = 0.841)

The high camber and inlet Mach number made the 50-degree airfoil very sensitive to choke incidence. Figure 46 illustrates this sensitivity for a circular arc compressor cascade design similar to the 50-degree EGV. It can be seen that an incidence of −6.6 degree is well beyond the choking point for the circular arc airfoil and hence, this level of negative incidence would result in high losses and low pressure rise coefficients as were obtained with the 50-degree EGV. Therefore, the data from tests of the 50-degree airfoil with −6.6 degree incidence are not representative of the airfoil's true potential.

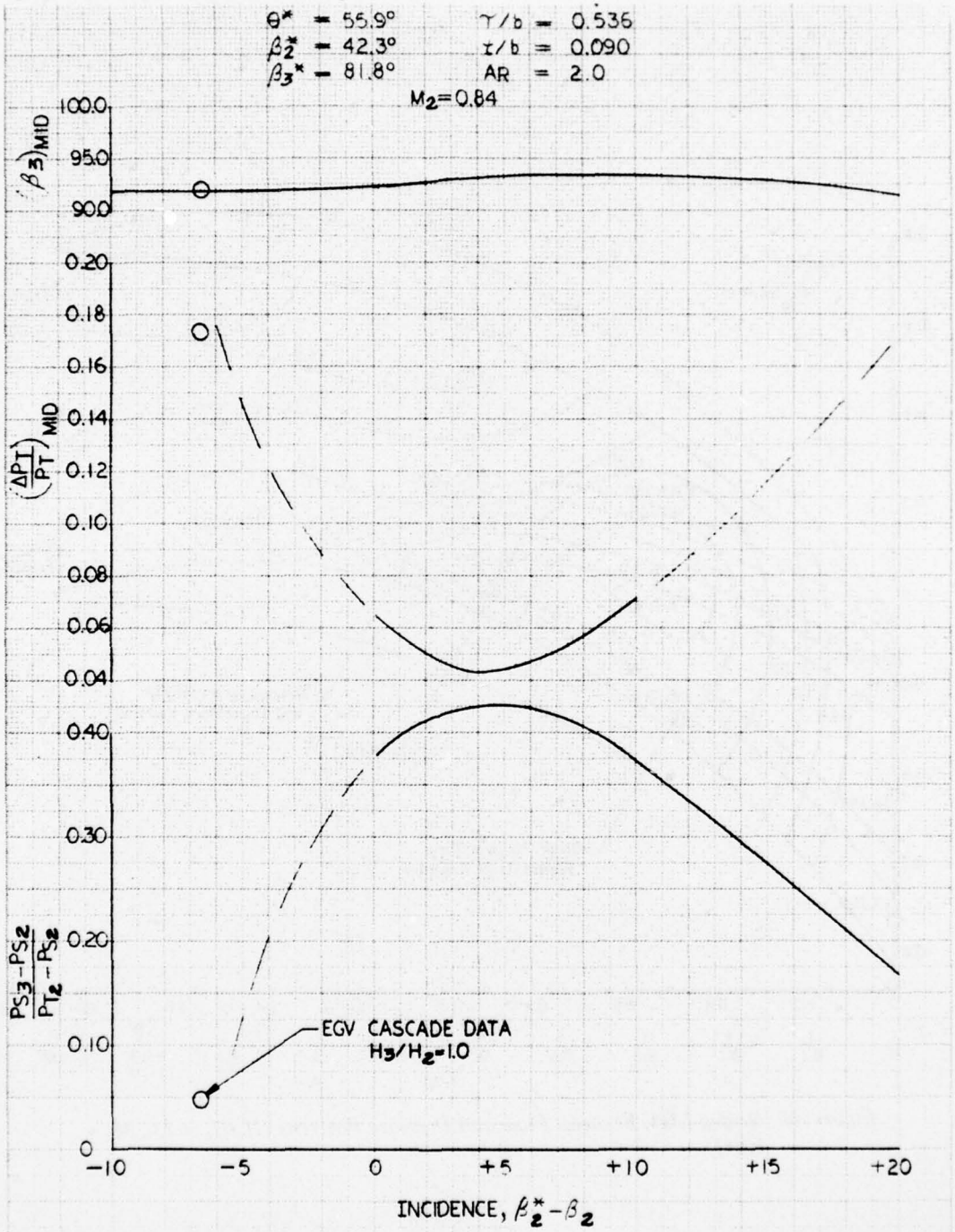


Figure 46. Effect of Incidence on Circular Arc Compressor Cascade Performance

4. 40-Degree Airfoil Performance Test Results

The 40-deg airfoil tests were conducted in two separate series, which occurred before and after the flow visualization tests (reported in Section B). In the first series of tests, the 40-deg airfoils were tested at inlet Mach numbers of approximately 0.25 and 0.675 (design) and with axial area expansion ratios of 1.0 and 1.1. In the first test series, data were obtained with positive and negative incidence. Figures 47 and 48 show the effect of positive and negative incidence on airfoil pressure distributions. In Figure 47, it can be seen that the pressure distributions, obtained with a 3.7 deg negative incidence angle (design incidence was +2 deg), are similar to those measured for the 30- and 50-deg airfoils, i.e., near the leading edge the static pressures are lower on the pressure side of the airfoil than those on the suction side. Figure 48 shows that a positive incidence of 7 deg causes very low static pressures on the suction side of the airfoil near the leading edge.

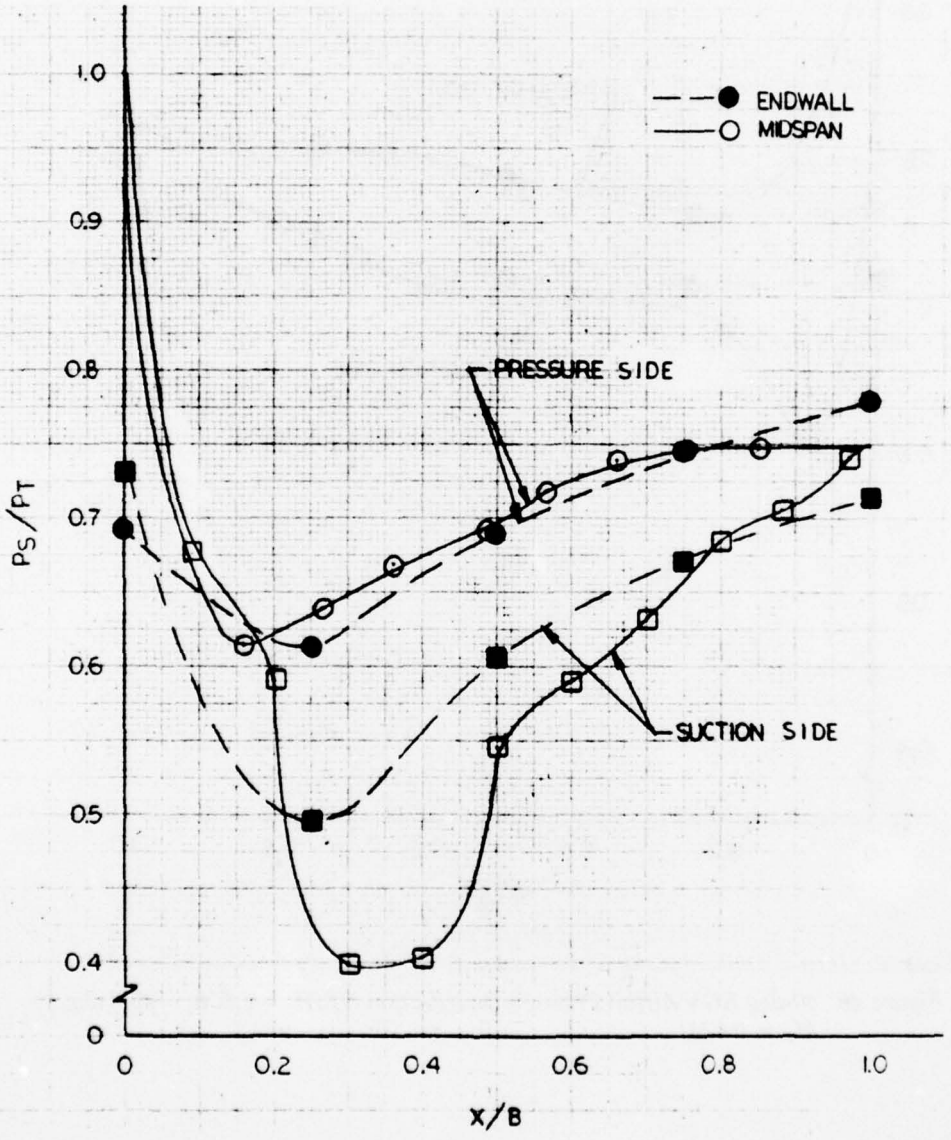


Figure 47. 40-deg EGV Airfoil Pressure Distribution ($H_3/H_2 = 1.1$, $\beta_2 = 55.7$ deg, $M_2 = 0.671$)

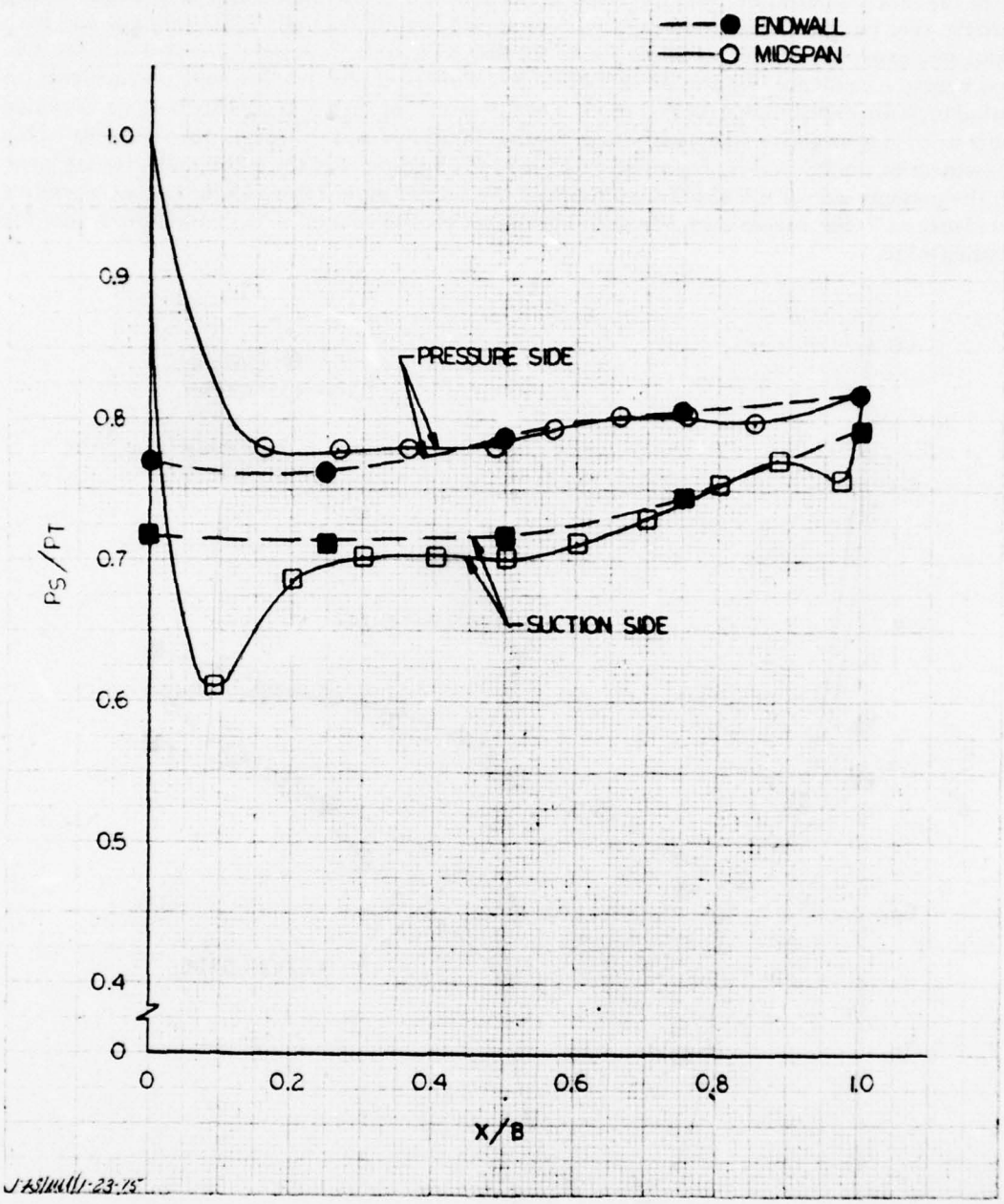


Figure 48. 40-deg EGV Airfoil Pressure Distribution (H_3/H_2 = 1.0, β_2 = 45.0 deg, M_2 = 0.634)

Average spanwise performance data for the initial 40-deg airfoil tests are summarized in Figure 49. The high loss and low pressure rise obtained at a Mach number of 0.671 and an axial area expansion ratio of 1.1 were attributed to negative incidence. At a comparable Mach number (0.634) and no axial area expansion ratio, but with positive incidence, the static pressure rise was higher, and the total pressure loss was less.

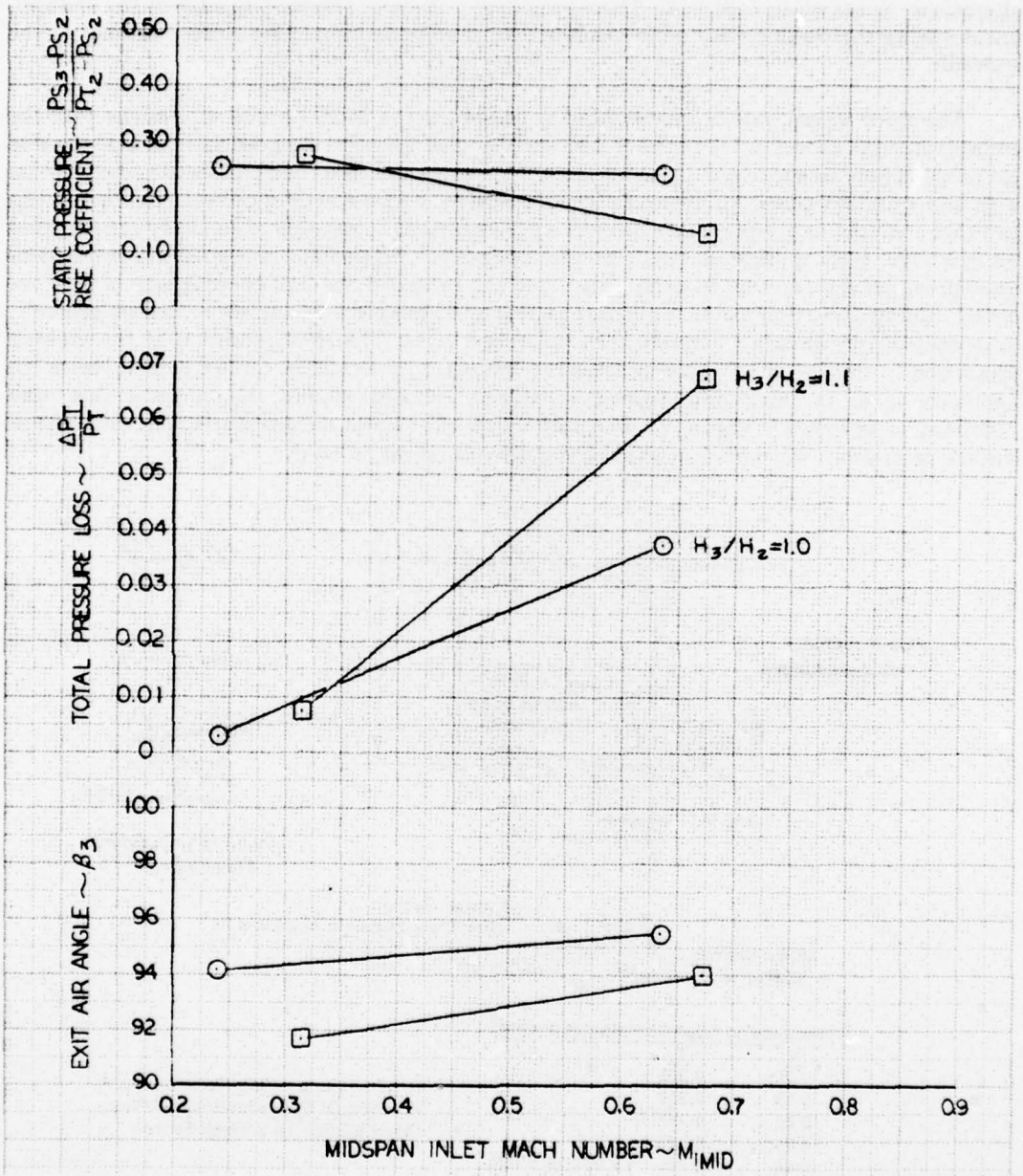
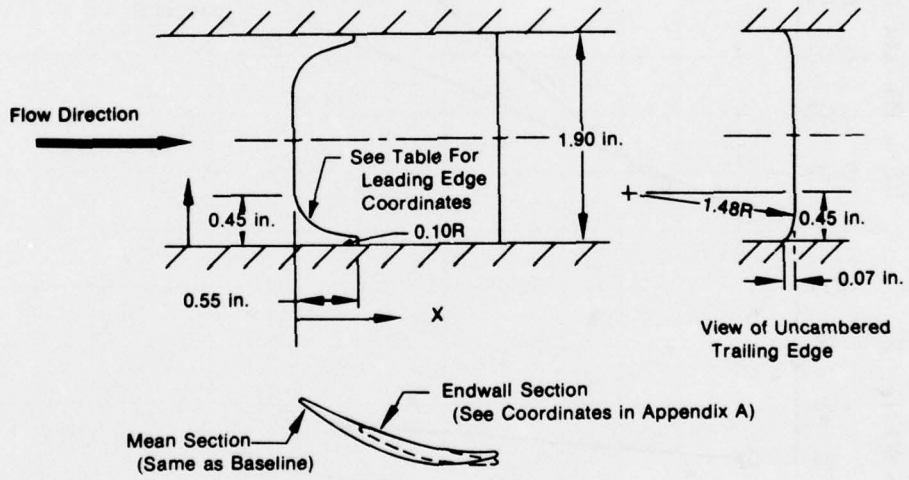


Figure 49. 40-deg EGV Average Performance Data Referenced to Midspan Inlet Total Pressure (7-Airfoil Cascade)

In the second series of tests with the 40-deg airfoil, the number of airfoils in the pack was increased from 7 to 13 to increase the width of the inlet flow channel and thereby obtain the design incidence flow angle (+2 deg). In this second series of tests, three configurations of a 40-deg straight endwall (H_3/H_2 = 1.0) cascade pack were evaluated. The first configuration was simply a retest of unmodified airfoils in the 13-airfoil pack.

The second model, referred to as Modification (Mod) 1, contained only airfoil geometry alterations, as shown in Figure 50. These included cutback of the leading edge at the endwall, uncambering the trailing edge at the endwall, and reduction of suction surface camber at the endwall.

The third model, referred to as Mod 2, combined the Mod 1 airfoil alterations with the endwall changes shown in Figure 51. These endwall changes were designed to minimize the rate of change of flow area through the airfoil pack. Figure 52 shows the channel flow area distribution with and without endwall protrusions. The channel flow area distribution was modified by the addition of a fillet on the pressure side on the airfoil at an axial position of about 65% chord. Flow visualization tests indicated that it was desirable to continue the endwall protrusions downstream of the cascade; therefore, the fillet was extended one-half chord length beyond the airfoil trailing edge. Channel flow conditions near an airfoil pressure surface corner are generally unseparated and have a relatively thin boundary layer. Therefore, addition of the endwall protrusion in this "healthy" flow location (as opposed to the suction surface corner, where the boundary layer is thick and nearing separation) should modify the effective flow area distribution, as shown in Figure 52. The desirability of pressure surface protrusions over suction surface protrusions was also indicated in the flow visualization study.



Airfoil Leading Edge Coordinates (Inches)

X	Y	
0.05	0.305	
0.15	0.210	
0.25	0.157	
0.35	0.124	
0.45	0.106	Blend to 0.10R As Shown
0.55	0.0	

Linearly Blend Airfoil Thickness As A Function Of Spanwise Position From Mean Section To Endwall Section

Figure 50. Description of Mod 1 Configuration

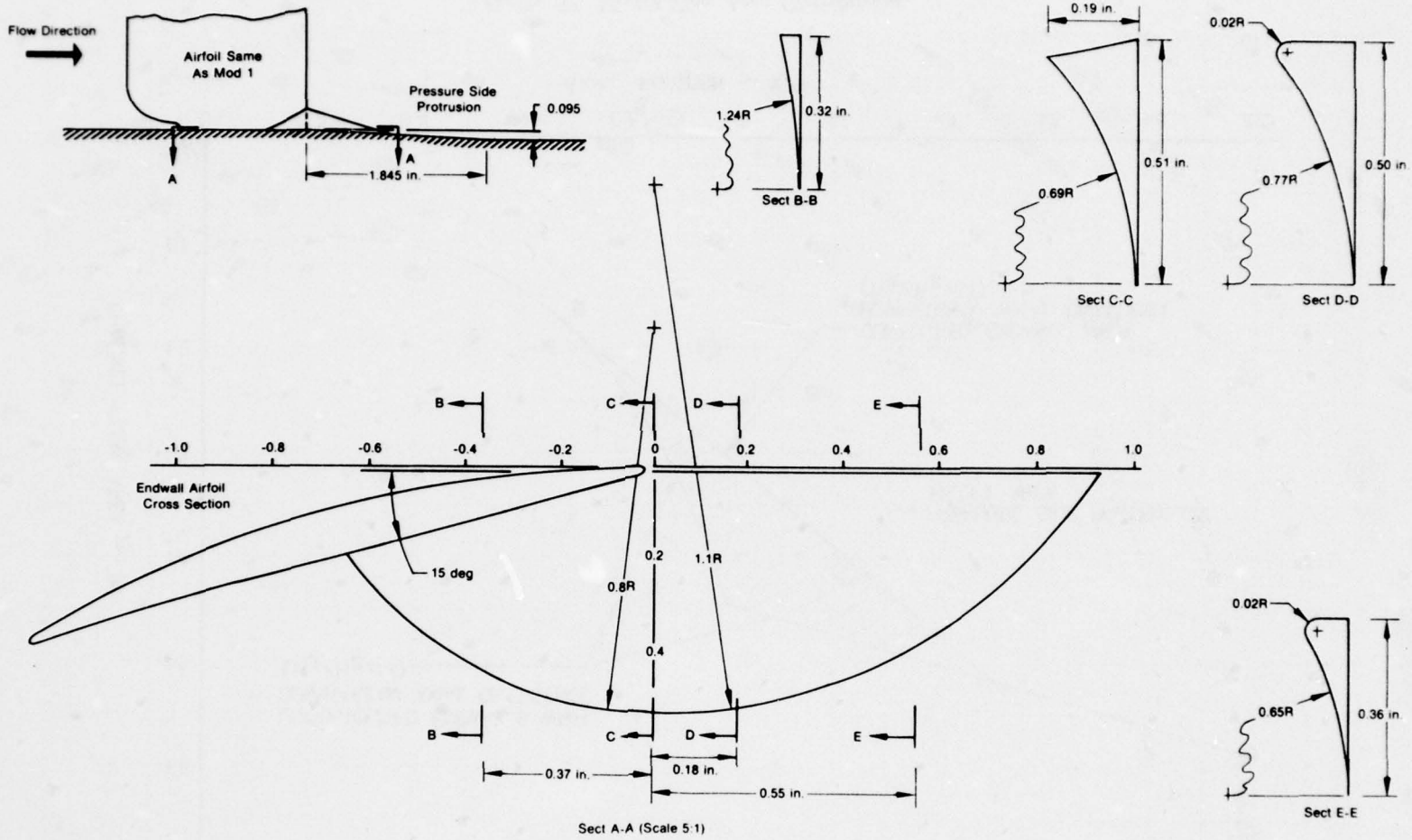


Figure 51. Description of Mod 2 Configuration

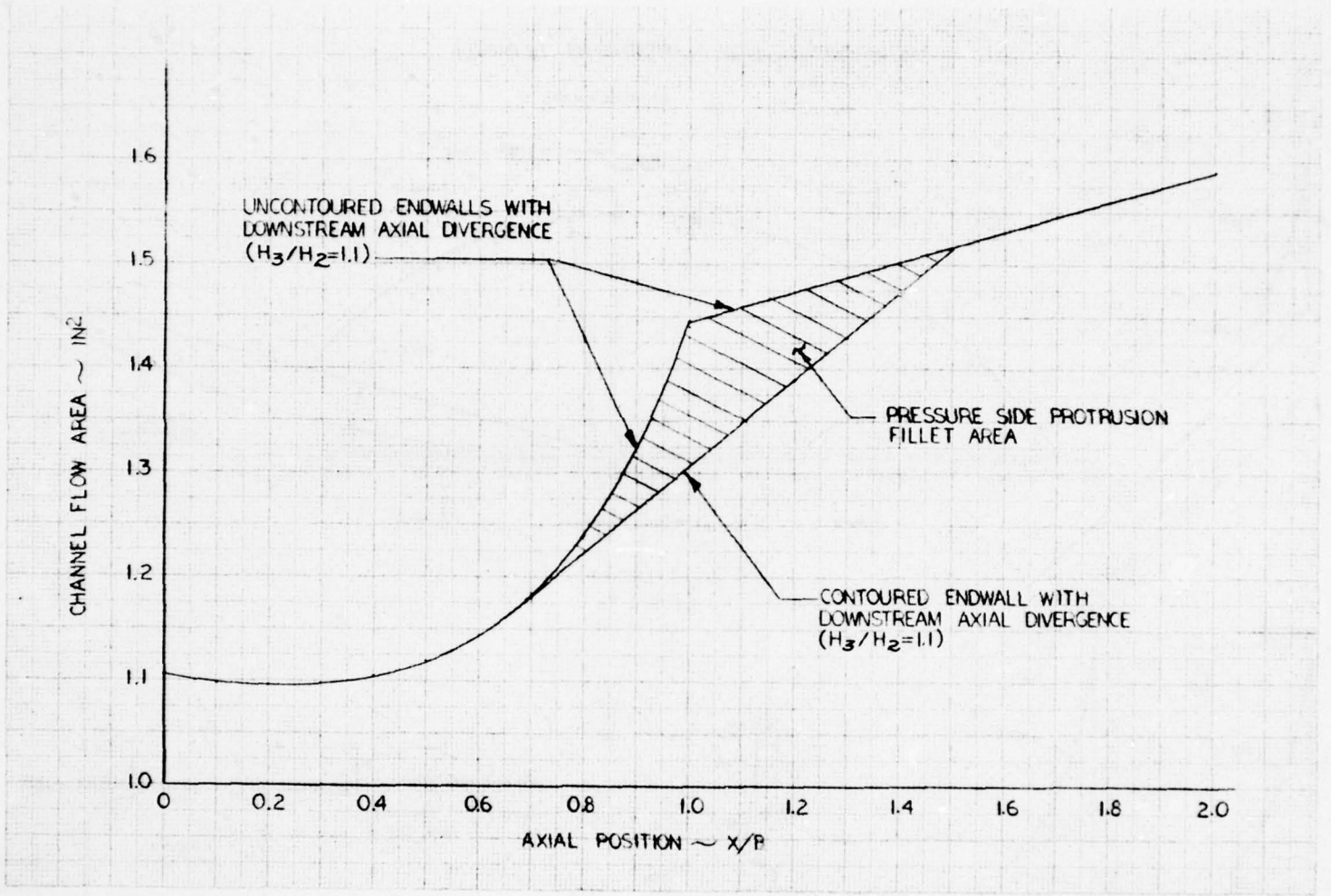


Figure 52. Mod 2 Flow Area Distribution

Figure 53 shows the static pressure distribution obtained with the baseline 40-deg airfoil in the second series of tests. Comparing this pressure distribution to those obtained in the first series of 40-deg airfoil tests with positive and negative incidence (and given in Figures 47 and 48) confirms that the airfoil was operating with near-design incidence.

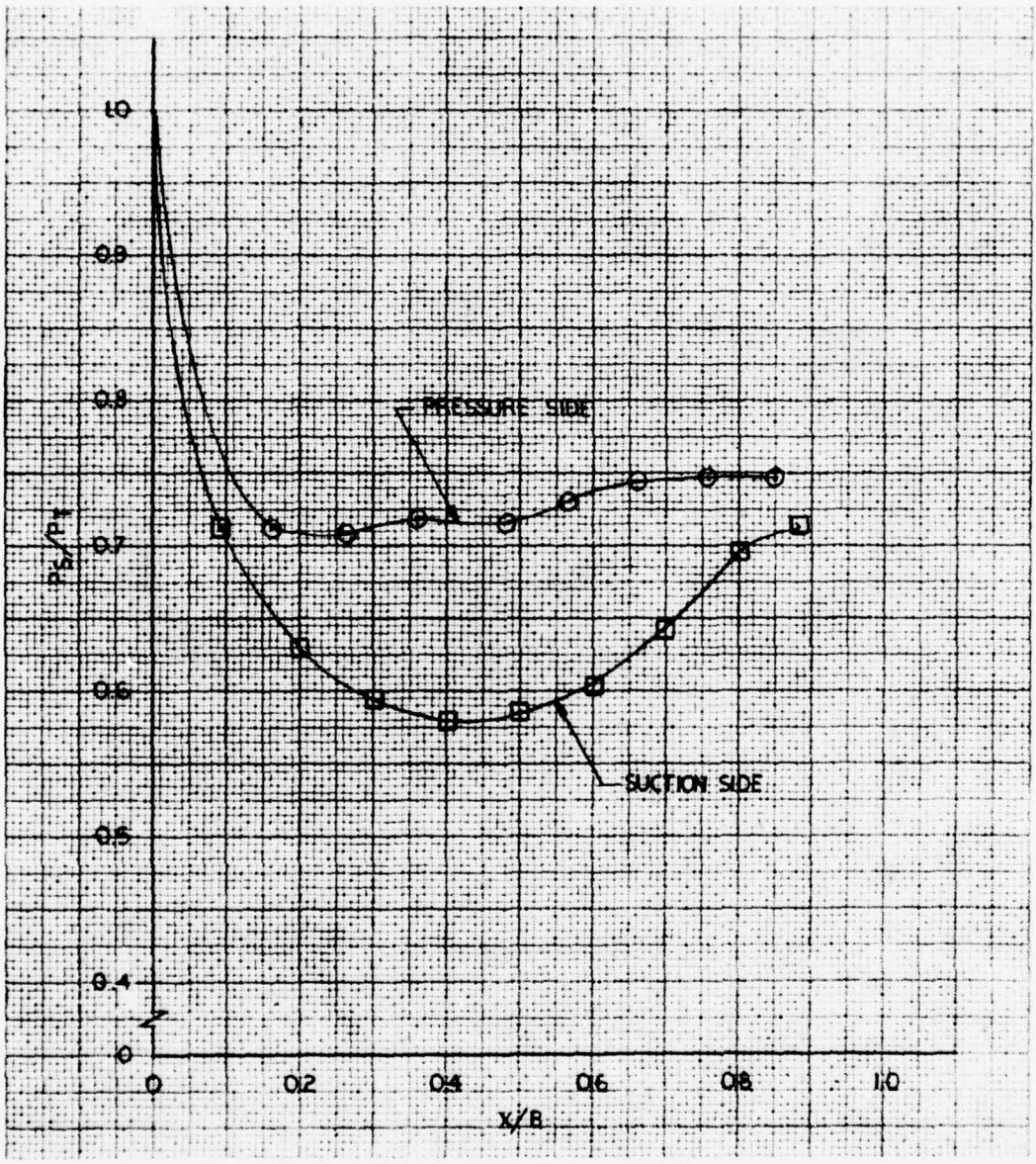


Figure 53. 40-deg EGV Airfoil Pressure Distribution (H_3/H_2 = 1.0, β_2 = 50 deg, M_2 = 0.702, Baseline Retest)

Figure 54 summarizes the average spanwise performance data obtained in the second series of tests with the 40-deg airfoil. It shows that static pressure rise was improved with modifications to both the airfoil and endwall. The largest improvement was obtained with alterations to both the airfoil and endwall, i.e., with the Mod 2 configuration.

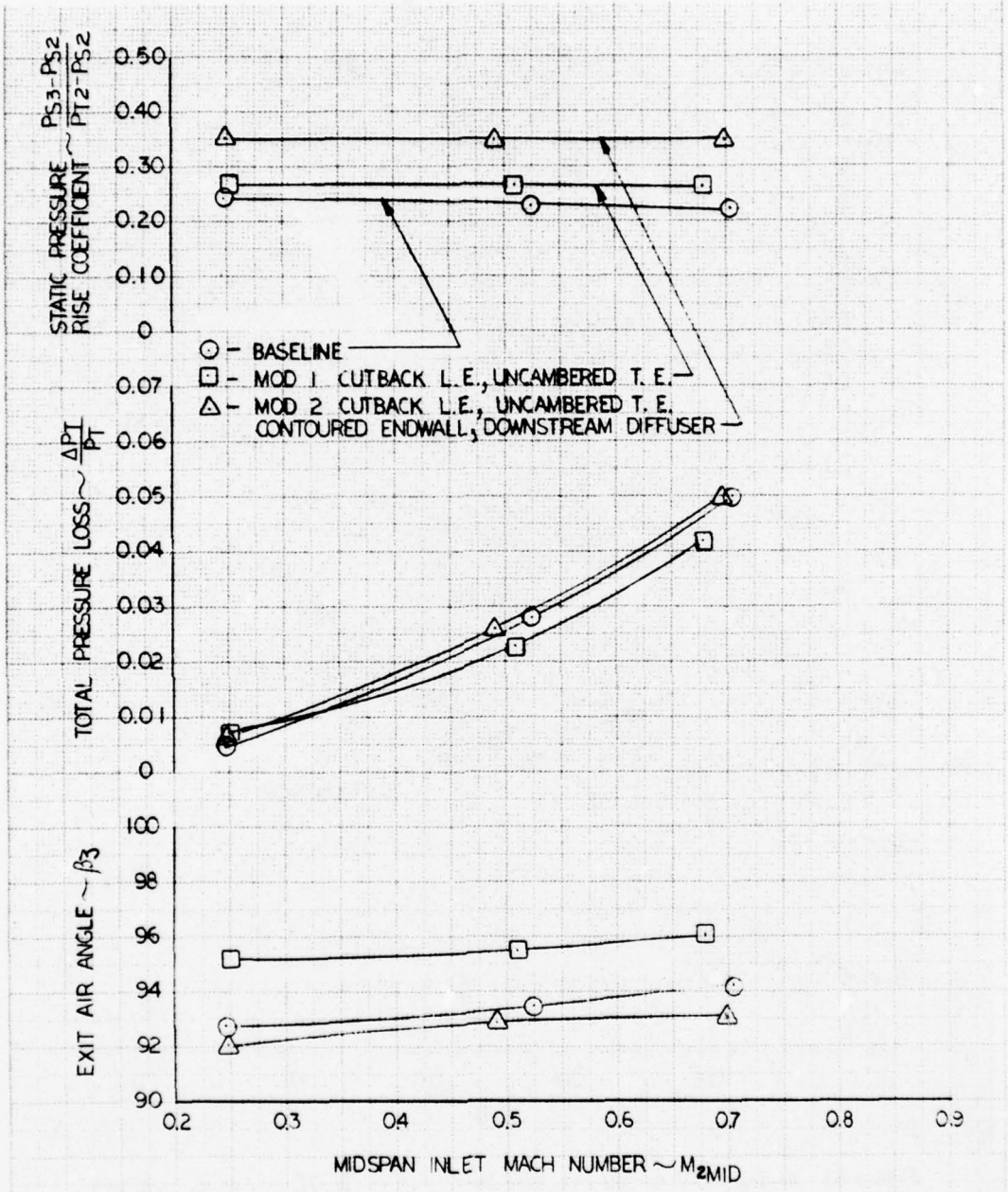


Figure 54. 40-deg EGV Average Performance Data Referenced to Midspan Inlet Total Pressure (13-Airfoil Cascade)

Spanwise distributions of total pressure loss and exit air angle presented in Figures 55 through 57 for inlet Mach numbers of 0.25, 0.50 and 0.675, respectively. It will be noted that data are presented for two exit measuring stations for the Mod 2 configuration. The first position was at the exit of the divergent section, and the second position was 0.2 in. behind the airfoil trailing edges. The traverse probe could get no closer than 9% span at the upstream position because of interference with the endwall protrusions.

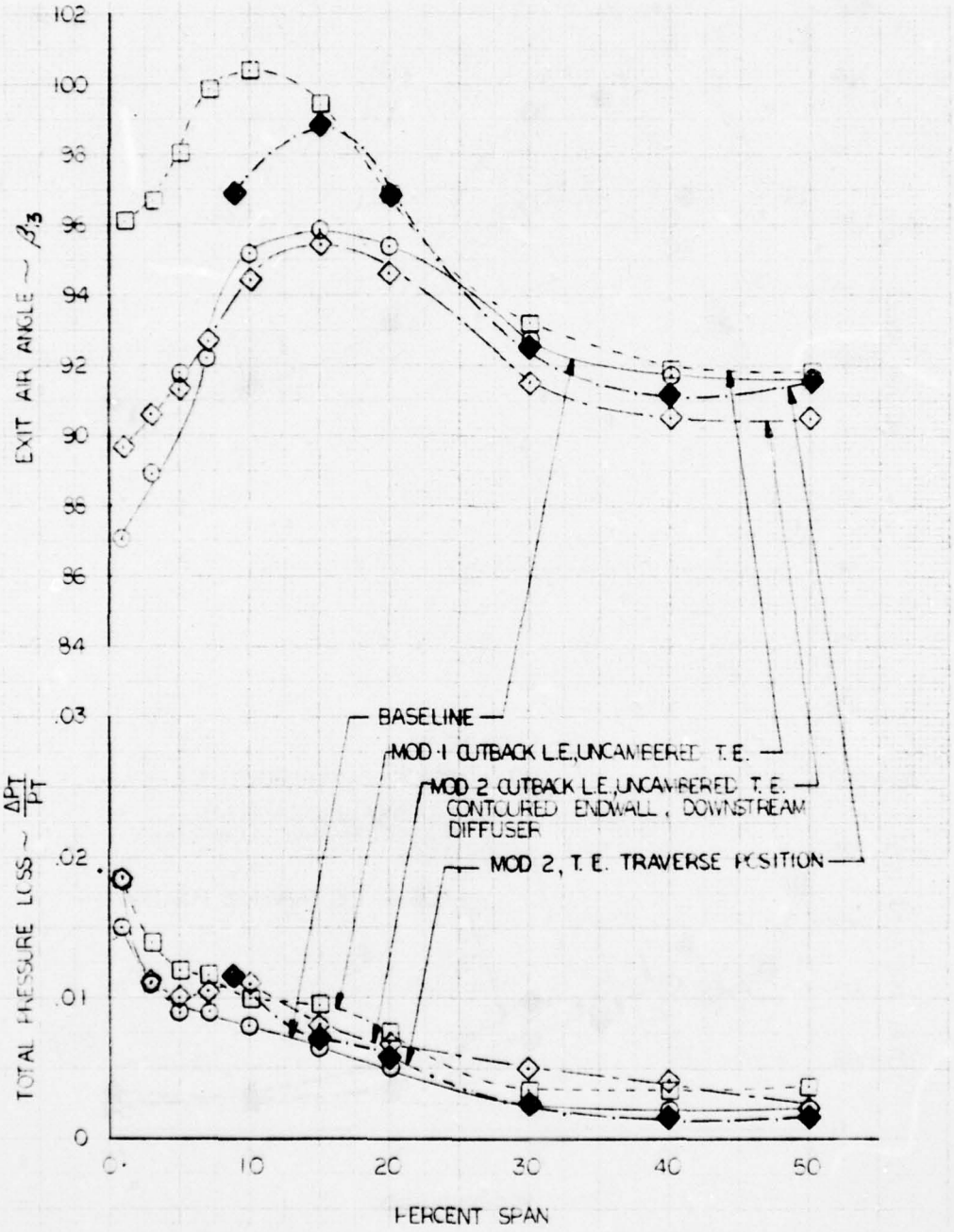


Figure 55. 40-deg EGV Spanwise Exit Air Angle and Loss Distribution (M_2 = 0.250)

Comparison of the total pressure loss distributions for the Mod 1 and baseline configurations shows that the airfoil modifications reduced the amount of span experiencing secondary loss, particularly at the higher Mach numbers. (See Figures 56 and 57.) Secondary loss extended all the way to midspan for the baseline configuration. However, with Mod 1, losses were nearly constant in the 30% to 50% span region. Similar loss measurements were obtained for the Mod 2 trailing edge traverse position.

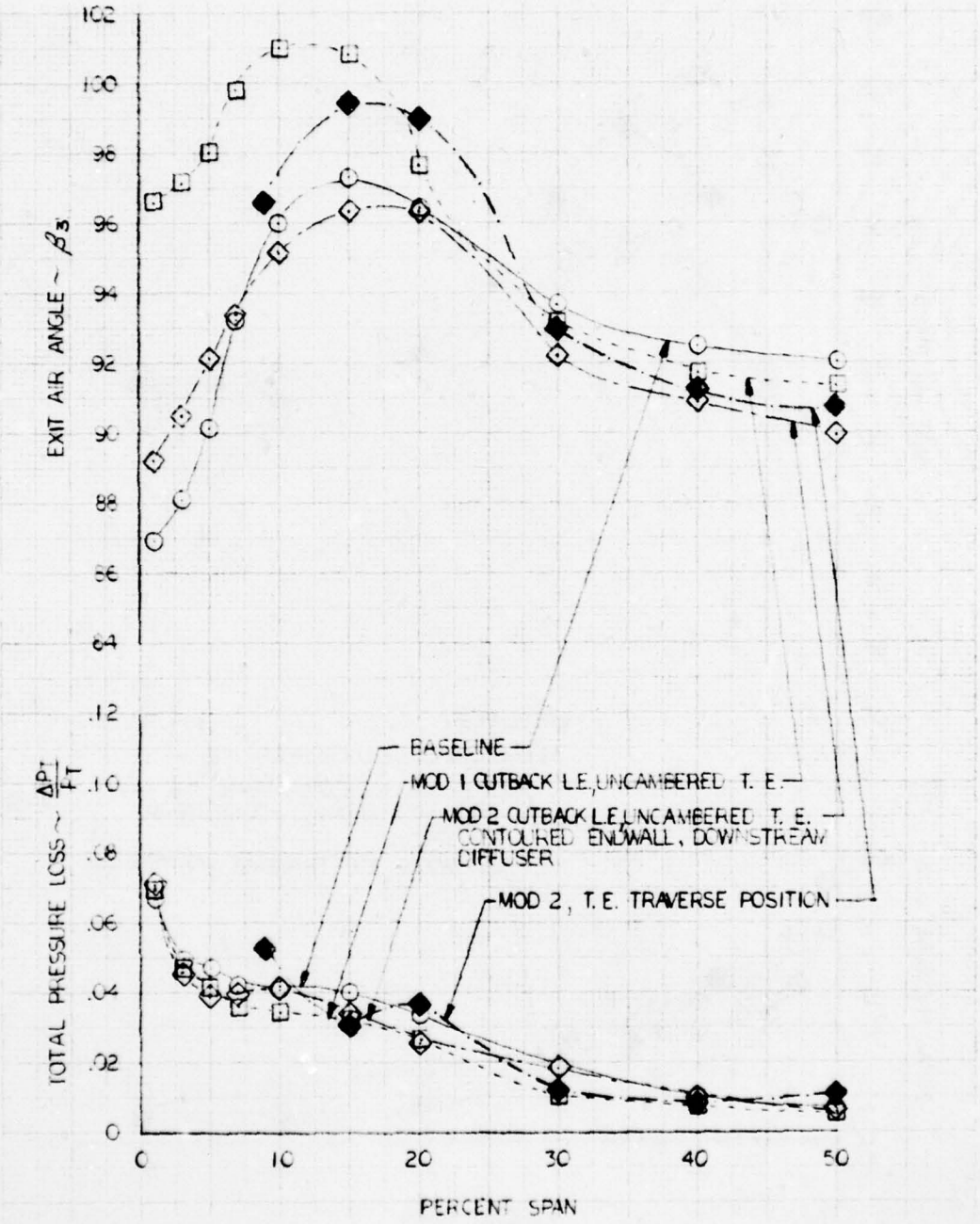


Figure 56. 40-deg EGV Spanwise Exit Angle and Loss Distribution (M_2 = 0.500)

Mod 1 overcompensated to airflow overturning near the endwall; however, midspan deviation was 1.25 deg less than the baseline at design conditions. Comparison of spanwise surveys of air angles taken near the Mod 2 cascade trailing edge at the exit of Mod 1 clearly shows that the air angle did not change appreciably from 30% to 50% span due to addition of endwall protrusions. However, between 9% and 20% span, two observations can be made: (1) the endwall protrusions reduced the underturning of Mod 1 by 2 to 3 deg; and (2) the Mod 2 flow became more axial as it moved downstream.

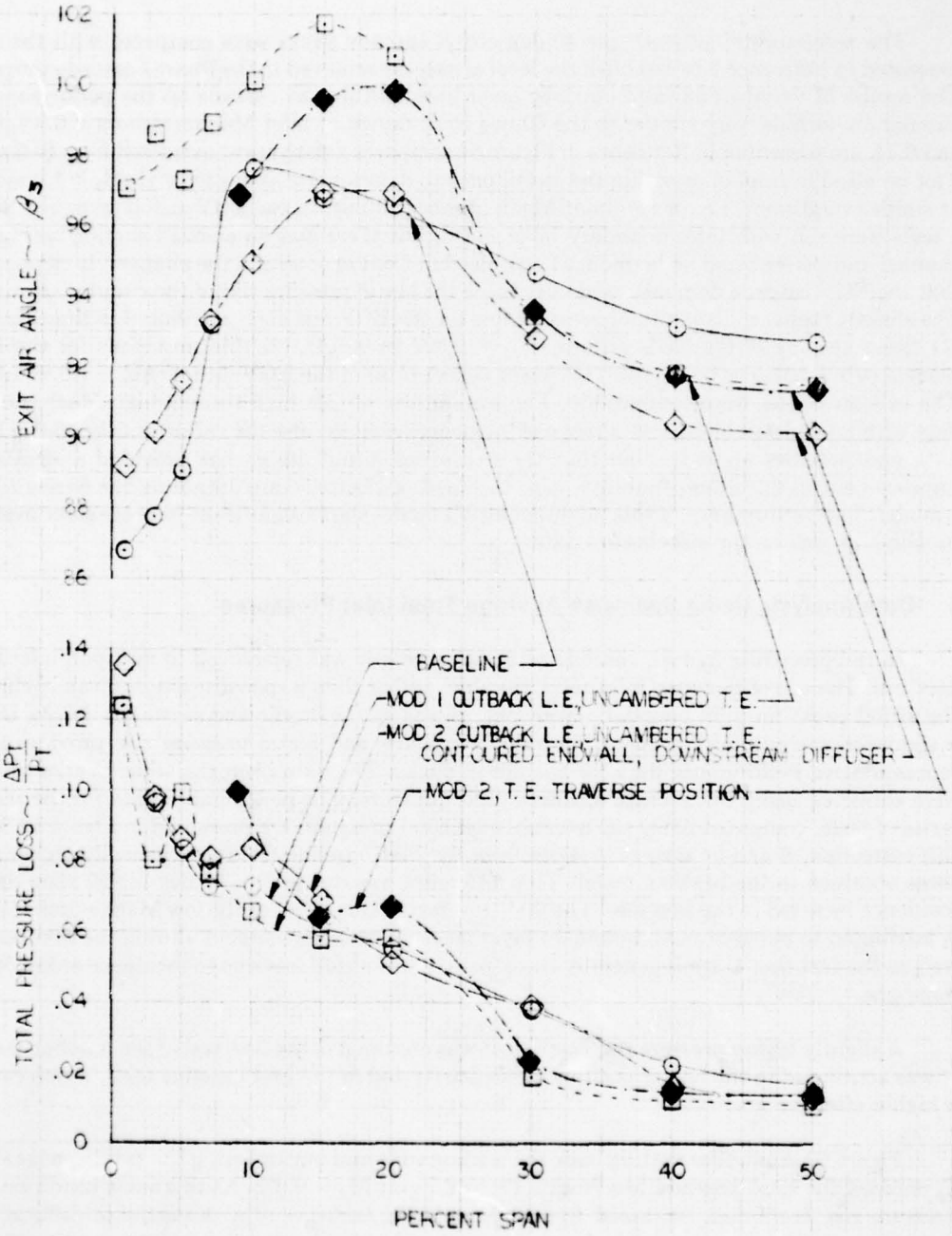


Figure 57. 40-deg EGV Spanwise Exit Air Angle and Loss Distribution (M_2 = 0.675)

AD-A060 343 PRATT AND WHITNEY AIRCRAFT GROUP WEST PALM BEACH FL G--ETC F/G 21/5
TURBINE EXIT GUIDE VANE PROGRAM.(U)
NOV 77 W S MITCHELL, J F SOILEAU F33615-74-C-2060
UNCLASSIFIED PWA-FR-8932 AFAPL-TR-77-75 NL

2 OF 4
AD
A060343



The Mod 2 total pressure loss was, as expected, somewhat higher than corresponding values for either the baseline model or the Mod 1 configurations, apparently due to additional wall friction and growth of the secondary flow vortex. In comparing the upstream and downstream data for Mod 2 in Figure 57, it can be seen that losses in the upstream position between 30% and 50% span are about the same as those obtained with the Mod 1 configuration. However, between 9% and 20% span, total pressure loss was higher with Mod 2. This additional loss is attributed to the presence of the endwall protrusions, as they represent the only difference between Mod 1 and Mod 2 at the upstream measuring station.

The results obtained with the 40-deg airfoil cascade packs were compared with the data presented in Reference 2 to establish the level of success achieved in the Phase I cascade program. The results of varying endwall boundary layer bleed within the cascade on the performance of circular arc airfoils, very similar to the 40-deg EGV design at inlet Mach numbers of 0.5.1, 0.64, and 0.74, are presented in Reference 2. Figure 58 compares a data curve extracted from Reference 2 for no bleed in front of or within the airfoil pack to data for the 40-deg EGV $H_3/H_2 = 1.0$ models at similar conditions, i.e., for an inlet Mach number of 0.64. In the EGV airfoil tests, the Series 1 tests were run with inlet boundary layer bleed, but there was no endwall suction within the channel and Series 2 had no boundary layer bleed in front of or within the channel. It can be seen that the EGV cascade demonstrated over twice the static pressure rise of the circular arc airfoil. The slightly higher midspan total pressure loss for the EGV airfoils is attributed to three factors: (1) closer spacing of the EGV airfoils (τ/b = 0.392 vs 0.614), (2) thicker airfoils for the EGV models (t/b + 0.075 vs 0.059), and (3) lower aspect ratio of the EGV airfoil (AR = 1.0 vs 1.855). The exit air angles were comparable. The availability of this high turning-high Mach number data without endwall bleed over a range of incidence levels verifies the validity of the 40-deg EGV data and provides an indication that the non-series airfoil design has provided a significant improvement in diffusion capability. Also included in Figure 58 are data from the Series 2 Mod 1 model. The performance of this modified airfoil model shows significant improvement over the baseline, as well as the circular arc data.

5. Data Analysis Using Spanwise Average Total Inlet Pressures

In the preceding figures, cascade total pressure loss was referenced to midspan inlet total pressure. The use of midspan inlet total pressure, rather than a spanwise average value, charges the airfoil packs for inlet boundary layer loss, as well as the profile and secondary losses. Use of a spanwise average inlet pressure for calculating loss and static pressure rise provides more representative performance data for the airfoil packs. The data from the second series of tests were corrected using the average spanwise inlet pressure. The performance data for the second series of tests, computed using the average inlet total pressure, are presented in Figure 59. With this correction, it can be seen that losses from the first baseline tests were geneally higher than those obtained in the baseline retest. This difference was due to the +5 deg higher than design incidence incurred in the first test. The 0.1% reversal of this effect at the low Mach number point is attributed to possible small boundary layer measurement inaccuracies during the first test, as well as the fact that there is generally less sensitivity of airfoil loss due to incidence at low Mach numbers.

A slightly higher pressure rise coefficient was obtained in the first test of the baseline model. It was attributed to the higher positive incidence (tested in the first baseline test), which caused a higher effective area ratio.

Figure 59 shows that cutting back the leading edge and uncambering the trailing edge (Mod 1) reduced the total pressure loss from 3.1% to 2.7% at $M_2 = 0.675$. At this same condition, the pressure rise coefficient increased from 0.24 to 0.28. Addition of a downstream diffuser and endwall protrusions to the modified airfoil cascade (Mod 2) resulted in a pressure rise coefficient

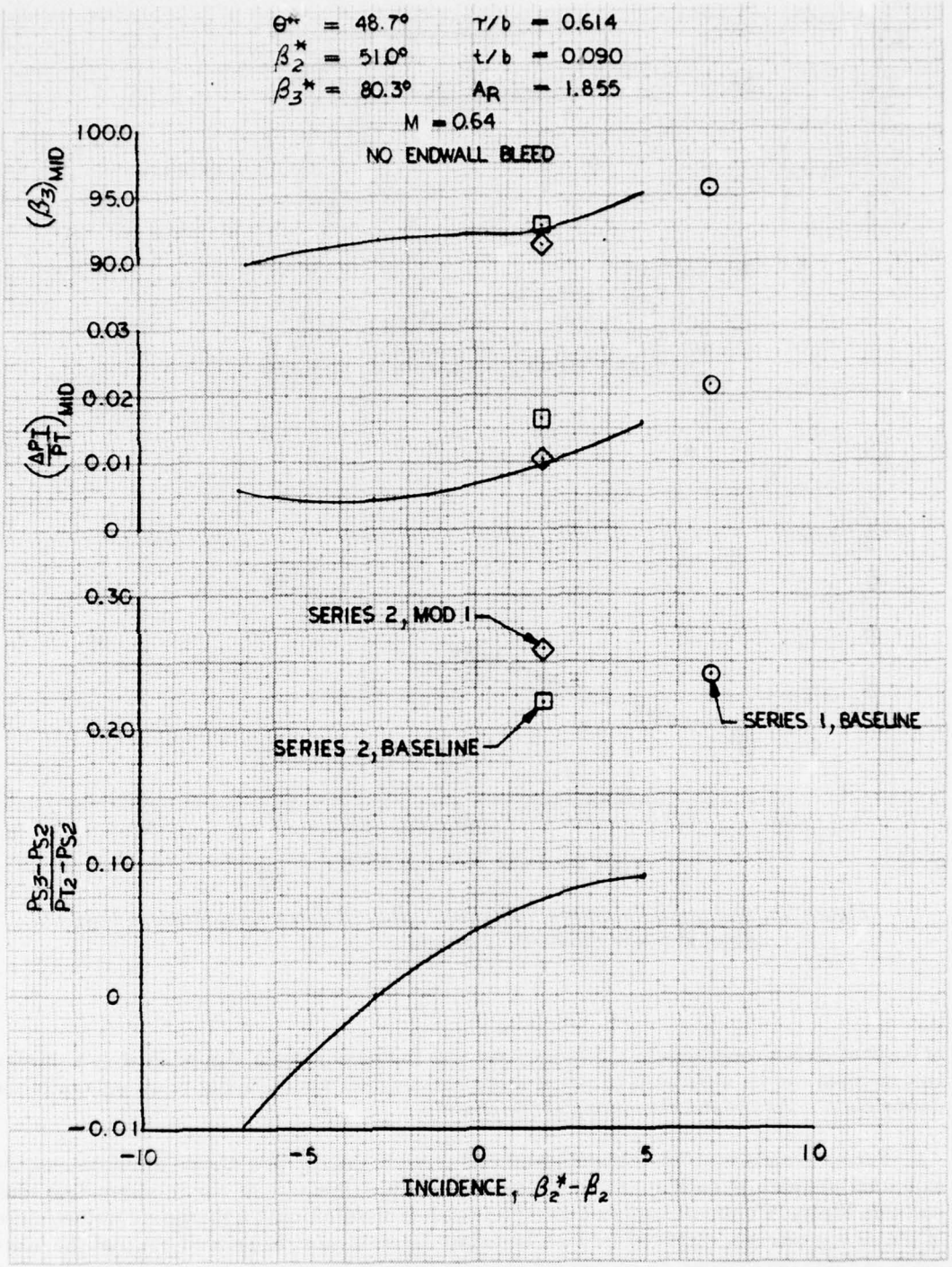


Figure 58. Effect of Incidence on Circular Arc Compressor Cascade Performance (Reference 2)

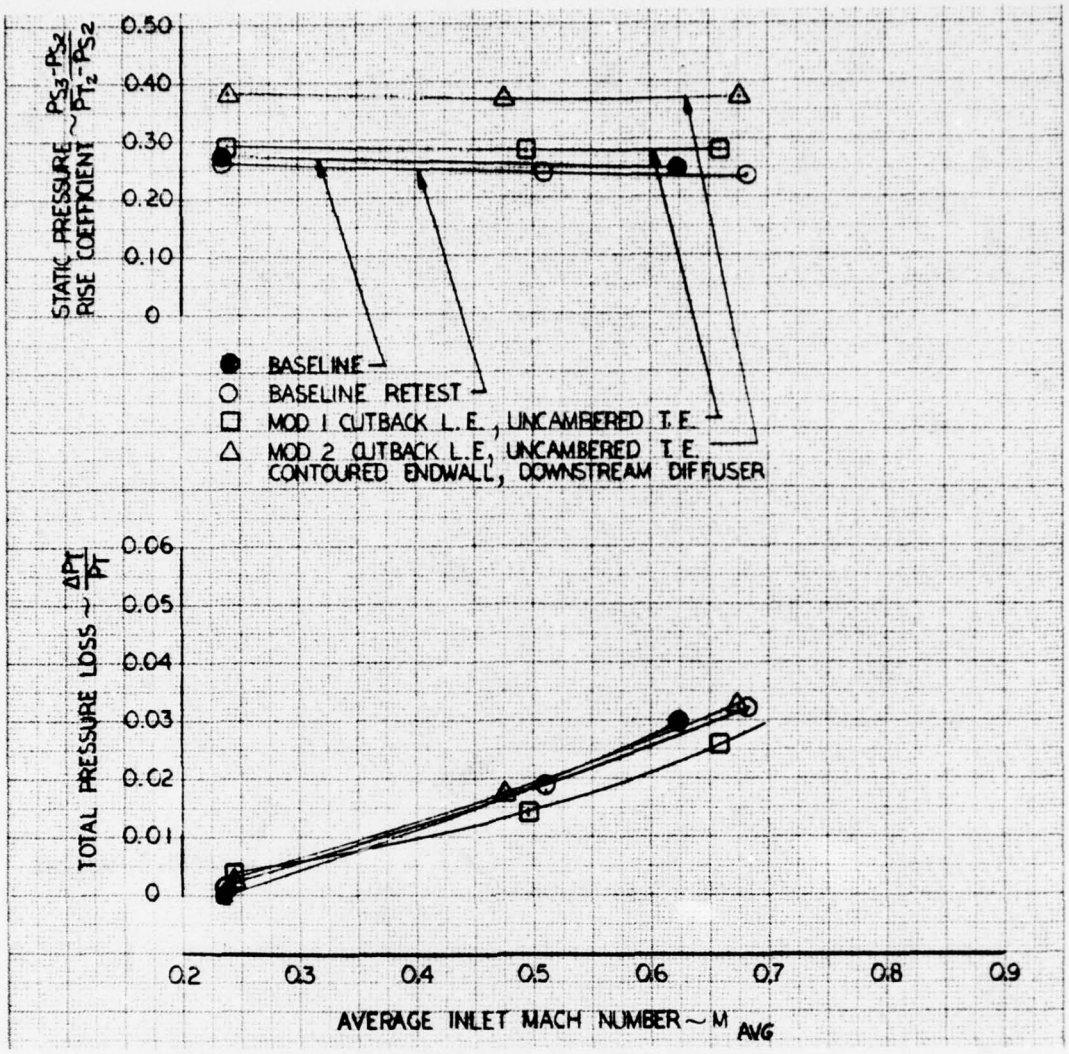


Figure 59. 40-deg EGV Average Performance Data Referenced to Average Inlet Total Pressure (13-Airfoil Cascade)

of 0.372 at design conditions or a 55% increase over the baseline case. Approximately a third of this increase can be attributed to airfoil modifications and the remainder to divergence of the downstream endwalls and contouring of the endwall.

Further insight into the distribution of total pressure loss can be obtained by referencing the exit total pressure at each spanwise position to the inlet pressure at the corresponding span location. Figure 60 presents spanwise total pressure loss distributions for the second test sequence of the 40-deg cascade, corrected for inlet boundary layer. It must be pointed out that the exact levels of these data cannot be considered accurate because an entering stream surface does not necessarily remain at the same spanwise location as it passes through the cascade. This is particularly true near the endwall, where the entering boundary layer is swept across the channel and up onto the airfoil suction surface. However, Figure 60 clearly shows that the concentration

of loss developed by highly loaded turbine EGV's located in a secondary flow vortex well off the endwall. For the models tested, the core of this vortex appears to be at about 10% to 15% span.

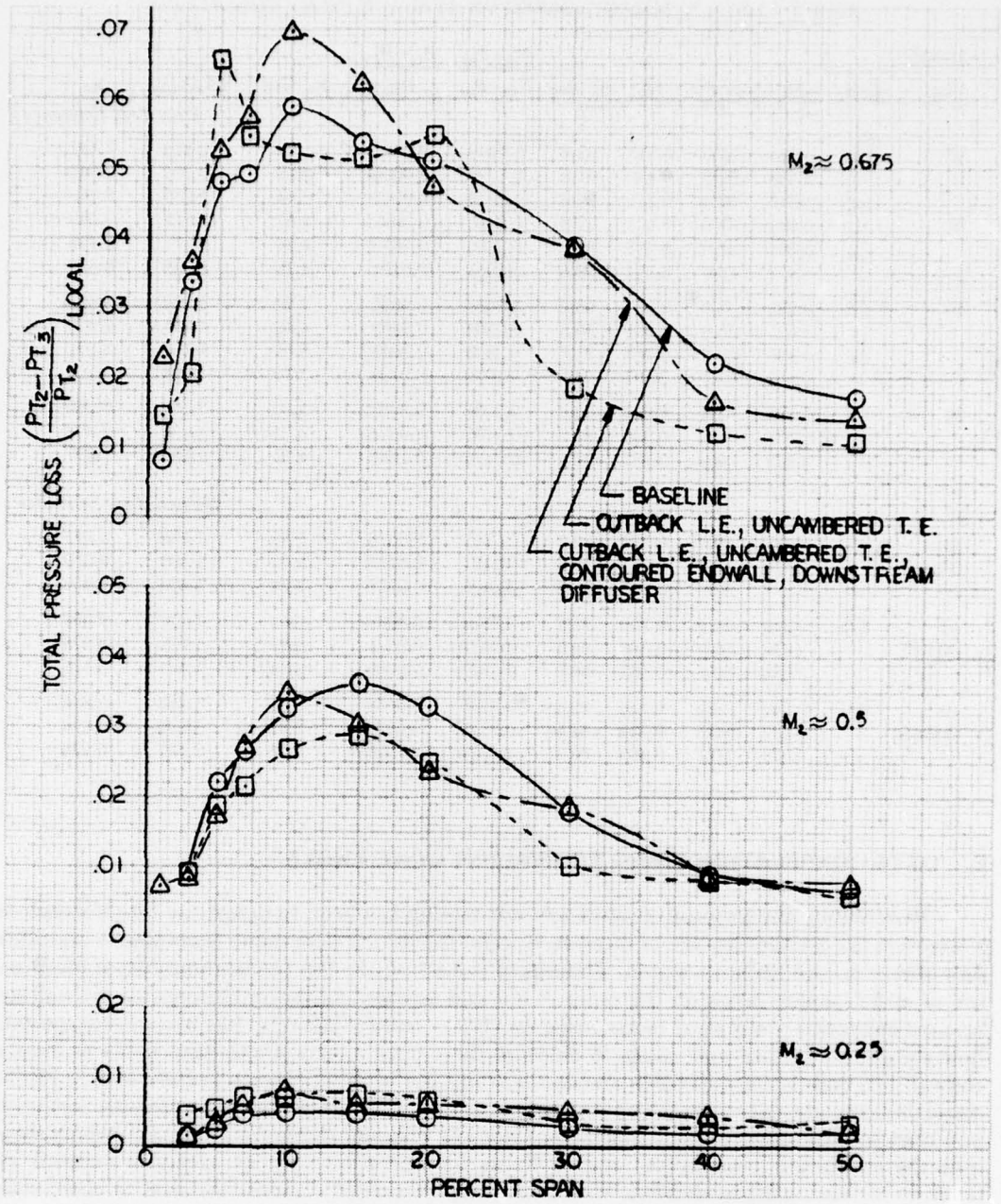


Figure 60. 40-deg EGV Total Pressure Loss Distribution Corrected for Inlet Total Pressure Distribution (13-Airfoil Cascade)

The performance values, computed using average spanwise inlet pressures, are given in Table 10 for all of the airfoil cascade tests.

TABLE 10
PHASE I DATA SUMMARY (BASED ON AVERAGE INLET CONDITIONS)

Airfoil (deg)	H_3/H_2	M_2	β_2, deg	M_3	β_3, deg	$\frac{P_{S3}-P_{S2}}{P_{T2}-P_{S2}}$	$\frac{P_{T2}-P_{T3}}{P_{T2}}$	θ_{eq}, deg	$(A_3/A_2)_{eq}$	η_D
										First Test Sequence
30	1.0	0.224	62.6	0.215	93.6	0.0935	0.0007	1.73	1.135	0.447
		0.489	62.6	0.432	94.8	0.1795	0.0030	2.08	1.164	0.763
	1.1	0.246	62.6	0.212	96.6	0.2623	0.0007	3.04	1.256	0.759
		0.499	62.6	0.421	97.8	0.2435	0.0092	3.57	1.311	0.643
	1.2	0.267	62.6	0.216	97.0	0.3306	0.0010	4.19	1.377	0.728
		0.493	62.6	0.374	99.6	0.2951	0.0171	4.78	1.449	0.613
40	1.0	0.235	45.0	0.207	95.2	0.2683	0.0010	3.34	1.437	0.489
		0.625	45.0	0.501	95.5	0.2504	0.0303	4.19	1.595	0.406
	1.1	0.306	50.3	0.287	91.7	0.2835	0.0048	3.52	1.468	0.521
		0.661	55.7	0.557	94.0	0.1373	0.0599	3.72	1.504	0.251
50	1.0	0.298	47.4	0.240	92.3	0.2086	0.0085	3.00	1.389	0.395
		0.507	48.6	0.390	91.2	0.1735	0.0372	3.25	1.431	0.328
		0.823	48.6	0.587	91.6	0.0478	0.1685	4.39	1.650	0.077
										Second Test Sequence
40	1.0	0.237	49.6	0.197	92.8	0.2647	0.0016	2.65	1.330	0.617
(Base)		0.510	49.9	0.404	93.5	0.2421	0.0188	3.04	1.392	0.520
		0.683	50.0	0.535	94.2	0.2405	0.0322	3.52	1.474	0.476
40	1.0	0.240	50.5	0.186	95.2	0.2946	0.0038	2.53	1.312	0.692
(Mod 1)		0.496	50.4	0.386	95.5	0.2839	0.0141	2.93	1.375	0.619
		0.658	50.7	0.503	96.0	0.2829	0.0260	3.33	1.441	0.573
40	1.0	0.240	49.8	0.176	92.1	0.3765	0.0033	2.57	1.463	0.875
(Mod 2)		0.478	49.5	0.334	92.9	0.3715	0.0177	2.91	1.545	0.810
		0.678	50.2	0.465	93.1	0.3725	0.0327	3.28	1.647	0.738

E. DATA CORRELATION USING EQUIVALENT CONE ANGLE

Historically, the purpose of plane cascade testing has been to determine two-dimensional characteristics for the cascade of interest. Special provisions were made to minimize secondary flow effects on the midspan region. These provisions took the form of boundary layer bleed and use of airfoil aspect ratios on the order of 2.0 and greater. As the importance of endwall loss became increasingly apparent (accounting for 50% or more of the total loss in a multistage axial flow compressor), tests were made to measure these effects, and efforts were made to develop endwall loss correlations. Notable among these was the work by Hanley in Reference 3. Hanley correlated cascade exit endwall displacement thickness as a function of static pressure coefficient and inlet endwall displacement thickness. Figure 61 presents Hanley's correlation, which shows that the maximum permissible loading limits for operation without excessive endwall loss (sharply increasing δ^*_3/b) decrease with increasing inlet-displacement-thickness to chord ratio. Data from the basic Phase I tests have been superimposed on Figure 61. It can be seen that generally good agreement was obtained. This is particularly significant since Hanley's original data were all with straight, nondiverging endwalls, at a constant inlet Mach number of 0.25, with aspect ratios of 2.75 or greater, and conventional airfoil designs. In fact, more than half of his data were taken with sheet metal, circular arc airfoils with a camber of 30 deg.

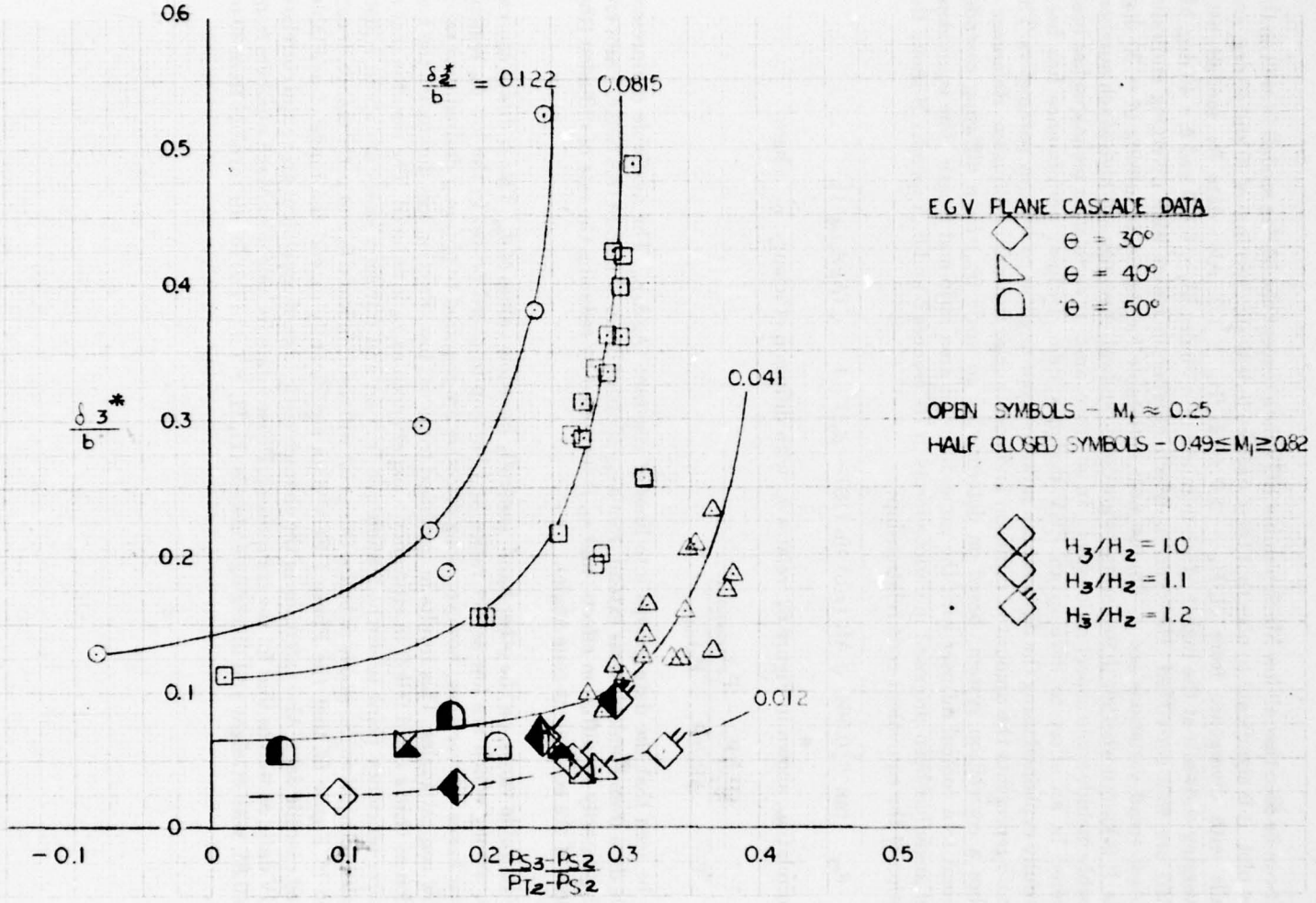


Figure 61. Correlation of Exit Endwall Boundary Layer Displacement Thickness

It can be seen that all low Mach number EGV data (except the 50-deg model) fit well on the Hanley plot. It is significant to note that these data include design turnings of 30 and 40 deg, and endwalls with divergence from $H_3/H_2 = 1.0$ to $H_3/H_2 = 1.2$. Also data for models with nondiverging endwalls at the higher Mach numbers ($\theta = 30$ deg $M_2 = 0.489$ and $\theta = 40$ deg, $M_2 = 0.625$) are well correlated. However, as Mach number increases with diverging endwalls, significant trend variations occur. This is most noticeable for the lower turning ($\theta = 30$ deg) models. It is known whether these variances are due to endwall divergence at high Mach numbers or possibly include some aspect ratio effects. In any case, another correlation technique has been considered in an effort to develop an EGV design system. Diffuser performance has been successfully explained using the diffuser area ratio and cone angle as correlating parameters. The area ratio represents the amount of diffusion and cone angle, the rate of diffusion. Reference 4 describes a correlation system, based on determining an angle (θ_{eq}) for a diffusing cascade, equivalent to a conical diffuser with the same diffusion area ratio and length. The equivalent conical angle has been proposed in various forms in References 5 and 6. Appendix B shows the derivation of the equivalent cone relationship:

$$\theta_{eq} \quad \tan^{-1}\left[0.564 \sqrt{AR\,(\tau/b)\sin(180 - \beta_3^*)}\left(1 - \sqrt{(A_2/A_3)_{eq}}\right)\right]$$

The correlation, shown in Figure 62, relates θ_{eq} with diffusion efficiency, η_D, where

$$\eta_D = \frac{\Delta P_S/(P_T - P_3)_{,measured}}{\Delta P_S/(P_T - P_S)_{,ideal}}$$

It can be seen that the data groups into lines of constant $(A_3/A_2)_{eq}$. The available compressor cascade data from Hanley's tests extend from a θ_{eq} of about 6.5 to 15 deg. In this range, losses are caused primarily by diffusion effects, and η_D is increased by reducing the rate of diffusion (the steepness of the equivalent cone angle).

Exit guide vanes, on the other hand, generally have low values of θ_{eq}. This is due to several factors, among which are low-aspect ratios and low-gap-to-chord ratios. In the low θ_{eq} region, diffusion losses are very low; however, long diffusers are required to obtain a desired area ratio with low conical angles. This results in increased frictional loss. Friction loss dominates the low θ_{eg} region so that a rapid falloff in efficiency is experienced as θ_{eq} is reduced. The result is that a maximum efficiency point is reached where the friction and diffusion losses are about equal. Equivalent conical angles above or below this point will result in less efficient performance. It can be seen in Figure 62 that the Phase I EGV data significantly extend the range of available diffusing cascade data. Also extension of the characteristic lines of equivalent area ratio correlate the EGV data, as well as that for the compressor. Phase I data include inlet Mach numbers from 0.25 to 0.85, with straight and diverging endwalls ($H_3/H_2 = 1.0$ to 1.2) for air turnings from 30 to 50 deg.

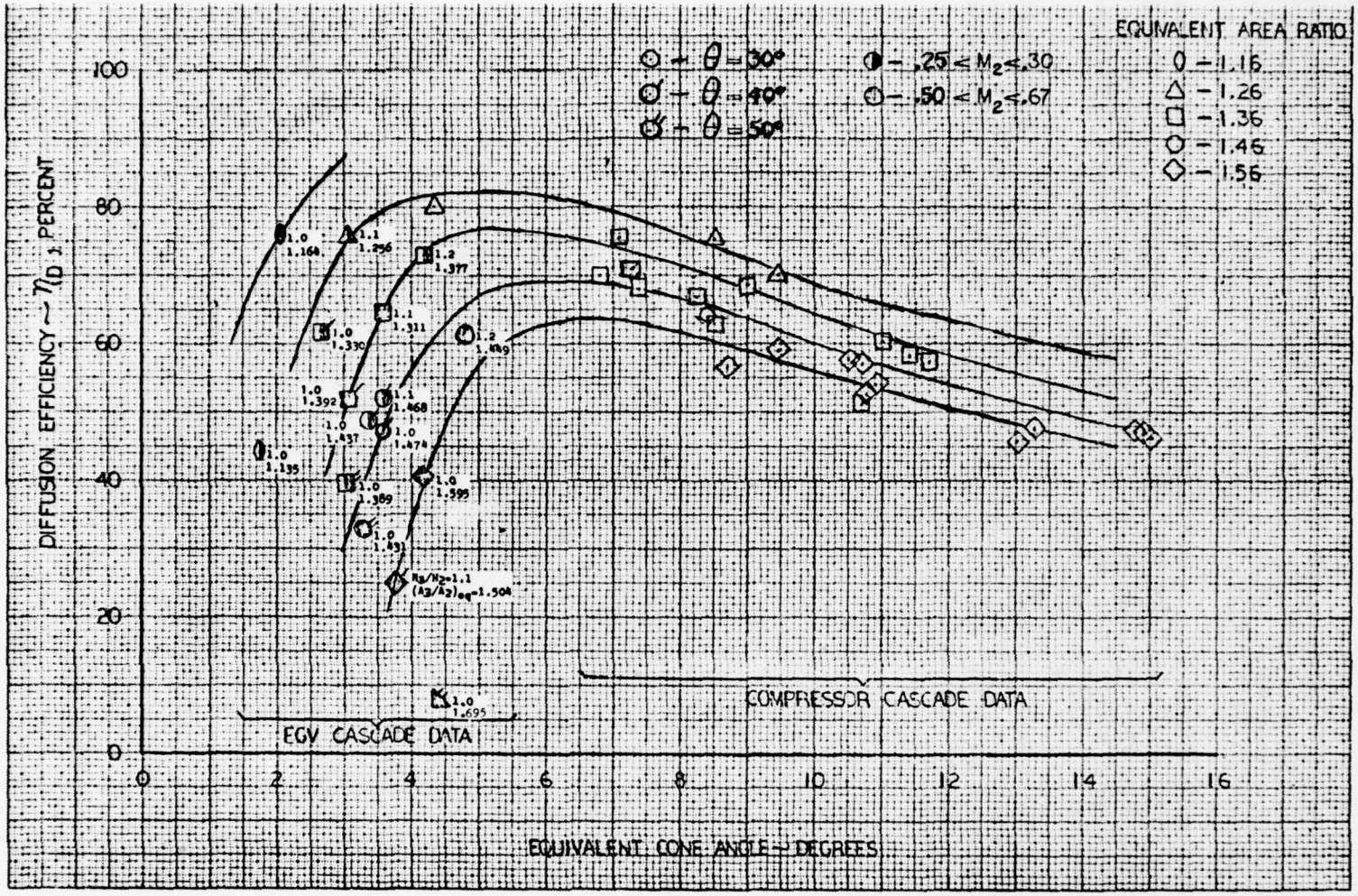


Figure 62. Equivalent Conical Angle Correlation of Diffusing Cascade Data

F. SUMMARY — PHASE I

Non-series airfoils, designed by tailoring camber and thickness distribution to minimize the potential for suction surface separation, demonstrated improved performance relative to state-of-the-art circular arc series airfoils, reducing total pressure loss and increasing diffusion. However, the non-series airfoils were found to be sensitive to incidence variations.

The airfoil modifications and endwall contours, identified in the flow visualization studies and subsequently tested in the 40-deg cascade, demonstrated improved performance by: reducing the amount of loss due to secondary flow; and/or increasing the static pressure rise coefficient. These modifications included (at the endwall): cutback leading edge, uncambered trailing edge, reduced suction surface camber, and addition of pressure surface protrusions.

Using a correlation system developed at P&WA, the Phase I cascade data has been correlated with previously reported compressor cascade data to provide an EGV design system. The correlation relates an equivalent conical angle (θeq) with diffusion efficiency (η_D) and defines an opimum diffusion efficiency for each equivalent diffuser area ratio (A_3/A_2)eq.

SECTION II
PHASE II — ANNULAR CASCADE DESIGN AND TESTING

Phase II of the EGV program was an experimental and analytical investigation conducted to: (1) evaluate and improve the accuracy of the Phase I design system (θeq), and (2) evaluate, in a three-dimensional flow environment, the effects of spanwise variations in Mach number, gas turning and gap/chord ratio. The Phase II experimental investigations were conducted in an annular cascade test facility designed to provide EGV inlet Mach number and swirl distributions which are typical of an advanced engine application.

In this phase, two EGV annular cascades were tested. The first airfoil was a non-series high aspect ratio design which did not have any airfoil or endwall modifications included in the design to reduce secondary losses. The second airfoil was exactly the same as the first except for endwall and airfoil modifications intended to reduce secondary losses. These modifications included (at or near the endwall): cutback leading edge, uncambered trailing edge and pressure side protrusions.

A. AIRFOIL AND ENDWALL ANALYSIS AND DESIGN

1. Design Point Selection

Design of the Phase II annular cascade models was based on inlet swirl and Mach number distributions, representative of conditions from an advanced, highly loaded fan-drive turbine. The selected turbine was from a preliminary design study for a single-stage, fan-drive turbine to be used in an advanced F100-sized engine. Table 11 presents meanline conditions for this turbine.

TABLE 11
MEANLINE CONDITIONS FOR THE
SELECTED SINGLE-STAGE,
LOW-PRESSURE TURBINE DESIGN

Stage Loading Parameter ($\Delta H_T/T_T$)	0.043
Inlet Flow Parameter [$W\sqrt{(T_T/P_T)_{inlet}}$]	68.2
Inlet Speed Parameter ($N/\sqrt{(T_T)}$)	222.5
Pressure Ratio (P_R)	2.12
Mean Velocity Ratio (V_{RM})	0.472
Exit Air Angle, (β_{Exit}) deg	52.0
Exit Mach Number [$(M_A)_{Exit}$]	0.539

The diffusion system (EGV and downstream diffuser) length and inlet-to-exit annulus area ratio were based on the F100 turbine flowpath shown in Figure 63. EGV inlet Mach number and air angle distributions are presented in Figure 64 or design conditions.

2. Selection of Model Scale and Swirl Vane Design

A schematic of the Phase II annular cascade test rig, showing its major components, is presented in Figure 65. Airlow to the rig plenum chamber was delivered through a 10-in.-diameter pipe. To reduce the possibility of flow distortion due to a high velocity jet from this pipe, design flowrate was set for a pipe exit Mach number of 0.3. The resulting flowrate of 16 lb/sec set the rig annulus area at about 1/6 of the engine EGV inlet annulus area. This rig annulus area could have been used to simulate either (1) a 60-deg sector of an engine size EGV or (2) a larger sector of a

reduced-scale EGV. The desirability of avoiding flow distortion caused by proximity of the annular segment side walls dictated that model scale be reduced to provide a sector are of 180 deg. This resulted in a model scale, which was 60% of full size.

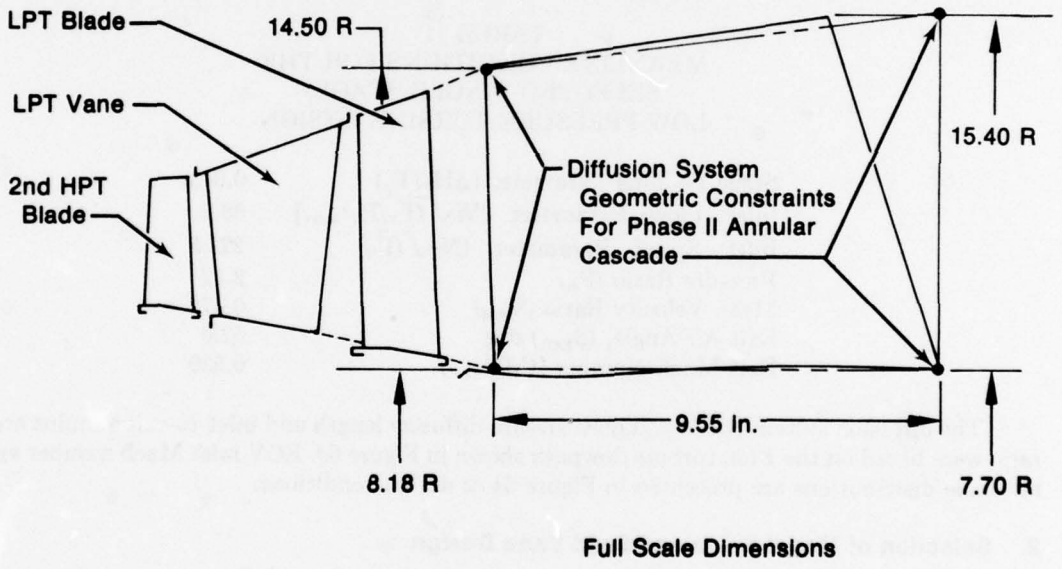


Figure 63. F100 Single Stage Low Pressure Turbine Flowpath

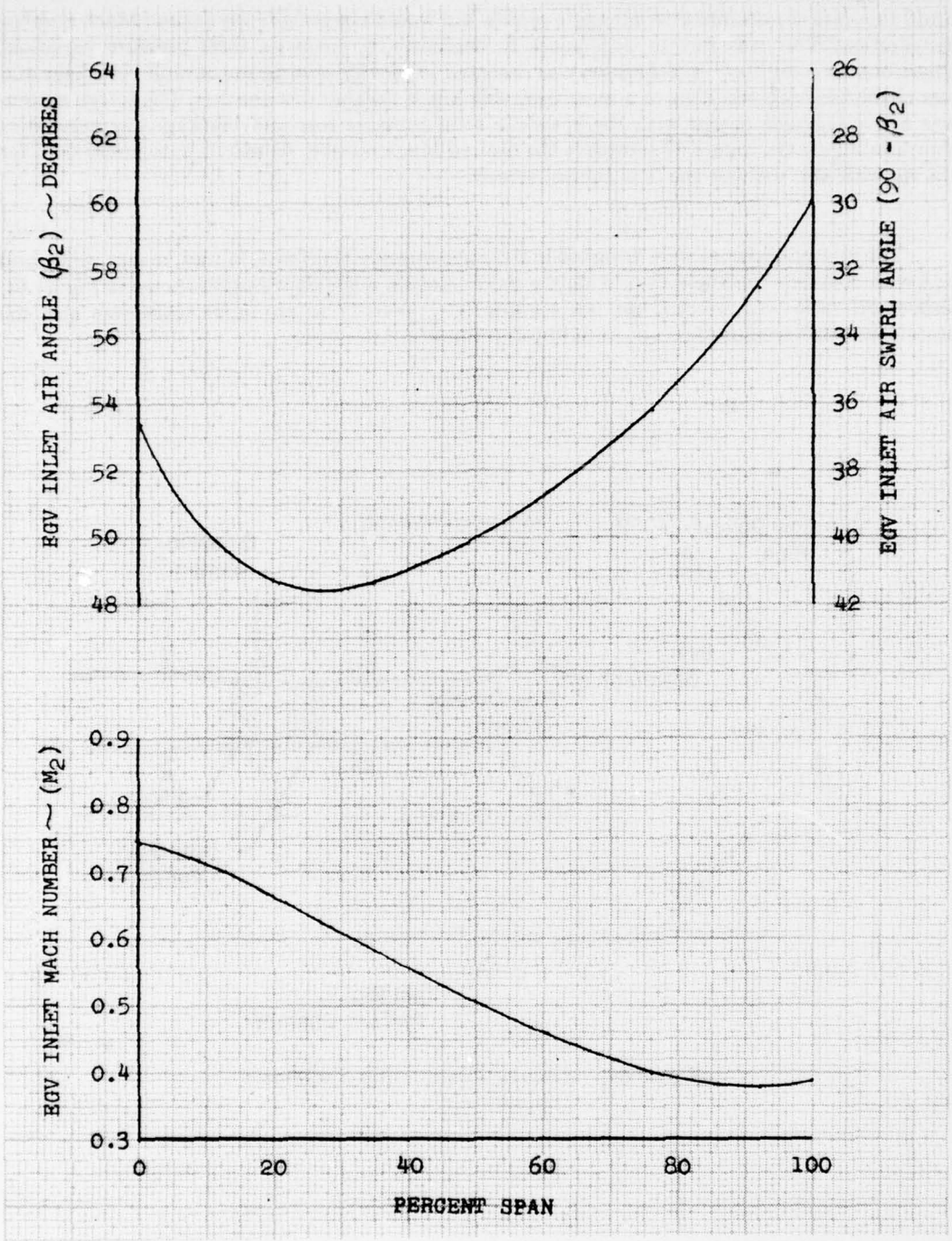


Figure 64. Annular Cascade Design Inlet Air Angle and Mach Number Distribution

A streamline anlaysis of the test rig flowpath indicated that inlet swirl vanes (Figure 65) could simulate the desired inlet air angle profile, but would not provide the desired Mach number distribution. This was due to differences in engine-to-rig spanwise total pressure variation. Therefore, an inlet flow control screen was designed to provide a variation of radial blockage and loss characteristics, resulting in a more desirable Mach number distribution. The screen system was a five-segment design with the spanwise total pressure loss and blockage characteristics shown in Figure 66. Figure 67 compares the desired Mach number distribution to predictions for the rig with and without the flow control screen.

The inlet swirl vanes were designed in five spanwise sections (root, ¼ root, mean, ¼ tip, and tip) with constant thickness to provide the EGV inlet air angle distribution shown in Figure 64. Gap/chord ratio was selected for low loading ($C_{L_{max}}$=0.71) to minimize wake size and the associated total pressure loss generated by the vanes.

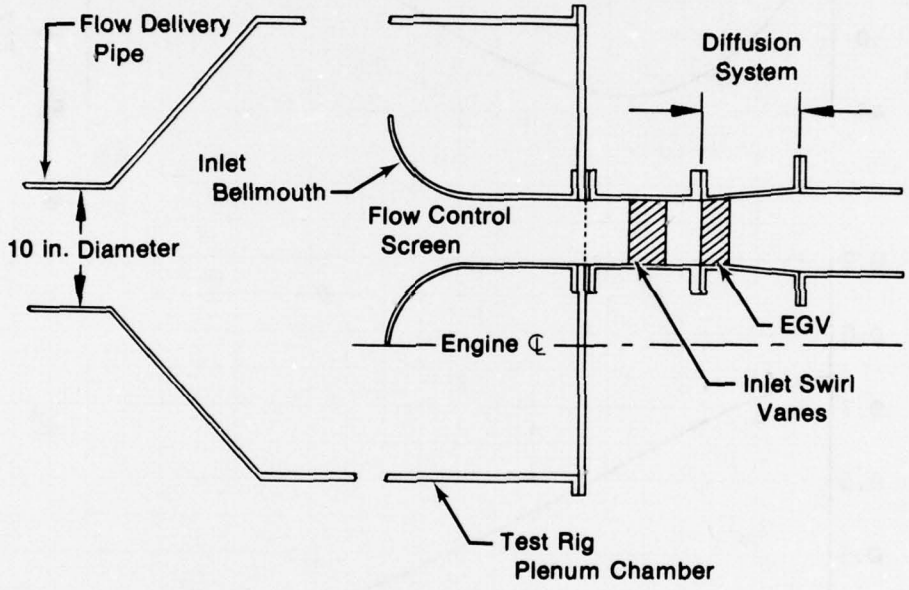


Figure 65. Annular Cascade Rig Schematic

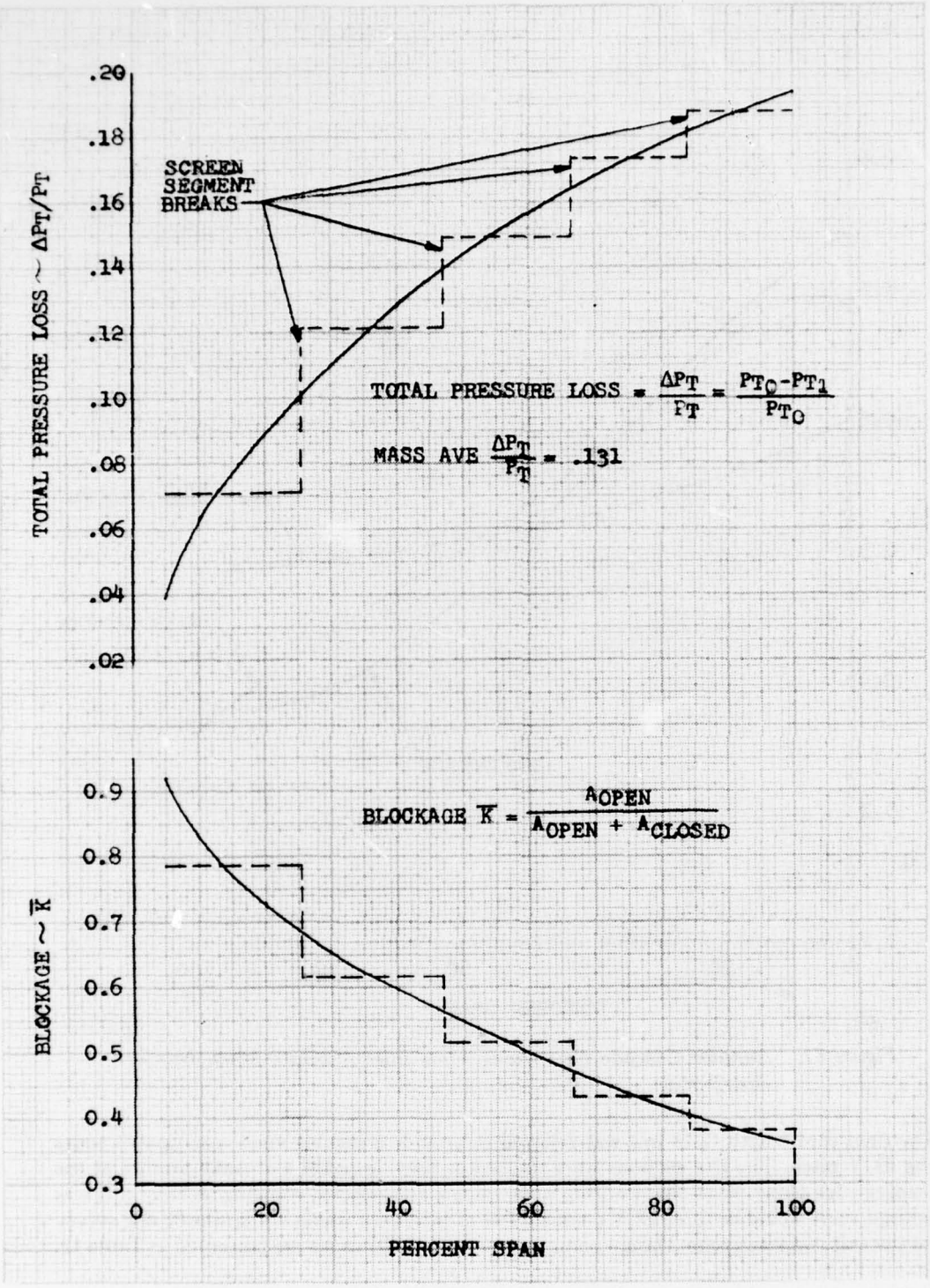


Figure 66. Annular Cascade Rig Inlet Screen Design Total Pressure Loss and Blockage Characteristics

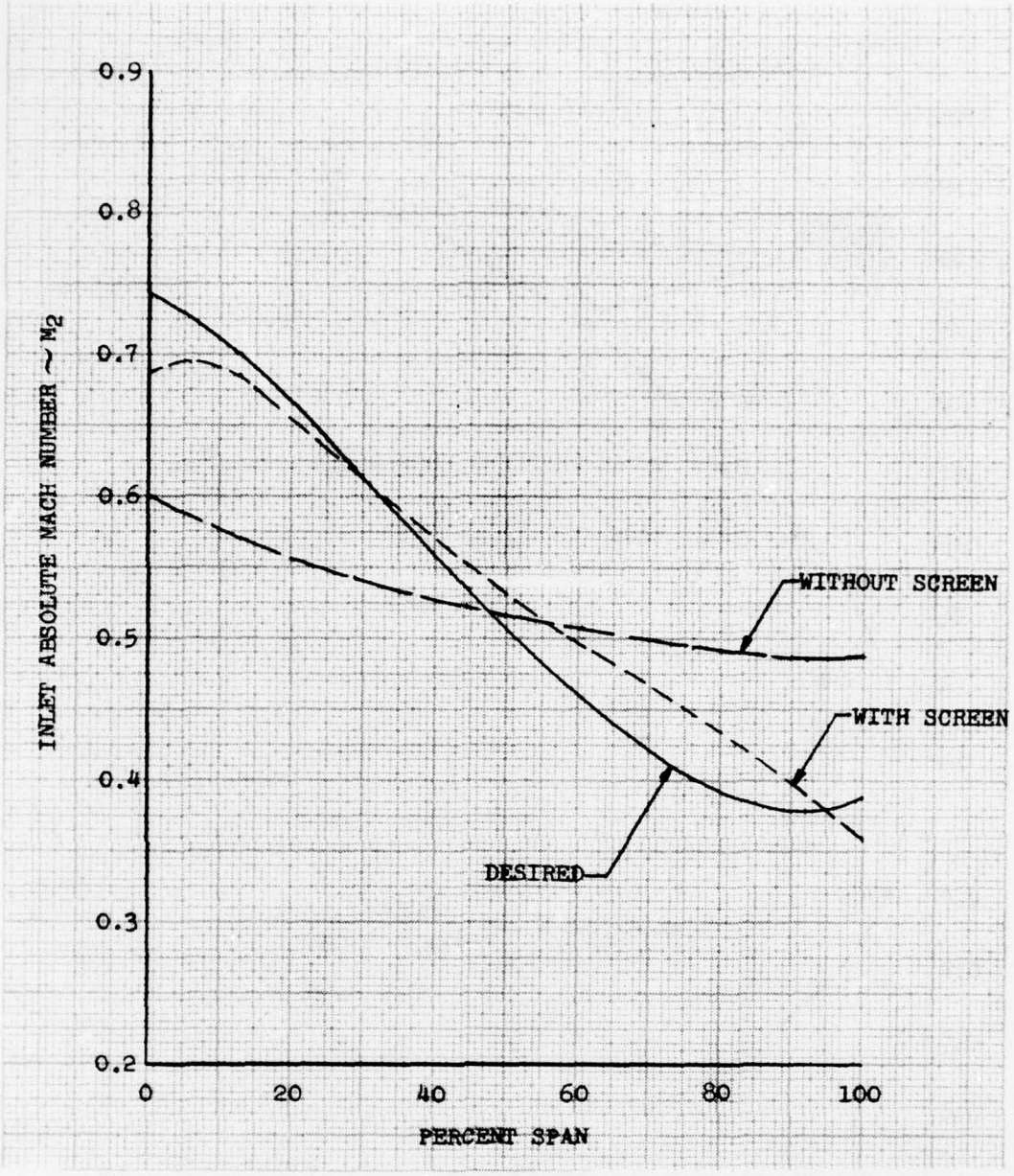


Figure 67. Annular Cascade Exit Guide Vane Inlet Absolute Mach Number Distribution

The final cord length (2.18 in.) was selected to provide a turning vane spacing 60% wider than the EGV pitch. The five sections were stacked to provide radial exit wake profiles at the EGV leading edge plane. With the resulting wide spacing and selected stacking technique, it was planned that there would be three EGV passages free of swirl vane wakes within the 60-deg survey range of the exit traverse probe. Design parameters for the swirl vanes are presented in Table 12.

TABLE 12
INLET SWIRL VANE DESIGN PARAMETERS

Percent Span	*0%*	*25%*	*50%*	*75%*	*100%*
Inlet Gas Angle (β_2), deg	90.0	90.0	90.0	90.0	90.0
Inlet Metal Angle (β_2*), deg	90.0	90.0	90.0	90.0	90.0
Exit Gas Angle (β_3), deg	53.4	48.4	50.0	53.6	60.0
Exit Metal Angle (β_3*), deg	53.4	48.4	50.0	53.6	60.0
Axial Chord (bx), in.	2.18	2.18	2.18	2.18	2.18
Thickness/Chord (t/bx)	0.014	0.014	0.014	0.014	0.014
Gap/Chord (τ/bx)	0.463	0.552	0.642	0.731	0.821
Zwiefel Load Coefficient (C_L)	0.443	0.549	0.632	0.699	0.711

3. Aerodynamic Design of Configuration 1 (EGV No. 1)

Overall dimensions of the model were selected for compatibility with the available space for an exit guide vane in an F100 engine, with a single-stage, fan-drive turbine. Figure 68 presents the assumed flowpath constraints. Divergence was permitted at the OD where Mach number was

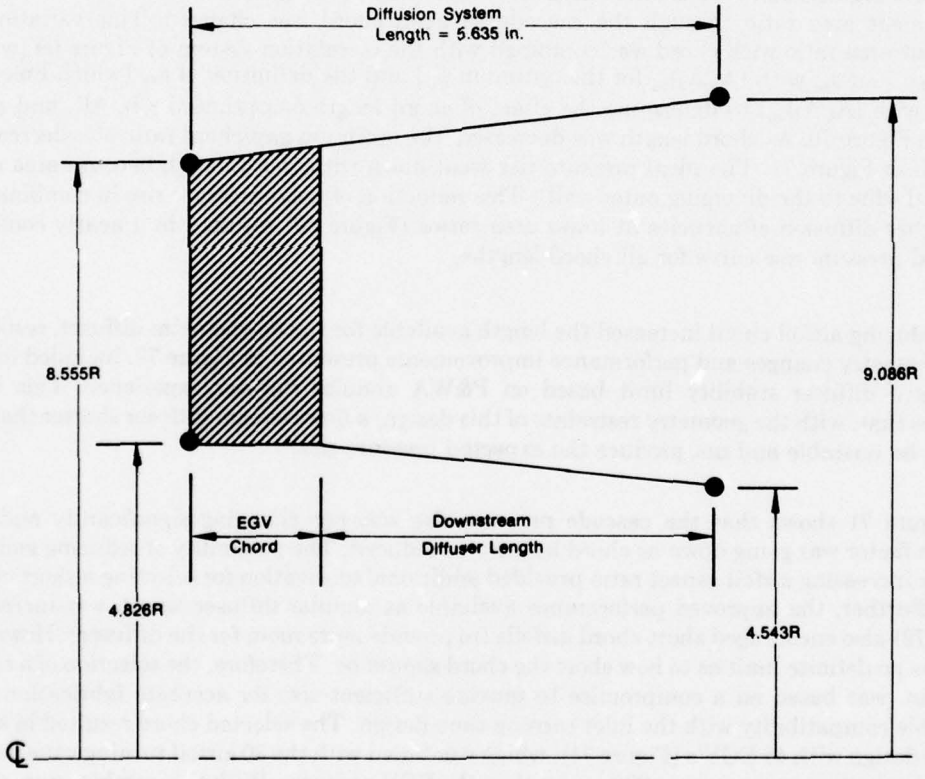


Figure 68. Annular Cascade Diffusion System Flowpath Restraints (Rig Scale)

low; however, the ID wall within the airfoil row was maintained constant (i.e., it had no divergence) to avoid excessive loading in the high Mach number, high turning root area. With these resulting dimensional constraints, the design process involved the selection of an EGV, which would provide the highest possible diffusion system efficiency with low total pressure loss.

The design was guided by results from the Phase I plane cascade tests, which provided data to verify and extend a P&WA diffusing cascade correlation system. The correlation system was based on an equivalent conical angle (θ_{eq}), determined by equating each cascade to a conical diffuser with the same diffusion area ratio and length. In Reference 1, θ_{eq} is shown to be:

$$\theta_{eq} = \theta_{eq} \quad \tan^{-1}\left[0.564\ \sqrt{AR\ (\tau/b)\ \sin\ (180 - \beta_3^*)}\left(\ 1 - \sqrt{(A_2/A_3)_{eq}}\ \right)\right]$$

Figure 69 presents the correlation, which related θ_{eq} with diffusion efficiency, η_D, where

$$\eta_D = \frac{\Delta P_S/(P_T - P_s)_{,measured}}{\Delta P_S/(P_T - P_S)_{,ideal}}$$

It can be seen that the data group into lines of constant equivalent area ratio, which correlate the Phase I data with the earlier compressor cascade data. The locus of peak efficiency points for each equivalent area ratio line is shown in Figure 69 as the maximum η_D line.

The design ground rule of constant ID and diverging OD (Figure 68) resulted in a variation of equivalent area ratio through the cascade as axial chord was changed. This variation of equivalent area ratio with chord was combined with the correlation system of Figure 69 [which relates η_D, and θ_{eq} with $(A_3/A_2)_{eq}$ for the optimum η_D] and the definition of θ_{eq} [which links τ/b, and AR with $(A_3/A_2)_{eq}$] to determine the effect of chord length on optimum τ/b, AR, and η_D as shown in Figure 70. As chord length was decreased, the optimum gap/chord ratio also decreased, as shown in Figure 71. The ideal pressure rise went down with chord length because area ratio decreased (due to the diverging outer wall). This reduction of ideal pressure rise in combination with higher diffusion efficiencies at lower area ratios (Figure 69) resulted in a nearly constant predicted pressure rise curve for all chord lengths.

Reducing airfoil chord increased the length available for the downstream diffuser, resulting in the geometry changes and performance improvements presented in Figure 72. Included in this figure is a diffuser stability limit based on P&WA annular diffuser experience. This limit indicates that, with the geometry restraints of this design, a downstream diffuser shorter than 2.3 in. may be unstable and not produce the expected pressure rise.

Figure 71 shows that the cascade pressure rise was not changing significantly and the diffusion factor was going down as chord length was reduced. The possibility of reducing endwall losses by increasing airfoil aspect ratio provided additional motivation for selecting a short chord design. Further, the improved performance available as annular diffuser length was increased (Figure 72) also encouraged short chord airfoils (to provide more room for the diffuser). However, there was no definite limit as to how short the chord should be. Therefore, the selection of a chord of 1.54 in. was based on a compromise to provide sufficient size for accurate fabrication and reasonable compatibility with the inlet turning vane design. The selected chord resulted in a full annulus design with 48 EGV's (Figure 71), which combined with the 30 airfoil turning vane design to provide turning vane passages 60% wider than the EGV passages. With this combination, there would be three EGV passages free of turning vane wakes in the 60-deg flow field segment to be surveyed during the tests.

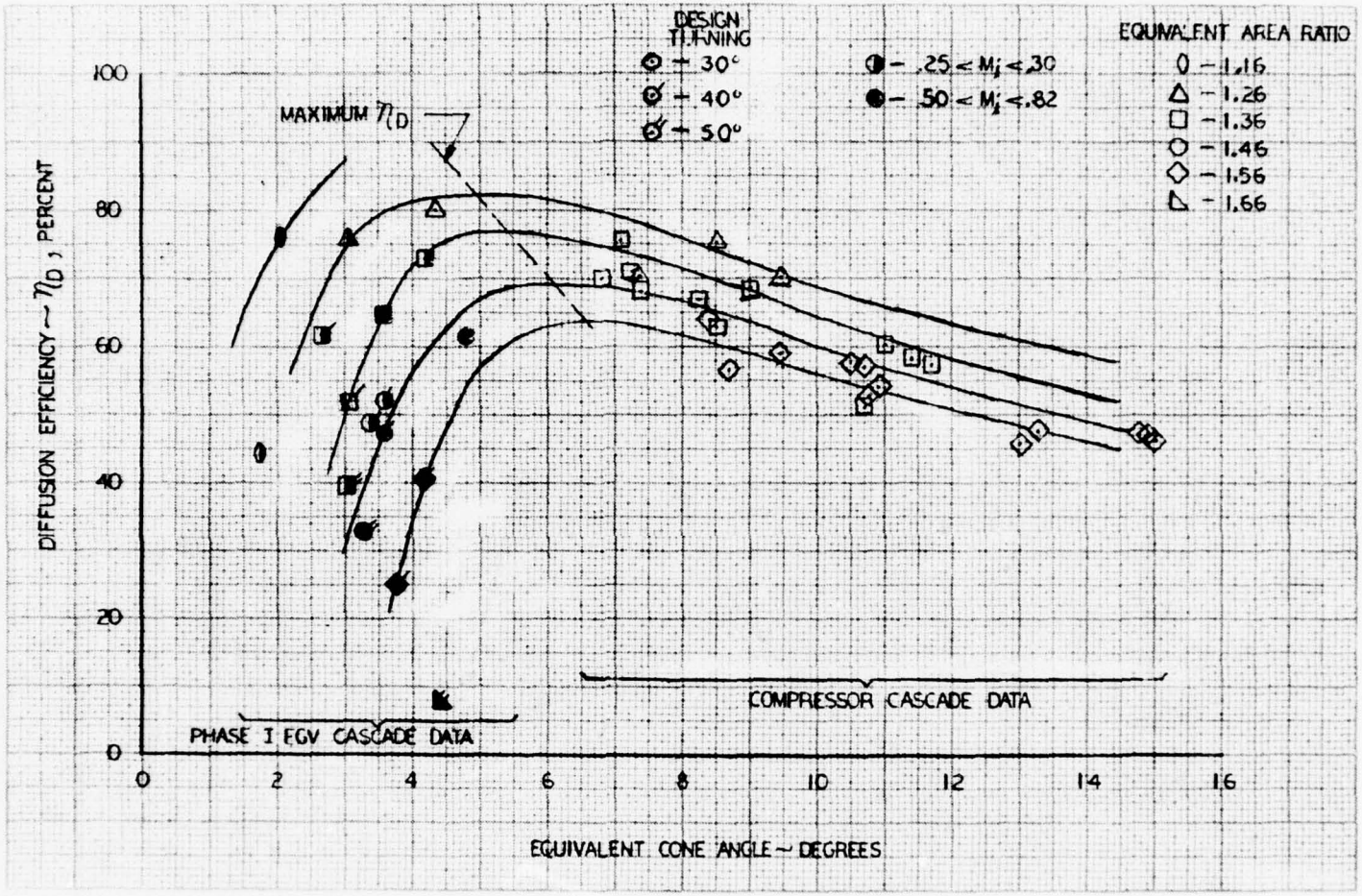


Figure 69. Equivalent Conical Angle Correlation of Diffusing Cascade Data

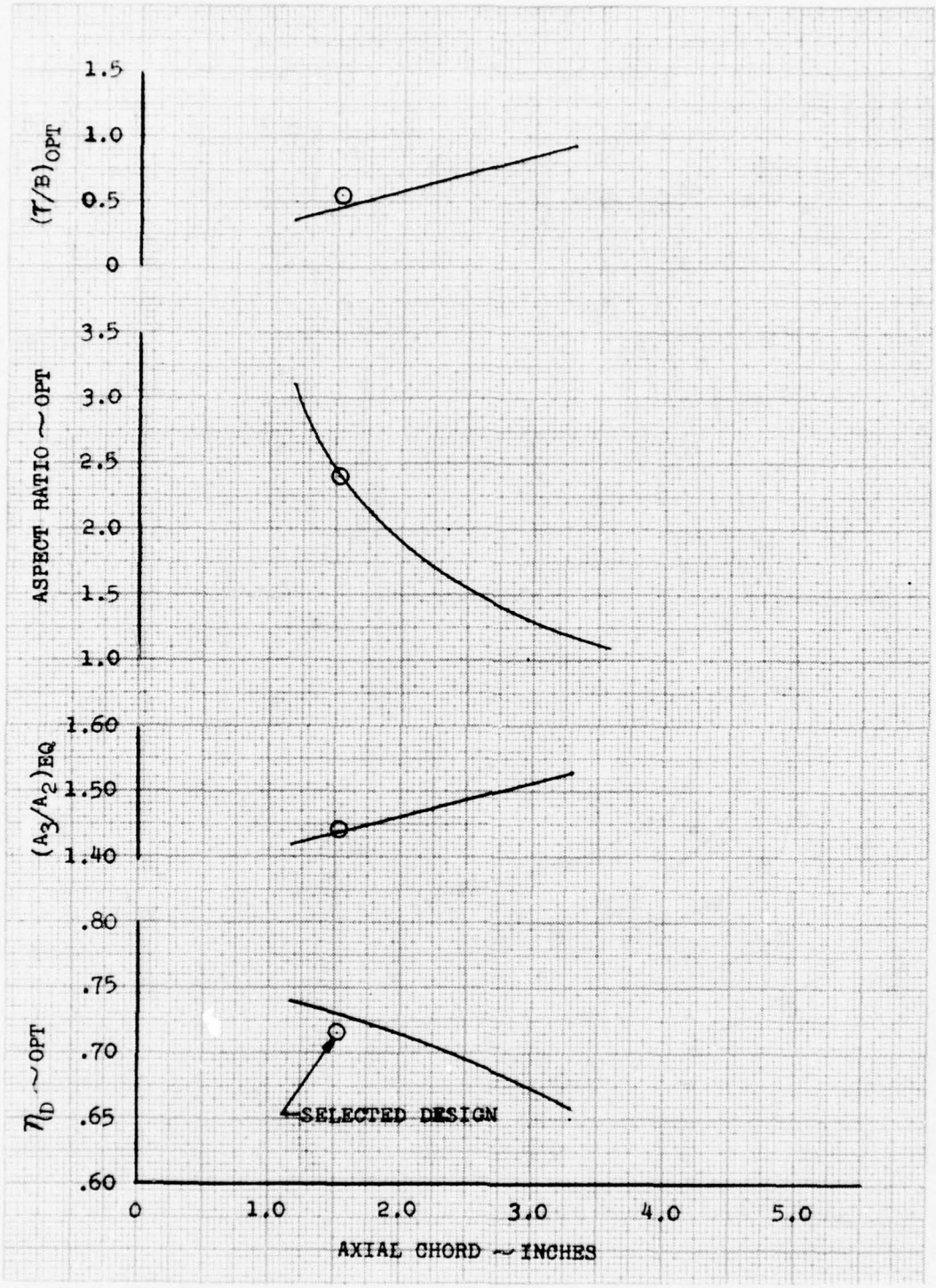


Figure 70. EGV Design Characteristics Based on Phase I Cascade Correlation at Optimum Diffuser Efficiency

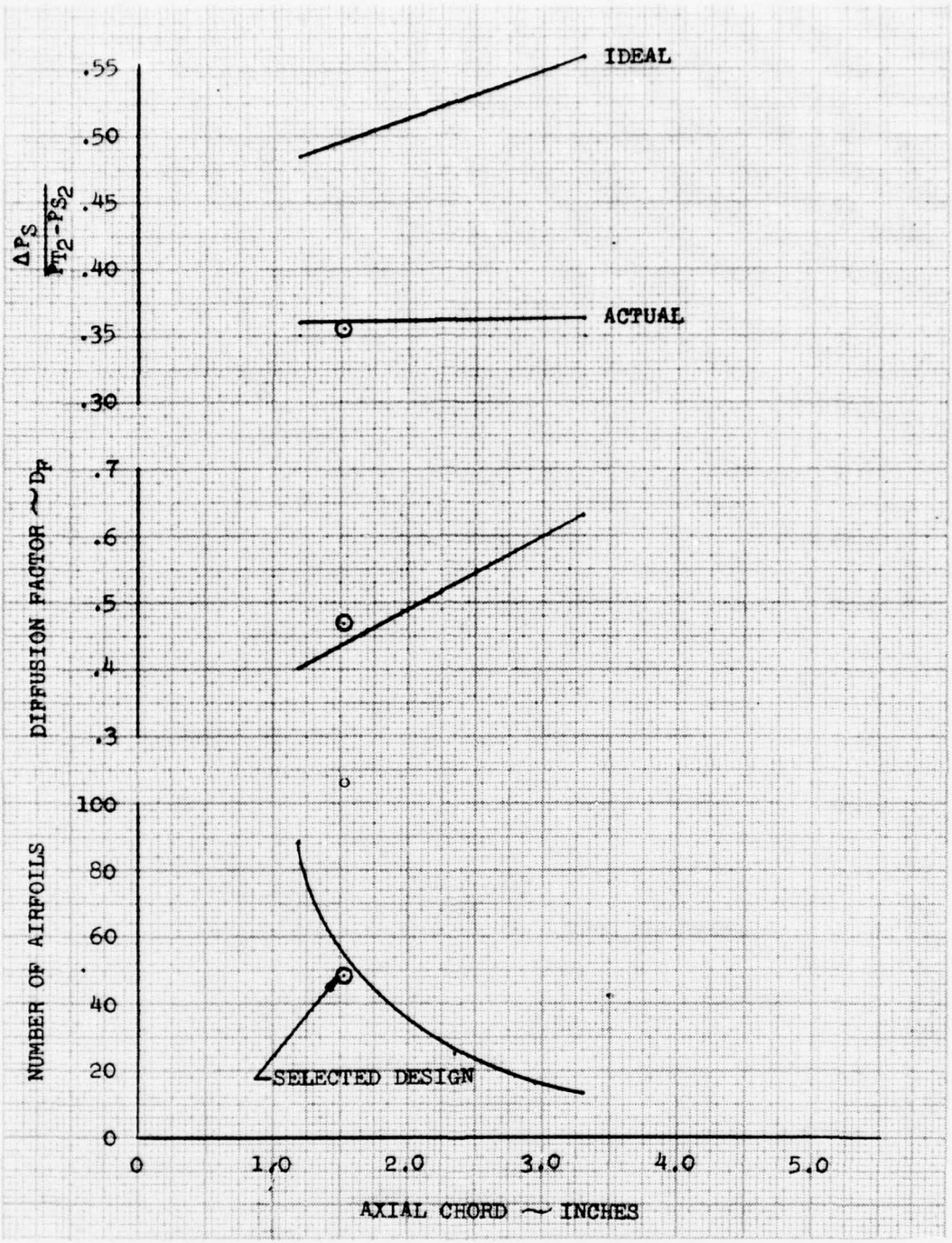


Figure 71. EGV Design Characteristics Based on Phase I Cascade Correlation at Optimum Diffuser Efficiency

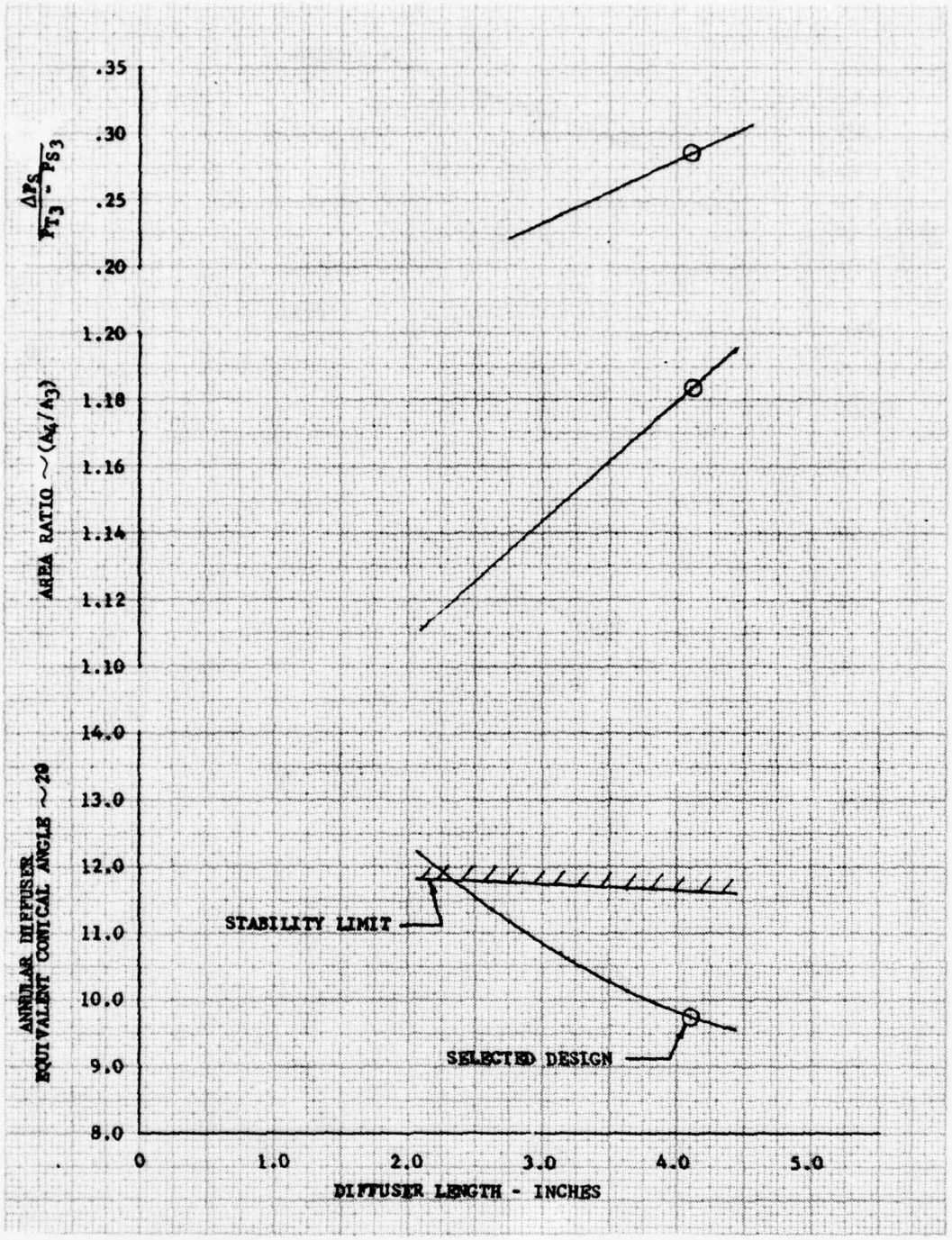


Figure 72. Downstream Diffuser Characteristics as a Function of Diffuser Length

With the selection of chord length, the airfoil gap/chord ratio was defined. Gap/chord ratio in combination with inlet and exit air angles provided sufficient information to design the EGV airfoil aerodynamic contour. The airfoil contour was designed at five span locations (root, ¼ root, mean, ¼ tip and tip) by tailoring the camber and thickness distributions to minimize separation potential, based on boundary layer analysis of the contour and calculated pressure distribution. The five airfoil cross-sections and defining coordinates are presented in Appendix D. Boundary layer analysis of the airfoil suction surface at rig conditions indicated transitional boundary layers with unseparated flow over 90 to 100% of the suction surface length. Results of the boundary layer analysis are presented in Figures 73 through 77.

4. Aerodynamic Design of Configuration 2 (EGV No. 2)

EGV No. 2 had the same basic cascade and downstream diffuser as the first model (discussed above). However, airfoil and endwall modifications, found to improve performance in Phase I, were incorporated. These modifications were:

1. Cutback of the airfoil leading edge by 30% near the endwalls
2. Locally uncambering the airfoil near the endwalls
3. Addition of endwall protrusions along the airfoil pressure surface, extending into the downstream diffuser.

The cutback and uncambered airfoil sections were designed for the same inlet air angle as the unmodified configurations. A 30% reduction of chord was selected based on results from the Phase I study. The trailing edges were set for an exit metal angle of 90 deg, which resulted in an uncambering of 6.5 deg at the root and 6.8 deg at the tip. Figures 78 and 79 present the modified root and tip sections, respectively, superimposed on the unmodified designs. An analysis of the endwall boundary layer growth up to the EGV leading edge indicated a relatively thin boundary layer (velocity boundary layer thickness = 0.26 in. on the OD and the 0.11 in. on the ID). Because it was not possible to accurately account for the effects of the inlet flow control screen and inlet turning vanes on the boundary layer growth, it was decided to begin the cutback 0.3 in. away from the endwall to ensure that it extended beyond the boundary layer.

The filleted pressure side protrusions were designed to minimize the rate of change of streamtube flow area near the endwalls. Examination of the predicted, spanwise loss distribution for EGV No. 1, presented in Figure 80, showed that endwall loses were restricted to about 30% of span near the ID and 20% of span near the OD. Therefore, the area distributions of interest were restricted to streamtubes containing 30% of the flow near the ID and 20% of the flow near the OD. It was assumed that these streamtubes included the endwall loss regions. Figure 81 presents the flow area distributions for the selected ID and OD streamtubes with and without endwall protrusions. It can be seen that the flow area distributions have been modified by the addition of pressure side fillet areas that begin within the cascade at an axial position about 1 in. behind the leading edge. These fillets were extended beyond the airfoil trailing edges by approximately ½ chord length. Figure 82 presents the selected design for EGV No. 2 showing the cutback leading edge and endwall protrusions.

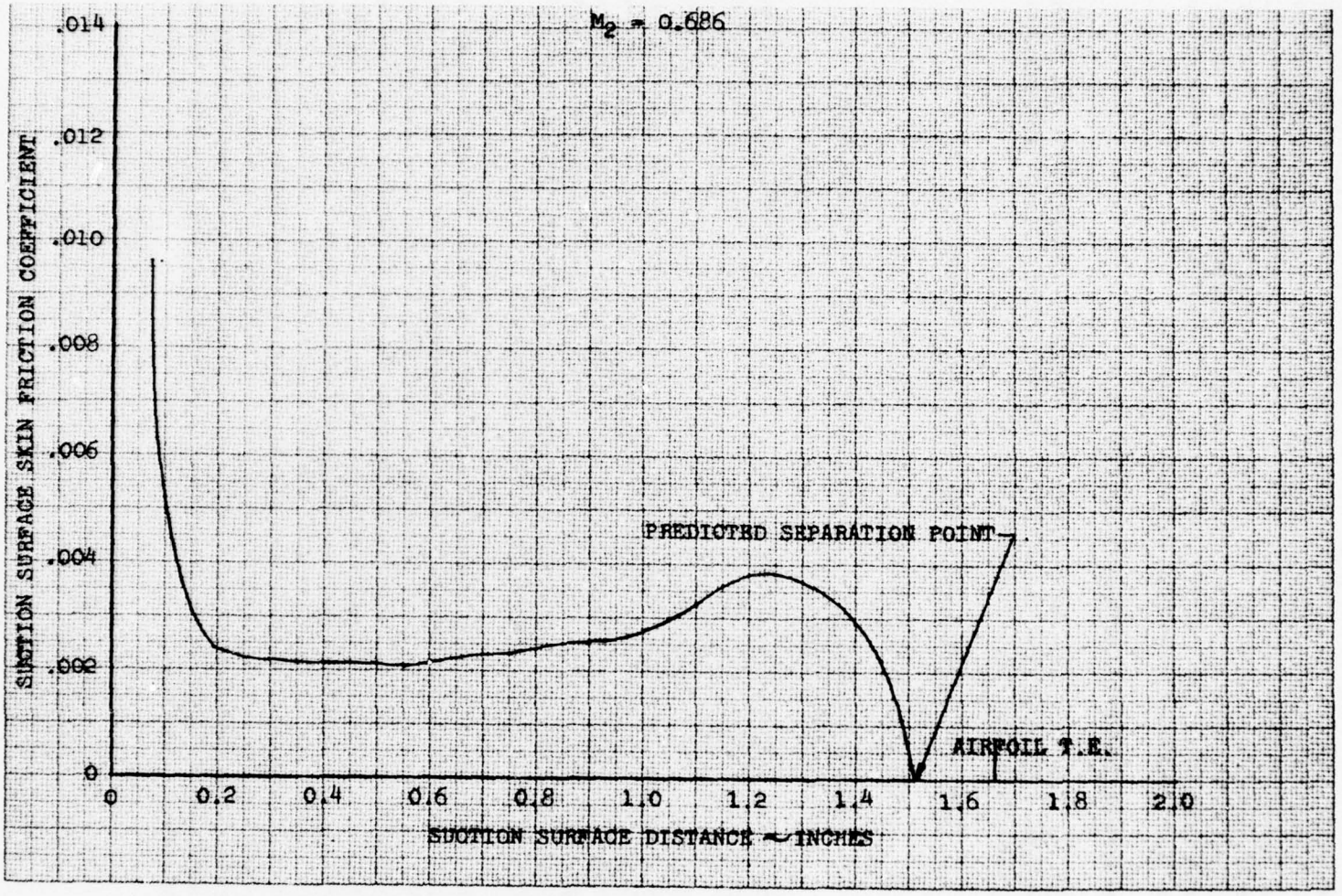


Figure 73. Annular Cascade EGV Root Section Boundary Layer Analysis (M_2 = 0.686)

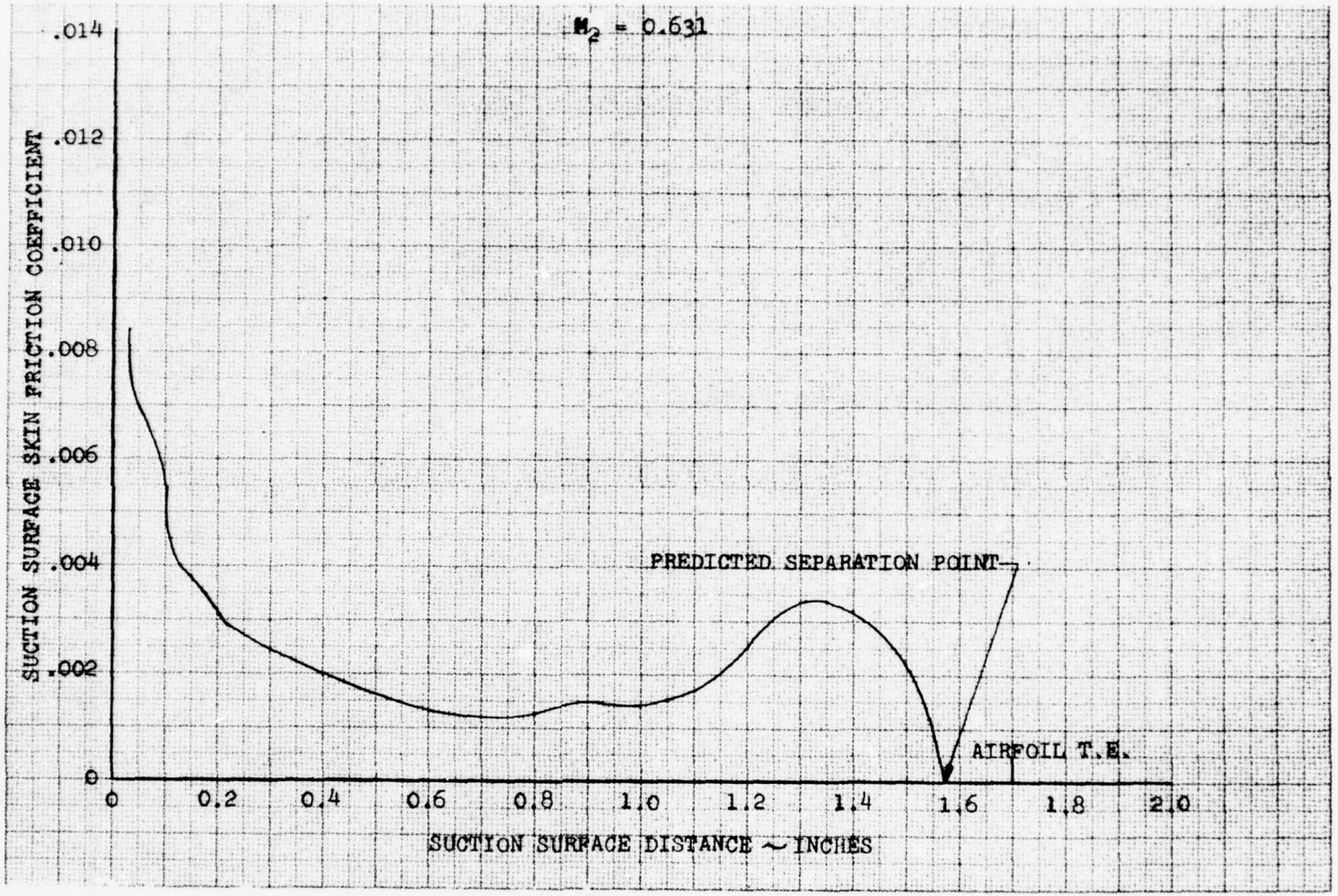


Figure 74. Annular Cascade EGV, ¼ Root Section Boundary Layer Analysis (M_2 = 0.631)

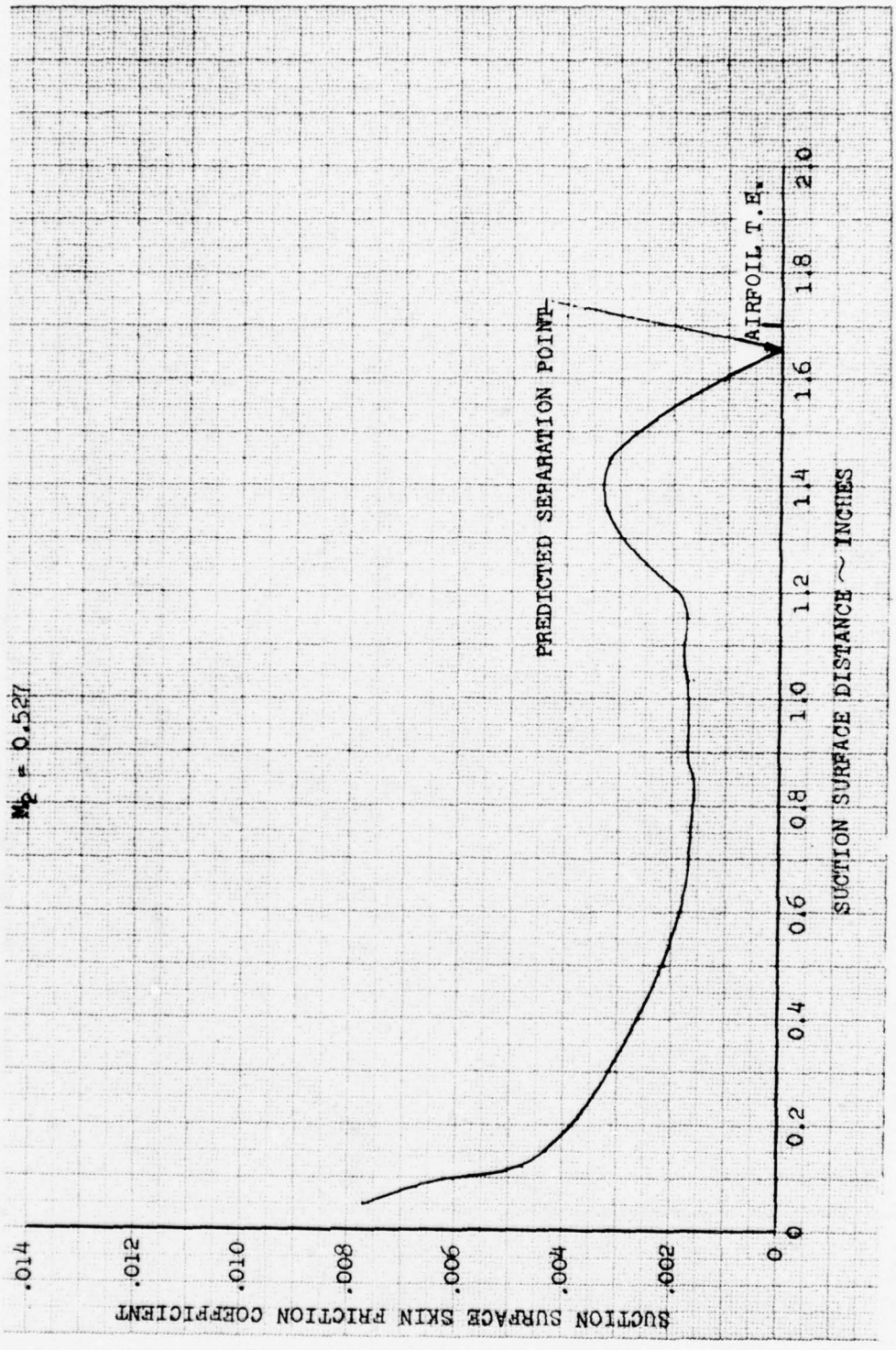


Figure 75. Annular Cascade EGV Mean Section Boundary Layer Analysis (M_2 = 0.527)

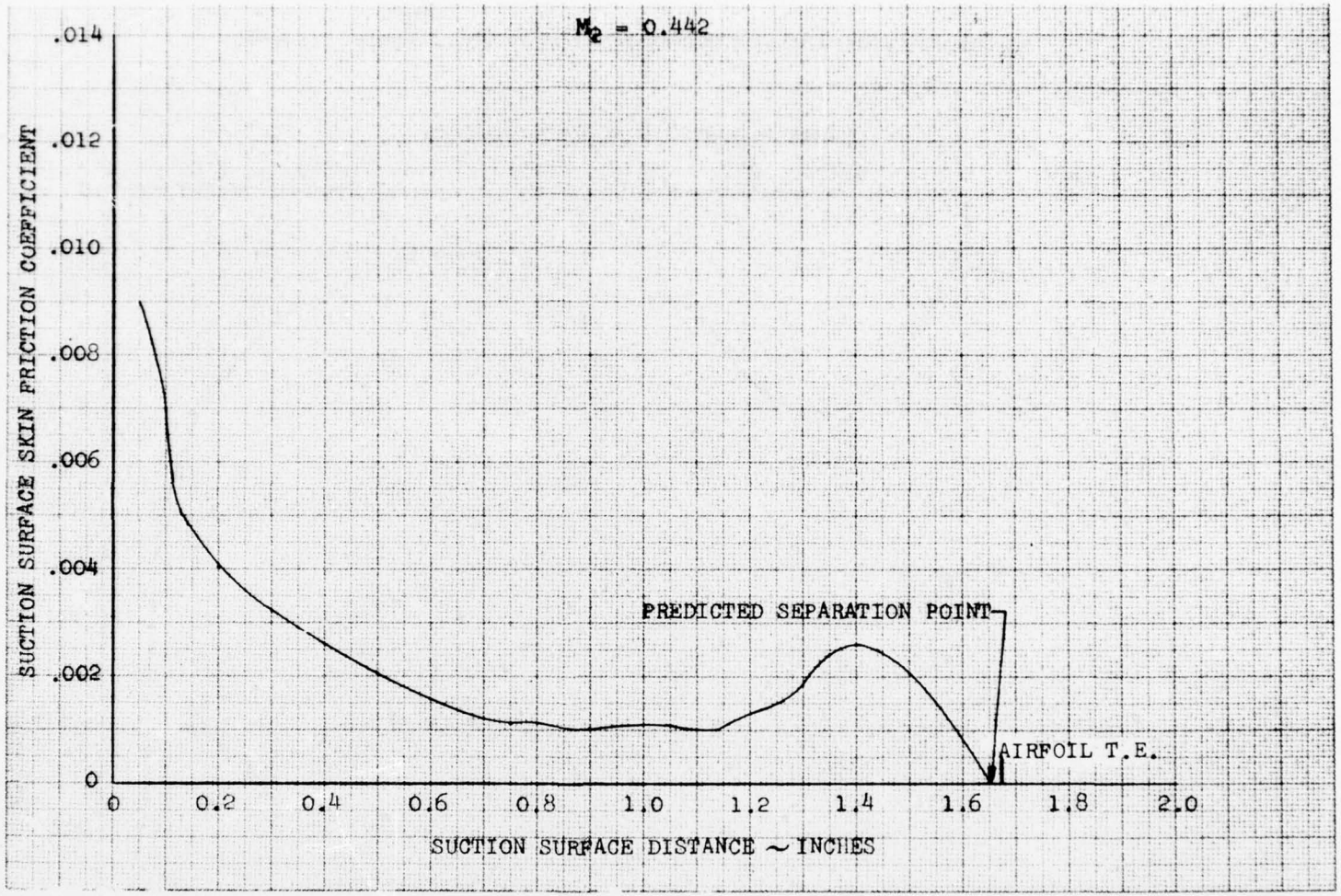


Figure 76. Annular Cascade EGV, ¼ Tip Section Boundary Layer Analysis (M_2 = 0.442)

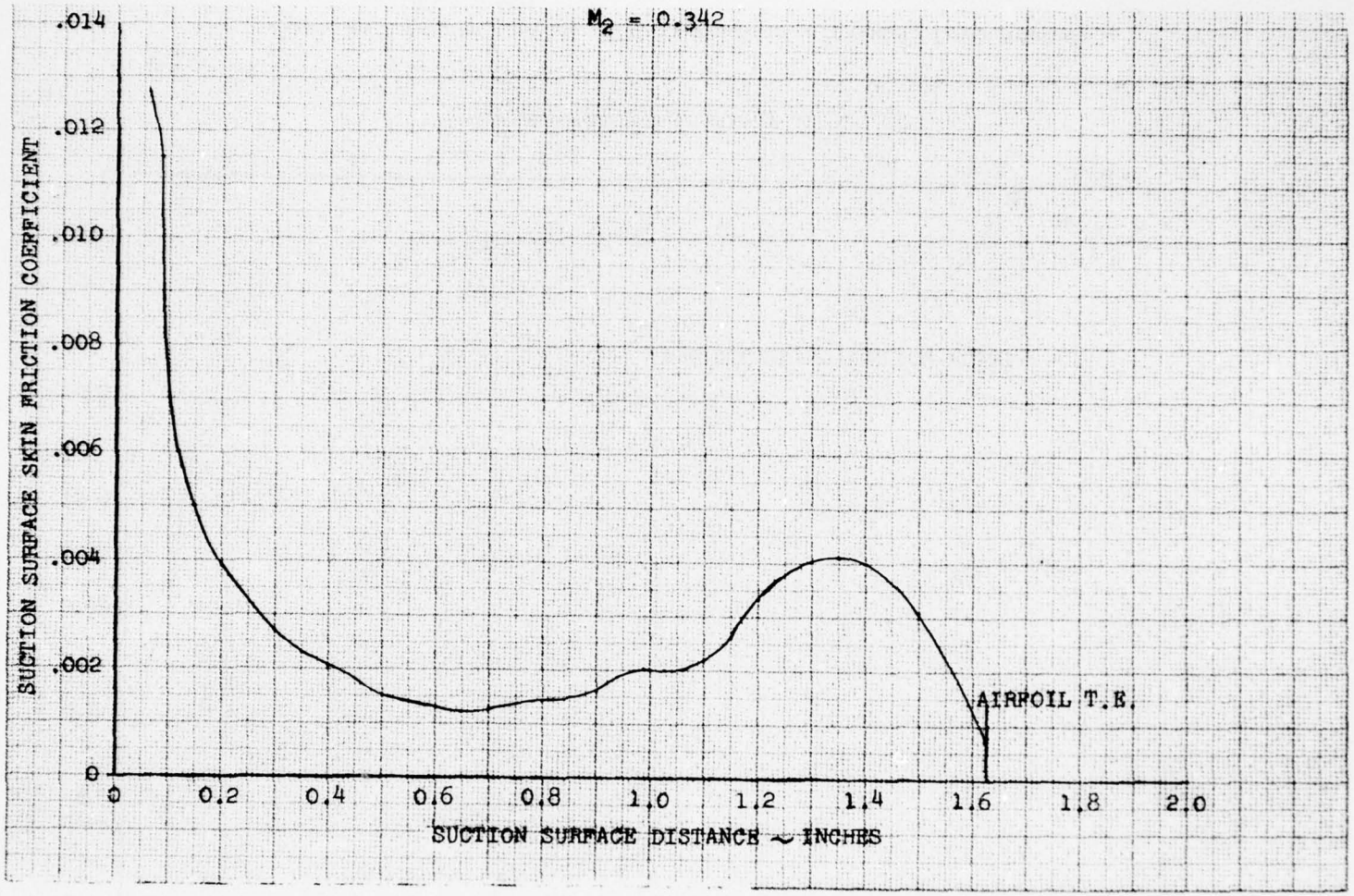


Figure 77. Annular Cascade EGV, Tip Section Boundary Layer Analysis (M_2 = 0.342)

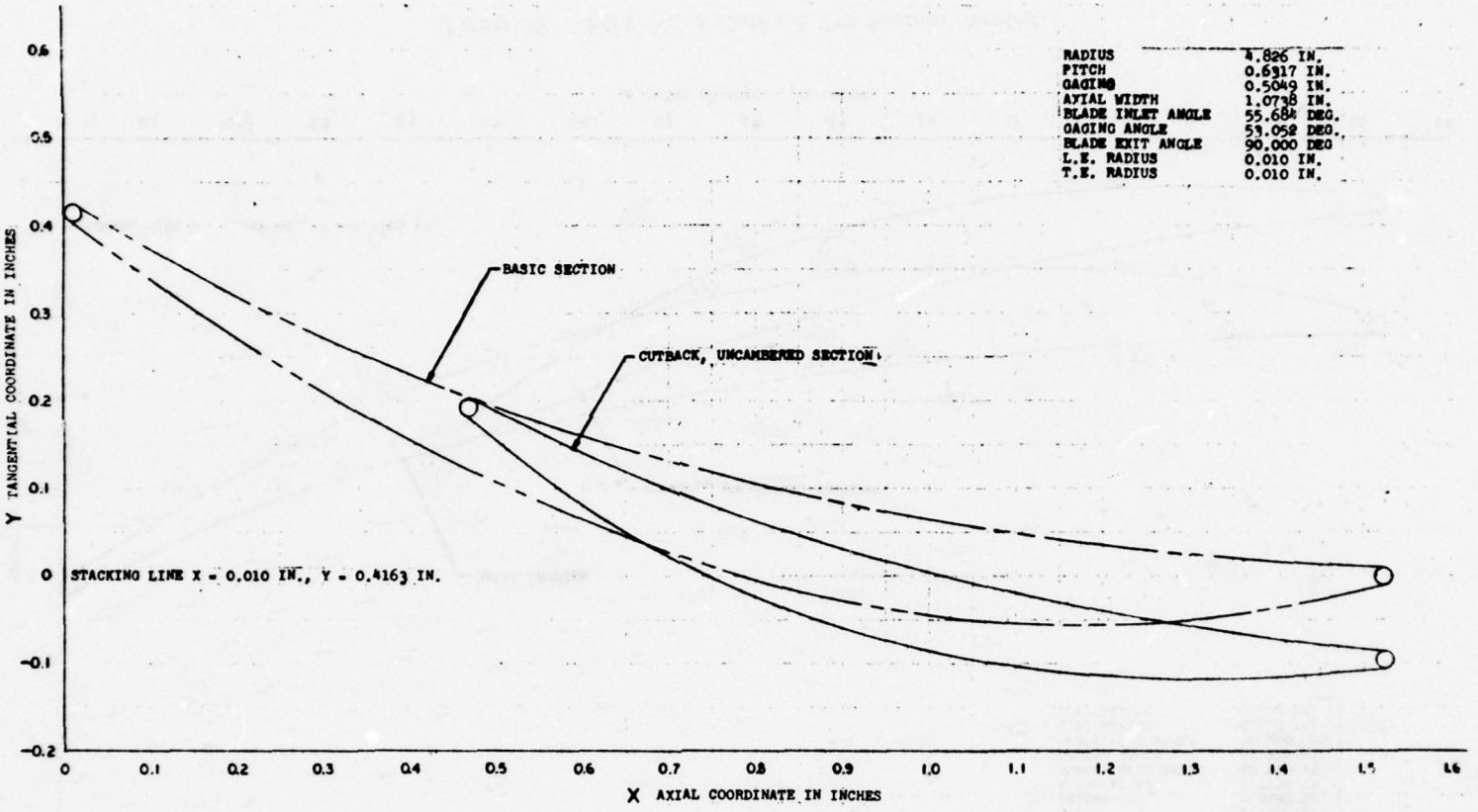


Figure 78. EGV No. 2 Cutback Root Section (Scaled)

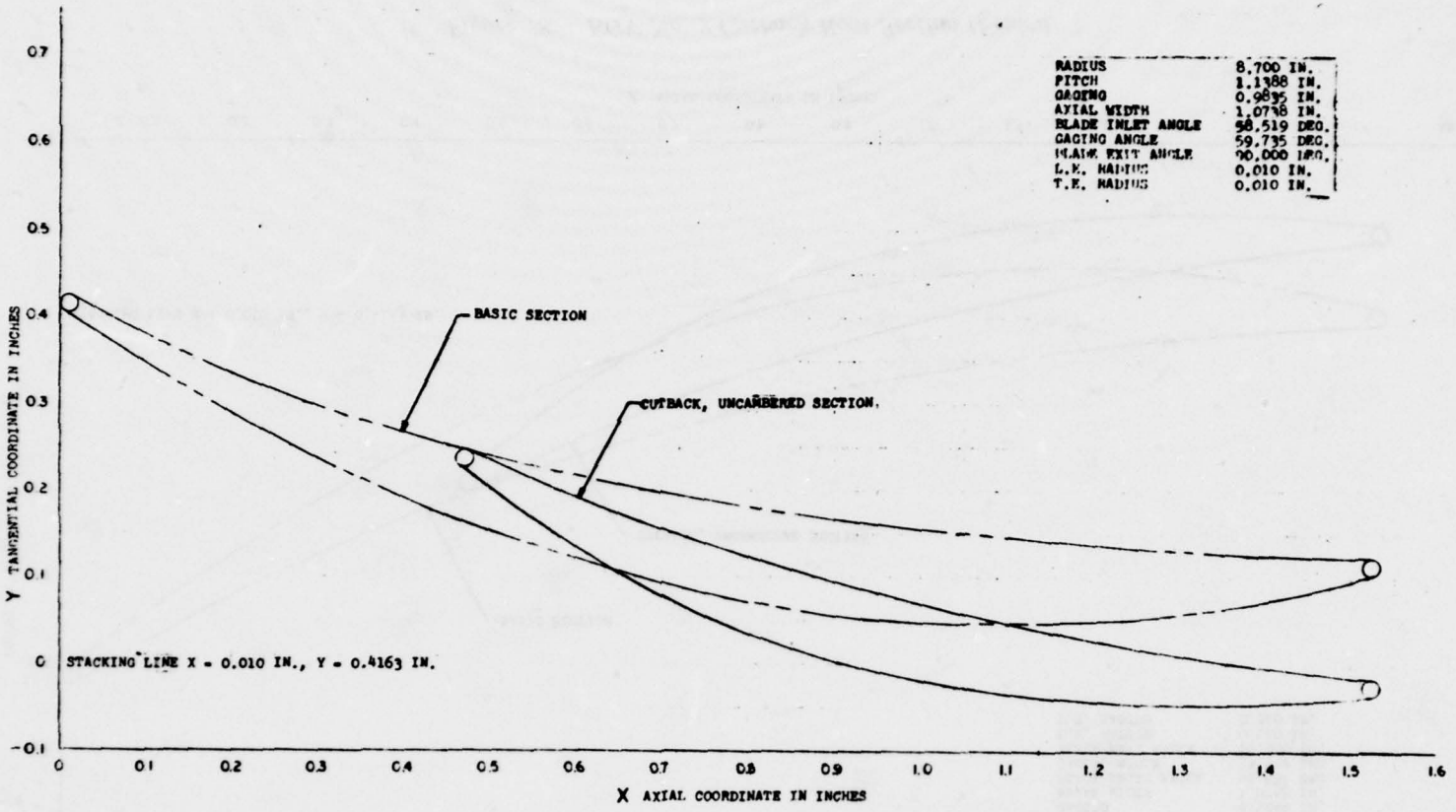


Figure 79. EGV No. 2 Cutback Tip Section (Scaled)

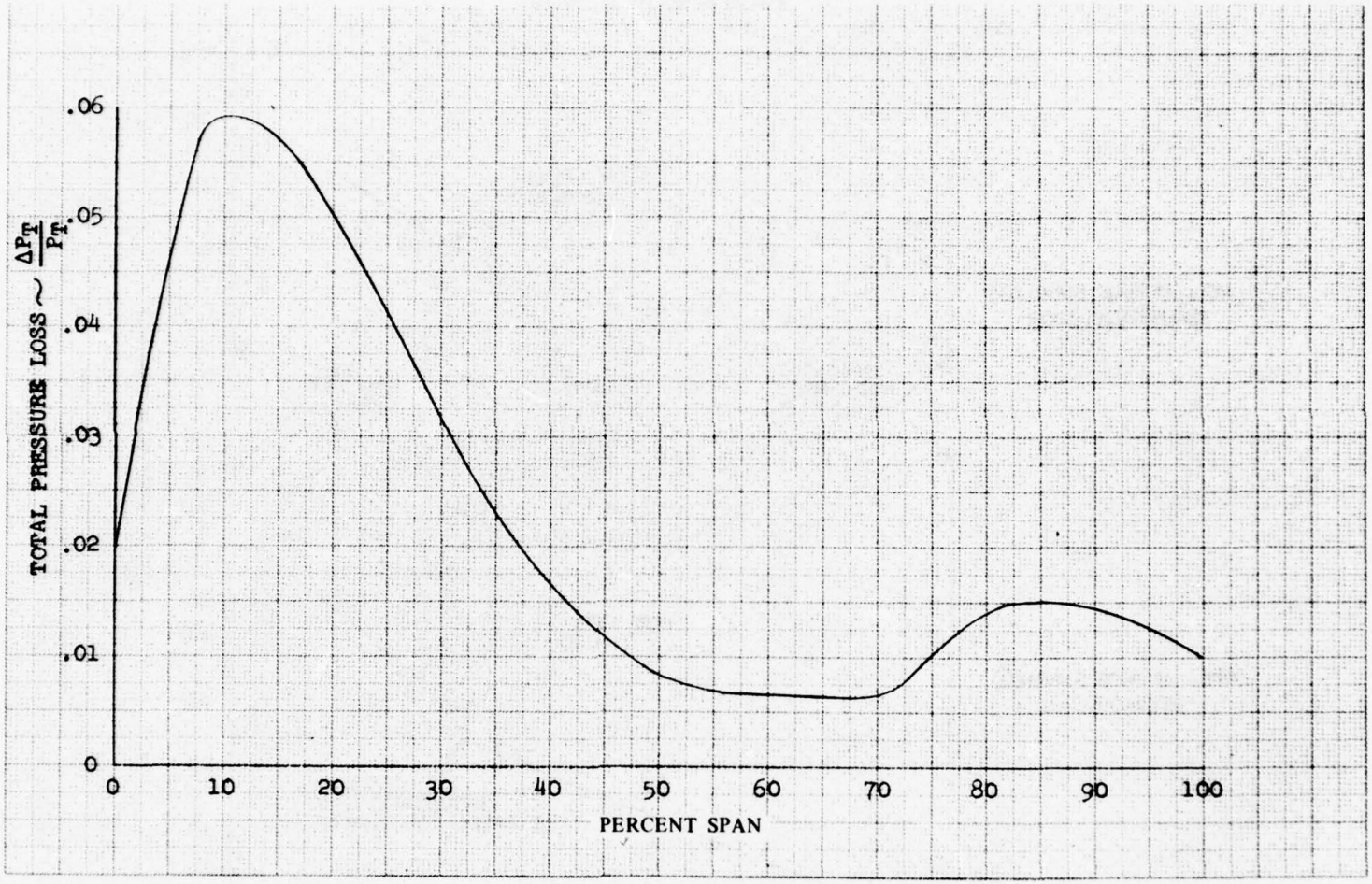


Figure 80. EGV No. 1 Predicted Spanwise Total Pressure Loss Distribution

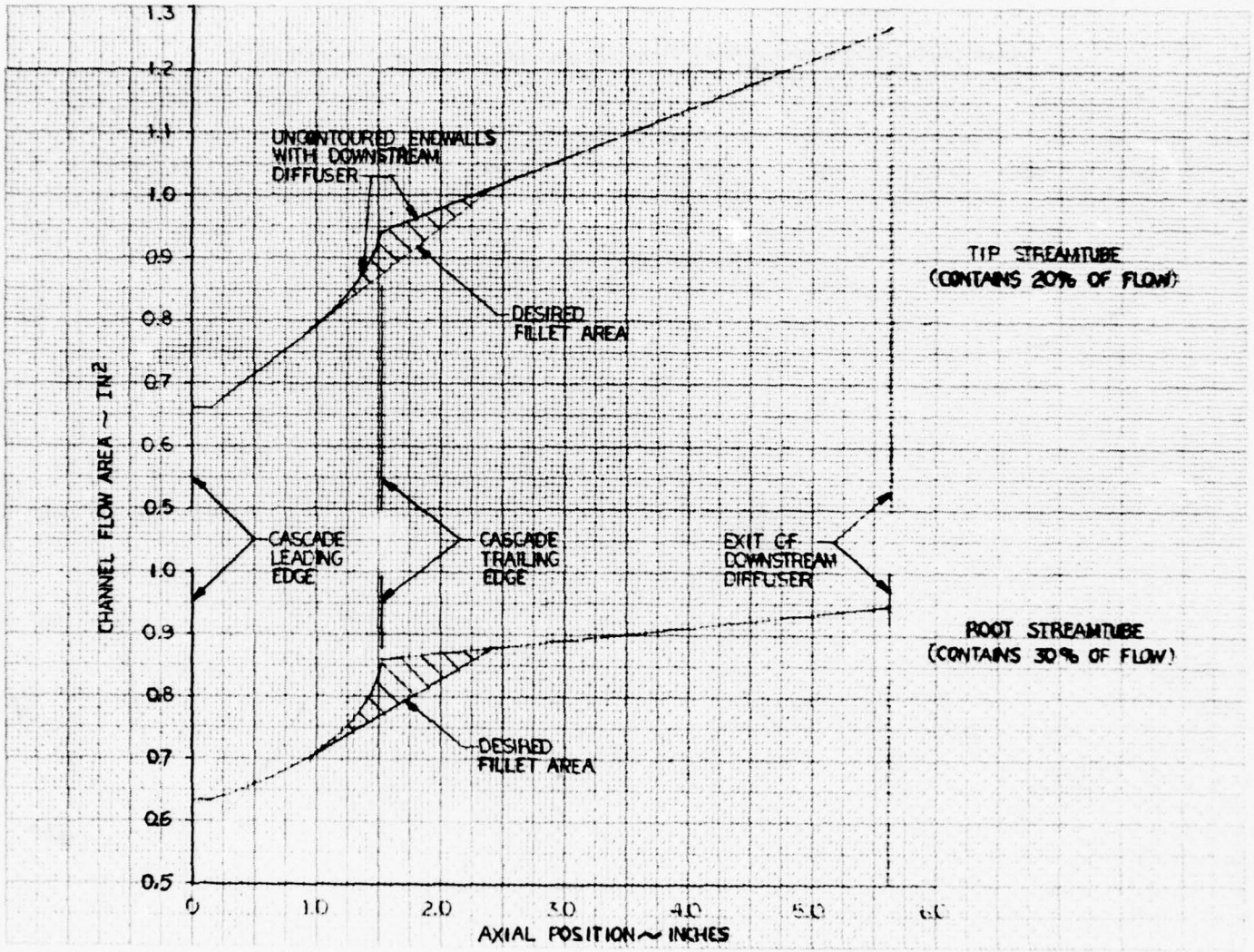


Figure 81. Flow Area Distributions for Selected Root and Tip Streamtubes

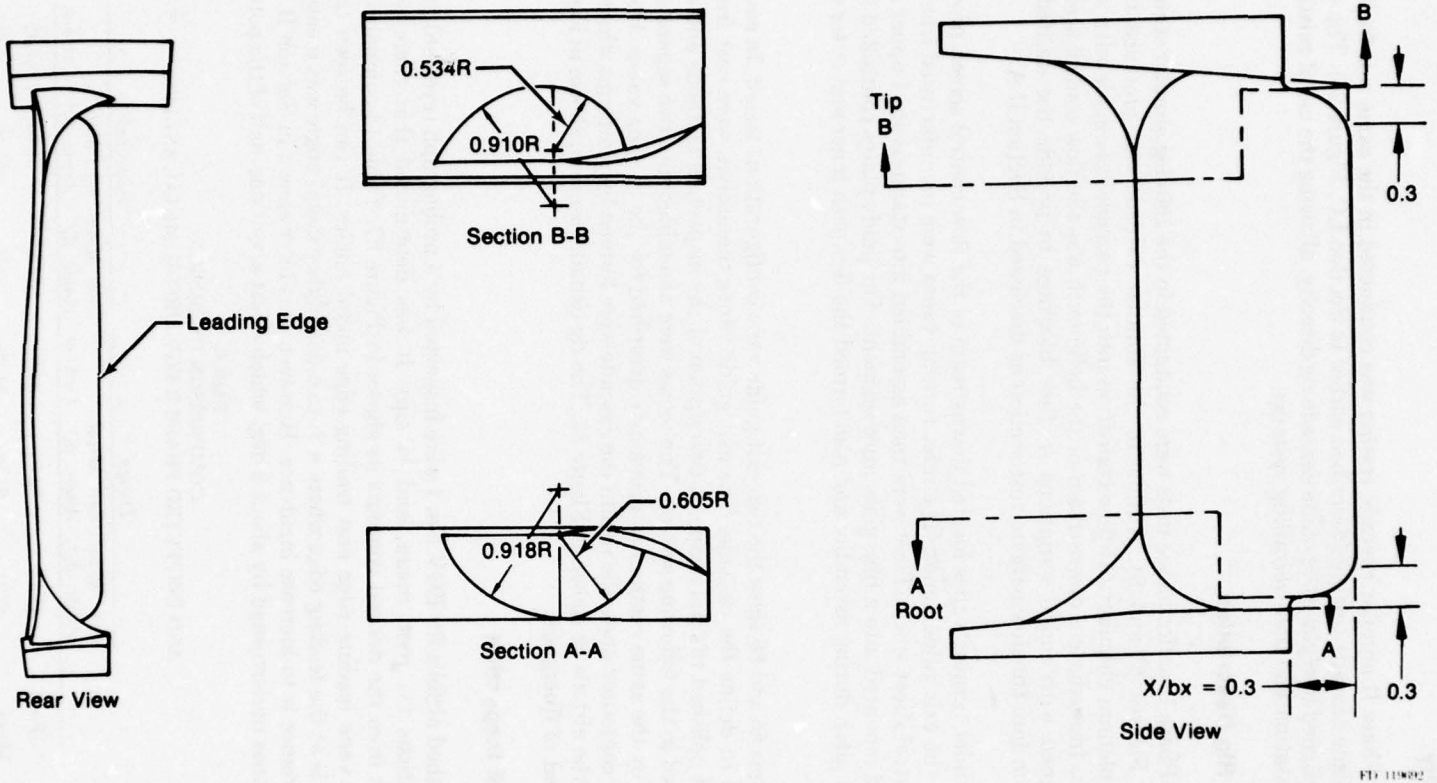


Figure 82. EGV No. 2 Configuration

B. ANNULAR CASCADE TEST SETUP AND DATA REDUCTION

1. Facility

The Phase II annular cascade testing was conducted in the same test facility used for the Phase I plane cascade testing (described earlier in Section I.C, Figure 26). The annular cascade rig was designed to replace the plane cascade rig directly, allowing the use of existing control room instrumentation and data recording systems.

2. Test Rig Description

The Phase II performance tests were conducted in the 180-deg annular segment cascade rig shown in Figures 83 and 84. Airflow to the annular cascade was provided through a 36-in. diameter plenum chamber. Airflow transition into the cascade was made with a fiberglass inlet bellmouth. Immediately downstream of the bellmouth was the flow control screen. This screen was designed with radial variations in flow blockage to provide the desired total pressure distribution into the downstream test section as discussed in Section II.A.

The inlet turning vanes located downstream of the flow control screen provide the desired swirl into the exit guide vanes. The inlet turning vanes were manufactured from 0.040-in. thick stainless steel sheet stock. They were then assembled into stainless steel upper and lower guide plates and mounted into a fiberglass duct segment. The guide plates controlled the vane stagger angle and pitch during assembly and also formed the flowpath inner and outer walls within the cascade.

Figures 85 and 86 show the two exit guide vane configurations tested. In each test, 23 vanes were used to define the cascade. The exit guide vanes themselves were cast from Kirksite and then hand polished to final shape. A description of the inspection methods and airfoil deviation is presented in the following section. The vanes were assembled into two separate fiberglass duct segments by the same method as previously described for the turning vanes. However, for EGV No. 2, the contoured endwalls within the cascade were formed by platforms which were integrally cast with the airfoils as shown in Figure 86. The rig exhaust section, shown in Figure 84, was also constructed of fiberglass.

3. Airfoil Inspection

Finished airfoils for EGV No. 1 were inspected by a probagraph (eyelash) machine at three span positions (¼ root, mean, and ¼ tip). It was determined that there were only minor deviations from the desired contours as shown in Figure 87. Table 13 compares the design and inspected vane leading edge and trailing edge metal angles. It can be seen that the greatest deviation is at the leading edge where a 3- to 6-deg higher metal angle was measured. The effect of this variance is to increase incidence. However, it is later shown in Section II.C that the inlet turning vanes underturned by about 2 deg, which offset about one-half of the potential incidence variation.

TABLE 13
COMPARISON OF DESIGN
AND INSPECTED PHASE II EGV AIRFOIL METAL ANGLES

	Design			*Inspected*		
	Inlet Metal Angle, β_2^*	*Exit Metal Angle, β_3^**	*Camber*	*Inlet Metal Angle, β_2^**	*Exit Metal Angle, β_3^**	*Camber*
¼-Root	47.18	82.00	50.82	52.83	81.75	45.42
Mean	47.11	81.50	51.39	51.67	84.58	43.75
¼-Tip	50.55	81.50	47.95	53.42	83.42	43.16

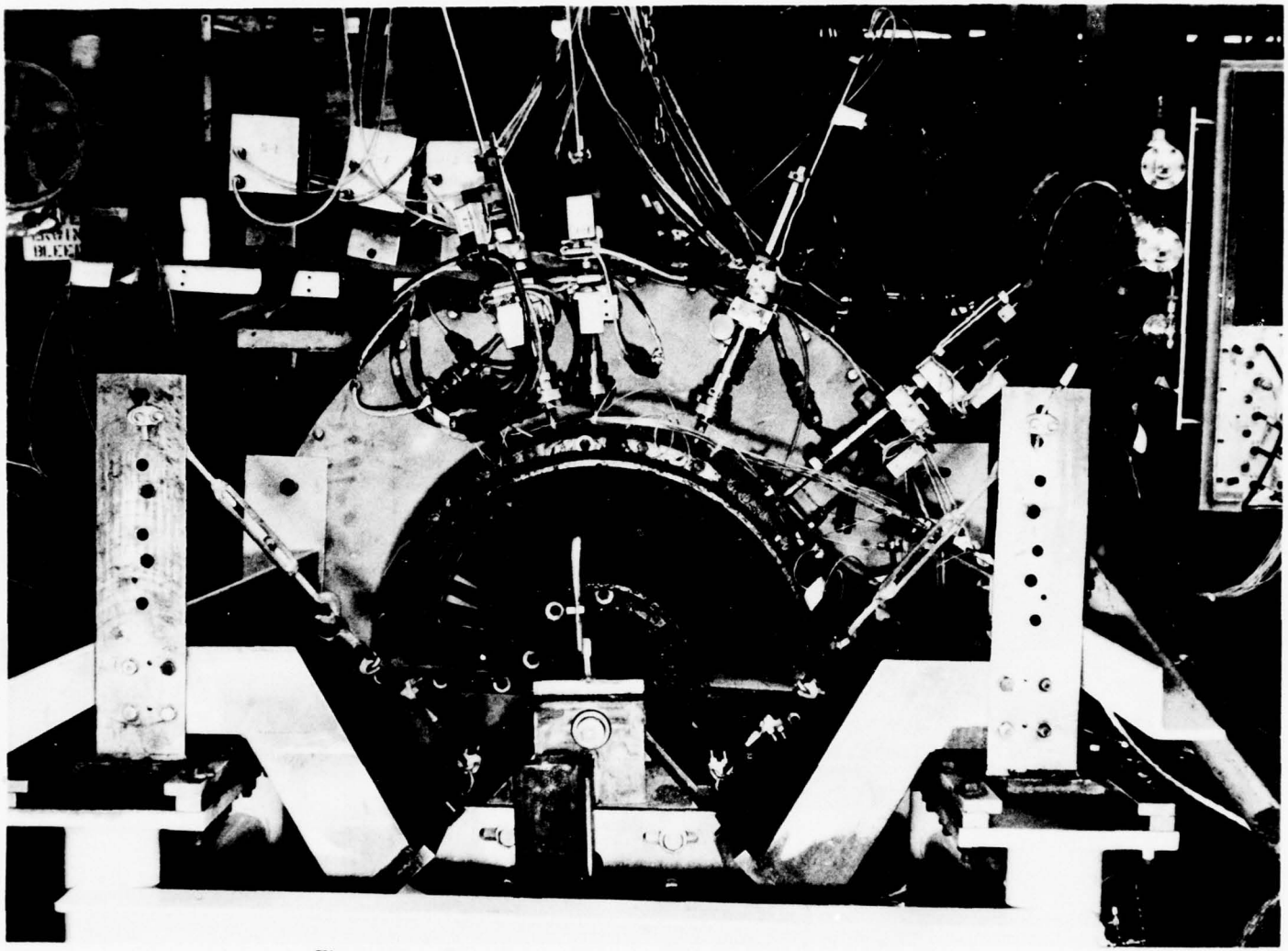


Figure 83. Rear View of 180-deg Segment Annular Cascade Rig

FAE 339691

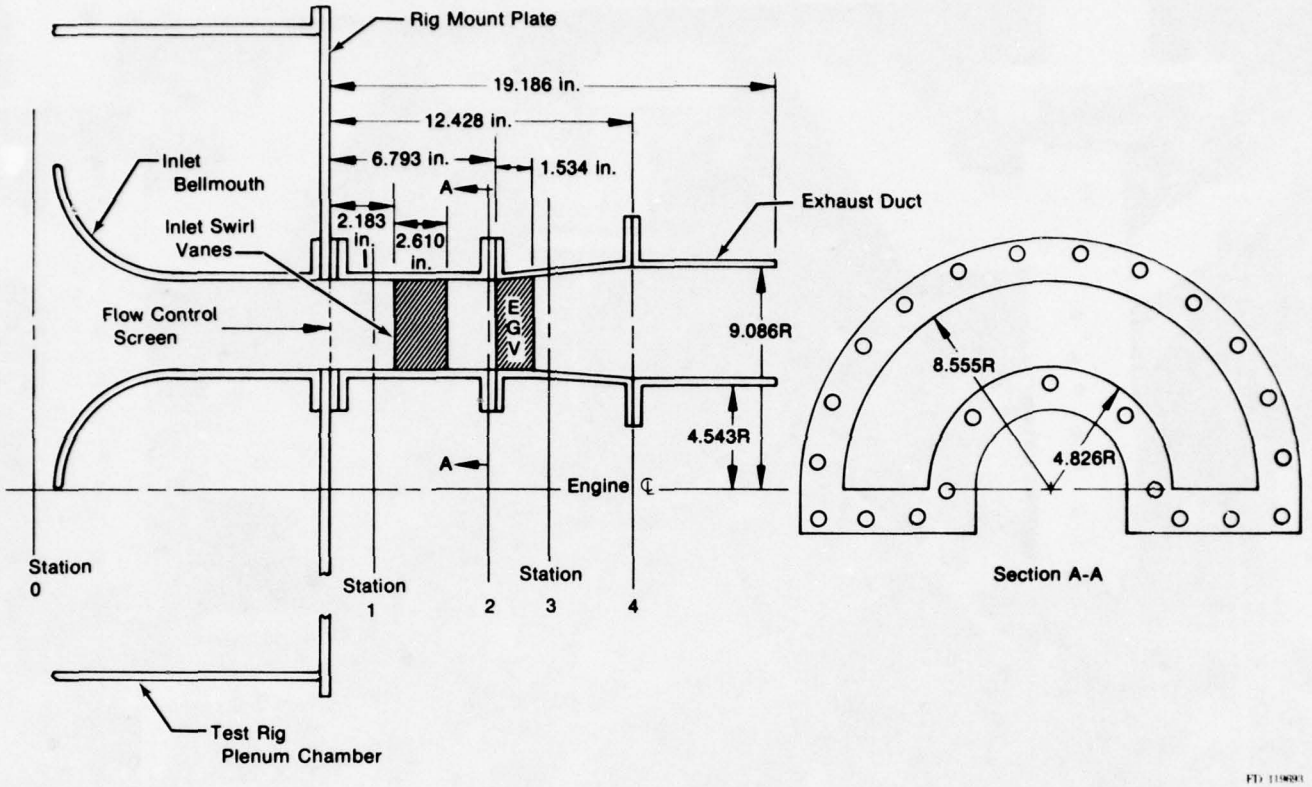


Figure 84. 180-deg Segment Annular Cascade Rig Schematic

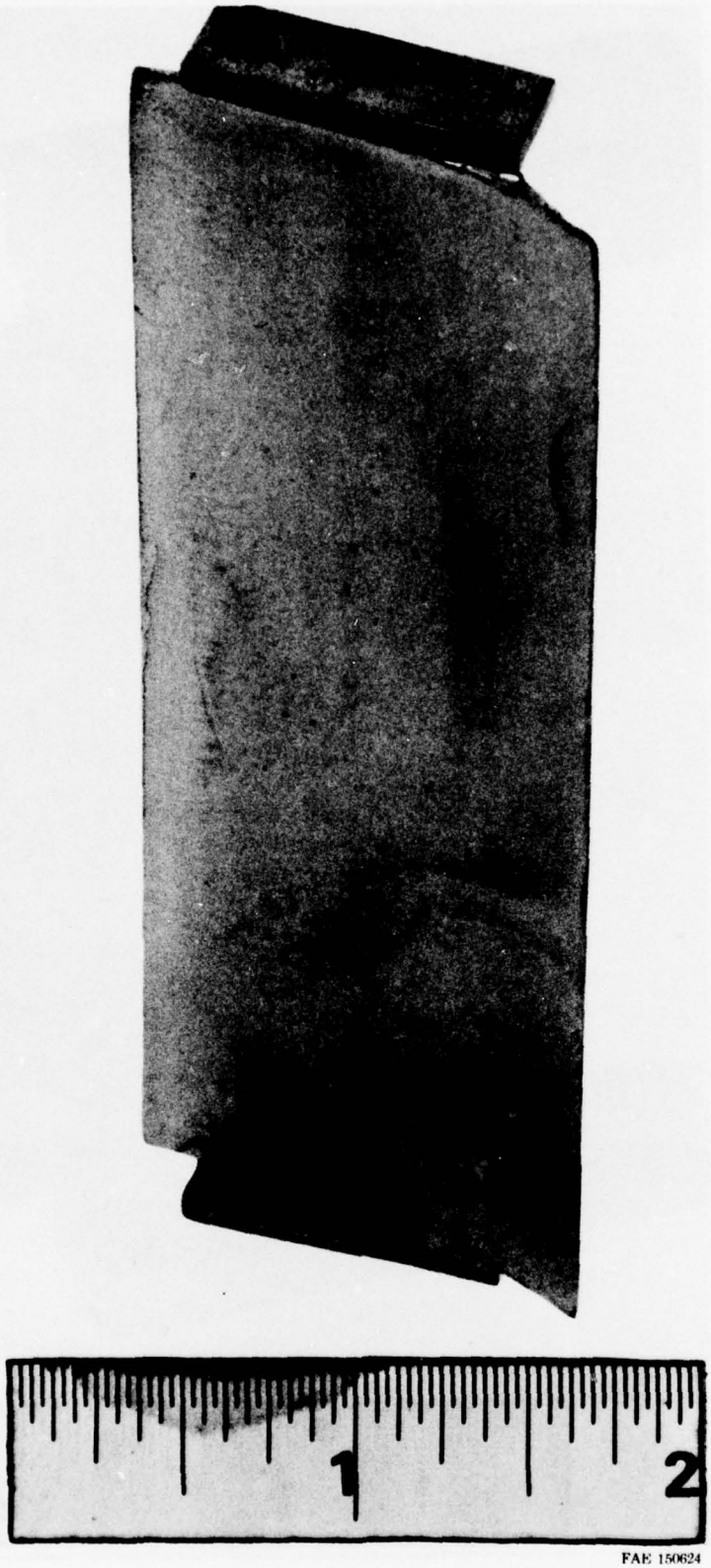
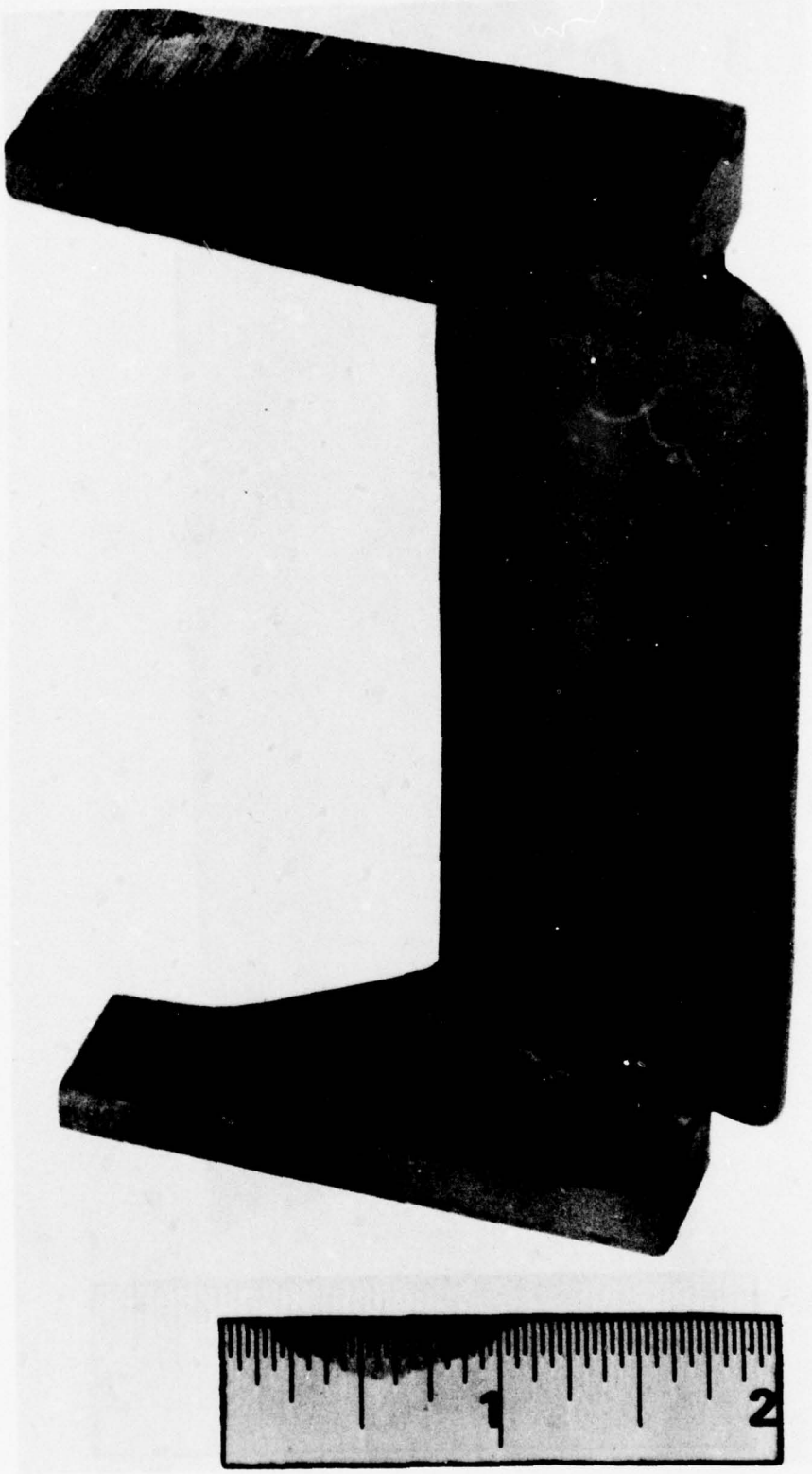


Figure 85. Annular Cascade Test Airfoil, EGV No. 1



AE 150625

Figure 86. Annular Cascade Test Airfoil, EGV No. 2

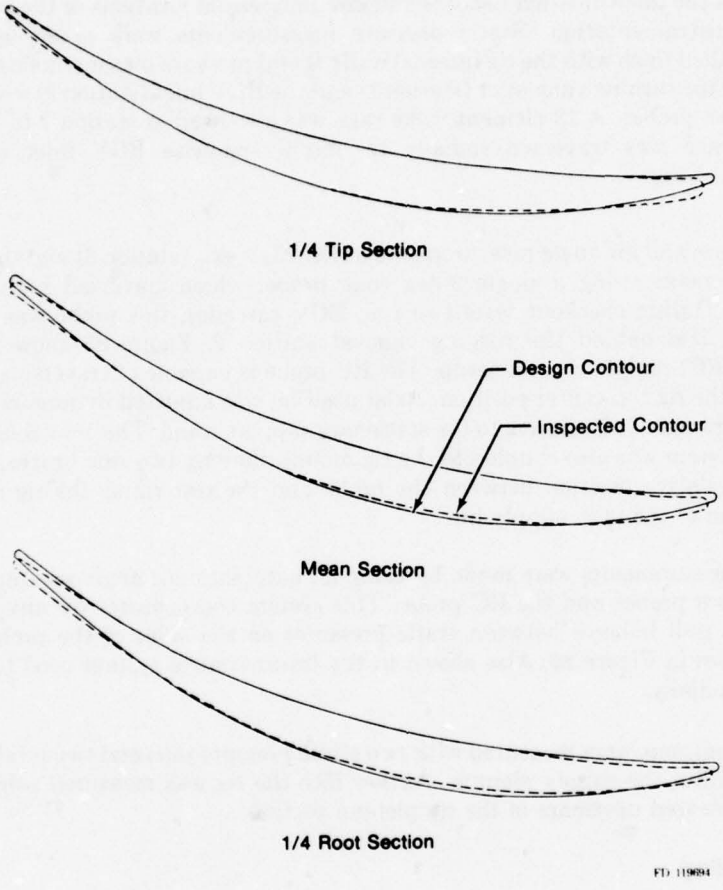


Figure 87. EGV No. 1 Airfoil Inspection

The modified endwall regions of EGV No. 2 were inspected by hand with templates and deviations were corrected by adding or removing material. The casting pattern for the central portion of EGV No. 2 was the EGV No. 1 pattern for the same section, so the inspected airfoil cross-sections presented in Figure 87 are also representative of EGV No. 2.

4. Test Rig Instrumentation

Exit guide vane performance was determined by measuring flow conditions at four different axial positions within the test rig. Figure 84 defines each of these axial positions or stations. At each station, static pressures, total pressures, and air angle measurements were recorded. Appendix E gives the identification headers and circumferential locations of the wall static and traverse probe instrumentation. Static pressure measurements were made using 0.062-in. hypotubing, installed flush with the rig internal walls. Total pressure measurements and air angle measurements at the turning vane inlet (station 1) and the EGV inlet (station 2) were made using minicobra traverse probes. A 13-element wake rake was also used at station 2 to measure total pressure. This rake was traversed radially to obtain spanwise EGV inlet total pressure distributions.

Total pressure and air angle measurements at the EGV exit (station 3) and the diffuser exit (station 4) were made using a single 9-deg cone probe, which traversed both radially and cirumferentially. During checkout tests (with no EGV cascade), this probe was positioned to survey the flow field behind the turning vane at station 2. Figure 88 shows the radially-circumferential (RC) probe actuator setup. The RC probe is capable of traversing 30 deg to the right and left of the rig top center position. Axial position was adjusted by manually sliding the probe actuator forward or aft relative to the stationary support stand. This movable section of the probe actuator system was also coupled to the rig mount plate by two side braces. These braces maintained the relative position between the probe and the test rig as the rig moved due to thermal expansion of the inlet supply line.

Air angle measurements were made by using an automatic air angle seeking system with both the minicobra probes and the RC probe. This system compensates for any change in air angle by using a null balance between static pressures on the sides of the probes. A system schematic is shown in Figure 89. Also shown in the linear control system used to position the traverse probes radially.

Rig inlet conditions were measured with two static pressure taps and two total temperature probes located within the supply plenum. Airflow into the rig was measured using a 7.250-in. diameter orifice located upstream of the rig plenum section.

5. Data Recording

All transient data measured with the traverse probes and a selected amount of steady-state data necessary to define rig inlet conditions and flowrates were recorded on the test stand's automatic data recording system. All remaining data were measured using manometers and gages. The data recorded with manometers were limited to steady-state wall static pressures. Some instrumentation monitored by the data system was also coupled to manometers and gages to define and set the test points. In such instances, the recorded data was used in the final data reduction.

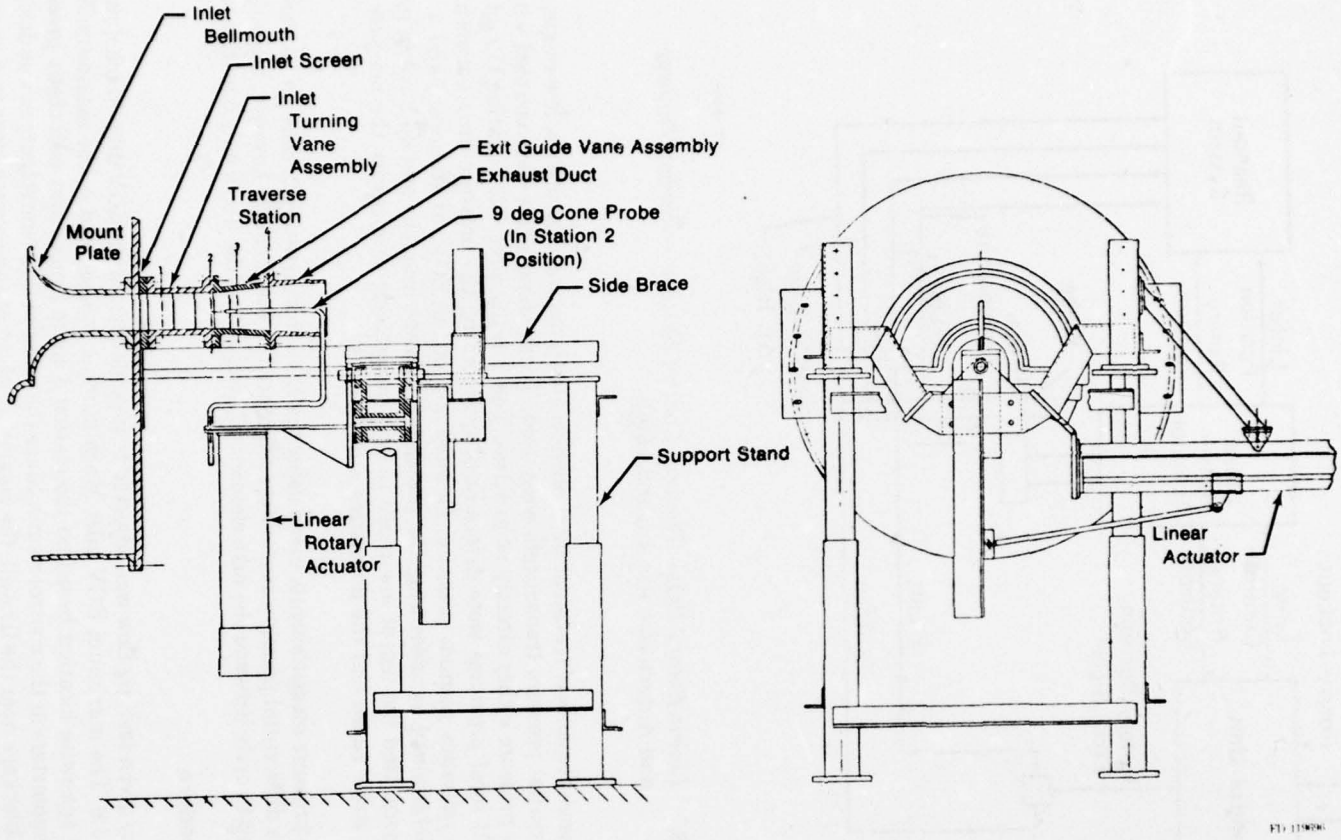


Figure 88. Annular Cascade Radial-Circumferential Probe Traverse System

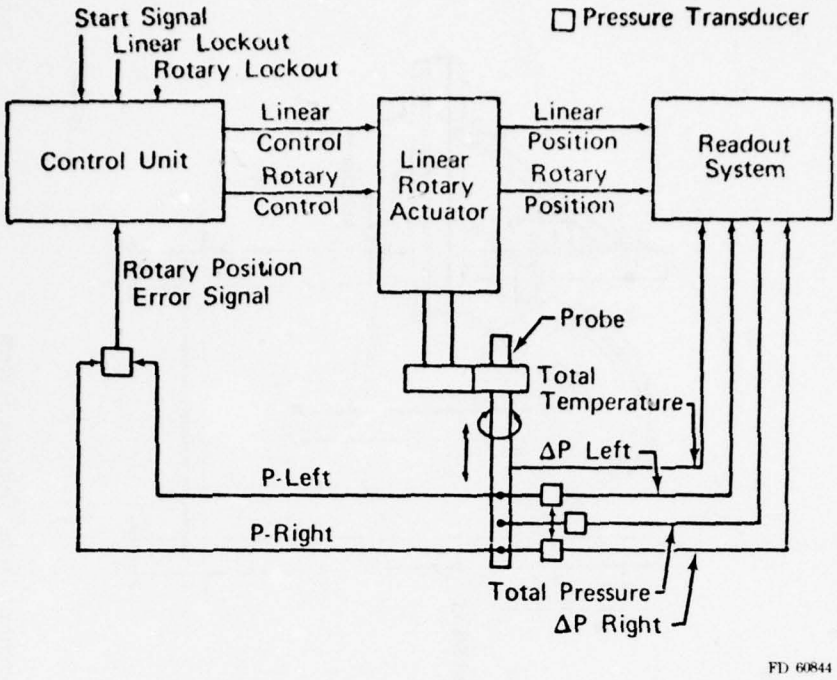


Figure 89. Linear-Rotary Probe Traverse Control System — Radial Traverse and Automotive Air Angle Seeking

During measurements of transient total pressures with the traverse probes, low-range, high-accuracy differential pressure transducers were used. These transducers were coupled with the known plenum pressure either directly or in series. The turning vane inlet (station 1) and EGV inlet (station 2) total pressures were determined by recording the pressure drop between each probe and the reference plenum pressure. Downstream of the EGV, at stations 3 and 4, total pressure was determined by measuring the pressure difference from the station 2 cobra probes. This method permitted the use of low-range (5 psi) transducers to measure the pressure drop across the exit guide vanes and the downstream diffuser.

The total pressure measurements made using the EGV inlet (station 2) rake probe were also recorded with a differential pressure transducer referenced to the plenum; however, a scanivalve system was used to cycle between the rake elements, necessitating the use of only one transducer.

6. Test Procedure

During any given test, rig flow was adjusted to provide maximum EGV inlet Mach numbers of 0.25, 0.7, or 0.9. The maximum EGV inlet Mach number was defined as the maximum Mach number at any spanwise location based on the station 2 cobra probes and wall static pressures (read out on manometers in the control room). Since the rig inlet flow control screen was designed with minimum blockage near the ID wall, the maximum Mach numbers were measured at or near the 10% span location. Once the desired condition was established, the upstream plenum pressure and temperature were noted and held constant.

The first test sequence in Phase II was conducted to verify that the rig adequately simulated the design EGV inlet conditions. During this rig checkout, the EGV test section and the exhaust section were not installed. It was, therefore, possible to move the radial-circumferential (RC) traverse probe upstream to the station 2 location and completely survey the flow field total pressure and air angle approaching the EGV models. Data from RC probe surveys obtained during the checkout test, also provided an accurate reference for comparison with the wake rake and cobra probes, located at station 2.

At each test point, the traverse probes (cobra and wake rake) at the EGV inlet (station 2) were positioned to correspond with the percent span position of the RC probe. The RC probe was then traversed circumferentially through an arc of 60 deg during the checkout test and early performance tests. The circumferential range was reduced to 45 deg during the later test points (to speed up testing) after examination of the data indicated there would be no loss of accuracy.

Performance tests were conducted with an EGV test section and the exhaust section in position (see Figure 84). During each test Mach number, the RC traverse probe was positioned to survey the flow field at the EGV exit (station 3) and then moved downstream to survey the diffuser exit at station 4. In this way, it was possible to isolate diffusion and pressure loss performance for the EGV cascade alone (stations 2-3), the combination cascade and diffuser (stations 2-4), and the downstream diffuser alone (stations 3-4).

7. Data Reduction

The performance evaluation of the Phase II annular cascade tests was based on total pressure, static pressure, and air angle data taken at the EGV inlet (station 2) and exit (station 3) and the downstream diffuser exit (station 4), as described earlier.

Data from the station 2 rake probe was used to define the EGV inlet total pressure. This 13-element wake rake was designed to survey across one pitch of the turning vane at the vane tip section. This required that only selected elements of the probe be used to determine the circumferential average pressure as the probe was radially traversed. Figure 90 shows the range of data sampling available with the rake probe and identifies the selected probe elements arithmetically averaged to obtain pressure at each span location. Average EGV inlet total pressure was based on an area weight average of the spanwise distribution. Static pressures at the station 2 OD and ID were obtained by arithmetically averaging data from the six OD and six ID static pressure taps, respectively. A linear distribution of static pressure from the ID to the OD was assumed for the use in the calculation of spanwise Mach number distributions. Air angle distributions at the EGV inlet were based on the checkout run surveys at station 2. Cobra probe air angle measurements were recorded to ensure that no variation of rig operation occurred between the checkout tests and the performance tests.

Total pressure and air angle measurements behind the EGV were obtained from radial-circumferential traverse probe surveys. Data from this probe were arithmetically averaged in the circumferential direction to obtain spanwise distributions. These profiles were then used to calculate area weight total pressure and air angles at the EGV exit (station 3) and the diffuser exit (station 4). Data from the static pressures taps at stations 3 and 4 were arithmetically averaged just as discussed above for station 2.

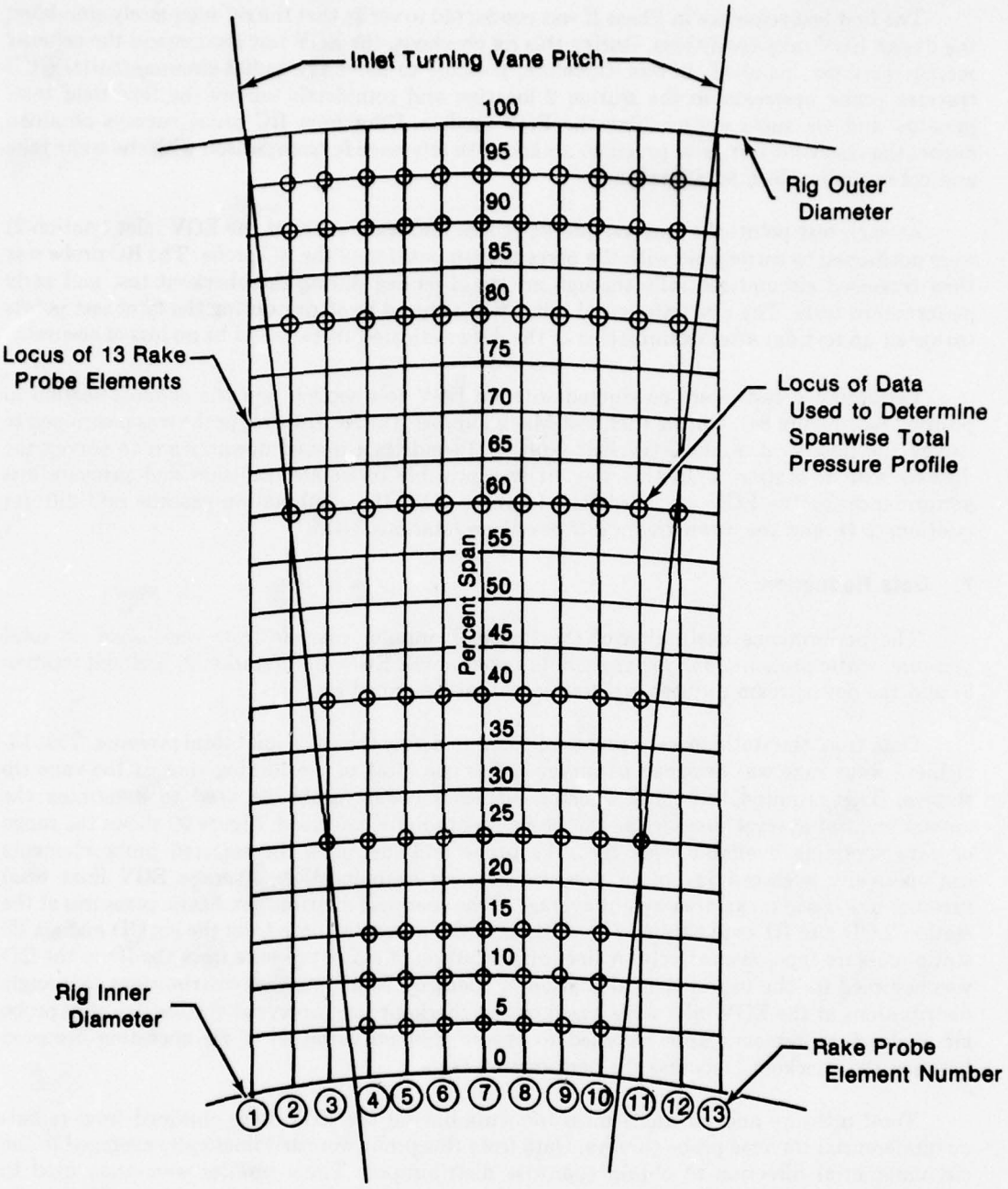


Figure 90. Annular Cascade Rig Wake Rake Element Traverse Positions (Station 2)

This data reduction process provided the information to calculate the following performance parameters:

$$\left(\frac{\Delta P_T}{P_T}\right)_{2-3} = \frac{P_{T_2}-P_{T_3}}{P_{T_2}} \quad \left(\frac{\Delta P_T}{P_T}\right)_{2-4} = \frac{P_{T_2}-P_{T_4}}{P_{T_2}} \quad \left(\frac{\Delta P_T}{P_T}\right)_{3-4} = \frac{P_{T_3}-P_{T_4}}{P_{T_3}}$$

$$\left(\frac{\Delta P_S}{P_T-P_S}\right)_{2-3} = \frac{P_{S_3}-P_{S_2}}{P_{T_2}-P_{S_2}} \quad \left(\frac{\Delta P_S}{P_T-P_S}\right)_{2-4} = \frac{P_{S_4}-P_{S_2}}{P_{T_2}-P_{S_2}} \quad \left(\frac{\Delta P_S}{P_T-P_S}\right)_{3-4} = \frac{P_{S_4}-P_{S_3}}{P_{T_3}-P_{S_3}}$$

$$M_2 = f\left(\frac{P_{S_2}}{P_{T_2}}\right)_{av} \qquad M_3 = f\left(\frac{P_{S_3}}{P_{T_3}}\right)_{av} \qquad M_4 = f\left(\frac{P_{S_4}}{P_{T_4}}\right)_{av}$$

$M_2max = f\left(\frac{P_{S_2local}}{P_{T_2max}}\right)$ P_{S_2local} obtained from a linear distribution between average ID and OD static pressure

θ_{eq} = Equivalent Conical Angle (See Section I and Appendix C)

$(A_3/A_2)_{eq}$ = Equivalent Area Ratio (See Section I and Appendix C)

$$\eta_D = \frac{\Delta P_S/(P_T-P_S)_{,measured}}{\Delta P_S/(P_T-P_S)_{,ideal}}$$

C. AIRFOIL PERFORMANCE TEST RESULTS

1. General

This section presents the Phase II test results for the rig checkout tests and for each of the two EGV test configurations. Each configuration was tested at three Mach numbers (0.25, 0.7, and 0.9). These test point Mach numbers were established at the EGV inlet (station 2) near the ID where the maximum Mach number occurred due to the simulated engine velocity distribution. The test Mach number was, therefore, referred to as M_2max, Table 14 presents the Phase II test

TABLE 14
TEST PROGRAM SUMMARY

Test No.	*Radial Circumferential Probe Survey Station*	*Configuration*	*Maximum Inlet Mach No.*
1	2	Check Case (No EGV)	0.7
2	2	Check Case (No EGV)	0.25
3	2	Check Case (No EGV)	0.90
4-3	3	EGV No. 1	0.7
4-4	4	EGV No. 1	0.7
5-3	3	EGV No. 1	0.25
5-4	4	EGV No. 1	0.25
6-3	3	EGV No. 1	0.90
6-4	4	EGV No. 1	0.90
7-3	3	EGV No. 2	0.7
7-4	4	EGV No. 2	0.7
8-3	3	EGV No. 2	0.25
8-4	4	EGV No. 2	0.25
9-3	3	EGV No. 2	0.90
9-4	4	EGV No. 2	0.90

sequence. It will be noted that test numbers for the performance configurations include the station at which the radial-circumferential probe was located. This was done because almost a complete set of data (total pressure, temperatures, air angles, and static pressures) was obtained during surveys with this probe when it was moved to each of its axial locations. The only information lacking was total pressure and air angle at the station not being surveyed. Table 15 presents all of the measured performance parameters for Phase II.

2. Checkout Tests

The objective of the checkout test was to verify that the test rig adequately simulated the design EGV inlet conditions. The checkout test configuration consisted of the rig inlet bellmouth, the flow control screen, and inlet swirl vanes. No EGV cascade was installed for these tests.

Figure 91 presents the swirl vane exit isobar plot from the checkout run at design conditions ($M_{2max} = 0.7$) for the 60-deg segment surveyed. The wakes from five swirl vanes and the two cobra probes can be identified. A total of 15 swirl vane passages were contained in the 180-deg annular segment so that each passage spanned a 12-deg segment. The periodicity of the inlet flow field was examined by comparing radial total pressure and air angle distributions obtained by averaging data from a single passage (a 12-deg segment) with averages from three passages (a 36-deg segment). Figure 92 shows the results of this study. It can be seen that EGV inlet total pressure agreed within 0.1 psi and air angle varied by only 1 deg.

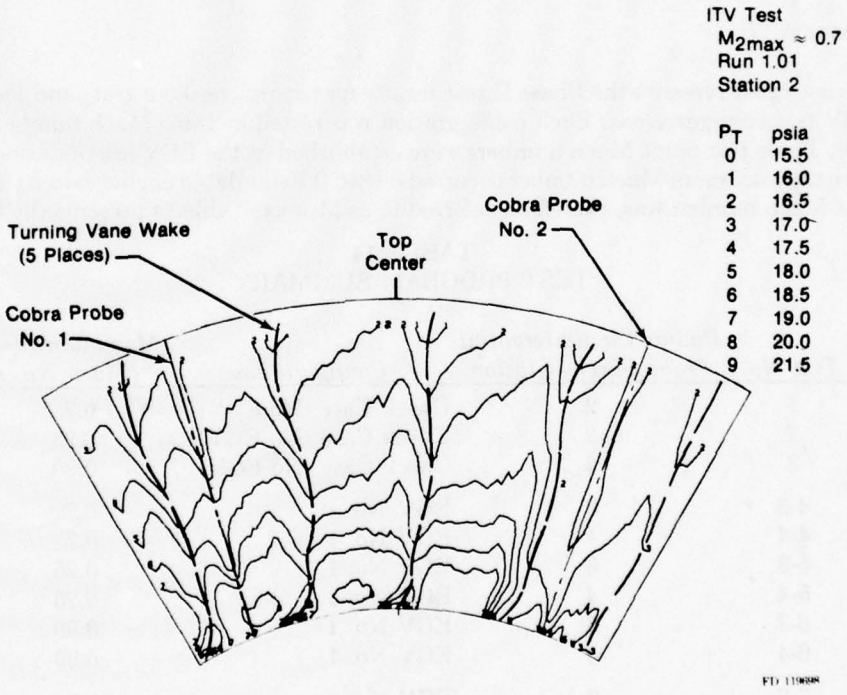


Figure 91. Annular Cascade Checkout Test, Swirl Vane Exit Flow Field Isobars at Design Conditions

TABLE 15
PHASE II DATA SUMMARY

Test No.	Configuration	M_{2max}	M_2	M_3	M_4	β_{2min} (deg)	β_2 (deg)	β_3 (deg)	β_4 (deg)	$(\Delta P_S/P_T-P_S)_{2-3}$
4-3	EGV No. 1	0.680	0.524	0.388	-	50.4	54.6	93.9	-	0.3626
4-4	EGV No. 1	0.687	0.531	-	0.337	50.4	54.6	-	92.6	0.3673
5-3	EGV No. 1	0.318	0.246	0.194	-	50.4	54.6	92.8	-	0.3166
5-4	EGV No. 1	0.325	0.253	-	0.168	50.4	54.6	-	91.6	0.3216
6-3	EGV No. 1	0.884	0.707	0.496	-	50.4	54.6	93.4	-	0.3495
6-4	EGV No. 1	0.894	0.710	-	0.426	50.4	54.6	-	93.5	0.3532
7-3	EGV No. 2	0.692	0.545	0.373	-	50.4	54.6	91.5	-	0.3761
7-4	EGV No. 2	0.685	0.540	-	0.299	50.4	54.6	-	91.6	0.3838
8-3	EGV No. 2	0.323	0.255	0.184	-	50.4	54.6	90.4	-	0.3343
8-4	EGV No. 2	0.315	0.251	-	0.200	50.4	54.6	-	90.3	0.3612
9-3	EGV No. 2	0.931	0.730	0.483	-	50.4	54.6	92.2	-	0.3672
9-4	EGV No. 2	0.914	0.728	-	0.406	50.4	54.6	-	92.4	0.3773

Test No.	Configuration	$(\Delta P_S/P_T-P_S)_{2-4}$	$(\Delta P_S/P_T-P_S)_{2-4}$	$(\Delta P_T/P_T)_{2-3}$	$(\Delta P_T/P_T)_{3-4}$	$(\Delta P_T/P_T)_{2-4}$
4-3	EGV No. 1	0.1505	0.4426	0.0110	-	-
4-4	EGV No. 1	-	0.4491	-	0.0087	0.0220
5-3	EGV No. 1	0.1528	0.4023	0.0025	-	-
5-4	EGV No. 1	-	0.4028	-	0.0022	0.0065
6-3	EGV No. 1	0.1349	0.4245	0.0350	-	-
6-4	EGV No. 1	-	0.4322	-	0.0187	0.0520
7-3	EGV No. 2	0.1560	0.4417	0.0240	-	-
7-4	EGV No. 2	-	0.4469	-	0.0092	0.0320
8-3	EGV No. 2	0.2171	0.4003	0.0060	-	-
8-4	EGV No. 2	-	0.4225	-	−0.0003	0.0047
9-3	EGV No. 2	0.1912	0.4484	0.0480	-	-
9-4	EGV No. 2	-	0.4457	-	0.0135	0.0640

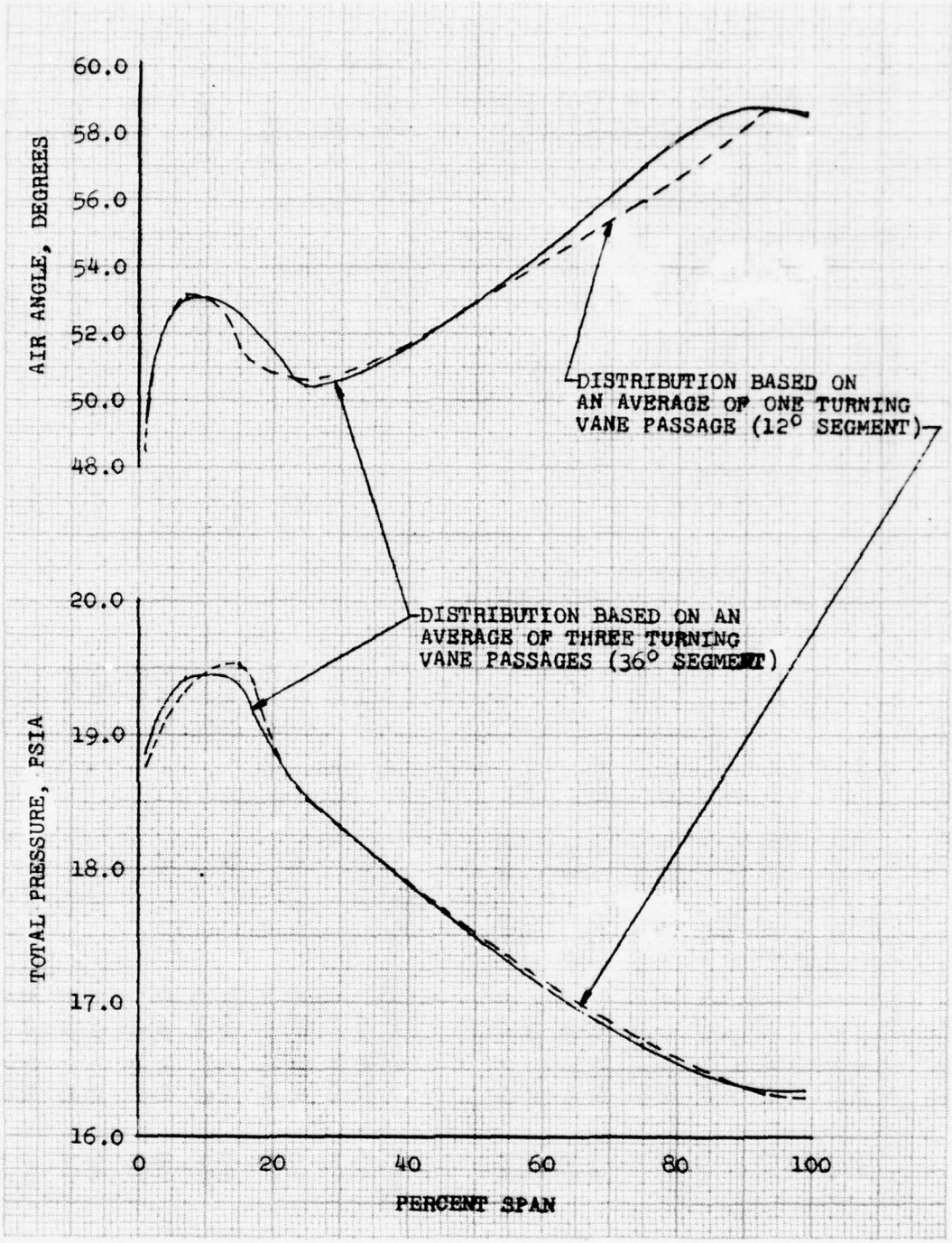


Figure 92. Annular Cascade Checkout Test, Evaluation of Flow Field Periodicity from Swirl Vanes at Design Conditions

It was possible to completely survey total pressure at the swirl vane exit (station 2) only with the EGV cascade removed. Therefore, part of the station 2 instrumentation was a 13-element wake rake that could be used to define total pressure during the performance tests. This probe was relatively large, so it was positioned outside the survey area to prevent its wake from distorting the flowfield being studies. Figure 93 compares the spanwise total pressure distributions measured by the wake rake and radial-circumferential probes for the design inlet conditions. It can be seen that the average wake rake data matches the traverse probe data within 0.1 psia. These results show that the rake provides adequate measurement of total pressure and that there is little circumferential variation of flow conditions between the survey area (±30 deg from the station centerline) and the wake rake position (42 deg from the station centerline).

The spanwise Mach number and air angle distributions measured in the checkout run are compared to the desired profiles in Figure 94 at design conditions. It can be seen that the desired profiles were closely simulated, indicating that the flow control screen and swirl vanes performed as expected. The small (2 to 3 deg) variance of air angle is due to a slight misalignment of swirl vane stagger angle during assembly. Figure 95 presents the Mach number and air angle distributions for the three checkout tests. It can be seen that the air angle distribution is not significantly affected by Mach number changes. Therefore, it was assumed that the average air angle distribution, shown in the figure, could be used for all performance runs.

3. EGV No. 1 Performance Test Results

The design of EGV No. 1 was discussed in Section II.A. Inspection of the finished airfoils was discussed in Section II.B. The effects of measured station 2 air angle and inspected EGV inlet metal angle are shown in Figure 96 as spanwise incidence distribution. It can be seen that incidence varies from 0 to 3.6 deg higher than design. The maximum variance occurs at the ¼ root location, where actual incidence is +2.4 deg, instead of −1.2 deg. This should be well within the loss bucket of these airfoils and is in the direction to increase choke margin in the high Mach number root region. The goal for Phase II was to diffuse the flow to an exit Mach number of 0.4 at design inlet conditions with less than 2% total pressure loss. Figure 97 presents the critical performance for EGV No. 1 to show that this performance goal was exceeded. Examination of Figure 97 shows that the flow was diffused to an exit Mach number less than 0.4 at the design inlet Mach number by passing through the EGV cascade alone (i.e., additional diffusion provided by the downstream diffuser was not necessary to achieve the 0.4 exit Mach number goal). However, by including the downstream diffuser, it was possible to increase inlet Mach number to 0.825 and still achieve an exit Mach number of 0.4. Total pressure loss from the EGV inlet to the EGV exit was below 2% until the inlet Mach number reached 0.78. At the design inlet Mach number total pressure loss for the EGV alone was only 1.2% (significantly better than the 2% goal). It can be seen that the exit air angle was only about 2 to 4 deg away from the axial direction (axial is 90 deg). The downstream diffuser further straightened the flow approximately 1 deg for the EGV No. 1 configuration.

4. EGV No. 2 Performance Test Results

The design of EGV No. 2 was identical to EGV No. 1 between 30% and 80% span. Near the endwalls the airfoil leading edge was cutback; the trailing edge was uncambered; and a fillet was added between the endwall and the pressure surface, extending downstream of the trailing edge. The design of this model is discussed in Section II.A. The spanwise incidence distribution for EGV No. 2 is the same as for EGV No. 1 and is shown in Figure 96.

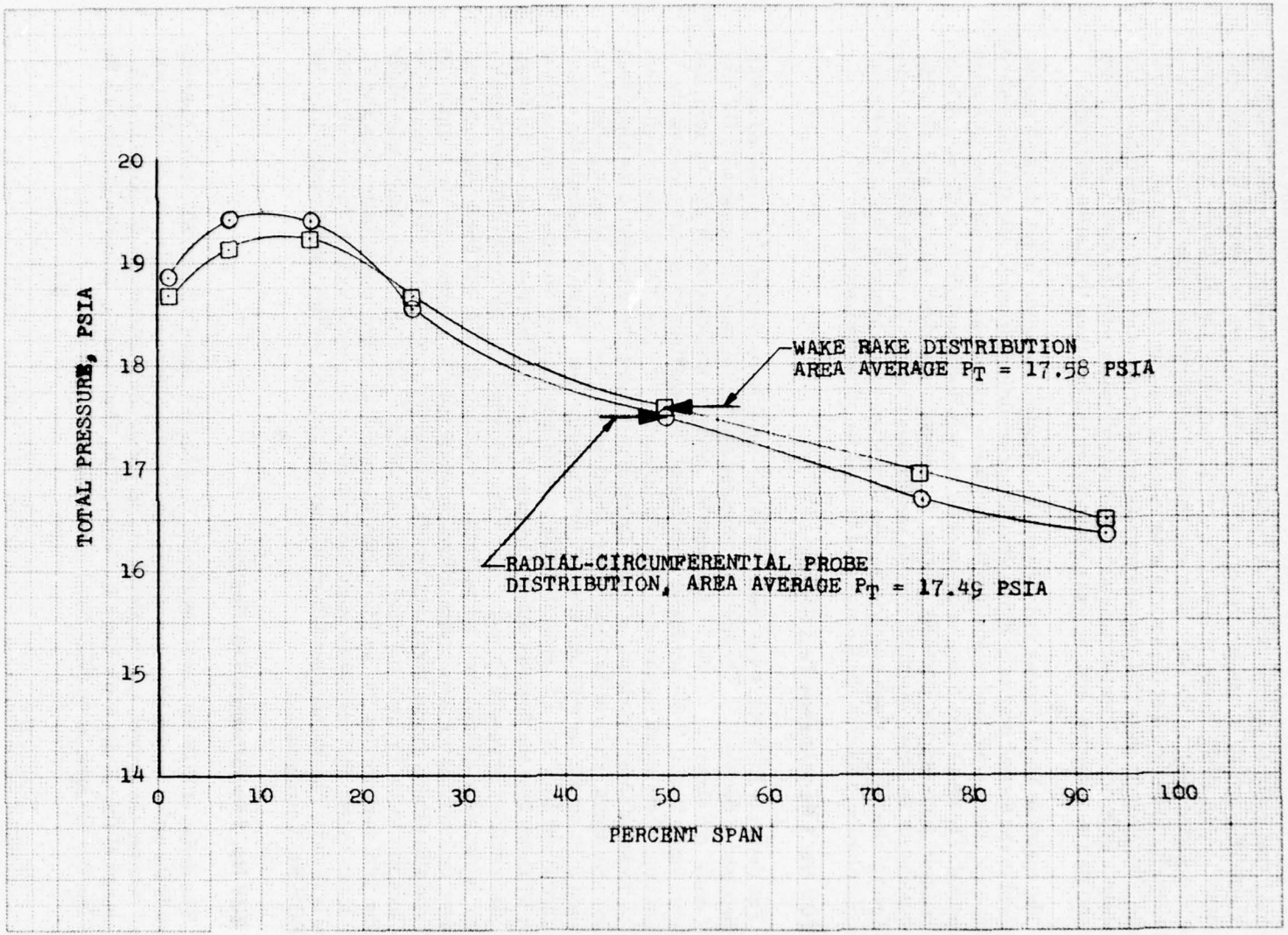


Figure 93. Comparison of EGV Inlet Spanwise Total Pressure Distributions, Measured by the Wake Rake and Radial-Circumferential Traverse Probe at Design Conditions

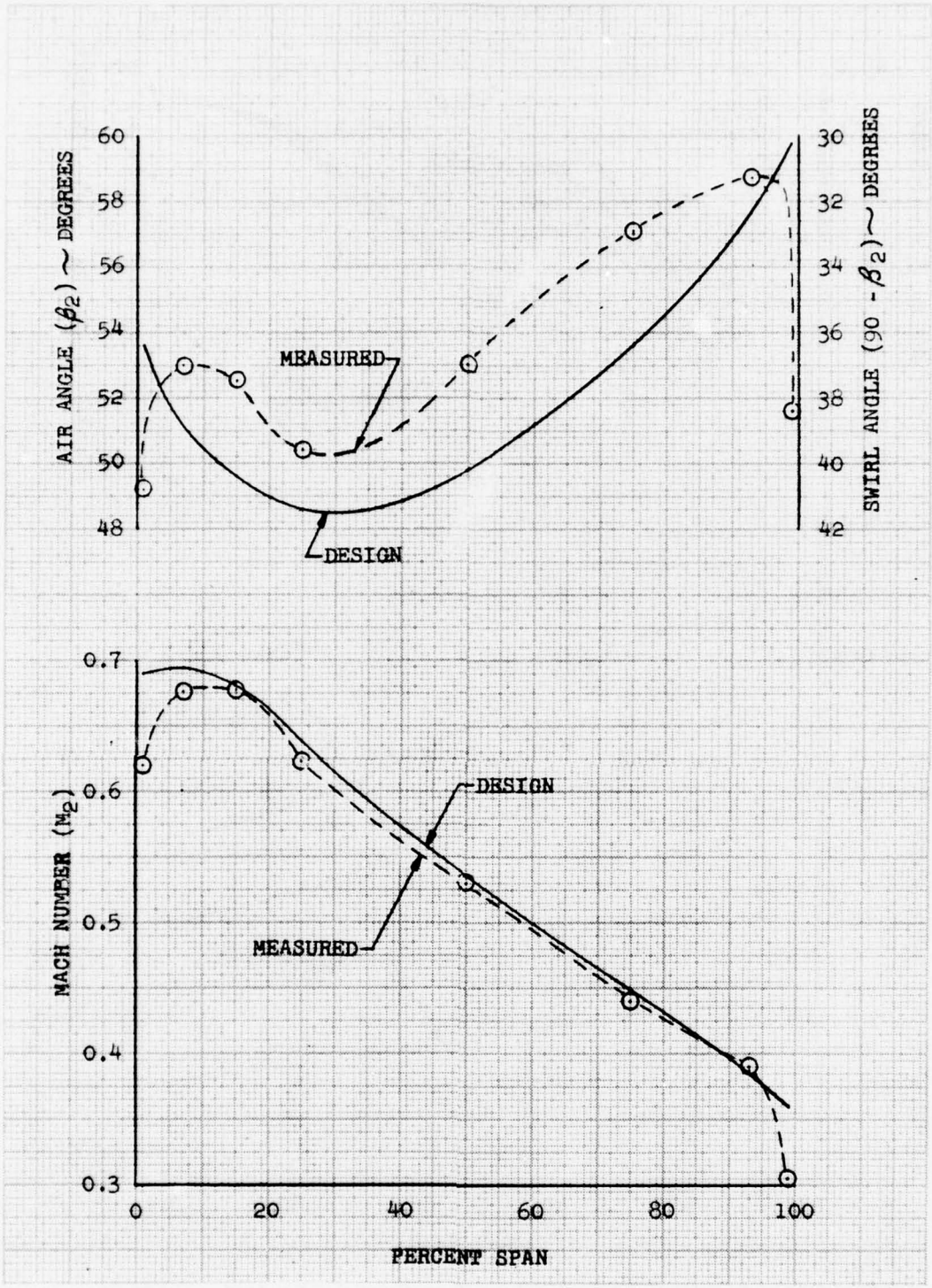


Figure 94. Annular Cascade Checkout Test, Spanwise Mach Number, and Air Angle Distribution at Design Conditions

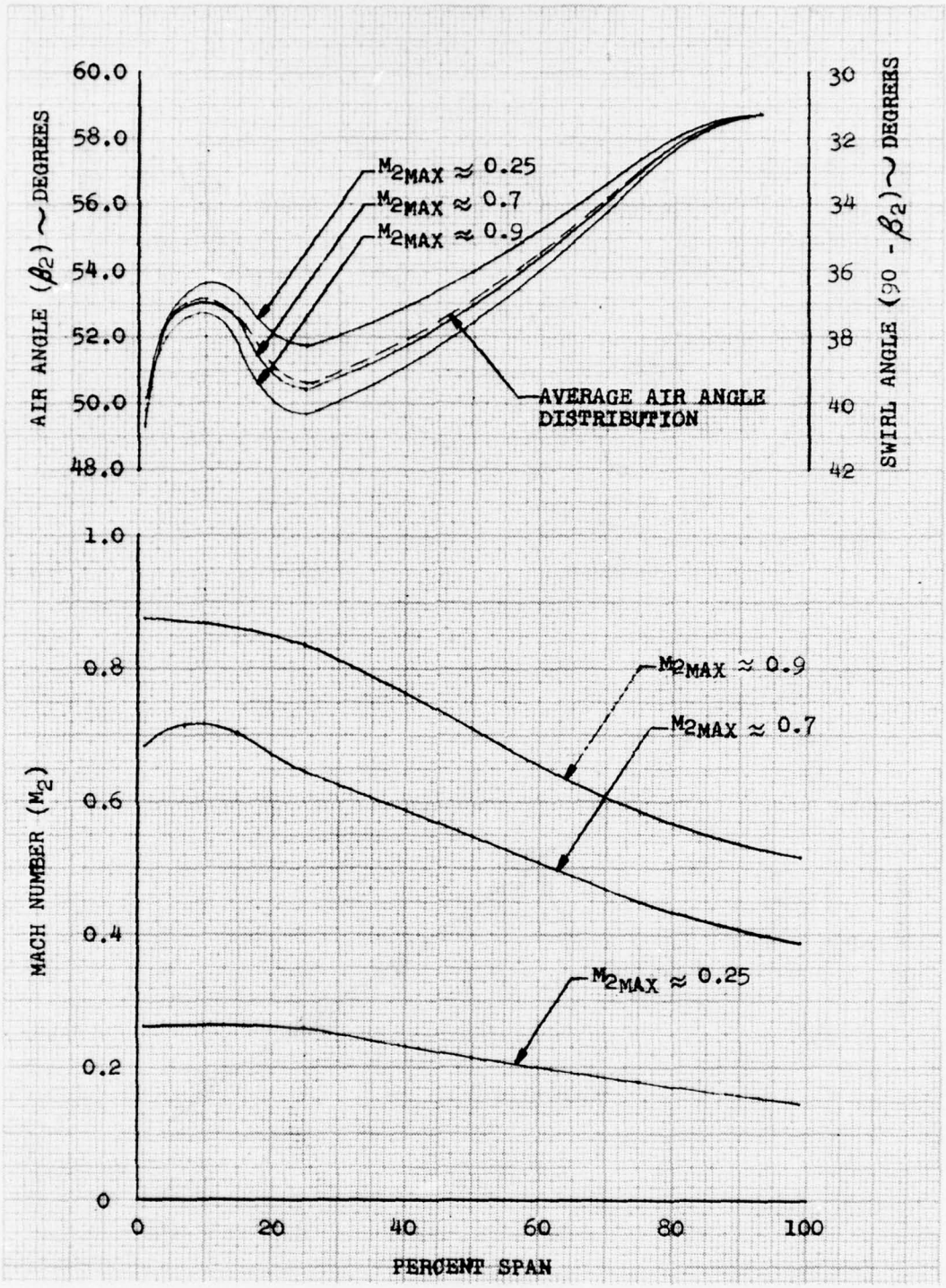


Figure 95. Annular Cascade Checkout Test, Spanwise Air Angle, and Mach Number Distributions

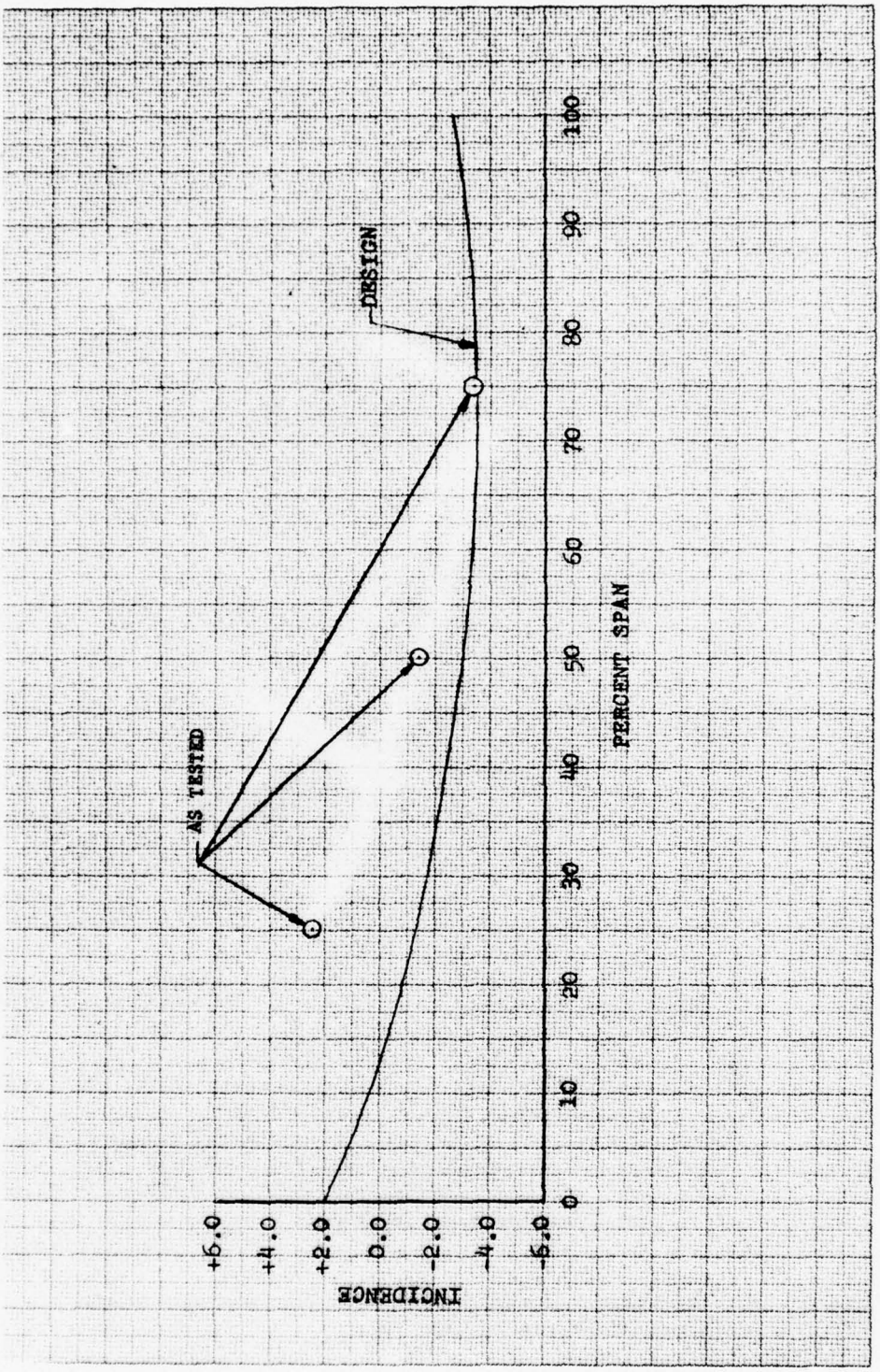


Figure 96. Annular Cascade Test EGV Incidence Distribution

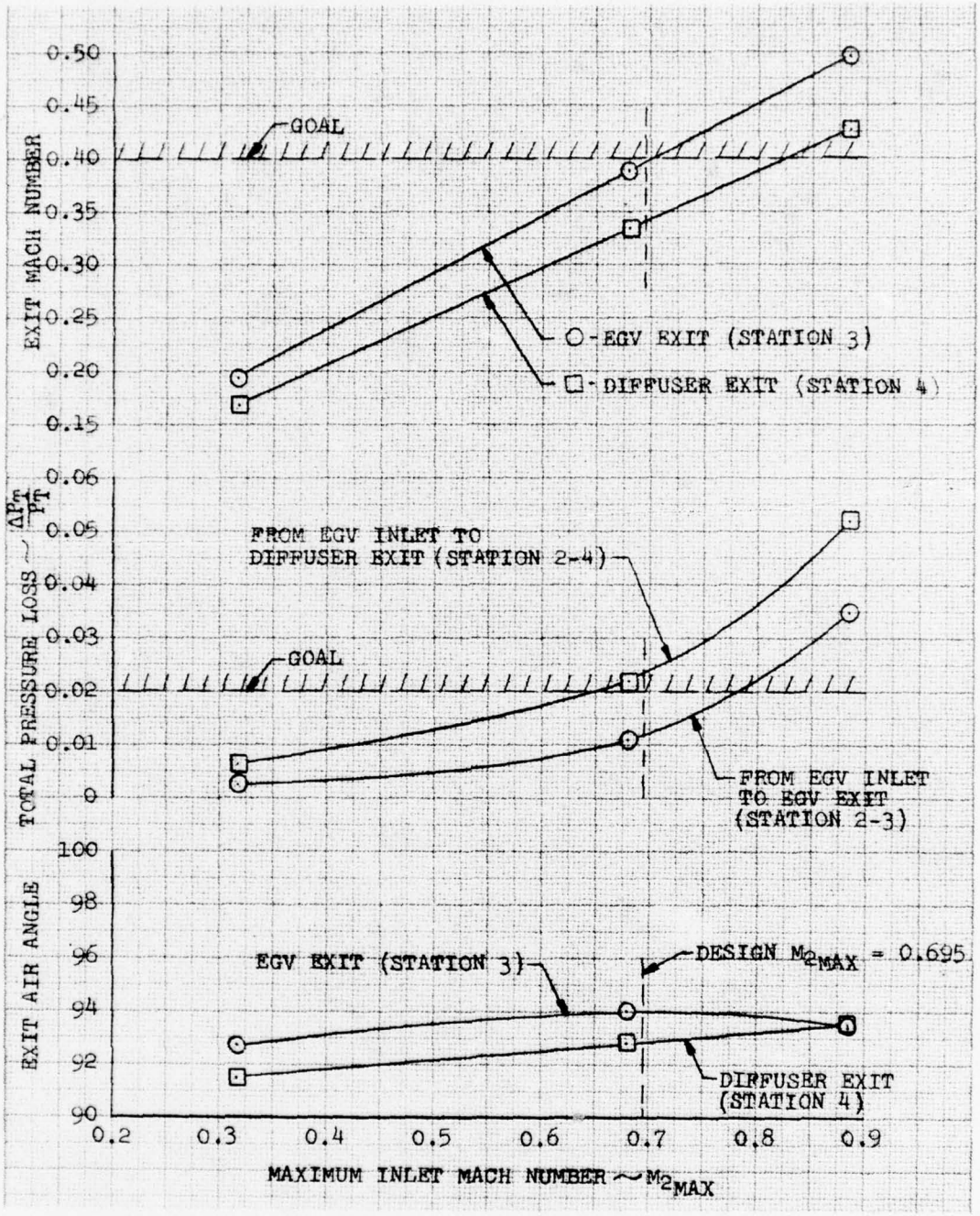


Figure 97. Annular Cascade Average Performance Data Referenced to Maximum Inlet Mach Number (EGV No. 1)

The modifications applied to EGV No. 2 redistributed the flow area and altered the airfoil near the endwalls to improve diffusion performance and reduce secondary losses. Figure 98 summarizes the performance characteristics of EGV No. 2. It can be seen that an inlet Mach number of nearly 0.75 (well above design) could be tolerated and still achieve diffusion to an exit Mach number of 0.4 with the modified EGV cascade alone. By including the downstream diffuser, inlet Mach number can be increased above 0.9 and satisfy the diffusion goal. The exit air angle was within 2 deg of axial with no variation between the EGV exit and the difuser exit. However, it was determined that total pressure loss was increased by the modifications applied to EGV No. 2. The higher loss is attributed to separation along the airfoil trailing edge, triggered by separation on the endwall fillets.

5. Performance Comparison

Predicted and measured performance at design inlet conditions are compared in Table 16. The comparison was made in three ways: across the EGV cascade alone (station 2 to 3); across the downstream diffuser alone (station 3 to 4); and across the cascade and diffuser combination (station 2 to 4). Predicted performance was based on Phase I plane cascade data.

TABLE 16

COMPARISON OF PREDICTED AND MEASURED PERFORMANCE AT DESIGN CONDITIONS (M_2=0.695)

Performance Parameter	*Prediction*	*Measured*	
		EGV No. 1	*EGV No.2*
	EGV Alone (Station 2-3)		
$(\Delta P_T/P_T)_{2-3}$	2.29%	1.20%	2.40%
M_3	0.380	0.395	0.374
$(\Delta P_S/P_T-P_S)_{2-3}$	0.354	0.362	0.376
η_D	0.715	0.733	0.749
	Downstream Diffuser Alone (Station 3-4)		
$(\Delta P_T/P_T)_{3-4}$	0.068%	0.87%	0.92%
M_4	0.313	0.344	0.300
$(\Delta P_S/P_T-P_S)_{3-4}$	0.300	0.140	0.134
η_D	0.975	0.596	0.628
	Combined System (Station 2-4)		
$(\Delta P_T/P_T)_{2-4}$	2.36%	2.30%	3.20%
M_4	0.313	0.344	0.300
$(\Delta P_S/P_T-P_S)_{2-4}$	0.455	0.449	0.447
η_D	0.917	0.723	0.716

It will be noted that across the cascade alone (station 2-3) EGV No. 1 provided superior diffusion efficiency with approximately one-half of the predicted total pressure loss. The high performance can be traced to low endwall loss. This is clearly shown in Figure 99, where spanwise loss distributions are compared with a prediction, based on Phase I plane cascade data. This effect is attributed to the relatively high aspect ratio (AR=2.4) of the Phase II design compared to the Phase I design (AR=1.0). The slightly higher Mach number measured at the EGV exit is due to higher available total pressure.

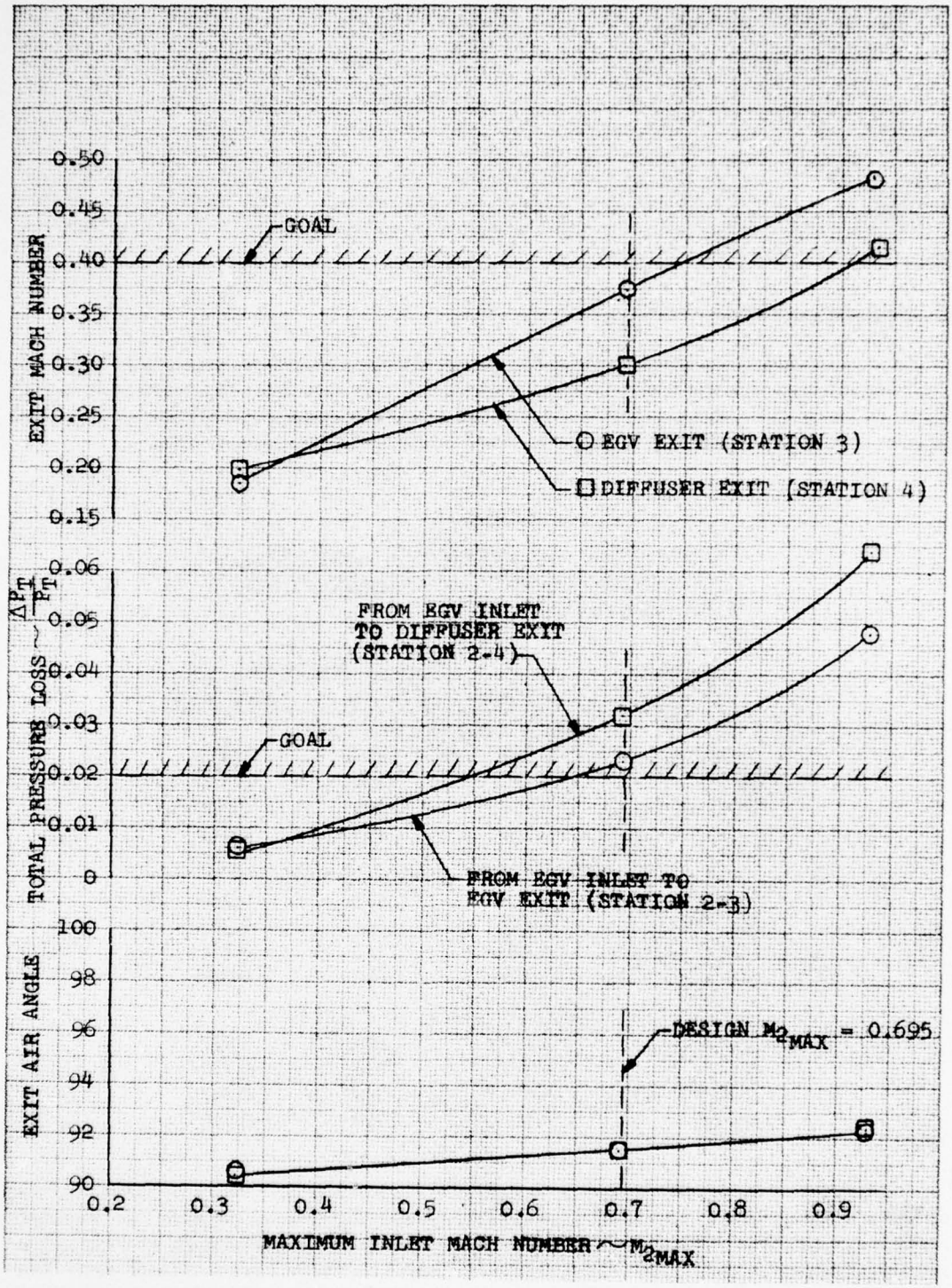


Figure 98. Annular Cascade Average Performance Data Reference to Maximum Inlet Mach Number (EGV No. 2)

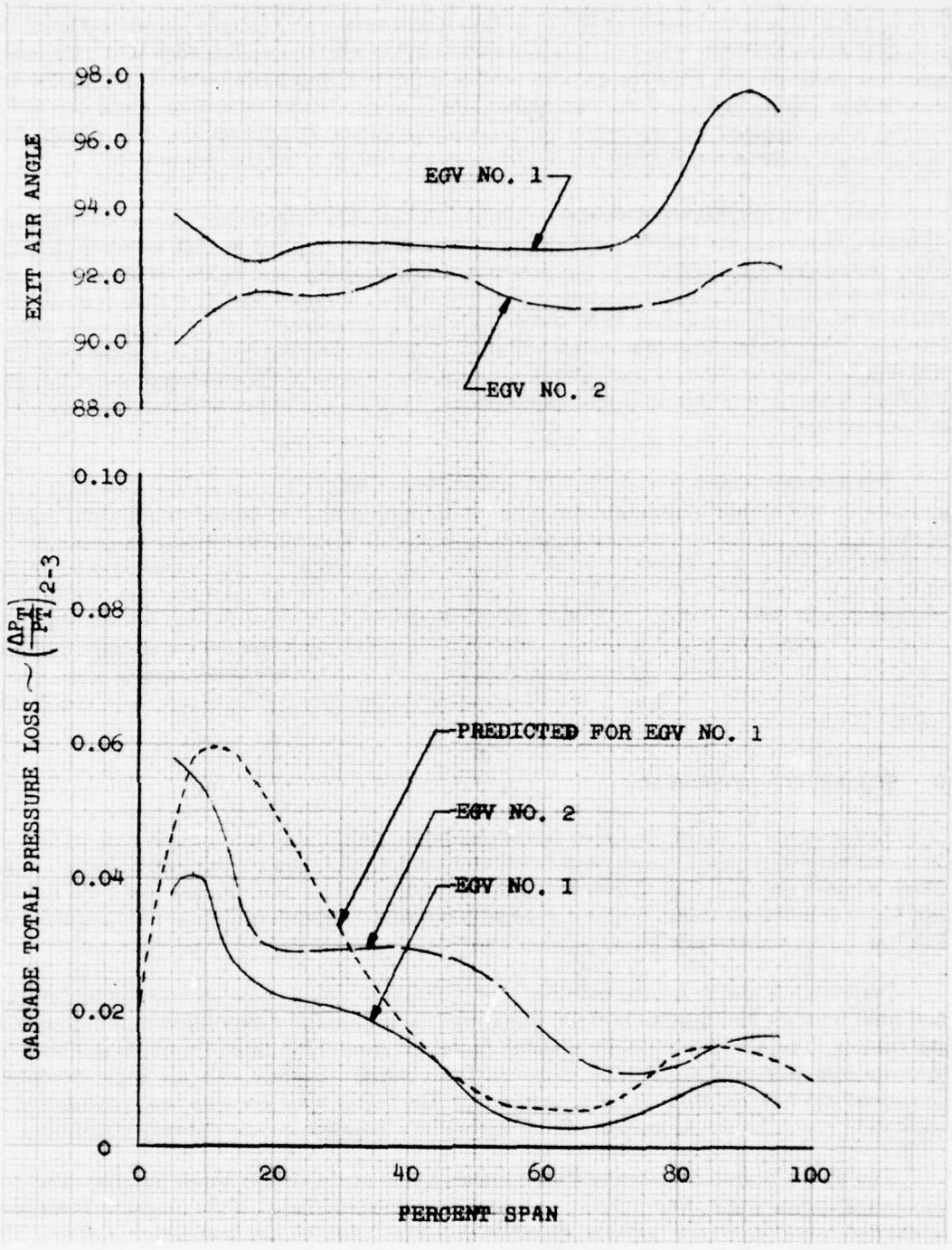


Figure 99. Comparison of Spanwise Distribution of Total Pressure Loss and Exit Air Angle (M_{2max} = 0.695)

The geometric modifications incorporated in EGV No. 2 resulted in improved diffusion performance (higher static pressure rise coefficient and diffusion efficiency). However, total pressure loss increased. Examination of the flow visualization photographs shown in Figure 100 reveals that the EGV No. 2 had a region of separated flow near the trailing edge across the entire span (not observed with EGV No. 1). This verifies the generally uniform increase of spanwise loss distribution shown in Figure 99. The higher loss is attributed to separation along the airfoil trailing edge triggered by separation on the endwall fillets. It appears that the closure rate (abruptness) of the endwall fillets should be more gradual to avoid this separation.

Table 16 shows that the downstream diffuser did provide a significant amount of additional diffusion. However, the overall performance of this diffuser was not as high as predicted. The lower performance is attributed to the presence of inlet turning vane wakes, which were clearly evident at stations 2, 3, and 4, as shown in the isobar plots of Figure 101. At station 4, it was very difficult to identify individual EGV wakes because of spreading by the turning vane wakes. However, it should be noted that no endwall separation was observed during any of the tests with this annular diffuser. And, it can be expected that the absence of the growing pressure loss and blockage from these wakes in a real engine would improve performance throughout the EGV diffuser system.

The system on which the Phase II models were designed is based on a correlation of compressor and Phase I cascade data. The correlation relates the cascade equivalent conical angle (θ_{eq}) and equivalent area ratio $(A_3/A_2)_{eq}$ with diffusion efficiency (η_D) as presented in Section II.A. The Phase II data (for the cascade alone, station 2-3) was superimposed on the equivalent conical angle correlation plot in Figure 102. It can be seen that, at design inlet conditions, diffusion efficiency exceeded the predicted level. A value for θ_{eq}, 0.5 deg less than design was actually measured because of small differences in the measured metal angle and inlet conditions. The Phase II data fit the correlation well except for the low Mach number tests, which appear to be about 10% low in η_D. It can be seen that the modified configuration (EGV No. 2) had higher efficiency at each test condition.

D. SUMMARY — PHASE II

Performance of the unmodified non-series high aspect ratio airfoil (EGV No. 1) met or exceeded the design performance goals (total pressure loss less than 2% while diffusing to an exit Mach number less than 0.4). Across the airfoil cascade (stations 2-3), the loss was 1.2% and the exit Mach number was 0.395. For the combined airfoil and downstream diffuser (stations 2-4), the loss was 2.35% and the exit Mach number was 0.34.

Performance results for the modified airfoil (EGV No. 2), showed an increase in diffusion and total pressure loss relative to EGV No. 1 with approximately a two degree improvement in gas turning. The airfoil exit Mach number decreased from 0.395 to 0.375; however, the total pressure loss increased from 1.2% to 2.3%. The spanwise average exit air angle decreased (increased gas turning) from 94.0 deg to 91.5 deg. The higher total pressure loss is attributed to separation along the airfoil trailing edge triggered by separation on the endwall protrusions.

The Phase II annular cascade data correlated well at the design Mach number using the equivalent conical angle (θeq) correlation system developed in Phase I of the program. The Phase II annular cascade results provide excellent substantiation to the correlation system. The correlation, although based on plane cascade data, can be applied directly to annular cascade designs. The off-design point performance correlation was not as good as the design point correlation. These differences may require minor modifications to the correlation once additional data becomes available.



EGV No. 1

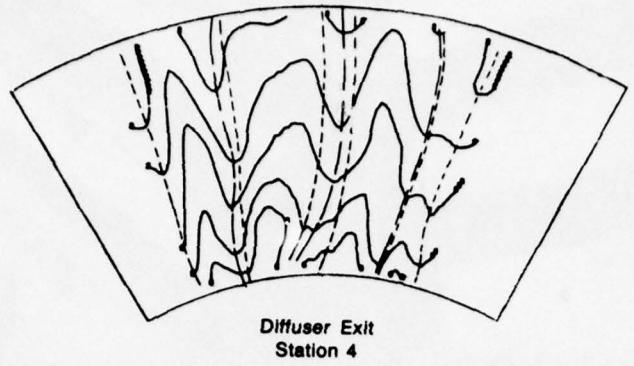
FAE 150628



EGV No. 2

FAE 150629

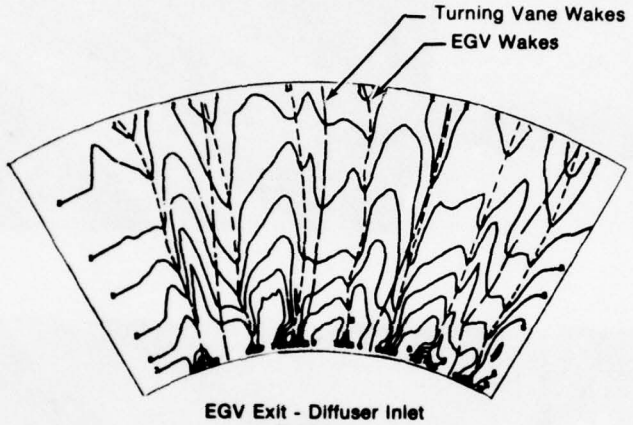
Figure 100. Boundary Layer Streamline Patterns from Annular Cascade Tests (M_2 = 0.695)



Diffuser Exit
Station 4

EGV No. 1
Run 1.03
Station 4

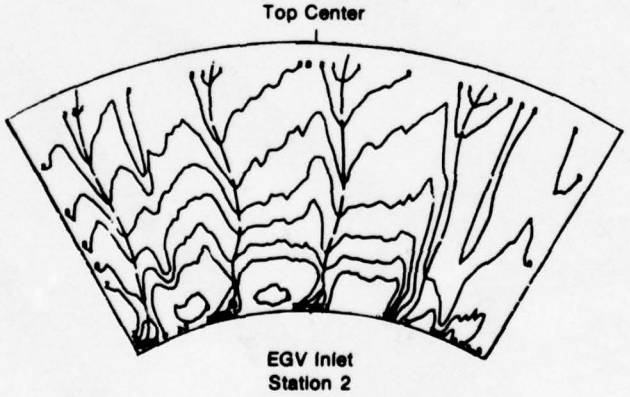
	P_T
0	14.5
1	14.7
2	15.0
3	15.5
4	16.0
5	16.5
6	17.0
7	17.5
8	18.0
9	18.5



EGV Exit - Diffuser Inlet
Station 3

EGV No. 1
Run 1.02
Station 3

	P_T
0	14.0
1	14.5
2	15.0
3	15.5
4	16.0
5	16.5
6	17.0
7	17.5
8	18.0
9	18.5



EGV Inlet
Station 2

ITV Test
Run 1.01
Station 2

	P_T
0	15.5
1	16.0
2	16.5
3	17.0
4	17.5
5	18.0
6	18.5
7	19.0
8	20.0
9	21.5

Figure 101. Flow Field Surveys for EGV No. 1 for $M_{2max} = 0.7$

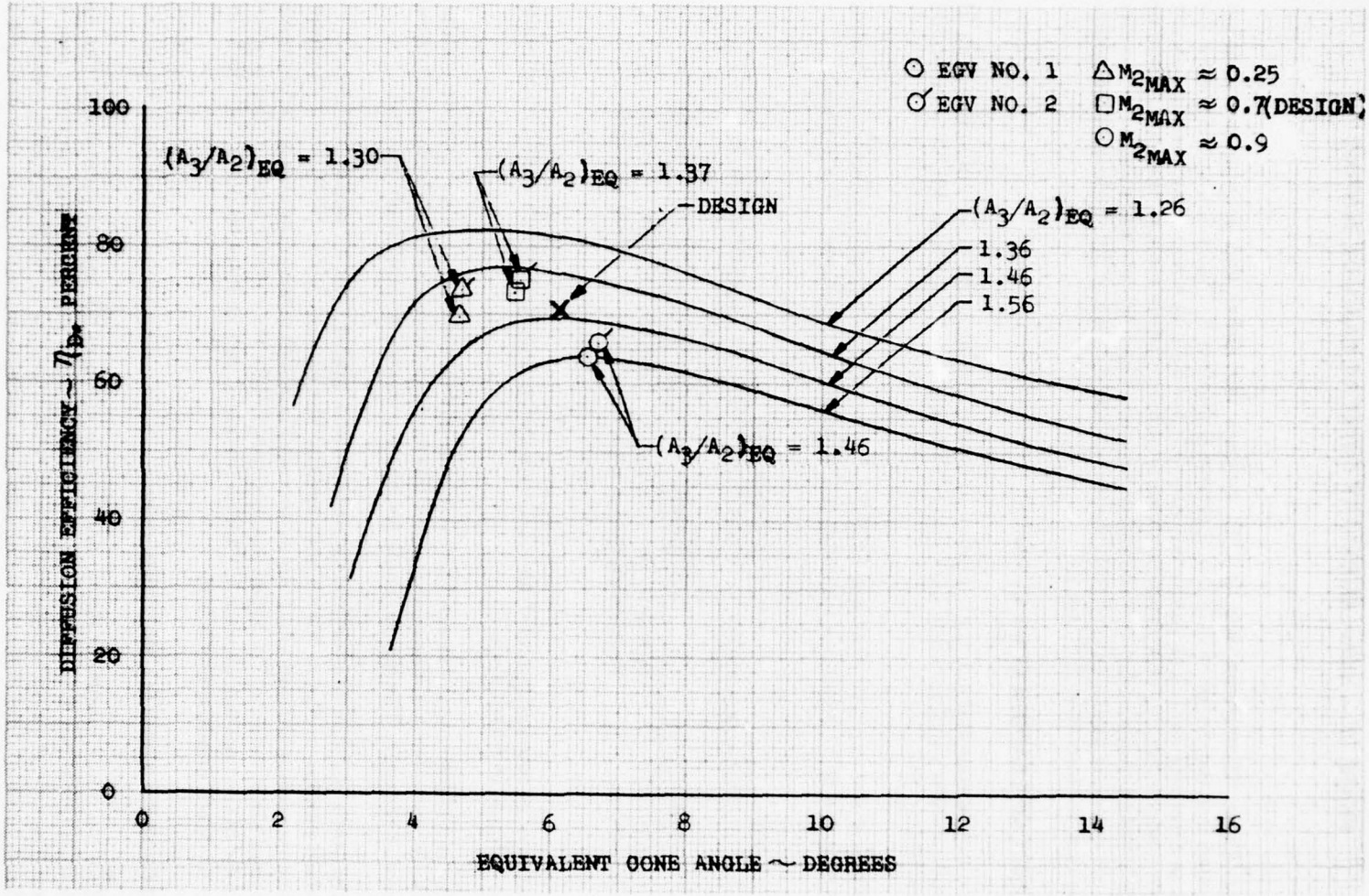


Figure 102. Equivalent Conical Angle Correlation of Diffusing Cascade Data

SECTION III
PHASE III — SUPPLEMENTARY ANNULAR CASCADE TESTING

The Phase III objective was to: (1) evaluate the airfoil and endwall modifications incorporated into the design of EGV No. 2 (Phase II, Section II, Figure 82), and (2) define the baseline performance level of an equivalent state-of-the-art series airfoil. Four annular cascade tests were conducted during this phase. Separate tests were made to evaluate the cutback leading edge, uncambered trailing edge and endwall protrusion. The final test was a test of a 65-series circular arc meanline airfoil. In each test, the facility setup, test and data reduction procedures were identical to those used in Phase II.

A. EFFECT OF LEADING EDGE CUTBACK

The leading edge cutback was evaluated by testing the basic non-series airfoil (EGV No. 1) modified to a cutback configuration, EGV No. 1-1. The leading edge cutback was identical to that incorporated into EGV No. 2.

Comparison of the EGV No. 1 and EGV No. 1-1 test results define the effects of the leading edge cutback. Table 17 presents a summary of the design point performance parameters.

TABLE 17
COMPARISON OF EGV NO. 1 AND NO. 1-1 PERFORMANCE

Configuration	*Description*	$\Delta P_T/P_T$	$\Delta P_S/Q$	θGAS
EGV No. 1	Basic Design	0.0118	0.361	31.4
EGV No. 1-1	Basic With Cutback LE	0.0221	0.331	31.2

The leading edge cutback increased the total pressure loss and decreased the static pressure rise. The gas turning decreased slightly.

Figure 103 presents the design point spanwise plots of total pressure loss and exit air angle for EGV No. 1 and No. 1-1. The total pressure loss for the cutback airfoil (EGV No. 1-1) increased over most of the span. The exit air angle distribution showed no significant changes.

The static pressure rise coefficients and spanwise average exit air angles are presented vs inlet Mach number in Figure 104 for both airfoils. The cutback airfoil (EGV No. 1-1) shows a reduction in pressure rise and a decrease in turning. Figure 105 presents the average total pressure loss vs inlet Mach number. The airfoil loss (stations 2-3) for the cutback configuration is greater at all inlet Mach numbers above 0.32. Across the airfoil and diffuser (stations 2-4) the loss is greater for Mach numbers above 0.44.

B. EFFECT OF ENDWALL PROTRUSIONS

EGV No. 2 was modified twice to evaluate the effects of the endwall protrusions. The first modification, EGV No. 2-1, reduced the endwall protrusion maximum cross-sectional area by one-half. The second modification, EGV No. 2-2, removed the endwall protrusion completely. EGV No. 2-2 had only the cutback leading edge and uncambered trailing edge. Comparing EGV

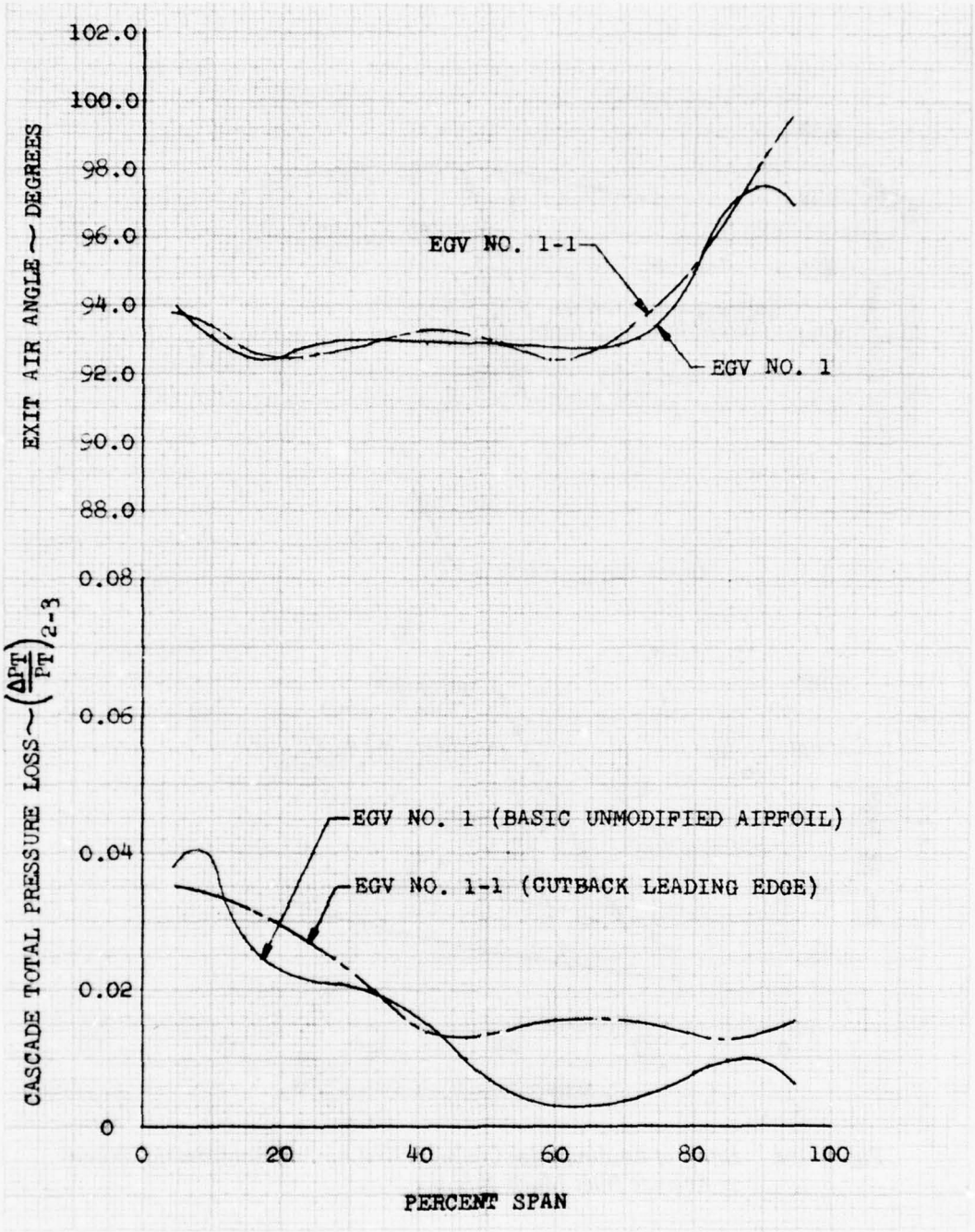


Figure 103. Effect of Leading Edge Cutback, Total Pressure Loss and Exit Air Angle vs Percent Span

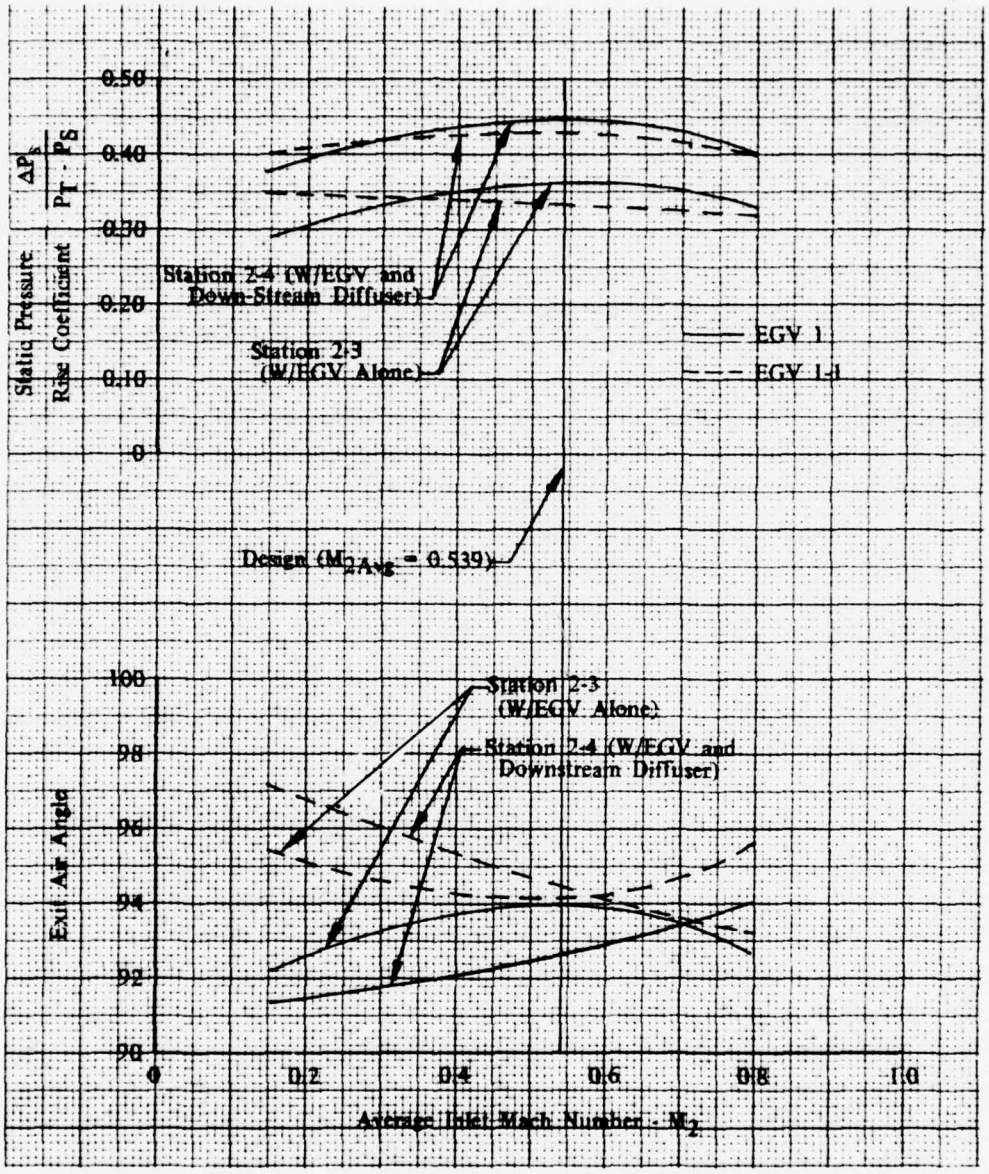


Figure 104. Effect of Leading Edge Cutback, Exit Air Angle and Static Pressure vs Average Inlet Mach Number

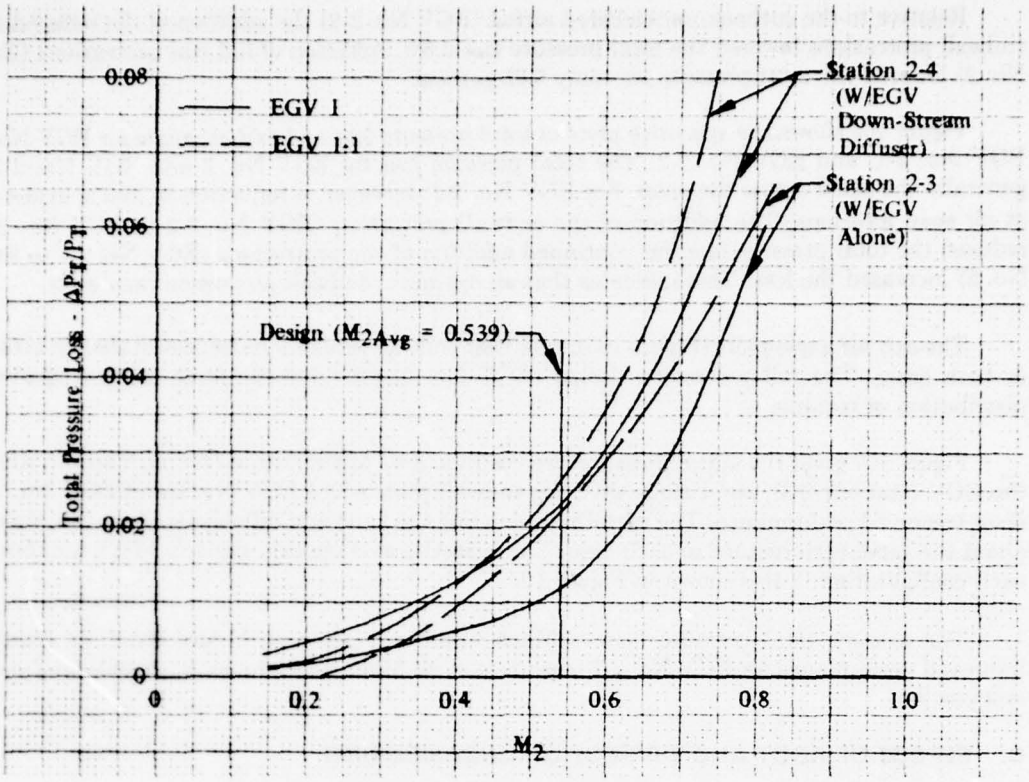


Figure 105. Effect of Leading Edge Cutback, Total Pressure Loss vs Average Inlet Mach Number

No. 2 with EGV No. 2-2 shows the relative effect of adding full size protrusions. Comparing EGV No. 2-1 with EGV No. 2-2 shows the relative effect of adding reduced size protrusions. In both cases, endwall protrusions decreased the total pressure loss and increased the static pressure rise and gas turning as shown in Table 18.

TABLE 18
COMPARISON OF EGV NOS. 2, 2-1, and 2-2 PERFORMANCE

Configuration	*Description*	$\Delta P_T/P_T$	$\Delta P_S/Q$	θGAS
EGV No. 2	Original Modified Design Cutback LE, Uncambered TE, Full Protrusion	0.0237	0.375	33.9
EGV No. 2-1	Cutback LE, Uncambered TE, Reduced Protrusion	0.0162	0.379	32.6
EGV No. 2-2	Cutback LE, Uncambered TE, No Protrusion	0.0242	0.337	31.0

Relative to the cutback-uncambered airfoil (EGV No. 2-2) the addition of the reduced size endwall protrusions lowered the total pressure loss 0.8%. Addition of full size protrusions (EGV No. 2) lowered the total pressure loss only 0.05 percent.

Figure 106 shows the spanwise plots of total pressure loss and exit air angle for EGV No. 2, EGV No. 2-1, and EGV No. 2-2. The total pressure loss for EGV No. 2 and EGV No. 2-2 is generally the same across the span. For EGV No. 2-1, however, a reduction in loss is evident at all span locations. The addition of the endwall protrusion (EGV No. 2-2 to EGV No. 2-1) reduced the total pressure loss but continued addition of the protrusions (EGV No. 2-1 to EGV No. 2) increased the loss. This indicates that an optimum endwall protrusion may exist.

The exit air angle plots (Figure 106) show that endwall protrusions improved the gas turning in both cases. The full protrusion design (EGV No. 2) provided the most uniform spanwise distribution of turning.

Figure 107 gives the static pressure rise coefficient vs Mach number for each airfoil. Across the EGV (stations 2-3), the airfoils with the endwall protrusions EGV No. 2 and EGV No. 2-1, show improved performance. The performance across the vane and diffuser, stations 2-4, showed about the same performance in each case. The spanwise average exit angle vs Mach number for each configuration is also shown in Figure 107.

The average total pressure loss vs Mach number is given in Figure 108. The trend of improved performance for EGV No. 2-1 is evident at all Mach numbers for both stations 2-3 and stations 2-4.

C. EFFECT OF ROOT AND TIP SECTION UNCAMBERING

Comparison of EGV No. 1-1 with EGV No. 2-2 shows the relative effect of the root and tip section uncambering. In both cases the airfoils had cutback leading edges. The uncambered airfoil (EGV No. 2-2) shows an increase in total pressure loss, a decrease in gas turning, and a slight increase in the static pressure rise. Average design point performance parameters are presented in Table 19.

TABLE 19
COMPARISON OF EGV NOS. 1-1 AND 2-2 PERFORMANCE

Configuration	*Description*	$\Delta P_T/P_T$	$\Delta P_s/Q$	θGAS
EGV No. 1-1	Basic Airfoil With Cutback LE	0.0221	0.331	31.2
EGV No. 2-2	Cutback Leading Edge Uncambered TE	0.0242	0.337	31.0

The spanwise plots of the total pressure loss and exit air angle are given in Figure 109 for EGV No. 1-1 and EGV No. 2-2. The uncambered airfoil (EGV No. 2-2) shows a significant increase in loss over the first 20% of the span. The spanwise exit air angle for EGV No. 2-2 showed an increase at both the root and tip sections while the midspan air angles agreed within one degree.

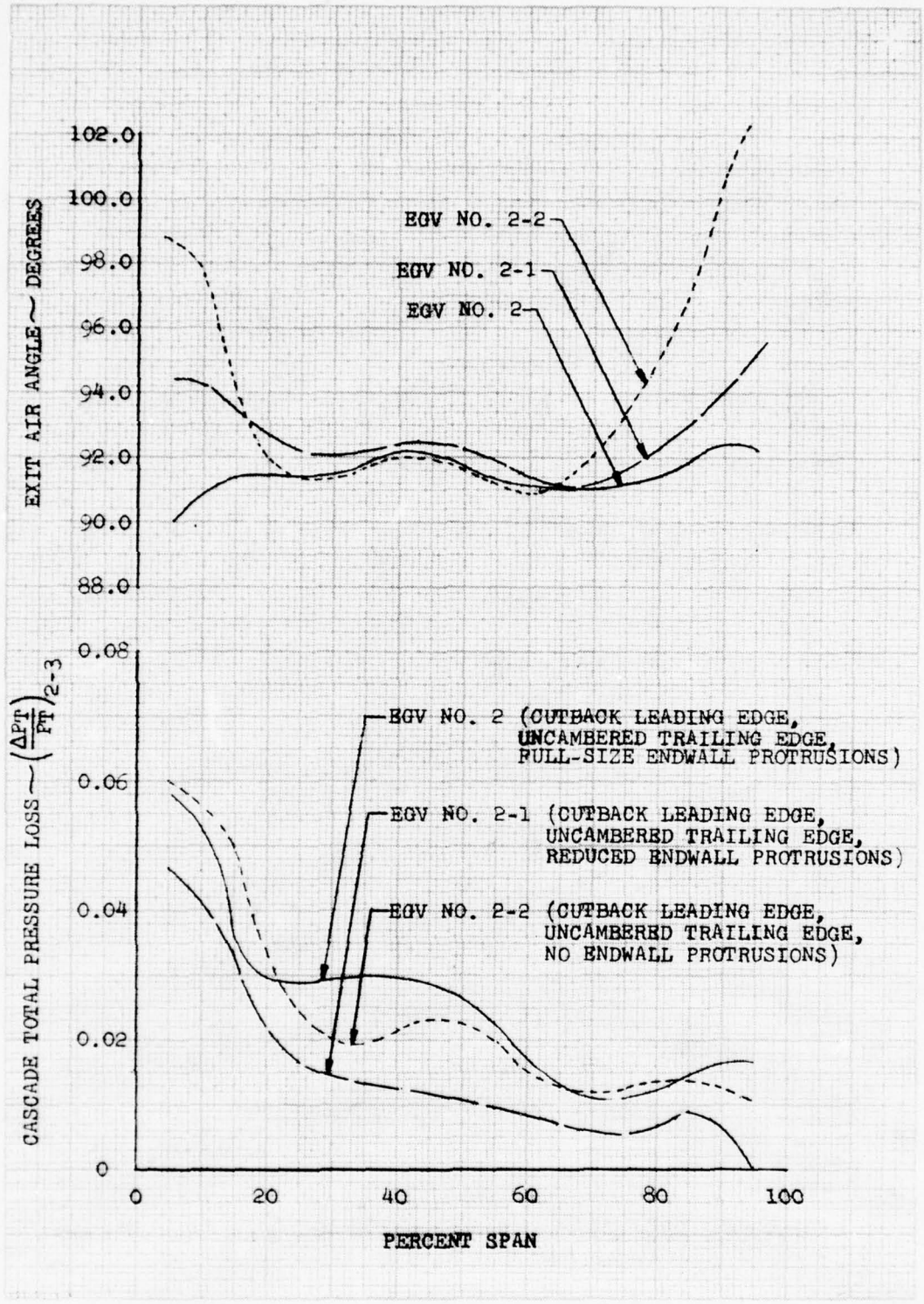


Figure 106. Effect of Endwall Protrusions, Total Pressure Loss and Exit Air Angle vs Percent Span

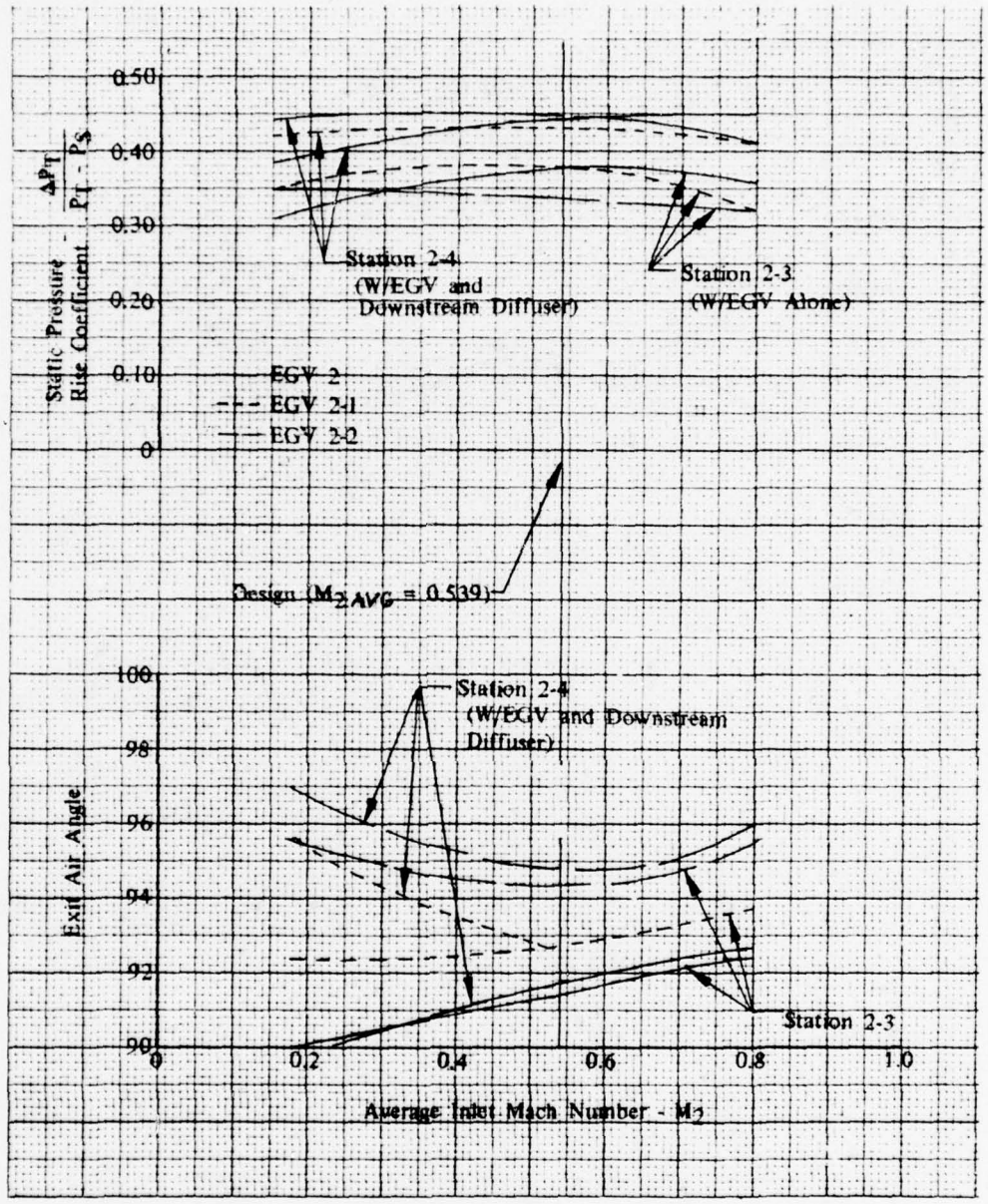


Figure 107. Effect of Endwall Protrusions, Exit Air Angle and Static Pressure vs Average Inlet Mach Number

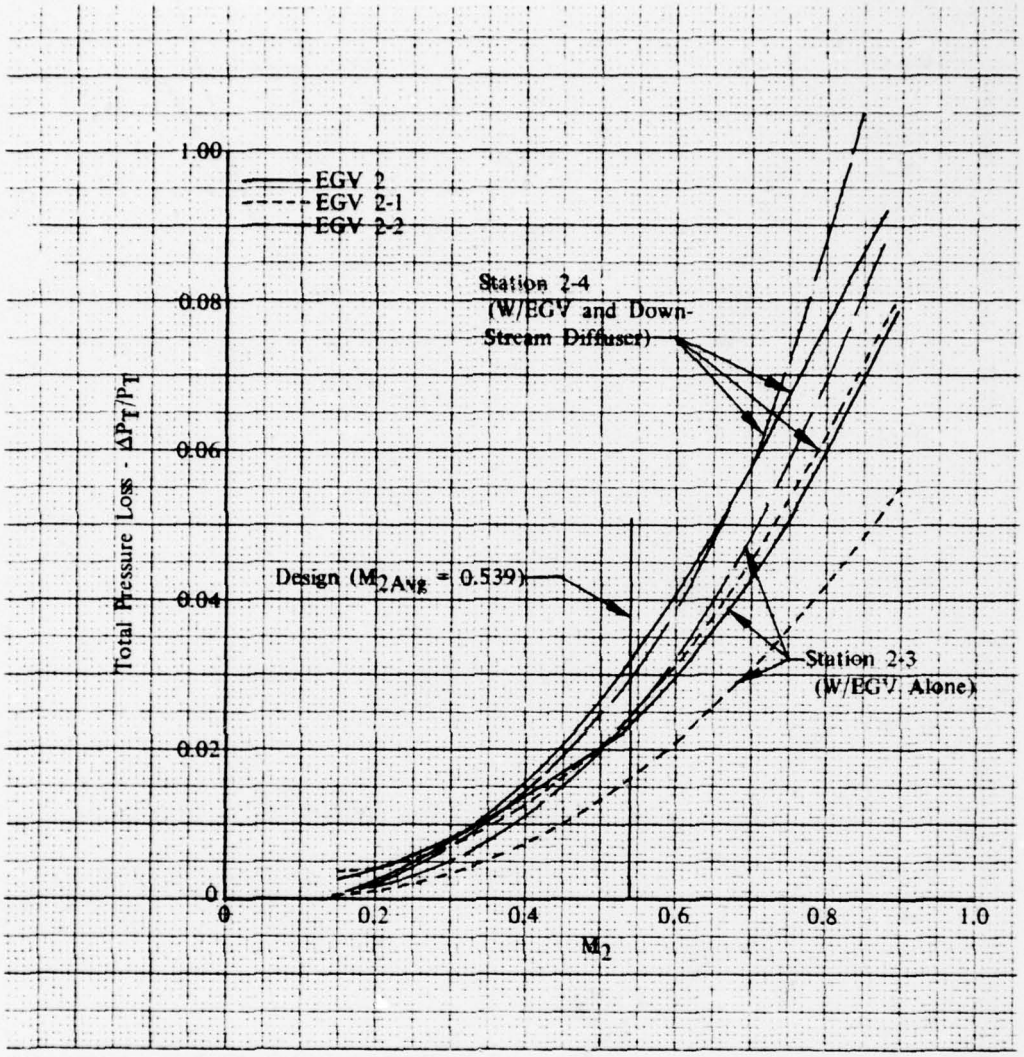


Figure 108. Effect of Endwall Protrusions, Total Pressure Loss vs Average Inlet Mach Number

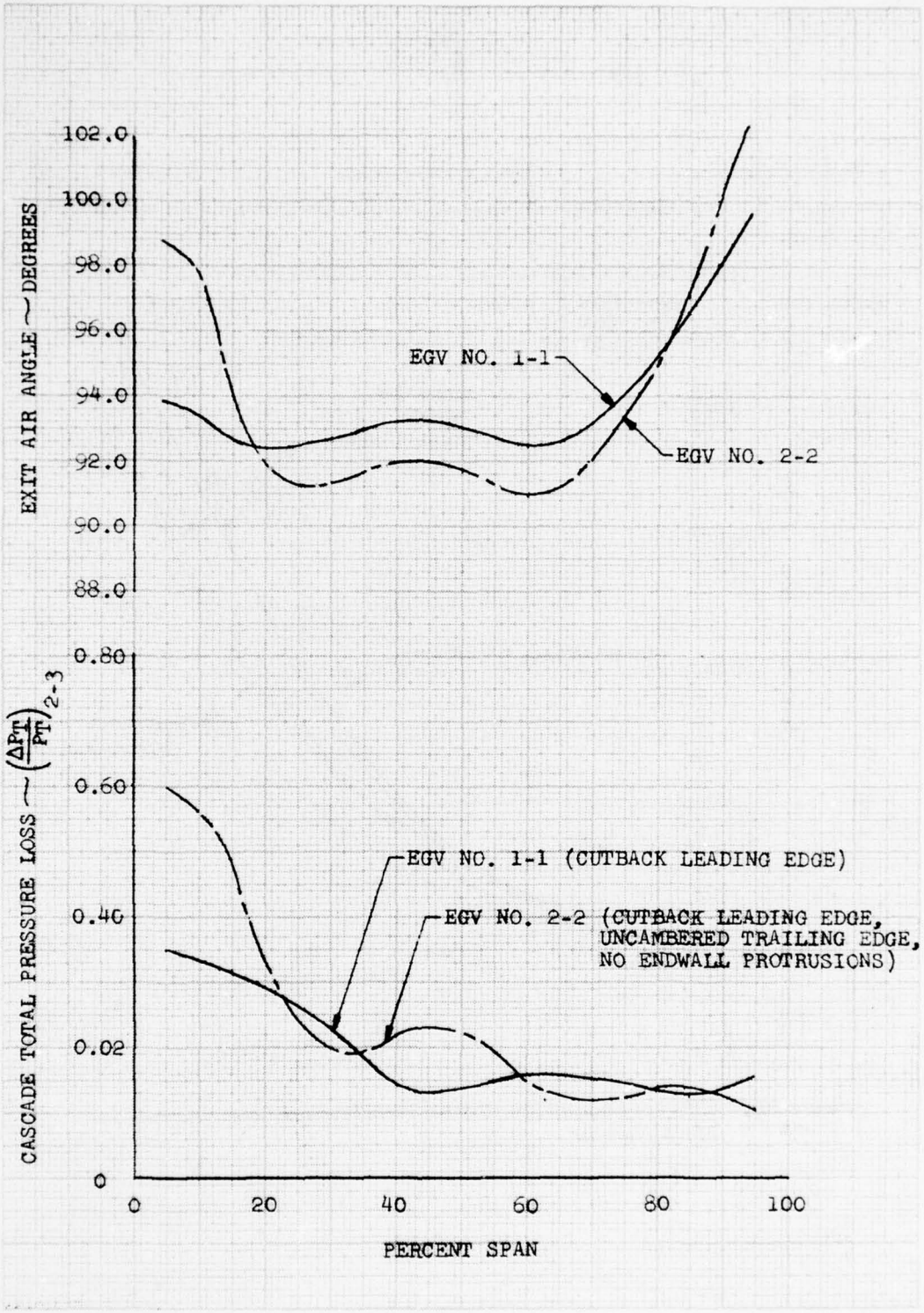


Figure 109. Effect of Uncambered Trailing Edge, Total Pressure Loss and Exit Air Angle vs Percent Span

Figure 110 gives the static pressure rise coefficient for the two airfoils. Across the exit guide vanes (stations 2-3), little or no change was evident, but for the combined EGV and downstream diffuser (stations 2-4), a slight increase was evident for EGV No. 2-2. Also shown in Figure 110 is the average exit air angle vs Mach number for each airfoil.

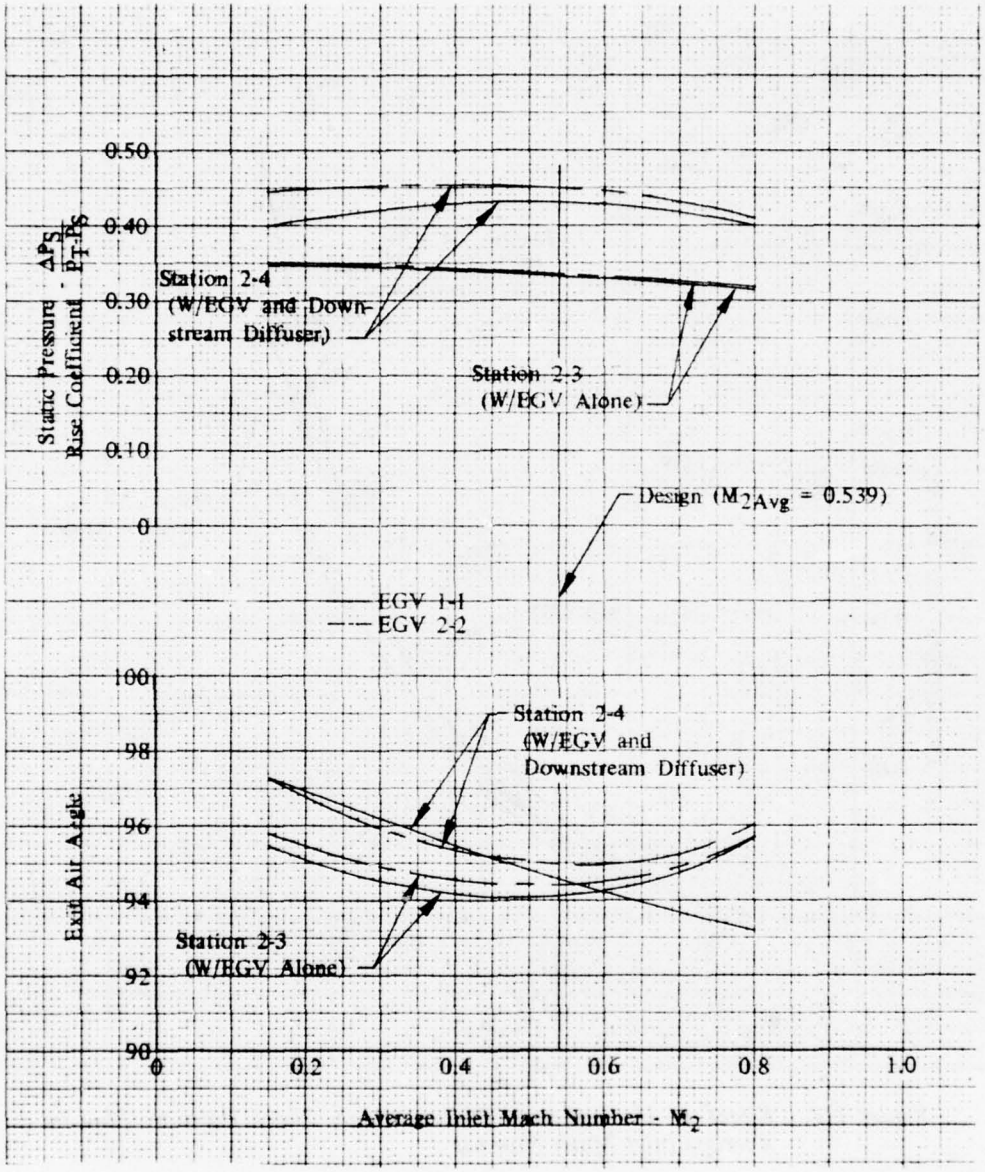


Figure 110. Effect of Uncambered Trailing Edge, Exit Air Angle and Static Pressure vs Average Inlet Mach Number

Figure 111 presents the average total pressure loss vs Mach number for each airfoil. At all Mach numbers, the loss for the uncambered airfoil between stations 2-3 is higher. This trend reverses, however, between stations 2-4. No reason for the reversal is apparent.

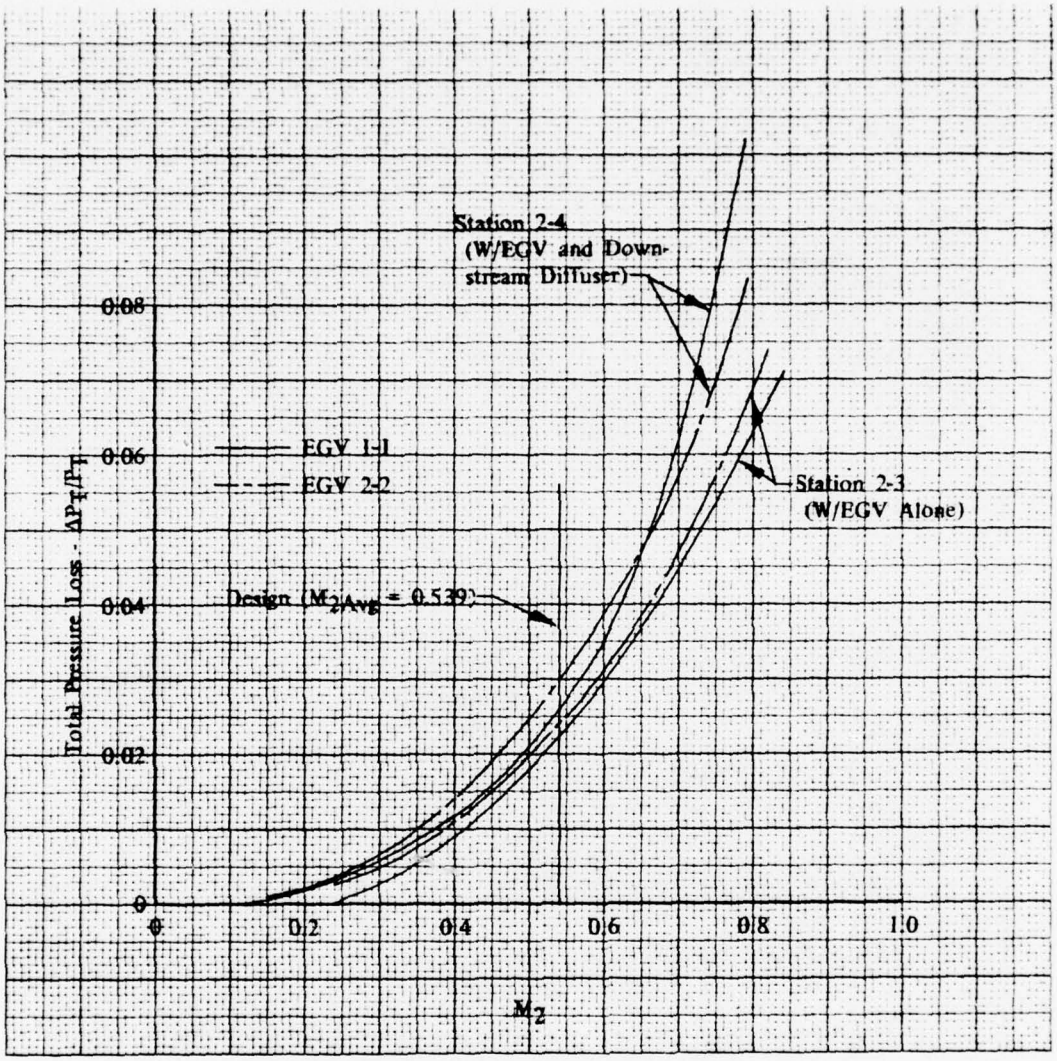


Figure 111. Effect of Uncambered Trailing Edge, Total Pressure Loss vs Average Inlet Mach Number

Table 20 summarizes the Phase II EGV airfoil configurations and the modified configurations tested in Phase III. Presented in Table 21 are the design point (average Mach number = 0.539) and the high Mach number (average Mach number = 0.7) performance gains and losses for the various airfoil modifications tested. Comparison of the design point and high Mach number data shows that the trends are consistent with Mach number. Table 22 presents a summary of the measured performance of each EGV configuration at the various test points recorded.

TABLE 20

EXIT GUIDE VANE CONFIGURATIONS

Configuration	*Description*
EGV No. 1	Basic Airfoil Design
EGV No. 1-1	Basic Airfoil Design (EGV No. 1) with a cutback leading edge.
EGV No. 2	Original Modified Airfoil Design, basic airfoil design (EGV No. 1) but with cutback leading edge, uncambered trailing edge and endwall protrusions.
EGV No. 2-1	Modified Airfoil (EGV No. 2) with 50% reduction in endwall protrusion size.
EGV No. 2-2	Modified Airfoil (EGV No. 2) with no protrusions (i.e., cutback leading edge — uncambered trailing edge).

TABLE 21

EXIT GUIDE VANE PERFORMANCE SUMMARY

Measured Performance Effects of Airfoil Modifications

Modification	*Total Pressure Loss*	*(ΔPT/PT)2-3**	*Diffusion*	*(ΔPS/Q)2-3*	*Gas Turning*	*θ2-3*
Average Mach No.	0.539	0.700	0.539	0.700	0.539	0.700
Leading Edge Cutback	+1.03%	+1.1%	−0.030	−0.026	−0.19°	−1.15°
Endwall Pressure Side Protrusions						
Full Size	−0.05%	−0.5%	+0.038	+0.044	+2.95°	+2.8°
Reduced Size	−0.8%	−1.7%	+0.042	+0.025	+1.56°	+1.4°
Trailing Edge Uncambering	+0.21%	+0.35%	+0.006	+0.004	−0.23°	−0.1°

*Station 2 denotes EGV Inlet
Station 3 denotes EGV Exit

TABLE 22
SUMMARY OF MEASURED PERFORMANCE OF EGV CONFIGURATIONS

Test No.	EGV No.	M_{2max}	M_2	M_3	M_4	β_{2min} (deg)	β_2 (deg)	β_3 (deg)	β_4 (deg)	$(\Delta P_2/P_1-P_2)_2$	$(\Delta P_2/P_1-P_2)_3$	$(\Delta P_2/P_1-P_2)_4$	$(\Delta P_3/P_3)_3$	$(\Delta P_3/P_3)_4$	$(\Delta P_3/P_3)_4$	ηD_2	ηD_3	ηD_4
4-3	1	0.680	0.524	0.388		50.4	54.6	93.9		0.3626	0.1505	0.4426	0.0110			0.733	0.596	
16-3	1-1	0.663	0.512	0.374				94.2		0.3341	0.1740	0.4272	0.0194			0.676	0.705	
4-4	1	0.687	0.531		0.337	50.4	54.6		92.6	0.3673		0.4491		0.0087	0.0220			0.723
16-4	1-1	0.641	0.510		0.329				94.7	0.3356		0.4307		0.0057	0.0217			0.700
5-3	1	0.318	0.246	0.194		50.4	54.6	92.8		0.3166	0.1528	0.4023	0.0025			0.701	0.655	
17-3	1-1	0.307	0.229	0.182				95.0		0.3451	0.0936	0.4048	0.0006			0.773	0.421	
5-4	1	0.325	0.253		0.168	50.4	54.6		91.6	0.3216		0.4028		0.0022	0.0065			0.694
17-4	1-1	0.287	0.220		0.150				96.6	0.3353		0.4405		0.0048	0.0030			0.771
6-3	1	0.884	0.707	0.496		50.4	54.6	93.4		0.3495	0.1349	0.4245	0.0350			0.640	0.503	
18-3	1-1	0.874	0.707	0.493				94.8		0.3234	0.1738	0.4130	0.0459			0.594	0.644	
6-4	1	0.894	0.710		0.426	50.4	54.6		93.5	0.3532		0.4322		0.0187	0.0520			0.650
18-4	1-1	0.876	0.697		0.404				93.7	0.3192		0.4107		0.0233	0.0640			0.621
7-3	2	0.692	0.545	0.373		50.4	54.6	91.5		0.3761	0.1560	0.4417	0.0240			0.749	0.628	
10-3	2-1	0.650	0.507	0.364				92.7		0.3787	0.1020	0.4334	0.0137			0.770	0.409	
13-3	2-2	0.680	0.532	0.381				94.5		0.3349	0.2020	0.4424	0.0235			0.676	0.467	
7-4	2	0.685	0.540		0.299	50.4	54.6		91.6	0.3838		0.4469		0.0092	0.0320			0.716
10-4	2-1	0.622	0.509		0.317				92.7	0.3617		0.4392		0.0137	0.0210			0.712
13-4	2-2	0.660	0.527		0.322				94.9	0.3441		0.4464		0.0084	0.0281			0.721
8-3	2	0.323	0.255	0.184		50.4	54.6	90.4		0.3343	0.2171	0.4003	0.0060			0.678	0.938	
11-3	2-1	0.295	0.232	0.178				92.4		0.3604	0.1100	0.4252	0.0019			0.799	0.460	
14-3	2-2	0.308	0.238	0.180				95.3		0.3454	0.1743	0.4456	0.0031			0.773	0.767	
8-4	2	0.315	0.251		0.200	50.4	54.6		90.3	0.3612		0.4225		−0.0003	0.0047			0.826
11-4	2-1	0.284	0.226		0.146				95.2	0.3350		0.4305		0.0060	0.0051			0.750
14-4	2-2	0.323	0.251		0.154				96.3	0.3359		0.4437		0.0018	0.0071			0.774
9-3	2	0.931	0.730	0.483		50.4	54.6	92.2		0.3672	0.1912	0.4484	0.0480			0.659	0.719	
12-3	2-1	0.861	0.693	0.491				93.3		0.3515	0.1390	0.4263	0.0306			0.649	0.519	
15-3	2-2	0.930	0.736	0.502				95.0		0.3237	0.2069	0.4260	0.0549			0.584	0.773	
9-4	2	0.914	0.728		0.406	50.4	54.6		92.4	0.3773		0.4457		0.0135	0.0640			0.664
12-4	2-1	0.820	0.676		0.416				93.3	0.3619		0.4327		0.0122	0.0419			0.660
15-4	2-2	0.930	0.717		0.418				95.3	0.3065		0.4163		0.0121	0.0636			0.626

D. STATE-OF-THE-ART SERIES AIRFOIL EVALUATION

The fourth annular cascade test conducted in Phase III was a test of a state-of-the-art series airfoil. This test was conducted for several reasons. First, to define the advanced technology improvements made in the EGV program, a test of a "state-of-the-art" series airfoil in the same EGV test facility was required. Secondly, the boundary layer analysis used in the design of the non-series airfoil (EGV No. 1), predicted that separation would not occur. This same analysis predicted early separation for the highly loaded series airfoils. The series airfoil test provides a means of identifying the importance of individual airfoil performance differences to the design system.

Six candidate series airfoils were evaluated in terms of predicted total pressure loss and minimum loss incidence range. Table 23 presents the predicted performance for each series considered. The following discussion comparing the various airfoils is based on the data presented in this table.

TABLE 23
SERIES AIRFOIL EVALUATION

$$\beta M = \frac{\beta R + \beta L}{2}$$

Total Pressure Loss $\Delta PT/PT$

Series	*400 Series*	*65 Series*	*Circular Arc*	*65 Series C/A Meanline*	*63 Series*	*Modified 65 Series*
Section						
Root	0.0075	0.0119	0.0111	0.0123	0.0125	0.0121
¼ Root	0.0069	0.0061	0.0076	0.0059	0.0066	0.0061
Mean	0.0040	0.0031	0.0044	0.0031	0.0033	0.0031
¼ Tip	0.0023	0.0017	0.0027	0.0017	0.0018	0.0017
Tip	0.0011	0.0009	0.0014	0.0009	0.0009	0.0009
Average	0.0044	0.0047	0.0054	0.0048	0.0050	0.0048

Minimum Loss Range

Range $\beta R - \beta L$ at $\beta M = \frac{\beta R + \beta L}{2}$

Root	6.24	8.87	8.79	7.33	10.02	9.04
¼ Root	10.89	12.71	11.52	10.92	11.28	12.59
Mean	15.80	13.67	12.98	13.68	12.66	13.55
¼ Tip	17.90	15.17	14.39	15.19	14.42	15.05
Tip	20.55	17.72	16.42	17.72	17.17	17.60
Average	14.28	13.63	12.82	12.86	13.11	13.59

βR: Maximum angle for minimum loss — choke direction
βL: Minimum angle for minimum loss — stall direction
βM: Mid range angle

The 400 series airfoil had the lowest average total pressure loss. However, it was not selected for the test airfoil because the root section loss (0.0075) was questionable. Except at the root section, each 400 series airfoil section indicated higher losses relative to the other low loss series airfoils. In addition, the 400 series root section loss was considerably lower than the typical (0.012) loss indicated for the other airfoils. Additional analytical design work would have been required to answer the questions about the low 400-series root section loss. It was felt that this work was beyond the scope of the contract objectives. In addition, the average 400-series loss was only slightly less than that of the 65-series airfoils. The 400-series, therefore, was not selected as the test airfoil.

The circular arc series and the 63-series airfoils had the highest average losses. Therefore, they were not selected as the test airfoil. This narrowed the selection to the three 65-series airfoils. These airfoils had about the same total pressure loss and minimum loss incidence range. Any one of the 65-series airfoils could have been selected as the test airfoil. The 65-series circular-arc meanline airfoil was selected because it is the easiest to fabricate. The airfoil curvature for this series was the smoothest, making curve-line fairing between sections slightly easier.

Figure 112 presents the geometric characteristics for the 65-series circular arc airfoil. The airfoil gap/chord, thickness/chord, and aspect ratios are the same as those of the non-series design, EGV No. 1. The series airfoil maximum thickness and axial chord were also kept the same.

The series airfoil was defined at five radial or spanwise locations. The five airfoil cross-sections and the defining coordinates are presented in Appendix F.

Figure 113 illustrates the differences between the mean sections of the series and non-series airfoils. The series airfoil has its turning and maximum thickness at the leading edge. The non-series airfoil is directly opposite with the turning and maximum thickness at the trailing edge. This difference results from tailoring the non-series airfoil curvature and thickness distribution to reduce suction surface diffusion. Similar comparisons can be made at the other cross sections of the two airfoils.

The 65 series airfoil sections were defined with an inlet metal angle which was midway or mid-range between the airfoil choke and stall inlet angles. The choke and stall inlet angles are defined as the angles where the total pressure loss ($\Delta P_T/P_T$) is 0.022 higher than the mid-range loss value. Figure 114A presents the loss vs inlet angle curve for the 65 series root section. Although not presented, similar curves can be generated for the other airfoil sections. Selecting the mid-range inlet angle permits the airfoil to operate efficiently at off-design gas inlet conditions. This range of operation is equal in both the stall and choke directions.

An alternative to selecting the mid-range inlet angle is to select the inlet angle which gives the lowest loss. This angle is defined as the minimum loss inlet angle. Figure 114B presents the minimum loss curve for a 65-series circular arc meanline root section. As shown, the minimum loss inlet angle does not provide equal margins between choke and stall. In Figure 114B, the choke and stall angles are defined at the angles where the loss is 0.022 higher than the minimum loss value.

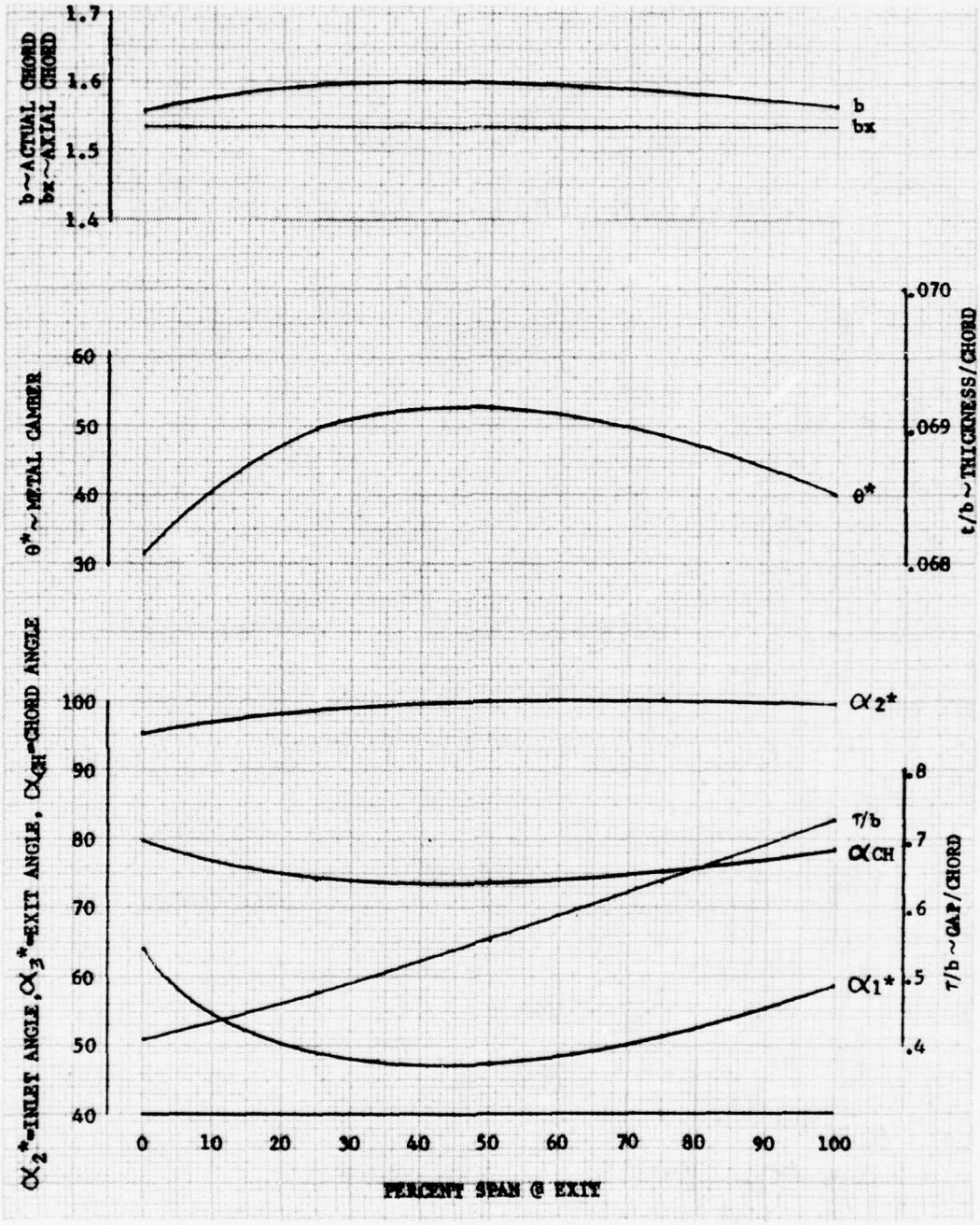


Figure 112. 65 Series — Circular Arc Meanline Airfoil Characteristics

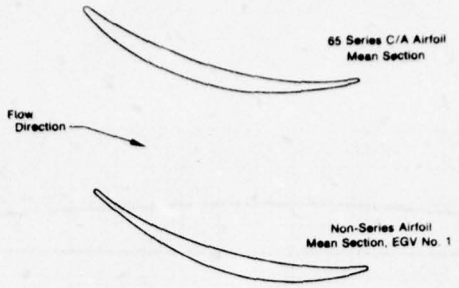
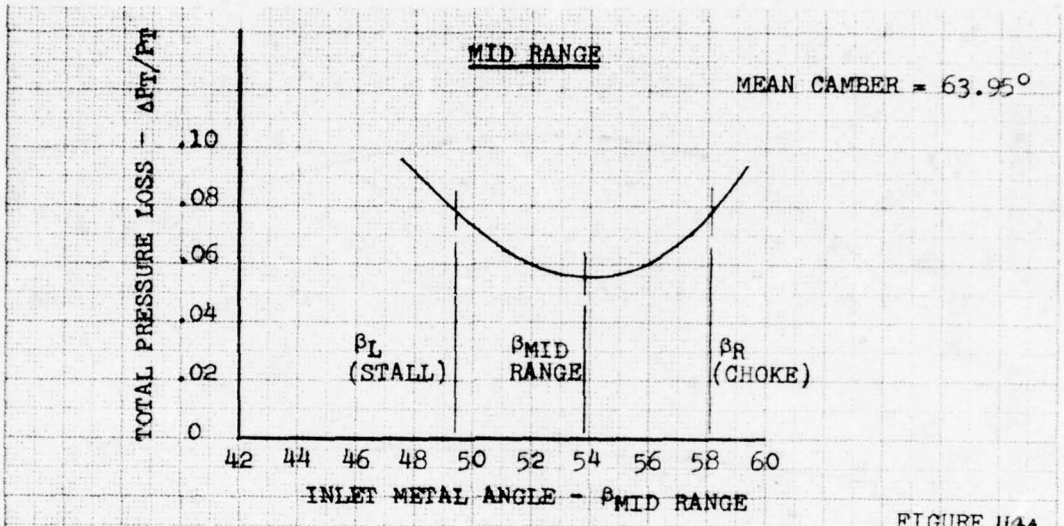


Figure 113. Mean Section Comparison, Series vs Non-series Airfoil



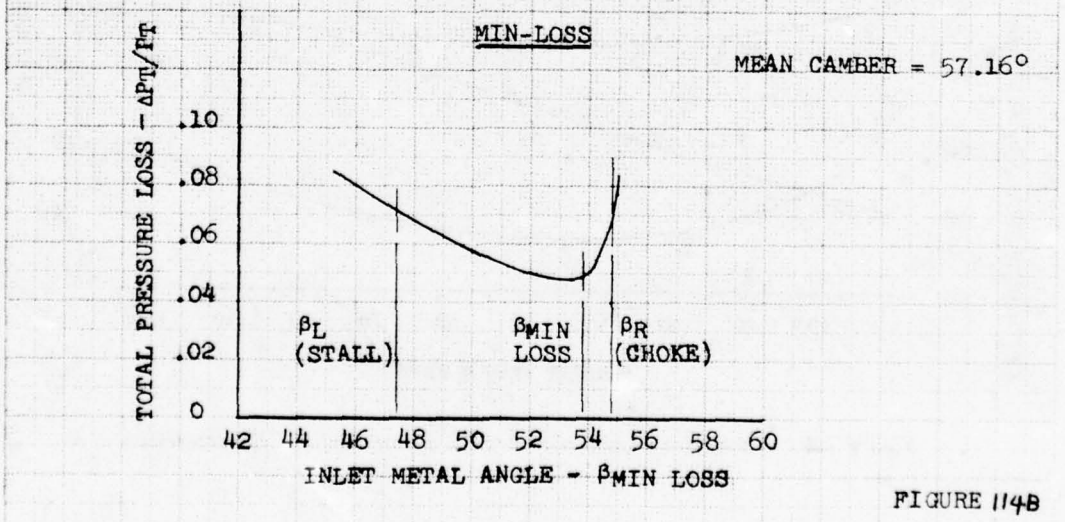


Figure 114. Mid Range Loss and Minimum Loss vs Inlet Angle, Root Section

Table 24 presents a summary of the minimum loss and mid-range performance predictions for each section of the 65-series airfoil. Because of the small choke margin ($\beta_R - \beta_{min}$) for the minimum loss root section, the 65-series airfoil was designed with the mid-range inlet angles. Except for the root and mean, each section showed the same loss at both the mid-range and minimum loss inlet angles. At the root, the selection of the mid-range angle resulted in an increased loss of 0.15%. The mean section loss increased 0.01%.

As shown in Table 24, selection of the mid-range inlet angle increases the root section incidence from 3.68 degrees to +10.19 degrees. Although the +10.19 degrees of incidence is higher than normal, it is acceptable since the actual area to choke area ratio for the series airfoil is about the same as that of the non-series airfoil, 1.092 vs 1.095 respectively. Table 25 presents a summary of the area ratios and additional geometric properties for the series and non-series airfoils.

TABLE 24
65 SERIES/CIRCULAR ARC MEANLINE
PERFORMANCE COMPARISON AT
MINIMUM LOSS AND MID-RANGE

At Minimum Loss

Section	*βR-βMin*	*βL-βMin*	*ΔPT/PT*	*i*
Root	1.02	6.38	0.0115	+3.68
¼ Root	6.28	4.92	0.0059	+0.84
Mean	8.51	5.70	0.0030	−0.98
¼ Tip	8.50	7.01	0.0017	−2.25
Tip	9.03	8.82	0.0009	−2.38

$$\text{At Mid-Range } \beta_{MID} = \frac{\beta R - \beta L}{2}$$

	βR-βMid	*βL-βMid*	*ΔPT/PT*	*i*
Root	4.33	4.33	0.0130	+10.19
¼ Root	5.47	5.47	0.0059	+ 0.14
Mean	6.81	6.81	0.0031	− 2.98
¼ Tip	7.63	7.63	0.0017	− 2.95
Tip	8.90	8.90	0.0009	− 2.69

βR: Maximum angle for minimum loss — choke direction
βL: Minimum angle for minimum loss — stall direction
βMin: Minimum loss angle
βMid: Mid-range angle
i: Incidence $\beta_{Metal} - \beta_{Gas}$

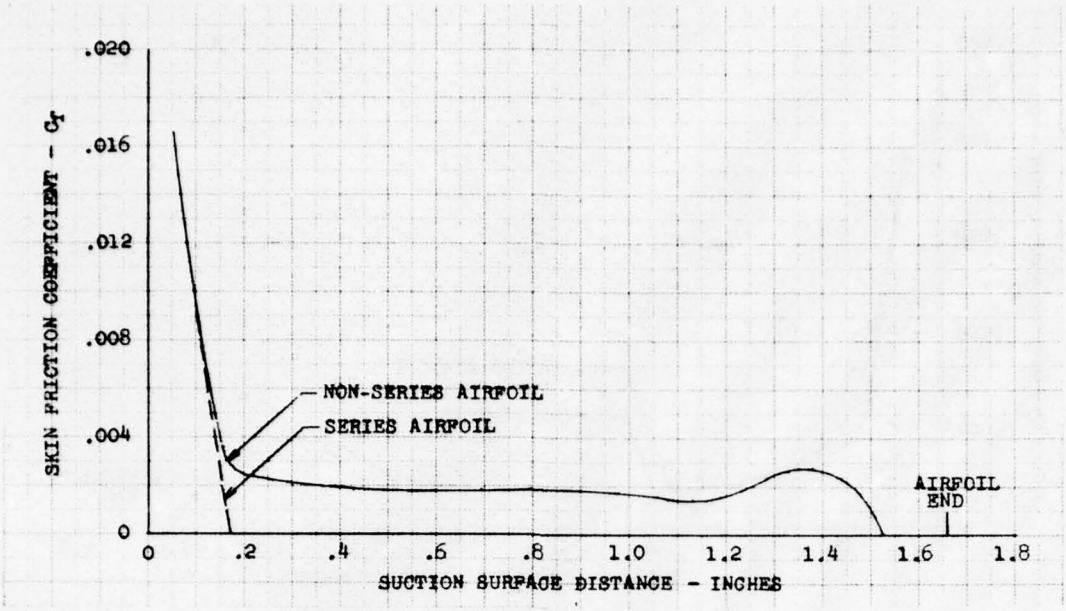
TABLE 25
COMPARISON OF SELECTED SERIES AIRFOIL AND NON-SERIES AIRFOIL

Section	β_1*	β_2*	θ*	B	τ/B	t/B	AR	i	$\lambda A/\lambda C$	LER	TER	H/L	$\Delta\beta_2$	$\Delta\beta_3$
Series Airfoil (Full size, scale by 0.59 for rig size)														
Root	63.95	95.68	31.73	2.639	0.406	0.070		+10.19	1.092	0.017	0.017	−0.1796	83.31	6.89
¼ Root	48.74	98.72	49.98	2.70	0.476	0.068		+ 0.14	1.142	0.017	0.017	−0.2918	77.12	6.37
Mean	47.12	99.82	52.70	2.707	0.55	0.068	2.38	− 2.98	1.262	0.017	0.017	−0.2968	75.98	6.15
¼ Tip	51.05	99.77	48.72	2.683	0.639	0.069		− 2.95	1.440	0.017	0.017	−0.2603	77.63	6.34
Tip	58.51	98.60	40.09	2.65	0.728	0.070		− 2.69	1.754	0.017	0.017	−0.2024	82.07	6.47
Nonseries Airfoil (Full size, scale by 0.59 for rig size)														
Root	55.68	96.5	40.82	2.671	0.401	0.069		+ 1.92	1.095	0.017	0.017	−0.275	5.0	18.0
¼ Root	47.18	98.0	50.82	2.717	0.473	0.068		− 1.42	1.159	0.017	0.017	−0.310	3.0	15.0
Mean	47.10	98.5	51.40	2.717	0.552	0.068	2.37	− 2.99	1.291	0.017	0.017	−0.310	2.0	14.0
¼ Tip	50.55	98.5	47.95	2.689	0.638	0.069		− 3.45	1.462	0.017	0.017	−0.270	3.0	13.5
Tip	58.52	96.8	38.28	2.627	0.735	0.070		− 2.68	1.789	0.017	0.017	−0.200	4.0	16.0

Figures 115 through 119 present the predicted surface pressure distributions and boundary layer skin friction coefficients for both the 65-series airfoil and the non-series airfoil, EGV No. 1. Comparing pressure distributions at each airfoil section shows the non-series airfoil reduced suction surface rate of diffusion. The non-series airfoil pressure surface rate of diffusion is also reduced. Comparing skin friction coefficients, the series airfoil root and tip sections separate near the leading edge; the ¼ root and ¼ tip sections separate about midway along the suction surface. The series airfoil mean section did not separate but the coefficient of friction (C_f) did approach zero at a surface distance of 0.85 in. Separation is assumed to occur when the friction coefficient equals zero. The non-series airfoil, except for the tip section, separates at or near the trailing edge. The tip section separates at a surface distance of 0.7 in., midway along the suction surface.

Based on the performance of the other sections of the non-series airfoil, the tip section was not expected to separate. However, the Reynolds number for the tip section is the lowest across the span and could have caused the predicted separation. The tip section Reynolds number is approximately one-half that of the root section, 154,000 vs 275,000.

The free stream turbulence used in the boundary layer analysis was set at 4%, which is typical of engine turbulence levels. Based on the size of the rig inlet distortion screen, the rig turbulence is estimated to be 3.8 percent.



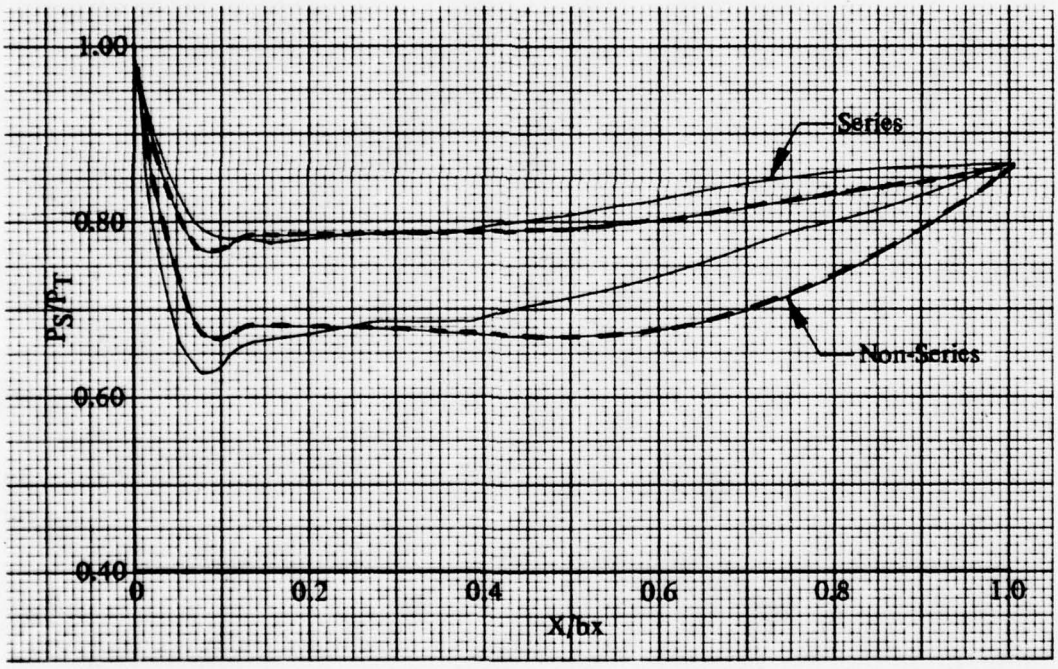
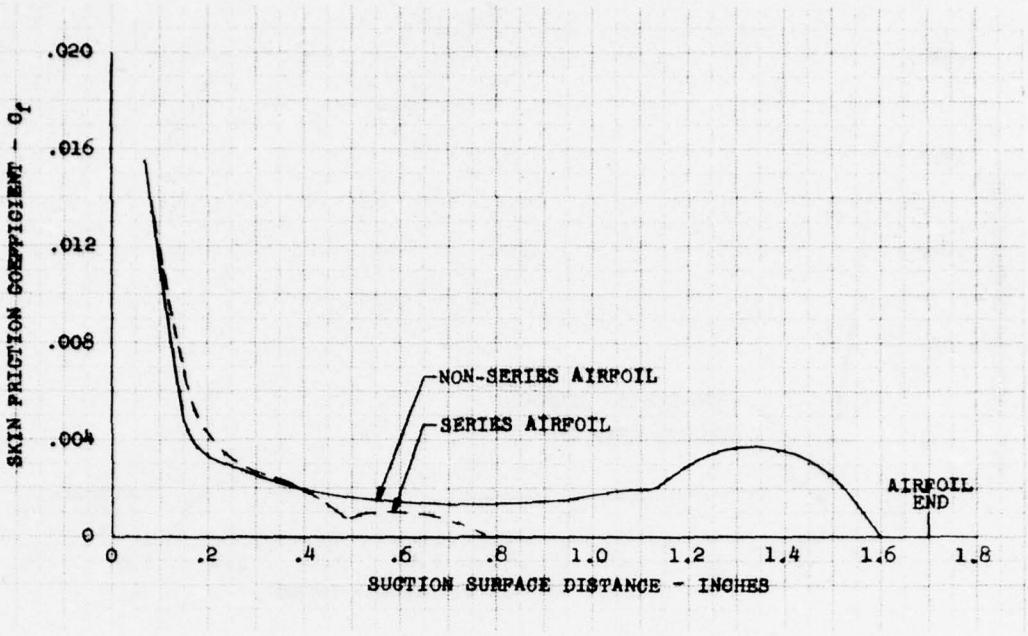


Figure 115. Series and Non-series Airfoil Root Section Surface Pressure Distributions and Skin Friction Coefficients



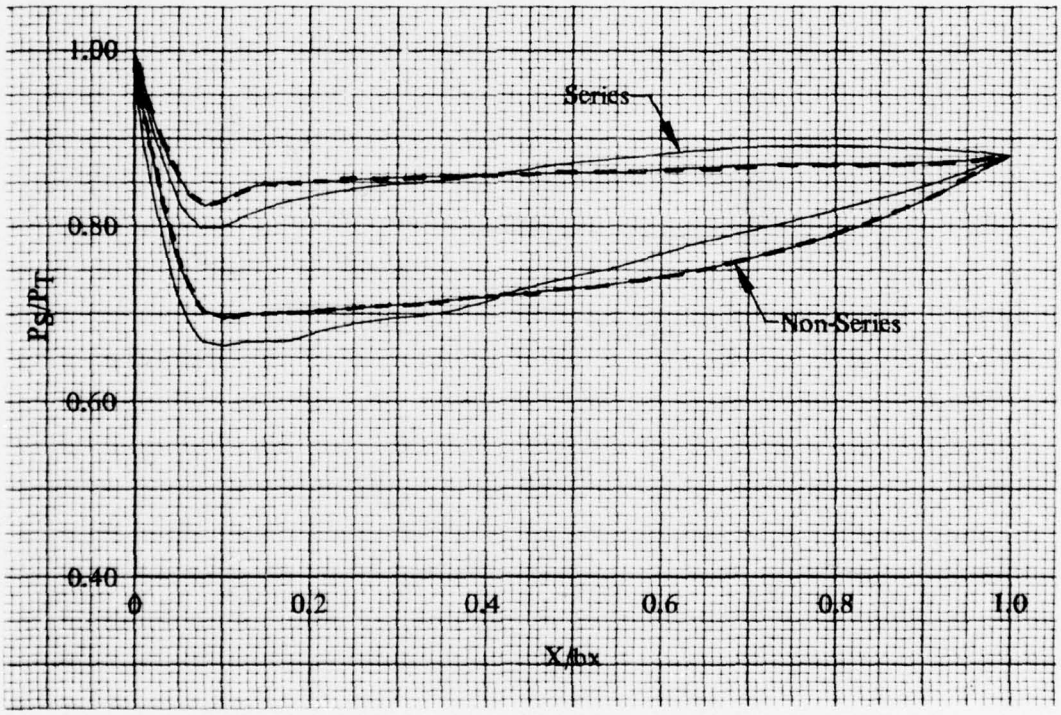
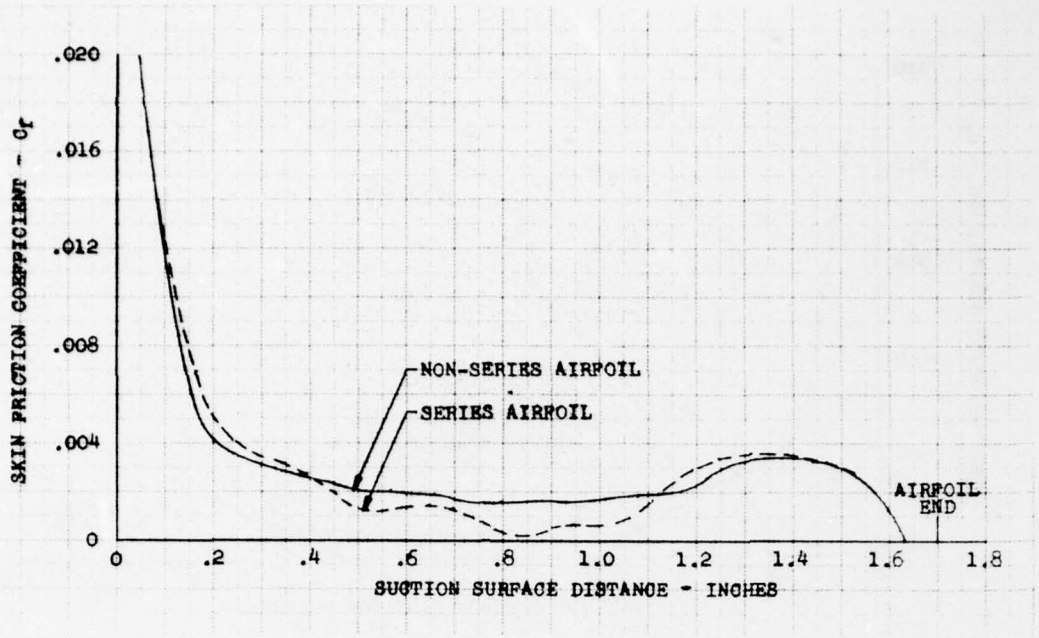


Figure 116. Series and Non-series Airfoil ¼ Root Section Surface Pressure Distributions and Skin Friction Coefficients



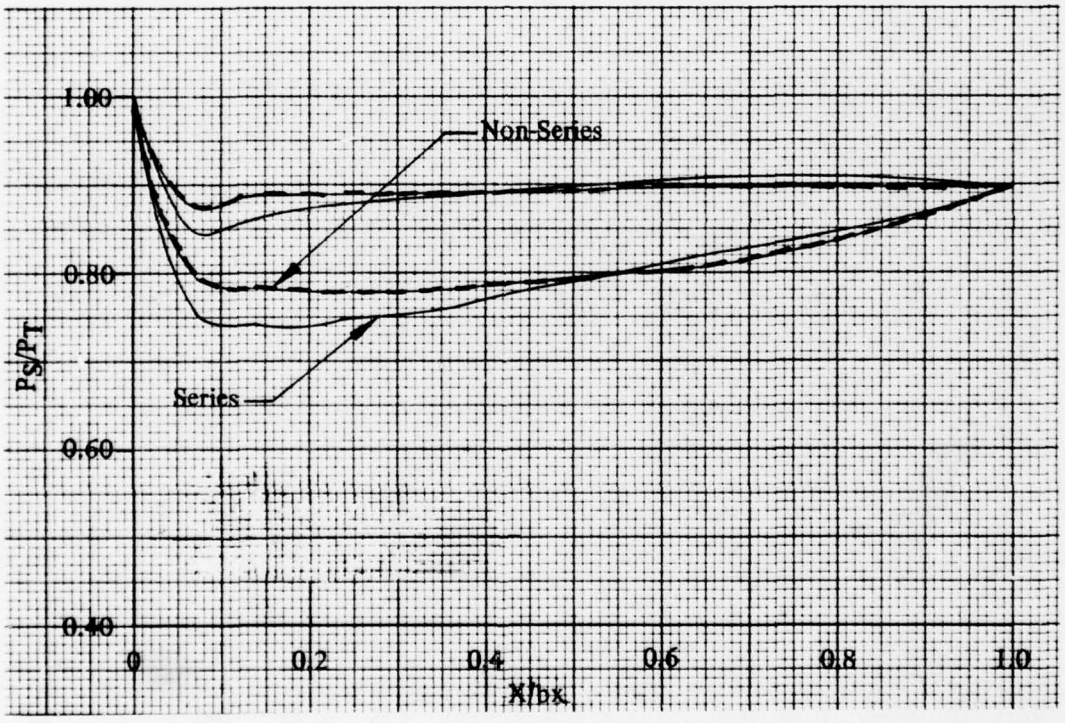
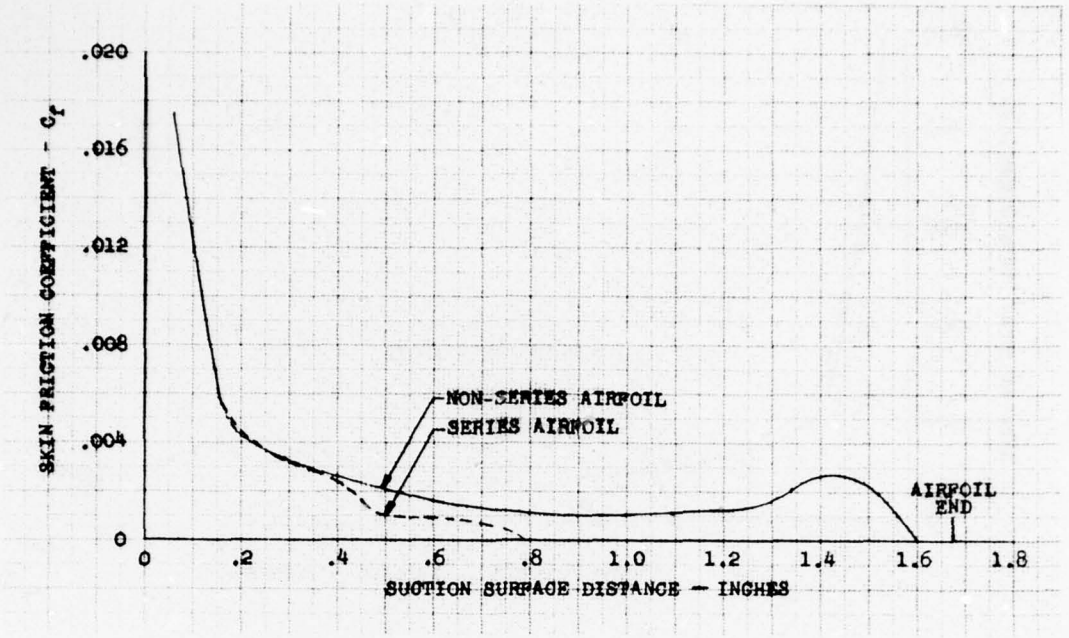


Figure 117. Series and Non-series Airfoil Mean Section Surface Pressure Distributions and Skin Friction Coefficients



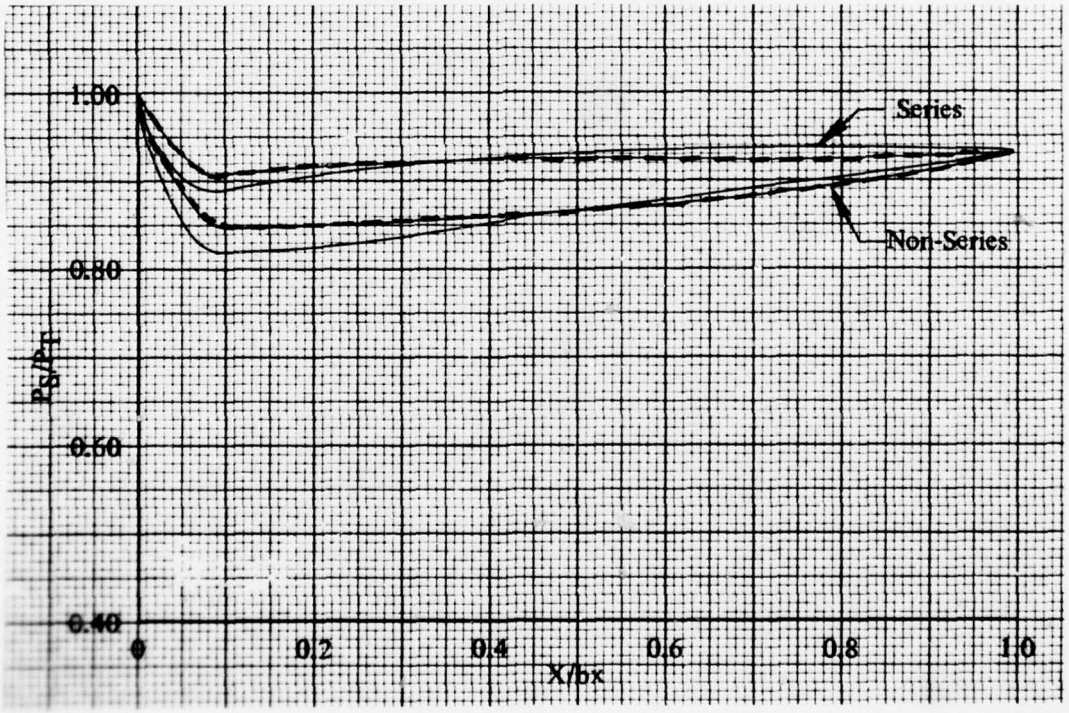
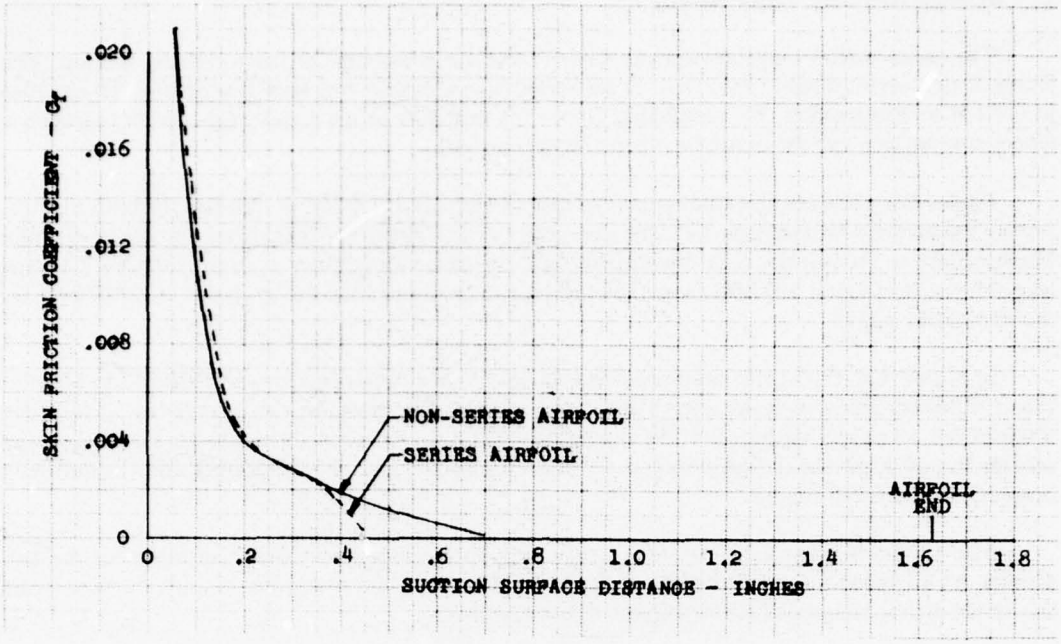


Figure 118. Series and Non-series Airfoil ¼ Tip Section Surface Pressure Distributions and Skin Friction Coefficients



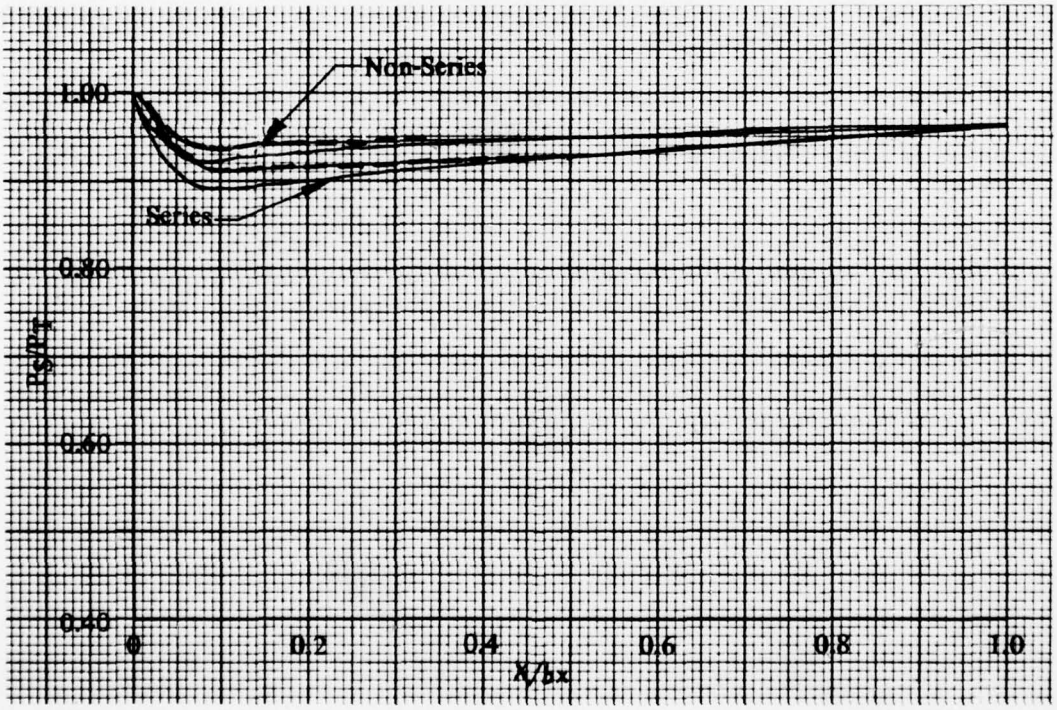


Figure 119. Series and Non-series Airfoil Tip Section Surface Pressure Distributions and Skin Friction Coefficients

E. SERIES AIRFOIL TEST RESULTS

The series airfoil annular cascade test results are presented in the following section. The Phase II non-series airfoil (EGV No. 1) test results (previously presented in Section II) are also presented in this section. By presenting the series and non-series airfoil test results together, a direct comparison can be made between the two airfoils.

Figure 120 presents the total pressure loss vs average inlet Mach number for both airfoils. Across the airfoil row (stations 2-3), the non-series airfoil has lower total pressure loss at all inlet Mach numbers. Across the combined airfoil and downstream diffuser system (stations 2-4), the non-series airfoil again has lower loss. In both cases, the loss at the design point is 1.0% lower for the non-series airfoil.

In Figure 121, the static pressure rise coefficients are presented for each airfoil. At all inlet Mach numbers the non-series airfoil has the higher static pressure rise across the airfoil row, stations 2-3. Between stations 2-4, the non-series airfoil pressure rise is higher for Mach numbers greater than 0.4. At the design point, the station 3 pressure rise is 0.015 higher and the station 4 pressure rise is 0.016 higher.

Also shown in Figure 121 is the average exit air angle vs inlet Mach number for the two airfoils. At all Mach numbers the non-series airfoil has about three degrees of underturning while the series airfoil has about three degrees of overturning.

Figure 122 presents the spanwise profiles of total pressure loss and exit air angle for the two airfoils. Comparing the loss profiles, the series airfoil shows higher loss at all span locations except between the 30-35 precent span locations. Comparing the exit air angle profiles, the underturning and overturning characteristics of each airfoil are evident at all span locations. Both airfoils have decreased turning near the endwalls.

Presented in Figure 123 are the diffusion efficiencies for the two airfoils. Except for the low Mach number points, the non-series airfoil has higher diffusion efficiencies. At the design point, the non-series airfoil efficiency is 3.6% higher between stations 2-3 and 2.2% higher between stations 2-4.

Figure 124 and 125 present the measured ¼ root and mean section pressure distributions. At all Mach numbers, the tangential loading is less for the non-series airfoil. The reduced loading is attributed to the difference in gas turning between the two airfoils.

Presented in Figure 126 for the ¼ root and mean sections is the average static pressure rise vs local maximum suction surface pressure rise or diffusion ($\Delta P/Q$). Both airfoil sections show that for a given average pressure rise, the non-series airfoil will have lower suction surface diffusion.

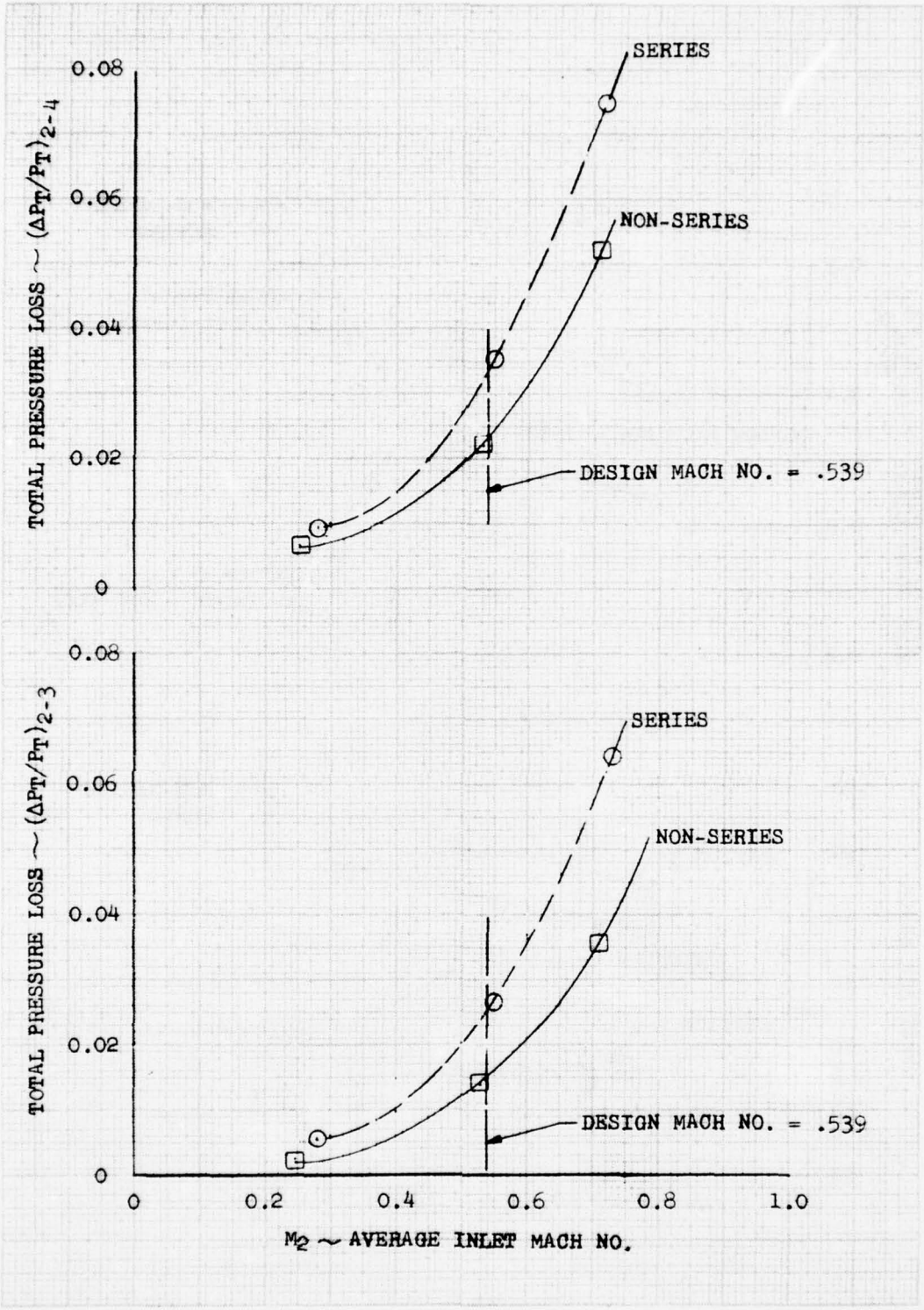


Figure 120. Series and Non-series EGV Total Pressure Loss vs Inlet Mach Number

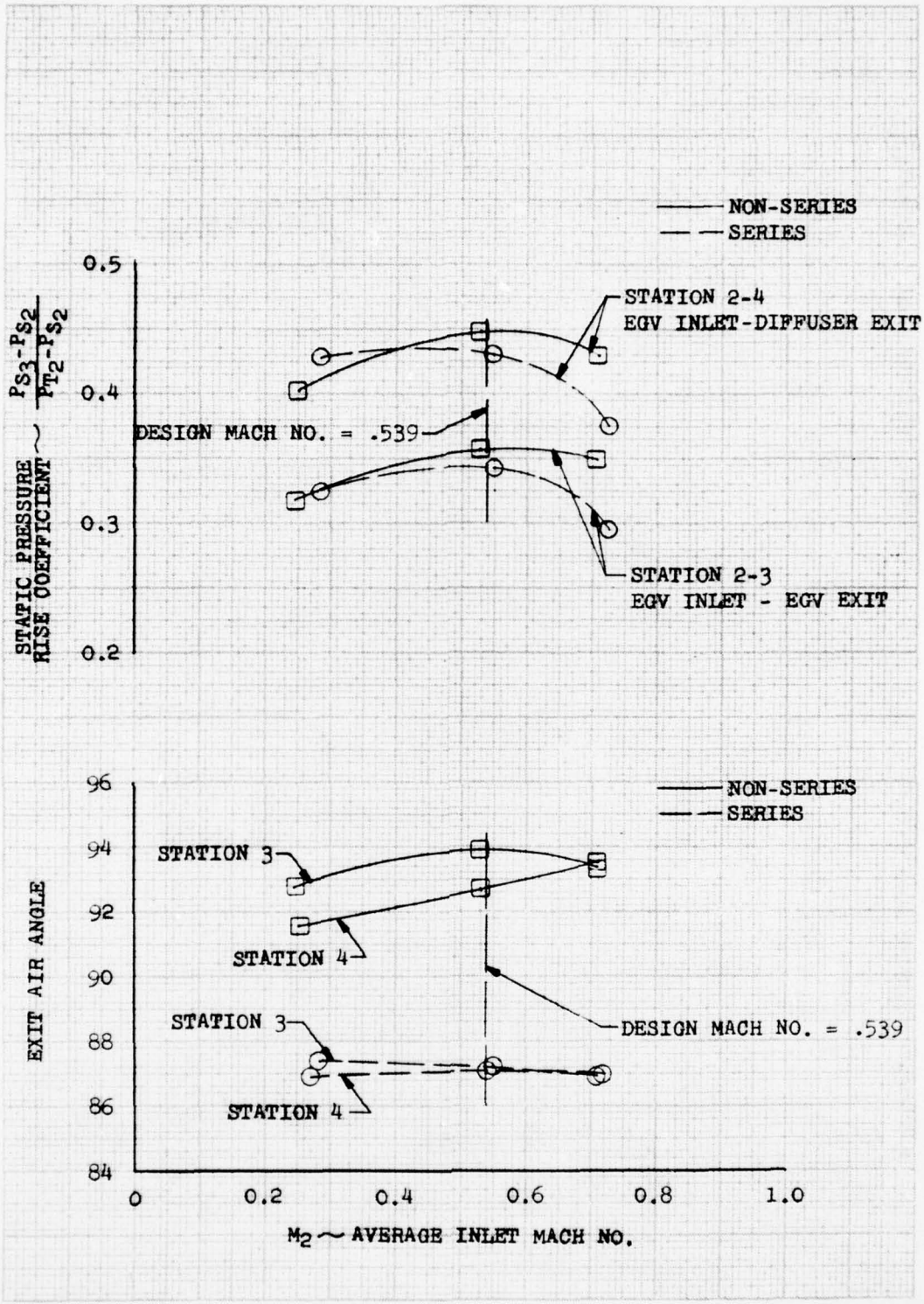


Figure 121. Series and Non-series EGV Static Pressure Rise, Exit Air Angle vs Inlet Mach Number

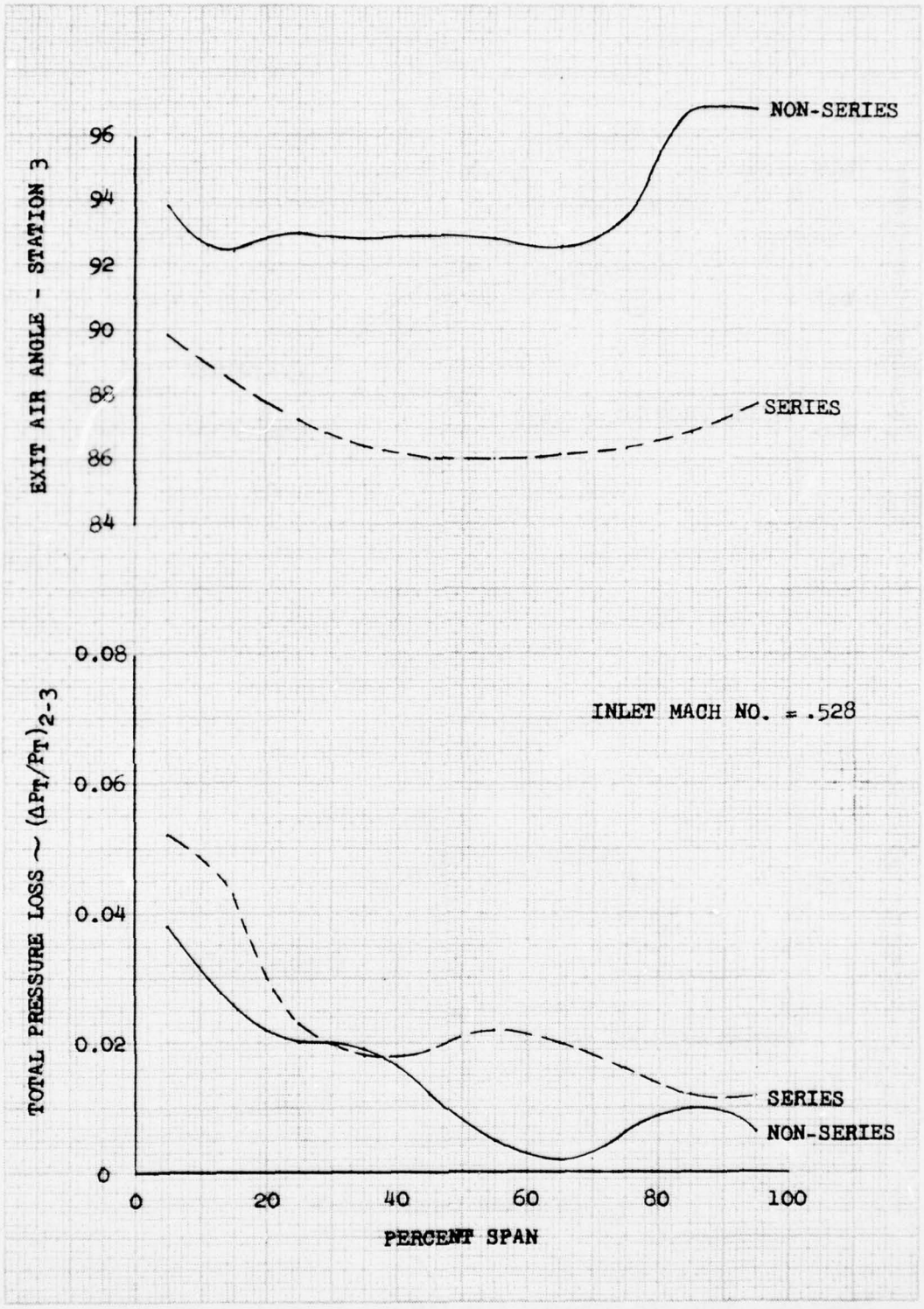


Figure 122. Series and Non-series EGV Exit Air Angle, Total Pressure Loss vs Percent Span

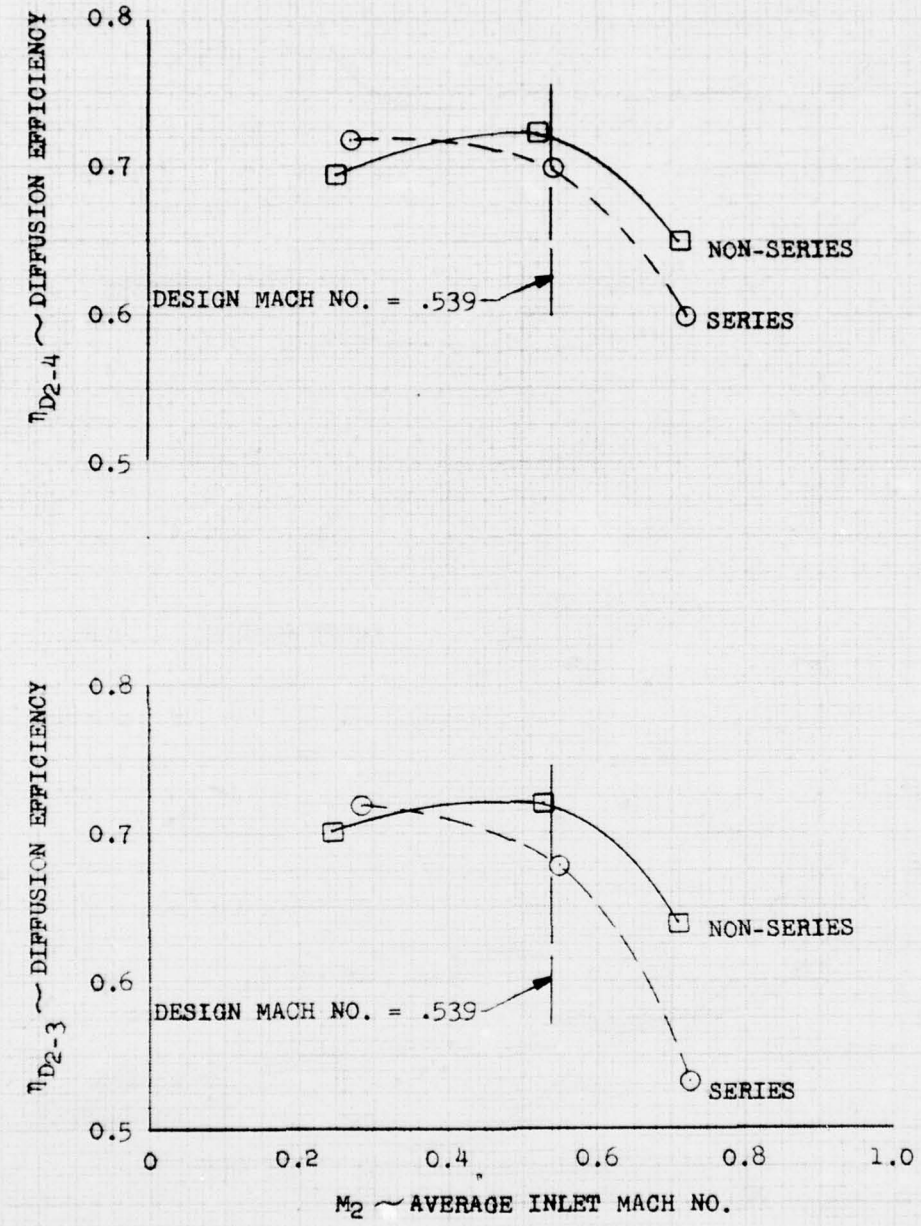


Figure 123. Series and Non-series EGV Diffusion Efficiency vs Inlet Mach Number

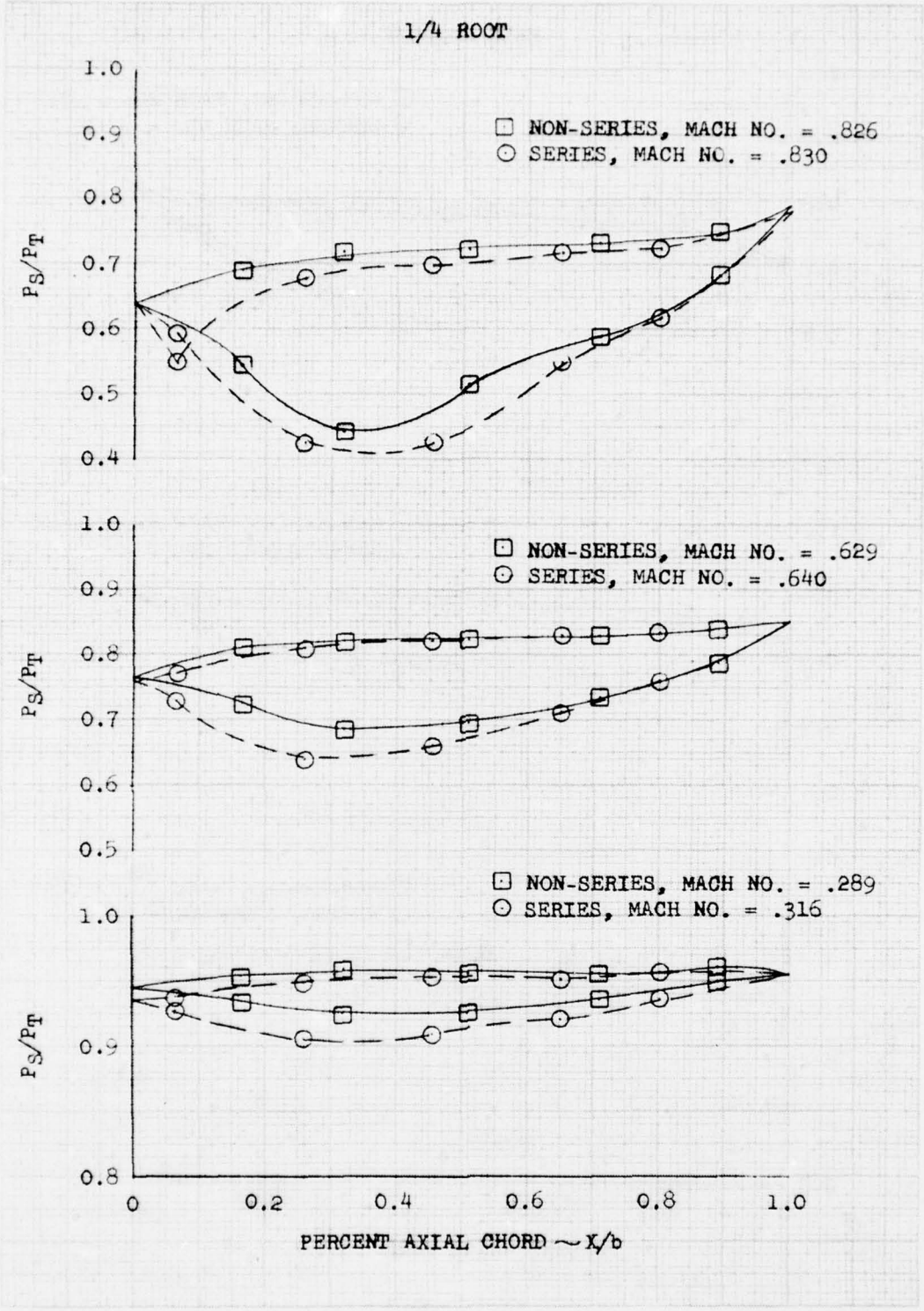


Figure 124. Series and Non-series EGV ¼ Root Section Measured Pressure Distributions

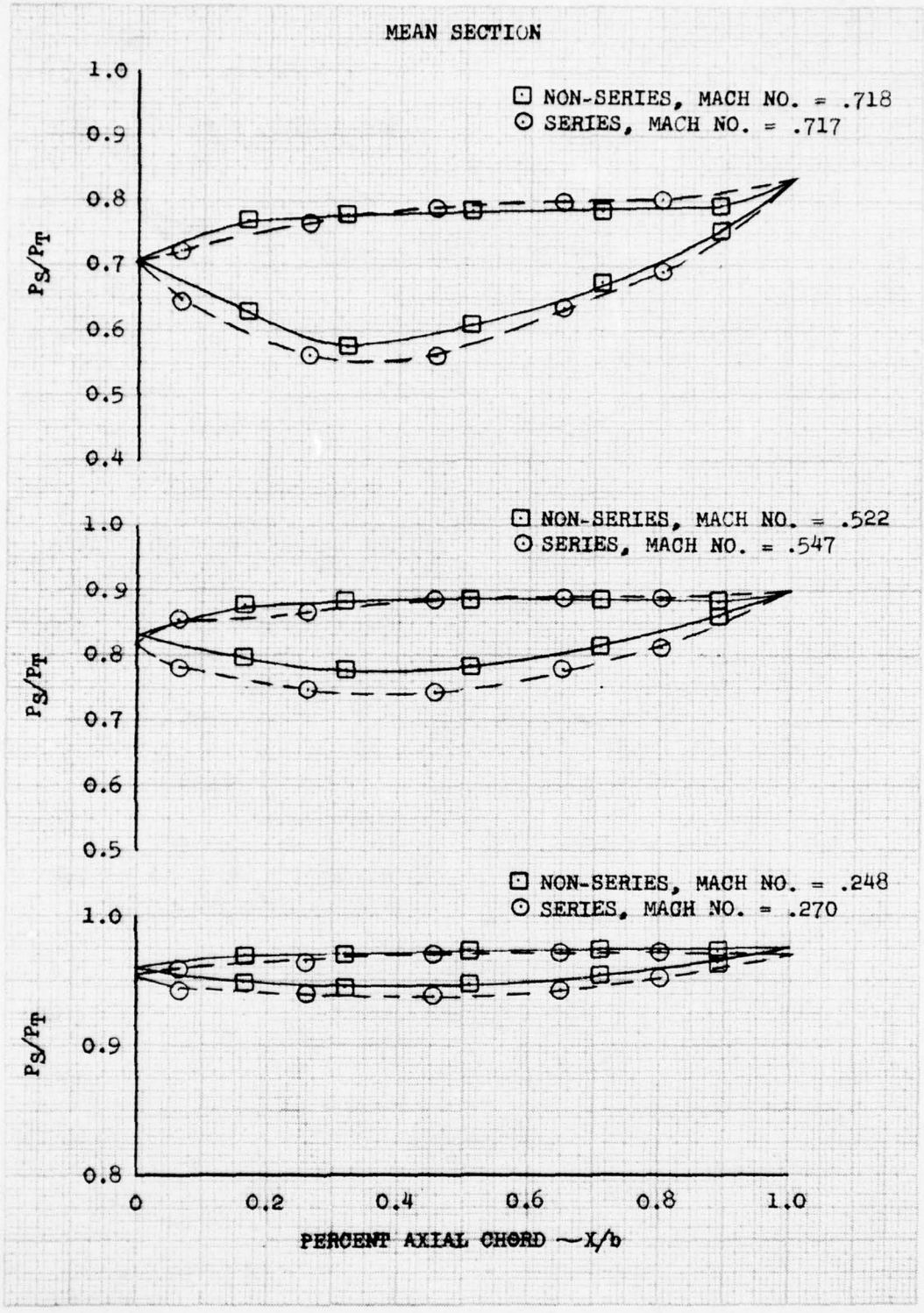


Figure 125. Series and Non-series EGV Mean Section Measurement Pressure Distributions

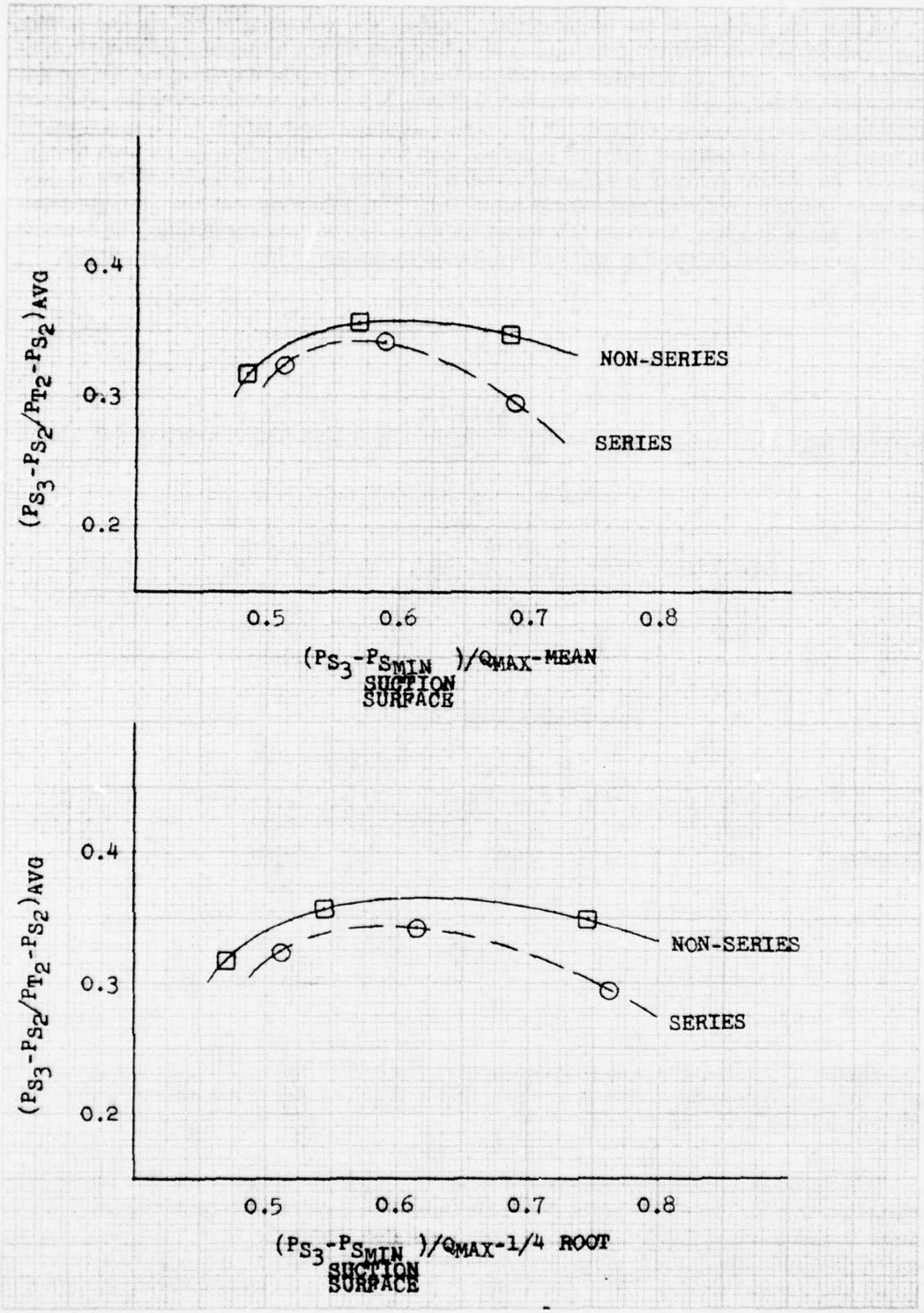


Figure 126. Series and Non-series EGV Average Static Pressure Rise vs Suction Surface Diffusion

Because the loading on the series airfoil is higher, any reduction in the suction surface diffusion which is a result of the difference in airfoil designs cannot be determined directly from the data. However, analytical predictions indicate that the design goal of reduced suction surface diffusion was achieved with the non-series airfoil. Table 26 presents a summary of the predicted and measured suction surface diffusion for the ¼ root sections of each airfoil. At the measured rig test conditions, the predicted diffusion is higher than the measured diffusion for both airfoils. However, the relative decrease in diffusion between the series and non-series airfoils shows good agreement (−0.081 predicted and −0.070 measured). This indicates that the absolute levels predicted should be lower. Applying this reasoning to the design point predictions, the decrease in diffusion predicted for the non-series airfoil should be decreased from −0.062 to −0.051.

TABLE 26
PREDICTED AND MEASURED SUCTION SURFACE DIFFUSION ¼ ROOT SECTION

Rig Test Conditions

	Inlet Mach No.	*Predicted* $(P_{s3} - P_{s\ min}/Q_{max})$	*Measured* $(P_{s3} - P_{s\ min}/Q_{max})$	*Difference*
Series	0.640	0.697	0.614	−0.083
Non-series	0.629	0.616	0.544	−0.072
		−0.081	−0.070	

Design Point Conditions

	Inlet Mach No.	*Predicted* $(P_{s3} - P_{s\ min}/Q_{max})$	*Predicted w/correction* $(P_{s3} - P_{s\ min}/Q_{max})$	*Correction*
Series	0.631	0.749	0.666	−0.083
Non-series	0.631	0.687	0.615	−0.072
		−0.062	−0.051	

Figure 127 presents the average static pressure rise coefficients vs total pressure loss for the series and non-series airfoils. This figure shows that for a given pressure rise, the non-series airfoil will have a lower loss.

A lamp black and oil flow visualization study was made on the series airfoil to identify any areas of separation. The results of this study are shown in Figure 128. Except for an isolated area at the ¼ root section, the airfoil is completely separated. From the ¼ root section to the tip section, the separation tends to move forward on the airfoil. A similar trend is shown between the ¼ root and the root section. These results agree with the spanwise loss profile shown earlier in Figure 122.

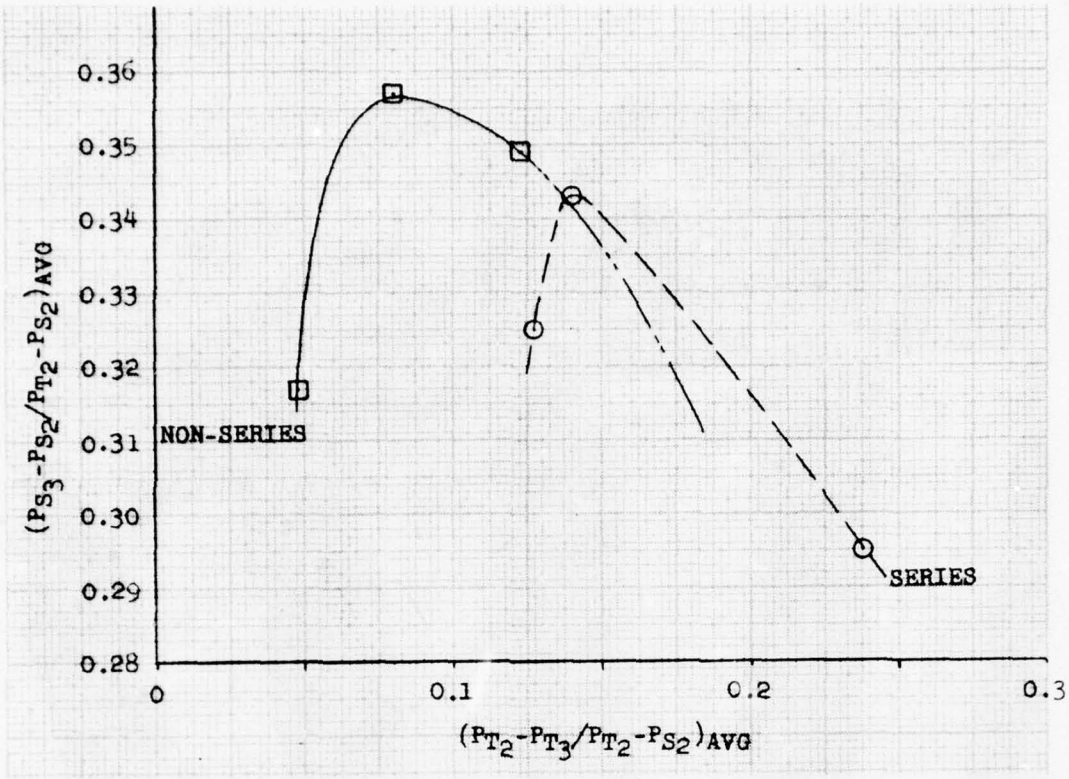


Figure 127. Series and Non-series EGV Average Static Pressure Rise vs Total Pressure Loss

Table 27 presents the design point performance summary for the series and non-series airfoils. The non-series airfoil is more efficient in terms of increased static pressure rise with reduced total pressure loss.

TABLE 27
DESIGN POINT PERFORMANCE SUMMARY

Parameter	*Series*	*Non-series*
Mach No. — Station 2	0.539	0.539
Air Angle — Station 2	54.6	54.6
Mach No. — Station 3	0.384	0.397
Air Angle — Station 3	87.2	93.9
Pressure Rise ($P_{s3} - P_{s2}/P_{t2} - P_{s3}$)	0.343	0.357
Pressure Loss ($\Delta P_t/P_{t2}$) 2-3	0.025	0.015
Mach No. — Station 4	0.327	0.342
Air Angle — Station 4	87.1	92.7
Pressure Rise ($P_{s4} - P_{s2}/P_{t2} - P_{s2}$)	0.432	0.448
Pressure Loss ($\Delta P_t/P_{t2}/P_{t2}$) 2-4	0.034	0.023



Figure 128. Flow Visualization — 65 Series Airfoil

Figure 129 presents the predicted effect on performance of the 6.7 degrees difference in gas turning between the two airfoils. Based on compressor cascade data, the difference in turning does not account for the differences in performance. Therefore, the differences in performance can be attributed to the differences in the airfoil designs.

Figures 130 and 131 present the predicted and measured static pressure distributions for the non-series and series EGV designs. In Figure 130, good agreement is evident at both airfoil sections for the non-series airfoil. For the series airfoil, shown in Figure 131, only the ¼ root section has good agreement. The poor agreement at the mean section is attributed to airfoil separation.

A comparison of the predicted and measured series airfoil separation is presented in Figure 132. In the midspan region, the predicted and measured separation are in good agreement. However, the agreement decreases towards the endwalls. The predicted separation was based on a two-dimensional analysis which neglected any endwall effects.

F. SUMMARY — PHASE III

Both the uncambered trailing edge and cutback leading edge modifications included in the design of EGV No. 2 resulted in a decrease in aerodynamic performance. Both modifications increased the total pressure loss and decreased the gas turning. The static pressure rise decreased slightly with the leading edge cutback and increased slightly with the uncambered trailing edge.

The endwall modifications (pressure surface protrusions) resulted in improved aerodynamic performance. Compared to the relatively high loss cutback-uncambered airfoil (EGV No. 2-2), addition of a reduced size and a full-size protrusion decreased the total pressure loss and increased the static pressure rise and gas turning. The reduced size protrusion, approximately one-half the size of the full protrusion, resulted in the largest reduction in total pressure loss and indicates that an optimum protrusion size exists.

The performance comparison made between the 65 series EGV airfoil and the unmodified non-series airfoil (EGV No. 1) indicated that, relative to the state-of-the-art series airfoil, the non-series airfoil improved performance, decreasing the total pressure loss (0.015 vs 0.025 percent) and increasing the static pressure rise (0.357 vs 0.343). Flow visualization tests made on the series airfoil indicated that the high total pressure loss was caused by flow separation. Analytical studies made to evaluate the series airfoils (prior to the testing) predicted the flow separation. The non-series airfoil, specifically designed with a reduced suction surface rate of diffusion, as predicted, did not separate.

AD-A060 343 PRATT AND WHITNEY AIRCRAFT GROUP WEST PALM BEACH FL G--ETC F/G 21/5
TURBINE EXIT GUIDE VANE PROGRAM.(U)
NOV 77 W S MITCHELL, J F SOILEAU F33615-74-C-2060
UNCLASSIFIED PWA-FR-8932 AFAPL-TR-77-75 NL

3 OF 4
AD
A060343



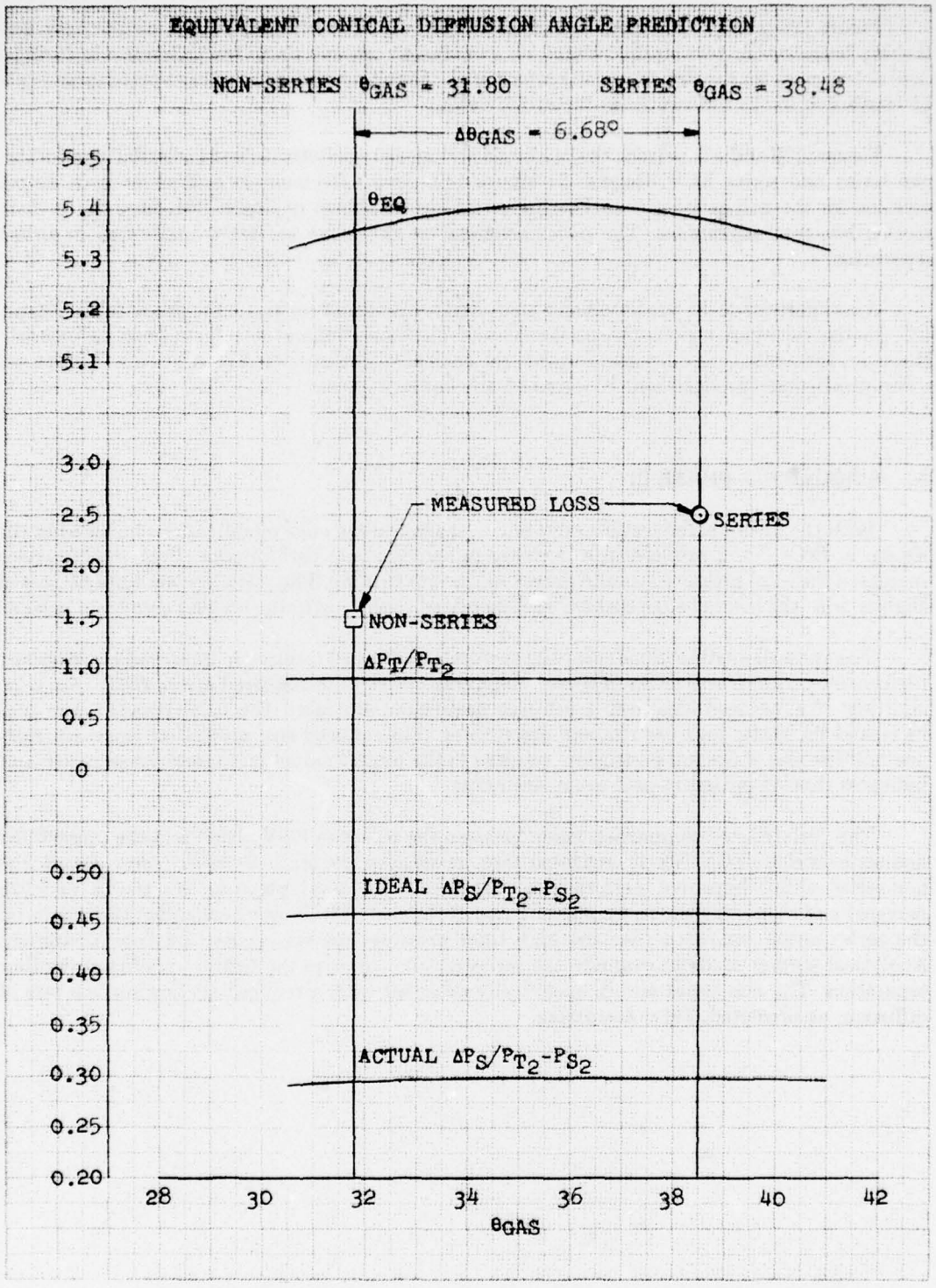


Figure 129. Predicted Effect of Gas Turning on Performance

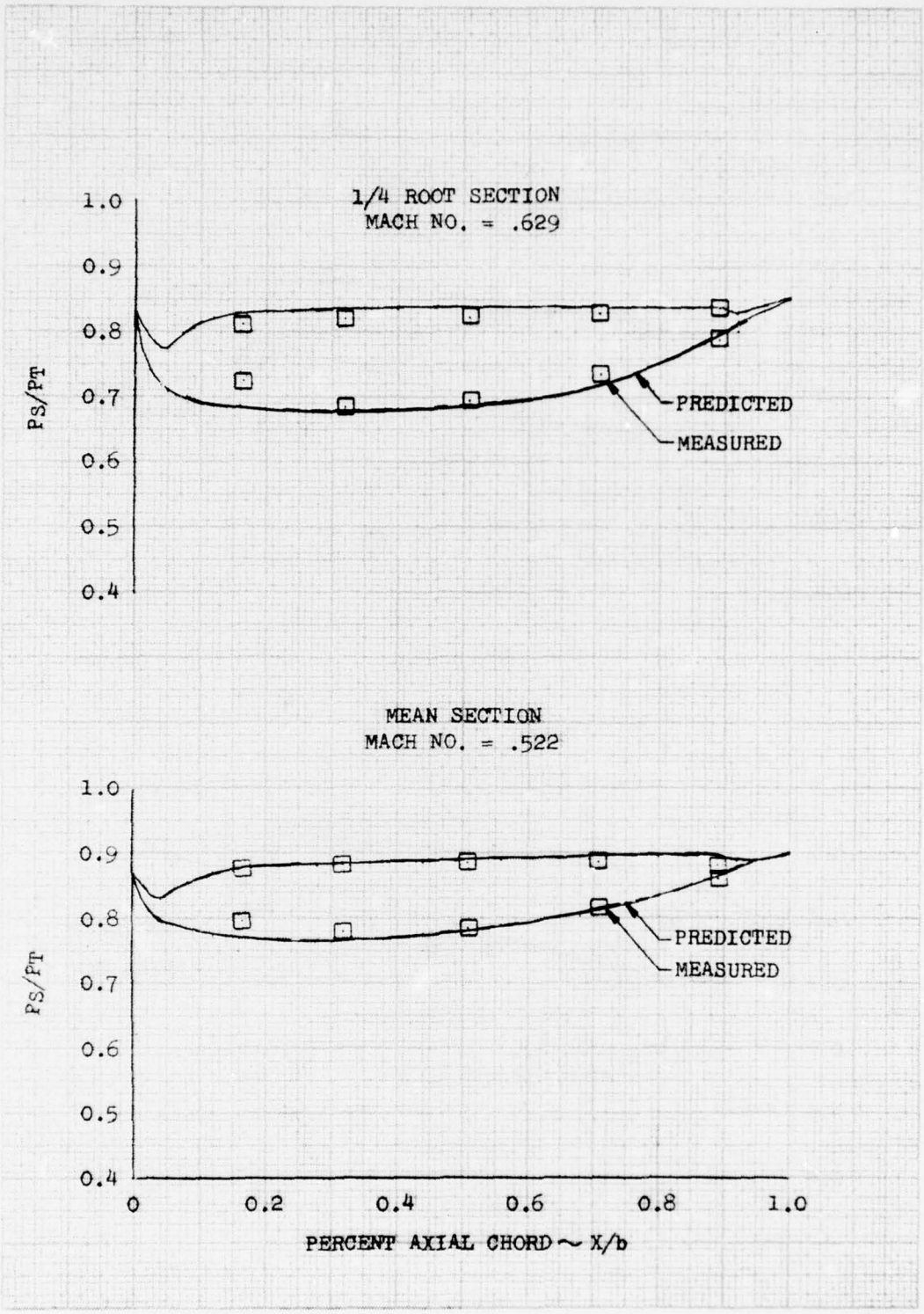


Figure 130. Non-series Predicted and Measured Static Pressure Distributions

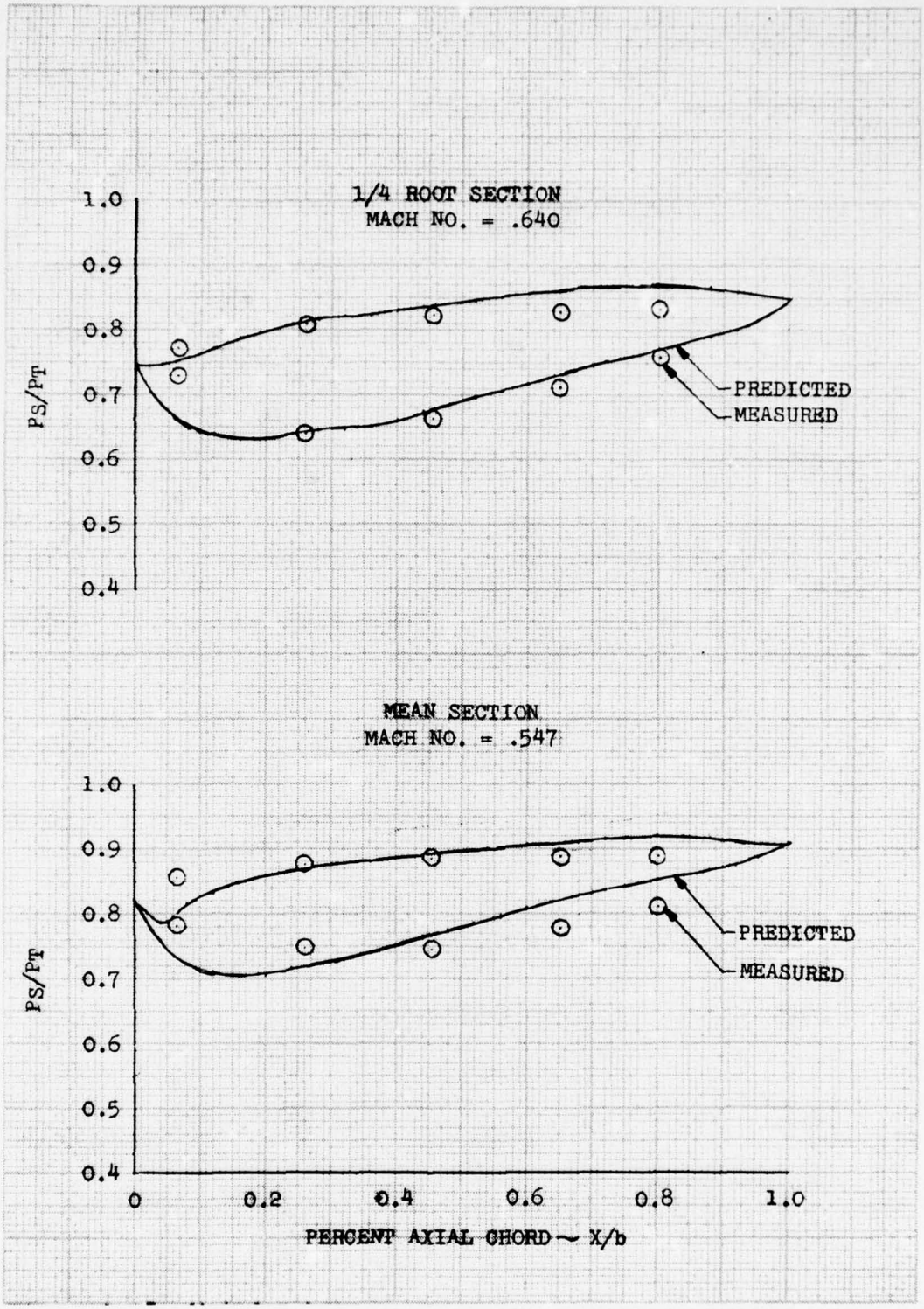


Figure 131. 65-Series EGV Predicted and Measured Static Pressure Distributions

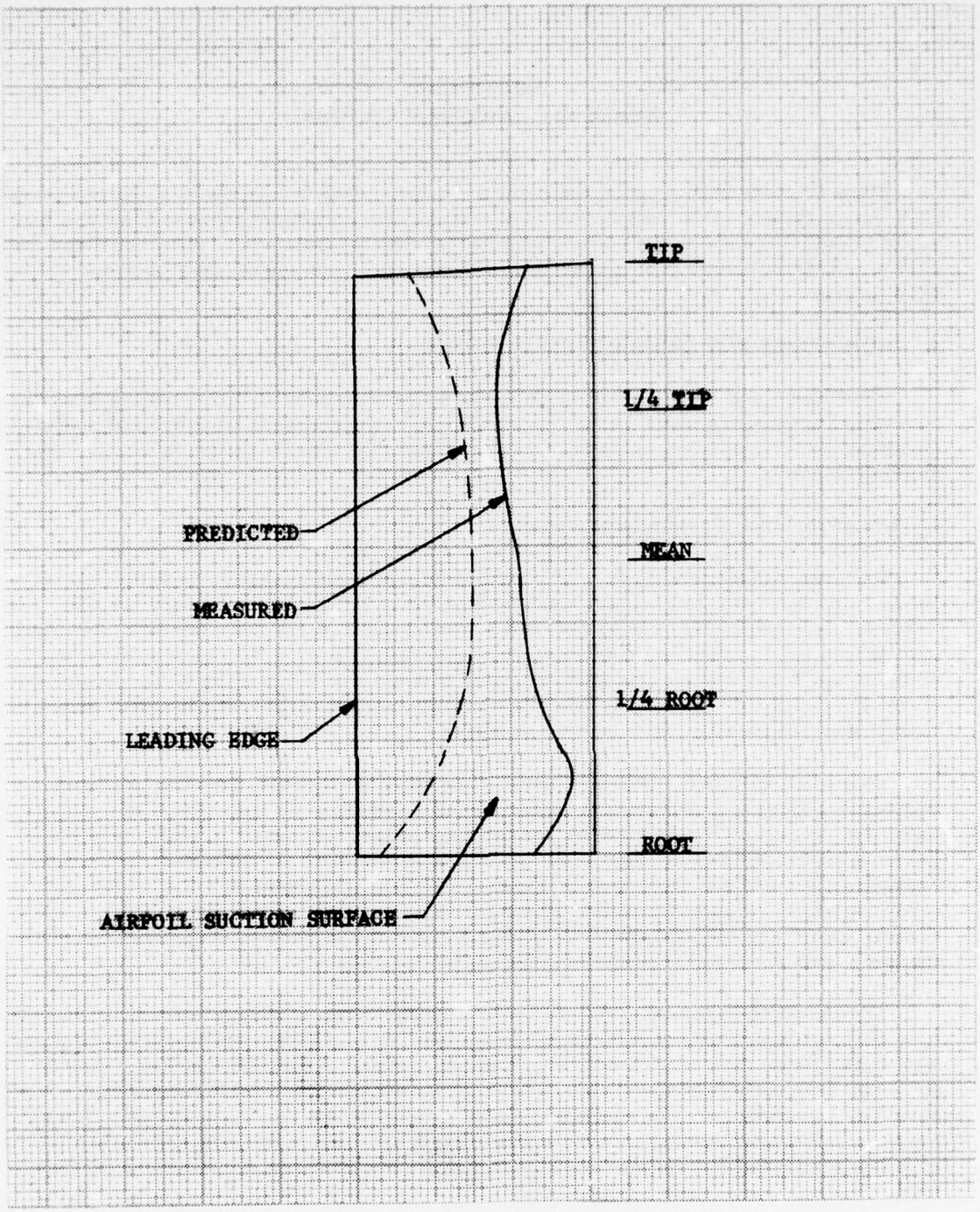


Figure 132. 65-Series EGV Series Airfoil Predicted/Measured Suction Surface Separation Line

SECTION IV
PHASE IV — PROGRAM CRITIQUE

Phase IV of the EGV program was a critique which included: (1) a review of the non-series EGV design system, (2) a design study of the advantages and disadvantages of low and high aspect ratio EGV's, (3) a design study comparing the incidence sensitivity of series and non-series EGV's, and (4) the definition of state-of-the-art technology advancements made as a result of the EGV program.

A. NON-SERIES EGV DESIGN SYSTEM REVIEW

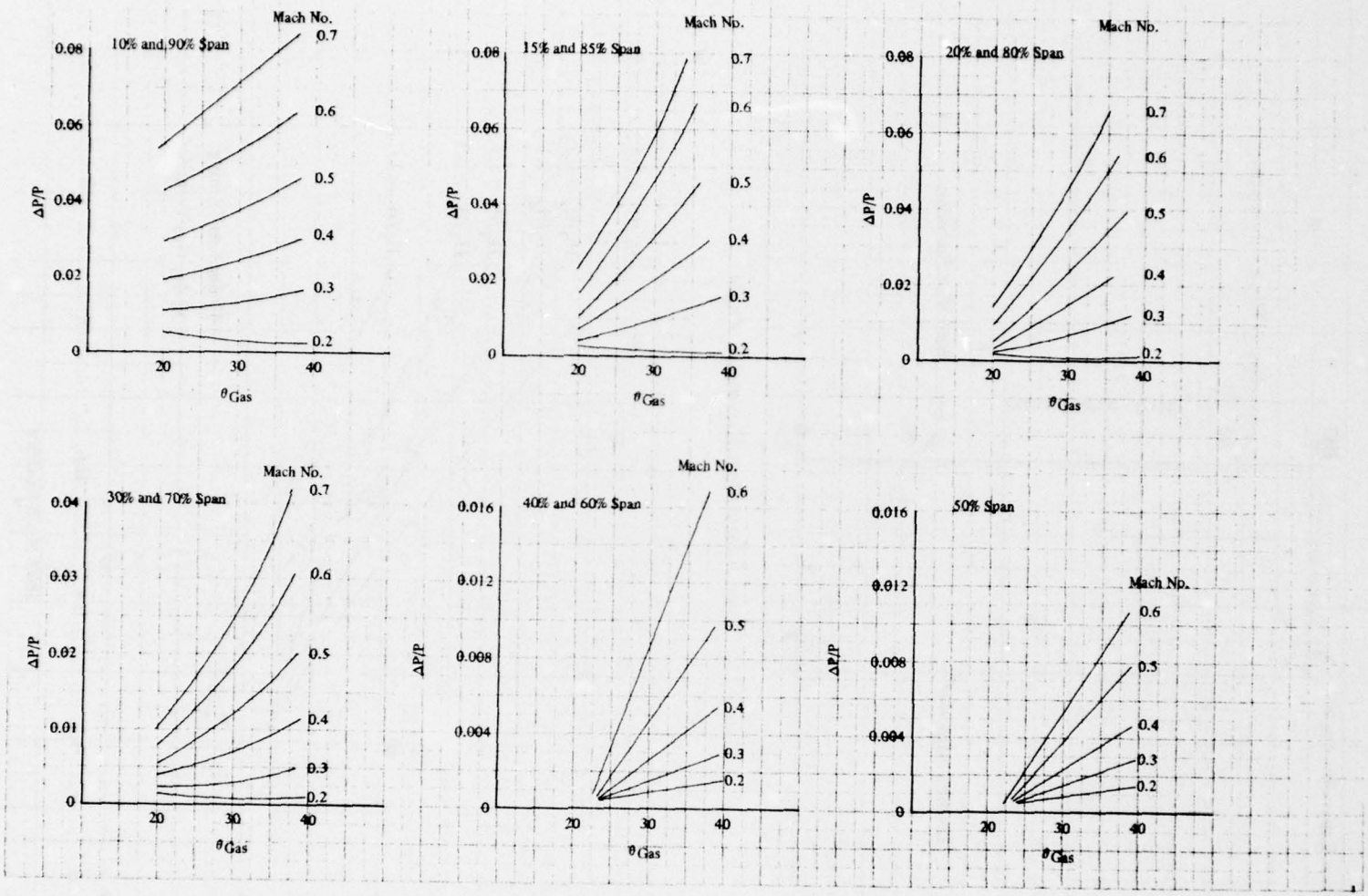
The Phase I and Phase II cascade data was reviewed in order to update and improve the non-series EGV design system. This review consisted of a comparison of measured and predicted (spanwise) total pressure loss and gas turning data to identify possible design system corrections and improvements.

1. Loss Prediction System Improvement

The Phase I 30-deg and 40-deg plane cascade total pressure loss data is presented in Figure 133 as a function of gas turning and Mach number for six different percent span locations. The loss data, presented in this form, can be used to predict spanwise loss distributions for any Mach number and gas turning. The data, however, was obtained only for an aspect ratio of one. In addition, the 30-deg cascade was tested at a gap/chord ratio of 0.77 and the 40-deg cascade was tested at a gap/chord ratio of 0.39. The Phase I 50-deg cascade data is not presented because of incidence variations which affected the test results.

To predict the annular cascade spanwise loss using the loss data presented in Figure 133 requires that gap/chord variations be neglected and a correction for aspect ratio be made. The aspect ratio correction can be made by first defining the spanwise locations where the secondary loss ends. A secondary flow expansion angle is used to define the secondary loss spanwise endpoints. This angle is illustrated in Figure 134. Figure 135 shows that the secondary flow expansion angle, based on measured Phase I data, expands spanwise, increasing with Mach number, gas turning and local area ratio (H_3/H_2). Between the secondary loss spanwise endpoints, the loss is profile loss and is estimated using the 50% span data in Figure 133.

The secondary losses are estimated by defining equivalent span locations which allow the secondary loss data presented in Figure 133 to be used. The equivalent span locations for the high aspect ratio Phase II annular cascade airfoil are illustrated in Figure 136. The high aspect ratio secondary loss spanwise endpoints (by percent span) are aligned parallel to the low aspect ratio secondary loss endpoints. The equivalent spanwise locations are then identified; e.g., the high aspect ratio 20% span location becomes equivalent to the 10% low aspect ratio span location. The high aspect ratio loss is estimated using its equivalent low aspect ratio loss correlation (Figure 133).



FD 121877

Figure 133. Phase I Plane Cascade Spanwise Loss Distributions

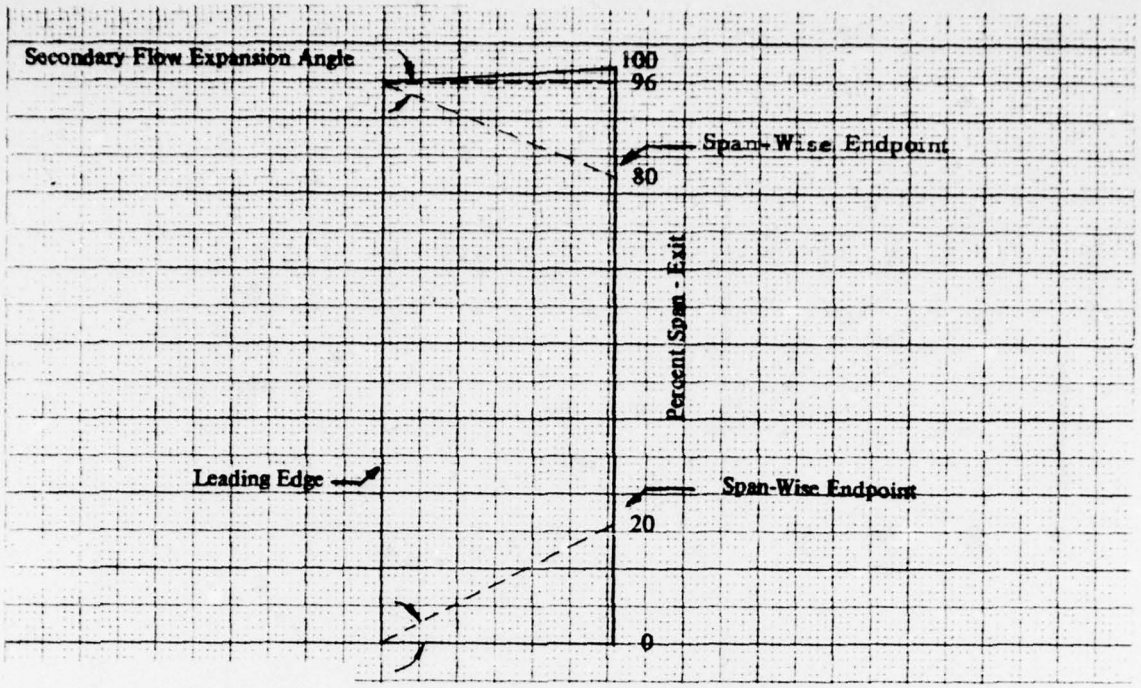


Figure 134. Secondary Flow Expansion Angle

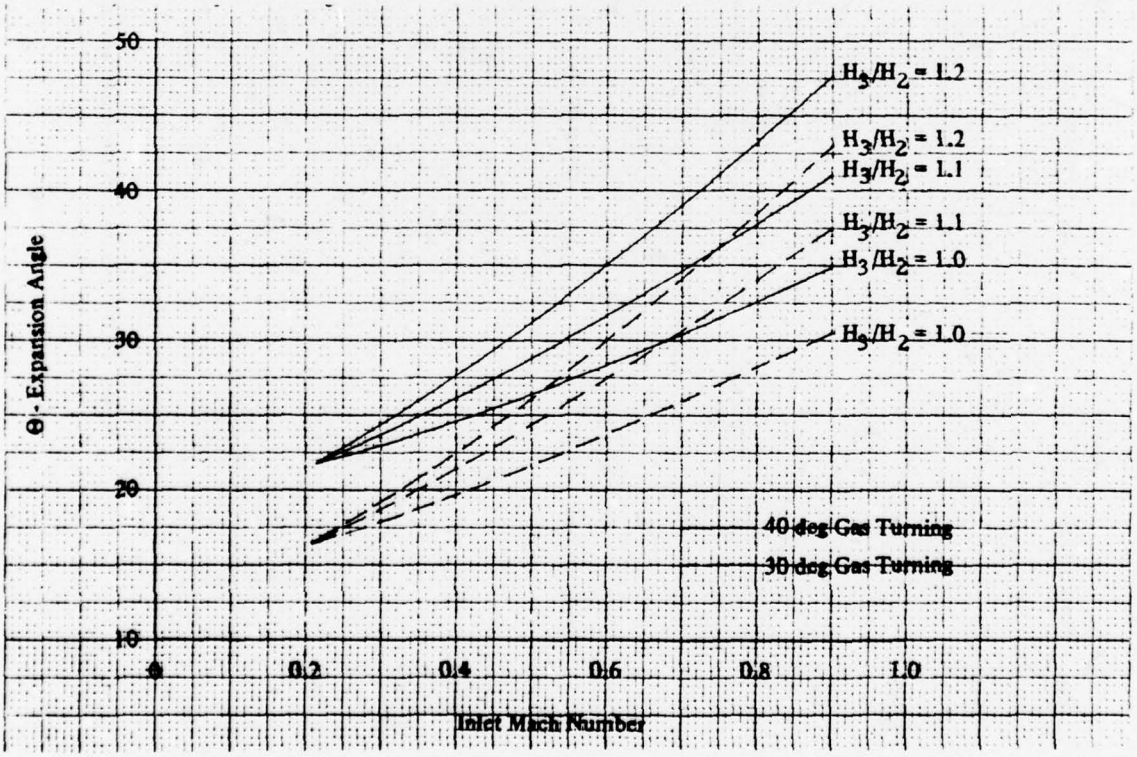


Figure 135. Secondary Flow Expansion Angle vs Inlet Mach Number

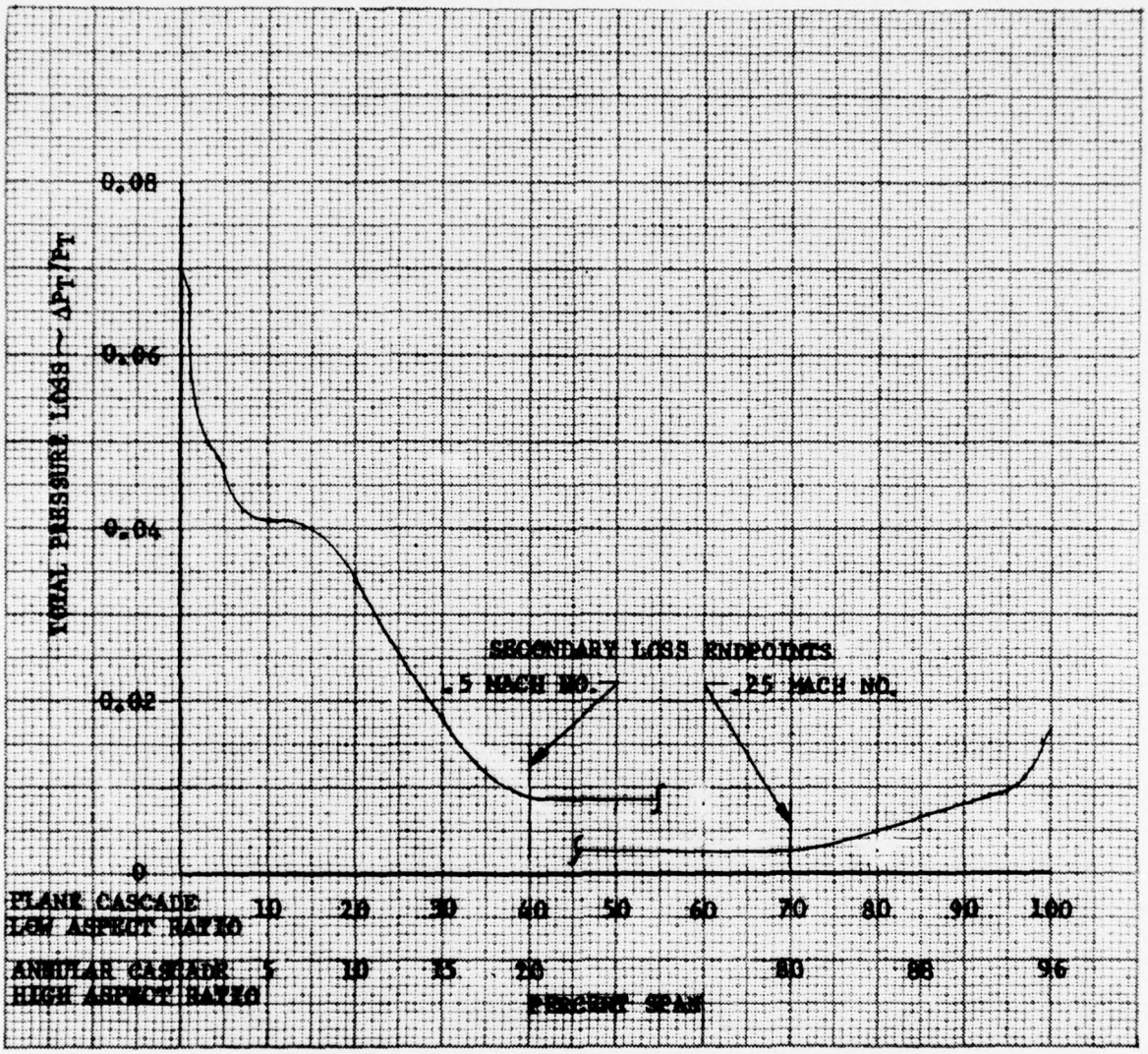


Figure 136. High and Low Aspect Ratio EGV Equivalent Percent Span Locations

Figure 137 presents the measured Phase II annular cascade spanwise loss and the predicted loss obtained using the loss prediction techniques just described. The predicted secondary loss endpoint at the ID wall (20% span) indicates excellent agreement, but the predicted loss level is too high. At the OD wall, the measured secondary loss endpoint is at 65% span compared to a predicted endpoint of 75% span. The predicted loss at the OD wall, like the ID loss prediction, is too high and indicates that the secondary loss prediction is too pessimistic. However, the secondary loss endpoint prediction (secondary flow expansion angle) shows relatively good agreement. Between the ID and OD secondary loss endpoints, the predicted profile loss was both higher and lower than the measured profile loss. Therefore, no conclusions can be made about the accuracy of the profile loss prediction. The annular cascade three-dimensional flow, with varying Mach number and turning distributions, may have resulted in a spanwise redistribution of losses which have not been considered.

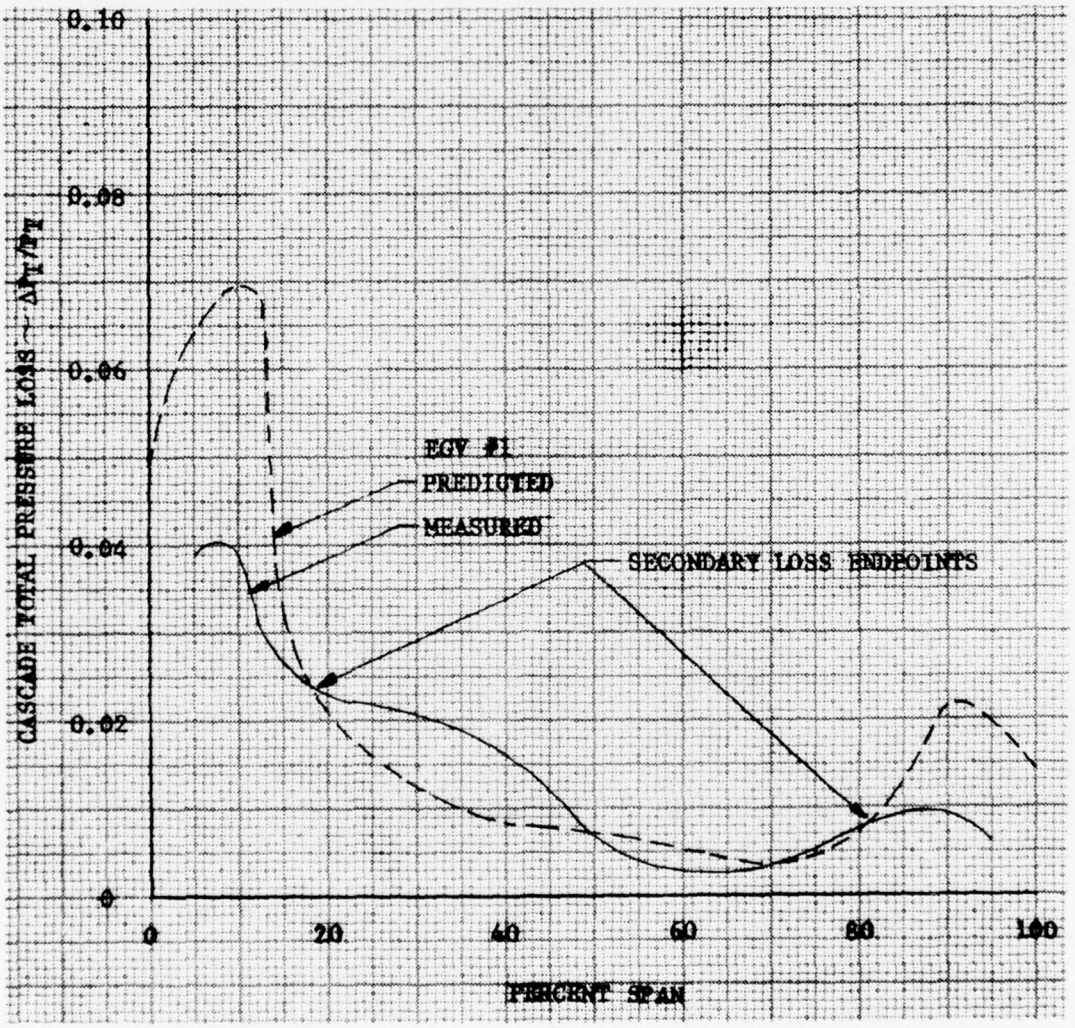


Figure 137. EGV No. 1 Predicted and Measured Spanwise Loss Distributions

2. Deviation System Improvement

In each non-series exit guide vane test conducted, the airfoil gas turning was less than the predicted turning. A summary of the design and measured airfoil deviation (exit gas angle – exit metal angle) is presented in Figure 138. The difference between measured and design deviation increases with increasing inlet Mach number as shown in Figure 139. This trend indicates that the correction (based on Mach number) shown in this figure should be made to the design deviation prediction. The design deviation prediction was based on a version of "Carter's rule" for series airfoils (Reference 7). Carter's rule, based on series airfoil low Mach number test data, correlated measured deviation with airfoil camber and gap/chord ratios. The design deviation prediction is presented in Appendix H.

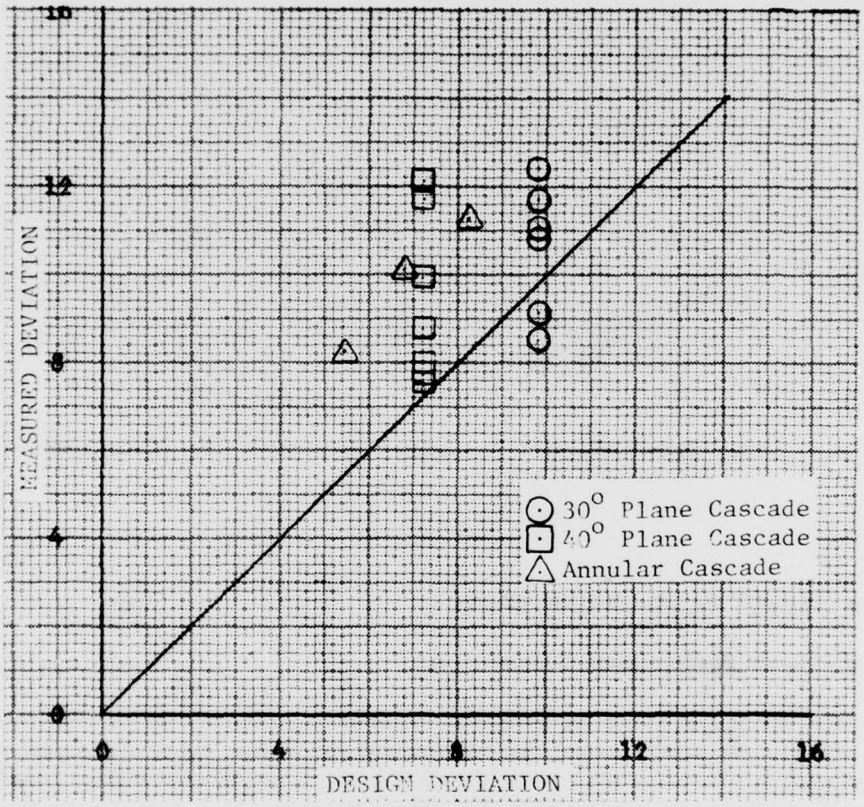


Figure 138. Non-series EGV Measured vs Design Deviation

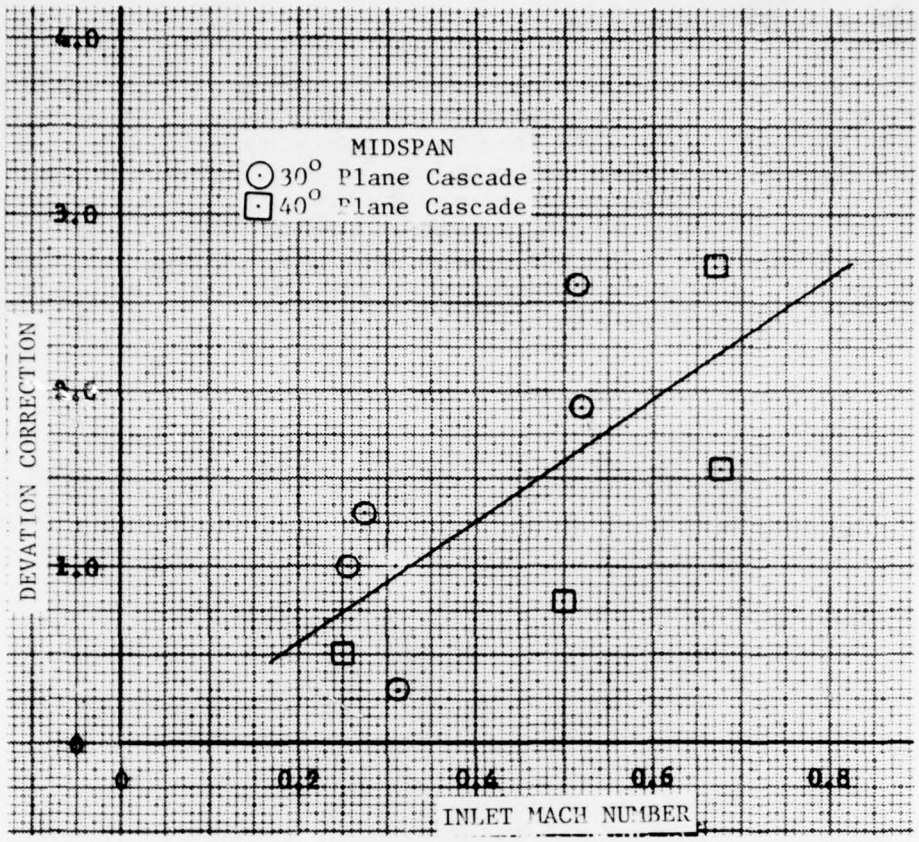


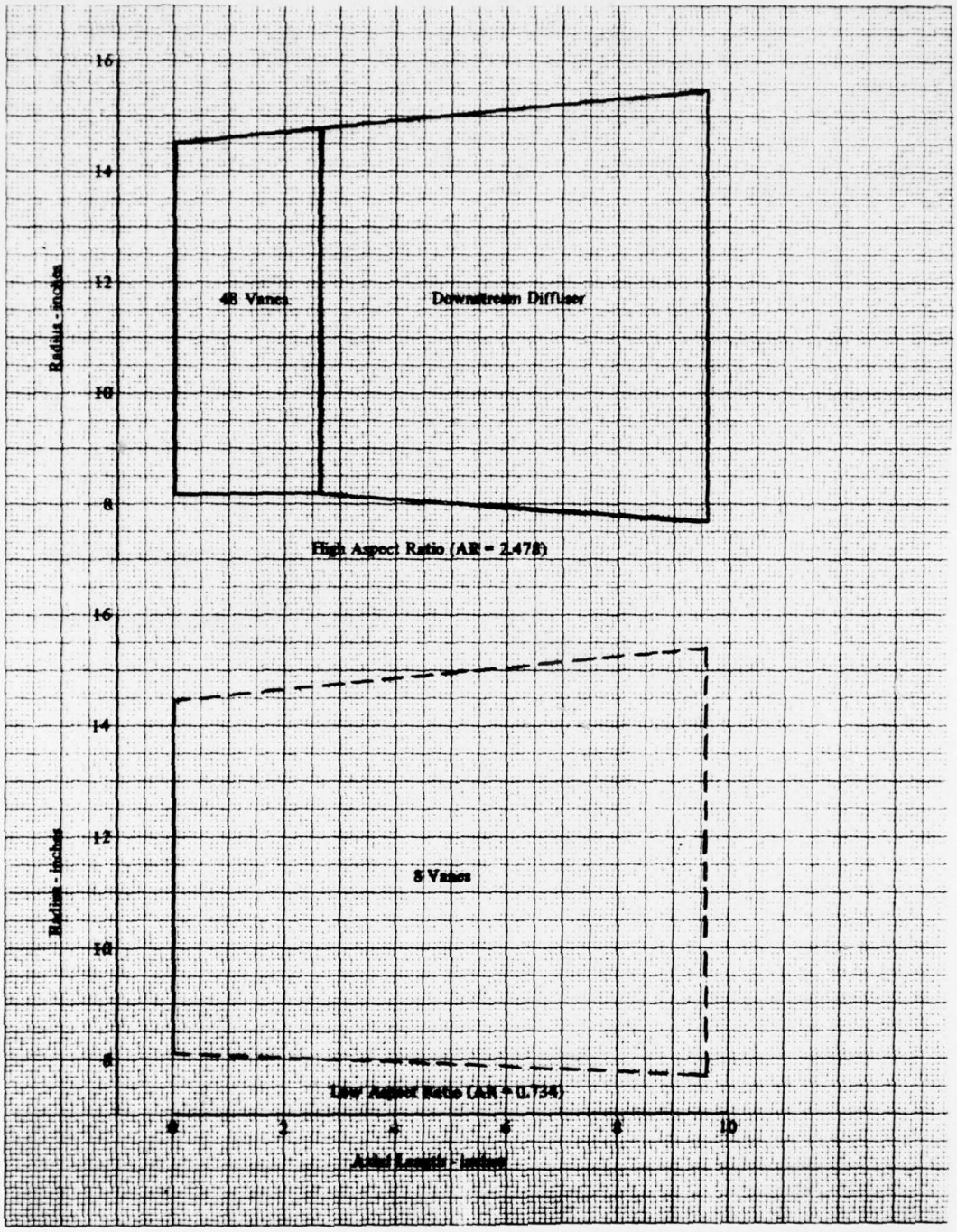
Figure 139. Non-series EGV Deviation Correction vs Inlet Mach Number

B. LOW ASPECT RATIO DESIGN STUDY

1. Aerodynamic Performance Comparison

Turbine exit guide vanes are generally required to accommodate bearing compartment support rods and oil lines. To meet this requirement, thick, long chord, low aspect ratio guide vanes are used. In Phase II of the contract, the EGV design was selected without considering any of the mechanical design requirements. The Phase II design (EGV No. 1) consisted of a high aspect ratio airfoil followed by a downstream diffuser.

As part of the Phase IV critique, a low aspect ratio EGV was designed for the purpose of identifying the advantages and disadvantages of high and low aspect ratio designs. The low aspect ratio EGV is equivalent aerodynamically to the combined high aspect ratio EGV and downstream diffuser system. Schematics of both designs are presented in Figure 140. Normal mechanical design restrictions were imposed on the low aspect ratio design. Non-series design techniques (pressure distribution and boundary layer analysis) were used to design the low aspect ratio airfoil.



FD 121880

Figure 140. High and Low Aspect Ratio EGV Schematics

Figure 141 summarizes, for the high and low aspect ratio designs, the number of airfoils required for varying gap/chord ratios. In Figure 142, the diffusion factor (D_F) and predicted total pressure loss ($\Delta P_T/P_T$) are presented versus mean gap/chord ratio for both airfoil designs. The low aspect ratio EGV total pressure loss is at a minimum for gap/chord ratios between 0.4 and 0.7. The high aspect ratio EGV total pressure loss is at a minimum between the 0.5 and 1.0 gap/chord ratios. In both designs, the total pressure loss increases sharply as the diffusion factor increases above 0.6. The total pressure loss data presented in Figure 142 was obtained from the correlations presented in Reference 7.

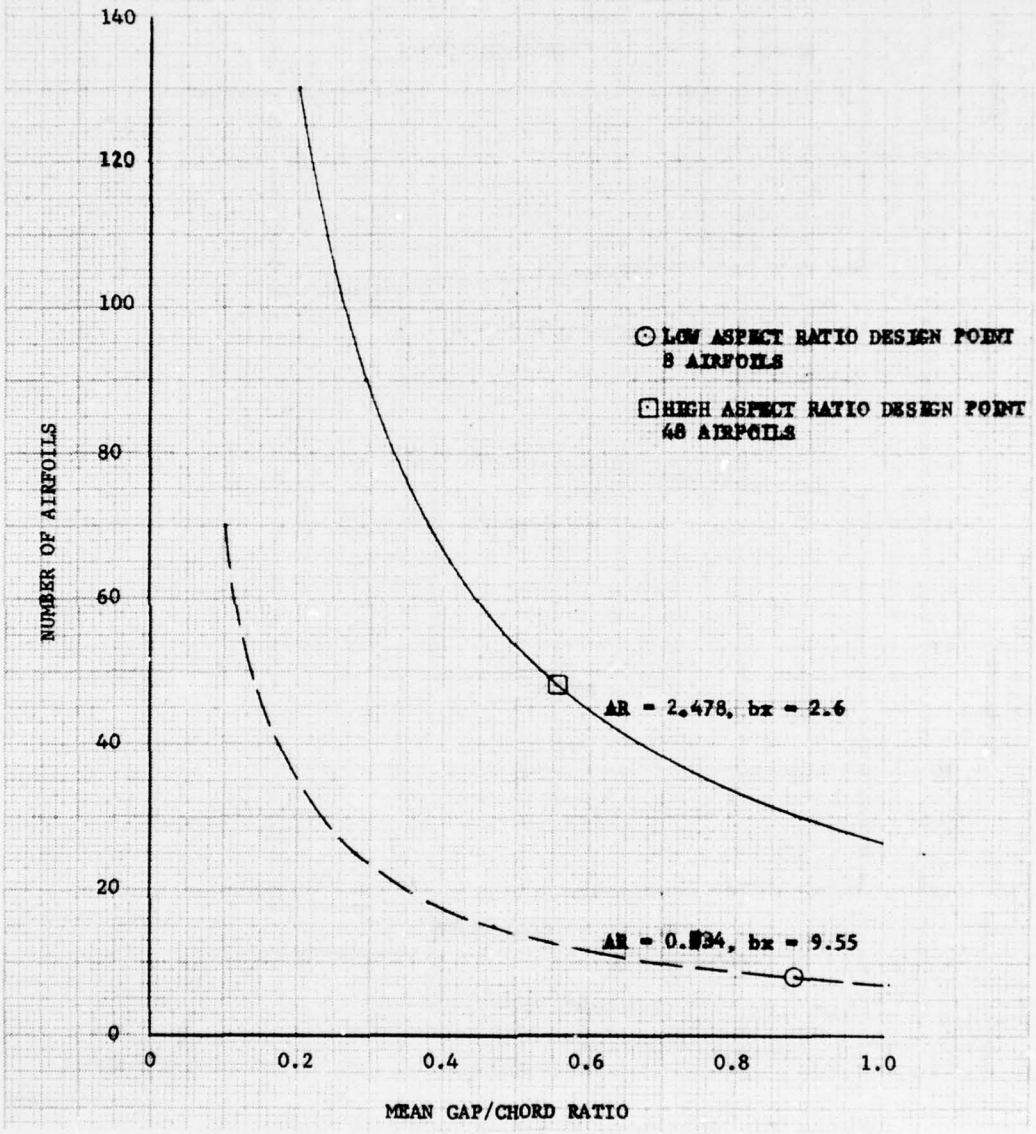


Figure 141. Number of High and Low Aspect Ratio Airfoils vs Mean Gap/Chord Ratio

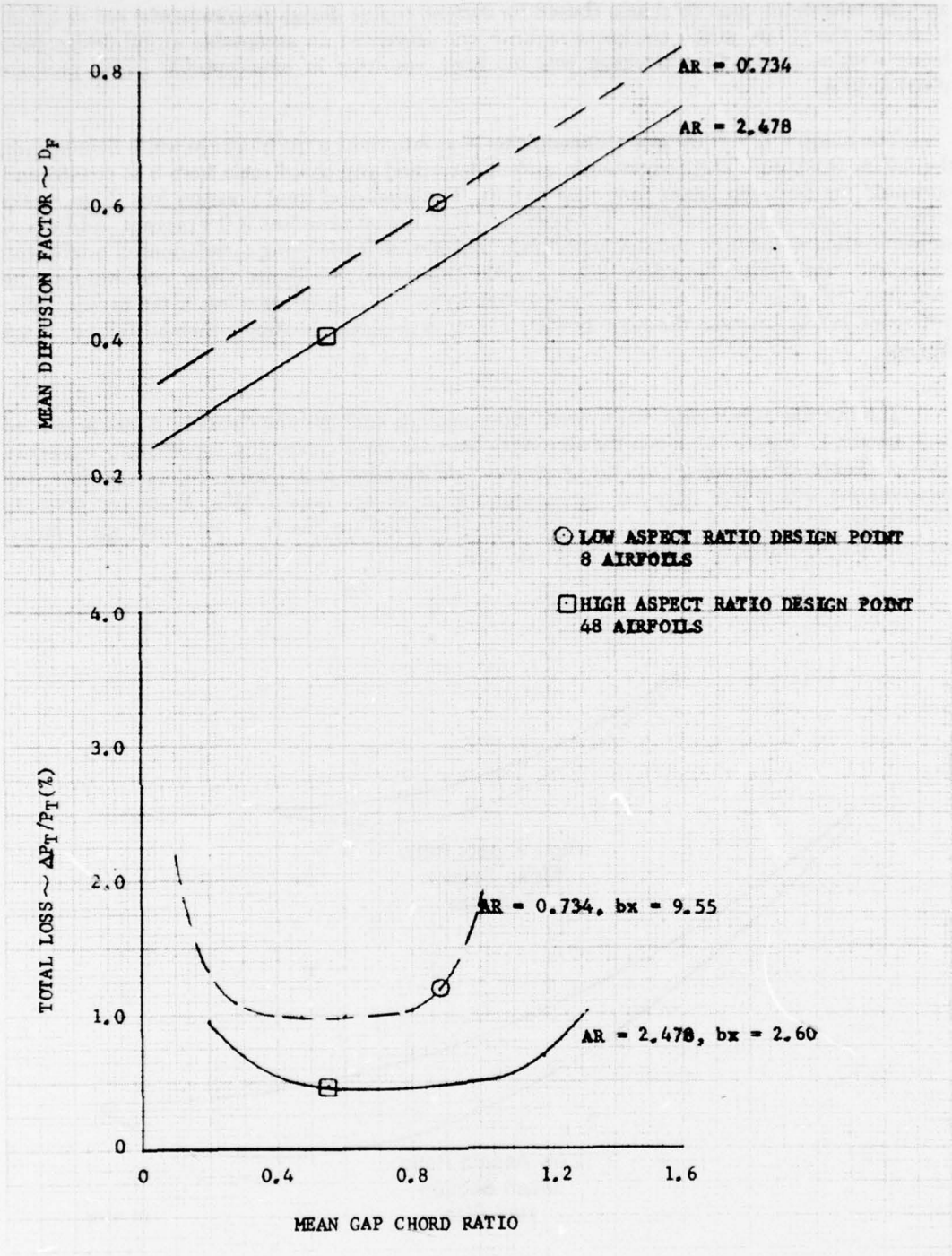


Figure 142. High and Low Aspect Ratio EGV Diffusion Factor and Total Pressure Loss vs Mean Gap/Chord Ratio

The low aspect ratio EGV design study was initiated with the number of airfoils set at 16 and the maximum vane thickness (based on current engine design requirements) set at 1.0 in. However, the 1.0 in. airfoil thickness requirement prevented an acceptable airfoil design from being obtained. The flow blockage was too high, resulting in unacceptable airfoil pressure distributions.

The number of airfoils was reduced from 16 to 8 to reduce the blockage while maintaining the 1.0 in. thickness. This reduction in airfoils increased gap/chord ratio from 0.44 to 0.89 and increased the diffusion factor from 0.46 to 0.61. The predicted total pressure loss (Figure 142) increased from 1.0 to 1.2 percent. The predicted high aspect ratio loss is 0.4 percent. Additional substantiation of the high and low aspect ratio losses were made using correlations of profile and secondary losses with boundary layer growth (Reference 8). Using these correlations, the predicted low aspect ratio loss is 1.4 percent and the high aspect ratio loss is 0.6 percent. The difference in loss between the high and low aspect ratio designs, using either prediction, is 0.8 percent.

The five low aspect ratio EGV airfoil cross-sections and defining coordinates are presented in Appendix G. Figure 143 shows the similarity between the high and low aspect ratio non-series EGV's. Table 28 summarizes the geometric differences and Table 29 summarizes the aerodynamic differences between the low and high aspect ratio EGV's. Predicted pressure distribution and boundary layer skin friction coefficients for the five low aspect ratio airfoil sections are presented in Figures 145 through 149.

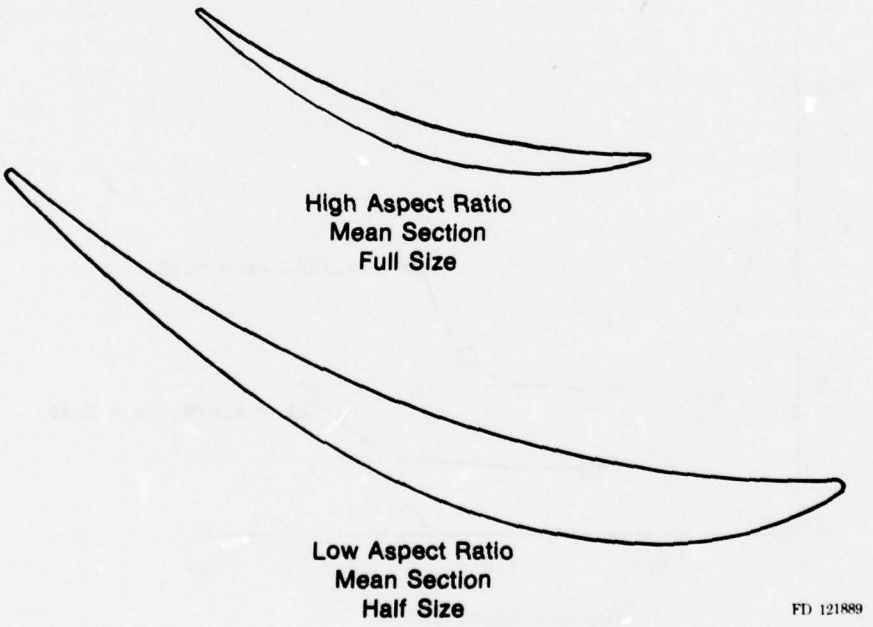


Figure 143. Comparison of High and Low Aspect Ratio EGV Mean Sections

TABLE 28
HIGH AND LOW ASPECT RATIO
AIRFOIL GEOMETRY

Low Aspect Ratio

	β_2^*	β_3^*	θ^*	B	τ/B	t/b	*AR*	*LER*	*TER*	*H/L*	$\Delta\beta_2$	$\Delta\beta_3$
Root	55.68	79.0	45.32	10.099	0.636	0.099		0.045	0.075	−0.350	9.0	36.0
¼ Root	47.18	76.5	56.32	10.158	0.759	0.098		0.045	0.075	−0.370	6.25	30.6
Mean	47.10	75.0	57.89	10.158	0.886	0.098	0.734	0.045	0.075	−0.370	5.0	23.0
¼ Tip	50.55	73.5	55.95	10.076	1.0214	0.099		0.045	0.075	−0.344	5.0	31.0
Tip	58.52	75.0	46.48	9.888	1.172	0.1011		0.045	0.075	−0.275	6.8	37.5

High Aspect Ratio

Root	55.68	83.5	40.82	2.671	0.401	0.069		0.017	0.017	−0.275	5.0	18.0
¼ Root	47.18	82.0	50.82	2.717	0.473	0.068		0.017	0.017	−0.310	3.0	15.0
Mean	47.10	81.5	51.4	2.717	0.552	0.068	2.478	0.017	0.017	−0.310	2.0	14.0
¼ Tip	50.55	81.5	47.95	2.689	0.638	0.069		0.017	0.017	−0.270	3.0	13.5
Tip	58.52	83.2	38.28	2.627	0.735	0.070		0.017	0.017	−0.200	4.0	16.0

TABLE 29
HIGH AND LOW ASPECT RATIO
AERODYNAMIC DESIGN

Low Aspect Ratio

	M_2	M_3	i	$(\Delta P_s/Q)_{min}$	D_F
Root	0.686	0.413	+1.92	0.7791	0.564
¼ Root	0.631	0.387	−1.42	0.7757	0.623
Mean	0.527	0.353	−2.99	0.7074	0.608
¼ Tip	0.442	0.249	−3.45	0.6841	0.745
Tip	0.342	0.132	−2.681	0.8218	0.920
					0.692 Avg

High Aspect Ratio

Root	0.686	0.461	+1.92	0.685	0.429
¼ Root	0.631	0.432	−1.42	0.686	0.461
Mean	0.527	0.403	−2.99	0.586	0.411
¼ Tip	0.442	0.317	−2.45	0.586	0.474
Tip	0.342	0.225	−2.68	0.605	0.547
					0.464 Avg

In designing the low aspect ratio EGV, several interactions were made on each airfoil section until the minimum suction surface diffusion ($\Delta P_s/Q$) was obtained. The final airfoil sections were then analyzed using boundary layer predictions to determine the location of the suction surface separation. As shown in Figures 144 through 148, each section of the low aspect ratio EGV is predicted to separate ahead of the trailing edge point. Table 30 presents a summary of the suction surface static pressure rise obtained prior to predicted separation for both the low and high aspect ratio EGV's. In both cases separation occurs at approximately the 90% chord location. The average low aspect ratio EGV suction surface static pressure rise obtained prior to separation is significantly less (by percentage) than the pressure rise obtained with the high aspect ratio EGV. The low aspect ratio EGV suction surface static pressure at the point of separation (90% chord) is 48% lower than the exit static pressure level (100% chord). This pressure rise, occurring within the last 10% span, may be too severe, increasing the total pressure loss and decreasing the diffusion and gas turning.

TABLE 30
SUCTION SURFACE STATIC PRESSURE RISE

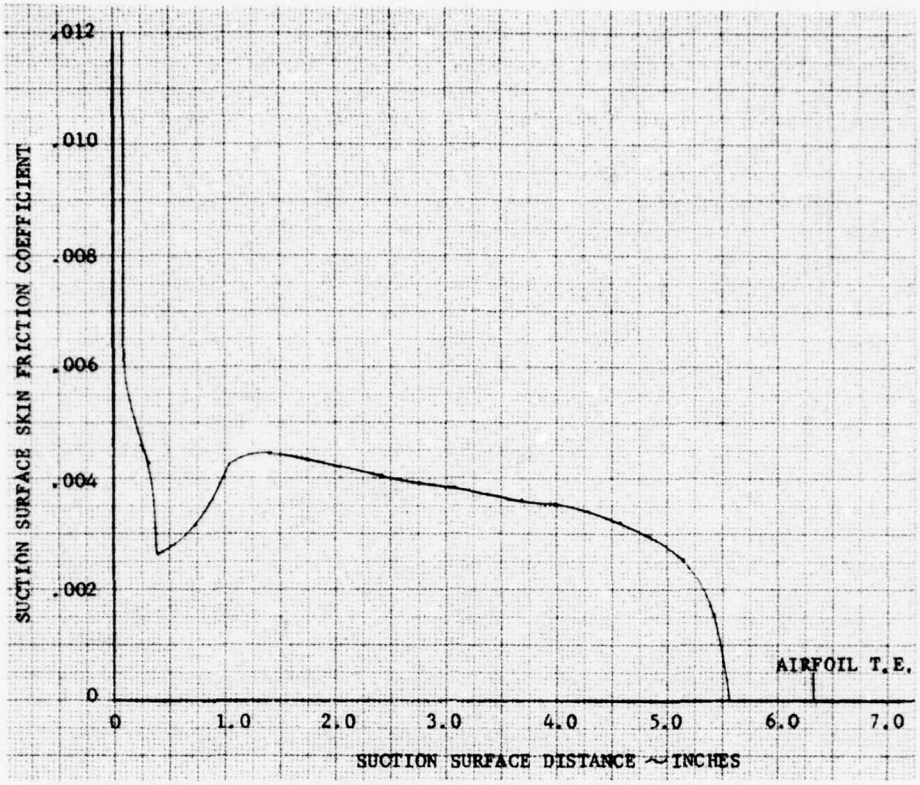
	Suction *Surface Separation Distance*	X/B_x *Weight Axial Chord*	*Separation Point Static Pressure (A)*	*Suction Surface Min. Static Pressure (B)*	*Exit Static Pressure (C)*	*Percent Pressure Rise (A−B/C−B)*	
Low Aspect Ratio							
Root	5.423	0.85	0.7318	0.6585	0.9360	26.4	
¼ Root	5.324	0.80	0.7751	0.6925	0.9380	33.6	
Mean	5.900	0.90	0.8757	0.7741	0.9430	60.1	
¼ Tip	5.775	0.90	0.9202	0.8501	0.9608	63.3	
Tip	5.553	0.90	0.9713	0.9141	0.9880	77.4	
						52.16	Avg
High Aspect Ratio							
Root	1.502	0.90	0.7932	0.6562	0.8626	66.4	
¼ Root	1.542	0.90	0.8380	0.7020	0.8815	75.8	
Mean	1.619	0.95	0.8792	0.7762	0.8957	86.2	
¼ Tip	1.639	0.98	0.9251	0.8419	0.9290	95.5	
Tip	1.628	1.00	0.9620	0.9071	0.9620	100.0	
						84.78	Avg

2. Weight Comparison

In order to estimate the weight differences between the high and low aspect ratio EGV designs, it was necessary to make several assumptions. The F100 engine was selected as the representative design baseline and to meet typical rear bearing compartment mechanical design requirements, four downstream struts were added to the high aspect ratio EGV design. The resulting estimated weights were 17lb for the low aspect ratio design and 41lb for the high aspect ratio design.

3. Cost Comparison

Cost estimates, again using the F100 engine as a baseline, were made for both EGV designs. Compared with the F100 engine, the two designs are each expected to cost an additional $3,000 per engine. This assumes that the 48 vane high aspect ratio EGV can be cast as a single piece; otherwise an additional $1,500 per engine would be required. The low aspect ratio design results in a cost increase when compared with the F100 engine because of increased chords and exhaust case lengths.



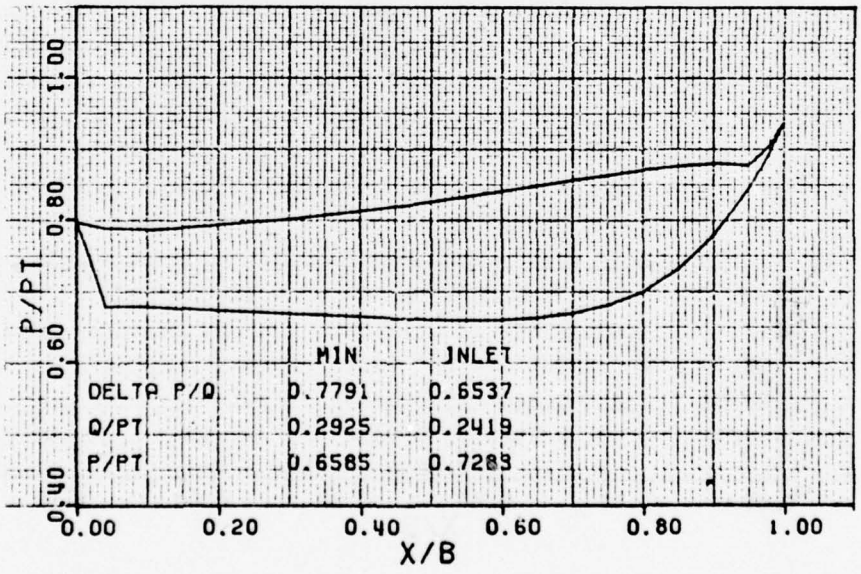
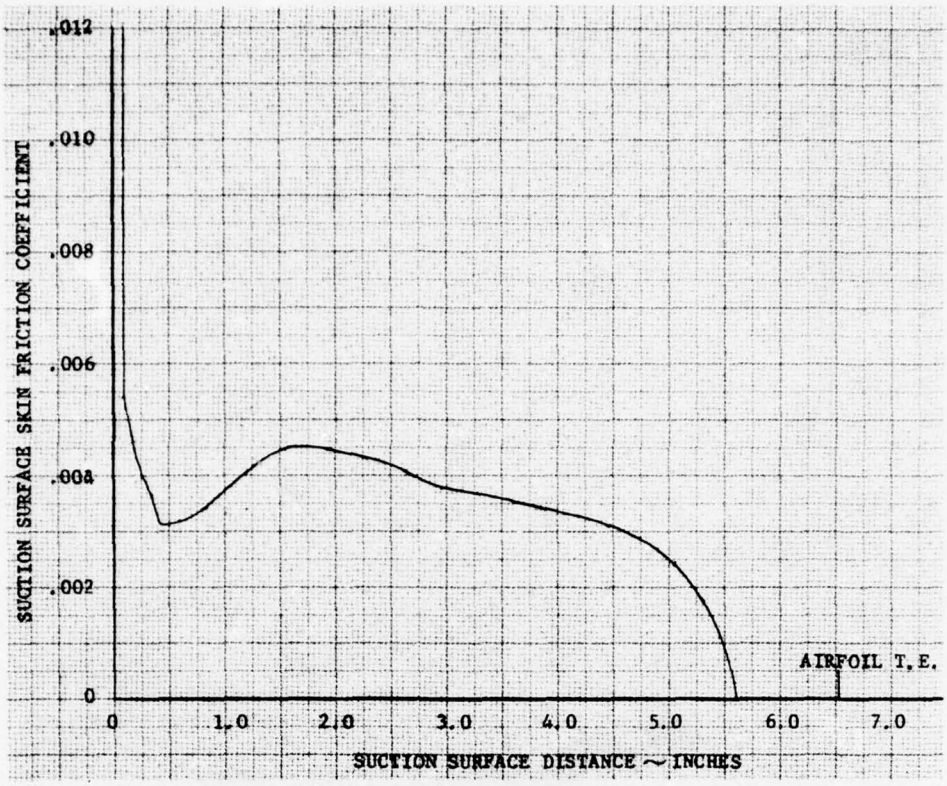


Figure 144. Low Aspect Ratio EGV Root Section Predicted Pressure Distribution and Skin Friction Coefficient



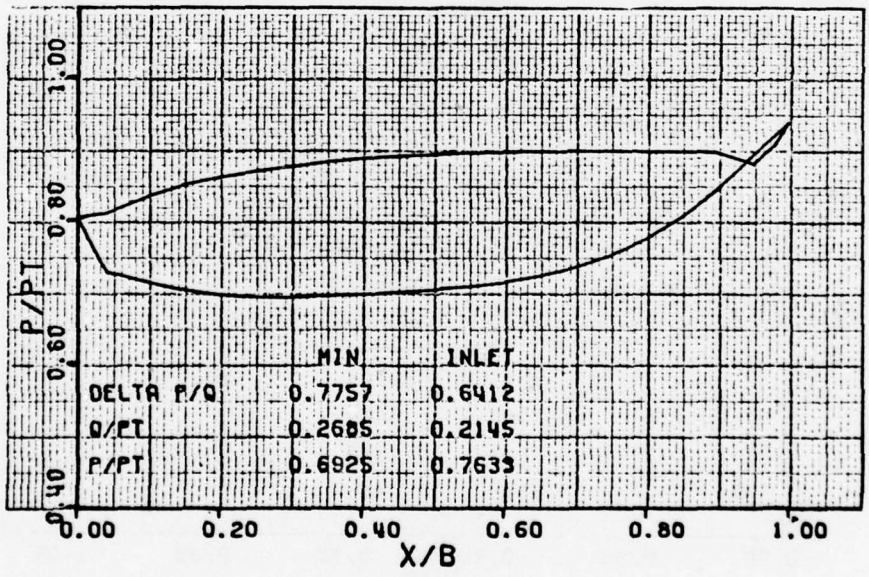
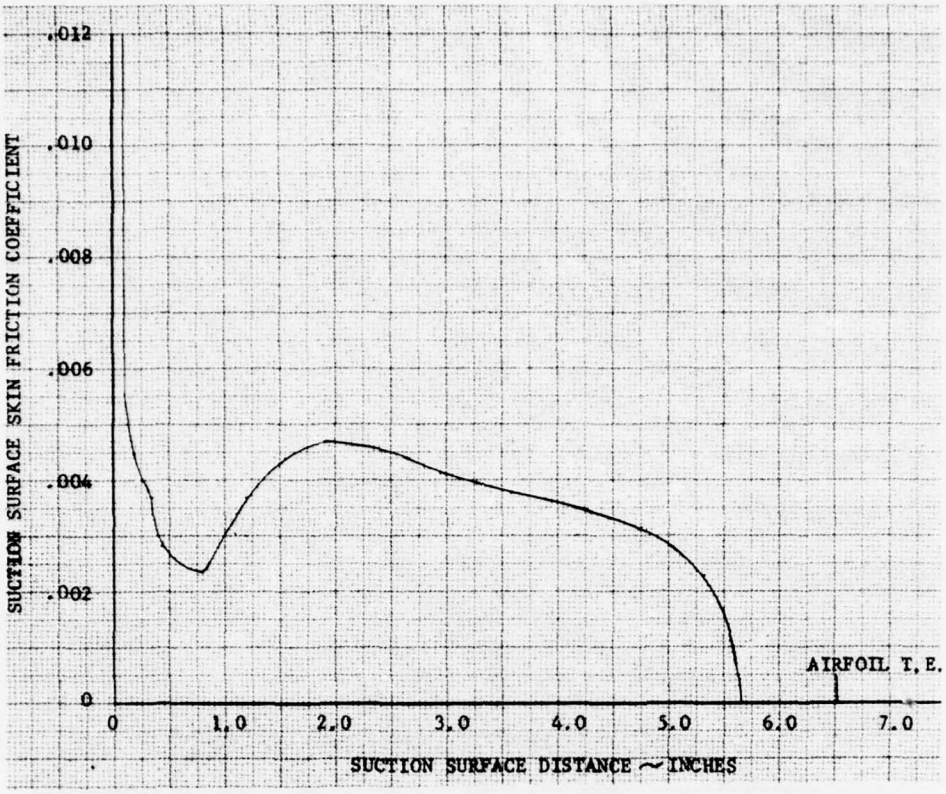


Figure 145. Low Aspect Ratio EGV ¼ Root Section Predicted Distribution and Skin Friction Coefficient



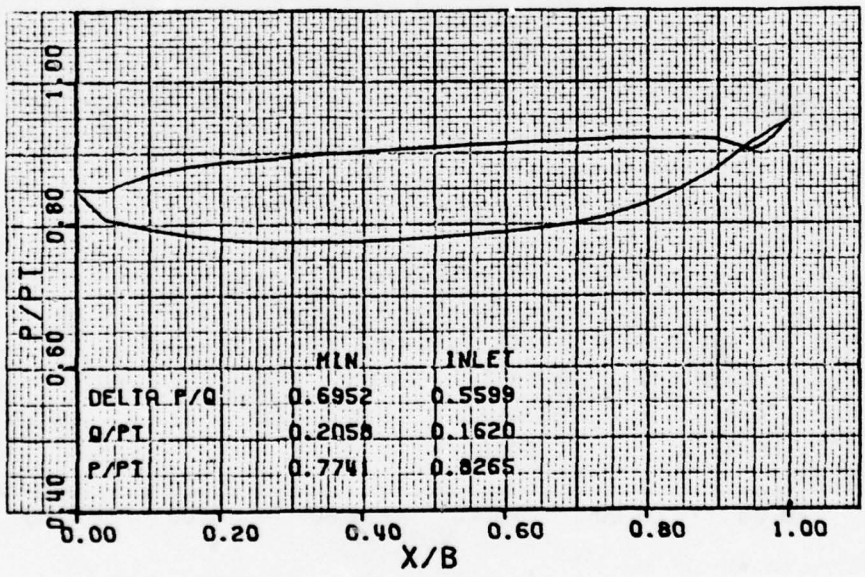
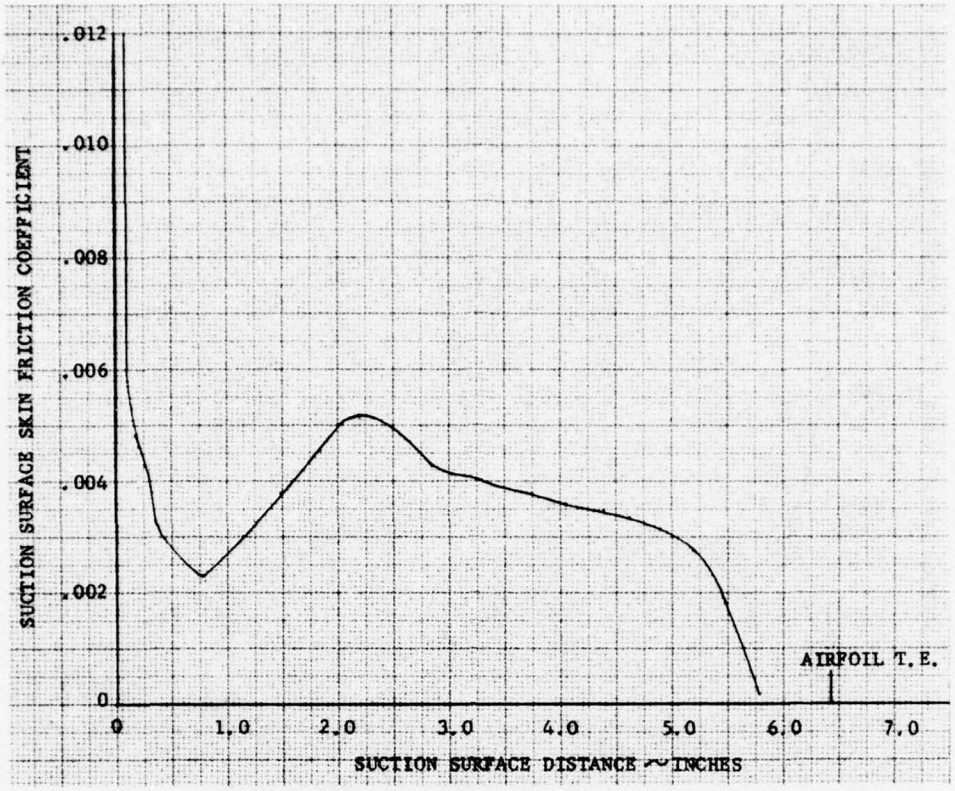


Figure 146. Low Aspect Ratio EGV Mean Section Predicted Distribution and Skin Friction Coefficient



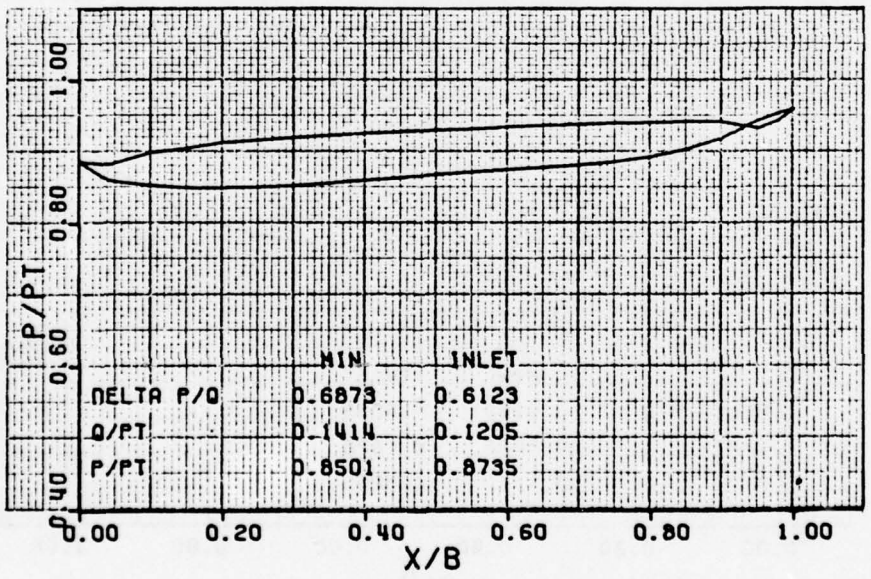
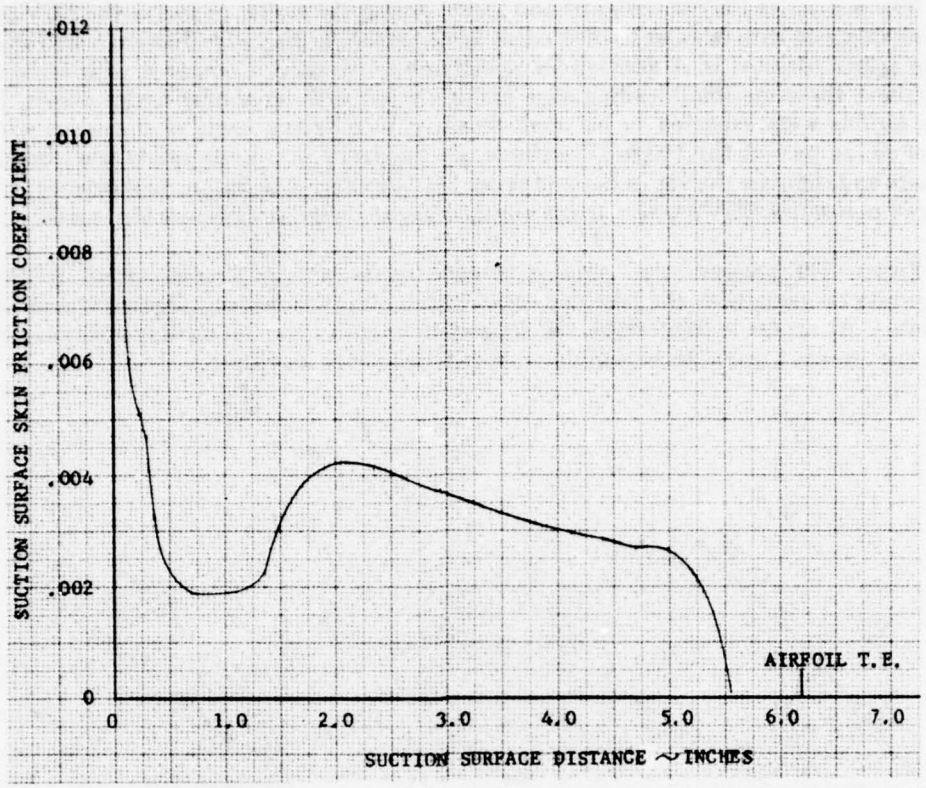


Figure 147. Low Aspect Ratio EGV ¼ Tip Section Predicted Pressure Distribution and Skin Friction Coefficient



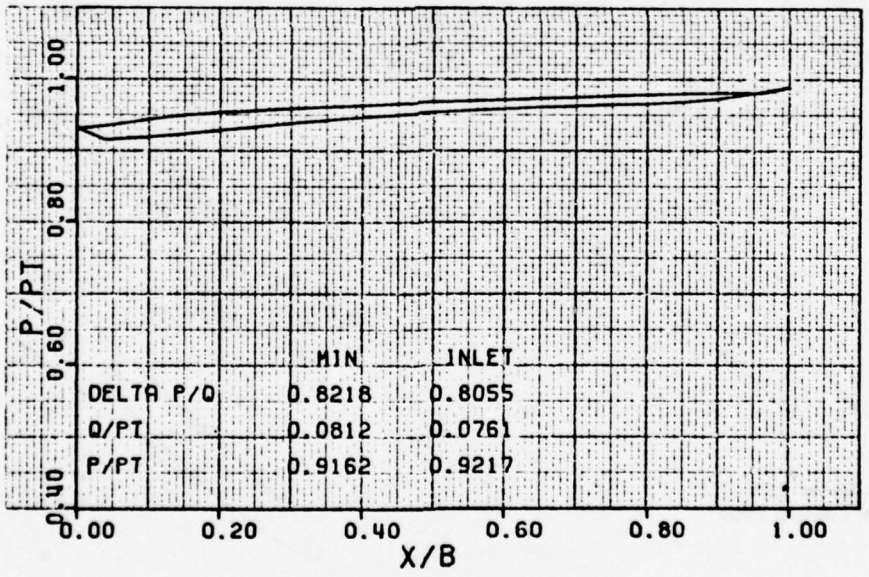


Figure 148. Low Aspect Ratio EGV Tip Section Predicted Pressure Distribution and Skin Friction Coefficient

C. SERIES AND NON-SERIES EGV INCIDENCE SENSITIVITY STUDY

The non-series EGV's, designed and tested during the earlier phases of the EGV program, were all designed with circular leading edges having small leading edge diameters and small inlet wedge angles (defined in Abbreviations and Symbols Section). Compared with series airfoils, which have the same small leading edge diameters but with large inlet wedge angles, the non-series airfoils were expected to be more sensitive to inlet gas angle or incidence variations. Therefore, as part of the Phase IV critique, an incidence sensitivity study was conducted to evaluate and compare the non-series and series EGV designs. In addition, an incidence sensitivity study of non-series EGV's with various eliptical leading edge designs was also made.

Figure 149 presents the annular cascade series and non-series airfoil leading edge configurations along with the four non-series airfoil elliptical leading edge designs which were evaluated. As shown in Figure 149, the series airfoil, with its small leading edge diameter and large inlet wedge angle, can be simulated very closely with an ellipse.

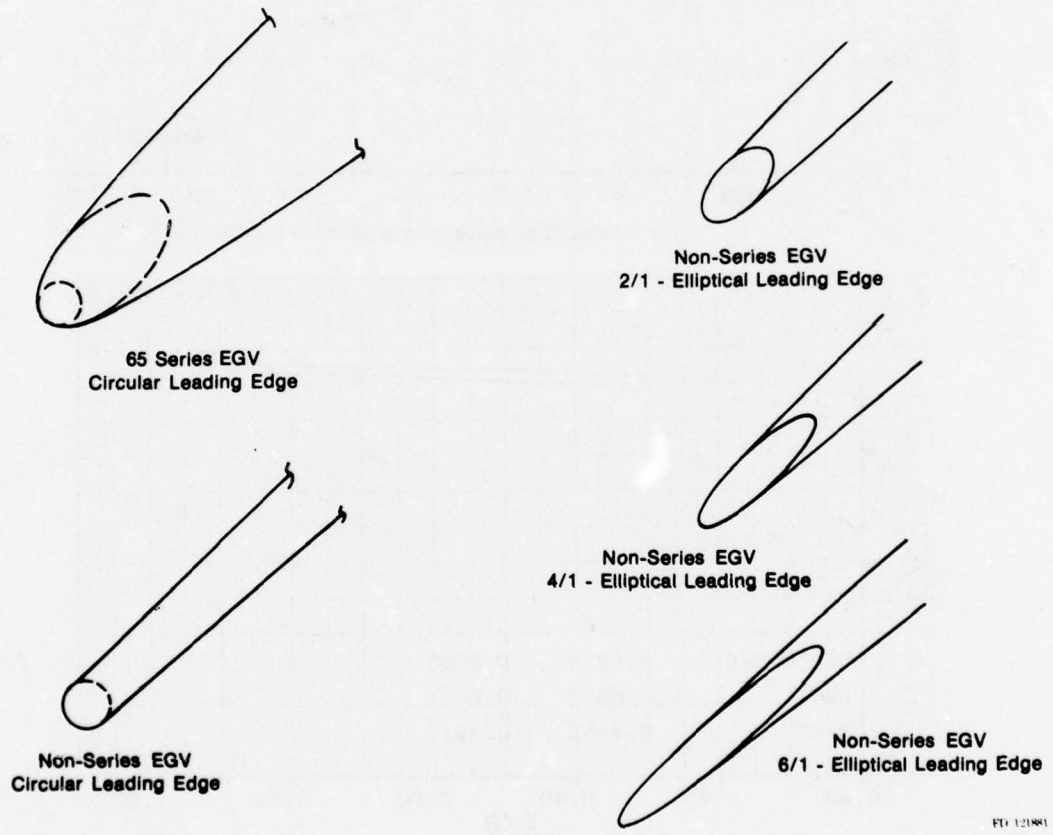


Figure 149. 65-Series and Non-series EGV Leading Edge Configurations

Presented in Figures 150 through 154 are the predicted pressure distributions for the series airfoil operating at incidence levels of −4.0, −2.0, 0.0, +2.0, and +4.0 deg, respectively. The pressure distributions were predicted using a P&WA compressible flow program with a leading edge region reanalysis calculation. In Figures 150 and 154, for incidence levels of −4.0 deg and +4.0 deg, the overspeed or minimum P_S/P_T is at or near that for sonic flow (P_S/P_T 0.528). In the incidence range comparison presented later, the overspeed limitng value was arbitrarily set at $(P_S/P_T)_{min} = 0.528$, slightly less than the sonic value.

Figures 155 through 158 present the predicted pressure distributions for the non-series airfoil with a circular leading edge at incidence levels of −4.0, −2.0, 0.0, and +2.0 deg. The +4.0 deg incidence level was also evaluated but the prediction did not converge properly for this case. The leading edge overspeed exceeds the sonic values at all incidence levels except for −2.0 deg of incidence (Figure 156). The overspeed predicted for 0.0 deg of incidence (Figure 157 is caused by displacement of the stagnation point away from the nose point towards the pressure surface. Stagnation point displacement is caused by cross-channel effects which influence the inlet flow field.

The nonseries EGV's with elliptical leading edges were evaluated at the design point incidence of −1.42 deg. Predicted leading edge region pressure distributions are presented in Figure 159. The 6/1 (major axis/minor axis) elliptical design has the best pressure distribution; however, as shown in Figure 149, this design results in a very sharp or pointed leading-edge which would be difficult to manufacture. The 2/1 elliptical design, when compared with the circular design, indicates only a slight reduction in the pressure surface overspeed and an increased overspeed on the suction surface. The 4/1 elliptical design reduces the pressure surface overspeed but does not alter the suction surface overspeed. The 4/1 elliptical design appears to be the best nonseries EGV design, considering the improved performance offered relative to the circular design and the fact that fabrication would be somewhat easier compared to the 6/1 design.

The 4/1 elliptical design was evaluated at incidence levels of −6.0, −5.0, −4.0, −2.0, 0.0, +2.0 and +4.0 deg. Figures 160 through 166, respectively, present the predicted pressure distributions.

Presented in Table 31 is a summary of the predicted minimum pressure levels, (P_S/P_T) min, for the series and non-series incidence levels evaluated. Both the circular and 4/1 elliptical non-series design predictions are presented.

TABLE 31
INCIDENCE SENSITIVITY STUDY MINIMUM LEADING EDGE P_S/P_T

Incidence (deg)	−6	−5	−4	−2	0	+2	+4
Series EGV	-	-	0.5078	0.6348	0.6566	0.6350	0.5602
Non-series EGV Circular LE	-	-	0.4772	0.5736	0.4705	0.4251	-
Non-series EGV 4/1 Elliptical LE	0.4027	0.4591	0.5832	0.7026	0.5565	0.3901	0.3140

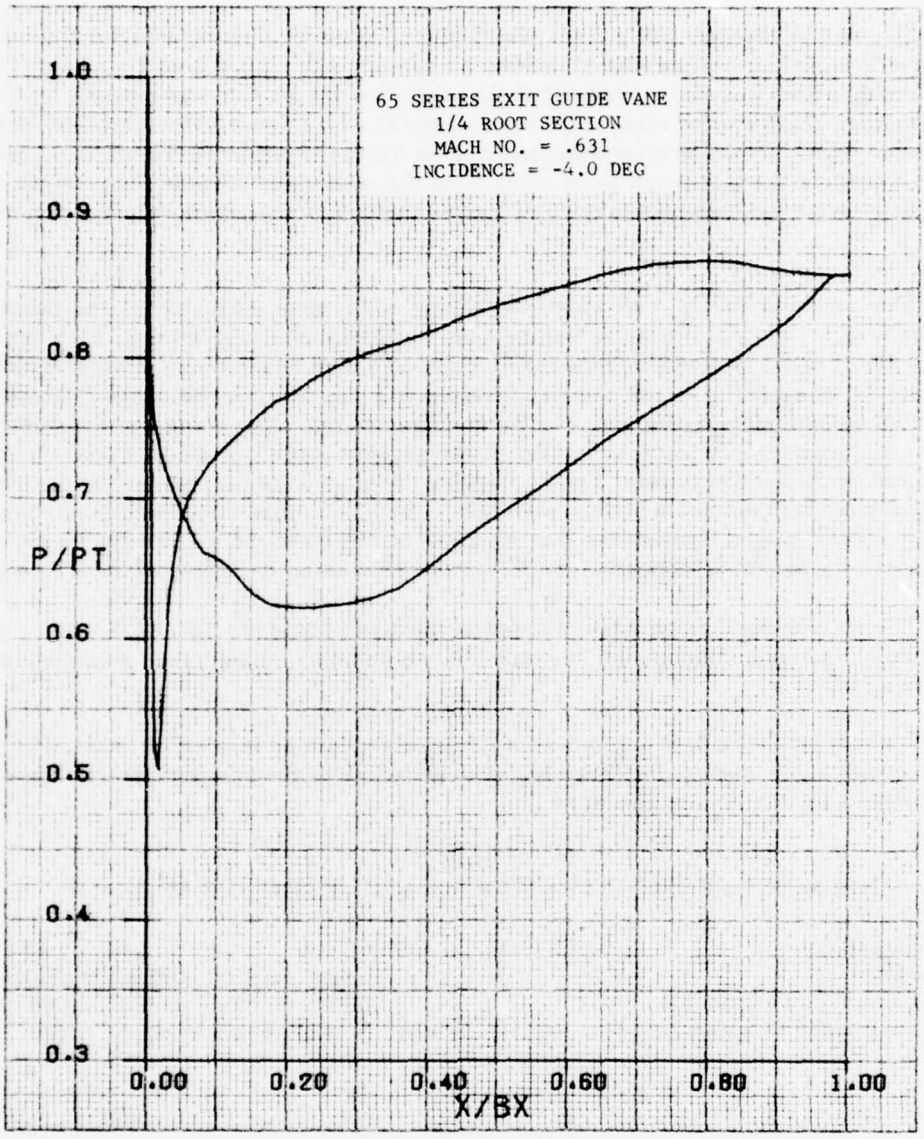


Figure 150. 65-Series EGV ¼ Root Section Predicted Pressure Distribution at −4.0 deg Incidence

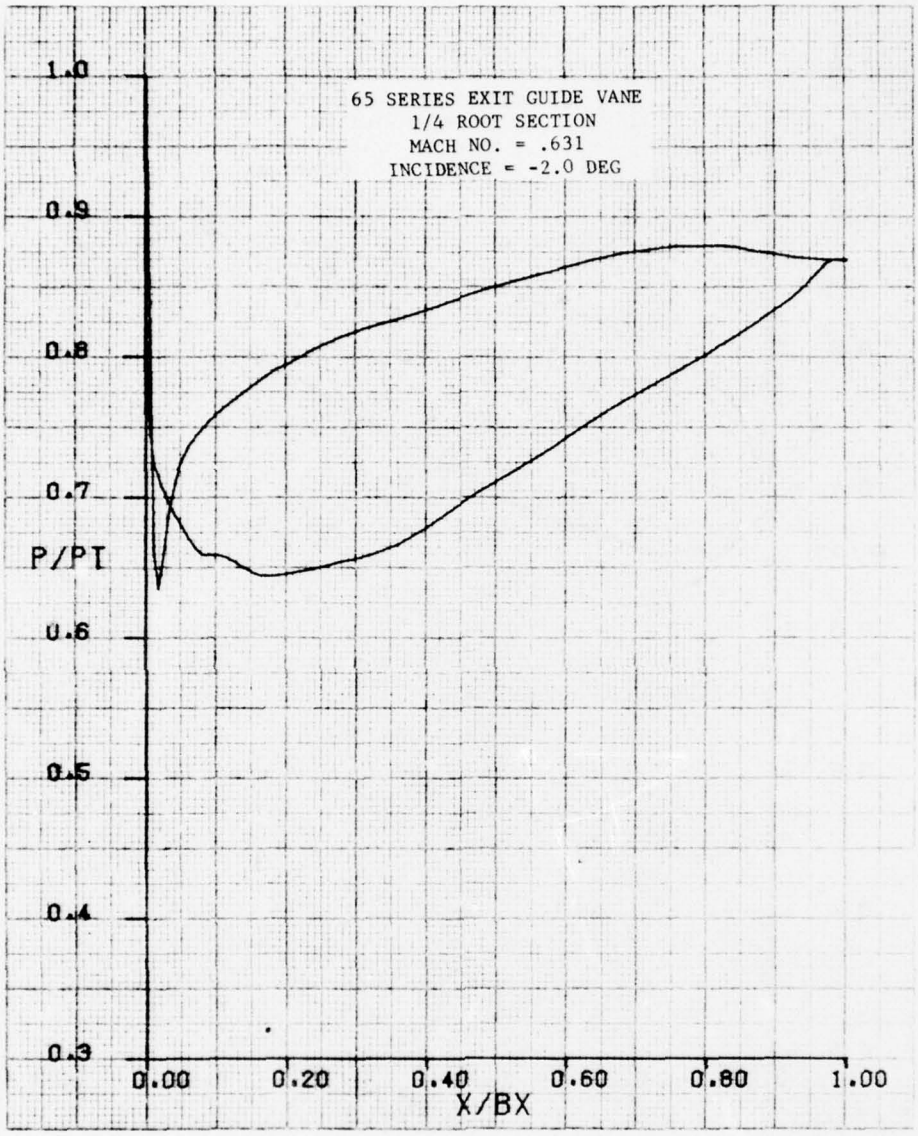


Figure 151. 65-Series EGV ¼ Root Section Predicted Pressure Distribution at −2.0 deg Incidence

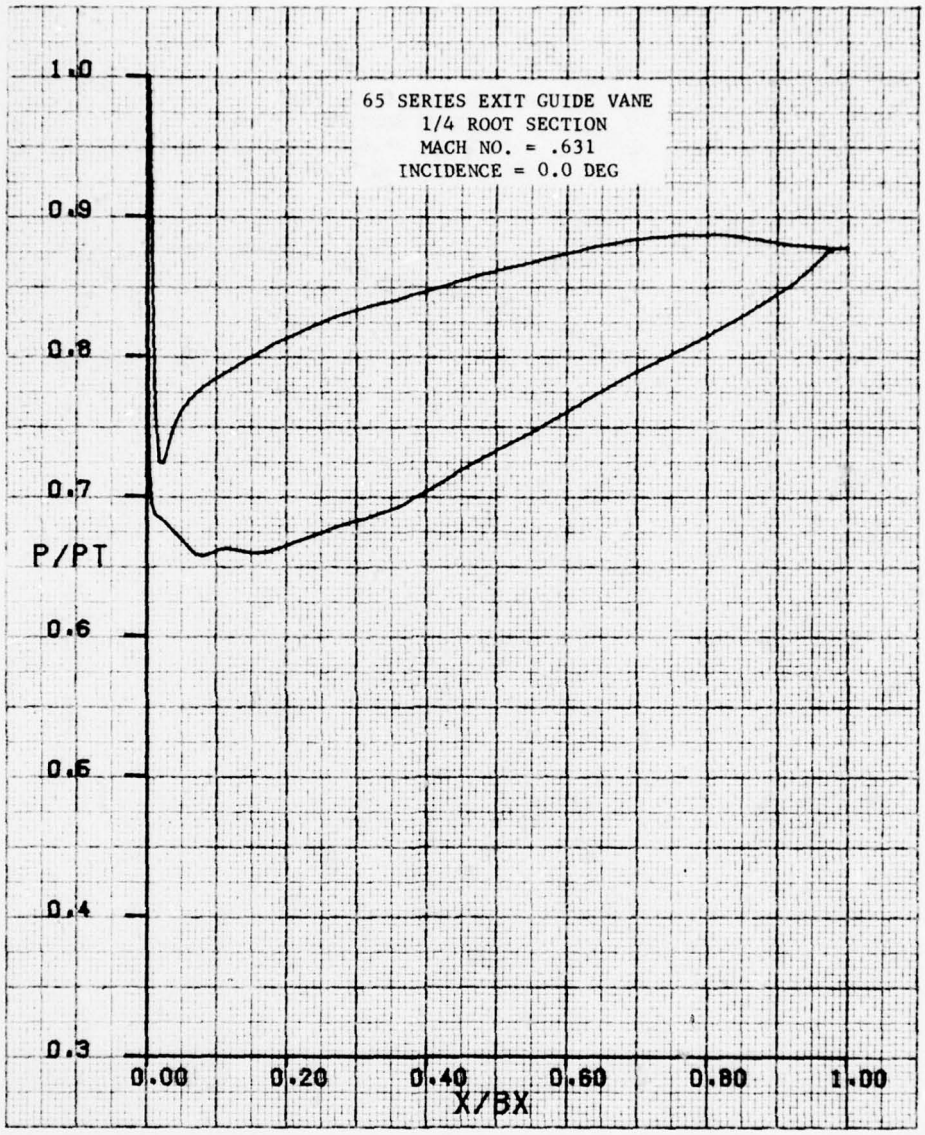


Figure 152. 65-Series EGV ¼ Root Section Predicted Pressure Distribution at 0.0 deg Incidence

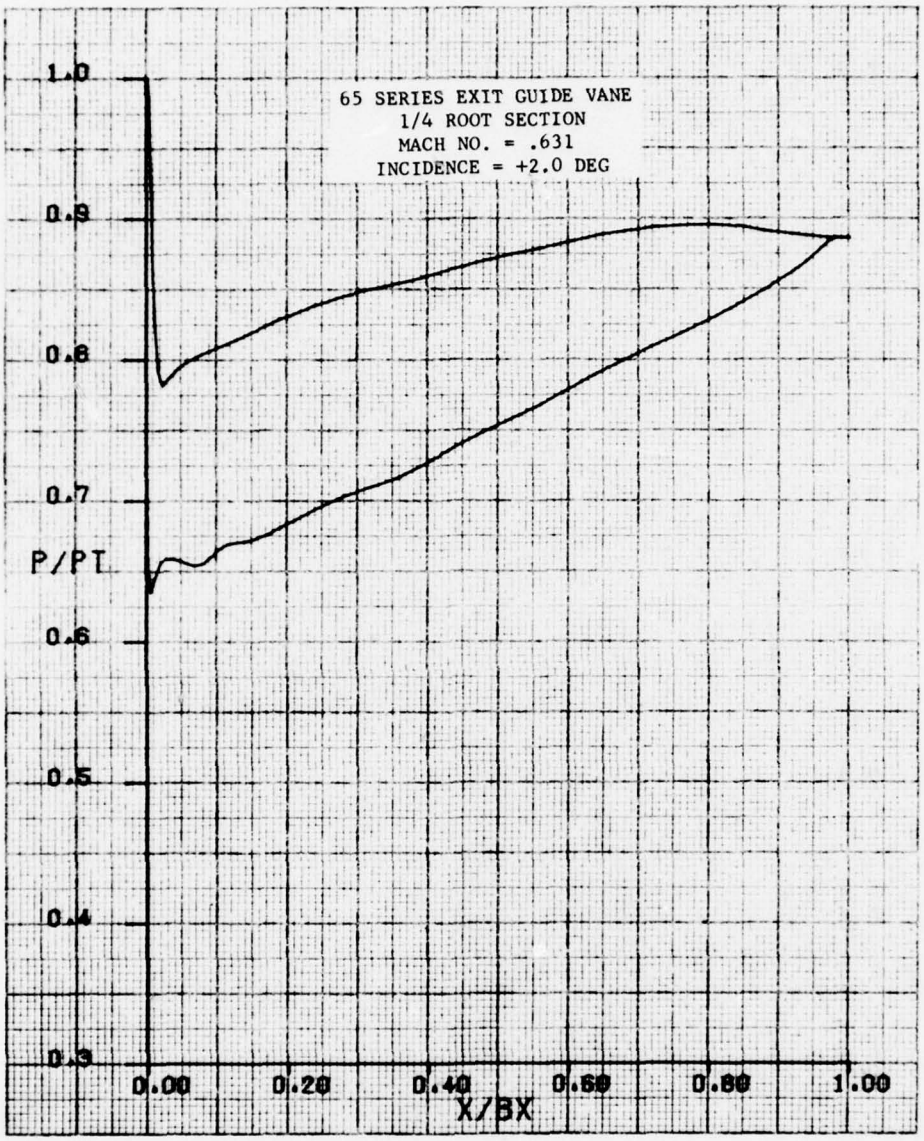


Figure 153. 65-Series EGV ¼ Root Section Predicted Pressure Distribution at +2.0 deg Incidence

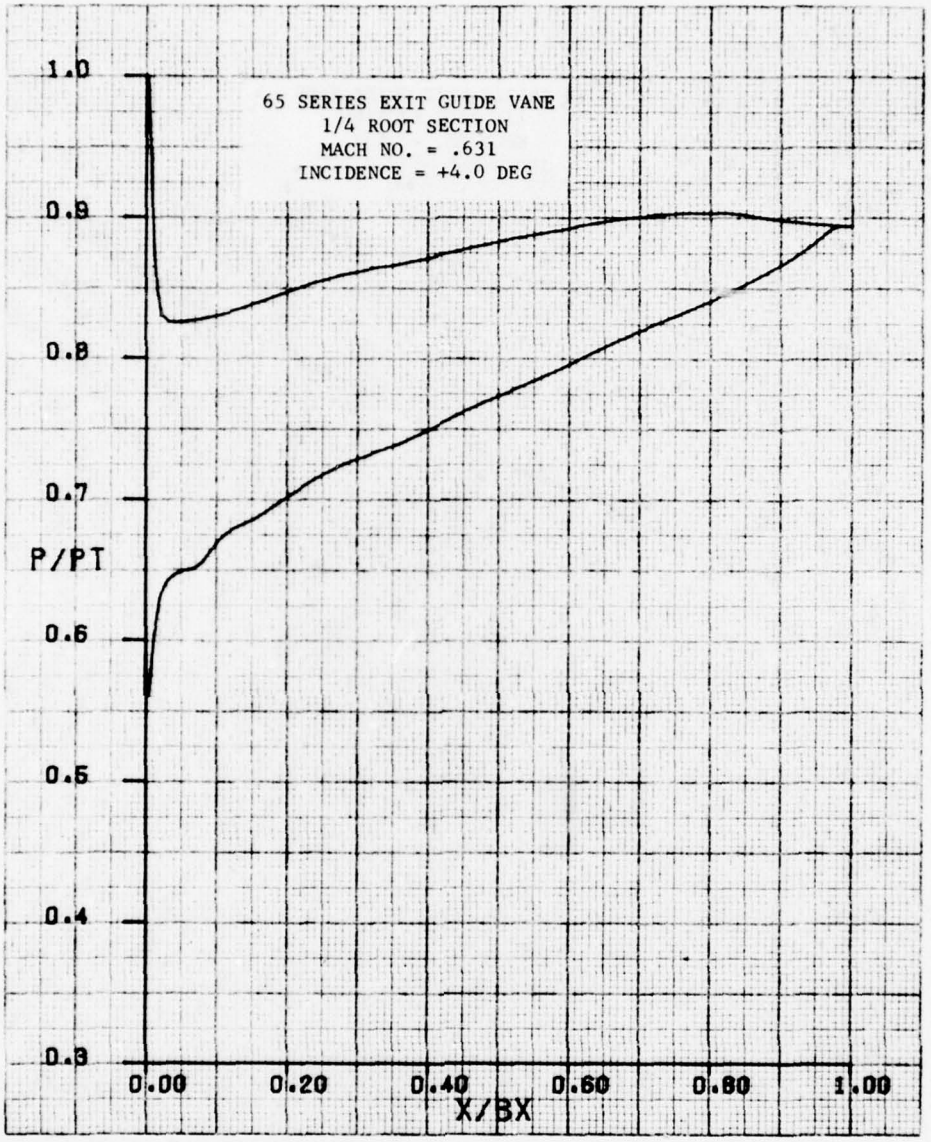


Figure 154. 65-Series EGV ¼ Root Section Predicted Pressure Distribution at +4.0 deg Incidence

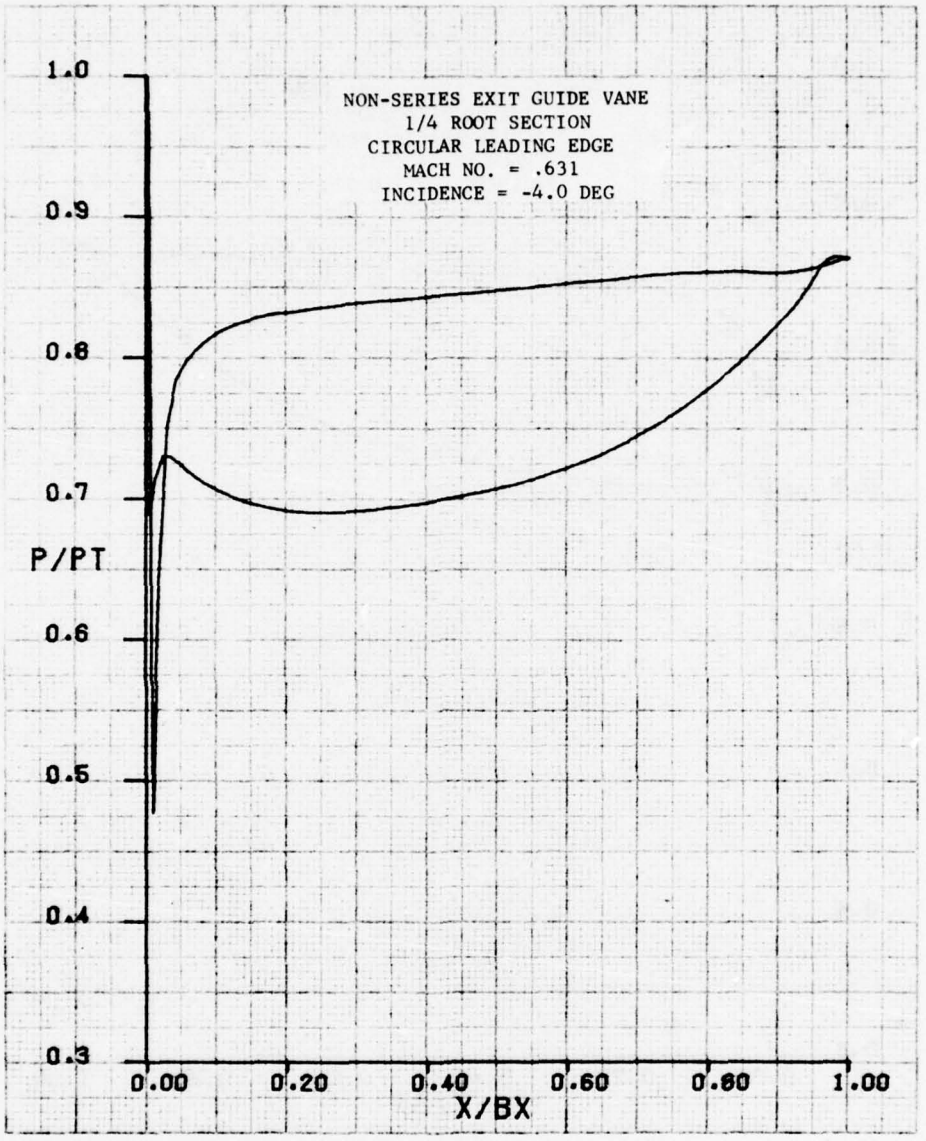


Figure 155. Non-series EGV ¼ Root Section Predicted Pressure Distribution at −4.0 deg Incidence

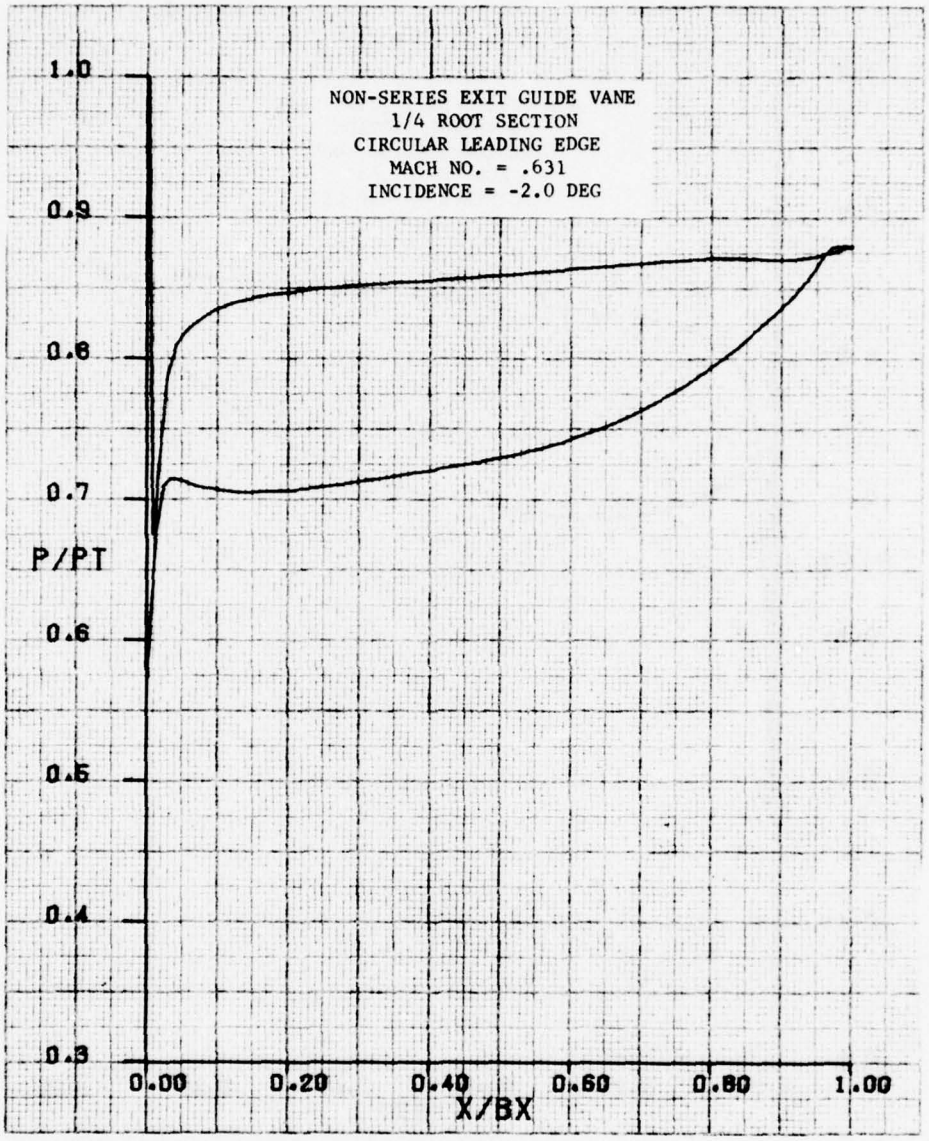


Figure 156. Non-series EGV ¼ Root Section Predicted Pressure Distribution at −2.0 deg Incidence

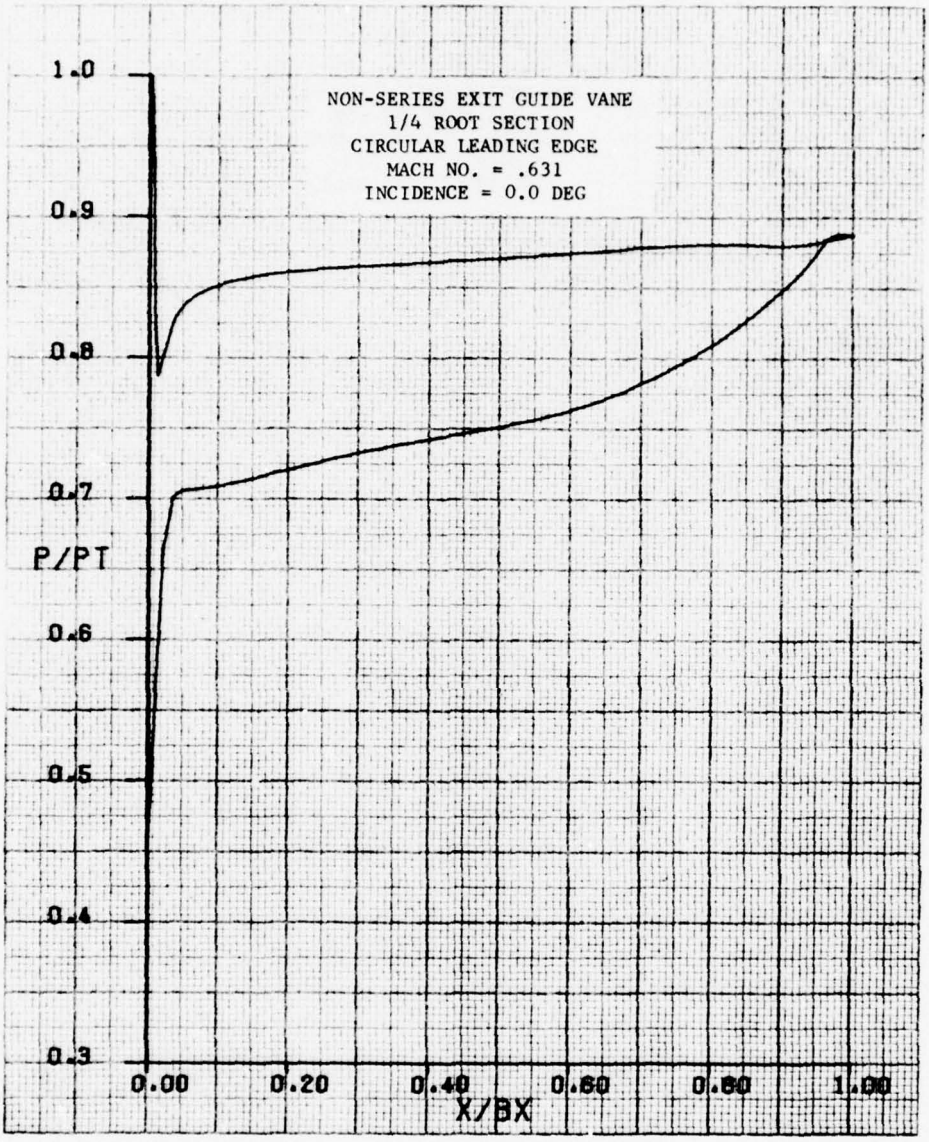


Figure 157. Non-series EGV ¼ Root Section Predicted Pressure Distribution at 0.0 deg Incidence

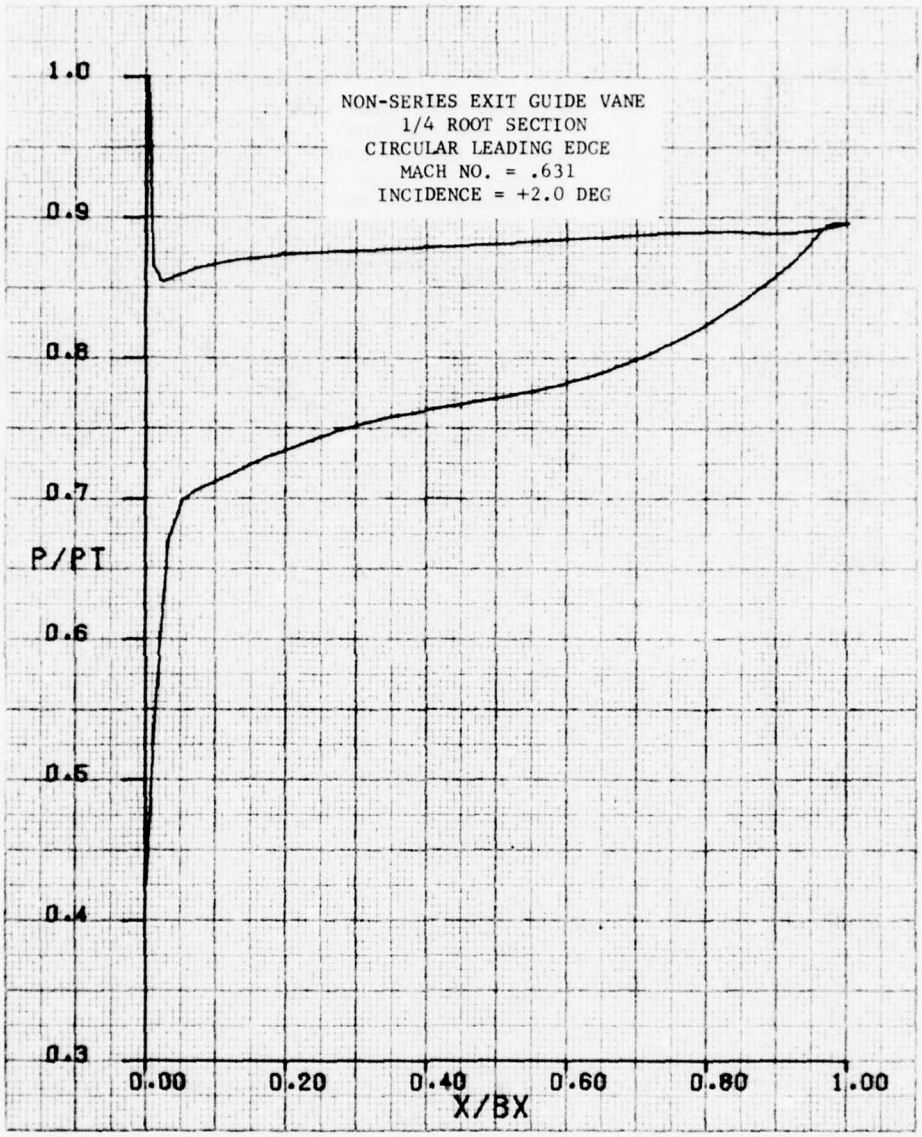


Figure 158. Non-series EGV ¼ Root Section Predicted Pressure Distribution at +2.0 deg Incidence

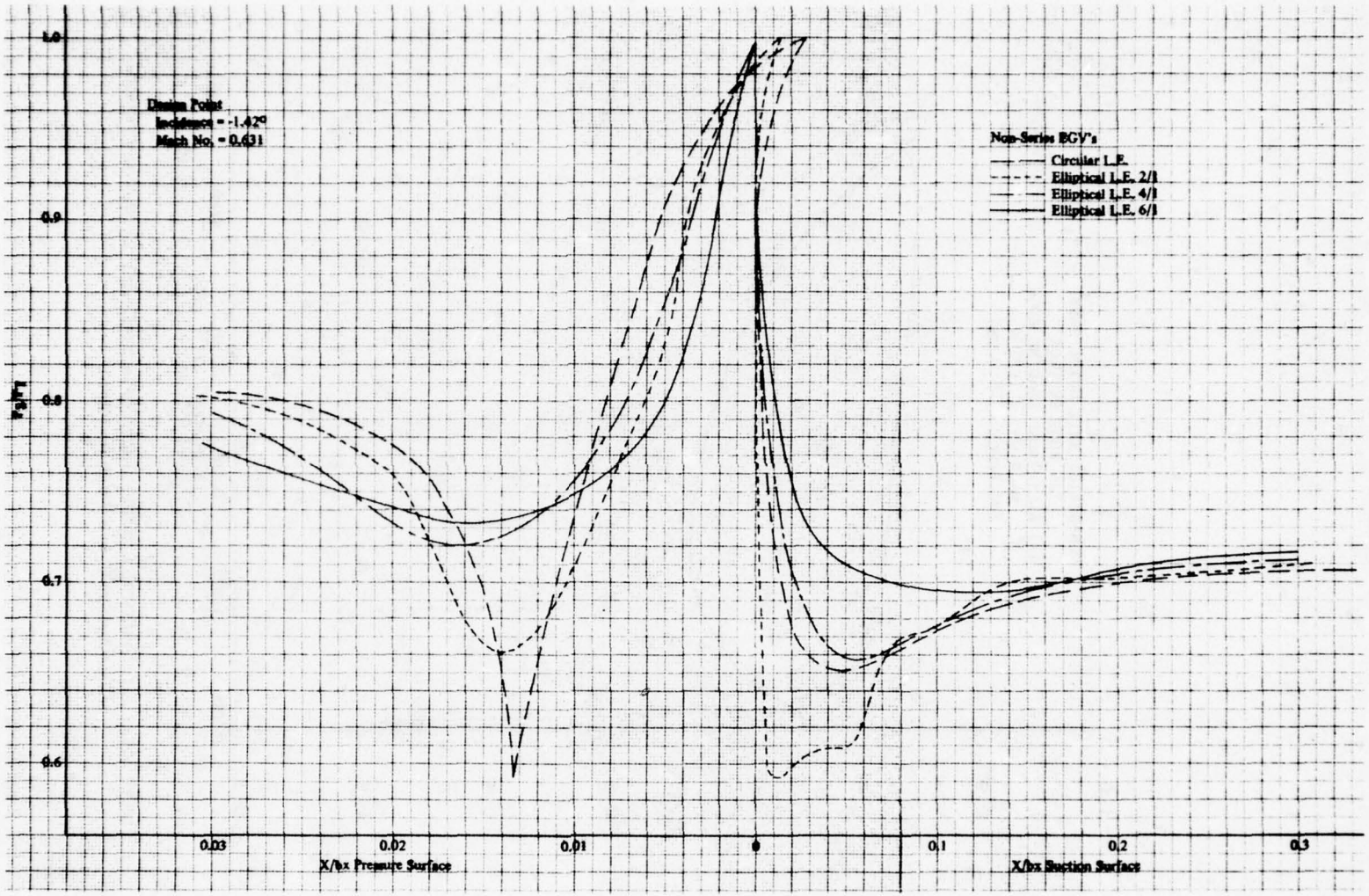


Figure 159. Non-series EGV ¼ Root Section Predicted Leading Edge Region Pressure Distribution for Circular 2/1, 4/1, and 6/1 Elliptical Leading Edges

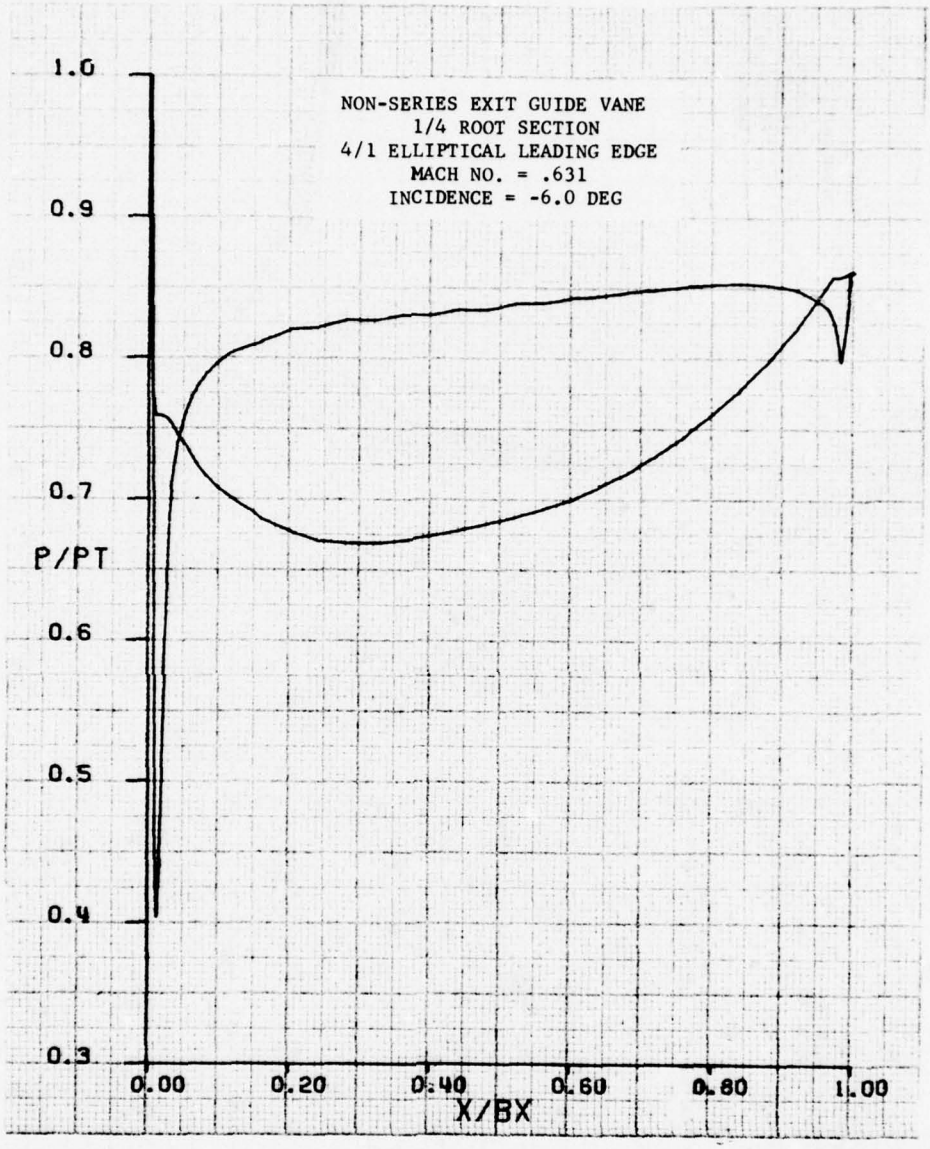


Figure 160. 4/1 Elliptical Leading Edge Non-series EGV Predicted Pressure Distribution at −6.0 deg Incidence

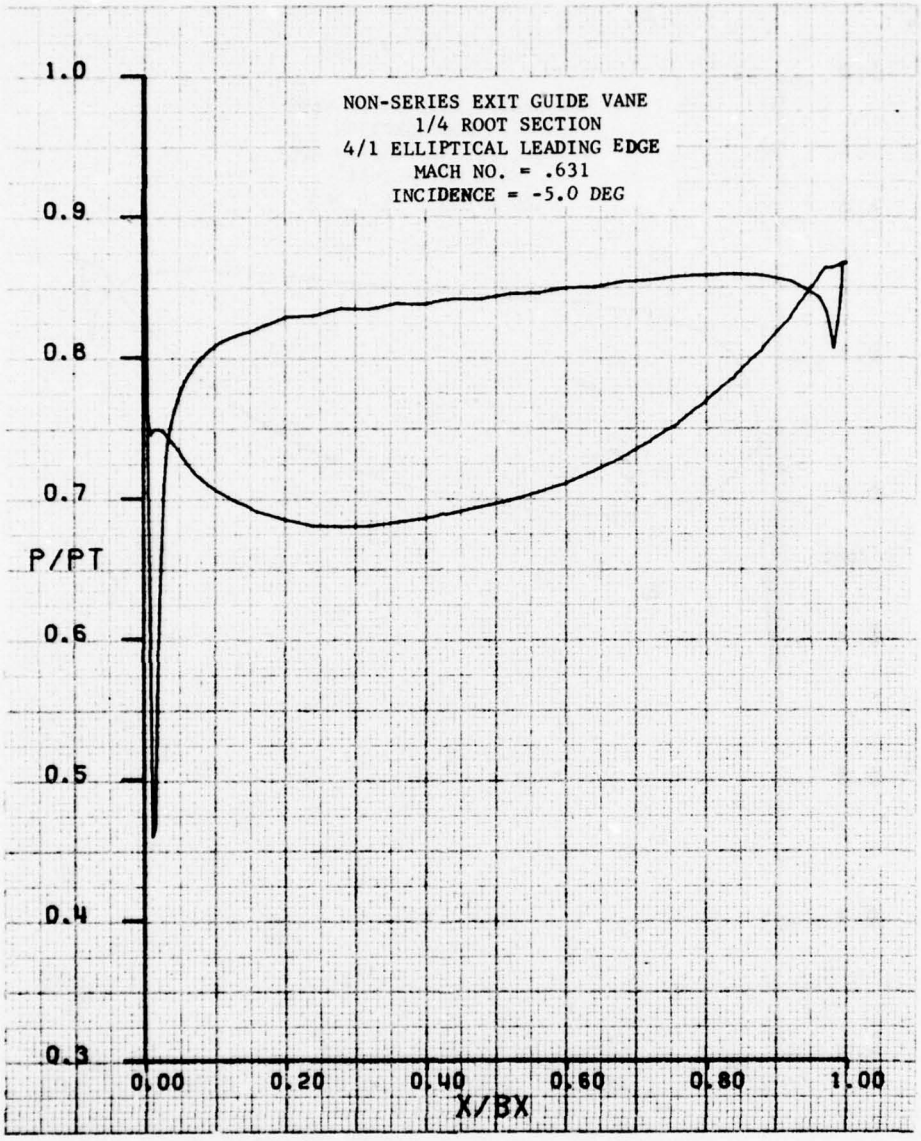


Figure 161. 4/1 Elliptical Leading Edge Non-series EGV Predicted Pressure Distribution at −5.0 deg Incidence

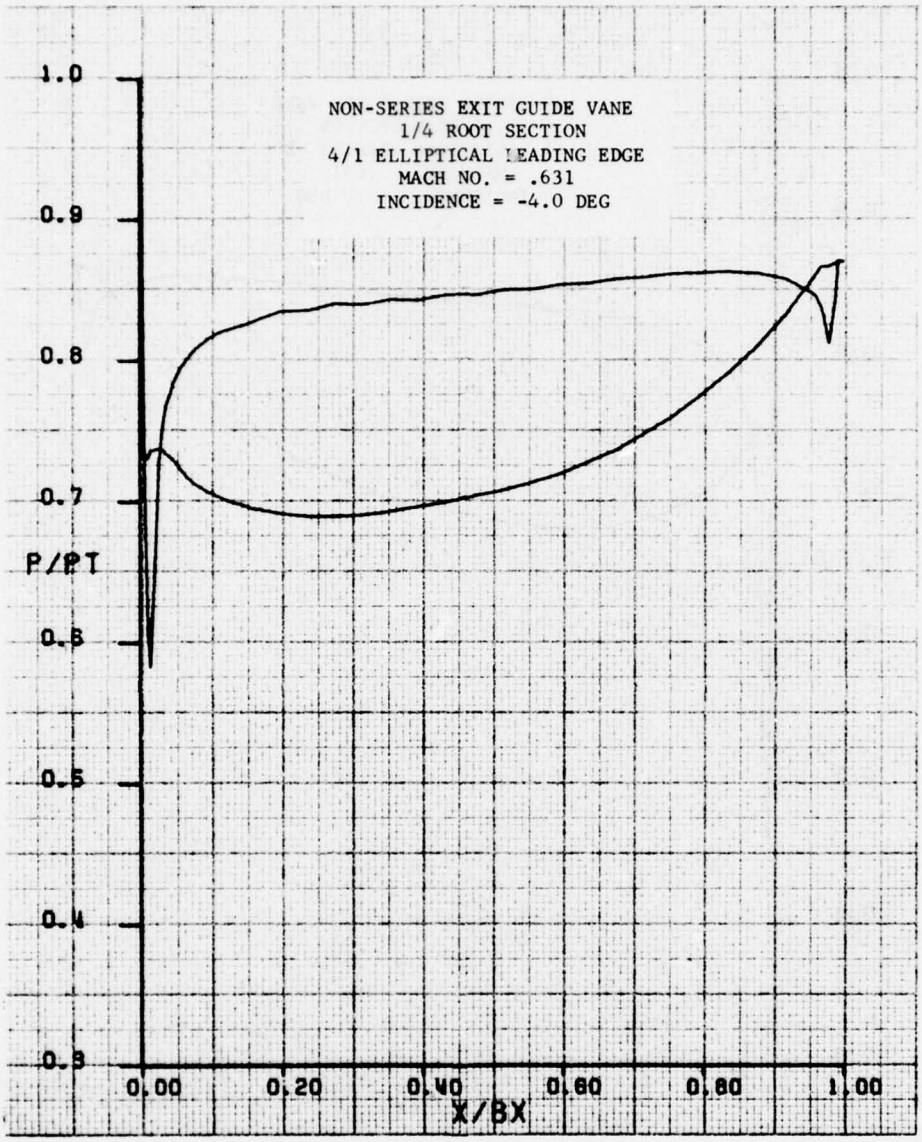


Figure 162. 4/1 Elliptical Leading Edge Non-series EGV Predicted Pressure Distribution at −4.0 deg Incidence

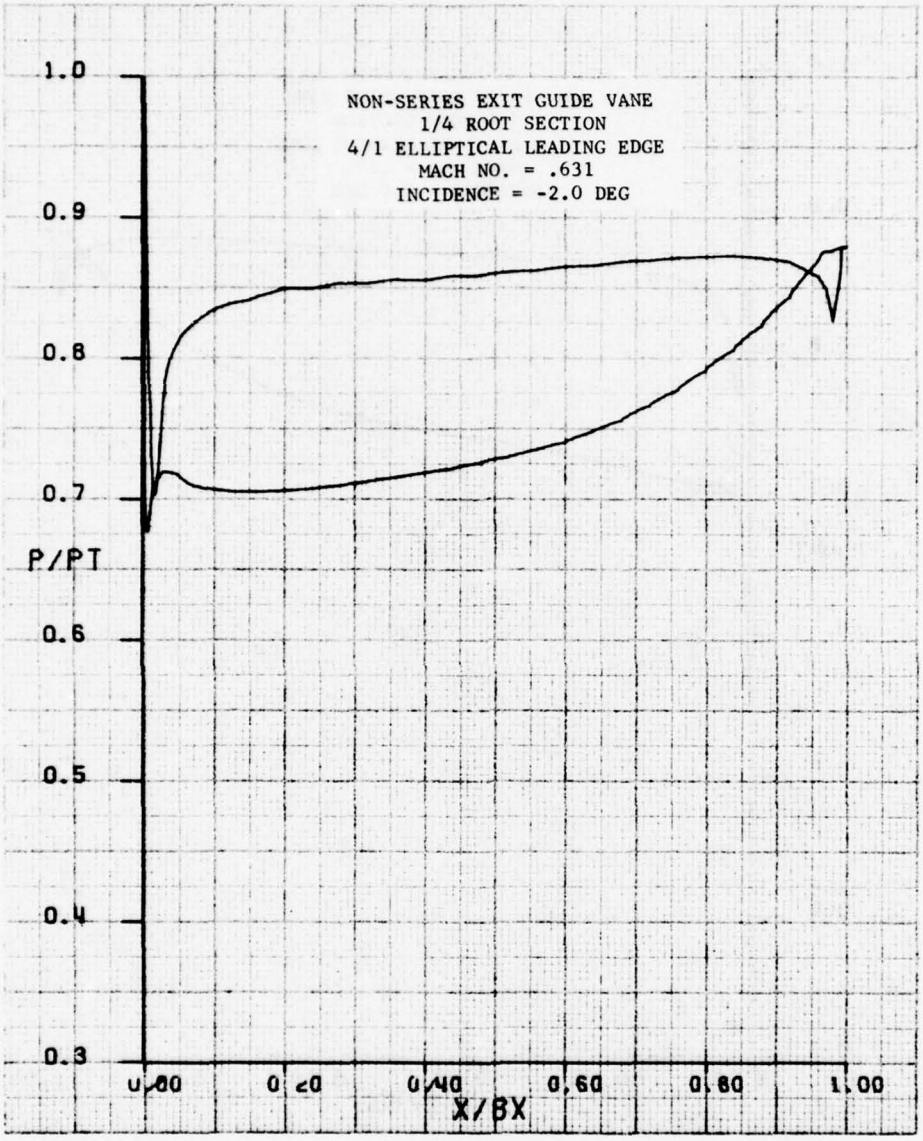


Figure 163. 4/1 Elliptical Leading Edge Non-series EGV Predicted Pressure Distribution at −2.0 deg Incidence

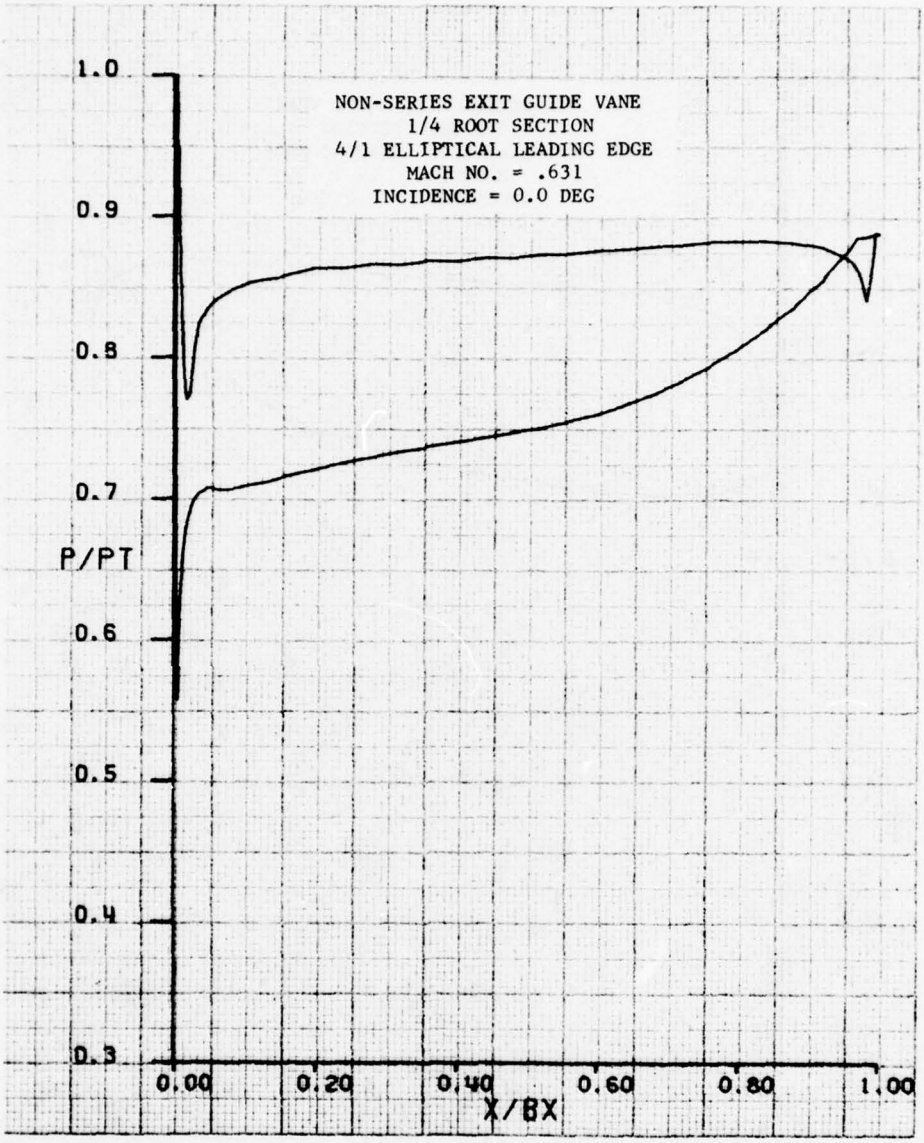


Figure 164. 4/1 Elliptical Leading Edge Non-series EGV Predicted Pressure Distribution at 0.0 deg Incidence

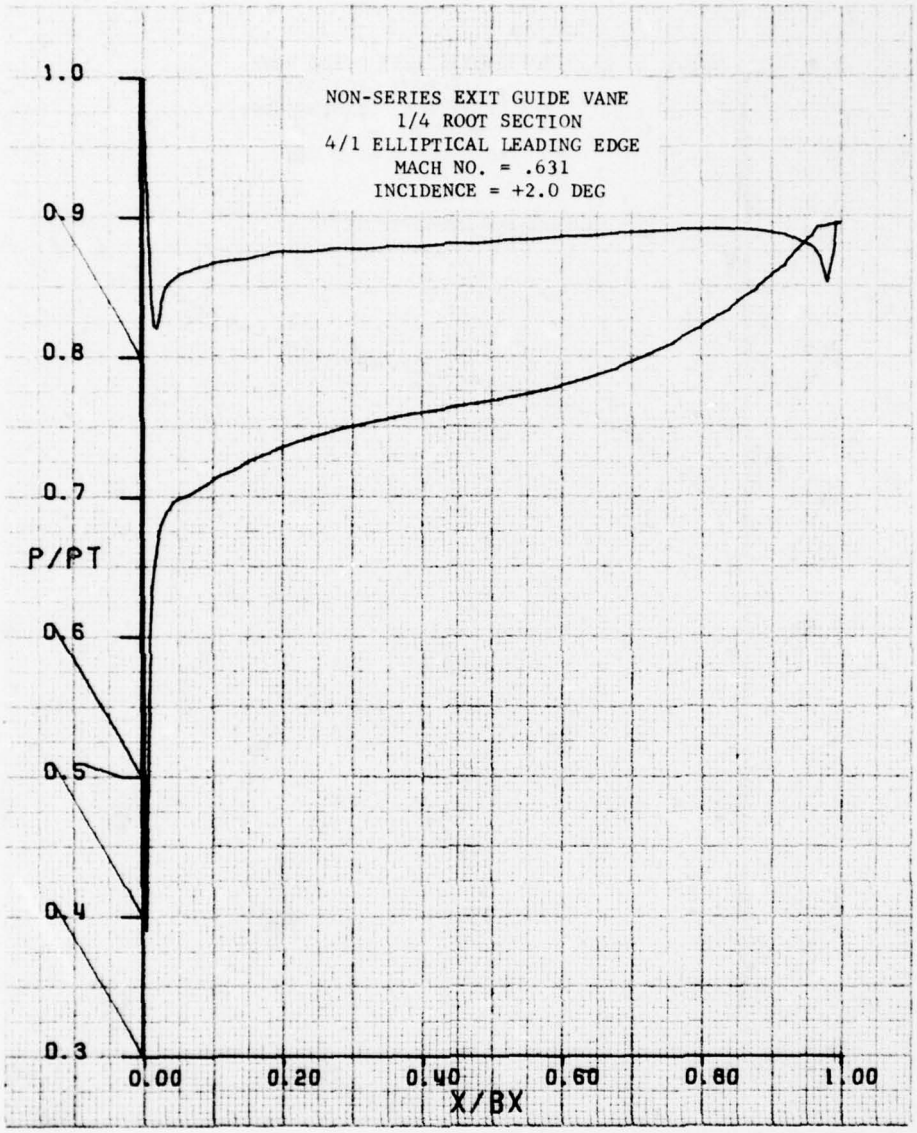


Figure 165. 4/1 Elliptical Leading Edge Non-series EGV Predicted Pressure Distribution at +2.0 deg Incidence

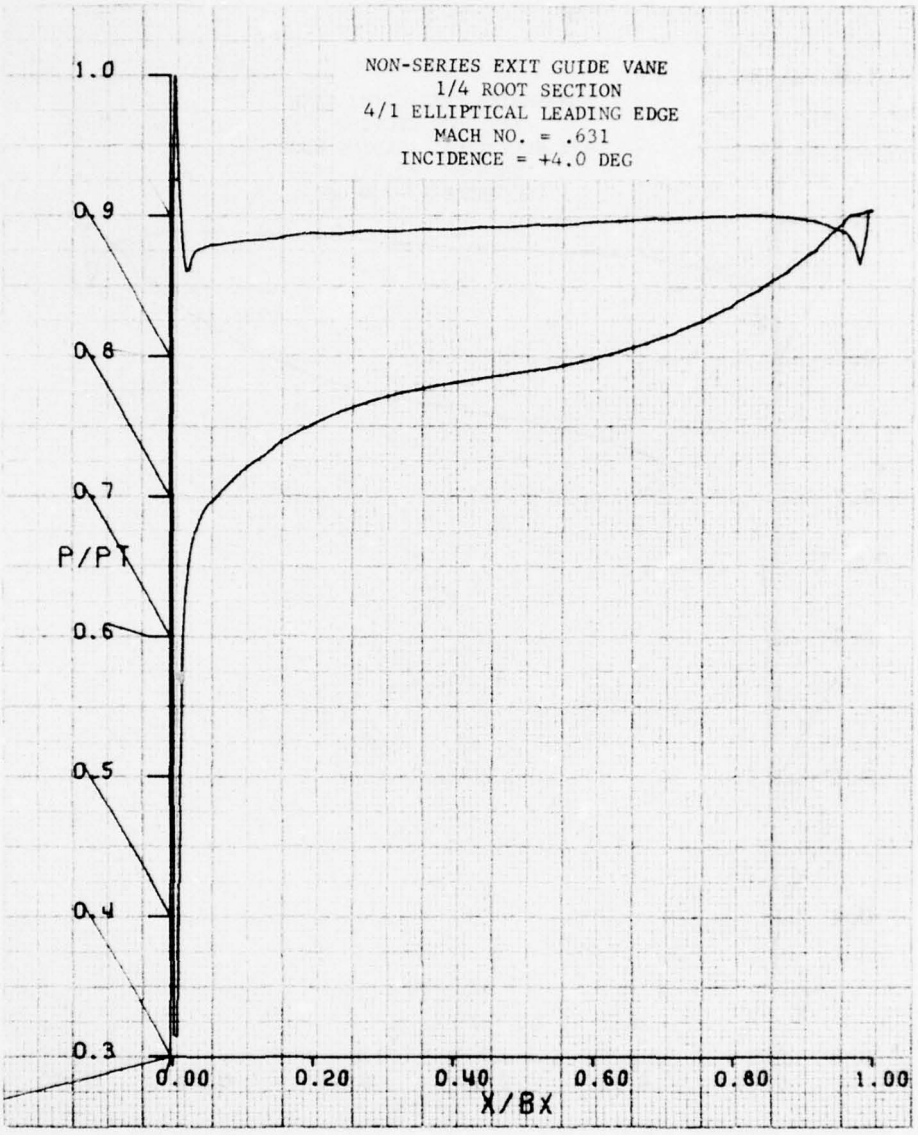


Figure 166. 4/1 Elliptical Leading Edge Non-series EGV Predicted Pressure Distribution at +4.0 deg Incidence

In order to compare the incidence range of the series and non-series EGV's, a minimum P_s/P_T value of 0.5 was arbitrarily selected as a limit. On this basis, the series airfoil range (table 31) is estimated to be 9.0 deg, −4.0 deg to +5.0 deg. The circular leading edge non-series EGV range (estimated) is 2.0 deg, −3.0 deg to −1.0 deg. The 4/1 elliptical leading edge non-series EGV (estimated) range is 6.0 deg, −4.5 deg to +1.0 deg.

The minimum P_s/P_T value of 0.5 was arbitrarily selected only to provide a basis for comparison. The minimum value may vary for each airfoil design application and it may also vary depending on which airfoil surface the overspeed occurs.

In multistage engine applications, turbine EGV's are required to operate through an incidence range of approximately 4 deg between intermediate and maximum power settings. In single-stage engine applications, the EGV's operate through an incidence range of approximately 6 deg. The results of the incidence range comparison indicate that the series airfoil incidence range (9.0 deg) exceeds both engine operating ranges. The 4/1 elliptical leading edge non-series incidence range (6.0 deg) exceeds the multistage operating range and just meets the single-stage operating range. The circular leading edge non-series airfoil incidence range (2.0 deg) is unsatisfactory for either application but it may be satisfactory in engine applications where variable position EGV's are used. In engine applications where the incidence range is critical, the non-series EGV airfoils can be designed with leading edges specifically designed for increased incidence ranges. This can be achieved by using larger leading edges, either circular or elliptical. However, the larger leading edge will cause the flow to accelerate up to the gage point, increasing the diffusion rate between the gage point and trailing edge. The potential for flow separation may increase.

D. STATE-OF-THE-ART ADVANCEMENTS

In the EGV program, non-series airfoils, designed for Mach number and gas turning levels above those typical of state-of-the-art EGV airfoils, demonstrated (relative to equivalent series airfoils) higher diffusion efficiencies, reduced total pressure losses and reduced tendencies for flow separation. The non-series EGV's were designed by optimizing the airfoil camber and thickness distributions to obtain the minimum rate of diffusion on the airfoil suction surface. Computer graphics airfoil design techniques with predicted airfoil pressure distributions and suction surface boundary layer characteristics were used to identify the optimum airfoil designs.

The EGV program Phase I cascade data extended a correlation system developed by P&WA for compressor casades (equivalent conical angle, θeq) into a range of conical angles applicable to advanced engine turbine EGV's. The θeq correlation equates each airfoil cascade to a conical diffuser with the same diffusion area ratio and length. The airfoil aspect ratio and gap/chord ratio are selected to obtain the optimum diffusion efficiency for each equivalent diffuser area ratio and equivalent conical angle. The Phase II annular cascade (designed using the θeq correlation) verified the correlation with measured diffusion efficiencies that equalled the predicted efficiencies.

Results of the Phase I low Mach number cascade testing and the Phases II and III high Mach number annular cascade testing indicated that secondary losses can be reduced with endwall protrusions. The endwall protrusions also improved the spanwise turning distributions, eliminating the underturning tendencies near the endwalls, and increased the average static pressure rise.

CONCLUSIONS

Highly loaded non-series turbine EGV's, designed by tailoring camber and thickness distributions to minimize the airfoil suction surface rate of diffusion, demonstrated the following characteristics relative to equivalent NASA series airfoils: a reduction in total pressure loss, higher diffusion efficiencies and reduced tendencies for flow separation. These results verified that the non-series airfoil design technology (computer graphics design techniques with predicted airfoil surface pressure distributions and predicted suction surface boundary layer characteristics) can be used to design optimum EGV airfoil geometries.

Designing the non-series EGV's to obtain the minimum suction surface rate of diffusion resulted in airfoils which were more sensitive to incidence variations than the equivalent series airfoils. However, the non-series EGV incidence sensitivity was predicted to be improved by redesigning the airfoils with elliptical leading edges rather than circular leading edges. With the redesigned leading edges, the non-series EGV incidence range was determined to be acceptable for both single stage and multistage turbine EGV applications.

Non-series airfoil design evaluation techniques, when used to evaluate candidate series airfoils, identified high suction surface rates of diffusion and predicted flow separation. Results of the 65 series annular cascade testing verified the predicted separation, thus emphasizing the importance of the non-series airfoil design evaluation techniques (pressure distribution and boundary layer analysis) to series airfoil design applications.

The P&WA equivalent cone angle correlation (θeq) for diffusing cascades was used to achieve optimum diffusion efficiencies in the annular cascade testing. This correlation permits selection of gap/chord and aspect ratios which yield the desired equivalent conical angle for optimum diffusion efficiency.

Endwall protrusions demonstrated reduced secondary losses with improved spanwise gas turning distributions and increased diffusion. These results, however, were obtained relative to a high loss airfoil (cutback leading edge and uncambered trailing edge). The uncambered and cutback airfoil modifications, in Phase I, demonstrated performance improvements. In Phase II, these same modifications resulted in decreased performance. Definite conclusions regarding the effects of the cutback and uncambered airfoil modifications cannot be made on the basis of the existing data.

RECOMMENDATIONS

The following recommendations are based on the results of the EGV technology development program:

1. The incidence range of non-series EGV's, with circular and elliptical leading edges, should be demonstrated experimentally.

2. The performance of the low aspect ratio non-series EGV should be measured in the annular cascade test rig. Direct performance comparisons between the high and low aspect ratio EGV's should then be made.

3. Endwall protrusions should be evaluated with available 3-D flow calculations to identify the optimum protrusion size. Annular cascade test evaluation of the optimum protrusion should be made.

4. The cutback leading edge and uncambered trailing edge airfoil modifications should be evaluated independently.

5. Optimum non-series EGV's with airfoil and endwall modifications designed to reduce secondary losses should be demonstrated in a full size rotating rig test, permitting measurement of both design point and off-design point performance.

REFERENCES

1. Schlichting, H., Boundary Layer Theory, 4th Edition, McGraw-Hill, New York, 1960.

2. Starken, H., F. A. E. Breugelmans, and P. Schimming, Investigation of the Axial Velocity Density Ratio in a High Turning Cascade, ASME 75-GT-25, March 2, 1975.

3. Hanley, W. T., A Correlation of Endwall Losses in Plane Compressor Cascades, Journal of Engineering for Power, Trans., ASME, July 1968, pp. 251-257.

4. Edmonds, S. A., B. E. Endsley, and M. G. Jones, Equivalent Conical Diffusion Angle Analogy Cascade Correlation and Meanline Program Formulation, P&WA Report FTDM No. 571, July 1974.

5. Kussoy, M. I., and D. Bachkin, Comparison of Performance of Two Aerodynamically Similar 14-Inch Diameter Single Stage Compressor Rotors of Different Chord Length, NACA RM E57103.

6. Howell, A. R., The Present Basis of Axial Flow Compressor Design, Part 1, Cascade Theory and Performance, Gt. Br. ARC.

7. Aerodynamic Design of Axial Flow Compressors, NASA SP-36, 1965.

8. Papailiou, K. D., Correlations Concerning the Process of Flow Deceleration, ASME 74-GT-87, 27 November 1973.

APPENDIX A
PHASE I AIRFOIL COORDINATES

THIS PAGE IS BEST QUALITY PRACTICABLE
FROM COPY FURNISHED TO DDC

TABLE A-1

30 DEGREES TURNING CASCADE SECTION DESIGN

GEOMETRY

		BETA1 (METAL)	57.500	PITCH	1.5199
AXIAL CHORD	1.8700	BETA2 (METAL)	85.000	GAGING	1.2554
M/L RATIO	-0.3250	DELTA BETA1	10.000	MAX THICK	0.1420
		DELTA BETA2	16.000	AREA	0.1988
L.E. DIAMETER	0.0250	GAGE ANGLE	55.690		
T.E. DIAMETER	0.0200	GAMMA	10.070		

	X	X/B	Y	Y/B	R	R/B
L.E. CIRCLE	0.0125	0.0067	-0.6004	-0.3211	0.0125	0.0067
L.E. SUCT. TANG. PT.	0.0049	0.0026	-0.5905	-0.3158		
L.E. PRESS. TANG. PT.	0.0183	0.0098	-0.6115	-0.3270		
GAGE POINT	0.5966	0.3190	-0.2059	-0.1101		
CTR. OF MAX THICK.	0.0	0.0	1.6638	0.8897		
CTR. OF GRAVITY	0.9290	0.4968	-0.1741	-0.0931		
T.E. CIRCLE	1.8600	0.9947	0.0	0.0	0.0100	0.0053
T.E. SUCT. TANG. PT.	1.8622	0.9959	0.0097	0.0052		
T.E. PRESS. TANG. PT.	1.8605	0.9949	-0.0100	-0.0053		
SUCT. INTERMED. PT.	1.2516	0.6693	0.0237	0.0127		
PRESS. INTERMED. PT.	1.1220	0.6000	-0.1485	-0.0794		

X	X/B	YS	YS/B	YP	YP/B	RC/P	A/AG
0.0	0.0	-0.6004	-0.3211	-0.6004	-0.3211	0.0067	1.00
0.0187	0.0100	-0.5800	-0.3101	-0.6113	-0.3269	3.0403	1.00
0.0374	0.0200	-0.5658	-0.3025	-0.6016	-0.3217	2.9694	1.00
0.0561	0.0300	-0.5517	-0.2950	-0.5919	-0.3165	2.9004	1.00
0.0748	0.0400	-0.5377	-0.2876	-0.5823	-0.3114	2.8333	1.00
0.0935	0.0500	-0.5239	-0.2802	-0.5728	-0.3063	2.7679	1.00
0.1870	0.1000	-0.4568	-0.2443	-0.5259	-0.2812	2.4674	1.00
0.2805	0.1500	-0.3931	-0.2102	-0.4805	-0.2569	2.2079	1.00
0.3740	0.2000	-0.3331	-0.1781	-0.4366	-0.2335	1.9860	1.00
0.4675	0.2500	-0.2769	-0.1481	-0.3942	-0.2108	1.7983	1.00
0.5610	0.3000	-0.2247	-0.1202	-0.3535	-0.1890	1.6419	1.01
0.6545	0.3500	-0.1767	-0.0945	-0.3144	-0.1681	1.5112	1.01
0.7480	0.4000	-0.1329	-0.0711	-0.2772	-0.1482	1.3935	1.02
0.8415	0.4500	-0.0936	-0.0500	-0.2418	-0.1293	1.2872	1.03
0.9350	0.5000	-0.0588	-0.0314	-0.2084	-0.1114	1.1919	1.04
1.0285	0.5500	-0.0286	-0.0153	-0.1770	-0.0947	1.1073	1.05
1.1220	0.6000	-0.0032	-0.0017	-0.1478	-0.0791	1.0331	1.07
1.2155	0.6500	0.0172	0.0092	-0.1209	-0.0647	0.9689	1.08
1.3090	0.7000	0.0325	0.0174	-0.0965	-0.0516	0.9147	1.09
1.4025	0.7500	0.0426	0.0228	-0.0745	-0.0399	0.8700	1.11
1.4960	0.8000	0.0473	0.0253	-0.0553	-0.0296	0.8348	1.13
1.5895	0.8500	0.0463	0.0248	-0.0390	-0.0209	0.8090	1.14
1.6830	0.9000	0.0396	0.0212	-0.0258	-0.0138	0.7926	1.16
1.7765	0.9500	0.0269	0.0144	-0.0159	-0.0085	0.7858	1.00
1.8326	0.9800	0.0163	0.0087	-0.0116	-0.0062	0.7864	1.00
1.8513	0.9900	0.0122	0.0065	-0.0105	-0.0056	0.7874	1.00
1.8700	1.0000	0.0	0.0	0.0	0.0	0.0053	1.00

THIS PAGE IS BEST QUALITY PRACTICABLE
FROM COPY FURNISHED TO DDC

TABLE A-2

40 DEGREES TURNING CASCADE SECTION DESIGN

GEOMETRY

		BETA1 (METAL)	52.079	PITCH	0.7600
AXIAL CHORD	1.8447	BETA2 (METAL)	84.000	GAGING	0.5771
H/L RATIO	-0.3250	DELTA BETA1	7.000	MAX THICK	0.141F
		DELTA BETA2	18.000	AREA	0.1898
L.E. DIAMETER	0.0200	GAGE ANGLE	49.410		
T.E. DIAMETER	0.0200	GAMMA	6.751		

	X	X/B	Y	Y/B	B	R/B
L.E. CIRCLE	0.0100	0.0054	-0.5930	-0.3215	0.0100	0.0054
L.E. SUCT. TANG. PT.	0.0034	0.0018	-0.5855	-0.3174		
L.E. PRESS. TANG. PT.	0.0157	0.0085	-0.6013	-0.3259		
GAGE POINT	0.3440	0.1865	-0.3159	-0.1713		
CTR. OF MAX THICK.	0.0	0.0	0.0000	0.0000		
CTR. OF GRAVITY	0.9443	0.5119	-0.1328	-0.0720		
T.E. CIRCLE	1.8347	0.9946	0.0	0.0	0.0100	0.0054
T.E. SUCT. TANG. PT.	1.8373	0.9960	0.0097	0.0052		
T.E. PRESS. TANG. PT.	1.8352	0.9949	-0.0100	-0.0054		
SUCT. INTERMED. PT.	1.0954	0.5938	0.0270	0.0146		
PRESS. INTERMED. PT.	0.8624	0.4675	-0.1850	-0.1003		

X	X/B	YS	YS/B	YP	YP/B	RC/B	A/AG
0.0	0.0	-0.5930	-0.3215	-0.5930	-0.3215	0.0054	1.00
0.0184	0.0100	-0.5723	-0.3102	-0.5994	-0.3249	2.6927	1.00
0.0369	0.0200	-0.5562	-0.3015	-0.5868	-0.3181	2.5876	1.00
0.0553	0.0300	-0.5403	-0.2929	-0.5745	-0.3114	2.4886	1.00
0.0738	0.0400	-0.5246	-0.2844	-0.5623	-0.3048	2.3952	1.00
0.0922	0.0500	-0.5090	-0.2759	-0.5503	-0.2983	2.3074	1.00
0.1845	0.1000	-0.4340	-0.2353	-0.4929	-0.2672	1.9454	1.00
0.2767	0.1500	-0.3638	-0.1972	-0.4397	-0.2383	1.6964	1.00
0.3689	0.2000	-0.2988	-0.1620	-0.3903	-0.2116	1.5403	1.00
0.4612	0.2500	-0.2391	-0.1296	-0.3446	-0.1868	1.4176	1.00
0.5534	0.3000	-0.1847	-0.1001	-0.3024	-0.1640	1.3085	1.00
0.6456	0.3500	-0.1355	-0.0735	-0.2637	-0.1429	1.2120	1.00
0.7379	0.4000	-0.0918	-0.0497	-0.2281	-0.1237	1.1277	1.00
0.8301	0.4500	-0.0533	-0.0289	-0.1956	-0.1060	1.0548	1.01
0.9223	0.5000	-0.0203	-0.0110	-0.1661	-0.0900	0.9929	1.02
1.0146	0.5500	0.0073	0.0040	-0.1394	-0.0755	0.9415	1.03
1.1068	0.6000	0.0295	0.0160	-0.1153	-0.0625	0.9000	1.04
1.1991	0.6500	0.0461	0.0250	-0.0939	-0.0509	0.8682	1.06
1.2913	0.7000	0.0573	0.0311	-0.0751	-0.0407	0.8457	1.09
1.3835	0.7500	0.0630	0.0342	-0.0588	-0.0318	0.8324	1.11
1.4758	0.8000	0.0632	0.0342	-0.0444	-0.0241	0.8282	1.13
1.5680	0.8500	0.0577	0.0313	-0.0325	-0.0178	0.8331	1.16
1.6602	0.9000	0.0467	0.0253	-0.0228	-0.0123	0.8471	1.20
1.7525	0.9500	0.0300	0.0163	-0.0151	-0.0082	0.8705	1.00
1.8078	0.9800	0.0173	0.0094	-0.0115	-0.0062	0.8892	1.00
1.8263	0.9900	0.0126	0.0068	-0.0105	-0.0057	0.8962	1.00
1.8447	1.0000	0.0	0.0	0.0	0.0	0.0054	1.00

0.0 1.0000 1.0000

THIS PAGE IS BEST QUALITY PRACTICABLE
FROM COPY FURNISHED TO DDC

TABLE A-3

50 DEGREES TURNING CASCADE SECTION DESIGN

GEOMETRY

		BETA1 (METAL)	42.319	PITCH	0.7790
AXIAL CHORD	1.8694	BETA2 (METAL)	81.800	GAGING	0.5028
H/L RATIO	-0.4500	DELTA BETA1	6.000	MAX THICK	0.1460
		DELTA BETA2	19.000	AREA	0.2077
L.E. DIAMETER	0.0200	GAGE ANGLE	40.200		
T.E. DIAMETER	0.0200	GAMMA	6.912		

	X	X/B	Y	Y/B	R	R/L
L.E. CIRCLE	0.0100	0.0053	-0.8322	-0.4452	0.0100	0.0053
L.E. SUCT. TANG. PT.	0.0023	0.0012	-0.8259	-0.4418		
L.E. PRESS. TANG. PT.	0.0170	0.0091	-0.8393	-0.4490		
GAGE POINT	0.3647	0.1951	-0.4236	-0.2266		
CTR. OF MAX THICK.	0.0	0.0	0.4729	0.2530		
CTR. OF GRAVITY	0.9406	0.5032	-0.1755	-0.0960		
T.E. CIRCLE	1.8594	0.9947	0.0	0.0	0.0100	0.0053
T.E. SUCT. TANG. PT.	1.8624	0.9963	0.0095	0.0051		
T.E. PRESS. TANG. PT.	1.8598	0.9948	-0.0100	-0.0053		
SUCT. INTERMED. PT.	1.0959	0.5862	0.0264	0.0141		
PRESS. INTERMED. PT.	1.0261	0.5489	-0.1496	-0.0800		

X	X/B	YS	YS/L	YP	YP/B	RC/B	A/AG
0.0	0.0	-0.8322	-0.4452	-0.8322	-0.4452	0.0053	1.00
0.0187	0.0100	-0.8059	-0.4311	-0.8377	-0.4481	5.1068	1.00
0.0374	0.0200	-0.7833	-0.4190	-0.8193	-0.4383	4.6880	1.00
0.0561	0.0300	-0.7608	-0.4070	-0.8011	-0.4285	4.3030	1.00
0.0748	0.0400	-0.7385	-0.3950	-0.7831	-0.4189	3.9497	1.00
0.0935	0.0500	-0.7163	-0.3832	-0.7652	-0.4093	3.6267	1.00
0.1869	0.1000	-0.6088	-0.3257	-0.6788	-0.3631	2.4104	1.00
0.2804	0.1500	-0.5078	-0.2718	-0.5974	-0.3196	1.7288	1.01
0.3739	0.2000	-0.4148	-0.2219	-0.5212	-0.2788	1.4270	1.03
0.4674	0.2500	-0.3304	-0.1787	-0.4506	-0.2411	1.2704	1.04
0.5608	0.3000	-0.2544	-0.1361	-0.3858	-0.2064	1.1361	1.05
0.6543	0.3500	-0.1866	-0.0998	-0.3289	-0.1749	1.0221	1.07
0.7478	0.4000	-0.1270	-0.0879	-0.2738	-0.1465	0.9266	1.10
0.8412	0.4500	-0.0753	-0.0403	-0.2266	-0.1212	0.8480	1.13
0.9347	0.5000	-0.0314	-0.0168	-0.1850	-0.0990	0.7850	1.15
1.0282	0.5500	0.0049	0.0026	-0.1488	-0.0796	0.7362	1.17
1.1216	0.6000	0.0336	0.0180	-0.1177	-0.0630	0.7007	1.21
1.2151	0.6500	0.0549	0.0294	-0.0914	-0.0489	0.6777	1.23
1.3086	0.7000	0.0689	0.0369	-0.0694	-0.0371	0.6666	1.26
1.4021	0.7500	0.0758	0.0406	-0.0515	-0.0275	0.6669	1.30
1.4955	0.8000	0.0757	0.0405	-0.0372	-0.0199	0.6785	1.32
1.5890	0.8500	0.0687	0.0367	-0.0262	-0.0140	0.7014	1.37
1.6825	0.9000	0.0548	0.0293	-0.0182	-0.0097	0.7357	1.41
1.7759	0.9500	0.0344	0.0184	-0.0128	-0.0068	0.7819	1.00
1.8320	0.9800	0.0189	0.0101	-0.0107	-0.0057	0.8154	1.00
1.8507	0.9900	0.0132	0.0071	-0.0102	-0.0055	0.8276	1.00
1.8694	1.0000	0.0	0.0	0.0	0.0	0.0053	1.00

THIS PAGE IS BEST QUALITY PRACTICABLE
FROM COPY FURNISHED TO DDC

TABLE A-4

40 DEGREES EGV PLANE CASCADE DESIGN, ROOT SECTION

GEOMETRY

		BETA1 (METAL)	60.000	PITCH	0.7600
AXIAL CHORD	1.2910	BETA2 (METAL)	37.000	GAGING	0.6515
M/L RATIO	-0.2750	DELTA BETA1	4.500	MAX THICK	0.1024
		DELTA BETA2	14.000	AREA	0.0975
L.E. DIAMETER	0.0200	GAGE ANGLE	59.000		
T.E. DIAMETER	0.0200	GAMMA	6.109		

	X	X/B	Y	Y/B	R	R/B
L.E. CIRCLE	0.0100	0.0077	-0.3495	-0.2707	0.0100	0.0077
L.E. SUCT. TANG. PT.	0.0047	0.0036	-0.3411	-0.2642		
L.E. PRESS. TANG. PT.	0.0147	0.0114	-0.3564	-0.2776		
GAGE POINT	0.2805	0.2173	-0.1931	-0.1496		
CTR. OF MAX THICK.	0.0	0.0	0.0	0.0000		
CTR. OF GRAVITY	0.6422	0.4975	-0.1326	-0.1027		
T.E. CIRCLE	1.2810	0.9923	0.0	0.0	0.0100	0.0077
T.E. SUCT. TANG. PT.	1.2810	0.9923	0.0100	0.0077		
T.E. PRESS. TANG. PT.	1.2834	0.9941	-0.0097	-0.0075		
SUCT. INTERMED. PT.	0.7573	0.5866	-0.0408	-0.0316		
PRESS. INTERMED. PT.	0.3903	0.3023	-0.2405	-0.1863		

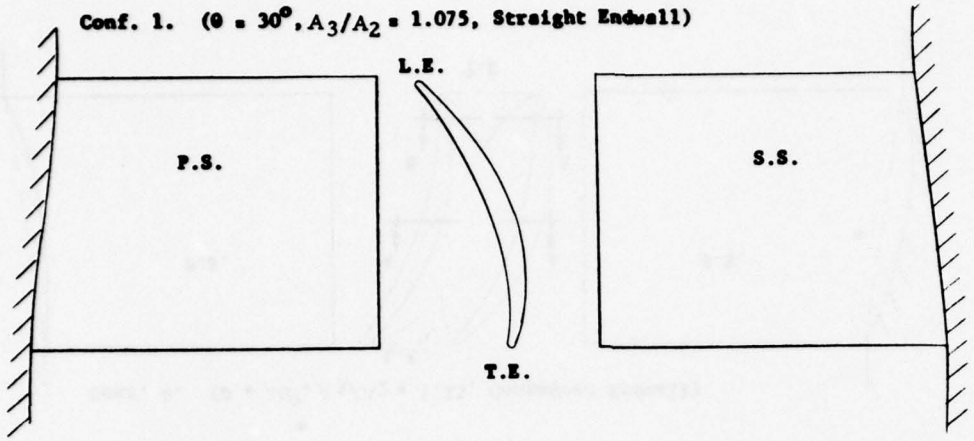
X	X/B	YS	YS/B	YP	YP/B	RC/B	A/AG
0.0	0.0	-0.3495	-0.2707	-0.3495	-0.2707	0.0077	1.00
0.0129	0.0100	-0.3359	-0.2602	-0.3591	-0.2782	1.7308	1.00
0.0258	0.0200	-0.3279	-0.2540	-0.3530	-0.2735	1.7282	1.00
0.0387	0.0300	-0.3200	-0.2479	-0.3476	-0.2692	1.7258	1.00
0.0516	0.0400	-0.3122	-0.2419	-0.3426	-0.2654	1.7235	1.00
0.0645	0.0500	-0.3046	-0.2359	-0.3379	-0.2617	1.7213	1.00
0.1291	0.1000	-0.2681	-0.2077	-0.3163	-0.2450	1.7129	1.00
0.1937	0.1500	-0.2344	-0.1815	-0.2965	-0.2296	1.7082	1.00
0.2582	0.2000	-0.2033	-0.1575	-0.2775	-0.2150	1.7070	0.99
0.3228	0.2500	-0.1747	-0.1353	-0.2592	-0.2008	1.7098	0.98
0.3873	0.3000	-0.1486	-0.1151	-0.2413	-0.1869	1.7177	0.98
0.4519	0.3500	-0.1246	-0.0966	-0.2237	-0.1733	1.7306	0.97
0.5164	0.4000	-0.1032	-0.0799	-0.2063	-0.1598	1.7481	0.97
0.5810	0.4500	-0.0837	-0.0648	-0.1891	-0.1465	1.7703	0.97
0.6455	0.5000	-0.0663	-0.0514	-0.1722	-0.1333	1.7970	0.97
0.7101	0.5500	-0.0509	-0.0394	-0.1553	-0.1203	1.8281	0.98
0.7746	0.6000	-0.0373	-0.0289	-0.1386	-0.1073	1.8635	0.99
0.8392	0.6500	-0.0256	-0.0198	-0.1219	-0.0945	1.9031	1.00
0.9037	0.7000	-0.0157	-0.0121	-0.1054	-0.0817	1.9468	1.01
0.9683	0.7500	-0.0075	-0.0058	-0.0890	-0.0689	1.9947	1.03
1.0328	0.8000	-0.0009	-0.0007	-0.0726	-0.0562	2.0467	1.04
1.0974	0.8500	0.0041	0.0032	-0.0563	-0.0436	2.1028	1.06
1.1619	0.9000	0.0075	0.0058	-0.0401	-0.0311	2.1628	1.09
1.2264	0.9500	0.0095	0.0074	-0.0239	-0.0185	2.2269	1.12
1.2652	0.9800	0.0100	0.0077	-0.0143	-0.0110	2.2673	1.13
1.2781	0.9900	0.0100	0.0077	-0.0110	-0.0085	2.2811	1.00
1.2916	1.0000	0.0	0.0	0.0	0.0	0.0077	1.00

APPENDIX B
PHASE I FLOW VISUALIZATION TEST CONFIGURATIONS AND RESULTS

TABLE B-1

FLOW VISUALIZATION TESTS

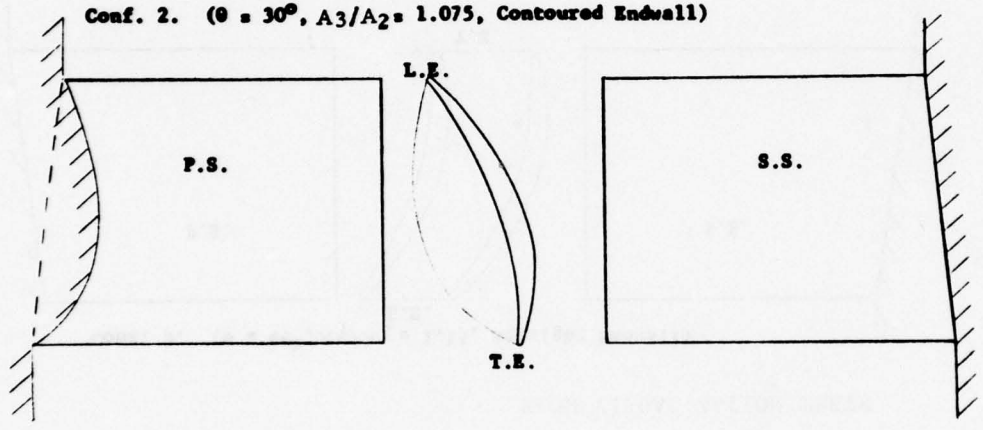
Conf. 1. ($\theta = 30^{\circ}$, $A_3/A_2 = 1.075$, Straight Endwall)



Results

Check out test. Demonstrated good flow visualization.

Conf. 2. ($\theta = 30^{\circ}$, $A_3/A_2 = 1.075$, Contoured Endwall)

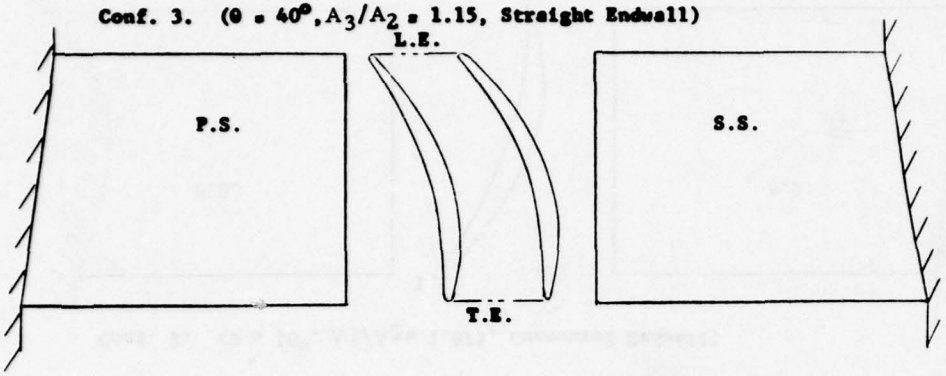


Pressure side protrusion. Reduced endwall crossflow. Apparent separation aft of protrusion.

TABLE B-1 (CONTINUED)

FLOW VISUALIZATION TESTS

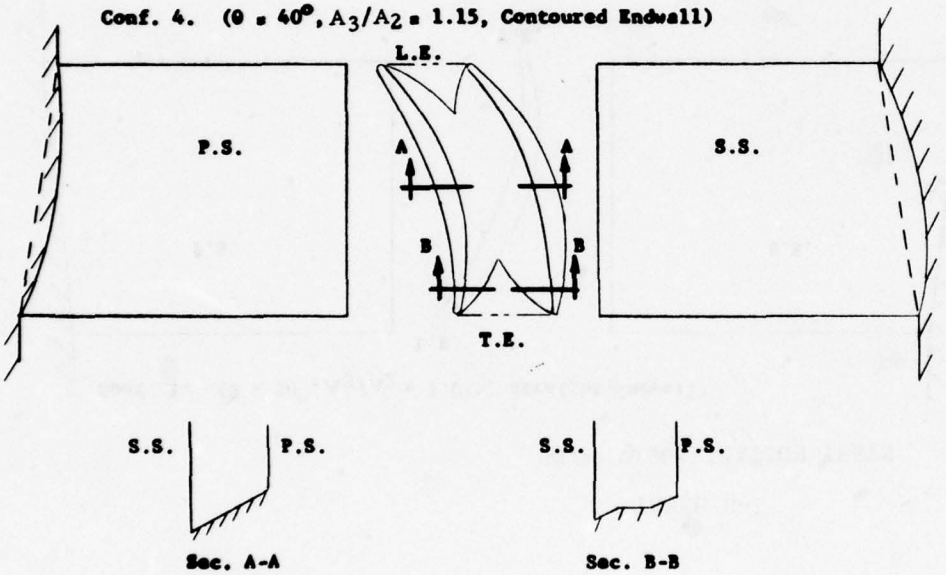
Conf. 3. (θ = 40°, A_3/A_2 = 1.15, Straight Endwall)



Results

Significant P.S. to S.S. crossflow with airfoil separation near endwall junction.

Conf. 4. (θ = 40°, A_3/A_2 = 1.15, Contoured Endwall)

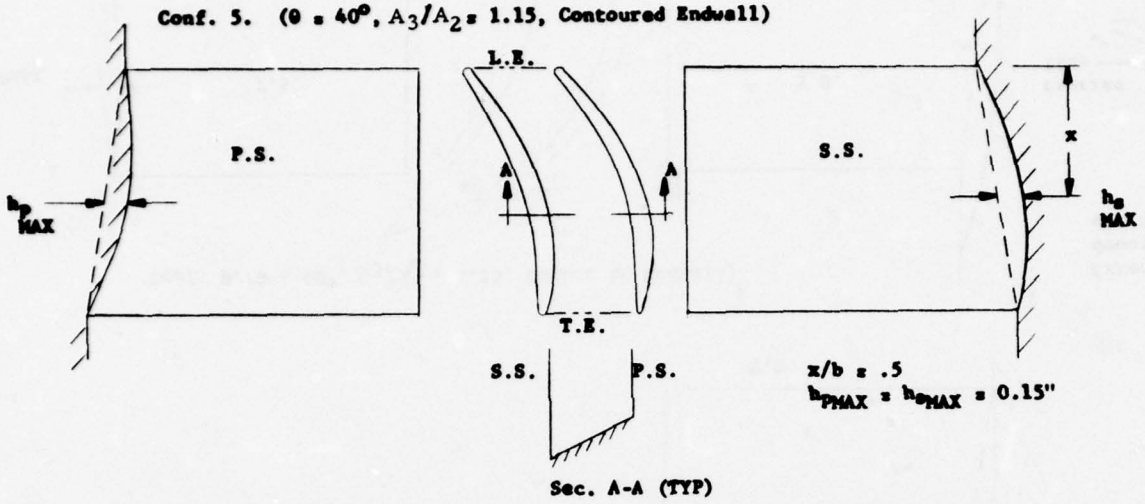


Reversed crossflow (S.S. to P.S.). Discontinuous endwall induced endwall separation near L.E. & T.E. BL flow migrated around T.E. from P.S. to S.S.

TABLE B-1 (CONTINUED)

FLOW VISUALIZATION TESTS

Conf. 5. (θ = 40°, A_3/A_2 = 1.15, Contoured Endwall)



Sec. A-A (TYP)

Results

Smoothed endwalls eliminated endwall separation near L.E. (still separated near T.E.).

Conf. 6. (θ = 40°, A_3/A_2 = 1.15, Contoured Endwall)

Same as Conf. 5 except: x/b = .3
$h_{PMAX} = h_{sMAX}$ = 0.1"

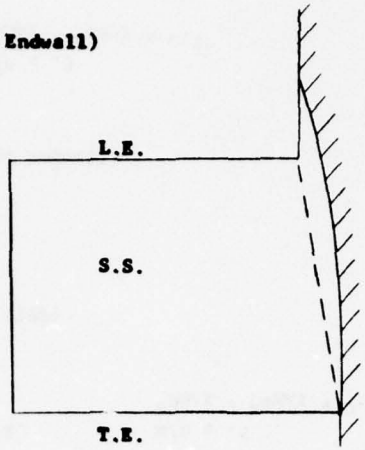
Crossflow shifted back somewhat from P.S. to S.S. Endwall had little separation but flow would not proceed past T.E. except near P.S. Airfoil still had appreciable corner separation starting at about 50% chord on S.S. Concluded airfoil separation caused by too much turning diffusion after significant axial diffusion. Decided to extend axial diffusion on S.S. ahead of airfoil.

TABLE B-1 (CONTINUED)

FLOW VISUALIZATION TESTS

Conf. 7. (θ = 40°, A_3/A_2 = 1.15, Contoured Endwall)

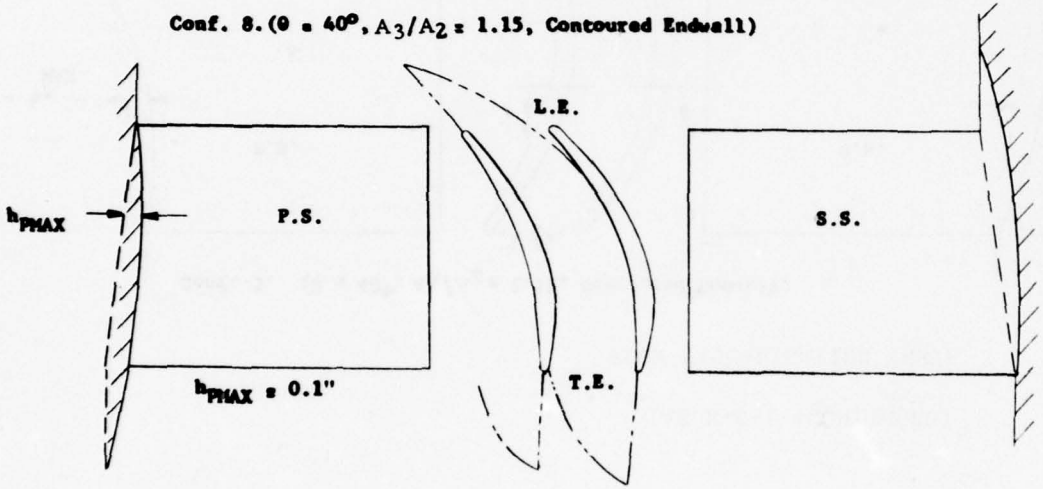
Same as Conf. 6 except:



Results

Airfoil separation possibly slightly retarded. Otherwise same as 6.

Conf. 8. (θ = 40°, A_3/A_2 = 1.15, Contoured Endwall)



Extension of P.S. protrusion downstream to reduce cross channel gradient near T.E.



TABLE B-1 (CONTINUED)

FLOW VISUALIZATION TESTS

Conf. 9. ($\theta = 40^{\circ}$, $A_3/A_2 = 1.15$, **Contoured Endwall**)

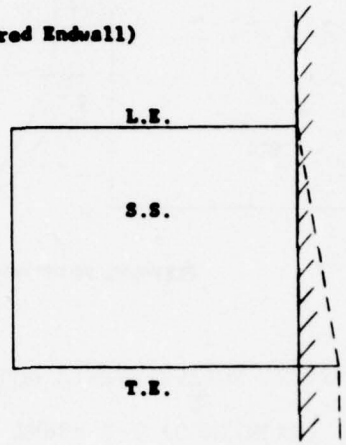
Same as Conf. 8 except: $h_{PMAX} = 0.15"$

Results

Flow did not curve to S.S. until about 70% chord. Reverse pressure gradient downstream of T.E. slightly worse.

Conf. 10. ($\theta = 40^{\circ}$, $A_3/A_2 = 1.15$, **Contoured Endwall**)

Same as Conf. 9 except:

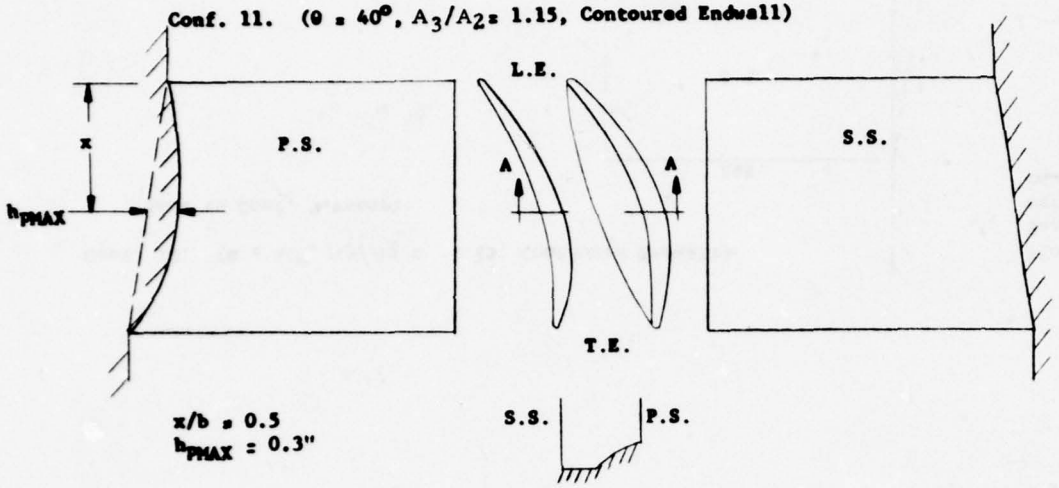


Flow at exit was better. Separation on airfoil S.S. extended 1/2" from endwall compared to 3/4".

TABLE B-1 (CONTINUED)

FLOW VISUALIZATION TESTS

Conf. 11. (θ = 40°, A_3/A_2 = 1.15, Contoured Endwall)



x/b = 0.5
h_{PMAX} = 0.3"

Sec. A-A

Results

Reversed crossflow (S.S. to P.S.). However endwall appears separated with a large area of back flow.



Conf. 12. (θ = 40°, A_3/A_2 = 1.15, Contoured Endwall)

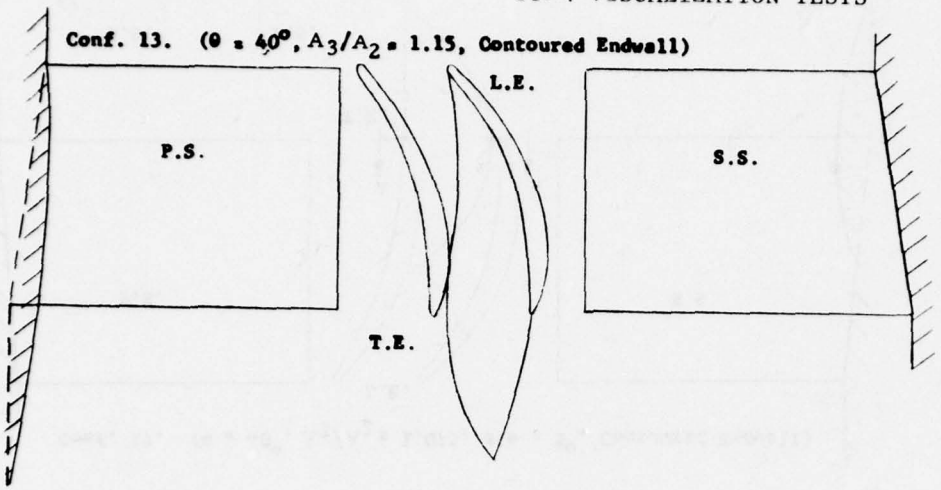
Same as Conf. 11 except: x/b = 0.3

Shifting of P.S. protrusion max. thickness forward aggrevated separation on airfoil S.S.

TABLE B-1 (CONTINUED)

FLOW VISUALIZATION TESTS

Conf. 13. ($\theta = 40^{\circ}$, $A_3/A_2 = 1.15$, Contoured Endwall)

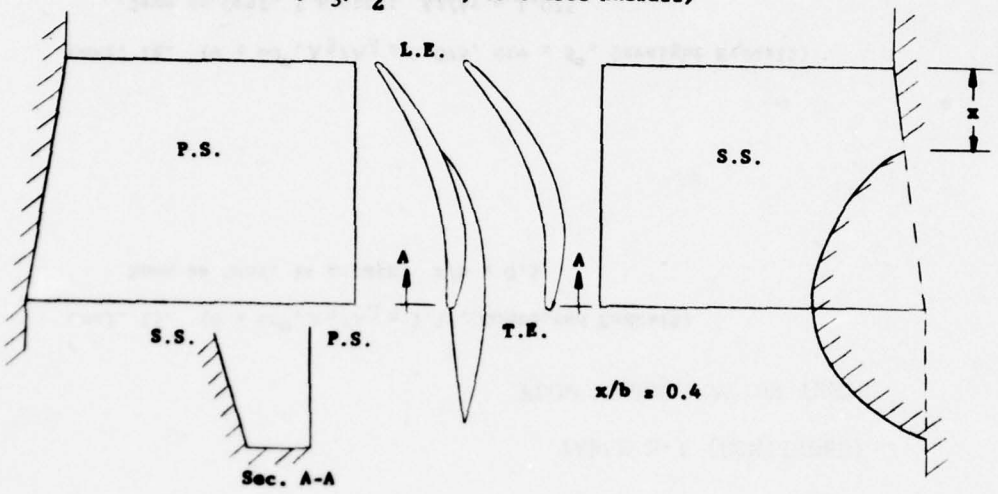


Results

Inlet streamlines funnelled toward S.S. streamlines on protrusion were straight or curved back toward P.S.



Conf. 14. ($\theta = 40^{\circ}$, $A_3/A_2 = 1.15$, Contoured Endwall)



Simulated undercamber near endwall starting at x/b = 0.4 faired downstream. Reduced airfoil separation and endwall crossflow

TABLE B-1 (CONTINUED)

FLOW VISUALIZATION TESTS

Conf. 15. ($\theta = 40^{\circ}$, $A_3/A_2 = 1.15$, Contoured Endwall)

Same as Conf. 14 except: $x/b = 0.5$

Results

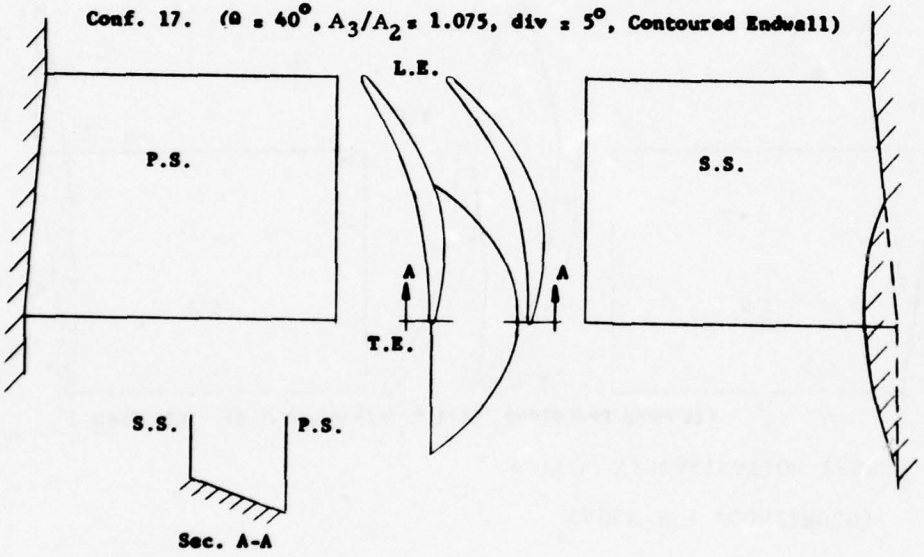
Starting under camber at $x/b = 0.5$ was less effective than $x/b = 0.4$ for Conf. 14.

Conf. 16. ($\theta = 40^{\circ}$, $A_3/A_2 = 1.075$, div = 5°, Straight Endwall)

Same as Conf. 3 except: $A_2/A_1 = 1.075$

Crossflow is less than with $A_3/A_2 = 1.15$. Airfoil separation is delayed.

Conf. 17. ($\theta = 40^{\circ}$, $A_3/A_2 = 1.075$, div = 5°, Contoured Endwall)



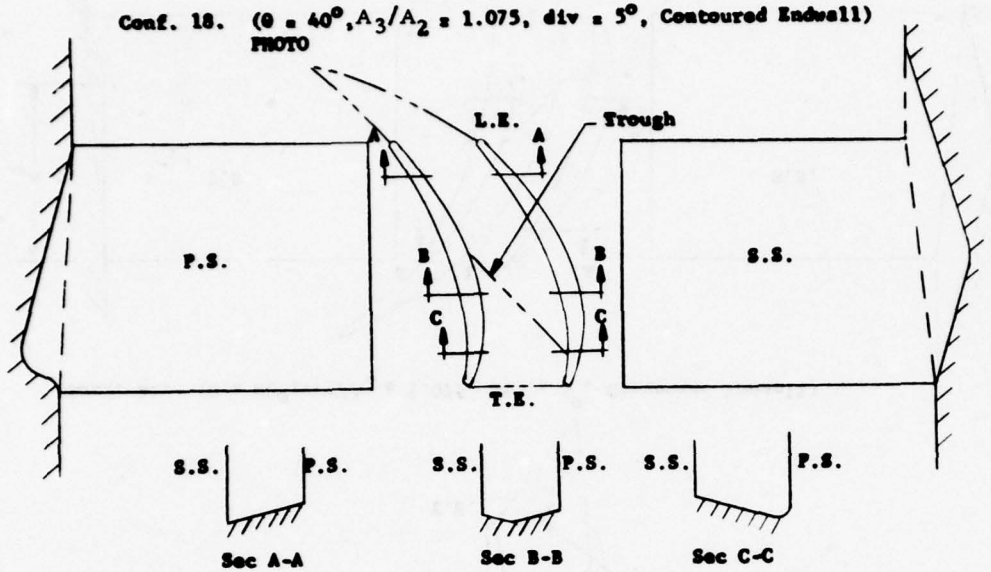
Retarded crossflow. Large reverse flow region formed on endwall downstream of T.E.

TABLE B-1 (CONTINUED)

FLOW VISUALIZATION TESTS

Conf. 18. ($\theta = 40^{\circ}, A_3/A_2 = 1.075$, div = 5°, Contoured Endwall)

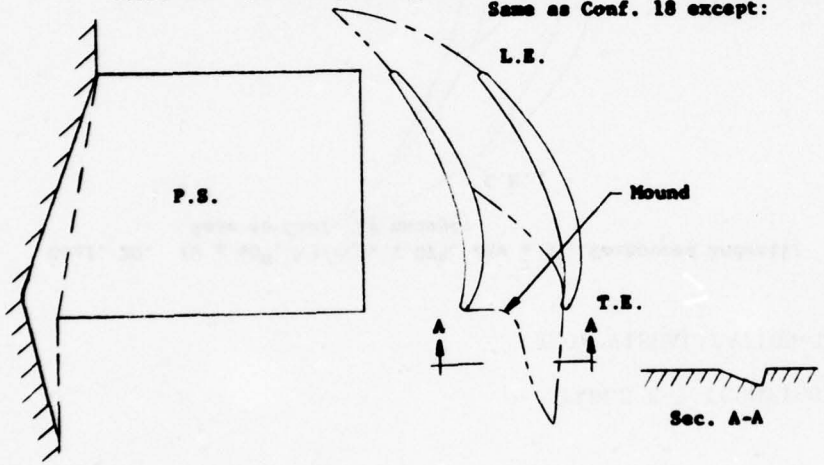
PHOTO



Results

Endwall cross flow began downstream of trough. Rise near P.S. T.E. drove crossflow abruptly toward S.S.

Conf. 19. ($\theta = 40^{\circ}, A_3/A_2 = 1.075$, div = 5°, Contoured Endwall)
Same as Conf. 18 except:

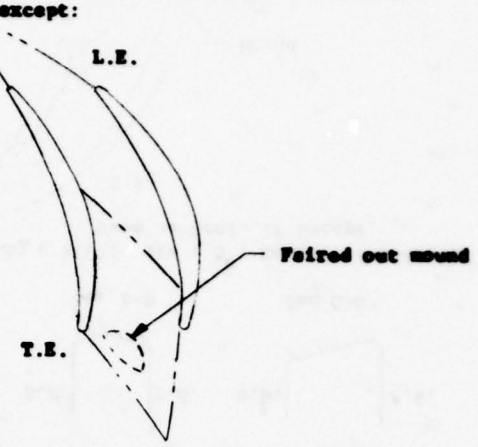


Flow better controlled near P.S. T.E. However endwall separation and reverse flow occurred near S.S. T.E. in area of mound.

TABLE B-1 (CONTINUED)

FLOW VISUALIZATION TESTS

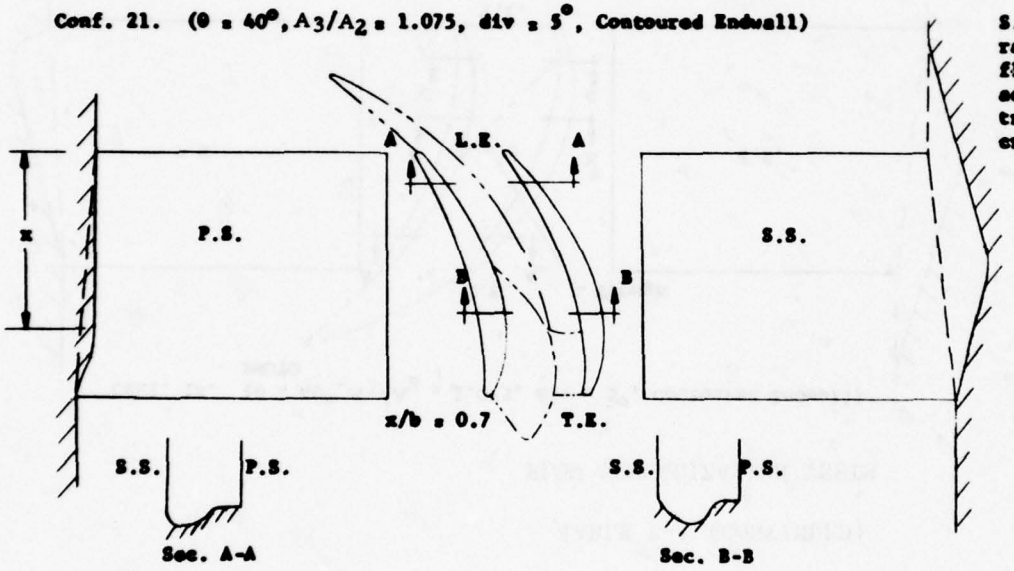
Conf. 20. (θ = 40°, A_3/A_2 = 1.075, div = 5°, Contoured Endwall)
Same as Conf. 19 except:



Results

Less downstream overturning (comparable to Conf. 16 with straight endwall). No significant change in cross channel flow. Conclusion from Conf. 18, 19 and 20 that pressure ramp on S.S. does not seem to control crossflow.

Conf. 21. (θ = 40°, A_3/A_2 = 1.075, div = 5°, Contoured Endwall)

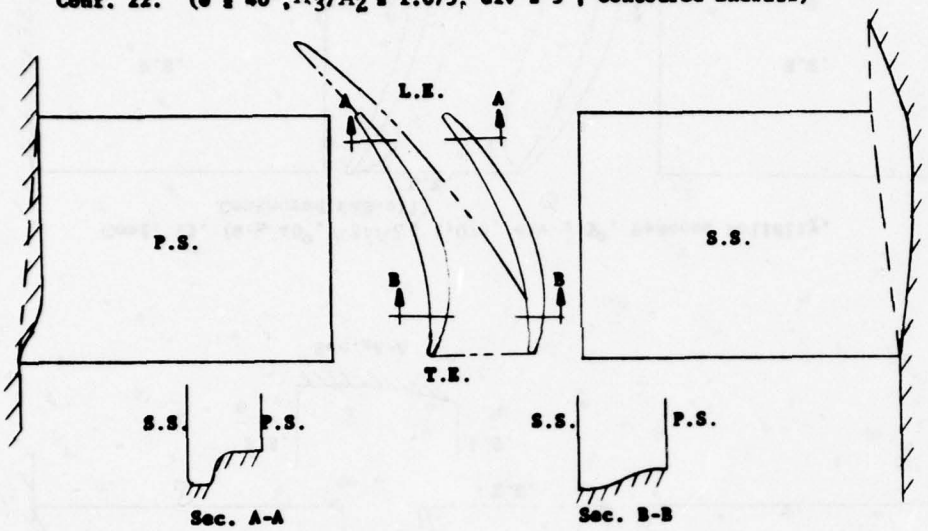


S.S. separation in area of S.S. ramp. P.S. bump seems to keep flow moving downstream. Flow accumulated in remaining trough but appeared to be less cross flow.

TABLE B-1 (CONTINUED)

FLOW VISUALIZATION TESTS

Conf. 22. ($\theta = 40^\circ$, $A_3/A_2 = 1.075$, div = 5°, Contoured Endwall)



Results

Significant endwall separation near S.S.

Conf. 23. ($\theta = 40^\circ$, $A_3/A_2 = 1.075$, div = 5°, Reduced Solidity, Straight Endwall)

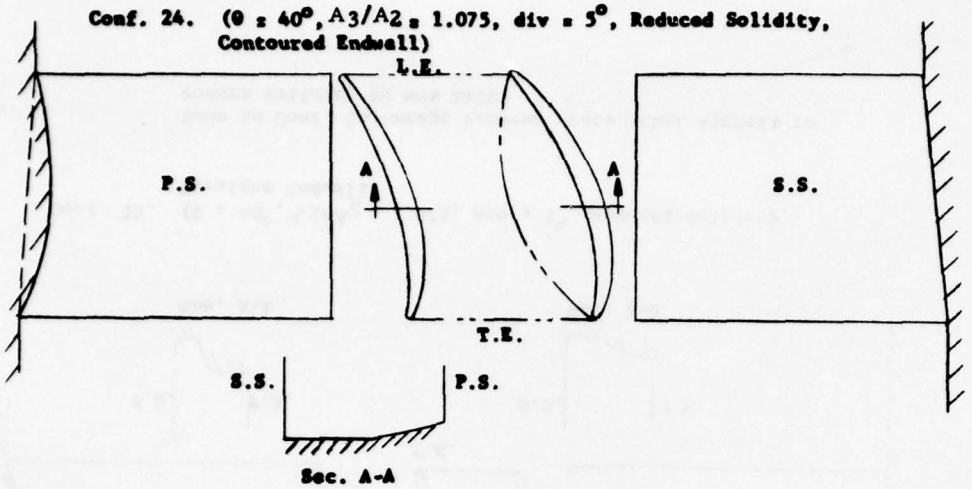
Same as Conf. 16 except removed every other airfoil to reduce solidity by one half.

About same quantity of cross flow reaches S.S., however the increased channel width results in more than half of inlet flow never reaching S.S. Demonstrated that half the design solidity is more than adequate to turn endwall boundary layer. Height of airfoil separation bubble about same as design solidity (5/8").

TABLE B-1 (CONTINUED)

FLOW VISUALIZATION TESTS

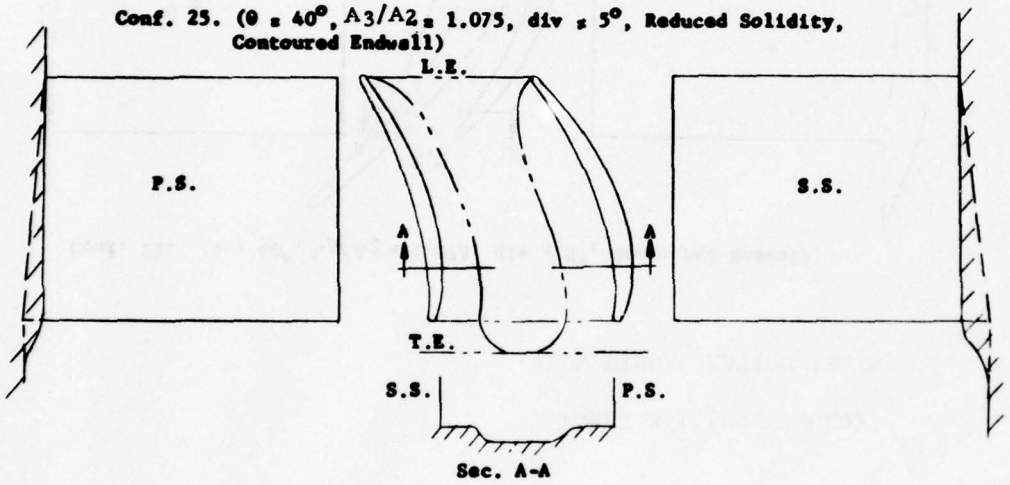
Conf. 24. ($\theta = 40^\circ$, $A_3/A_2 = 1.075$, div = 5°, Reduced Solidity, Contoured Endwall)



Results

Flow near P.S. was better controlled resulting in less overturning. Most noticeable downstream.

Conf. 25. ($\theta = 40^\circ$, $A_3/A_2 = 1.075$, div = 5°, Reduced Solidity, Contoured Endwall)

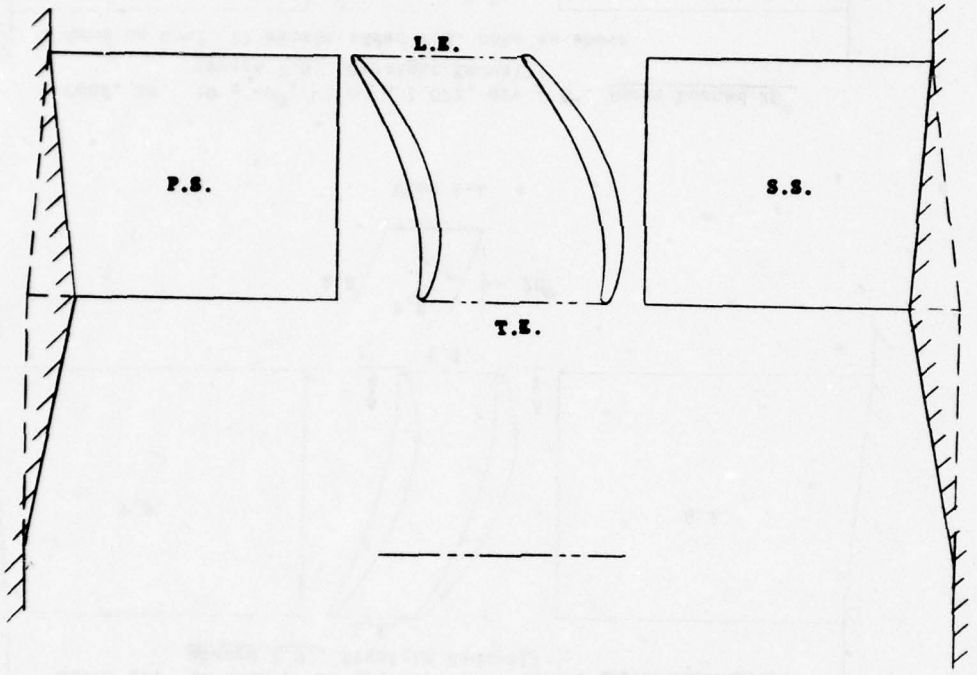


Significant endwall separation as S.S. and P.S. ramps fair into original contour near T.E.

TABLE B-1 (CONTINUED)

FLOW VISUALIZATION TESTS

Conf. 26. ($\theta = 40^{\circ}$, $A_3/A_2 = 1.075$, div $= 5^{\circ}$, Reduced Solidity, Contoured Endwall) PHOTO



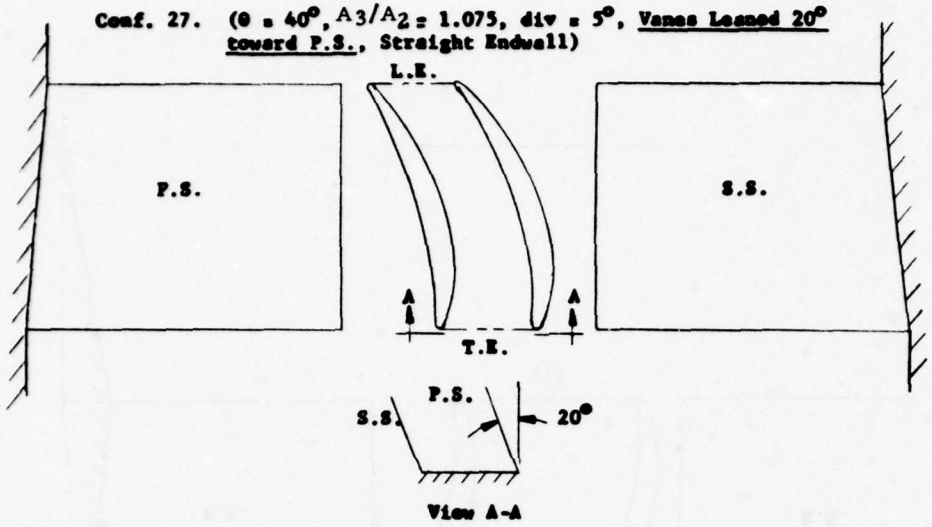
Results

Airfoil corner separation reduced from 5/8" to 1/2". Little or no endwall separation within the channel or downstream.

TABLE B-1 (CONTINUED)

FLOW VISUALIZATION TESTS

Conf. 27. (θ = 40°, A_3/A_2 = 1.075, div = 5°, <u>Vanes Leaned 20° toward P.S.</u>, Straight Endwall)

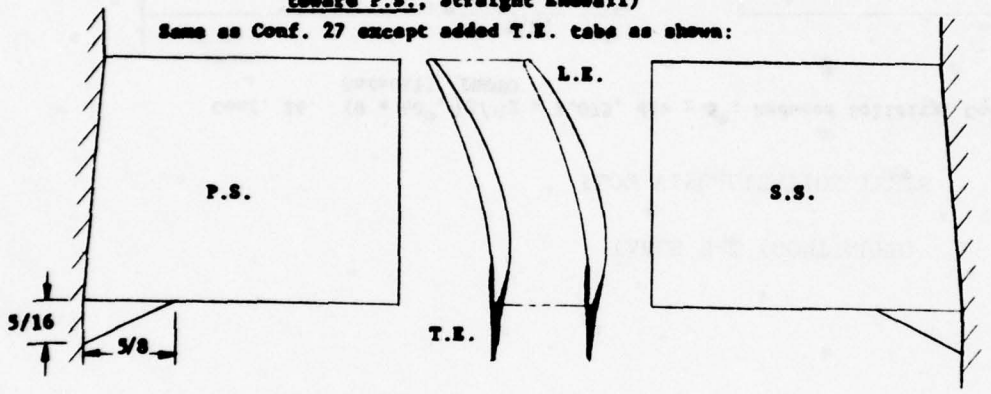


Results

Endwall flow downstream of exit nearly parallel and axial. Channel crossflow is significant but no endwall separation. Airfoil corner separation is large (5/8").

Conf. 28. (θ = 40°, A_3/A_2 = 1.075, div = 5°, <u>Vanes Leaned 20° toward P.S.</u>, Straight Endwall)

Same as Conf. 27 except added T.E. tabs as shown:



Added tabs to uncamber trailing edges. There was no significant benefit.

TABLE B-1 (CONTINUED)

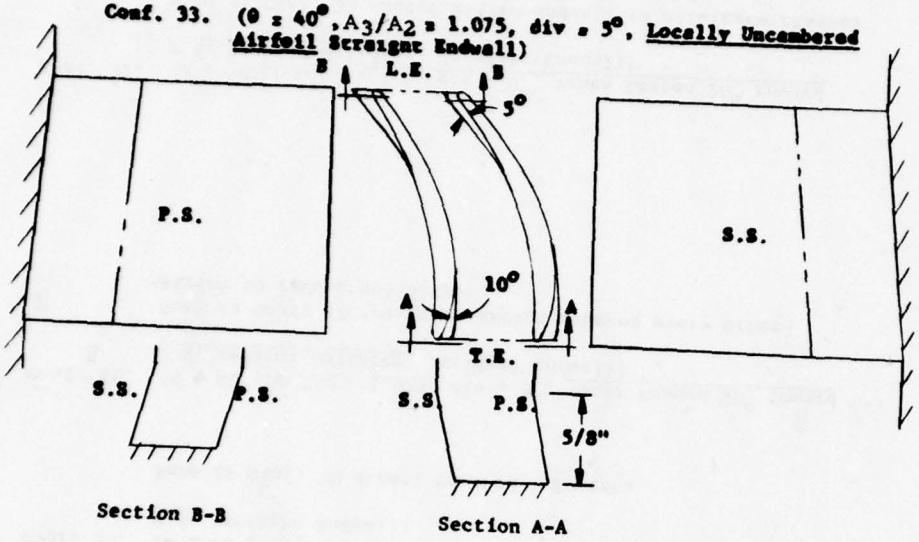
FLOW VISUALIZATION TESTS

		Results
Conf. 29.	(θ = 40°, A_3/A_2 = 1.075, div = 5°, Vanes Leaned 20° toward P.S. straight Endwall)	
	Same as Conf. 28, except added L.E. tabs near endwall with about 5° negative incidence.	No Significant benefit.
Conf. 30.	(θ = 40°, A_3/A_2 = 1.075, div = 5°, Vanes Leaned 20° toward P.S. Straight Endwall)	
	Same as Conf. 29 except removed T.E. tabs.	No significant benefit.
Conf. 31.	(θ = 40°, A_3/A_2 = 1.075, div = 5°, Vanes Leaned 20° toward P.S. Reduced Solidity, Straight Endwall)	
	Same as Conf. 27 (no tabs) except removed every other airfoil to reduce solidity.	Airfoil corner separation as large as before. Crossflow contacting suction surface about the same, however only about 2/3 of channel endwall boundary layer reached suction.
Conf. 32.	(θ = 40°, A_3/A_2 = 1.0, div = 0°, Vanes Leaned 20° toward P.S., Reduced Solidity, Straight Endwall)	
	Same as Conf. 31 except filled endwall to eliminate channel and downstream divergence to give A_2/A_1 = 1.0.	Corner separation essentially eliminated. Apparently eliminated convergence of main flowfield along suction surface. Aft 10% chord separated for most of span. Appears that Airfoil loading has been increased significantly by combination of leaning and reducing A_3/A_2 to 1.0. Crossflow not changed.

TABLE B-1 (CONTINUED)

FLOW VISUALIZATION TESTS

Conf. 33. ($\theta = 40^\circ$, $A_3/A_2 = 1.075$, div = 5°, **Locally Uncambered Airfoil** Straight Endwall)



Results

No significant benefit.

Conf. 34. ($\theta = 40^\circ$, $A_3/A_2 = 1.075$, div = 5°, **Locally Uncambered Airfoil Reduced Solidity**, Straight Endwall)

Same as Conf. 33 except every other airfoil removed to reduce solidity by one half.

Results similar to Conf. 23.

TABLE B-1 (CONTINUED)

FLOW VISUALIZATION TESTS

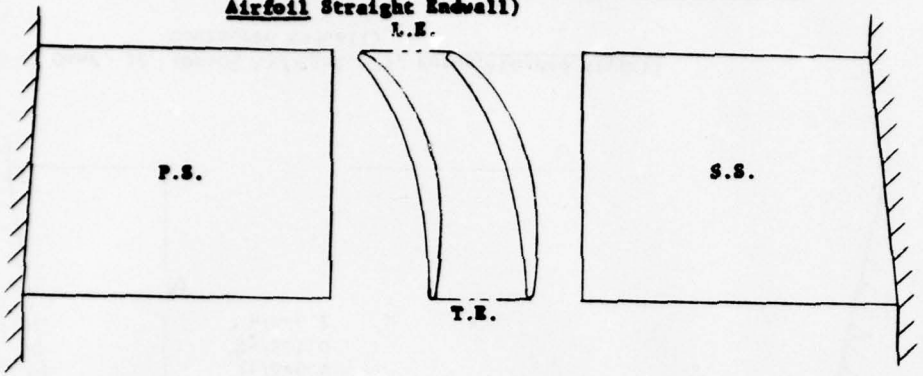
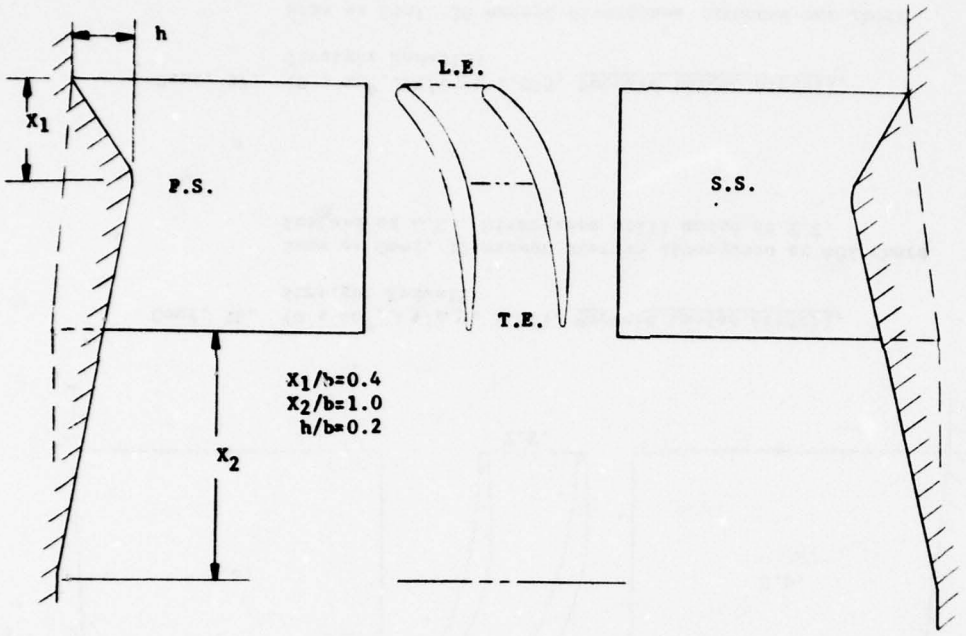
Conf. 35.	($\theta = 40^\circ$, $A_3/A_2 = 1.075$, div = 5°, Forward Loaded Airfoil Straight Endwall) 	Channel cross flow was significantly increased. Airfoil corner separation appears to have increased.
Conf. 36.	($\theta = 40^\circ$, $A_3/A_2 = 1.075$, Forward Loaded Airfoil, Straight Endwall) Same as Conf. 35 except started divergence at 40% chord instead of L.E. Divergence still ended at T.E.	Channel endwall flow separated from suction surface at beginning of divergence resulting in significant reverse flow. Airfoil corner separation initiated at divergence point and extended to nearly 7/8" at T.E.
Conf. 37.	($\theta = 40^\circ$, $A_3/A_2 = 1.075$, Forward Loaded Airfoil, Straight Endwall) Same as Conf. 36 except divergence extended one chord length past T.E.	A noticeable improvement over Conf. 36. No significant endwall separation within channel, but some reverse flow near T.E. Airfoil corner separation 5/8".

TABLE B-1 (CONTINUED)

FLOW VISUALIZATION TESTS

Conf. 38 ($\Theta=40^{\circ}$, $A_3/A_2=1.075$, **Forward Loaded**



Results

L.E. ramp was too abrupt, causing endwall separation ahead of cascade. Flow separated from the endwall as soon as divergence started. Evidently the change in direction from convergence to divergence was much too abrupt. Strong recirculation and reverse flow from downstream of T.E. was observed in separated regions.

Conf. 39. ($\Theta=40^{\circ}$, $A_3/A_2=1.075$, **Forward Loaded Airfoil Contoured Endwall)**

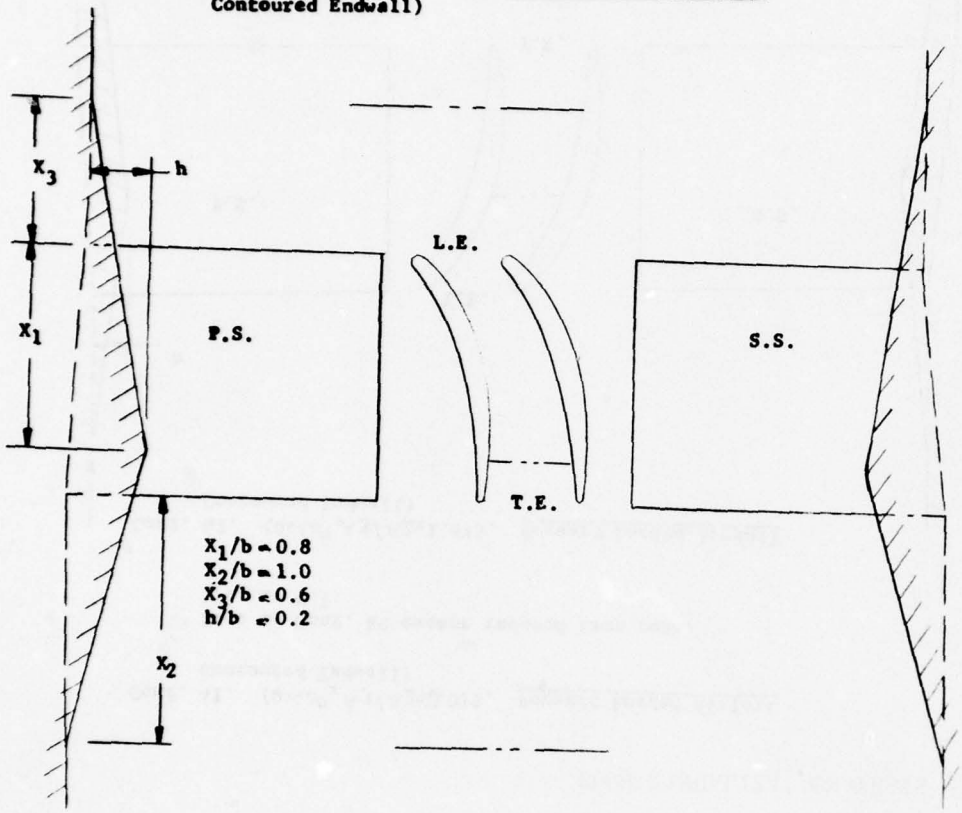
Same as Conf.38 except convergent ramp began 0.6b ahead of L.E.

Inlet flow was good up to peak of ramp. Airfoil corner separation started at peak on suction surface. The separated region extended across the entire channel on the endwall and about 0.4b downstream of T.E. Airfoil corner separation extended about 0.9 inches above endwall at T.E. Strong recirculation and reverse flow from downstream of T.E was observed in separated regions.

TABLE B-1 (CONTINUED)

FLOW VISUALIZATION TESTS

Conf. 40. (θ=40°, A_3/A_2=1.075, **Forward Loaded Airfoil Contoured Endwall**)



Results

Endwall flow was well controlled upstream of convergence peak. Airfoil corner separation started slightly ahead of peak and extended about 0.75 inches above endwall at T.E. Endwall was grossly separated downstream of peak with strong recirculation and reverse flow from downstream of the T.E.

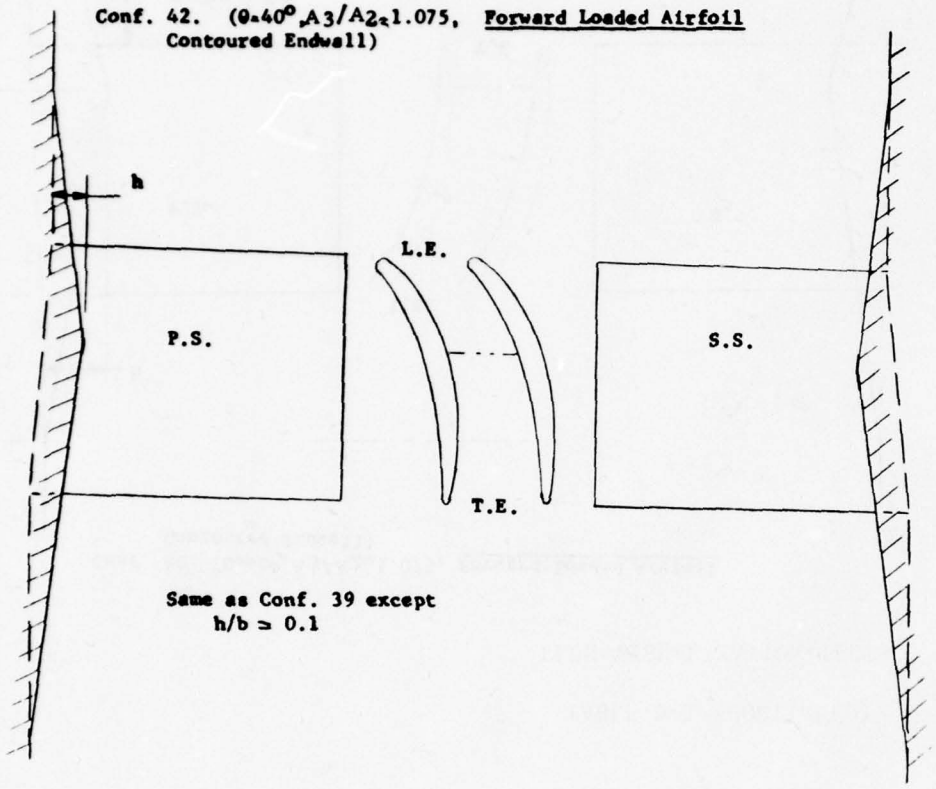
TABLE B-1 (CONTINUED)

FLOW VISUALIZATION TESTS

Conf. 41. (θ=40°, A_3/A_2=1.075, Forward Loaded Airfoil Contoured Endwall)

Same as Conf. 40 except reduced ramp peak, h/b, to 0.1.

Conf. 42. (θ=40°, A_3/A_2=1.075, Forward Loaded Airfoil Contoured Endwall)



Same as Conf. 39 except h/b ≥ 0.1

Results

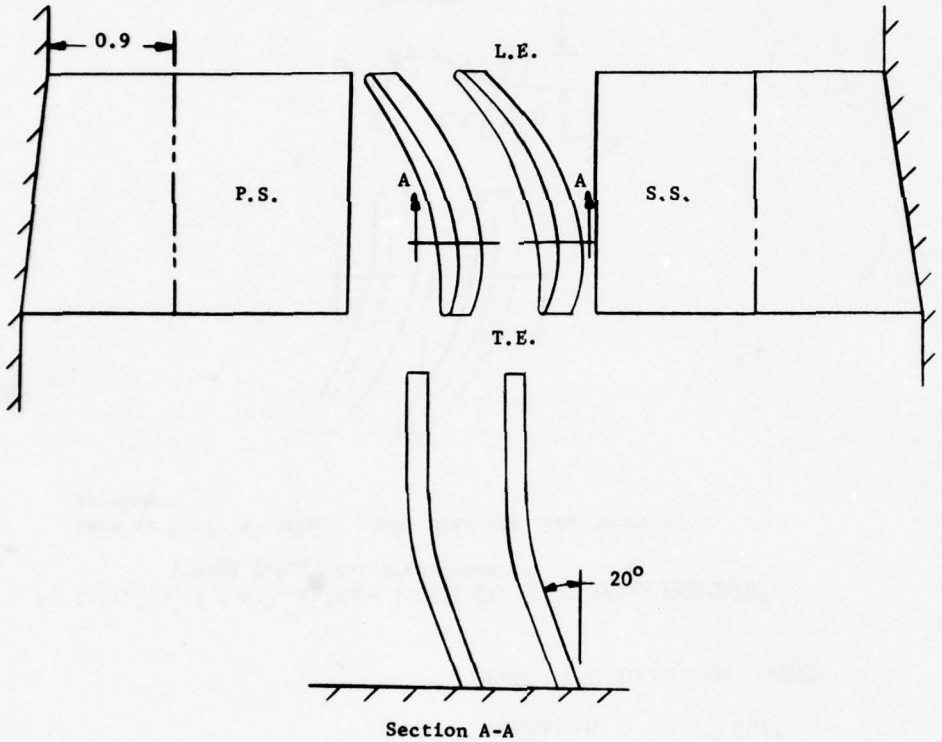
Similar to Conf. 40 except that endwall only separated across half the channel at T.E. Airfoil corner and endwall continued to have strong recirculation and reverse flow from downstream of T.E.

Similar to Conf. 39 with same airfoil corner separation. Endwall separation extended across only half of channel at T.E. All separated regions had strong recirculation and reverse flow from downstream of T.E.

TABLE B-1 (CONTINUED)

FLOW VISUALIZATION TESTS

Conf. 43 ($\theta = 40^{\circ}$, $A_3/A_2 = 1.075$, div = 5°, Vanes Bowed 20° toward P.S., Straight Endwall)



Results

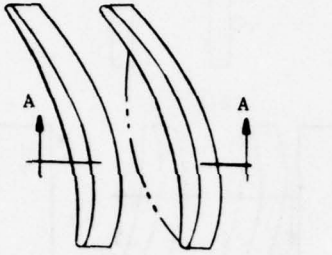
Strong channel crossflow, but no endwall separation. Airfoil corner separation is large extending to bend at TE.

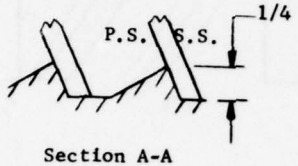
TABLE B-1 (CONTINUED)

FLOW VISUALIZATION TESTS

Conf. 44 ($\theta = 40^{o}$, $A_3/A_2 = 1.075$, div = 5^{o}, Vanes Bowed 20^{o} toward P.S., Contoured Endwall)

Same as Conf. 43 except added pressure side protrusion as shown:





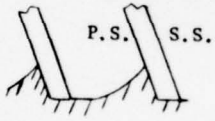
Section A-A

Results

Airfoil corner separation was aggravated. Endwall flow downstream of airfoil reversed toward suction surface from about 1/4 inch behind airfoil.

Conf. 45 ($\theta = 40^{o}$, $A_3/A_2 = 1.075$, div = 5^{o}, Vanes Bowed 20^{o} toward P.S., Contoured Endwall)

Same as Conf. 44 except pressure side protrusion modified to be concave as shown:



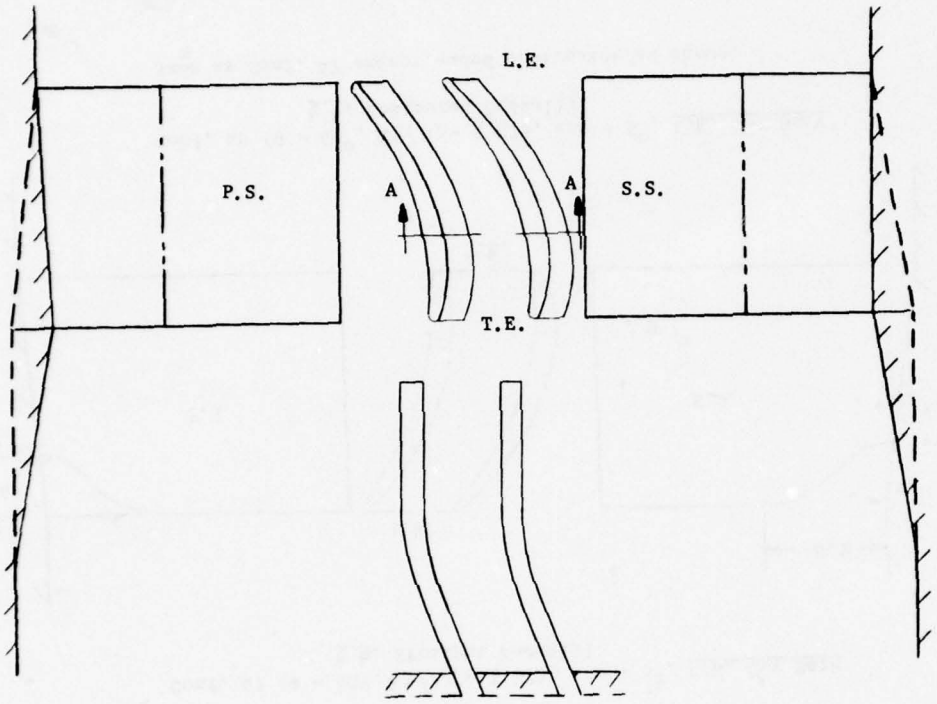
Results

Channel flow improved to exit of cascade. Some downstream reverse flow still occurred.

TABLE B-1 (CONTINUED)

FLOW VISUALIZATION TESTS

Conf. 46 ($\theta = 40^{o}$, $A_3/A_2 = 1.075$, div = 5^{o}, Vanes Bowed 20^{o} toward P.S., Contoured Endwall)



Section A-A

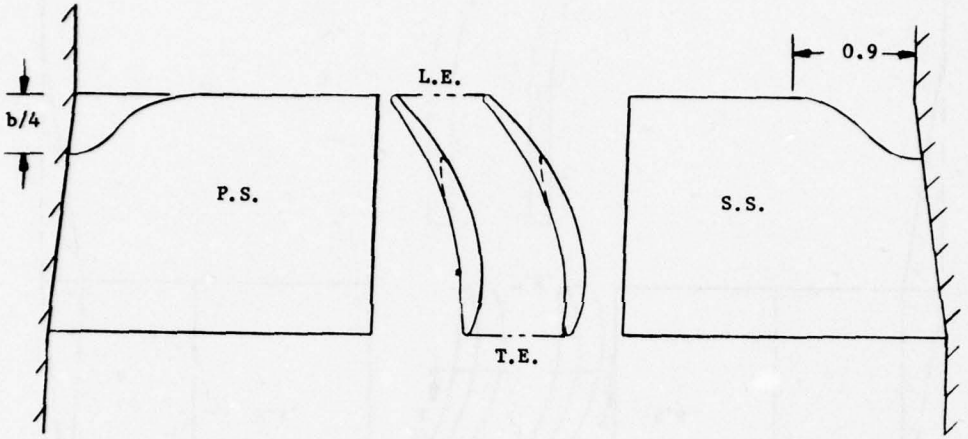
Results

Channel crossflow was low. Corner separation on suction surface was reduced significantly. Airfoils separated uniformly over span about 1/4 inch from TE. Downstream endwall flow was separated in wake projections from airfoils and flow was overturned where not separated.

TABLE B-1 (CONTINUED

FLOW VISUALIZATION TESTS

Conf. 47 ($\theta = 40^{\circ}$, $A_3/A_2 = 1.075$, div = 5°, L.E. Cut Back ½ b, Straight Endwall)

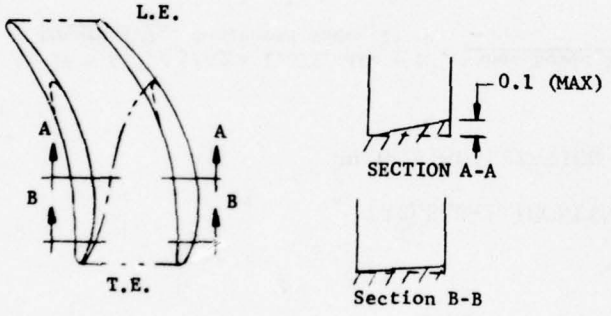


Results

Reduced channel crossflow. Crossflow did not begin until cut back L.E. Moderate suction surface corner separation. Slight downstream reverse flow.

Conf. 48 ($\theta = 40^{\circ}$, $A_3/A_2 = 1.075$, div = 5°, L.E. Cut Back ½ b, Contoured Endwall)

Same as Conf. 47 except added protrusion as shown:



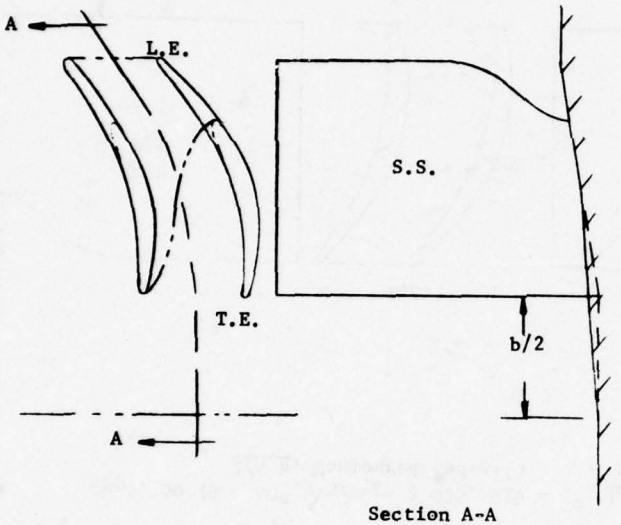
Channel endwall flow diverted toward suction surface by forward edge of protrusion. Very little crossflow on protrusion surface. Endwall flow would not continue beyond T.E. plane.

TABLE B-1 (CONTINUED)

FLOW VISUALIZATION TESTS

Conf. 49 ($\theta = 40^{o}$, $A_3/A_2 = 1.075$, div = 5^{o}, L.E. Cut Back 1/4 b, Contoured Endwall)

Same as Conf. 48 except filled in endwall at T.E. to extend divergent section by 1/2 b as shown:



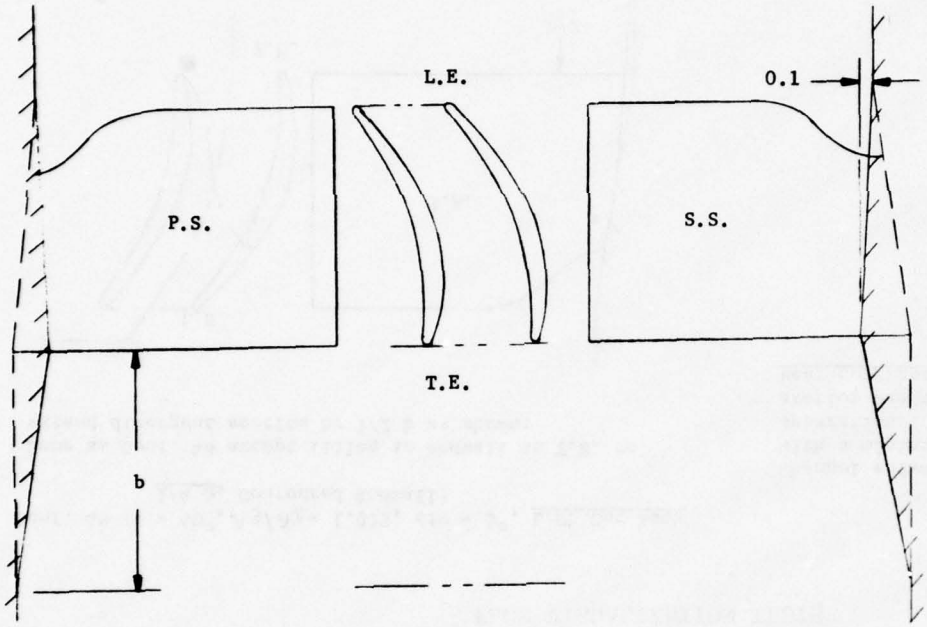
Section A-A

Channel endwall flow proceeded downstream with a minimum of crossflow. No endwall separation. Suction surface corner separation was relatively small. This is best configuration so far.

TABLE B-1 (CONTINUED)

FLOW VISUALIZATION TESTS

Conf. 50 ($\theta = 40^{\circ}$, $A_3/A_2 = 1.075$, div = 5°, L.E. Cut Back 1/4 b, Contoured Endwall)



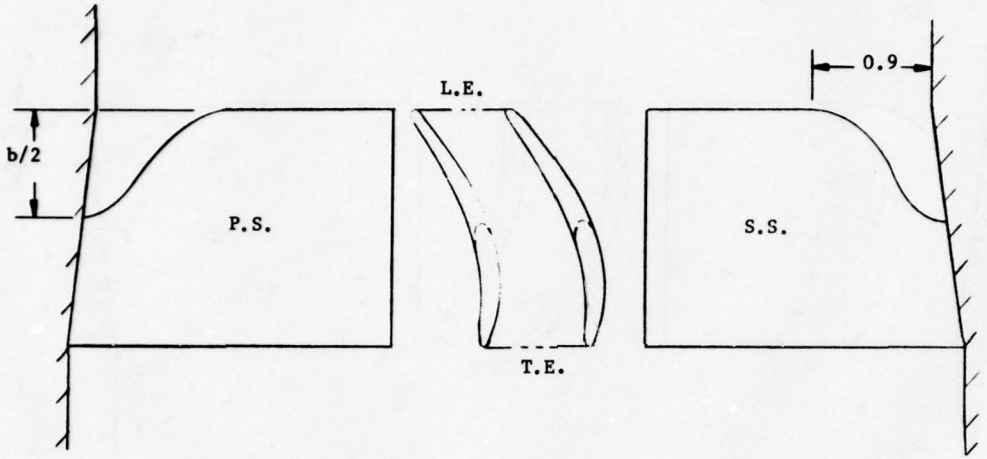
Results

Very little channel cross flow. Small suction surface corner separation. Flow separated badly from divergent section downstream of T.E.

TABLE B-1 (CONTINUED)

FLOW VISUALIZATION TESTS

Conf. 51 ($\theta = 40^{\circ}$, $A_3/A_2 = 1.075$, div = 5°, L.E. Cut Back ½ b, Straight Endwall)



Results

Cross flow retarded until cut back L.E. Strong channel cross-flow downstream of cut back was aggravated by relative high local incidence and large L.E. diameter. Reverse flow on endwall downstream of T.E. to about .2 b.

Conf. 52 ($\theta = 40^{\circ}$, $A_3/A_2 = 1.075$, div = 5°, L.E. Cut Back ½ b, Contoured Endwall)

No significant benefit.

Same as Conf. 51 except added protrusion as shown:

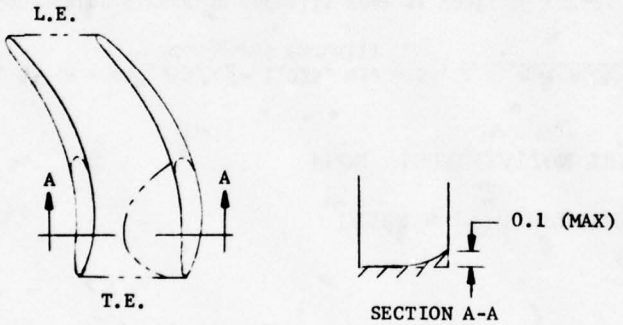


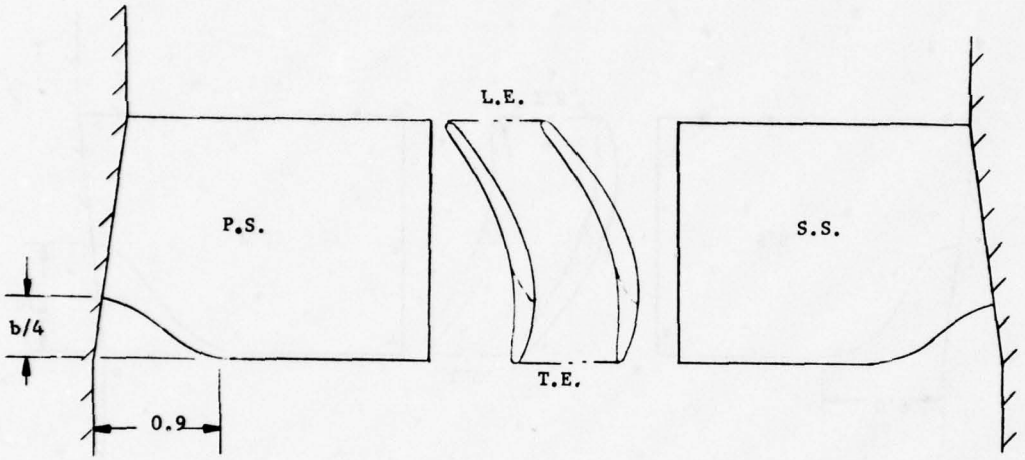
TABLE B-1 (CONTINUED)

FLOW VISUALIZATION TESTS

Conf. 53 ($\theta = 40^{o}$, $A_3/A_2 = 1.025$, div = 5^{o}, L.E. Cut Back ½ b, Contoured Endwall)

Converging-diverging endwalls same as Conf. 50 except L.E. Cut back ½ b instead of ¼ b.

Conf. 54 ($\theta = 40^{o}$, $A_3/A_2 = 1.075$, div = 5^{o}, T.E. Cut Back ½ b, Straight Endwall)



Results

Still appreciable channel crossflow in rear half of channel. No endwall or airfoil reverse flow. Suction surface corner separation was very small.

Very large suction surface corner separation. Channel crossflow was low with no endwall separation. Endwall flow downstream of airfoil was underturned with reverse flow toward suction surface - endwall interface.

TABLE B-1 (CONTINUED)

FLOW VISUALIZATION TESTS

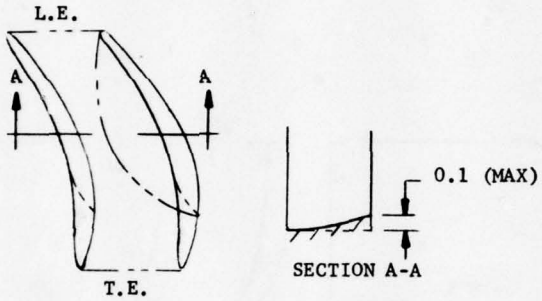
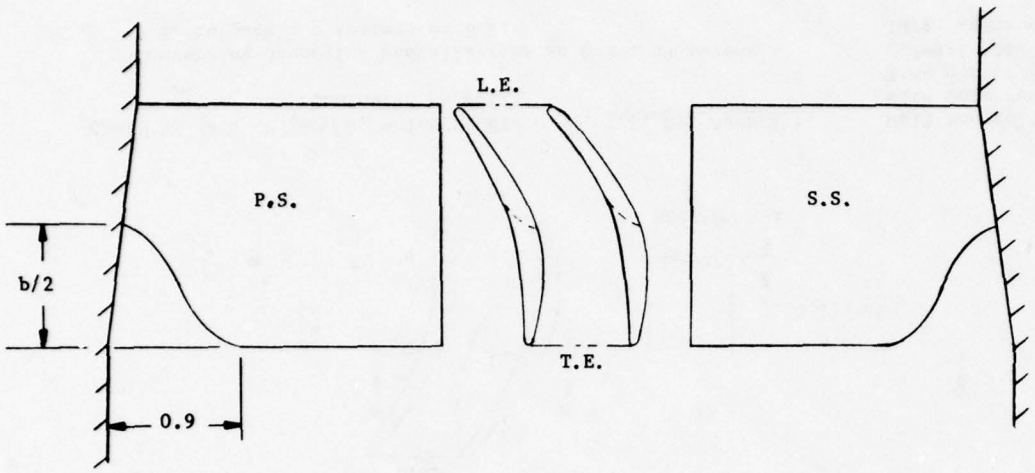
	Results
Conf. 55 ($\theta = 40^{o}, A_3/A_2 = 1.075$, div = 5^{o}, T.E. Cut Back ½ b, Contoured Endwall) Same as Conf. 54 except added protrusion as shown:  	Large endwall separation region near suction surface T.E. blocked flow and diverted it toward pressure surface. Suction side corner had large separation region. Large amount of reverse flow on endwall downstream of airfoil.
Conf. 56 ($\theta = 40^{o}, A_3/A_2 = 1.075$, div = 5^{o}, T.E. Cut Back ½ b, Contoured Endwall) Converging-diverging endwalls same as Conf. 50 except T.E. cutback ½ b instead of L.E.	Well controlled channel endwall flow with most turning in first ½ b. Suction side corner had small separation region. Endwall flow downstream of T.E. indicates large wakes with much separation.

TABLE B-1 (CONTINUED)

FLOW VISUALIZATION TESTS

Conf. 57 ($\theta = 40^{o}, A_3/A_2 = 1.075$, div = 5^{o}, T.E. Cut Back ½ b, Straight Endwall)

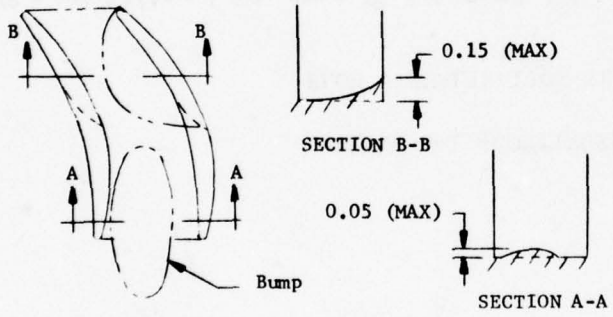


Results

Exit flow field squeezed to center of passage by adjacent unmodified airfoils. Channel endwall flow was slightly underturned with wakes starting from cut back trailing edges. Very little suction surface separation ahead of cut back.

Conf. 58 ($\theta = 40^{o}, A_3/A_2 = 1.075$, div = 5^{o}, T.E. Cut Back ½ b, Contoured Endwall)

Same as Conf. 57 except modified endwall as shown:

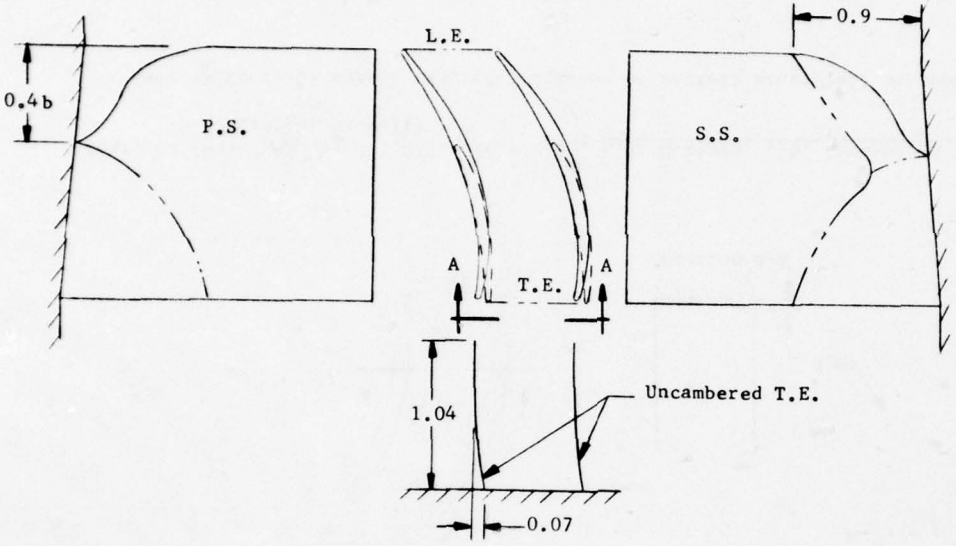


Eliminated some endwall separation by locating bump in wake region.

TABLE B-1 (CONTINUED)

FLOW VISUALIZATION TESTS

Conf. 59 (θ=40°, A_3/A_2 = 1.075, div = 4.3°, L.E. Cutback .4b, Uncambered T.E., Straight Endwall)



VIEW A-A

RESULTS

Improved flow pattern on endwall near cutback L.E. Suction side corner had small separation region. Small amount of reverse flow on endwall downstream of airfoil.

Conf. 60 (θ=40°, A_3/A_2 = 1.075, div = 4.3°, L.E. Cutback .4b, Uncambered T.E., Straight Endwall)

Same results as Conf. 59.

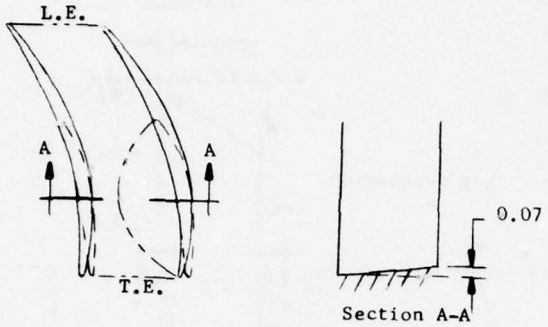
Repeat run of Conf. 59 with smoothed endwalls to improve passage similarity.

TABLE B-1 (CONTINUED)

FLOW VISUALIZATION TESTS

Conf. 61 (θ=40°, A_3/A_2 = 1.075, div = 4.3°, L.E. Cutback .4b, Uncambered T.E., Contoured Endwall)

Same as Conf. 60 except added pressure side protrusion as shown:

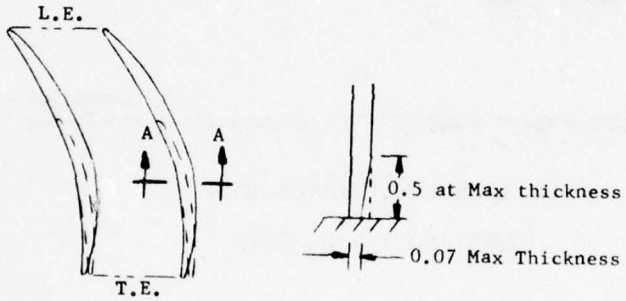


RESULTS

No significant benefit. Appeared to aggrevate endwall reverse flow.

Conf. 62 (θ=40°, A_3/A_2 = 1.075, div = 4.3°, L.E. Cutback .4b, Uncambered T.E. Straight Endwall)

Same as Conf. 59 except reduced thickness of airfoil at endwall as shown:



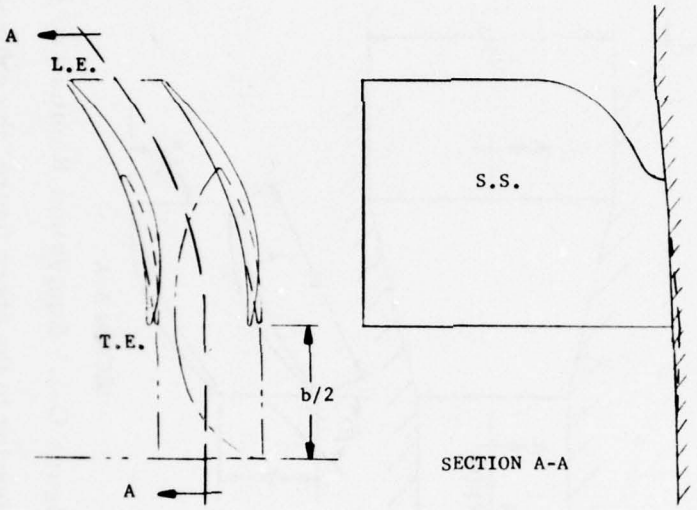
RESULTS

No endwall separation. Reduced amount of endwall reverse flow. No benefit to airfoil suction side corner separation.

TABLE B-1 (CONTINUED)

FLOW VISUALIZATION TESTS

Conf. 63 (θ=40°, A_3/A_2 = 1.075, div = 4.3°, L.E. Cutback .4b, Uncambered T.E., Contoured Endwall)	Results
Same as Conf. 62 except added pressure side protrusion and filled in endwall at T.E. to extend divergent section by 1/2 b as shown:	No endwall separation on reverse flow. Good control of downstream flow. Slightly improved suction side corner separation.



APPENDIX C
DERIVATION OF EQUIVALENT CONICAL ANGLE

DERIVATION OF EQUIVALENT CONICAL ANGLE (θ_{eq})

The equivalent cone angle is found by equating the cascade to a conical diffuser with the same area ratio and length as the cascade.

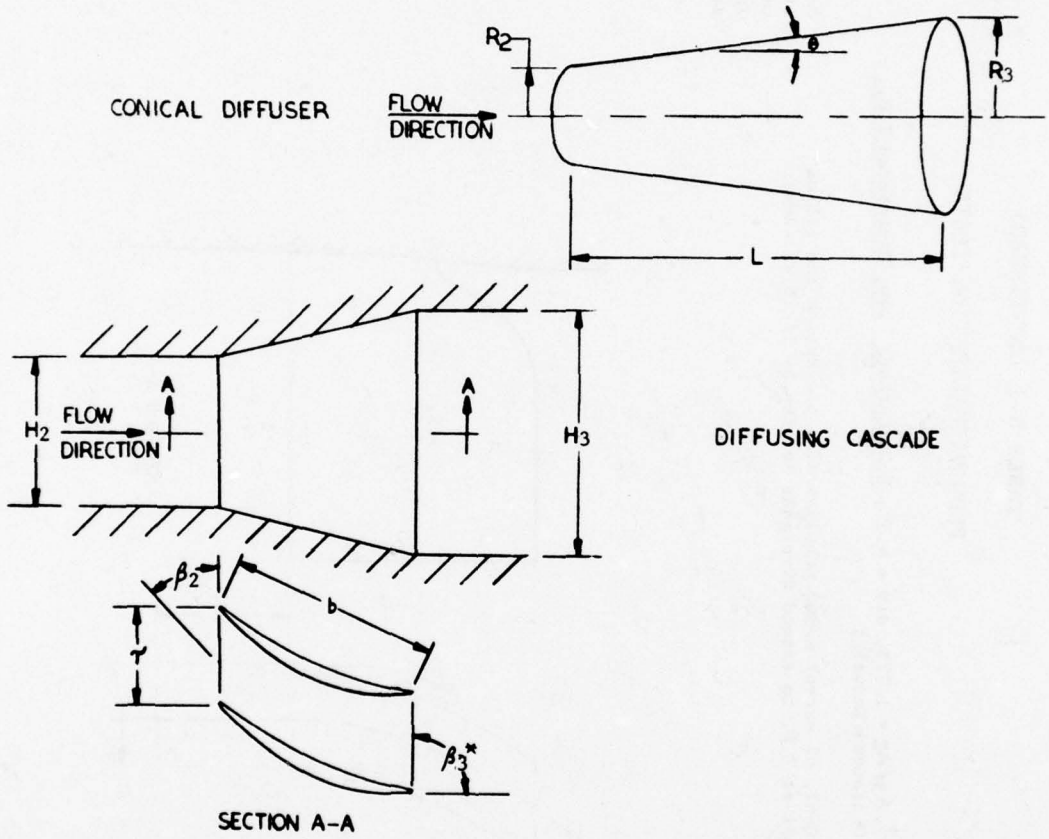


Figure C-1. Equivalent Radius and Cone Angle Derivation

Referring to the above figure, the equivalent radius and cone angle can be defined as:

$$R_{eq} \quad \left(\frac{A}{\pi}\right)^{1/2} \qquad\qquad \tan \theta_{eq} \quad \frac{R3_{eq} - R2_{eq}}{L}$$

where A normal flow area.

For a cascade of airfoils

$$\tan \theta_{eq} = \frac{\left(\frac{A_3}{\pi}\right)^{1/2} - \left(\frac{A_2}{\pi}\right)^{1/2}}{b} = \frac{0.564\left[1 - \left(\frac{A_2}{A_3}\right)^{1/2}\right]}{b/A_3^{1/2}}$$

now

$$A_3 = \tau H_3 \sin (180 - \beta_3^*)$$

or

$$\tan \theta_{eq} = \frac{0.564}{b}\left[\tau H_3 \sin (180 - \beta_3^*)\right]^{1/2}\left[1 - \left(\frac{A_2}{A_3}\right)^{1/2}\right]$$

A compressibility correction is made to θ_{eq} to account for the increase in velocity ratio that accompanies an increase in Mach number for a given conical angle. So that exit Mach number (M_3) can be iteratively solved as a function of area ratio from the isentropic relationship

$$\frac{A_3}{A_2} = \frac{H_3 \sin (180 - \beta_3^*)}{H_2 \sin \beta_2} = \frac{M_2}{M_3}\sqrt{\left[\frac{\left(1 + \frac{\gamma-1}{2} M_3^2\right)}{\left(1 + \frac{\gamma-1}{2} M_2^2\right)}\right]^{\frac{\gamma+1}{\gamma-1}}}$$

The equivalent area ratio $(A_2/A_3)_{eq}$ is then solved as the actual velocity ratio of the cascade for incompressible flow as

$$\left(\frac{A_2}{A_3}\right)_{eq} = \frac{V_3}{V_2} = \frac{M_3}{M_2}\sqrt{\frac{1 + \frac{\gamma-1}{2} M_2^2}{1 + \frac{\gamma-1}{2} M_3^2}}$$

so that the equation for θ_{eq} becomes

$$\theta_{eq} \text{ (deg)} = \tan^{-1}\left\{\frac{0.564}{b}\left[\tau H_3 \sin (180 - \beta_3^*)\right]^{1/2}\left[1 - \left(\frac{A_2}{A_3}\right)_{eq}^{1/2}\right]\right\}$$

or if aspect ratio (AR) is defined as H_2/b

$$\theta_{eq} \text{ (deg)} = \tan^{-1}\left\{0.564\left[\frac{\tau}{b} \text{ AR} \sin (180 - \beta_3^*)\right]^{1/2}\left[1 - \left(\frac{A_2}{A_3}\right)_{eq}^{1/2}\right]\right\}$$

APPENDIX D
PHASE II ANNULAR CASCADE NON-SERIES EGV AIRFOIL SECTIONS AND AIRFOIL COORDINATES

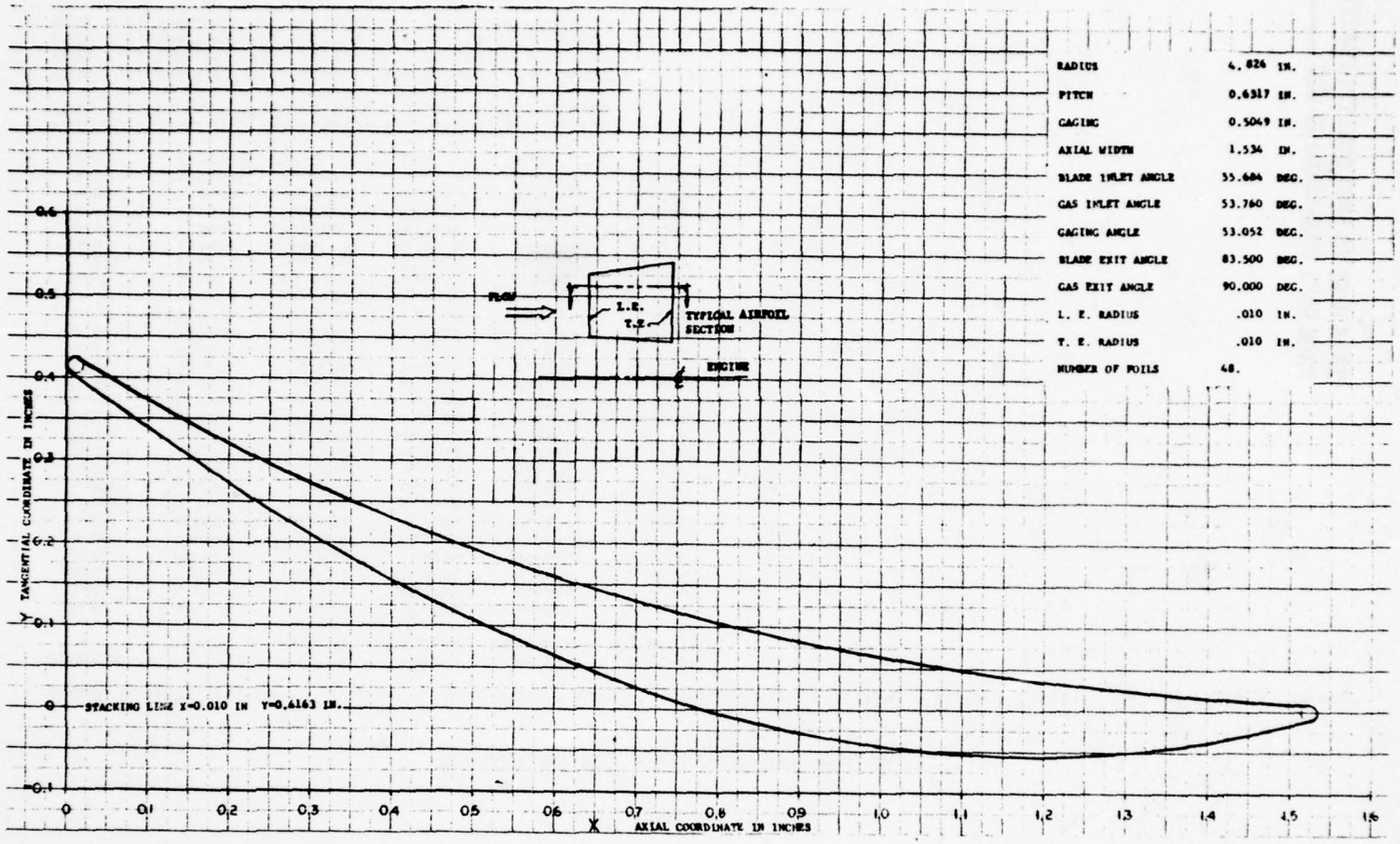


Figure D-1. Phase II Annular Cascade Non-Series EGV Design, Root Section (Scaled)

TABLE D-1

NON-SERIES EGV ROOT SECTION DESIGN

RADIUS OF ROOT SECTION = 4.6260 AXIAL CHORD = 1.5340 ACTUAL CHORD = 1.5759 PITCH = 0.6317 NO. OF FOILS = 48.00

PERCENT X	FOIL X	FOIL Y SUCTION	FOIL Y (CIRCLE)	FOIL Y PRESSURE	FOIL Y (CIRCLE)
0.0	0.0	0.4163	0.4163	0.4163	0.4163
0.01	0.0153	0.3999	0.3999	0.4248	0.4248
0.02	0.0307	0.3885	0.3885	0.4154	0.4154
0.03	0.0460	0.3774	0.3774	0.4061	0.4061
0.04	0.0614	0.3663	0.3663	0.3970	0.3970
0.05	0.0767	0.3554	0.3554	0.3880	0.3880
0.10	0.1534	0.3028	0.3028	0.3455	0.3455
0.15	0.2301	0.2534	0.2534	0.3064	0.3064
0.20	0.3068	0.2074	0.2074	0.2707	0.2707
0.25	0.3835	0.1648	0.1648	0.2380	0.2380
0.30	0.4602	0.1257	0.1257	0.2081	0.2081
0.35	0.5369	0.0901	0.0901	0.1810	0.1810
0.40	0.6136	0.0582	0.0582	0.1563	0.1563
0.45	0.6903	0.0300	0.0300	0.1340	0.1340
0.50	0.7670	0.0056	0.0056	0.1138	0.1138
0.55	0.8437	-0.0150	-0.0150	0.0958	0.0958
0.60	0.9204	-0.0315	-0.0315	0.0797	0.0797
0.65	0.9971	-0.0440	-0.0440	0.0654	0.0654
0.70	1.0738	-0.0522	-0.0522	0.0529	0.0529
0.75	1.1505	-0.0562	-0.0562	0.0420	0.0420
0.80	1.2272	-0.0558	-0.0558	0.0327	0.0327
0.85	1.3039	-0.0508	-0.0508	0.0249	0.0249
0.90	1.3806	-0.0412	-0.0412	0.0185	0.0185
0.95	1.4573	-0.0269	-0.0269	0.0134	0.0134
0.98	1.5033	-0.0159	-0.0159	0.0110	0.0110
0.99	1.5187	-0.0119	-0.0119	0.0103	0.0103
1.00	1.5340	0.0	0.0	0.0	0.0

FOIL L.E. CIRCLE X = 0.0100, Y = 0.4163, R = 0.0100
FOIL T.E. CIRCLE X = 1.5240, Y = 0.0 , R = 0.0100

FOIL L.E. TANGENCY PT. SUCTION X = 0.0040, Y = 0.4083
FOIL L.E. TANGENCY PT. PRESSURE X = 0.0153, Y = 0.4249
FOIL T.E. TANGENCY PT. SUCTION X = 1.5266, Y =-0.0047
FOIL T.E. TANGENCY PT. PRESSURE X = 1.5235, Y =-0.0100

THIS PAGE IS BEST QUALITY PRACTICABLE
FROM COPY FURNISHED TO DDC

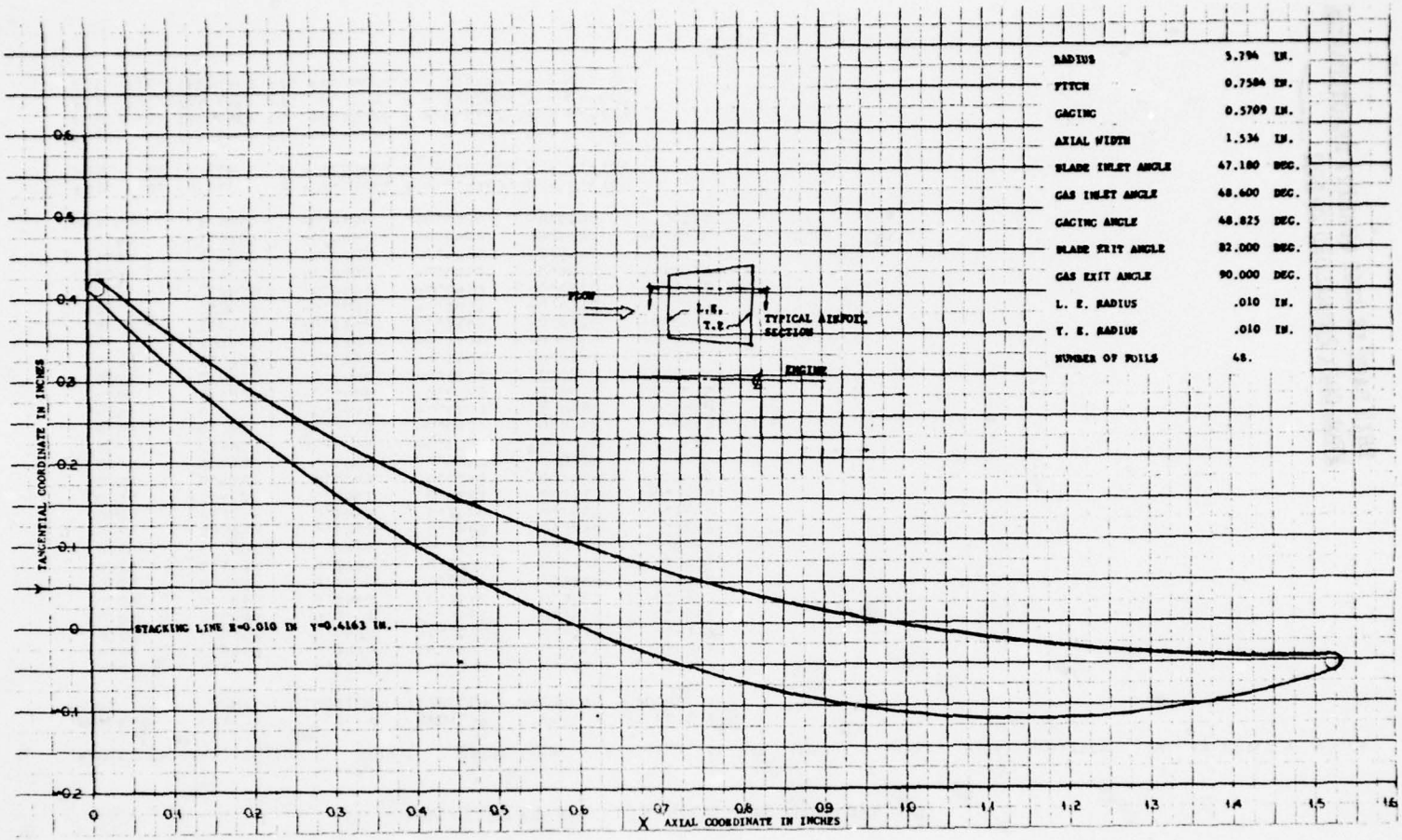


Figure D-2. Phase II Annular Cascade Non-Series EGV Design, Root Section (Scaled)

TABLE D-2

NON-SERIES EGV 1/4 ROOT SECTION DESIGN

RADIUS OF 1/4R SECTION = 5.7940 AXIAL CHORD = 1.5340 ACTUAL CHORD = 1.6031 PITCH = 0.7584 NO. OF FOILS = 48.00

PERCENT °X	FOIL X	FOIL Y SUCTION	FOIL Y (CIRCLE)	FOIL Y PRESSURE	FOIL Y (CIRCLE)
0.0	0.0	0.4163	0.4163	0.4163	0.4163
0.01	0.0153	0.3972	0.3972	0.4248	0.4248
0.02	0.0307	0.3826	0.3826	0.4117	0.4117
0.03	0.0460	0.3681	0.3681	0.3988	0.3988
0.04	0.0614	0.3540	0.3540	0.3862	0.3862
0.05	0.0767	0.3400	0.3400	0.3740	0.3740
0.10	0.1534	0.2739	0.2739	0.3178	0.3178
0.15	0.2301	0.2134	0.2134	0.2685	0.2685
0.20	0.3068	0.1583	0.1583	0.2248	0.2248
0.25	0.3835	0.1086	0.1086	0.1859	0.1859
0.30	0.4602	0.0641	0.0641	0.1513	0.1513
0.35	0.5369	0.0247	0.0247	0.1204	0.1204
0.40	0.6136	-0.0097	-0.0097	0.0929	0.0929
0.45	0.6903	-0.0392	-0.0392	0.0685	0.0685
0.50	0.7670	-0.0638	-0.0638	0.0469	0.0469
0.55	0.8437	-0.0837	-0.0837	0.0280	0.0280
0.60	0.9204	-0.0988	-0.0988	0.0116	0.0116
0.65	0.9971	-0.1094	-0.1094	-0.0024	-0.0024
0.70	1.0738	-0.1154	-0.1154	-0.0143	-0.0143
0.75	1.1505	-0.1170	-0.1170	-0.0240	-0.0240
0.80	1.2272	-0.1142	-0.1142	-0.0316	-0.0316
0.85	1.3039	-0.1071	-0.1071	-0.0373	-0.0373
0.90	1.3806	-0.0957	-0.0957	-0.0410	-0.0410
0.95	1.4573	-0.0802	-0.0802	-0.0429	-0.0429
0.98	1.5033	-0.0689	-0.0689	-0.0431	-0.0431
0.99	1.5187	-0.0648	-0.0648	-0.0430	-0.0430
1.00	1.5340	-0.0530	-0.0530	-0.0530	-0.0530

FOIL L.E. CIRCLE X = 0.0100, Y = 0.4163, R = 0.0100
FOIL T.E. CIRCLE X = 1.5240, Y =-0.0530, R = 0.0100

FOIL L.E. TANGENCY PT. SUCTION X = 0.0030, Y = 0.4092
FOIL L.E. TANGENCY PT. PRESSURE X = 0.0167, Y = 0.4239
FOIL T.E. TANGENCY PT. SUCTION X = 1.5266, Y =-0.0627
FOIL T.E. TANGENCY PT. PRESSURE X = 1.5234, Y =-0.0430

THIS PAGE IS BEST QUALITY PRACTICABLE
FROM COPY FURNISHED TO DDC

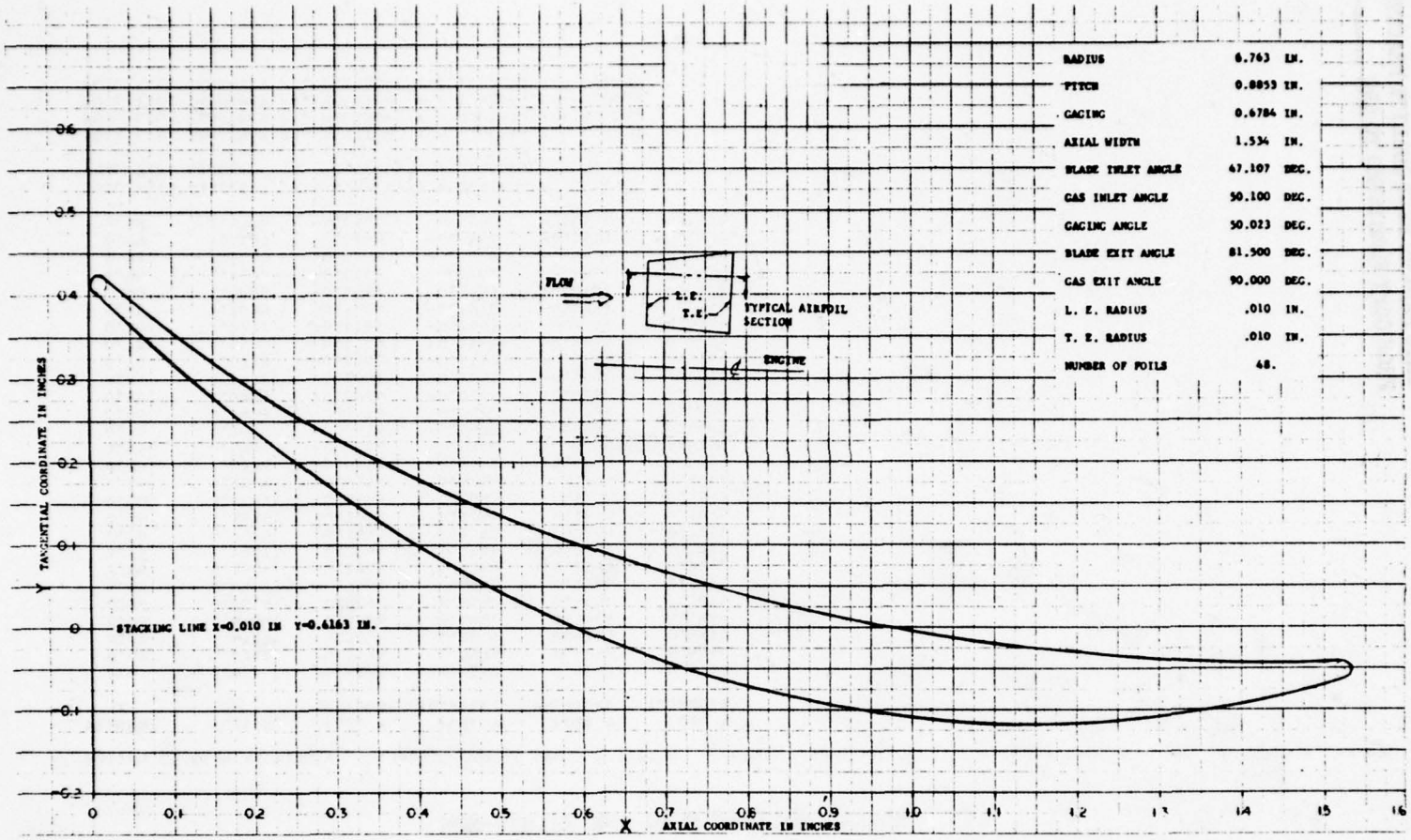


Figure D-3. Phase II Annular Cascade Non-Series EGV Design, 1/4 Root Section (Scaled)

TABLE D-3

NON-SERIES EGV MEAN SECTION DESIGN

RADIUS OF MEAN SECTION = 0.7630 AXIAL CHORD = 1.5340 ACTUAL CHORD = 1.6031 PITCH = 0.8853 NO. OF FOILS = 48.00

PERCENT X	FOIL X	FOIL Y SUCTION	FOIL Y (CIRCLE)	FOIL Y PRESSURE	FOIL Y (CIRCLE)
0.0	0.0	0.4163	0.4163	0.4163	0.4163
0.01	0.0153	0.3974	0.3974	0.4248	0.4248
0.02	0.0307	0.3829	0.3829	0.4115	0.4115
0.03	0.0460	0.3686	0.3686	0.3984	0.3984
0.04	0.0614	0.3546	0.3546	0.3858	0.3858
0.05	0.0767	0.3408	0.3408	0.3735	0.3735
0.10	0.1534	0.2749	0.2749	0.3177	0.3177
0.15	0.2301	0.2144	0.2144	0.2689	0.2689
0.20	0.3068	0.1593	0.1593	0.2259	0.2259
0.25	0.3835	0.1095	0.1095	0.1875	0.1875
0.30	0.4602	0.0649	0.0649	0.1532	0.1532
0.35	0.5369	0.0254	0.0254	0.1224	0.1224
0.40	0.6136	-0.0091	-0.0091	0.0947	0.0947
0.45	0.6903	-0.0386	-0.0386	0.0700	0.0700
0.50	0.7670	-0.0633	-0.0633	0.0481	0.0481
0.55	0.8437	-0.0833	-0.0833	0.0286	0.0286
0.60	0.9204	-0.0985	-0.0985	0.0116	0.0116
0.65	0.9971	-0.1091	-0.1091	-0.0030	-0.0030
0.70	1.0738	-0.1152	-0.1152	-0.0154	-0.0154
0.75	1.1505	-0.1169	-0.1169	-0.0255	-0.0255
0.80	1.2272	-0.1141	-0.1141	-0.0334	-0.0334
0.85	1.3039	-0.1070	-0.1070	-0.0391	-0.0391
0.90	1.3806	-0.0957	-0.0957	-0.0426	-0.0426
0.95	1.4573	-0.0802	-0.0802	-0.0438	-0.0438
0.98	1.5033	-0.0689	-0.0689	-0.0434	-0.0434
0.99	1.5187	-0.0648	-0.0648	-0.0431	-0.0431
1.00	1.5340	-0.0530	-0.0530	-0.0530	-0.0530

FOIL L.E. CIRCLE X = 0.0100, Y = 0.4163, R = 0.0100
FOIL T.E. CIRCLE X = 1.5240, Y =-0.0530, R = 0.0100

FOIL L.E. TANGENCY PT. SUCTION X = 0.0031, Y = 0.4091
FOIL L.E. TANGENCY PT. PRESSURE X = 0.0167, Y = 0.4236
FOIL T.E. TANGENCY PT. SUCTION X = 1.5266, Y =-0.0627
FOIL T.E. TANGENCY PT. PRESSURE X = 1.5237, Y =-0.0430

THIS PAGE IS BEST QUALITY PRACTICABLE
FROM COPY FURNISHED TO DDC

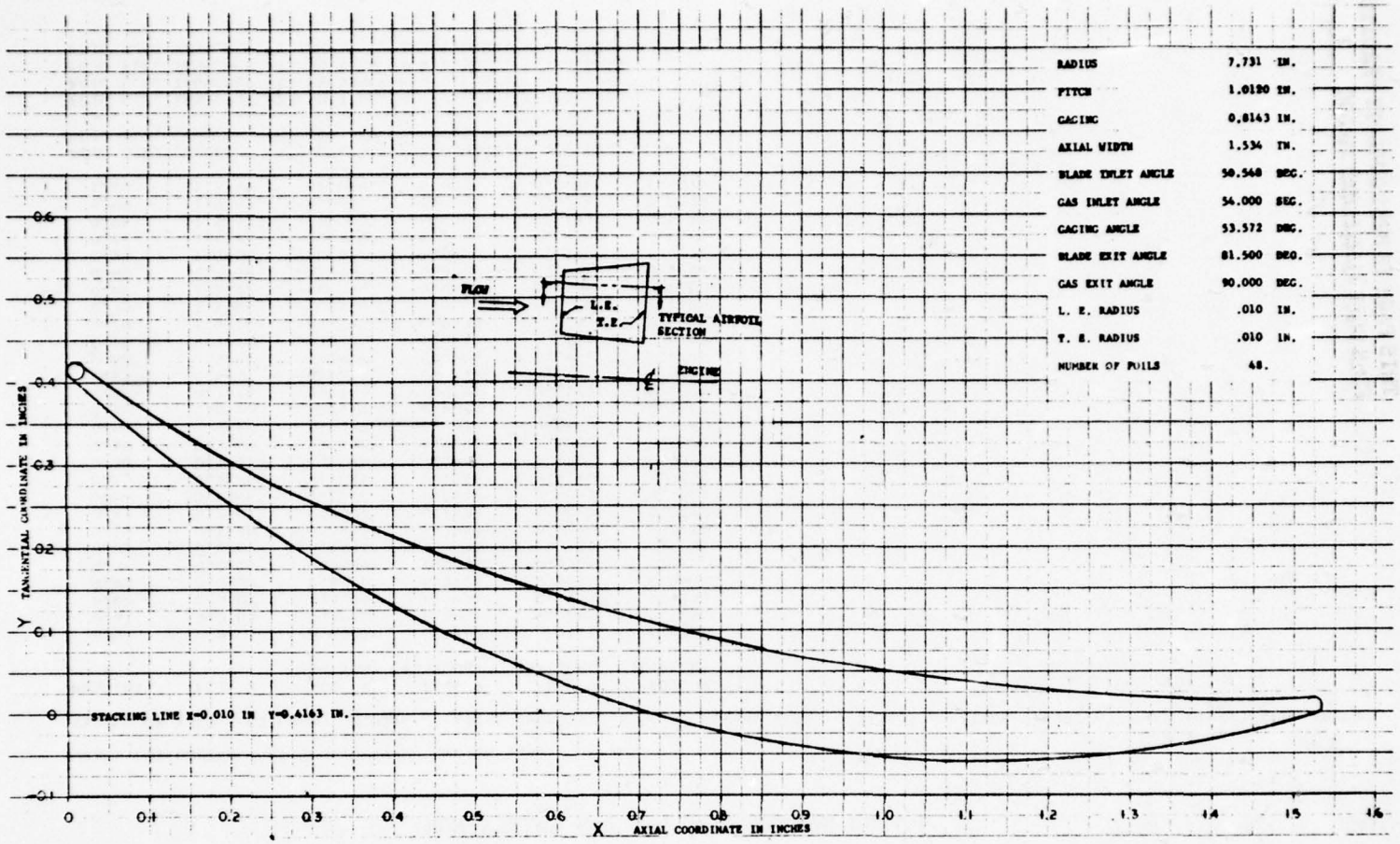


Figure D-4. Phase II Annular Cascade Non-Series EGV Design, ¼ Tip Section (Scaled)

TABLE D-4

NON-SERIES EGV 1/4 TIP SECTION DESIGN

WPAFB EGV CONTRACT EXIT GUIDE VANE DESIGN SCALED SF=.59

RADIUS OF 1/4T SECTION = 7.7310 AXIAL CHORD = 1.5340 ACTUAL CHORD = 1.5665 PITCH = 1.0120 NO. OF FOILS = 48.00

PERCENT X	FOIL X	FOIL Y SUCTION	FOIL Y (CIRCLE)	FOIL Y PRESSURE	FOIL Y (CIRCLE)
0.0	0.0	0.4163	0.4163	0.4163	0.4163
0.01	0.0153	0.3985	0.3985	0.4248	0.4248
0.02	0.0307	0.3854	0.3854	0.4131	0.4131
0.03	0.0460	0.3726	0.3726	0.4018	0.4018
0.04	0.0614	0.3599	0.3599	0.3909	0.3909
0.05	0.0767	0.3475	0.3475	0.3803	0.3803
0.10	0.1534	0.2881	0.2881	0.3319	0.3319
0.15	0.2301	0.2337	0.2337	0.2897	0.2897
0.20	0.3068	0.1842	0.1842	0.2523	0.2523
0.25	0.3835	0.1395	0.1395	0.2190	0.2190
0.30	0.4602	0.0996	0.0996	0.1891	0.1891
0.35	0.5369	0.0643	0.0643	0.1622	0.1622
0.40	0.6136	0.0337	0.0337	0.1380	0.1380
0.45	0.6903	0.0075	0.0075	0.1163	0.1163
0.50	0.7670	-0.0141	-0.0141	0.0970	0.0970
0.55	0.8437	-0.0314	-0.0314	0.0799	0.0799
0.60	0.9204	-0.0444	-0.0444	0.0648	0.0648
0.65	0.9971	-0.0531	-0.0531	0.0519	0.0519
0.70	1.0738	-0.0576	-0.0576	0.0409	0.0409
0.75	1.1505	-0.0580	-0.0580	0.0320	0.0320
0.80	1.2272	-0.0543	-0.0543	0.0250	0.0250
0.85	1.3039	-0.0466	-0.0466	0.0200	0.0200
0.90	1.3806	-0.0350	-0.0350	0.0172	0.0172
0.95	1.4573	-0.0194	-0.0194	0.0164	0.0164
0.98	1.5033	-0.0083	-0.0083	0.0171	0.0171
0.99	1.5187	-0.0043	-0.0043	0.0174	0.0174
1.00	1.5340	0.0076	0.0076	0.0076	0.0076

FOIL L.E. CIRCLE X = 0.0100, Y = 0.4163, R = 0.0100
FOIL T.E. CIRCLE X = 1.5240, Y = 0.0076, R = 0.0100

FOIL L.E. TANGENCY PT. SUCTION X = 0.0035, Y = 0.4088
FOIL L.E. TANGENCY PT. PRESSURE X = 0.0162, Y = 0.4242
FOIL T.E. TANGENCY PT. SUCTION X = 1.5206, Y =-0.0021
FOIL T.E. TANGENCY PT. PRESSURE X = 1.5237, Y = 0.0178

THIS PAGE IS BEST QUALITY PRACTICABLE
FROM COPY FURNISHED TO DDC

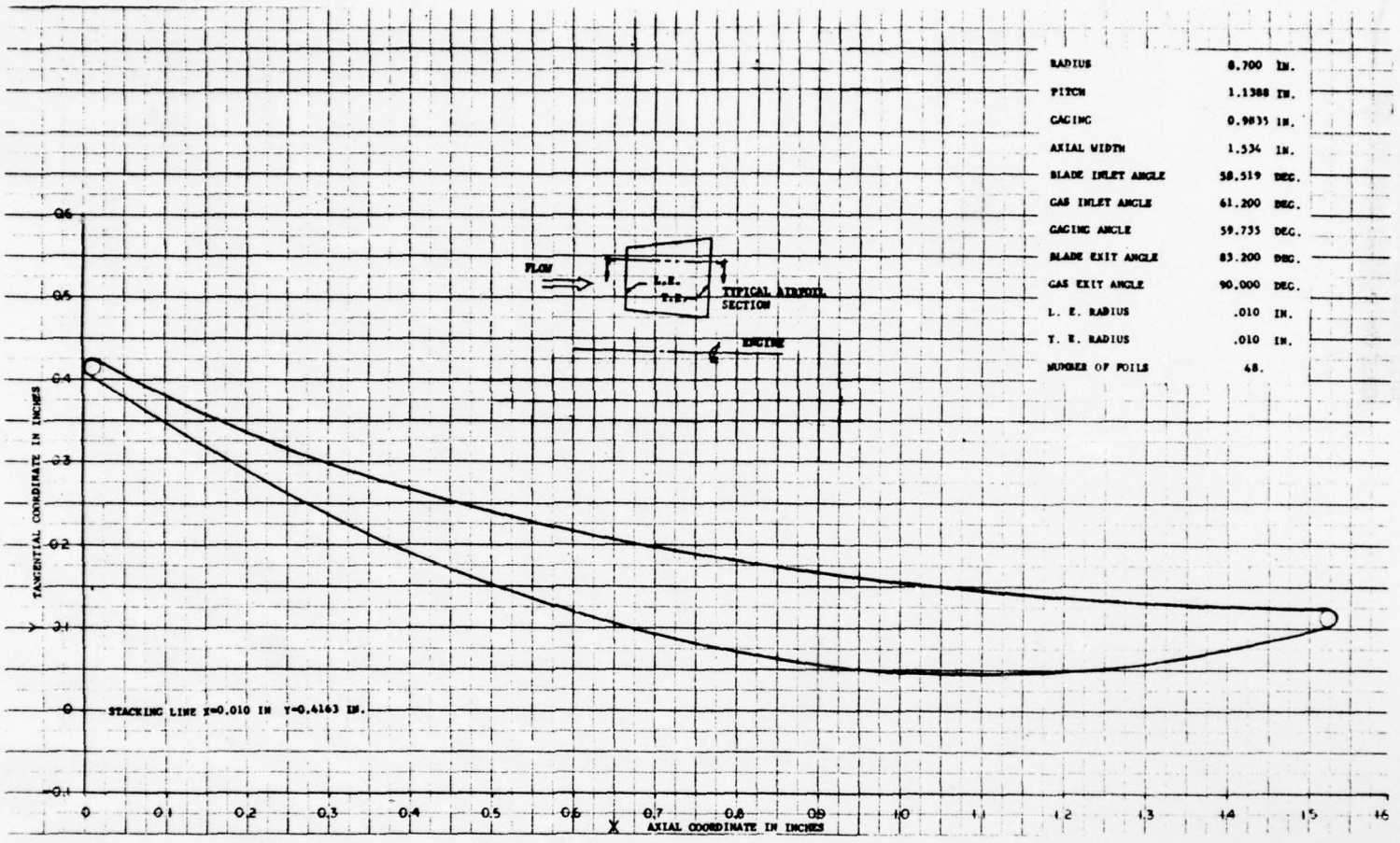
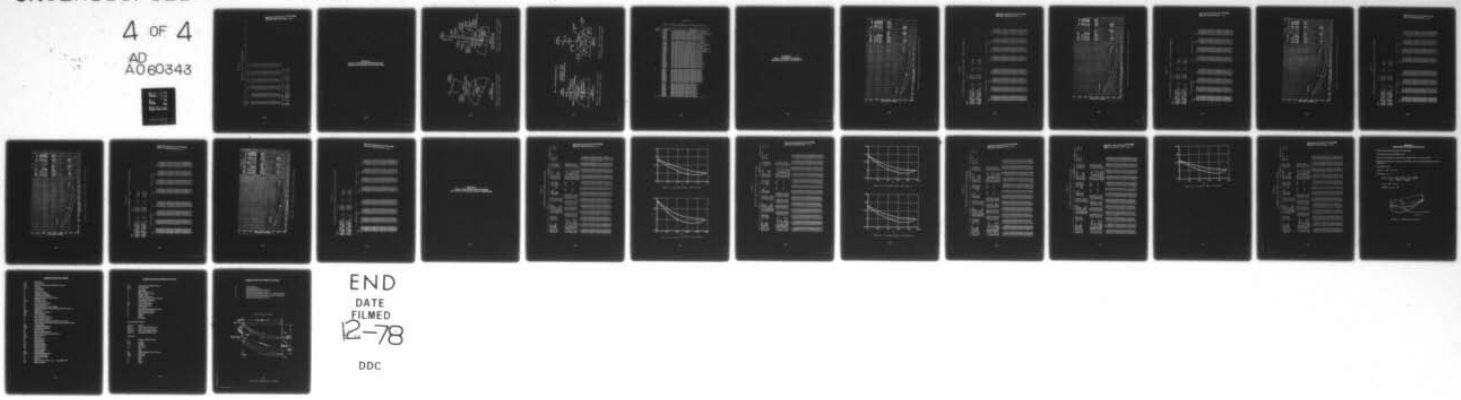


Figure D-5. Phase II Annular Cascade Non-Series EGV Design, Tip Section (Scaled)

AD-A060 343 PRATT AND WHITNEY AIRCRAFT GROUP WEST PALM BEACH FL G--ETC F/G 21/5
TURBINE EXIT GUIDE VANE PROGRAM.(U)
NOV 77 W S MITCHELL, J F SOILEAU F33615-74-C-2060

UNCLASSIFIED PWA-FR-8932 AFAPL-TR-77-75 NL

4 OF 4
AD
A060343



END
DATE
FILMED
12-78
DDC

TABLE D-5

NON-SERIES EGV TIP SECTION DESIGN

RADIUS OF TIP SECTION = 8.7000 AXIAL CHORD = 1.5340 ACTUAL CHORD = 1.5502 PITCH = 1.13[illegible] NO. OF FOILS = 48.00

PERCENT X	FOIL X	FOIL Y SUCTION	FOIL Y (CIRCLE)	FOIL Y PRESSURE	FOIL Y (CIRCLE)
0.0	0.0	0.4163	0.4163	0.4163	0.4163
0.01	0.0153	0.4008	0.4008	0.4249	0.4249
0.02	0.0307	0.3908	0.3908	0.4163	0.4163
0.03	0.0460	0.3810	0.3810	0.4080	0.4080
0.04	0.0614	0.3712	0.3712	0.3999	0.3999
0.05	0.0767	0.3616	0.3616	0.3921	0.3921
0.10	0.1534	0.3155	0.3155	0.3559	0.3559
0.15	0.2301	0.2729	0.2729	0.3242	0.3242
0.20	0.3068	0.2339	0.2339	0.2963	0.2963
0.25	0.3835	0.1985	0.1985	0.2717	0.2717
0.30	0.4602	0.1669	0.1669	0.2500	0.2500
0.35	0.5369	0.1390	0.1390	0.2308	0.2308
0.40	0.6136	0.1147	0.1147	0.2138	0.2138
0.45	0.6903	0.0941	0.0941	0.1988	0.1988
0.50	0.7670	0.0772	0.0772	0.1856	0.1856
0.55	0.8437	0.0639	0.0639	0.1740	0.1740
0.60	0.9204	0.0542	0.0542	0.1639	0.1639
0.65	0.9971	0.0482	0.0482	0.1551	0.1551
0.70	1.0738	0.0457	0.0457	0.1476	0.1476
0.75	1.1505	0.0469	0.0469	0.1412	0.1412
0.80	1.2272	0.0516	0.0516	0.1358	0.1358
0.85	1.3039	0.0598	0.0598	0.1314	0.1314
0.90	1.3806	0.0717	0.0717	0.1279	0.1279
0.95	1.4573	0.0870	0.0870	0.1253	0.1253
0.98	1.5033	0.0979	0.0979	0.1240	0.1240
0.99	1.5187	0.1018	0.1018	0.1237	0.1237
1.00	1.5340	0.1135	0.1135	0.1135	0.1135

FOIL L.E. CIRCLE X = 0.0160, Y = 0.4163, R = 0.0160
FOIL T.E. CIRCLE X = 1.5240, Y = 0.1135, R = 0.0100

FOIL L.E. TANGENCY PT. SUCTION X = 0.0045, Y = 0.4080
FOIL L.E. TANGENCY PT. PRESSURE X = 0.0150, Y = 0.4251
FOIL T.E. TANGENCY PT. SUCTION X = 1.5265, Y = 0.1039
FOIL T.E. TANGENCY PT. PRESSURE X = 1.5238, Y = 0.1035

THIS PAGE IS BEST QUALITY PRACTICABLE
FROM COPY FURNISHED TO DDC

APPENDIX E
ANNULAR CASCADE RIG INSTRUMENTATION HEADERS AND INSTRUMENTATION LOCATIONS

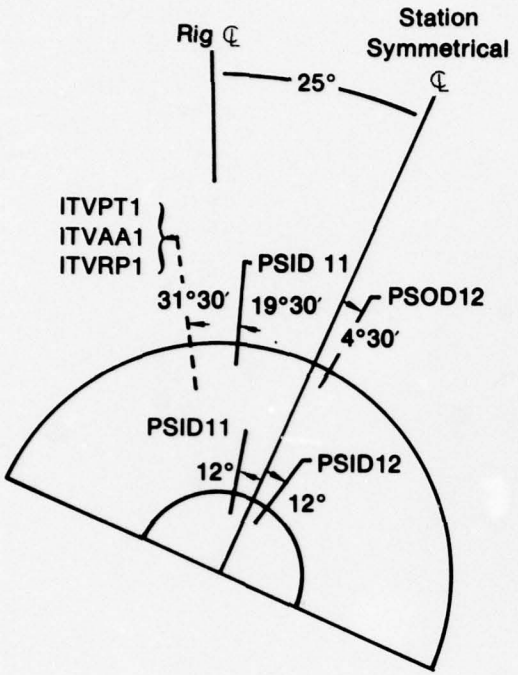


Figure E-1. Phase II Annular Cascade Instrumentation Location, Station 1

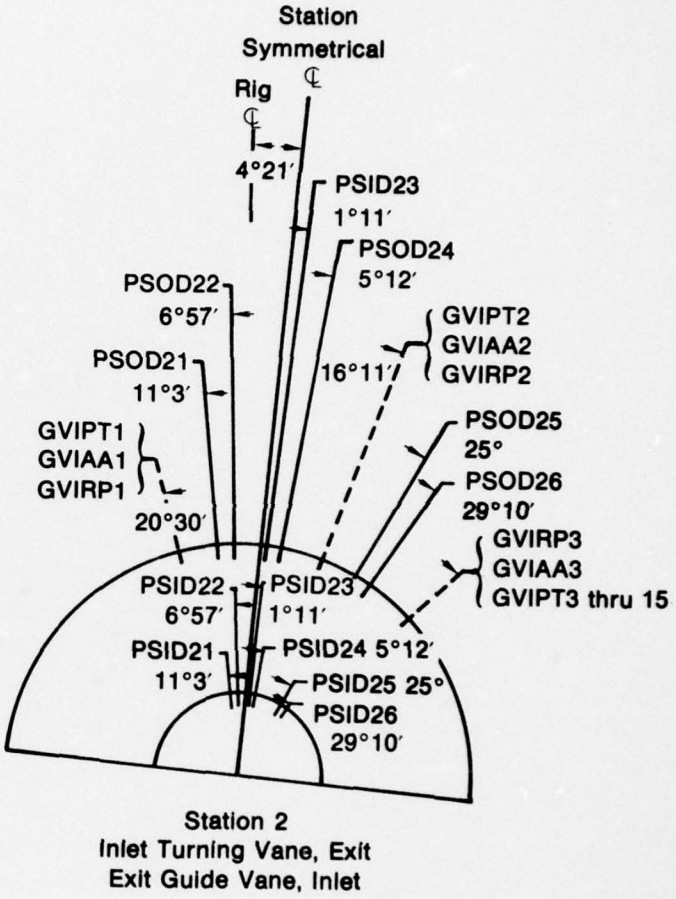


Figure E-2. Phase II Annular Cascade Instrumentation Location, Station 2

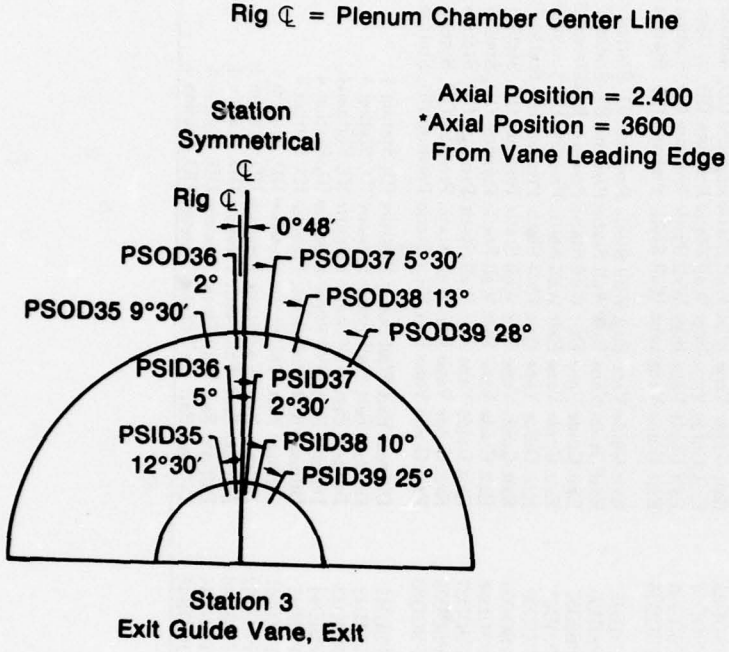


Figure E-3. Phase II Annular Cascade Instrumentation Location, Station 3

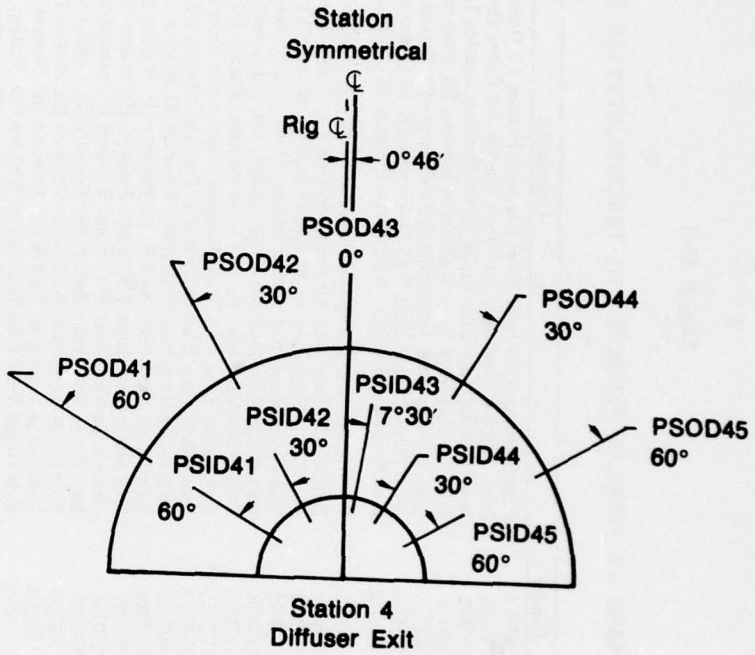


Figure E-4. Phase II Annular Cascade Instrumentation Location, Station 4

TABLE E-1

PHASE II ANNULAR SEGMENT RIG INSTRUMENTATION LIST

Station	*Header*	*Description*
1	ITVPT1	Inlet Turning Vane Inlet Total Pressure, Station 1-1 Cobra Probe
	ITVAA1	Inlet Turning Vane Inlet Air Angle, Station 1-1 Cobra Probe
	ITVRP1	Inlet Turning Vane Inlet Probe Radial Position, Station 1-1 Cobra Probe
	PSID11	Inlet Turning Vane Inlet Wall Static Pressure ID, Station 1
	PSID12	Inlet Turning Vane Inlet Wall Static Pressure ID, Station 1
	PSOD11	Inlet Turning Vane Inlet Wall Static Pressure OD, Station 1
	PSOD12	Inlet Turning Vane Inlet Wall Static Pressure OD, Station 1
2	GVIPT1	Exit Guide Vane Inlet Total Pressure, Station 2-1, Cobra Probe
	GVIAA1	Exit Guide Vane Inlet Air Angle, Station 2-1, Cobra Probe
	GVIRP1	Exit Guide Vane Inlet Probe Radial Position, Station 2-1, Cobra Probe
	GVIPT2	Exit Guide Vane Inlet Total Pressure, Station 2-2, Cobra Probe
	GVIAA2	Exit Guide Vane Inlet Air Angle, Station 2-2, Cobra Probe
	GVIRP2	Exit Guide Vane Inlet Probe Radial Position, Station 2-2, Cobra Probe
	GVIPT3-15	Exit Guide Vane Inlet Total Pressure, Station 2-3, Rake Probe
	GVIRP3	Exit Guide Vane Inlet Probe Radial Position, Station 2-3, Rake Probe
	PSID21	Exit Guide Vane Inlet Wall Static Pressure ID, Station 2
	PSID22	Exit Guide Vane Inlet Wall Static Pressure ID, Station 2
	PSID23	Exit Guide Vane Inlet Wall Static Pressure ID, Station 2
	PSID24	Exit Guide Vane Inlet Wall Static Pressure ID, Station 2
	PSID25	Exit Guide Vane Inlet Wall Static Pressure ID, Station 2
	PSID26	Exit Guide Vane Inlet Wall Static Pressure ID, Station 2
	PSOD21	Exit Guide Vane Inlet Wall Static Pressure OD, Station 2
	PSOD22	Exit Guide Vane Inlet Wall Static Pressure OD, Station 2
	PSOD23	Exit Guide Vane Inlet Wall Static Pressure OD, Station 2
	PSOD24	Exit Guide Vane Inlet Wall Static Pressure OD, Station 2
	PSOD25	Exit Guide Vane Inlet Wall Static Pressure OD, Station 2
	PSOD26	Exit Guide Vane Inlet Wall Static Pressure OD, Station 2
3	PSID35	Exit Guide Vane Exit Wall Static Pressure ID, Station 3
	PSID36	Exit Guide Vane Exit Wall Static Pressure ID, Station 3
	PSID37	Exit Guide Vane Exit Wall Static Pressure ID, Station 3
	PSID38	Exit Guide Vane Exit Wall Static Pressure ID, Station 3
	PSID39	Exit Guide Vane Exit Wall Static Pressure ID, Station 3
	PSOD35	Exit Guide Vane Exit Wall Static Pressure OD, Station 3
	PSOD36	Exit Guide Vane Exit Wall Static Pressure OD, Station 3
	PSOD37	Exit Guide Vane Exit Wall Static Pressure OD, Station 3
	PSOD38	Exit Guide Vane Exit Wall Static Pressure OD, Station 3
	PSOD39	Exit Guide Vane Exit Wall Static Pressure OD, Station 3
4	PSID41	Diffuser Exit Wall Static Pressure ID, Station 4
	PSID42	Diffuser Exit Wall Static Pressure ID, Station 4
	PSID43	Diffuser Exit Wall Static Pressure ID, Station 4
	PSID44	Diffuser Exit Wall Static Pressure ID, Station 4
	PSID45	Diffuser Exit Wall Static Pressure ID, Station 4
	PSOD41	Diffuser Exit Wall Static Pressure OD, Station 4
	PSOD42	Diffuser Exit Wall Static Pressure OD, Station 4
	PSOD43	Diffuser Exit Wall Static Pressure OD, Station 4
	PSOD44	Diffuser Exit Wall Static Pressure OD, Station 4
	PSOD45	Diffuser Exit Wall Static Pressure OD, Station 4

APPENDIX F
PHASE III 65-SERIES EGV AIRFOIL SECTIONS AND AIRFOIL COORDINATES

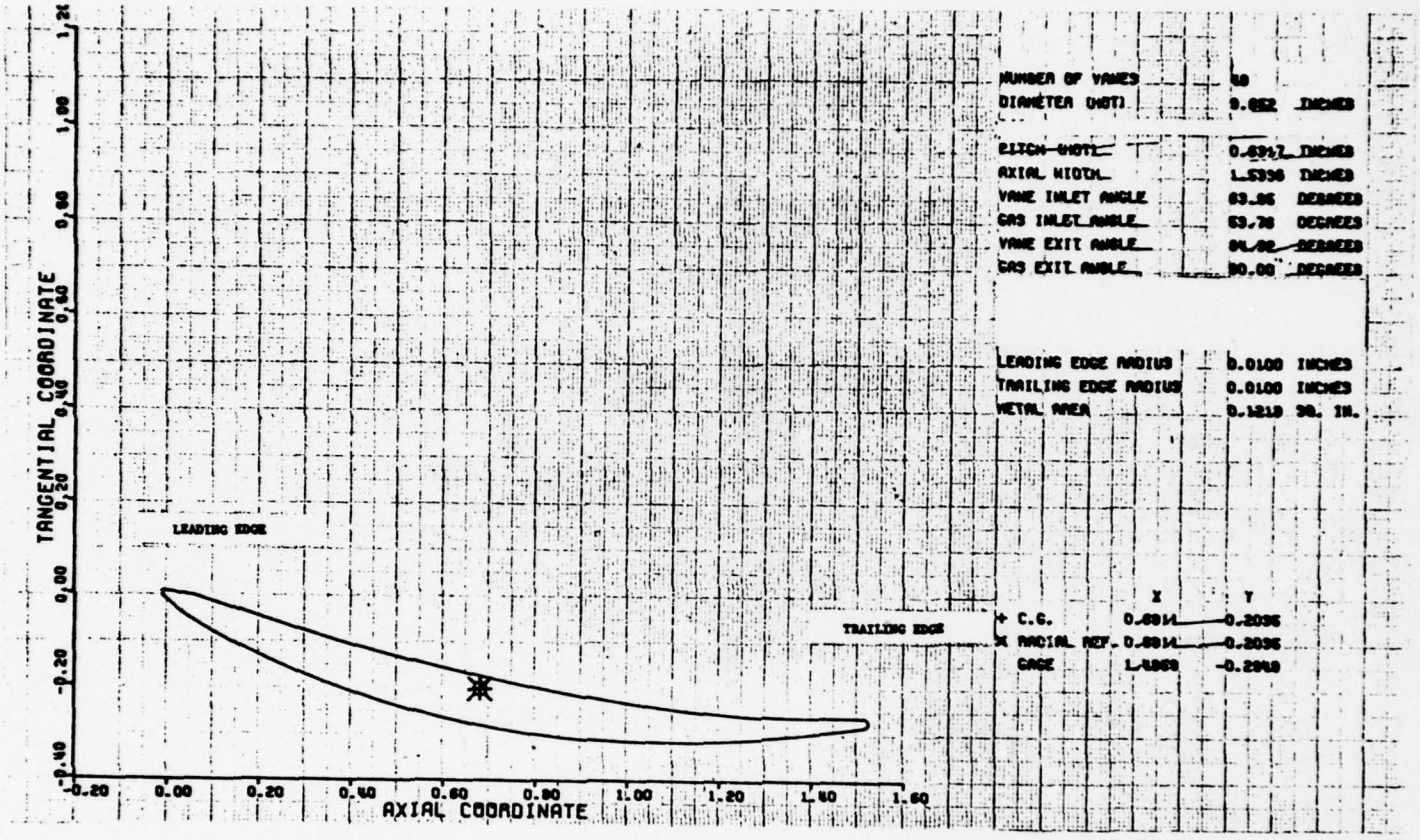


Figure F-1. 65 Circular-Arc Series Airfoil, Root Section

TABLE F-1

EGV CASCADE AIRFOIL 65 CIRCULAR-ARC SERIES ROOT SECTION DESIGN

AREA		0.1218		
L.E. CIRCLE RADIUS		0.0100		
L.E. CIRCLE CENTER	X =	-0.0000	Y =	0.0
SUCTION TANGENCY PT.	X =	-0.0093	Y =	-0.0038
PRESSURE TANGENCY PT.	X =	-0.0027	Y =	0.0097
T.E. CIRCLE RADIUS		0.0100		
T.E. CIRCLE CENTER	X =	1.5136	Y =	-0.2719
SUCTION TANGENCY PT.	X =	1.5152	Y =	-0.2818
PRESSURE TANGENCY PT.	X =	1.5132	Y =	-0.2619

SUCTION SURFACE				PRESSURE SURFACE			
X/B	X	Y/B	Y	X/B	X	Y/B	Y
-0.0065	-0.0100	0.0	0.0	-0.0065	-0.0100	0.0	0.0
0.0035	0.0053	-0.0192	-0.0294	0.0035	0.0053	0.0073	0.0112
0.0135	0.0206	-0.0265	-0.0406	0.0135	0.0206	0.0069	0.0106
0.0235	0.0360	-0.0292	-0.0448	0.0235	0.0360	0.0045	0.0069
0.0335	0.0513	-0.0329	-0.0505	0.0335	0.0513	0.0010	0.0015
0.0435	0.0667	-0.0387	-0.0594	0.0435	0.0667	-0.0026	-0.0040
0.0935	0.1433	-0.0684	-0.1049	0.0935	0.1433	-0.0177	-0.0271
0.1435	0.2200	-0.0920	-0.1410	0.1435	0.2200	-0.0336	-0.0515
0.1935	0.2967	-0.1131	-0.1734	0.1935	0.2967	-0.0491	-0.0753
0.2435	0.3734	-0.1316	-0.2018	0.2435	0.3734	-0.0639	-0.0979
0.2935	0.4501	-0.1480	-0.2270	0.2935	0.4501	-0.0777	-0.1191
0.3435	0.5267	-0.1627	-0.2495	0.3435	0.5267	-0.0903	-0.1384
0.3935	0.6034	-0.1750	-0.2684	0.3935	0.6034	-0.1021	-0.1565
0.4435	0.6801	-0.1850	-0.2838	0.4435	0.6801	-0.1134	-0.1739
0.4935	0.7568	-0.1932	-0.2962	0.4935	0.7568	-0.1239	-0.1900
0.5435	0.8335	-0.1995	-0.3059	0.5435	0.8335	-0.1334	-0.2046
0.5935	0.9102	-0.2038	-0.3125	0.5935	0.9102	-0.1422	-0.2180
0.6435	0.9868	-0.2062	-0.3162	0.6435	0.9868	-0.1502	-0.2303
0.6935	1.0635	-0.2070	-0.3174	0.6935	1.0635	-0.1571	-0.2410
0.7435	1.1402	-0.2064	-0.3165	0.7435	1.1402	-0.1627	-0.2496
0.7935	1.2169	-0.2043	-0.3133	0.7935	1.2169	-0.1670	-0.2562
0.8435	1.2936	-0.2008	-0.3080	0.8435	1.2936	-0.1700	-0.2608
0.8935	1.3702	-0.1962	-0.3008	0.8935	1.3702	-0.1717	-0.2633
0.9435	1.4469	-0.1902	-0.2917	0.9435	1.4469	-0.1716	-0.2632
0.9735	1.4929	-0.1860	-0.2853	0.9735	1.4929	-0.1712	-0.2625
0.9835	1.5083	-0.1845	-0.2829	0.9835	1.5083	-0.1709	-0.2621
0.9935	1.5236	-0.1773	-0.2719	0.9935	1.5236	-0.1773	-0.2719

THIS PAGE IS BEST QUALITY PRACTICABLE
FROM COPY FURNISHED TO DDC

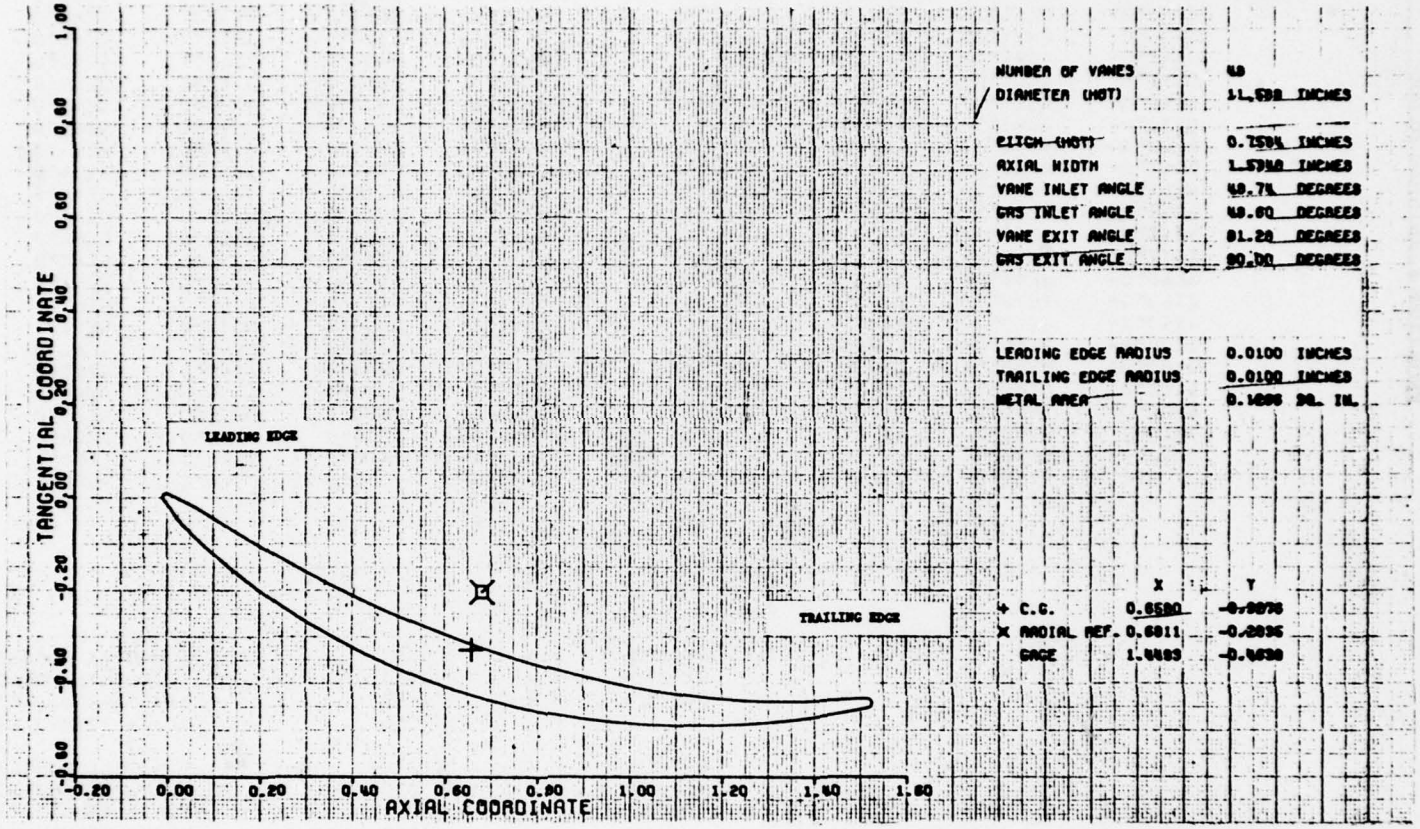


Figure F-2. 65 Circular-Arc Series Airfoil, 1/4 Root Section

TABLE F-2

EGV CASCADE AIRFOIL 65 CIRCULAR-ARC SERIES 1/4 ROOT SECTION DESIGN

AREA		0.1266		
L.E. CIRCLE RADIUS		0.0100		
L.E. CIRCLE CENTER	X =	-0.0000	Y =	0.0
SUCTION TANGENCY PT.	X =	-0.0099	Y =	-0.0018
PRESSURE TANGENCY PT.	X =	0.0005	Y =	0.0100
T.E. CIRCLE RADIUS		0.0100		
T.E. CIRCLE CENTER	X =	1.5139	Y =	-0.4418
SUCTION TANGENCY PT.	X =	1.5160	Y =	-0.4516
PRESSURE TANGENCY PT.	X =	1.5130	Y =	-0.4318

SUCTION SURFACE				PRESSURE SURFACE			
X/B	X	Y/B	Y	X/B	X	Y/B	Y
-0.0065	-0.0100	0.0	0.0	-0.0065	-0.0100	0.0	0.0
0.0035	0.0053	-0.0342	-0.0525	0.0035	0.0053	0.0062	0.0095
0.0135	0.0206	-0.0388	-0.0595	0.0135	0.0206	0.0032	0.0049
0.0235	0.0360	-0.0383	-0.0587	0.0235	0.0360	-0.0021	-0.0032
0.0335	0.0513	-0.0456	-0.0700	0.0335	0.0513	-0.0086	-0.0132
0.0435	0.0667	-0.0579	-0.0888	0.0435	0.0667	-0.0152	-0.0234
0.0935	0.1434	-0.1038	-0.1592	0.0935	0.1434	-0.0454	-0.0697
0.1435	0.2201	-0.1414	-0.2170	0.1435	0.2201	-0.0750	-0.1150
0.1935	0.2968	-0.1738	-0.2665	0.1935	0.2968	-0.1027	-0.1576
0.2435	0.3735	-0.2019	-0.3098	0.2435	0.3735	-0.1284	-0.1970
0.2935	0.4502	-0.2270	-0.3482	0.2935	0.4502	-0.1518	-0.2328
0.3435	0.5269	-0.2489	-0.3818	0.3435	0.5269	-0.1727	-0.2649
0.3935	0.6036	-0.2673	-0.4101	0.3935	0.6036	-0.1920	-0.2945
0.4435	0.6803	-0.2826	-0.4335	0.4435	0.6803	-0.2097	-0.3217
0.4935	0.7570	-0.2952	-0.4528	0.4935	0.7570	-0.2256	-0.3461
0.5435	0.8337	-0.3052	-0.4682	0.5435	0.8337	-0.2397	-0.3677
0.5935	0.9104	-0.3125	-0.4793	0.5935	0.9104	-0.2522	-0.3868
0.6435	0.9871	-0.3172	-0.4866	0.6435	0.9871	-0.2630	-0.4035
0.6935	1.0638	-0.3199	-0.4907	0.6935	1.0638	-0.2718	-0.4170
0.7435	1.1405	-0.3205	-0.4916	0.7435	1.1405	-0.2786	-0.4273
0.7935	1.2172	-0.3190	-0.4893	0.7935	1.2172	-0.2832	-0.4345
0.8435	1.2939	-0.3154	-0.4839	0.8435	1.2939	-0.2859	-0.4385
0.8935	1.3706	-0.3101	-0.4757	0.8935	1.3706	-0.2864	-0.4393
0.9435	1.4473	-0.3026	-0.4642	0.9435	1.4473	-0.2844	-0.4363
0.9735	1.4933	-0.2974	-0.4561	0.9735	1.4933	-0.2828	-0.4335
0.9835	1.5086	-0.2954	-0.4531	0.9835	1.5086	-0.2818	-0.4322
0.9935	1.5240	-0.2880	-0.4418	0.9935	1.5240	-0.2880	-0.4418

THIS PAGE IS BEST QUALITY PRACTICABLE
FROM COPY FURNISHED TO DDC

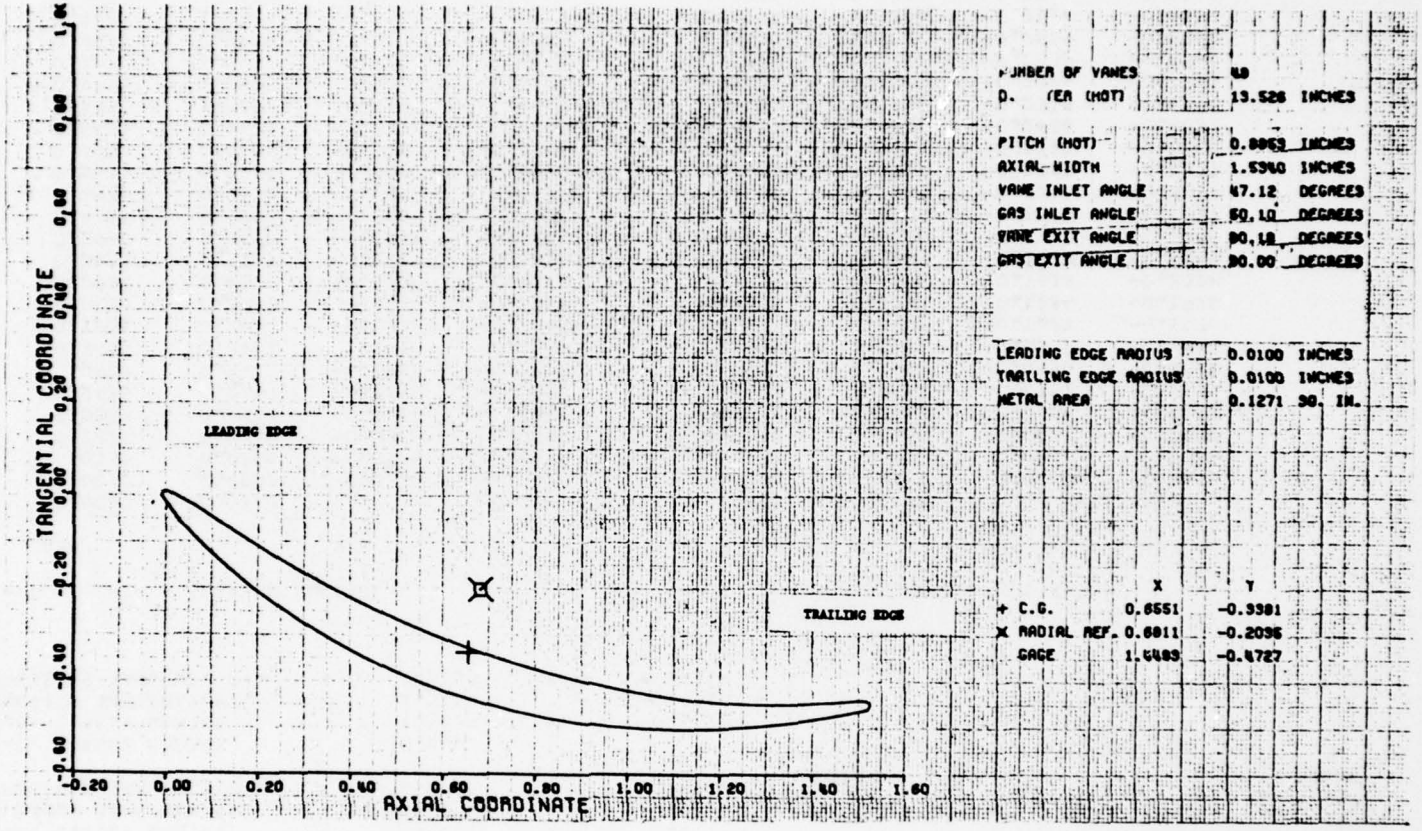


Figure F-3. 65 Circular-Arc Series Airfoil, Mean Section

TABLE F-3

EGV CASCADE AIRFOIL 65 CIRCULAR-ARC SERIES MEAN SECTION DESIGN

AREA		0.1271		
L.E. CIRCLE RADIUS		0.0100		
L.E. CIRCLE CENTER	X =	-0.0001	Y =	0.0
SUCTION TANGENCY PT.	X =	-0.0100	Y =	-0.0016
PRESSURE TANGENCY PT.	X =	0.0008	Y =	0.0100
T.E. CIRCLE RADIUS		0.0100		
T.E. CIRCLE CENTER	X =	1.5139	Y =	-0.4493
SUCTION TANGENCY PT.	X =	1.5161	Y =	-0.4591
PRESSURE TANGENCY PT.	X =	1.5127	Y =	-0.4394

SUCTION SURFACE				PRESSURE SURFACE			
X/B	X	Y/B	Y	X/B	X	Y/B	Y
-0.0066	-0.0101	0.0	0.0	-0.0066	-0.0101	0.0	0.0
0.0034	0.0053	-0.0370	-0.0567	0.0034	0.0053	0.0061	0.0094
0.0134	0.0206	-0.0402	-0.0617	0.0134	0.0206	0.0027	0.0042
0.0234	0.0359	-0.0390	-0.0599	0.0234	0.0359	-0.0029	-0.0045
0.0334	0.0513	-0.0472	-0.0724	0.0334	0.0513	-0.0098	-0.0150
0.0434	0.0666	-0.0606	-0.0930	0.0434	0.0666	-0.0168	-0.0258
0.0934	0.1433	-0.1081	-0.1658	0.0934	0.1433	-0.0488	-0.0748
0.1434	0.2200	-0.1473	-0.2259	0.1434	0.2200	-0.0798	-0.1224
0.1934	0.2967	-0.1806	-0.2771	0.1934	0.2967	-0.1088	-0.1669
0.2434	0.3734	-0.2096	-0.3215	0.2434	0.3734	-0.1355	-0.2078
0.2934	0.4501	-0.2353	-0.3610	0.2934	0.4501	-0.1596	-0.2448
0.3434	0.5268	-0.2576	-0.3952	0.3434	0.5268	-0.1811	-0.2778
0.3934	0.6035	-0.2763	-0.4239	0.3934	0.6035	-0.2008	-0.3081
0.4434	0.6802	-0.2918	-0.4476	0.4434	0.6802	-0.2189	-0.3358
0.4934	0.7569	-0.3045	-0.4671	0.4934	0.7569	-0.2350	-0.3605
0.5434	0.8336	-0.3144	-0.4823	0.5434	0.8336	-0.2492	-0.3822
0.5934	0.9103	-0.3216	-0.4933	0.5934	0.9103	-0.2615	-0.4012
0.6434	0.9870	-0.3262	-0.5003	0.6434	0.9870	-0.2722	-0.4176
0.6934	1.0637	-0.3285	-0.5040	0.6934	1.0637	-0.2807	-0.4306
0.7434	1.1404	-0.3287	-0.5042	0.7434	1.1404	-0.2870	-0.4403
0.7934	1.2171	-0.3267	-0.5011	0.7934	1.2171	-0.2912	-0.4467
0.8434	1.2938	-0.3226	-0.4949	0.8434	1.2938	-0.2932	-0.4497
0.8934	1.3705	-0.3166	-0.4857	0.8934	1.3705	-0.2930	-0.4494
0.9434	1.4472	-0.3084	-0.4730	0.9434	1.4472	-0.2902	-0.4451
0.9734	1.4932	-0.3026	-0.4641	0.9734	1.4932	-0.2878	-0.4415
0.9834	1.5086	-0.3004	-0.4608	0.9834	1.5086	-0.2867	-0.4399
0.9934	1.5239	-0.2929	-0.4493	0.9934	1.5239	-0.2929	-0.4493

THIS PAGE IS BEST QUALITY PRACTICABLE
FROM COPY FURNISHED TO DDC

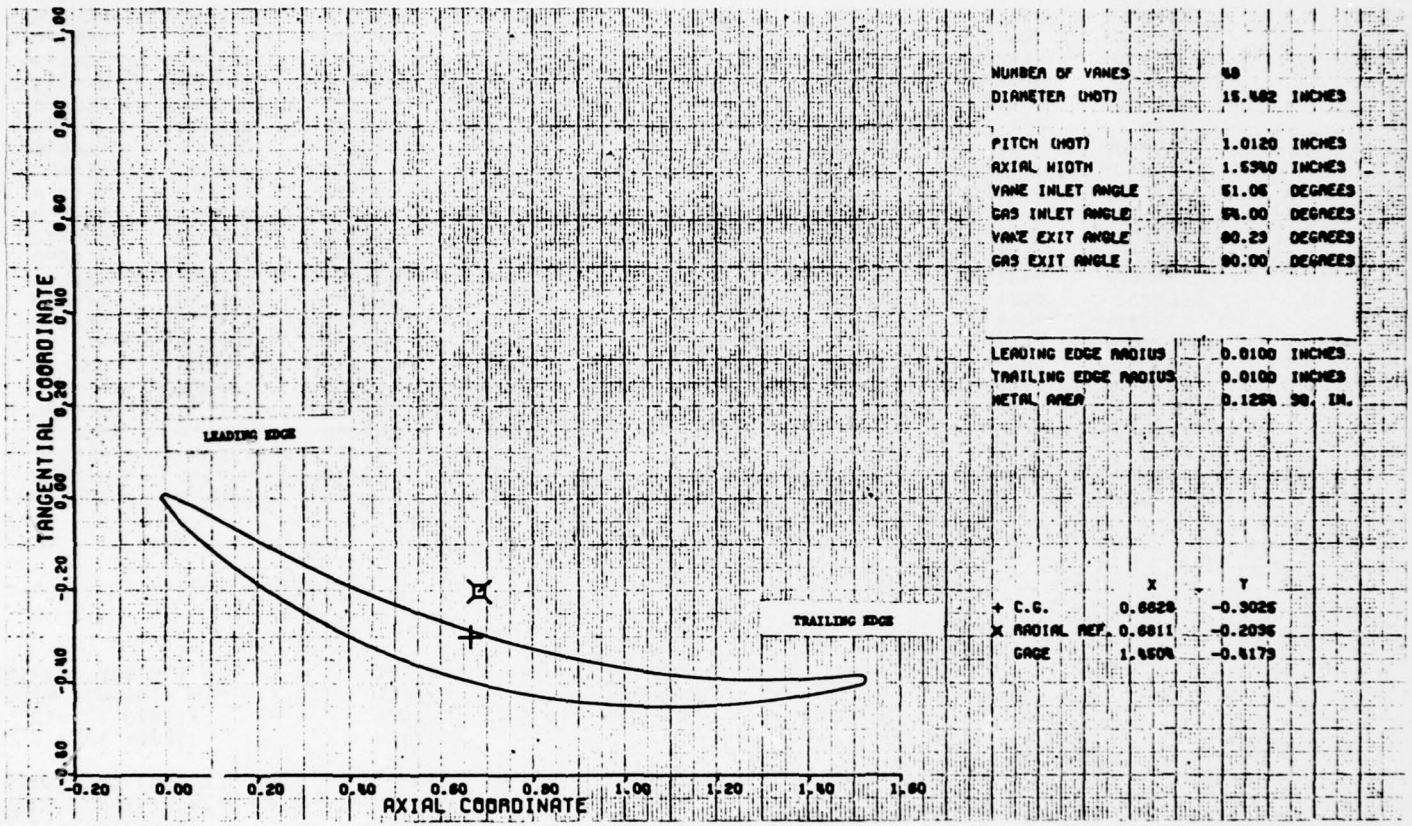


Figure F-4. 65 Circular-Arc Series Airfoil, 1/4 Tip Section

TABLE F-4

EGV CASCADE AIRFOIL 65 CIRCULAR-ARC SERIES 1/4 TIP SECTION DESIGN

AREA		0.125-		
L.E. CIRCLE RADIUS		0.0100		
L.E. CIRCLE CENTER	X =	-0.0000	Y =	0.0
SUCTION TANGENCY PT.	X =	-0.0098	Y =	-0.0021
PRESSURE TANGENCY PT.	X =	0.0000	Y =	0.0100
T.E. CIRCLE RADIUS		0.0100		
T.E. CIRCLE CENTER	X =	1.5134	Y =	-0.3941
SUCTION TANGENCY PT.	X =	1.5162	Y =	-0.4038
PRESSURE TANGENCY PT.	X =	1.5128	Y =	-0.3841

SUCTION SURFACE				PRESSURE SURFACE			
X/B	X	Y/B	Y	X/B	X	Y/B	Y
-0.0065	-0.0100	0.0	0.0	-0.0065	-0.0100	0.0	0.0
0.0035	0.0053	-0.0300	-0.0460	0.0035	0.0053	0.0063	0.0097
0.0135	0.0206	-0.0362	-0.0555	0.0135	0.0206	0.0037	0.0057
0.0235	0.0360	-0.0371	-0.0569	0.0235	0.0360	-0.0011	-0.0017
0.0335	0.0513	-0.0437	-0.0670	0.0335	0.0513	-0.0070	-0.0108
0.0435	0.0667	-0.0543	-0.0833	0.0435	0.0667	-0.0132	-0.0202
0.0935	0.1434	-0.0974	-0.1494	0.0935	0.1434	-0.0407	-0.0624
0.1435	0.2201	-0.1324	-0.2031	0.1435	0.2201	-0.0677	-0.1039
0.1935	0.2968	-0.1626	-0.2495	0.1935	0.2968	-0.0932	-0.1430
0.2435	0.3735	-0.1889	-0.2898	0.2435	0.3735	-0.1166	-0.1791
0.2935	0.4502	-0.2122	-0.3256	0.2935	0.4502	-0.1382	-0.2120
0.3435	0.5269	-0.2326	-0.3568	0.3435	0.5269	-0.1573	-0.2413
0.3935	0.6036	-0.2496	-0.3828	0.3935	0.6036	-0.1749	-0.2682
0.4435	0.6803	-0.2635	-0.4042	0.4435	0.6803	-0.1910	-0.2930
0.4935	0.7570	-0.2748	-0.4216	0.4935	0.7570	-0.2055	-0.3152
0.5435	0.8337	-0.2836	-0.4351	0.5435	0.8337	-0.2182	-0.3346
0.5935	0.9104	-0.2897	-0.4444	0.5935	0.9104	-0.2293	-0.3517
0.6435	0.9871	-0.2934	-0.4501	0.6435	0.9871	-0.2389	-0.3665
0.6935	1.0638	-0.2949	-0.4524	0.6935	1.0638	-0.2465	-0.3782
0.7435	1.1405	-0.2944	-0.4516	0.7435	1.1405	-0.2522	-0.3869
0.7935	1.2172	-0.2918	-0.4477	0.7935	1.2172	-0.2558	-0.3924
0.8435	1.2939	-0.2873	-0.4407	0.8435	1.2939	-0.2574	-0.3949
0.8935	1.3706	-0.2809	-0.4309	0.8935	1.3706	-0.2570	-0.3942
0.9435	1.4473	-0.2724	-0.4179	0.9435	1.4473	-0.2541	-0.3898
0.9735	1.4933	-0.2665	-0.4088	0.9735	1.4933	-0.2517	-0.3862
0.9835	1.5086	-0.2644	-0.4055	0.9835	1.5086	-0.2507	-0.3846
0.9935	1.5240	-0.2569	-0.3941	0.9935	1.5240	-0.2569	-0.3941

THIS PAGE IS BEST QUALITY PRACTICABLE
FROM COPY FURNISHED TO DDC

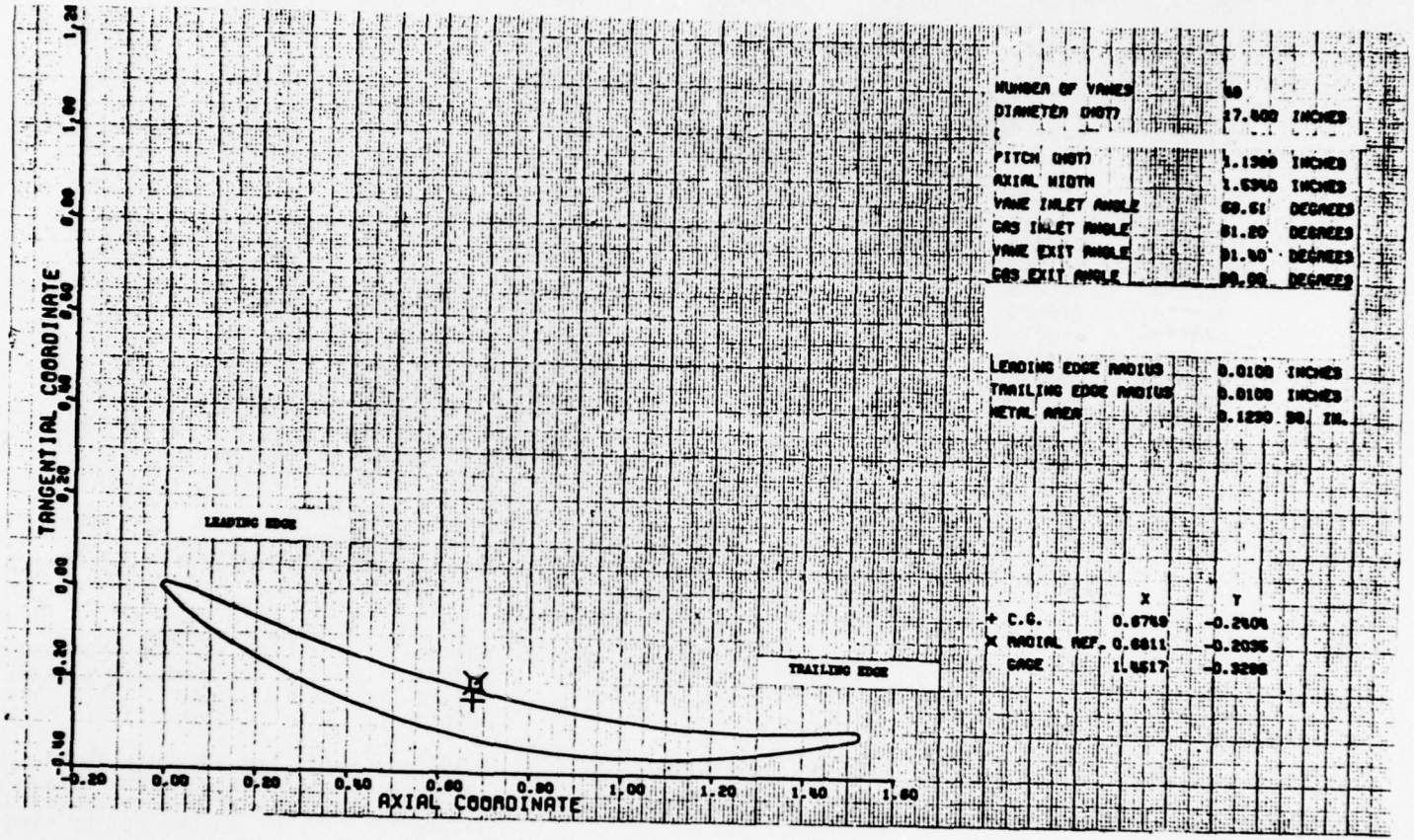


Figure F-5. 65 Circular-Arc Series Airfoil, Tip Section

TABLE F-5

EGV CASCADE AIRFOIL 65 CIRCULAR-ARC SERIES TIP SECTION DESIGN

AREA		0.1230		
L.E. CIRCLE RADIUS		0.0100		
L.E. CIRCLE CENTER	X =	0.0000	Y =	0.0
SUCTION TANGENCY PT.	X =	-0.0096	Y =	-0.0030
PRESSURE TANGENCY PT.	X =	-0.0017	Y =	0.0099
T.E. CIRCLE RADIUS		0.0100		
T.E. CIRCLE CENTER	X =	1.5139	Y =	-0.3061
SUCTION TANGENCY PT.	X =	1.5160	Y =	-0.2163
PRESSURE TANGENCY PT.	X =	1.5130	Y =	-0.2965

SUCTION SURFACE				PRESSURE SURFACE			
X/B	X	Y/B	Y	X/B	X	Y/B	Y
-0.0065	-0.0100	0.0	0.0	-0.0065	-0.0100	0.0	0.0
0.0035	0.0053	-0.0230	-0.0353	0.0035	0.0053	0.0069	0.0105
0.0135	0.0206	-0.0304	-0.0466	0.0135	0.0206	0.0056	0.0086
0.0235	0.0360	-0.0325	-0.0498	0.0235	0.0360	0.0022	0.0034
0.0335	0.0513	-0.0370	-0.0568	0.0335	0.0513	-0.0023	-0.0035
0.0435	0.0667	-0.0444	-0.0681	0.0435	0.0667	-0.0068	-0.0105
0.0935	0.1434	-0.0796	-0.1221	0.0935	0.1434	-0.0268	-0.0411
0.1435	0.2201	-0.1076	-0.1650	0.1435	0.2201	-0.0471	-0.0722
0.1935	0.2968	-0.1322	-0.2029	0.1935	0.2968	-0.0664	-0.1019
0.2435	0.3735	-0.1538	-0.2359	0.2435	0.3735	-0.0845	-0.1297
0.2935	0.4502	-0.1728	-0.2650	0.2935	0.4502	-0.1012	-0.1553
0.3435	0.5269	-0.1895	-0.2907	0.3435	0.5269	-0.1162	-0.1782
0.3935	0.6036	-0.2035	-0.3122	0.3935	0.6036	-0.1300	-0.1994
0.4435	0.6803	-0.2148	-0.3295	0.4435	0.6803	-0.1429	-0.2192
0.4935	0.7570	-0.2238	-0.3434	0.4935	0.7570	-0.1546	-0.2372
0.5435	0.8337	-0.2307	-0.3539	0.5435	0.8337	-0.1650	-0.2531
0.5935	0.9104	-0.2353	-0.3609	0.5935	0.9104	-0.1742	-0.2672
0.6435	0.9871	-0.2376	-0.3645	0.6435	0.9871	-0.1822	-0.2795
0.6935	1.0638	-0.2381	-0.3652	0.6935	1.0638	-0.1888	-0.2896
0.7435	1.1405	-0.2368	-0.3633	0.7435	1.1405	-0.1937	-0.2971
0.7935	1.2172	-0.2338	-0.3586	0.7935	1.2172	-0.1970	-0.3021
0.8435	1.2939	-0.2290	-0.3513	0.8435	1.2939	-0.1985	-0.3046
0.8935	1.3706	-0.2227	-0.3417	0.8935	1.3706	-0.1984	-0.3044
0.9435	1.4473	-0.2147	-0.3294	0.9435	1.4473	-0.1962	-0.3010
0.9735	1.4933	-0.2092	-0.3209	0.9735	1.4933	-0.1944	-0.2982
0.9835	1.5086	-0.2072	-0.3178	0.9835	1.5086	-0.1936	-0.2969
0.9935	1.5240	-0.1998	-0.3065	0.9935	1.5240	-0.1998	-0.3065

THIS PAGE IS BEST QUALITY PRACTICABLE
FROM COPY FURNISHED TO DDC

APPENDIX G
PHASE IV LOW ASPECT RATIO NON-SERIES EGV AIRFOIL SECTIONS AND AIRFOIL COORDINATES

TABLE G-1

LOW ASPECT RATIO EGV DESIGN, ROOT SECTION

GEOMETRY						CASCADE PRESSURE DISTRIBUTION		BOUNDARY LAYER	
SECTION RADIUS	8.1800	BETA1 (METAL)	55.084	PITCH	0.4240	MACH NO. (IN)	0.6860	TOTAL PRESS.	0.0
AXIAL CHORD	9.5300	BETA2 (METAL)	79.000	GAGING	0.1344	TOTAL TEMP.	660.00	CP	0.0
R/C RATIO	-0.3500	DELTA BETA1	9.000	MAX THICK	1.0341	M1/M0	1.00000	PRANDL	0.0
NO. OF FOILS	8.00	DELTA BETA2	30.000	AREA	0.7877	M2/M1	1.12200	TL	0.0
L.E. DIAMETER	0.0900	GAGE ANGLE	53.052	IMIN	0.0910095	M3/M2	1.00000	VELOCITY	0.0
T.E. DIAMETER	0.1300	GAMMA	6.809	IMAX	38.2008043	BETA1 (GAS)	53.760		
THROAT	0.0	ROTATION	0.0	ALPHA	19.854	BETA2 (GAS)	90.000		
		DEVIATION	11.200			DELTA P/P	0.0		
		BETA2 (CALC)	90.200						
		CAMBER/CHORD	0.5800						
		CHORD	10.0992						

	X	X/B	Y	Y/B	R	R/B
L.E. CIRCLE	0.0450	0.0047	-3.3005	-0.3450	0.0450	0.0047
L.E. SUCT. TANG. PT.	0.0168	0.0018	-3.2854	-0.3419		
L.E. PRESS. TANG. PT.	0.0674	0.0071	-3.3393	-0.3491		
GAGE POINT	2.7962	0.2922	-1.2886	-0.1328		
CTR. OF MAX THICK.	6.4130	0.6717	-0.1369	-0.0184		
CTR. OF GRAVITY	5.2226	0.5469	-0.7341	-0.0769		
T.E. CIRCLE	9.4750	0.9921	0.0	0.0	0.0750	0.0079
T.E. SUCT. TANG. PT.	9.5214	0.9980	0.0650	0.0069		
T.E. PRESS. TANG. PT.	9.4684	0.9731	-0.0744	-0.0078		
SUCT. INTERMED. PT.	0.0134	0.0021	0.4001	0.0425		
PRESS. INTERMED. PT.	4.7032	0.4988	-1.1313	-0.1237		

CP/CV	1.4114
MACH NO. (EX)	0.4169
DELTA P/Q (IN)	0.6537
Q/PT (IN)	0.2419
P/PT (IN)	0.7283
DELTA P/Q (MIN)	0.7791
Q/PT (MIN)	0.2925
P/PT MIN (MIN)	0.6585
P/PT (AVE)	0.7973
MACH NO. (AVE)	0.5701
FLOW PAR (AVE)	0.4380
UNBAL. FP/FM	0.0
BALANCED FP/FM	0.0

X	X/B	YS	YS/B	YP	YP/B	RC/B	A/A6	SS	SP	PS/PI	PP/PI	YMC
0.0	0.0	-3.3005	-0.3450	-3.3005	-0.3450	0.0047	1.00	0.0285	-0.0285	0.7964	0.7964	-3.3149
0.0955	0.0100	-3.2623	-0.3353	-3.3234	-0.3486	4.0348	1.00	0.1052	0.0698	0.7066	0.7942	-3.2766
0.1910	0.0200	-3.1201	-0.3273	-3.2691	-0.3423	3.9596	1.00	0.2876	0.1791	0.7369	0.7920	-3.2020
0.2865	0.0300	-3.0504	-0.3194	-3.2151	-0.3367	3.8852	1.00	0.4095	0.2893	0.7072	0.7899	-3.1375
0.3820	0.0400	-2.9753	-0.3115	-3.1610	-0.3311	3.8114	1.00	0.5310	0.3988	0.6774	0.7877	-3.0734
0.4775	0.0500	-2.9000	-0.3037	-3.1068	-0.3253	3.7385	1.00	0.6522	0.5080	0.6778	0.7869	-3.0106
0.5730	0.0600	-2.8253	-0.2959	-3.0524	-0.2984	3.6650	1.00	1.2534	1.0511	0.6783	0.7854	-2.6996
1.4325	0.1500	-2.1839	-0.2287	-2.6024	-0.2725	3.0509	1.00	1.0403	1.5889	0.6756	0.7892	-2.4012
1.9100	0.2000	-1.8470	-0.1934	-2.3659	-0.2477	2.7350	1.00	2.4387	2.1218	0.6726	0.7929	-2.1153
2.3875	0.2500	-1.5259	-0.1598	-2.1404	-0.2241	2.4389	0.99	3.0001	2.6499	0.6708	0.7968	-1.8425
2.8650	0.3000	-1.2214	-0.1279	-1.9258	-0.2017	2.1622	0.99	3.5724	3.1734	0.6687	0.8008	-1.5832
3.3425	0.3500	-0.9350	-0.0979	-1.7223	-0.1803	1.9035	0.99	4.1242	3.6924	0.6665	0.8063	-1.3379
3.8200	0.4000	-0.6679	-0.0699	-1.5297	-0.1602	1.6640	0.99	4.6763	4.2073	0.6646	0.8123	-1.1075
4.2975	0.4500	-0.4218	-0.0442	-1.3488	-0.1412	1.4427	0.99	5.2155	4.7182	0.6620	0.8187	-0.8925
4.7750	0.5000	-0.1985	-0.0208	-1.1772	-0.1233	1.2385	0.99	5.7407	5.2253	0.6600	0.8257	-0.6941
5.2525	0.5500	-0.0000	-0.0000	-1.0174	-0.1065	1.0502	1.00	6.2578	5.7269	0.6586	0.8330	-0.5133
5.7300	0.600	0.1711	0.0179	-0.8684	-0.0909	0.9236	1.01	6.7650	6.2291	0.6586	0.8405	-0.3514
6.2075	0.6500	0.3121	0.0327	-0.7303	-0.0765	0.7865	1.02	7.2629	6.7201	0.6613	0.8482	-0.2101
6.6850	0.7000	0.4195	0.0439	-0.6031	-0.0631	0.6667	1.03	7.7523	7.2203	0.6680	0.8558	-0.0914
7.1625	0.7500	0.4892	0.0512	-0.4867	-0.0510	0.5649	1.05	8.2349	7.7118	0.6798	0.8629	-0.0020
7.6400	0.8000	0.5183	0.0541	-0.3811	-0.0399	0.4899	1.08	8.7132	8.2008	0.6992	0.8704	0.0686
8.1175	0.8500	0.4945	0.0518	-0.2863	-0.0300	0.4281	1.11	9.1912	8.6876	0.7318	0.8754	0.1019
8.5950	0.9000	0.4139	0.0435	-0.2022	-0.0212	0.3867	1.15	9.6791	9.1725	0.7802	0.8795	0.1025
9.0725	0.9500	0.2703	0.0283	-0.1290	-0.0135	0.3631	1.00	10.1793	9.6556	0.8474	0.8755	0.0639
9.3590	0.9800	0.1452	0.0152	-0.0962	-0.0094	0.3631	1.00	10.4869	9.9447	0.8940	0.9048	0.0212
9.4545	0.9900	0.0964	0.0101	-0.0781	-0.0082	0.3699	1.00	10.5941	10.0409	0.9175	0.9204	0.0005
9.5500	1.0000	0.0	0.0	0.0	0.0	0.0079	1.00	10.7298	10.1643	0.9360	0.9360	-0.0097

THIS PAGE IS BEST QUALITY PRACTICABLE
FROM COPY FURNISHED TO DDC

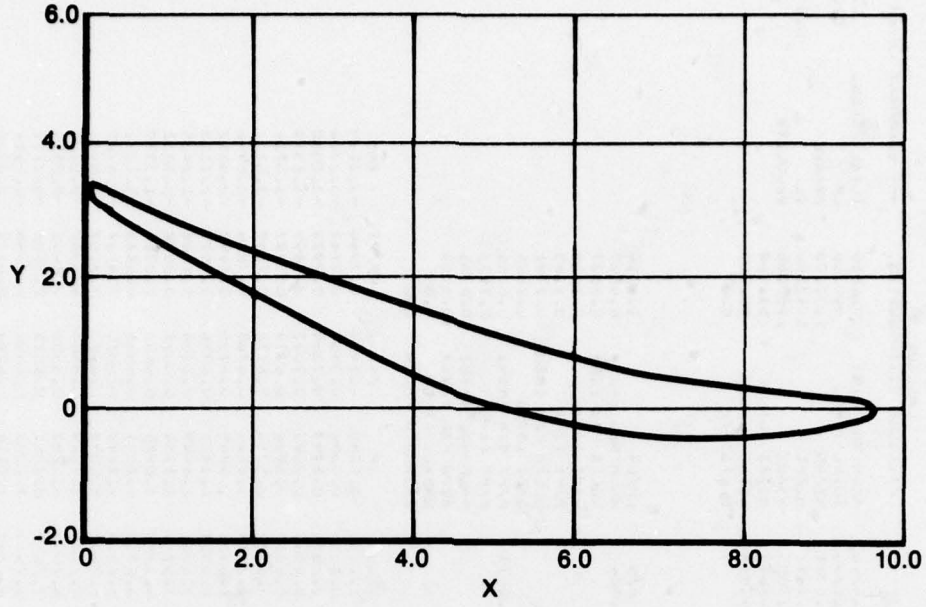


Figure G-1. Low Aspect Ratio, Root Section

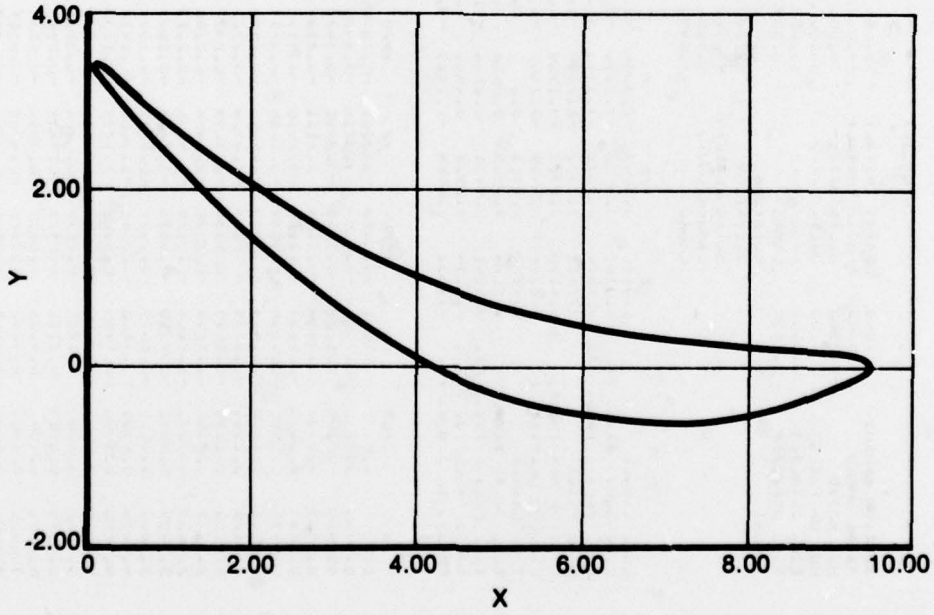


Figure G-2. Low Aspect Ratio, ¼ Root Section

TABLE G-2

LOW ASPECT RATIO EGV DESIGN, 1/4 ROOT SECTION

GEOMETRY						CASCADE PRESSURE DISTRIBUTION		BOUNDARY LAYER	
SECTION RADIUS	9.8210	BETA1 (METAL)	47.180	PITCH	7.7134	MACH NO. (IN)	0.6310	TOTAL PRESS.	0.0
AXIAL CHORD	9.5500	BETA2 (METAL)	76.500	GAGING	5.8060	TOTAL TEMP.	660.00	CP	0.0
H/L RATIO	-0.3700	DELTA BETA1	6.250	MAX THICK	1.0000	M1/M0	1.00000	PRANDL	0.0
NO. OF FOILS	8.00	DELTA BETA2	30.600	AREA	6.5509	M2/M1	1.00000	TL	0.0
L.E. DIAMETER	0.0900	GAGE ANGLE	48.826	IMIN	1.0206757	M3/M2	1.00000	VELOCITY	0.0
T.E. DIAMETER	0.1500	GAMMA	12.634	IMAX	36.5796051	BETA1 (GAS)	48.000		
THROAT	0.0	ROTATION	0.0	ALPHA	19.671	BETA2 (GAS)	90.000		
		DEVIATION	13.675			DELTA P/P	0.0		
		BETA2 (CALC)	90.175						
		CAMBER/CHORD	0.5500						
		CHORD	10.1587						

	X	X/B	Y	Y/B	R	R/B
L.E. CIRCLE	0.0450	0.0047	-3.4891	-0.3654	0.0450	0.0047
L.E. SUCT. TANG. PT.	0.0127	0.0013	-3.4578	-0.3621		
L.E. PRESS. TANG. PT.	0.0737	0.0077	-3.5237	-0.3690		
GAGE POINT	3.2583	0.3412	-0.6654	-0.0697		
CTR. OF MAX THICK.	6.3194	0.6617	0.1100	0.0115		
CTR. OF GRAVITY	5.2180	0.5464	-0.4843	-0.0507		
T.E. CIRCLE	9.4750	0.9921	0.0	0.0	0.0750	0.0079
T.E. SUCT. TANG. PT.	9.5111	0.9959	0.0657	0.0069		
T.E. PRESS. TANG. PT.	9.4774	0.9924	-0.0750	-0.0078		
SUCT. INTERMED. PT.	6.5485	0.6857	0.6523	0.0683		
PRESS. INTERMED. PT.	4.7652	0.4990	-0.7957	-0.0833		

CP/CV	1.4114
MACH NO. (EX)	0.3876
DELTA P/Q (IN)	0.6412
Q/PT (IN)	0.2145
P/PT (IN)	0.7633
DELTA P/Q (MIN)	0.7757
Q/PT (MIN)	0.2265
P/PT MIN (MIN)	0.6925
P/PT (AVE)	0.8154
MACH NO. (AVE)	0.5459
FLOW PAR (AVE)	0.4231
UNBAL. FP/FM	0.0
BALANCED FP/FM	0.0

X	X/B	YS	YS/B	YP	YP/B	RC/P	A/AG	SS	SP	PS/PT	PP/PT	YML
0.0	0.0	-3.4891	-0.3654	-3.4891	-0.3654	0.0047	1.00	0.0325	-0.0325	0.8050	0.8050	-3.5086
0.0955	0.0100	-3.3725	-0.3531	-3.5057	-0.3671	3.4603	1.00	0.1832	0.0644	0.7862	0.8066	-3.4471
0.1910	0.0200	-3.2749	-0.3429	-3.4270	-0.3588	3.3540	1.00	0.3198	0.1881	0.7673	0.8083	-3.3554
0.2865	0.0300	-3.1781	-0.3328	-3.3492	-0.3507	3.2507	1.00	0.4557	0.3113	0.7484	0.8099	-3.2683
0.3820	0.0400	-3.0822	-0.3227	-3.2722	-0.3426	3.1504	1.00	0.5911	0.4340	0.7296	0.8115	-3.1820
0.4775	0.0500	-2.9871	-0.3128	-3.1961	-0.3347	3.0531	1.00	0.7259	0.5561	0.7270	0.8150	-3.0971
0.9550	0.1000	-2.5252	-0.2644	-2.8288	-0.2962	2.6082	1.00	1.3902	1.1585	0.7144	0.8355	-2.6840
1.4325	0.1500	-2.0870	-0.2185	-2.4850	-0.2602	2.2284	1.00	2.0383	1.7470	0.7041	0.8516	-2.2940
1.9100	0.2000	-1.6746	-0.1754	-2.1659	-0.2268	1.9075	1.01	2.6692	2.3213	0.6968	0.8619	-1.9293
2.3875	0.2500	-1.2899	-0.1351	-1.8724	-0.1961	1.6392	1.02	3.2825	2.8817	0.6935	0.8702	-1.5910
2.8650	0.3000	-0.9346	-0.0979	-1.6052	-0.1681	1.4179	1.04	3.8778	3.4269	0.6927	0.8772	-1.2862
3.3425	0.3500	-0.6105	-0.0639	-1.3643	-0.1429	1.2379	1.06	4.4547	3.9637	0.6938	0.8830	-0.9977
3.8200	0.4000	-0.3189	-0.0334	-1.1492	-0.1203	1.0841	1.07	5.0142	4.4875	0.6962	0.8878	-0.7438
4.2975	0.4500	-0.0611	-0.0064	-0.9590	-0.1004	0.9503	1.08	5.5568	5.0014	0.6993	0.8913	-0.5167
4.7750	0.5000	0.1614	0.0169	-0.7925	-0.0830	0.8355	1.10	6.0836	5.5071	0.7031	0.8938	-0.3226
5.2525	0.5500	0.3471	0.0363	-0.6483	-0.0679	0.7387	1.11	6.5960	6.0059	0.7075	0.8958	-0.1557
5.7300	0.6000	0.4944	0.0516	-0.5246	-0.0549	0.6589	1.13	7.0957	6.4992	0.7132	0.8969	-0.0160
6.2075	0.6500	0.6015	0.0630	-0.4196	-0.0439	0.5955	1.14	7.5850	6.9881	0.7223	0.8979	0.0899
6.6850	0.7000	0.6665	0.0698	-0.3316	-0.0347	0.5477	1.15	8.0670	7.4736	0.7344	0.8985	0.1670
7.1625	0.7500	0.6873	0.0720	-0.2588	-0.0271	0.5150	1.17	8.5449	7.9567	0.7516	0.8988	0.2148
7.6400	0.8000	0.6618	0.0693	-0.1998	-0.0209	0.4974	1.18	9.0231	8.4378	0.7751	0.8971	0.2290
8.1175	0.8500	0.5875	0.0615	-0.1529	-0.0160	0.4949	1.21	9.5063	8.9176	0.8067	0.8981	0.2157
8.5950	0.9000	0.4618	0.0484	-0.1169	-0.0122	0.5085	1.22	10.0001	9.3964	0.8450	0.8955	0.1658
9.0725	0.9500	0.2817	0.0295	-0.0906	-0.0095	0.5394	1.00	10.5104	9.8747	0.8938	0.8799	0.0886
9.3590	0.9800	0.1463	0.0153	-0.0789	-0.0083	0.5671	1.00	10.8273	10.1614	0.9213	0.9068	0.0274
9.4545	0.9900	0.0964	0.0101	-0.0757	-0.0079	0.5780	1.00	10.9351	10.2570	0.9297	0.9225	-0.0000
9.5500	1.0000	0.0	0.0	0.0	0.0	0.0079	1.00	11.0708	10.3788	0.9382	0.9382	-0.0118

THIS PAGE IS BEST QUALITY PRACTICABLE
FROM COPY FURNISHED TO DDC

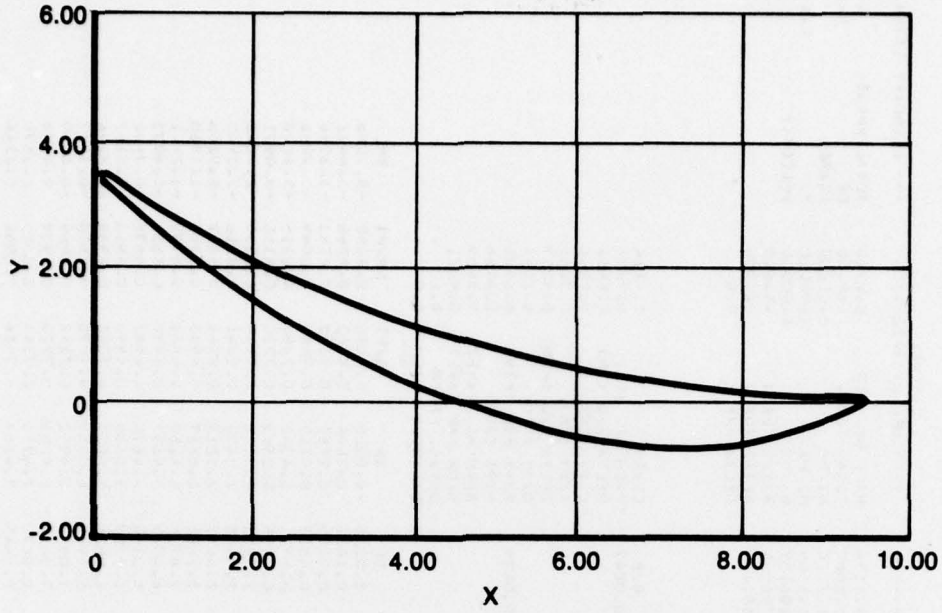


Figure G-3. Low Aspect Ratio, Mean Section

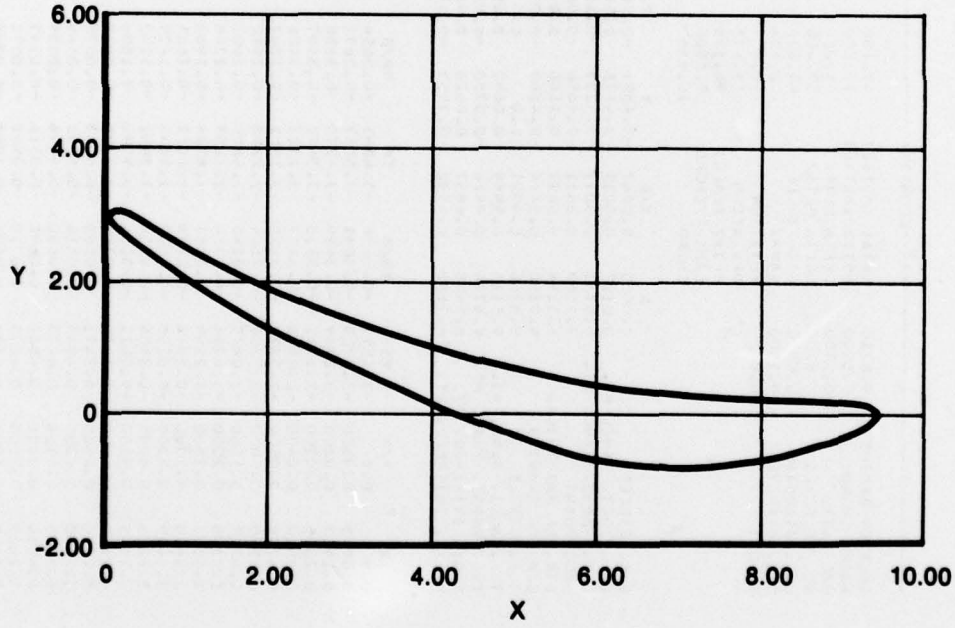


Figure G-4. Low Aspect Ratio, ¼ Tip Section

TABLE G-3

LOW ASPECT RATIO EGV DESIGN, MEAN SECTION

GEOMETRY						CASCADE PRESSURE DISTRIBUTION		BOUNDARY LAYER	
SECTION RADIUS	11.4630	BETA1 (METAL)	47.107	PITCH	9.0090	MACH NO. (IN)	0.5270	TOTAL PRESS.	0.0
AXIAL CHORD	9.5500	BETA2 (METAL)	75.000	GAGING	6.8990	TOTAL TEMP.	660.00	CP	0.0
H/L RATIO	-0.3700	DELTA BETA1	5.000	MAX THICK	1.0000	H1/H0	1.00000	PRANDL	0.0
NO. OF FOILS	8.00	DELTA BETA2	28.000	AREA	6.5838	H2/H1	1.05000	TL	0.0
L.E. DIAMETER	0.0900	GAGE ANGLE	50.023	IMIN	0.9998016	H3/H2	1.00000	VELOCITY	0.0
T.E. DIAMETER	0.1500	GAMMA	14.123	IMAX	36.1498566	BETA1 (GAS)	50.100		
THROAT	0.0	ROTATION	0.0	ALPHA	19.949	BETA2 (GAS)	40.000		
		DEVIATION	15.189			DELTA P/P	0.0		
		BETA2 (CALC)	90.189						
		CAMBER/CHORD	0.5500						
		CHORD	10.1576						

	X	X/B	Y	Y/B	P	R/B
L.E. CIRCLE	0.0450	0.0047	-3.4891	-0.3654	0.0450	0.0047
L.E. SUCT. TANG. PT.	0.0130	0.0014	-3.4575	-0.3620		
L.E. PRESS. TANG. PT.	0.0742	0.0078	-3.5234	-0.3689		
GAGE POINT	3.6495	0.3821	-0.4214	-0.0441		
CTR. OF MAX THICK.	5.9031	0.6181	0.0268	0.0028		
CTR. OF GRAVITY	5.1816	0.5426	-0.4919	-0.0515		
T.E. CIRCLE	9.4750	0.9921	0.0	0.0	0.0750	0.0079
T.E. SUCT. TANG. PT.	9.5114	0.9960	0.0656	0.0069		
T.E. PRESS. TANG. PT.	9.4737	0.9920	-0.0750	-0.0079		
SUCT. INTERMED. PT.	6.7232	0.7040	0.6771	0.0709		
PRESS. INTERMED. PT.	4.7652	0.4990	-0.8241	-0.0863		

CP/CV	1.4114
MACH NO. (EX)	0.5523
DELTA P/Q (IN)	0.5599
Q/PT (IN)	0.1620
P/PT (IN)	0.8265
DELTA P/Q (MIN)	0.6952
Q/PT (MIN)	0.2056
P/PT MIN (MIN)	0.7741
P/PT (AVE)	0.8585
MACH NO. (AVE)	0.4701
FLOW PAR (AVE)	0.3808
UNBAL. FP/FM	0.0
BALANCED FP/FM	0.0

X	X/B	YS	YS/B	YP	YP/B	RC/B	A/AC	SS	SP	PS/PT	PP/PT	YMC
0.0	0.0	-3.4891	-0.3654	-3.4891	-0.3654	0.0047	1.00	0.0313	-0.0313	0.8503	0.8503	-3.5185
0.0955	0.0100	-3.3741	-0.3533	-3.5052	-0.3670	4.0654	1.00	0.1808	0.0655	0.8396	0.8496	-3.4470
0.1910	0.0200	-3.2782	-0.3433	-3.4249	-0.3586	3.9227	1.00	0.3162	0.1903	0.8293	0.8490	-3.3555
0.2865	0.0300	-3.1829	-0.3333	-3.3459	-0.3504	3.7844	1.00	0.4510	0.3142	0.8189	0.8484	-3.2684
0.3820	0.0400	-3.0884	-0.3234	-3.2682	-0.3422	3.6506	1.00	0.5854	0.4374	0.8084	0.8477	-3.1825
0.4775	0.0500	-2.9947	-0.3136	-3.1918	-0.3342	3.5211	1.00	0.7193	0.5597	0.8060	0.8513	-3.0982
0.9550	0.1000	-2.5372	-0.2657	-2.8276	-0.2961	2.9353	1.00	1.3805	1.1602	0.7949	0.8699	-2.6893
1.4325	0.1500	-2.1008	-0.2200	-2.4922	-0.2610	2.4447	1.00	2.0274	1.7437	0.7862	0.8811	-2.3048
1.9100	0.2000	-1.6877	-0.1767	-2.1837	-0.2287	2.0391	1.00	2.6588	2.3122	0.7799	0.8872	-1.9455
2.3875	0.2500	-1.3007	-0.1362	-1.9004	-0.1990	1.7084	1.02	3.2734	2.8675	0.7766	0.8912	-1.6115
2.8650	0.3000	-0.9423	-0.0987	-1.6409	-0.1718	1.4436	1.04	3.8705	3.4109	0.7745	0.8948	-1.3031
3.3425	0.3500	-0.6147	-0.0644	-1.4042	-0.1470	1.2360	1.05	4.4495	3.9438	0.7742	0.8995	-1.0207
3.8200	0.4000	-0.3200	-0.0335	-1.1892	-0.1245	1.0764	1.06	5.0107	4.4675	0.7757	0.9027	-0.7649
4.2975	0.4500	-0.0596	-0.0062	-0.9949	-0.1042	0.9424	1.08	5.5546	4.9830	0.7777	0.9058	-0.5359
4.7750	0.5000	0.1651	0.0173	-0.8208	-0.0859	0.8277	1.10	6.0823	5.4913	0.7806	0.9085	-0.3345
5.2525	0.5500	0.3524	0.0369	-0.6660	-0.0697	0.7312	1.11	6.5952	5.9932	0.7838	0.9113	-0.1612
5.7300	0.6000	0.5008	0.0524	-0.5301	-0.0555	0.6520	1.13	7.0952	6.4897	0.7876	0.9135	-0.0169
6.2075	0.6500	0.6086	0.0637	-0.4125	-0.0432	0.5892	1.14	7.5847	6.9815	0.7931	0.9159	0.0975
6.6850	0.7000	0.6737	0.0705	-0.3129	-0.0328	0.5421	1.16	8.0667	7.4692	0.8005	0.9178	0.1862
7.1625	0.7500	0.6943	0.0727	-0.2309	-0.0242	0.5103	1.17	8.5446	7.9537	0.8111	0.9193	0.2822
7.6400	0.8000	0.6681	0.0700	-0.1662	-0.0174	0.4936	1.19	9.0228	8.4356	0.8263	0.9198	0.2465
8.1175	0.8500	0.5927	0.0621	-0.1186	-0.0124	0.4923	1.20	9.5062	8.9155	0.8479	0.9199	0.2329
8.5950	0.9000	0.4655	0.0487	-0.0878	-0.0092	0.5071	1.22	10.0004	9.3940	0.8757	0.9175	0.1817
9.0725	0.9500	0.2836	0.0297	-0.0739	-0.0077	0.5394	1.00	10.5114	9.8717	0.9136	0.9013	0.0976
9.3590	0.9800	0.1470	0.0154	-0.0735	-0.0077	0.5680	1.00	10.8288	10.1582	0.9325	0.9198	0.0303
9.4545	0.9900	0.0967	0.0101	-0.0747	-0.0078	0.5792	1.00	10.9367	10.2537	0.9377	0.9314	0.0000
9.5500	1.0000	0.0	0.0	0.0	0.0	0.0079	1.00	11.0726	10.3749	0.9430	0.9430	-0.0131

THIS PAGE IS BEST QUALITY PRACTICABLE
FROM COPY FURNISHED TO DDC

TABLE G-4

LOW ASPECT RATIO EGV DESIGN, 1/4 TIP SECTION

GEOMETRY						CASCADE PRESSURE DISTRIBUTION		BOUNDARY LAYER	
SECTION RADIUS	13.1040	BETA1 (METAL)	50.548	PITCH	10.2918	MACH NO. (IN)	0.4422	TOTAL PRESS.	0.0
AXIAL CHORD	9.5500	BETA2 (METAL)	73.500	GAGING	0.2809	TOTAL TEMP.	660.00	CP	0.0
H/L RATIO	-0.3250	DELTA BETA1	5.000	MAX THICK	0.9999	M1/M0	1.00000	PRANDL	0.0
NO. OF FOILS	8.00	DELTA BETA2	31.000	AREA	6.4699	M2/M1	1.20000	TL	0.0
L.E. DIAMETER	0.0900	GAGE ANGLE	53.572	IMIN	0.9062653	M3/M2	1.00000	VELOCITY	0.0
T.E. DIAMETER	0.1500	GAMMA	14.245	IMAX	34.5617523	BETA1 (GAS)	54.000		
TMAUAI	0.0	ROTATION	0.0	ALPHA	17.629	BETA2 (GAS)	90.000		
		DEVIATION	17.008			DELTA P/P	0.0		
		BETA2 (CALC)	90.508						
		CAMBER/CHORD	0.5700						
		CHORD	10.0192						

	X	X/B	Y	Y/B	R	R/B
L.E. CIRCLE	0.0450	0.0047	-3.0647	-0.3209	0.0450	0.0047
L.E. SUCT. TANG. PT.	0.0149	0.0016	-3.0313	-0.3174		
L.E. PRESS. TANG. PT.	0.0721	0.0075	-3.1007	-0.3247		
GAGE POINT	3.9161	0.4101	-0.1441	-0.0151		
CTR. OF MAX THICK.	6.2795	0.6575	0.1733	0.0181		
CTR. OF GRAVITY	5.2738	0.5522	-0.3494	-0.0366		
T.E. CIRCLE	9.4750	0.9921	0.0	0.0	0.0750	0.0079
T.E. SUCT. TANG. PT.	9.5147	0.9963	0.0636	0.0067		
T.E. PRESS. TANG. PT.	9.4737	0.9920	-0.0750	-0.0079		
SUCT. INTERMED. PT.	6.6833	0.6998	0.7320	0.0766		
PRESS. INTERMED. PT.	4.4940	0.4706	-0.7855	-0.0823		

CP/CV	1.4114
MACH NO. (EX)	0.2782
DELTA P/Q (IN)	0.0123
Q/PT (IN)	0.1205
P/PT (IN)	0.8735
DELTA P/Q (MIN)	0.6873
Q/PT (MIN)	0.1414
P/PT MIN (MIN)	0.8501
P/PT (AVE)	0.9054
MACH NO. (AVE)	0.3779
FLOW PAR (AVE)	0.3203
UNBAL. FP/FM	0.0
BALANCED FP/FM	0.0

X	X/B	YS	YS/B	YP	YP/B	RC/B	A/AG	SS	SP	PS/PT	PP/PT	YMC
0.0	0.0	-3.0647	-0.3209	-3.0647	-0.3209	0.0047	1.00	0.0283	-0.0283	0.8870	0.8870	-3.0818
0.0955	0.0100	-2.9590	-0.3098	-3.0831	-0.3228	4.4829	1.00	0.1707	0.0690	0.8806	0.8862	-3.0280
0.1910	0.0200	-2.8739	-0.3009	-3.0121	-0.3154	4.3225	1.00	0.2987	0.1880	0.8742	0.8853	-2.9461
0.2865	0.0300	-2.7892	-0.2921	-2.9421	-0.3081	4.1672	1.00	0.4263	0.3064	0.8677	0.8844	-2.8689
0.3820	0.0400	-2.7052	-0.2833	-2.8732	-0.3009	4.0168	1.00	0.5535	0.4242	0.8613	0.8836	-2.7926
0.4775	0.0500	-2.6216	-0.2745	-2.8053	-0.2937	3.8713	1.00	0.6804	0.5413	0.8606	0.8866	-2.7175
0.5550	0.1000	-2.2130	-0.2317	-2.4812	-0.2598	3.2130	1.00	1.3089	1.1184	0.8543	0.9010	-2.3523
1.4325	0.1500	-1.8209	-0.1907	-2.1618	-0.2285	2.6618	1.00	1.9267	1.6820	0.8512	0.9070	-2.0077
1.9100	0.2000	-1.4477	-0.1516	-1.9061	-0.1996	2.2064	1.00	2.5328	2.2334	0.8501	0.9148	-1.6844
2.3875	0.2500	-1.0960	-0.1148	-1.6550	-0.1731	1.8359	1.01	3.1258	2.7738	0.8510	0.9184	-1.3830
2.8650	0.3000	-0.7684	-0.0805	-1.4218	-0.1489	1.5400	1.03	3.7049	3.3044	0.8532	0.9221	-1.1040
3.3425	0.3500	-0.4673	-0.0489	-1.2115	-0.1269	1.3090	1.04	4.2694	3.8261	0.8563	0.9250	-0.8483
3.8200	0.4000	-0.1952	-0.0204	-1.0213	-0.1069	1.1344	1.05	4.8190	4.3401	0.8604	0.9279	-0.6166
4.2975	0.4500	0.0401	0.0048	-0.8505	-0.0891	1.0004	1.06	5.3540	4.8472	0.8642	0.9302	-0.4093
4.7750	0.5000	0.2552	0.0267	-0.6984	-0.0731	0.8827	1.08	5.8753	5.3484	0.8683	0.9326	-0.2272
5.2525	0.5500	0.4303	0.0451	-0.5644	-0.0591	0.7798	1.08	6.3839	5.8443	0.8719	0.9341	-0.0708
5.7300	0.6000	0.5697	0.0597	-0.4477	-0.0469	0.6915	1.10	6.8813	6.3359	0.8755	0.9369	0.0589
6.2075	0.6500	0.6711	0.0703	-0.3478	-0.0364	0.6174	1.11	7.3695	6.8237	0.8786	0.9389	0.1605
6.6850	0.7000	0.7322	0.0767	-0.2642	-0.0277	0.5574	1.12	7.8508	7.3085	0.8822	0.9407	0.2339
7.1625	0.7500	0.7499	0.0785	-0.1964	-0.0206	0.5114	1.13	8.3287	7.7908	0.8867	0.9424	0.2749
7.6400	0.8000	0.7208	0.0755	-0.1437	-0.0151	0.4793	1.14	8.8071	8.2711	0.8933	0.9428	0.2858
8.1175	0.8500	0.6409	0.0671	-0.1059	-0.0111	0.4616	1.15	9.2912	8.7501	0.9042	0.9443	0.2608
8.5950	0.9000	0.5053	0.0529	-0.0823	-0.0086	0.4592	1.00	9.7876	9.2282	0.9202	0.9437	0.2022
9.0725	0.9500	0.3079	0.0322	-0.0727	-0.0076	0.4735	1.00	10.3043	9.7058	0.9447	0.9342	0.1075
9.3590	0.9800	0.1569	0.0164	-0.0734	-0.0077	0.4912	1.00	10.6281	9.9923	0.9555	0.9460	0.0333
9.4545	0.9900	0.1006	0.0105	-0.0747	-0.0078	0.4988	1.00	10.7390	10.0878	0.9581	0.9534	0.0004
9.5500	1.0000	0.0	0.0	0.0	0.0	0.0079	1.00	10.8777	10.2091	0.9608	0.9608	-0.0146

THIS PAGE IS BEST QUALITY PRACTICABLE
FROM COPY FURNISHED TO DDC

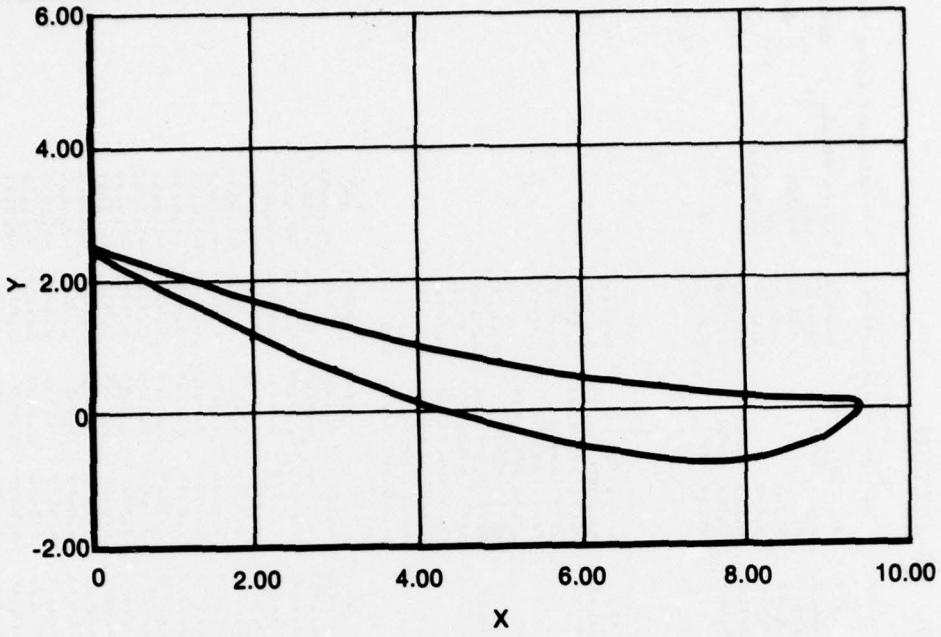


Figure G-5. Low Aspect Ratio, Tip Section

TABLE G-5

LOW ASPECT RATIO EGV DESIGN, TIP SECTION

GEOMETRY						CASCADE PRESSURE DISTRIBUTION		BOUNDARY LAYER	
SECTION RADIUS	14.7430	BETA1 (METAL)	56.519	PITCH	11.5807	MACH NO. (IN)	0.3420	TOTAL PRESS.	0.0
AXIAL CHORD	9.5300	BETA2 (METAL)	73.000	GAGING	10.0023	TOTAL TEMP.	660.00	CP	0.0
M/L RATIO	-0.2750	DELTA BETA	0.000	MAX THICK	0.9999	M1/M0	1.00000	PRANDL	0.0
NO. OF BLDS	0.00	DELTA BETA2	37.500	AREA	0.4077	M2/M1	1.81560	IL	0.0
L.E. DIAMETER	0.0300	GAGE ANGLE	54.735	IMIN	0.6175079	M3/M2	1.00000	VELOCITY	0.0
T.E. DIAMETER	0.1500	GAMMA	11.248	IMAX	34.4339752	BETA1 (GAS)	61.200		
THKDAT	0.0	ROTATION	0.0	ALPHA	15.000	BETA2 (GAS)	90.000		
		DEVIATION	15.032			DELTA P/P	0.0		
		BETA2 (CALC)	90.032						
		CAMBER/CHORD	0.5000						
		CHORD	9.8800						

	A	X/B	Y	Y/B	R	R/B		
L.E. CIRCLE	0.0450	0.0047	-2.5932	-0.2715	0.0450	0.0047	CP/CV	1.4114
L.E. SUCT. TANG. PT.	0.0193	0.0020	-2.5565	-0.2677			MACH NO. (EX)	0.1303
L.E. PRESS. TANG. PT.	0.0002	0.0000	-2.6330	-0.2757			DELTA P/Q (IN)	0.8055
GAGE POINT	4.0727	0.4262	-0.2172	-0.0227			W/PT (IN)	0.0761
CIR. OF MAX THICK.	0.3803	0.0681	0.0137	0.0016			P/PT (IN)	0.9217
CIR. OF GRAVITY	0.3396	0.0591	-0.4218	-0.0442			DELTA P/Q (MIN)	0.8218
T.E. CIRCLE	9.4750	0.9921	0.0	0.0	0.0750	0.0079	W/PT (MIN)	0.0812
T.E. SUCT. TANG. PT.	9.5167	0.9965	0.0624	0.0065			P/PT MIN (MIN)	0.9102
T.E. PRESS. TANG. PT.	9.4799	0.9927	-0.0748	-0.0078			P/PT (AVE)	0.9523
SUCT. INTERMED. PT.	7.2649	0.7609	0.0277	0.0029			MACH NO. (AVE)	0.2041
PRESS. INTERMED. PT.	4.7852	0.4990	-0.6031	-0.0904			FLOW PAR (AVE)	0.2337
							UNBAL. FP/FM	0.0
							BALANCED FP/FM	0.0

X	X/B	YS	YS/B	YP	YP/B	RC/B	A/AC	SS	SP	PS/PT	PP/PT	YML
0.0	0.0	-2.5932	-0.2715	-2.5932	-0.2715	0.0047	1.00	0.0226	-0.0226	0.9307	0.9307	-2.6059
0.0955	0.0100	-2.5835	-0.2705	-2.6114	-0.2734	3.9224	1.00	0.1338	0.0759	0.9265	0.9314	-2.5871
0.1910	0.0200	-2.6334	-0.2757	-2.5871	-0.2708	3.4816	1.00	0.2698	0.1838	0.9224	0.9322	-2.5852
0.2865	0.0300	-2.5720	-0.2693	-2.5178	-0.2636	3.4403	1.00	0.3850	0.2913	0.9182	0.9330	-2.4479
0.3820	0.0400	-2.5676	-0.2688	-2.4693	-0.2586	3.3980	1.00	0.5011	0.3984	0.9141	0.9338	-2.3914
0.4775	0.0500	-2.5625	-0.2683	-2.4217	-0.2536	3.3568	1.00	0.6163	0.5051	0.9146	0.9356	-2.3358
0.5730	0.0601	-1.9271	-0.2019	-2.1940	-0.2298	3.1404	1.00	1.1883	1.0338	0.9176	0.9437	-2.0659
1.4325	0.1500	-1.6258	-0.1702	-1.9847	-0.2078	2.9102	1.00	1.7532	1.5554	0.9218	0.9490	-1.8106
1.9100	0.2000	-1.3572	-0.1420	-1.7893	-0.1874	2.6859	1.00	2.3112	2.0714	0.9269	0.9528	-1.5692
2.3875	0.2500	-1.0822	-0.1133	-1.6071	-0.1683	2.4917	1.00	2.8620	2.5825	0.9320	0.9557	-1.3411
2.8650	0.3000	-0.8024	-0.0840	-1.4308	-0.1498	2.2156	1.01	3.4058	3.0894	0.9369	0.9585	-1.1262
3.3425	0.3500	-0.5380	-0.0564	-1.2778	-0.1338	1.9799	1.01	3.9422	3.5927	0.9414	0.9609	-0.9243
3.8200	0.4000	-0.3304	-0.0346	-1.1268	-0.1180	1.7470	1.01	4.4712	4.0925	0.9459	0.9632	-0.7351
4.2975	0.4500	-0.1211	-0.0127	-0.9899	-0.1037	1.5223	1.02	4.9926	4.5902	0.9492	0.9654	-0.5608
4.7750	0.5000	0.0084	0.0009	-0.8605	-0.0901	1.3178	1.02	5.5063	5.0849	0.9523	0.9673	-0.4004
5.2525	0.5500	0.2358	0.0247	-0.7403	-0.0775	1.1308	1.03	6.0122	5.5773	0.9551	0.9692	-0.2534
5.7300	0.6000	0.3765	0.0394	-0.6291	-0.0659	0.9638	1.03	6.5100	6.0676	0.9577	0.9711	-0.1273
6.2075	0.6500	0.4936	0.0517	-0.5268	-0.0552	0.8166	1.04	7.0018	6.5559	0.9599	0.9729	-0.0177
6.6850	0.7000	0.5774	0.0605	-0.4334	-0.0454	0.6875	1.05	7.4866	7.0424	0.9617	0.9746	0.0719
7.1625	0.7500	0.6254	0.0655	-0.3490	-0.0365	0.5761	1.06	7.9665	7.5273	0.9634	0.9763	0.1572
7.6400	0.8000	0.6317	0.0661	-0.2738	-0.0287	0.4886	1.07	8.4440	8.0107	0.9647	0.9779	0.1761
8.1175	0.8500	0.5886	0.0617	-0.2079	-0.0218	0.4175	1.08	8.9234	8.4928	0.9669	0.9793	0.1852
8.5950	0.9000	0.4869	0.0509	-0.1517	-0.0159	0.3672	1.09	9.4118	8.9730	0.9715	0.9804	0.1577
9.0725	0.9500	0.3109	0.0325	-0.1056	-0.0111	0.3391	1.00	9.9207	9.4533	0.9794	0.9793	0.0905
9.5500	0.9800	0.1022	0.0107	-0.0831	-0.0087	0.3343	1.00	10.2437	9.7407	0.9846	0.9836	0.0291
9.6542	0.9900	0.1029	0.0108	-0.0765	-0.0080	0.3351	1.00	10.3350	9.8304	0.9866	0.9860	0.0026
9.5500	1.0000	0.0	0.0	0.0	0.0	0.1079	1.00	10.4960	9.9588	0.9884	0.9884	-0.0134

THIS PAGE IS BEST QUALITY PRACTICABLE
FROM COPY FURNISHED TO DDC

APPENDIX H
DESIGN DEVIATION PREDICTION METHOD

Determine nose points at leading and trailing edge.

Connect nose points with straight line B.

Determine from airfoil mean camber line coordinates point of maximum camber.

Determine distance from nose point to point closest to point of maximum camber along line B - define as A.

Calculate ratio A/B.

Camber $\sigma^* = 180 - (\beta_2^* + \beta_3^*)$

Calculate $\beta_{3\ \text{corrected}} =$

$$\frac{\beta_2^* + \sigma^* \left[1.0 - (0.23\ [2\ A/B]^2 + 0.18)\ \sqrt{Tau}/B\right]}{(1.0 - 0.002\ \sigma^*\ \sqrt{Tau}/B)}$$

$\beta_{3\ (gas)} = 180 - \beta_{3\ \text{corrected}}$

Deviation $= \beta_{3\ (gas)} - \beta_3^*$

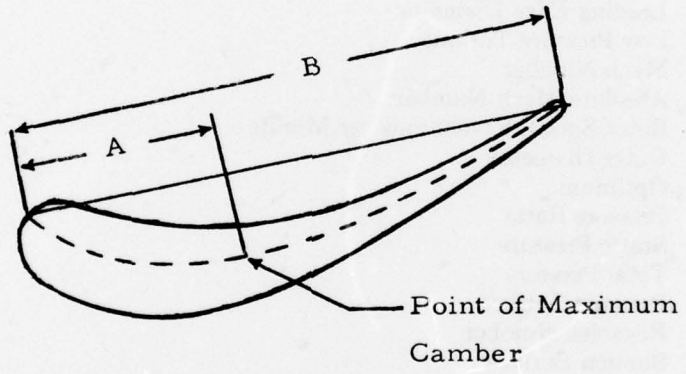


Figure H-1. Maximum Camber Location

ABBREVIATIONS AND SYMBOLS

A	Flow Area
AA	Annulus Area
AR	Aspect Ratio, Exit Span Height/Axial Chord
AVE	Average
b	Actual Chord
bx	Axial Chord
C	Absolute Velocity
C_f	Coefficient of Friction
C_L	Zwiefel Load Coefficient
C_x	Absolute Velocity Axial Direction
D_f	Diffusion Factor
EGV	Exit Guide Vane
g	Gravitational Constant
H	Specific Enthalpy
H	Two-dimensional Channel Height
H	Tangential distance between LE and TE circle centers
ΔH_T	Stage Work
HPT	High Pressure Turbine
ID	Inner Diameter
ITV	Inlet Turning Vane
J	Heat Equivalent of Work
K	Screen Blockage Factor
L	Axial distance between LE and TE circle centers
L	Plane Cascade Total Width between top and bottom plates
LE	Leading Edge
LED	Leading Edge Diameter
LPT	Low Pressure Turbine
M	Mach Number
M_A	Absolute Mach Number
N	Rotor Speed, Revolutions per Minute
OD	Outer Diameter
OPT	Optimum
P_R	Pressure Ratio
P_s	Static Pressure
P_T	Total Pressure
PS	Pressure Surface
R_N	Reynolds Number
SS	Suction Surface
t	Airfoil Thickness
TE	Trailing Edge
TED	Trailing Edge Diameter
T_T	Total Temperature
U	Blade Wheel Speed
V	Velocity
V_{RM}	Mean Velocity Ratio, $V_{RM} = (U_M/\sqrt{2gJ\Delta H})$
W	Mass Flow Rate

W_{BL}	Boundary Layer Bleed Flowrate
W_{TOT}	Total Flowrate
β	Air Angle
β^*	Metal Angle
γ	Ratio of Specific Heats
γ	Stagger Angle
Δ	Differential Quantity
δ	Velocity Boundary Layer Thickness
δ	Displacement Thickness
ΔP_T	Total Pressure Loss
ΔP_S	Static Pressure Rise
η_D	Diffusion Efficiency
θ	Air Turning
θ	Secondary Flow Expansion Angle
θ^*	Metal Turning (Camber)
θ_{eq}	Equivalent Cone Angle
λ	Gaging
ρ	Density
τ	Pitch-Gap

Instrumentation Stations

Station 0	Plenum
Station 1	Inlet to Inlet Turning Vanes
Station 2	Inlet to Exit Guide Vanes
Station 3	Inlet to Downstream Diffuser
Station 4	Downstream Diffuser Exit

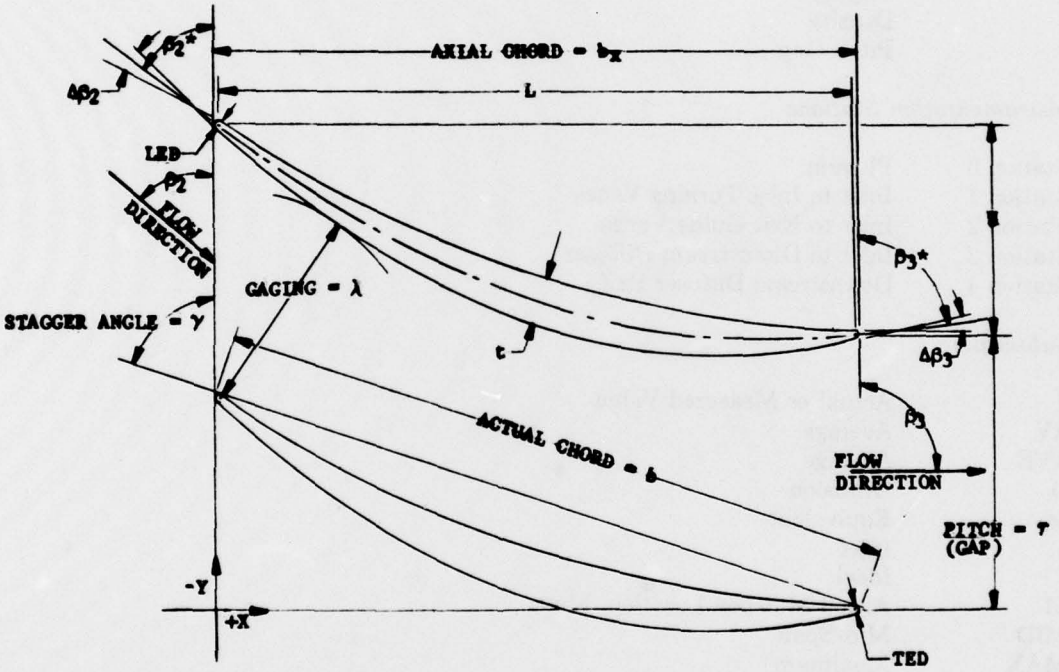
Subscripts

a	Actual or Measured Value
AV	Average
AVE	Average
D	Diffusion
eq	Equivalent
i	Inlet
I	Ideal
M	Airfoil Midspan Location, Mean
MID	Mid-Span
MAX	Maximum
r	Ratio
R	Ratio
S	Static
T	Total

ABBREVIATIONS AND SYMBOLS (Continued)

X	Axial Direction
Y	Tangential Direction
0	Denotes Instrumentation Station, 0
1	Denotes Instrumentation Station, 1
2	Denotes Instrumentation Station, 2 or EGV Airfoil Inlet
3	Denotes Instrumentation Station, 3 or EGV Airfoil Exit
4	Denotes Instrumentation Station, 4

Airfoil Nomenclature



*U.S.Government Printing Office: 1978 — 757-080/80